Food Poisoning

Outbreaks, Bacterial Sources and Adverse Health Effects

Paresh C. Ray
Editor

Food and Beverage Consumption and Health

NOVA

FOOD POISONING

OUTBREAKS, BACTERIAL SOURCES AND ADVERSE HEALTH EFFECTS

FOOD AND BEVERAGE CONSUMPTION AND HEALTH

Additional books in this series can be found on Nova's website under the Series tab.

Additional e-books in this series can be found on Nova's website under the e-book tab.

FOOD POISONING

OUTBREAKS, BACTERIAL SOURCES AND ADVERSE HEALTH EFFECTS

PARESH C. RAY
EDITOR

nova publishers
New York

Library of Congress Cataloging-in-Publication Data

ISBN: 978-1-63463-366-6 (eBook)

Library of Congress Control Number: 2014951978

Published by Nova Science Publishers, Inc. † New York

CONTENTS

PREFACE

Outbreaks of pathogens and chemical food poisoning occur regularly in this world. There is no doubt that the source of food poisoning and adverse health effects are fast growing research and technology areas in the last twenty years. Food recalls due to the presence of food-borne pathogens and toxic chemicals are the nightmares for economic growth of the world. Due to the lack of highly sensitive methods for the identification of pathogens and toxic chemicals in food sample, our society needs rapid, sensitive, and reliable assay to identify the harmful pathogens and toxic chemicals from food. The first volume in the "*Food Poisoning: Outbreaks, Bacterial Sources and Adverse Health Effects"* series contains ten chapters covering from basic science to possible device design which can have immense applications in our society. This book is unique in its design and content, providing depth of science about different causes of food poison, possible health effects and the latest research about how to detect those food-borne pathogens and toxic chemicals. I believe that the readers will be very pleased to read the wide range of start-of-the art techniques, which can be used to find pathogen source and to overcome adverse health effects. We thank all the expert scientists for their contributions and Nova Science Publishers, Inc for printing and timely publishing of the book for the future readers.

In the first chapter, Prof. Peter Fu from the National Center for Toxicological Research, Jefferson, Arkansas, USA discusses about food poisoning caused by pyrrolizidine alkaloid-containing plants. It is now well documented that pyrrolizidine alkaloid-containing plants are probably the most common type of poisonous plants affecting livestock, wildlife and humans. Since the use of dietary supplements and functional foods has grown rapidly in the last twenty years, we have to ensure that commercial herbal plants and herbal products are free from pyrrolizidine alkaloids. Current chapter entitled *"Pyrrolizidine Alkaloids: Toxic Phytochemicals Found in Food"* deals with the sources, routes of human exposure, and underlying mechanisms leading to hepatototoxicity of pyrrolizidine alkaloids present in herbal plants and herbal products. It also discusses the underlying mechanism by which pyrrolizidine alkaloids induce liver tumors in experimental animals. As an outlook, authors discuss the development of practical and liable methods for determining genotoxicity and tumorigenicity mechanism is very important.

Second chapter entitled *"Nanosilver-Based Antibacterial Agents for Food Safety"* by Shareena et, al. from USA reports the importance of food safety issues, the use of silver and nanosilver as antibacterial agents and the mechanism of action on microbial pathogens and parasites. Extensive research reports indicate that nanosilver, an ancient antibiotic, can be

reconsidered to be used as an antibiotic in combination with some of the outdated antibiotics for the treatment of infections. Current chapter summarizes bacteria-related food safety issues, mechanisms of antimicrobial/antiparasitic properties of nanosilver, and the use of nanosilver-based antimicrobials. It also discusses the synergistic effects and mechanistic pathways of combined antibiotics and nanosilver on microbial pathogens and parasites. At the end, they conclude that the antibacterial effect of nanosilver-antibiotic combination is greatly dependent on the size, stabilizer of nanosilver as well as the type of antibiotic molecules. Silver nano technology with combination of antibiotics has good potential to overcome microbial drug resistance, which is the main theme of this chapter.

In the third chapter entitled *"Laser-Induced Breakdown Spectroscopy (LIBS) as a potential tool for food safety",* Prof. Rosalie A. Multari from Applied Research Associates, Albuquerque, New Mexico, USA discusses the potential of LIBS as a tool for food safety applications. Over last few decades, LIBS has been shown to be useful for the detection of toxic metals from soil. It has been also reported that LIBS can be used for biological and chemical elements from fresh vegetables and food powders. Current chapter deals with the use of LIBS as a diagnostic tool for certain food safety applications. It discusses in detail the analysis of LIBS spectra for accurate identification of chemical and biological moieties in food. At the end, they conclude that after better design, the use of LIBS for food safety would allow for near real-time detection of both chemical and bacterial contaminations, thereby enhancing food safety.

Chapter 4 entitled *"Two Dimensional Graphene material for Food Pathogen Diagnosis"* by Bhanu Priya et al. illustrates the current status of the use of graphene material for food-borne pathogen sensing. Current chapter focuses on the basic concepts and critical properties of graphene materials that are useful for the pathogen sensing from food sample. Due to the remarkable electronic and structural properties, graphene based device may have immense applications in food industry. At the end, authors discuss about the possible future research in this area for the next generation scientific community.

In the fifth chapter *entitled "Plasmonic Nano-Probe and Nano-Medicine for Selective Detection, Ultrasensitive Quantification, and Untrendy Treatment for Food-borne Bacterial Infection"* by Dulal Senapati from Saha Institute of Nuclear Physics, India, reviews the plasmonic nanomaterials-based optical and spectroscopic techniques for strain-specific detection, quantification and efficient destruction of different food-borne bacteria. Since last ten years, intense research has been performed on how to use nanomaterial's size and shape dependent plasmonic properties for selective food-pathogen detection and photothermal killing. Current chapter reviews different types of food-borne bacterial species and their possible adverse health effects. It discusses about recent development on nano-materials based optical and spectroscopic techniques for detection, diagnosis and use of plasmonic nanoparticle for the treatment for food-borne bacterial infection. At the end, the author concludes that continuous research activity will likely lead to the development of exciting plasmonic based techniques which can resolve our society's problem on food poisoning.

Chapter 6, entitled *"Pseudomonas and Arsenic mediated endemic outbreaks of food and water"* by Debashis Chatterjee et al. from India discusses about a brief history of different factors such as lack of food storage and transport facilities, which causes contamination of food by several microorganisms and chemicals. Current chapter deals with food spoilage by *Pseudomonas* and arsenic which affects fresh water source of life for several millions people, mainly in Asia. This chapter also highlights several issues and concerns on public health of

food spoilage. At the end, authors discuss few thoughts on future affordable and user friendly technology needs to be developed.

In the 7th chapter, Dr. Brian G. Yust from University of Texas-Pan American, USA and others, discuss the possible mechanisms and operating principle for the targeted separation, imaging, and photothermal destruction of Mulidrug Resistance Bacteria (MDRB) from food sample using magnetic-plasmonic nanotechnology. Since last two decades, infectious disease outbreaks due to MDRB infections have been one of the leading causes of death globally. Current chapter entitled "*Hybrid Multifunctional Nanoparticles as Platforms for Targeted Detection, Separation, and Photothermal Destruction of Food Pathogens"* reviews the synthesis path for iron magnetic core–shell gold nanoparticle and how to use them for the targeted magnetic separation and enrichment, imaging, and the photothermal destruction of MDR Salmonella DT104. The reported method in this chapter can be used as an alternative way to destroy MDRB. At the end, they conclude that after the optimization of different parameters, hybrid nanotechnology-driven assay could have enormous potential for applications in the rapid MDRB separation and detection from food sample.

Chapter 8 by Prof. Ashton T. Hamme et al. from USA presents a summary of the development of plasmonic carbon nanotube (CNT) nanotechnology-based bioassays, which can used for the detection and photo thermal destruction of foodborne pathogens. Current chapter entitled "*Multifunctional SERS-Based SWCNT & Gold Nanostructures for Targeted Detection and Photothermal Destruction of Foodborne Pathogens*" discusses the fundamental concepts and novel properties of the nanomaterials that are useful for the detection and killing of the food-borne pathogens. This chapter provides an overview of strategies that applies SWCNT and gold nanotechnology to detect and destroy MDRB for food safety. As an outlook, they believe that properly chosen combinations of plasmonic and carbon nanomaterials can be used as multifunctional nanomedical platforms for multimodal diagnosis of MDRB from food sample.

In the ninth chapter Kanchanapally et al. discuss the development of hybrid SERS platform, which can be used for highly selective and ultra-sensitive detection of melamine in parts per quadrillion level. Since melamine from food are known to form insoluble crystals in the kidney, which causes renal failure and even death for child, a device which can detect very low concentration of melamine will be very useful for society. Current chapter entitled "*Detection of Melamine from Food in Parts Per Quadrillion Level Using Functionalized Graphene Oxide- Gold Nanoparticle Hybrid SERS Platform"* discusses about how the hybrid graphene oxide based SERS platform can be used as an excellent SERS substrate for the ultra-sensitive melamine detection from melamine contaminated milk product. At the end, they conclude that reported plasmonic graphene based assay could have enormous potential applications in rapid, on-site screening of melamine in food samples.

Chapter 10 by Louis Z G Touyz from McGill University, Montreal QC, discusses about the toxicity of naphthalene vapor to human cells and tissues. This chapter entitled "*Naphthalene Mothballs: A silent killer*" discusses about various signs and symptoms derived from acute or chronic naphthalene poisoning. It also reports different methods of avoidance and palliative care of mothball poisoning. Author also suggested possible sociological strategies for people to minimize risks from mothball poisoning.

I hope that all the readers will be as excited as I am with the board range of coverage on food technology. We would value feedback from all readers of this book. Your comments are

very important for us to improve the next edition. So please feel free to e-mail your suggestion to me via e-mail: paresh.c.ray@jsums.edu.

Thank you for reading.

Paresh C. Ray, 08/26/2014
Professor of Chemistry & Biochemistry
Jackson State University
P. O. Box 17910
Jackson, MS 39217
Tel: (601) 979-3486
Fax: (601) 979-3674
E-mail: paresh.c.ray@jsums.edu

In: Food Poisoning
Editor: Paresh C. Ray
ISBN: 978-1-63463-166-2

Chapter 1

PYRROLIZIDINE ALKALOIDS: TOXIC PHYTOCHEMICALS FOUND IN FOOD

Peter Fu [*] ***and Qingsu Xia***
Division of Biochemical Toxicology, National Center for Toxicological Research, Jefferson, Arkansas, US

ABSTRACT

There are more than 660 structurally different pyrrolizidine alkaloids and pyrrolizidine alkaloid *N*-oxides present in over 6,000 plants worldwide and about half of those plants are hepatotoxic. In addition, many pyrrolizidine alkaloids are genotoxic and tumorigenic. Pyrrolizidine alkaloid-containing plants are probably the most common type of poisonous plants affecting livestock, wildlife, and humans. Humans are exposed to toxic pyrrolizidine alkaloids through intake of contaminated staple foods, herbal medicines, herbal dietary supplements, and herbal teas, and this may result in acute poisoning, chronic poisoning, and epidemic outbreaks. While this is a serious health concern, to date, there are no practical analytical methods that can quantify the total quantity of toxic pyrrolizidine alkaloids present in herbal plants, herbal products, or contaminated foods, such as honey and milk**.** Very recently, the mechanism by which pyrrolizidine alkaloids induce liver tumors in experimental animals was determined at the molecular level, and the structures of the resulting exogenous DNA adducts were fully elucidated. The results of further studies indicate that a set of DNA adducts is a common biological biomarker of pyrrolizidine alkaloid tumorigenicity and exposure.

INTRODUCTION

Pyrrolizidine alkaloids are heterocyclic compounds containing a necine base with a characteristic bicyclic nitrogen-containing heterocyclic ring [1-3]. Upon hydrolysis, pyrrolizidine alkaloids produce a necic acid and a necine base. Structurally, different types of necine bases constitute different types of toxic and nontoxic pyrrolizidine alkaloids.

[*] Email: peter.fu@fda.hhs.gov, Tel: 870-543-7207, Fax: 870-543-7136.

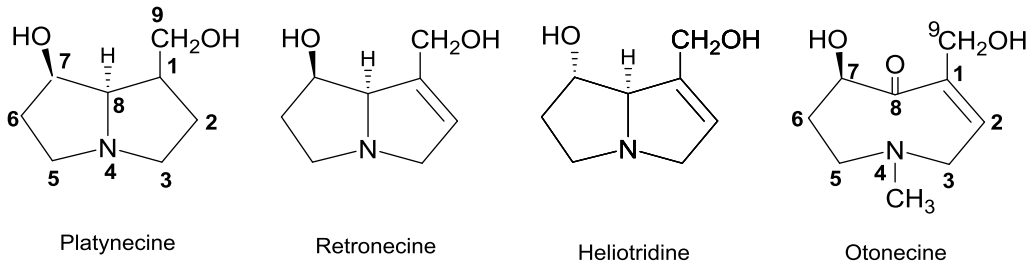

Figure 1. The common-necine bases of pyrrolizidine alkaloids.

The most common necine bases of pyrrolizidine alkaloids are platynecine, retronecine, heliotridine, and otonecine (Figure 1). Retronecine and heliotridine are enantiomers, with the former possessing a 7R-hydroxyl group and the latter having a 7S-hydroxyl group. Pyrrolizidine alkaloid *N*-oxides, *N*-oxidized derivatives of retronecine-type and heliotridine-type pyrrolizidine alkaloids, are also natural plant constituents. The quantity of pyrrolizidine alkaloid *N*-oxides in a plant can be higher, nearly equal to, or lower than the corresponding parent pyrrolizidine alkaloids [2]. Due to the presence of a methyl group at the nitrogen atom of the necine base, otonecine-type pyrrolizidine alkaloids cannot biologically form the corresponding pyrrolizidine alkaloid *N*-oxides. Pyrrolizidine alkaloid *N*-oxides exhibit a variety of physical, chemical, and biological properties different from pyrrolizidine alkaloids. For example, pyrrolizidine alkaloids are generally lipophilic, but pyrrolizidine alkaloid *N*-oxides are very water-soluble. Pyrrolizidine alkaloids derived from other necine bases, such as crotanecine and supinidine, are less studied [2].

There are approximately 660 pyrrolizidine alkaloids and pyrrolizidine alkaloid *N*-oxides present in more than 6000 plants. Retronecine-type, heliotridine-type, and otonecine-type pyrrolizidine alkaloids have a double bond at the C1 and C2 positions of the necine base. Most, if not all, of them exhibit hepatotoxicity and genotoxicity, and many possess carcinogenicity [1, 2, 4]. The names and structures of representative pyrrolizidine alkaloids are shown in Figure 2. Plant-generated pyrrolizidine alkaloids are typically esterified necines.

It has been recognized since the eighteenth century that pyrrolizidine alkaloids are highly toxic. Livestock were poisoned by grazing on pyrrolizidine alkaloid-containing plants, particularly the plant genuses *Senecio, Crotalaria,* and *Heliotropium*. Pyrrolizidine alkaloid poisoning affects most species of domestic livestock, and causes tremendous livestock loss worldwide [2, 5-12]. Pyrrolizidine alkaloids are also toxic to a variety of animal species [9, 13-17]. The toxic effects of pyrrolizidine alkaloids gained further attention when a series of pyrrolizidine alkaloids were found to be genotoxic and tumorigenic in experimental animals [1, 2, 4]. It became even more serious when human poisoning caused by pyrrolizidine alkaloids was reported [1, 3, 18-24]. The International Programme on Chemical Safety (IPCS) determined that pyrrolizidine alkaloids present in food are a threat to human health and safety [25] A number of countries around the world have enacted regulatory decisions for limiting the use of toxic pyrrolizidine alkaloids [25]. In 2011, the U.S. National Toxicology Program (NTP) classified riddelliine as "reasonably anticipated to be a human carcinogen" in the NTP 12th Report of Carcinogens [26]. Because of their widespread occurrence and high toxicity, pyrrolizidine alkaloid-containing plants are probably the most common poisonous plants affecting livestock, wildlife, and humans [2-4, 27-29].

Many reviews, book chapters, and books on the chemistry, toxicity, and mechanisms of pyrrolizidine alkaloids have been published [1, 2, 18, 20, 22, 28, 30-47]. In this review, the sources, routes of human exposure, and underlying mechanisms leading to hepatototoxicity of pyrrolizidine alkaloids contained in herbal plants and herbal products are described. The underlying mechanism by which pyrrolizidine alkaloids induce liver tumors in experimental animals, which was recently determined at the molecular level, is also reviewed.

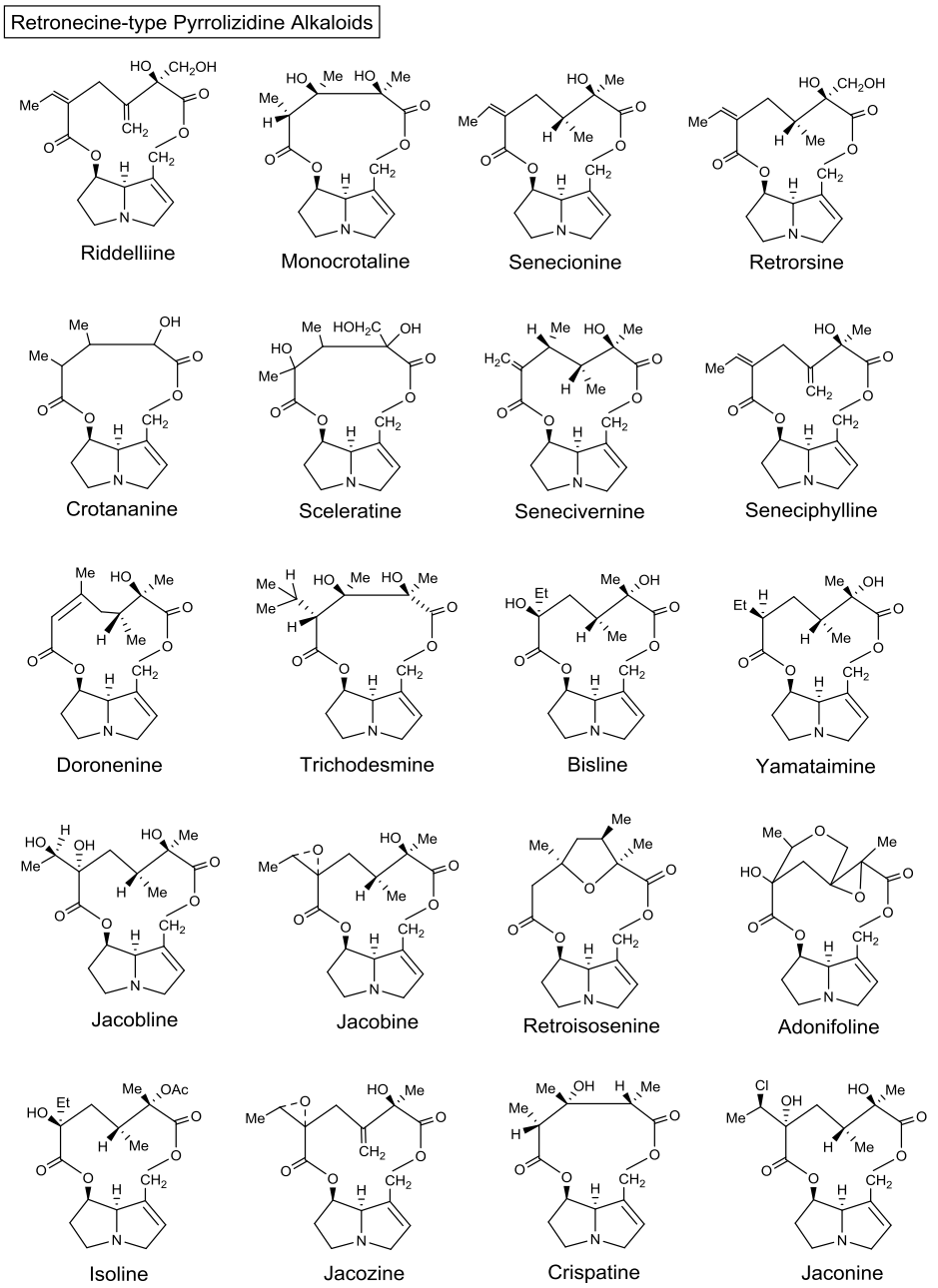

Figure 2. (Continued).

Heliotridine-type Pyrrolizidine Alkaloids

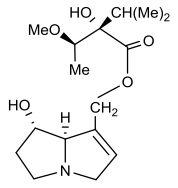
Heliotrine

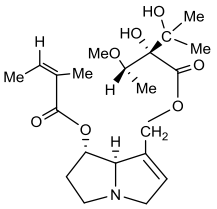
Lasiocarpine

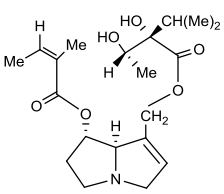
Trachelanthate

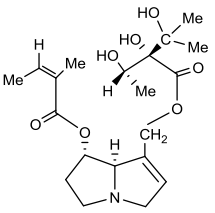
Asperumine

Otonecine-type Pyrrolizidine Alkaloids

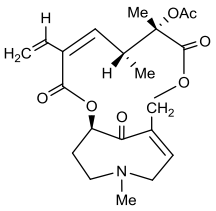
Clivorine

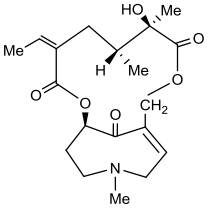
Senkirkine

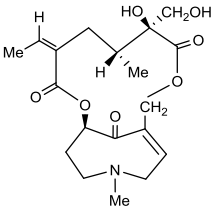
Hydroxysenkirkine

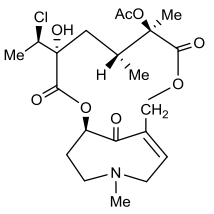
Doronine

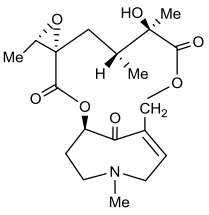
Otosenine

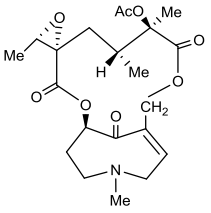
Florosenine

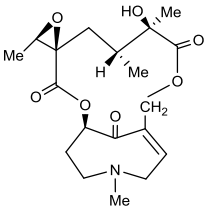
Petasitenine

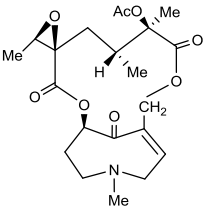
Neopetasitenine

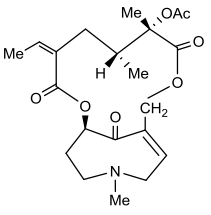
Ligularidine

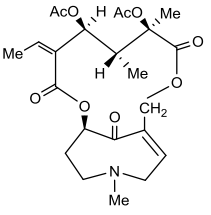
Ligularine

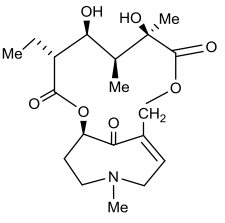
Syneilesine

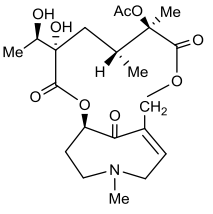
Floriidanine

Platynecine-type Pyrrolizidine Alkaloids

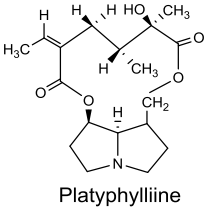
Platyphylliine

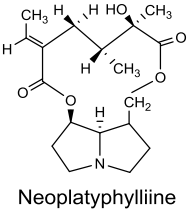
Neoplatyphylliine

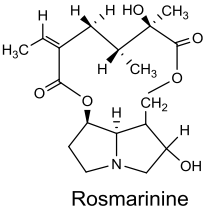
Rosmarinine

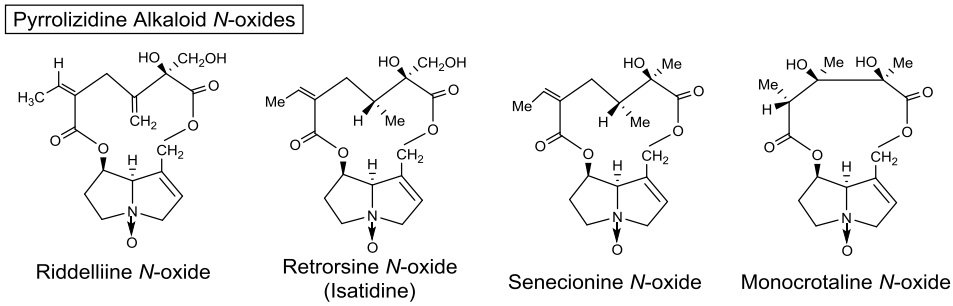

Figure 2. The names and structures of different types of pyrrolizidine alkaloids and pyrrolizidine alkaloid *N*-oxides.

SOURCES OF PYRROLIZIDINE ALKALOID-CONTAINING PLANTS

Like other phytochemicals, pyrrolizidine alkaloids are produced by plants as secondary metabolites to play a defensive role for against insect herbivores, vertebrates invasion, and severe environmental conditions, particular drought [1-3, 29, 48-52]. Thus, pyrrolizidine alkaloids are common constituents of hundreds of plant species of different unrelated botanical families and are widespread in the world [2, 3, 25, 29, 40]. To date, more than 660 pyrrolizidine alkaloids and pyrrolizidine alkaloid *N*-oxides have been identified in over 6,000 plants. Among the flowering plants in the world, it was estimated that there are about 3% that contain toxic pyrrolizidine alkaloids [53]. Pyrrolizidine alkaloids have been identified in more than twelve higher plant families of the Angiosperms, with the *Compositae* (*Asteraceae*), *Boraginaceae*, and *Legumionsae* (*Fabaceae*) families containing the most toxic pyrrolizidine alkaloids.

The genus *Senecio* contains a variety of toxic pyrrolizidine alkaloids and pyrrolizidine alkaloid *N*-oxides and is most studied. For example, *Senecio jacobaea*, the most widespread jacobine chemotype, contains at least seven individual alkaloids, jacobine, jacoline, jaconine, jacozine, retrorsine, senecionine, and seneciphylline. Another species, *S. longilobus*, contains four tumorigenic pyrrolizidine alkaloids, retrorsine, riddelliine, senecionine, and seneciphylline. In some cases, a plant species contains only one major pyrrolizidine alkaloid. Molynuex et al. [45] reported that *S. riddellii* contains essentially only a single pyrrolizidine alkaloid, riddelliine, with retrorsine in trace quantities.

Toxic pyrrolizidine alkaloid-containing plants grow worldwide, including Australia, Europe, South Africa, Central Africa, West Indies, China, Japan, Mongolia, Nepal, Jamaica, Canada, New Zealand, and the United States [3, 22, 29, 54, 55]. It is noteworthy that pyrrolizidine alkaloids and pyrrolizidine alkaloid *N*-oxides can invade from originated lands to other regions. An example is the recent report by Le Roux et al. [56] that fireweed (*Senecio madagascariensis*) probably originated in southern Africa was found in Australia, and most recently invaded Hawaii, having infested ranching areas [45, 57].

LIVESTOCK POISONING BY PYRROLIZIDINE ALKALOIDS

The first reported livestock poisoning by grazing upon pyrrolizidine alkaloid-containing plants occurred more than two hundred and twenty years ago [45]. It was in 1787 that in

Great Britain livestock consumed tansy ragwort (*Senecio jacobaea*), a toxic pyrrolizidine alkaloid-containing plant, and were poisoned [45]. The earliest report of poisoning to livestock in the United States was in 1884, caused by grazing upon prairie ragwort (*Senecio plattensis*) and/or arrowhead rattlebox (*Crotalaria sagittalis*). The 1903 Annual Report of the New Zealand Department of Agriculture stated that horses and cattle grazing pyrrolizidine alkaloid-containing plants developed hepatic cirrhosis that was called "Winton disease" [58]. Similar livestock poisoning by pyrrolizidine alkaloid-containing plants, predominantly the Senecio species, was reported in Australia [18] and South America [59]. Numerous incidents have occurred continuously, including those concomitantly occurring with the human epidemic outbreaks described in the following section.

ROUTES OF HUMAN EXPOSURE TO PYRROLIZIDINE ALKALOIDS

Toxic pyrrolizidine alkaloids contaminate many different human food sources, such as wheat, milk, honey, eggs, herbal medicines, and herbal teas [3, 8, 19-21, 23, 39, 42, 60-63]. In contrast to poisoning animals occurring exclusively by grazing upon toxic pyrrolizidine alkaloid-containing plants, ingestion by humans most frequently occurs through intake of contaminated foodstuffs from many different sources, such as grains, honey, eggs, and milk, [37] or through deliberate use of herbal remedies that contain toxic pyrrolizidine alkaloids [3, 45].

The same toxic pyrrolizidine alkaloids can expose humans through different routes. One example is the tumorigenic riddelliine, a constituent in the tansy ragwort (*Senecio jacobaea*) [52]. Riddelliine may contaminate human food sources, such as flour, milk, and honey [52, 64]. Riddelliine was also found in the herbal tea named "gordolobo yerba", which was popularly used in the American Southwest [65].

A. As Staple Food Contaminations and Cause of Human Epidemic Outbreaks

There are many reported human poisoning outbreaks caused by pyrrolizidine alkaloids [18, 20, 22, 24, 45, 66]. Large scale human poisonings by intake of food contaminated with toxic pyrrolizidine alkaloids took place in many countries [20, 22, 25, 66]. The first incidence occurred in 1920 a large scale food poisoning incidence in South Africa associated with consumption of bread made from wheat flour contaminated with toxic pyrrolizidine alkaloids, Senecio ilicifolius and/or S. burchellii [67, 68].

The pyrrolizidine alkaloid-caused human outbreak involving the highest mortality (7200 inhabitants) occurred in north-western Afghanistan during a 2-year severe drought in the period 1970-1972 [45, 69, 70].

The outbreak was attributed to consumption of bread made from wheat contaminated with seeds of Heliotropium popovii subsp. gillianum (family Boraginaceae). It was estimated that about 35000 inhabitants exposed to pyrrolizidine alkaloids, mainly the heliotrine and heliotrine N-oxide.

Similar human outbreaks in Afghanistan occurred in 1990 – 2000. More recently, another serious outbreak in Afghanistan occurred during the period November 2007 to December 2008.

More than 270 people suffered with hepatic veno-occlusive disease (VOD) and 44 people died [45, 71, 72]. Again, the outbreak was determined to be associated with consumption of bread made from flour contaminated with weed seeds of Heliotropium species [73] and with milk products from goats grazing contaminated plants in the area [73]. Using NMR spectroscopy, Molyneux et al. [74] determined that the seeds contained heliotrine and lasiocarpine.

Disruption of crop harvest can also result in contamination [45]. In 1922, a blockade in southern Tadjikistan led to a delay of wheat harvest about two months, resulting in seeds of the weed Heliotropium lasiocarpum to contaminate the crop harvested. Consumption of the contaminated flour as bread resulted in 3906 people suffering from hepatotoxicity [66, 75]. In 1973, an outbreak of "veno-occlusive disease" in the Sarguja district of India was due to consumption of cereals contaminated with seeds of Crotalaria nana. A total of 486 people died of veno-occlusion disease [70, 76, 77].

Human poisoning by exposure to pyrrolizidine alkaloids occurs more frequently in under-developing countries, such as in central and south Asia, by intake of contaminated staple food. It occurs much more frequently during the drought weather, because under such conditions, grains easily invaded by weeds of pyrrolizidine alkaloid-containing plants [45]. The people in developed countries take a variety of staple foods, and thus, human outbreaks due to intake of pyrrolizidine alkaloid-contaminated foods occur much less frequently.

B. As Food

Prakash et al. [20] reported that in the past people in Europe, North America, Japan, and Australia frequently consumed salads that contained the leaves of comfrey. Comfrey contains up to nine pyrrolizidine alkaloids, at least two of which, symphytine and lasiocarpine, are carcinogenic [78]. Pyrrolizidine alkaloid-containing plants, including Senecio cannabifolius, Petasites japonicus, Tussilago farfara, Farfugium japonicum, and Symphytum officinale, were consumed as vegetables in Japan [79]. Senecio jacobaea [80] and Echium plantagineum [81] were consumed as food in Oregon and Southeastern Australia, respectively. Even more recently, in 2007, salads sold in Germany were contaminated with Senecio vulgaris, a toxic pyrrolizidine alkaloid-containing plant [47].

The human intake of meat and dairy products from animals grazing on plants containing toxic pyrrolizidine alkaloids is another route of food contamination. This route results in the production of honey [37, 61, 80-82] eggs [83] and milk [43, 84] contaminated with toxic pyrrolizidine alkaloids [37, 39, 41]. In 1990, the potential risk of human intake of pyrrolizidine alkaloid-contaminated milk was reviewed by Molyneux and James [84].

In 1977, Deinzer et al. [80] first reported the detection of toxic pyrrolizidine alkaloids in honeys from different sources. Since then, it was found that honey contaminated with toxic pyrrolizidine alkaloids is widespread, and can seriously cause human health effects.

Table 1 is mainly the summarized information concerning pyrrolizidine alkaloid-containing plants known in honey products published in a review by Edgar in 2002 and several additional recent findings [61, 82, 85].

Table 1. Pyrrolizidine Alkaloid-Containing Plants Reported in Honey Products[a]

Country	Plant Family	Plant Genus
	Boraginaceae Family	
Argentina		*Echium*
Austria		*Myosotis*
Australia		*Echium, Heliotropium*
Canada		*Borago*
Denmark		*Borago*
Egypt		*Borago*
Finland		*Borago*
Germany		*Borago, Myosotis*
Italy		*Echium, Myosotis, Borago, Cynoglossum*
Lithuania		*Symphytum*
Morocco		*Echium*
New Zealand		*Echium*
Poland		*Echium*
Portugal		*Echium*
South Africa		*Echium*
Spain		*Echium*
Switzerland		*Myosotis*
Turkey		*Myosotis*
Ukraine		*Symphytum*
United Kingdom		*Borago, Myosotis*
Uruguay		*Echium*
USA		*Borago*
USSR		*Echium, Symphytum, Borago, Cynoglossum*
Yugoslavia		*Echium*
	Asteraceae Family	
Albania		*Senecio*
Argentina		*Eupatorium* [82]
Australia		*Ageratum, Ageratum* [85]
Brazil		*Senecio, Eupatorium; Chromolaena* [82]
Burma		*Chromolaena*
Germany		*Petasites*
India		*Senecio, Ageratum*
Italy		*Senecio, Petasites, Tussilago*
Mexico		*Eupatorium, Senecio*
Netherlands		*Tussilago*
Nigeria		*Ageratum, Chromolaena*
Poland		*Tussilago*
Somalia		*Eupatorium*
South Africa		*Ageratum*
Switzerland		*Senecio*
Thailand		*Chromolaena (Eupatorium)*
Taiwan		*Ageratum*
United Kingdom		*Senecio*
Uruguay		*Eupatorium* [82]
USA		*Senecio*
Zimbabwe		*Senecio*
	Fabaceae Family	
India		*Crotalaria*
Senegal		*Crotalaria*
Venezuela		*Crotalaria*

[a]Data summarized by Edgar et al. in 2002,[61] or reported as cited.

This information indicates that pyrrolizidine alkaloid-contaminated honey is widespread in the world. Furthermore, pyrrolizidine alkaloid-containing honey and pollen used as ingredients in food processing can also cause a downstream contamination in the food chain, reported having been detected in mead, candy, and fennel honey [86]. In general, the levels of contamination are usually low, not sufficient to cause acute or sub-acute poisoning. However, long-time continuous intake can easily reach a level above the maximum tolerable daily intakes set by risk assessment authorities, and potentially lead to chronic diseases, including cancer [37].

C. As Herbal Teas

Herbal teas have been a route of human exposure to toxic pyrrolizidine alkaloids [1, 25, 87, 88]. In both under-developed and developed countries, including South Africa, India, Japan, China, Jamaica, Mexico, Europe, South America, Sri-Lanka, and the United States, folk teas have been used for medicinal purposes; unfortunately, many of which contain toxic and tumorigenic pyrrolizidine alkaloids [8, 25, 29]. For example, it was found the herbal tea named "gordolobo yerba", which was popularly used in the American Southwest, contained the carcinogen riddelliine [65].

Several human outbreaks have been caused by the intake of Bush-teas containing toxic pyrrolizidine alkaloids. The incidences were in Jamaica in 1954 and 1970 [89, 90], South Africa in 1968 [91] and Martinique in 1975 [92]. Similar human outbreaks caused by intake of herbal teas containing toxic pyrrolizidine alkaloids were in Ecuador in 1973 [93], China in 1985 [94], Switzerland in 1985 and 1986 [95, 96], the United Kingdom in 1986 [97], Peru in 1994 [98], Austria in 1995 [99], and Argentina in 1999 [100].

D. As Herbal Medicines

In the ancient time, people took herbal medicines for treatment of illness. In the twenty century, modern Western medicine has replaced herbal medicines as the principal approach for curing illness. However, herbal medicine is still popular in many under-developed countries, including China, and also sporadically used in the developed countries, including in the United States and Europe. Unfortunately, many herbal medicinal plants contain toxic pyrrolizidine alkaloids [39, 41, 62, 101, 102]. To date, there are over 50 species of Chinese herbal plants containing pyrrolizidine alkaloids have been identified [29, 41, 87]. Among these plants, those from the *Asteraceae* (*Compositae*) family dominate, followed by the *Boraginaceae* and *Fabaceae* (*Leguminosae*) families, with the *Orchidaceae* family the least.

To date, more than 90 pyrrolizidine alkaloids were identified in herbal plants grown in China, among which about 20 induced tumors in experimental animals [1, 29, 62]. At the present, it is not known the total number of herbal plants in China that contain pyrrolizidine alkaloids.

The lack of this important information mainly attributed to the fact that it has not been systematically studied. Consequently, human health risk posed by consumption of pyrrolizidine alkaloid-containing Chinese herbal plants is a big concern.

E. As Herbal Dietary Supplements and Functional Products

Pyrrolizidine alkaloid-induced hepatotoxicity in humans in developing countries has been increasing during the recent decades because the use of traditional herbal remedies has increased considerably [3]. For example, pyrrolizidine alkaloid-containing herbal plants, such as comfrey, coltsfoot, and borage, have been sold as dietary supplements [8, 29, 40, 42, 60, 61]. Comfrey and coltsfoot are Chinese herbal medicines and produced in many countries. Chow and Fu [103] determined that pyrrolizidine alkaloid-derived DNA adducts were formed in livers of female F344 rats gavaged with three dietary supplements, comfrey root extract, comfrey compound oil, and coltsfoot root extract, sold in the United States.

TOXICITY OF PYRROLIZIDINE ALKALOIDS

Most pyrrolizidine alkaloids and pyrrolizidine alkaloid *N*-oxides with a 1,2-double bond exhibit toxic effects, including hepatotoxicity, carcinogenicity, genotoxicity, pneumotoxicity, and teratogenicity [2]. Pyrrolizidine alkaloids themselves are not toxic and require metabolic activation to form the "pyrrolic" metabolites, dehydropyrrolizidine alkaloids, to exert acute toxicity, chronic toxicity, genotoxicity, and carcinogenicity [2, 43, 63, 104, 105]. The determined genotoxicities of pyrrolizidine alkaloids include DNA binding, DNA cross-linking, DNA-protein cross-linking, sister chromatid exchange, chromosomal aberrations, and mutagenicity [106].

ACUTE AND CHRONIC POISONING

Pyrrolizidine alkaloid-induced acute poisoning causes massive hepatotoxicity, resulting in haemorrhagic necrosis, hepatomegaly, and ascites [2, 20, 25, 41, 107, 108]. Severe liver necrosis and dysfunction can lead to death. Sub-acute poisoning causes hepatomegaly, ascites, and endothelial proliferation. Further liver damage can lead to occlusion of hepatic veins, resulting in the veno-occlusion disease (VOD), which represents a characteristic histological sign of pyrrolizidine alkaloid poisoning [1, 20, 25, 107, 108]. At the end-stage of chronic poisoning by pyrrolizidine alkaloids, the VOD causes centrilobular congestion, necrosis, fibrosis, and liver cirrhosis.

Chronic poisoning by pyrrolizidine alkaloids also affects other tissues and organs, including lungs, blood vessels, kidneys, pancreas, gastrointestinal tract, bone marrow, and brain [2, 41]. Exposure over a longer period of time causes cell enlargement (megalocytosis), veno-occlusion in liver and lungs, fatty degeneration, nuclei enlargement with increasing nuclear chromatin, loss of metabolic function, inhibition of mitosis, proliferation of biliary tract epithelium, liver cirrhosis, nodular hyperplasia, and liver adenomas or carcinomas [2, 41].

As hepatotoxicity is the principal effect induced by pyrrolizidine alkaloids, it has been determined that pyrrolizidine alkaloids exhibit markedly different hepatotoxicity potency and acute toxicity (LD_{50}) [2]. Pyrrolizidine alkaloids without a double bond in the necine moiety in general are not toxic. Among the pyrrolizidine alkaloids, macrocyclic diester pyrrolizidine

alkaloids are most toxic. Open chain diester pyrrolizidine alkaloids are generally less toxic. Among macrocyclic diester pyrrolizidine alkaloids, those derived from retronecine exhibit the greatest hepatotoxicity. Accordingly, macrocyclic diester pyrrolizidine alkaloids of retronecine-type pyrrolizidine alkaloids are the most studied pyrrolizidine alkaloids.

A. Genotoxicity

Upon metabolism, pyrrolizidine alkaloids exhibit a variety of genotoxicities, resulting in DNA damage, chromosomal damage, and mutations [2, 8, 18, 63, 106, 109]. Both plant extracts and pure pyrrolizidine alkaloids have been extensively studied for genotoxicity in different systems. The resulting DNA damage includes DNA strand breakage, unscheduled DNA synthesis, DNA-DNA cross-linking, DNA-protein cross-linking [1, 4, 27, 110-112], and DNA adduct formation [1, 4, 27].

Pyrrolizidine alkaloids induce unscheduled DNA synthesis in rat hepatocytes and peripheral blood polychromatic erythrocytes of Swiss mice [113-115]. Bruggeman and van der Hoeven [116] determined that several pyrrolizidine alkaloids induced SCEs in V79 Chinese hamster cells co-cultured with chick embryo hepatocytes. Riddelliine induced unscheduled DNA synthesis, S-phase synthesis, and micronuclei [117].

Chromosomal damage induced by pyrrolizidine alkaloids was commonly studied by measuring micronucleus induction. This assay clearly shows that pyrrolizidine alkaloids and pyrrolizidine alkaloid-containing plants produce micronuclei in hepatocytes, bone marrow erythrocytes, and peripheral blood cells, validating that they are clastogenic agents [106, 118]. Pyrrolizidine alkaloids caused chromosome rearrangements in Drosophila melanogaster [119]. Chan [120] determined that in the presence of S9, riddelliine induced chromosomal aberrations in Chinese hamster ovary (CHO) cells. Pyrrolizidine alkaloids induce sister chromatid exchange and chromosomal aberrations in Chinese hamster ovary cells [121]. Heliotrine was found to induce somatic and teratogenic effects in Drosophila [122].

Frei et al. [38]. studied the induction of somatic mutation and recombination in wing cells of Drosophila melanogaster by a series of pyrrolizidine alkaloids. They determined that the mutagenic potency was in the order: senkirkine > monocrotaline > seneciphylline > senecionine > retrorsine > 7-acetyllycopsamine > symphytine > jacoline > symlandine > intermedine > indicine > lycopsamine > indicine N-oxide > supinine.

The mutagenicity of clivorine, heliotrine, lasiocarpine, senkirkine, retrorsine, seneciphylline, and riddelliine in Salmonella typhimurium TA100 in the presence of S9 enzymes was determined [78, 123-126]. Comfrey (Symphytum Officinale) extract was determined to be mutagenic in rat liver in vivo [106]. Mei et al. [127] found that riddelliine exhibited differential mutagenicity in liver endothelial and parenchymal cells of transgenic Big Blue rats.

B. Carcinogenicity

Pyrrolizidine alkaloids are among the first naturally occurring carcinogens to be discovered [2]. A number of pyrrolizidine alkaloid-containing plant extracts and pyrrolizidine alkaloids have been determined to induce tumors in experimental animals (Table 2) [64, 79, 120, 128-135]. The tumorigenic pyrrolizidine alkaloids are mainly from three plant families, Compositae, Boraginaceae, and Leguminosae (Table 2). Based on chemical structures, these

tumorigenic pyrrolizidine alkaloids belong to retronecine-type, heliotridine-type, and otonecine-type pyrrolizidine alkaloids. Their structures are shown in Figure 2.

As shown in Table 2, only one pyrrolizidine alkaloid N-oxide, retrorsine N-oxide (or isatidine) has so far been tested and shown to be carcinogenic. Consequently, the tumorigenicity of more pyrrolizidine alkaloid N-oxides warrants further investigation.

Table 2. Carcinogenic pyrrolizidine alkaloids and pyrrolizidine alkaloid *N*-oxides in rats

Pyrrolizidine Alkaloids	Plant species (Family)[a]	Tumor types	References
Retronecine - Type Pyrrolizidine Alkaloids			
Retrorsine	*Senecio* (Compositae)	Liver carcinoma	[134, 136-138]
Riddelliine	*Senecio* (Compositae), *Crotalaria* (Leguminosae)	Hepatocarcinoma	[136, 138, 139]
Monocrotaline	*Crotalaria* (Leguminosae)	Liver carcinoma, pulmonary adenoma, adrenal adenoma	[140, 141]
Senecionine[b]	*Senecio* (Compositae)	Liver tumor	[134, 138, 142]
Seneciphylline	*Senecio* (Compositae)	Hemangioendothelial sarcoma, liver adenoma	[136, 142]
Jacobine	*Senecio* L. (Compositae)	Liver tumor	[134, 143]
Symphytine	*Symphytum officinale* L (Boraginaceae)	Liver tumor	[144, 145]
Intermedine	*Amsinckia* (Boraginaceae)	Lslet cell adenoma, bladder papillary tumor	[133, 137]
Lycopasamine	*Amsinckia* (Boraginaceae)	Islet cell adenoma, bladder papillary tumor	[133, 137]
Retronecine	*Crotalaria* (Leguminosae)	Spinal cord tumor	[132]
Retronecine – Type Pyrrolizidine Alkaloid *N*-Oxide			
Retrorsine *N*-oxide (Isatidine)	*Senecio* (Compositae), *Crotalaria* (Leguminosae)	Liver carcinoma,	[134, 137, 138]
Heliotridine - Type Pyrrolizidine Alkaloids			
Lasiocarpine	*Heliotropium* (Boraginaceae)	Liver angiosarcoma, liver carcinoma, skin carcinoma, pulmonary adenoma	[130, 135, 146, 147]
Heliotrine	*Heliotropium* (Boraginaceae)	Pancreatic islet cell tumor, hepatoma	[131]
Otonecine - Type Pyrrolizidine Alkaloids			
Clivorine	*Ligularia dentata* Hara (Compositae)	Hemangioendothelial sarcoma, liver adenoma	[128]
Senkirkine	*Senecio* (Compositae) *Petasites* (Compositae)	Hemangioendothelial sarcoma, liver adenoma	[79, 142, 144]
Patasitenine	*Senecio* (Compositae)	Liver hemangio-enthdothelial sacrcoma, liver adenoma	[79, 148, 149]
Hydroxy-senkirkine	*Senecio* (Compositae)	Bladder papillary tumor	[132, 150]

Pyrrolizidine Alkaloids	Plant species (Family)[a]	Tumor types	References
Dehydropyrrolizidine Alkaloid Metabolites			
Dehydro-heliotridine[c]	--	Liver cystadenoma, lung adenocarcinoma, pancreas islet cell tumor	[108]
Dehydro-monocrotaline[c]	--	Skin tumor	[129]
Dehydro-retronecine (DHR)[c]	--	Rhabdomyosarcoma, skin tumor	[129, 140, 141, 151]

[a]Represents one of the main sources. [b]Not based on testing of the pure compound, but based on testing of the *Senecio* plants (such as *Senecio jacobaea* L.) that contain senecionine. [c]Prepared from organic synthesis.

METABOLIC ACTIVATION OF PYRROLIZIDINE ALKALOIDS LEADING TO TOXICITIES

Pyrrolizidine alkaloids are in most cases require metabolic activation to exert their toxicities [1, 2, 8]. Metabolism of pyrrolyzidine alkaloids occurs mainly in the liver. Metabolism and determination of metabolic activation pathways leading to cytotoxicity, genotoxicity, and tumorigenicity have been extensively studied [1, 2, 4, 8, 27, 152]. Retronecine-type, heliotridine-type, and otonecine-type pyrrolizidine alkaloids are most toxic. With retronecine-type and heliotridine-type pyrrolizidine alkaloids, there are three principal Phase I metabolic pathways: (i) dehydrogenation of the necine base, (ii) hydrolysis of the ester functional groups, and (iii) *N*-oxidation of the necine bases to the corresponding pyrrolizidine alkaloid *N*-oxides.

The first pathway involves the initial hydroxylation at the C-3 or C-8 position, catalyzed by cytochromes P-450, specifically by CYP2B6 and CPY3A isozymes [1, 153-156], to form 3- or 8-hydroxynecine derivative, which upon dehydration, generates the corresponding dehydropyrrolizidine (pyrrolic) alkaloid metabolites. Dehydropyrrolizidine alkaloid metabolites are highly unstable, with half-lives of about 0.3-5.1 seconds [157] in aqueous medium, and therefore have never been isolated from any *in vitro* or *in vivo* experimental systems. These reactive primary metabolites are facilely hydrolyzed to (+/-)-6,7-dihydro-7-hydroxy-1-hydroxymethyl-5*H*-pyrrolizine (DHP), or react with cellular proteins and DNA to form protein-DHP and DNA-DHP adducts as secondary metabolites, leading to pyrrolizidine alkaloid-induced toxicity [1, 2]. These reactive metabolites also react with cellular glutathione (GSH) to form GSH-DHP adducts which are trans-located in the urine and bile, and excreted [1, 2].

The second metabolic pathway, hydrolysis of the ester functional groups at C7 and C9 positions of the necine bases produces retronecine [153, 158-160], catalyzed by liver microsomal and cytosolic carboxyesterases [1, 2, 41, 155, 161, 162]. Since retronecine exhibits very low or no toxicity, this biotransformation is generally considered a detoxification pathway. The third principal pathway, metabolic *N*-oxidation to pyrrolizidine alkaloid *N*-oxides is catalyzed by both cytochrome P-450 (2B6 and 3A) and flavin-containing monooxygenase [16, 153, 163, 164]. Taking riddelliine as an example, these three metabolic pathways are shown in Figure 3.

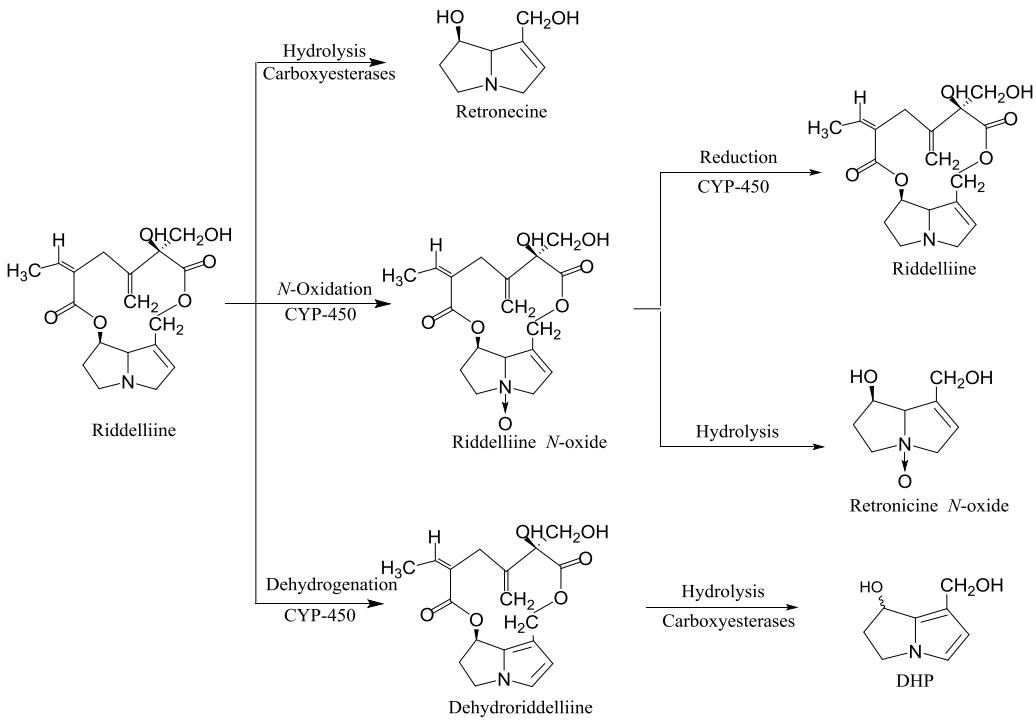

Figure 3. Metabolism pathways of riddelline.

Due to a methyl group at the nitrogen position of the necine base (Figure 1), metabolic *N*-oxidation of otonecine-type pyrrolizidine alkaloids to generate pyrrolizidine alkaloid N-oxides does not occur. Thus, otonecine-type pyrrolizidine alkaloids possess only two principal metabolic pathways. The first pathway is oxidative *N*-demethylation of the necine base, followed by ring closure through the elimination of a formaldehyde molecule, and the subsequent dehydration to generate dehydropyrrolizidine alkaloid metabolites. The C7 position of otonecine-type pyrrolizidine alkaloids possesses an *R* absolute configuration. Thus, the resulting dehydropyrrolizidine alkaloid metabolites all have a necine base identical to that of retronecine-type pyrrolizidine alkaloids [1, 165-168]. The second metabolic pathway is hydrolysis of the ester functional group(s) to form the corresponding necine bases and acids. As an example, the principal Phase I metabolism pathways of clivorine are shown in Figure 4.

Dehydropyrrolizidine alkaloids are principle metabolites that exert cytotoxicity, genotoxicity, and tumorigenicity [169, 170].

Therefore, the relative ease of dehydropyrrolizidine alkaloid formation compared to hydrolysis of dehydropyrrolizidine alkaloid is crucial in determining the toxicity of pyrrolizidine alkaloids. Several structural features, in particular steric hindrance, have been found to be important factors with related to dehydropyrrolizidine alkaloid metabolite formation and the metabolic hydrolysis pathway [111, 162, 171].

Pyrrolizidine alkaloid *N*-oxides are less toxic than the corresponding pyrrolizidine alkaloids and consequently are considered as detoxification metabolites [1-3, 22, 134, 161]. The toxicity of pyrrolizidine alkaloid *N*-oxides in animals is largely due to their conversion to the parent alkaloids in the gut [169, 170]. Recent studies determined that metabolism of

riddelliine *N*-oxide, monocrotaline *N*-oxide, and retrorsine *N*-oxide by rat and or human liver microsomes generated their carcinogenic parent pyrrolizidine alkaloids, riddelliine, monocrotaline, and retrorsine, respectively [172-174]. These results provide the alternative genotoxic mechanism by which pyrrolizidine alkaloid *N*-oxides induce toxicity.

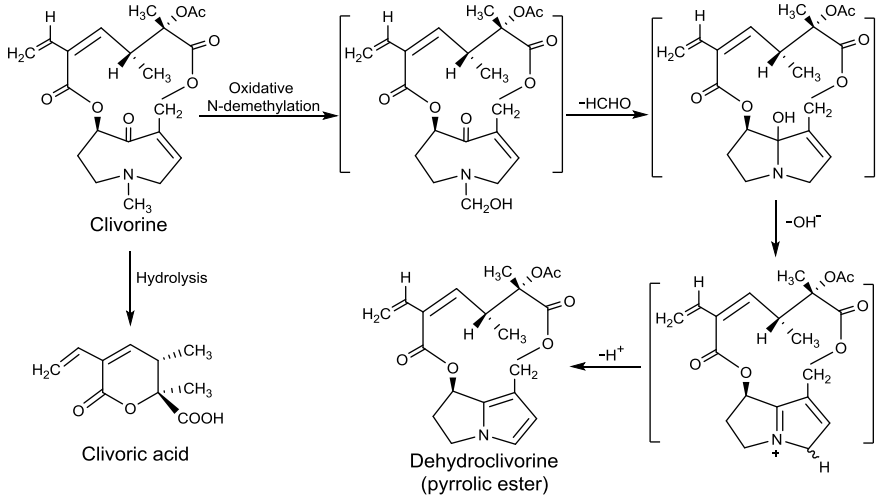

Figure 4. Principal phase I metabolism pathways of clivorine.

MECHANISMS OF PYRROLIZIDINE ALKALOIDS INDUCTION OF TUMORS

Pyrrolizidine alkaloids have been shown to induce tumors, primarily liver tumors, in experimental animals (Table 2). The mechanisms by which pyrrolizidine alkaloids induce tumors have been studied over the past several decades, and the formation of endogenous DNA adducts, exogenous DNA adducts, and DNA-DNA cross-links has been reported.

A. Formation of Endogenous DNA Adducts

Liver microsomal metabolism of senecionine generated trans-4-hydroxy-2-hexenal as a metabolite [175-179]. It is known that lipid peroxidation generates trans-4-hydroxy-2-hexenal that can react with deoxyguanosine and produce two adducts [179]. The overall results suggest that trans-4-hydroxy-2-hexenal may be a tumogenic metabolite of senecionine, although the mechanism has not been fully elucidated. These findings implicate that induction of lipid peroxidation by pyrrolizidine alkaloids may be involved in pyrrolizidine alkaloid-induced genotoxicity and tumorigenicity.

B. Formation of DNA Cross-linking and DNA-protein Cross-linking

Dehydropyrrolizidine alkaloids and DHP metabolites have two electrophilic sites at the C7 and C9 positions of the necine base, capable of binding to DNA and protein to form

DNA-DNA cross-linking, protein-protein cross-linking, and/or DNA-protein cross-linking [110-113, 178, 180-182].

Coulombe and co-workers compared the extent of DNA cross-linking formation induced by eight representative pyrrolizidine alkaloids, which included five macrocycle diesters (seneciphylline, senecionine, riddelliine, retrorsine, and monocrotaline), two open diesters (heliosupine and latifoline), and one necine base (retronecine), in cultured bovine kidney epithelial cells in the presence of an external metabolizing system [110, 111, 171]. The relative potency in causing DNA cross-linking and DNA-protein linking was determined to be: seneciphylline > riddelliine > retrorsine > senecionine > heliosupine > monocrotaline > latifoline > retronecine. In addition, the level of DNA cross-linking was higher than the DNA-protein cross-linking [111].

Kim et al. [112] studied five dehydropyrrolizidine alkaloid metabolites in mammalian cells, and found that the four macrocyclic diesters, dehydrosenecionine, dehydroseneciphylline, dehydroriddelliine, and dehydromonocrotaline, induced protein-DNA cross-links, with the levels higher than that from dehydroretronecine. Furthermore, the level of DNA-protein cross-linking formation correlated with the animal toxicity induced by the parent pyrrolizidine alkaloids. Thus, Kim et al. [112] concluded that DNA-protein cross-linking activity is probably involved in pyrrolizidine alkaloid-induced tumor induction and other related diseases.

To date, the structures of DNA crosslink adducts have not been fully characterized. The correlation between levels of adducts formation and tumor potency of treated animals has not been determined. These data gaps warrant further investigation.

C. Formation of Exogenous DNA Adducts

1. Mechanism by which Riddelliine Induces Tumors

The tumorigenicity of riddelliine was determined by the National Toxicology Program (NTP). The NTP two-year tumorigenicity study found that riddelliine induced liver hemangiosarcomas in male and female F344 rats and male B6C3F$_1$ mice [120]. Riddelliine is the first pyrrolizidine alkaloid for which a mechanism of induction of liver tumors was determined in experimental animals [183]. The mechanistic study and DNA adduct formation in vitro and in vivo were first determined by using the ^{32}P-postlabeling/HPLC method. A highly sensitive ^{32}P-postlabeling/HPLC method was developed by Yang et al. [184] and then used it for identification and quantitation of riddelliine-derived DNA adducts. Reaction of the synthetically prepared dehydroretronecine (DHR) with calf thymus DNA produced eight DHP-derived DNA adducts [183], of which two were identified as enantiomers of DHP-derived 7'-deoxyguanosin-N^2-yl adducts and the other six adducts were DHP-modified dinucleotides [183, 185]. Subsequent studies revealed that the same set of DHP-derived DNA adducts was formed from (i) metabolism of riddelliine by liver microsomes of male and female mice and rats in the presence of calf thymus DNA; and (ii) in the livers of F344 female rats administered riddelliine [183].

The studies by Yang et al. [183]. and Chou et al. [185, 186]. determined that there was a dose-response relationship between the extent of liver tumors of rats administered riddelliine and the levels of the eight DHP-derived adducts. DNA adduct levels in rat endothelial cells, the cells of origin for the hemangiosarcomas, were significantly greater than in the

parenchymal cells [185, 186]. Furthermore, the metabolic pattern and DNA adduct profile from metabolism of riddelliine by human liver microsomes were very similar to those formed in rat liver, indicating that the results of in vivo and in vitro mechanistic studies with experimental rodents are highly relevant to humans [187]. These results suggest that riddelliine can be genotoxic to humans via DHP-derived DNA adduct formation.

Although ^{32}P-postlabeling/HPLC method can be used to identify and quantify DHP-derived DNA adducts in vitro and in vivo, this method lacks of structural information about the resulting DHP-derived DNA adducts. As a result, a highly accurate and precise HPLC-ES-MS/MS methodology was developed for the identification and quantitation of DHP-derived DNA adducts in vivo and in vitro [27]. The levels of DHP-2′-deoxyguanosine (DHP-dG) and DHP-2′-deoxyadenosine (DHP-dA) adducts formed in vivo were determined by multiple reaction monitoring (MRM) analysis, using the synthesized isotopically labeled DHP-[$^{15}N_5$]dG and DHP-[$^{15}N_5$, $^{13}C_{10}$]dA adducts of known quantities as internal standards [27]. For structural identification of the DHP-derived DNA adducts formed in vitro and in vivo, five DHP-dG adducts (designated as DHP-dG-1, DHP-dG-2, DHP-dG-3, DHP-dG-4, and DHP-dG-5) and four DHP-dA adducts (designated as DHP-dA-1, DHP-dA-2, DHP-dA-3, and DHP-dA-4) were prepared from reactions of dehydroriddelliine with dG or dA, respectively [27, 152]. The reactions, names, and structures of these adducts are shown in Figure 5 and Figure 6. In these adducts, DHP-dG-4 is 7-hydroxy-9-(deoxyguanosin-N2-yl)dehydrosupinidine, an epimer of DHP-dG-3; DHP-dA-3 and DHP-dA-4 are another pair of epimers of 7-hydroxy-9-(deoxyadenosin-N6-yl) dehydrosupinidine. Similarly, DHP-dG-1 and DHP-dG-2 adducts are a pair of epimers; and DHP-dA-1 and DHP-dA-2 are another pair of epimers.

HPLC-ES-MS/MS analysis determined that in the liver of rats treated with the riddelliine produced DHP-dG-3 and DHP-dG-4 as predominant products, and DHP-dA-3 and DHP-dA-4 as minor adducts. The unequivocal DNA adduct structural determination provided the conclusion that cellular DNA preferentially binds to the reactive dehydroriddelliine metabolite at the C9 position of the necine base, rather than at the C7 position. This represents the first study with detailed structural assignments of pyrrolizidine alkaloid-derived DNA adducts, which are responsible for pyrrolizidine alkaloid tumor induction [152]. Thus, the mechanism of tumor initiation by a tumorigenic pyrrolizidine alkaloid, riddelliine, was fully determined (Figure 7). Partly because of these mechanistic findings, the NTP has classified riddelliine as "reasonably anticipated to be a human carcinogen" in 2011 [26].

2. General Metabolic Pathway for Activation of Pyrrolizidine Alkaloids and DNA Adducts as Biomarkers of Tumorigenicity

The mechanistic studies from Fu and co-workers indicated that all different types of tumorigenic pyrrolizidine alkaloids generated the same set of DHP-derived DNA adducts in vivo, but these adducts were not formed from a non-tumorigenic pyrrolizidine alkaloid (platyphylliine) or vehicle control [4, 103, 160, 173, 174, 188-191]. The initial studies were conducted using ^{32}P-postlabeling/HPLC analysis.

The results indicate that the same set of DHP-derived DNA adducts was found from metabolism of a series of tumorigenic pyrrolizidine alkaloids and pyrrolizidine alkaloid N-oxides, including clivorine [190], retrorsine [173], monocrotaline [188], lasiocarpine [189], heliotrine [160], retronecine [191], retronecine N-oxide [191], retrorsine N-oxide [174], and

monocrotaline N-oxide [174] in vitro and/or in vivo. In addition, the same set of adducts was identified from metabolism of the Ligularia hodgsonnii hook plant extract in vitro [190] and in the liver of female F344 rats gavaged with dietary supplements, comfrey root extract, comfrey compound oil, and coltsfoot root extract, and with a Chinese herbal plant extract, flos farfara (Kuan Tong Hua) [103].

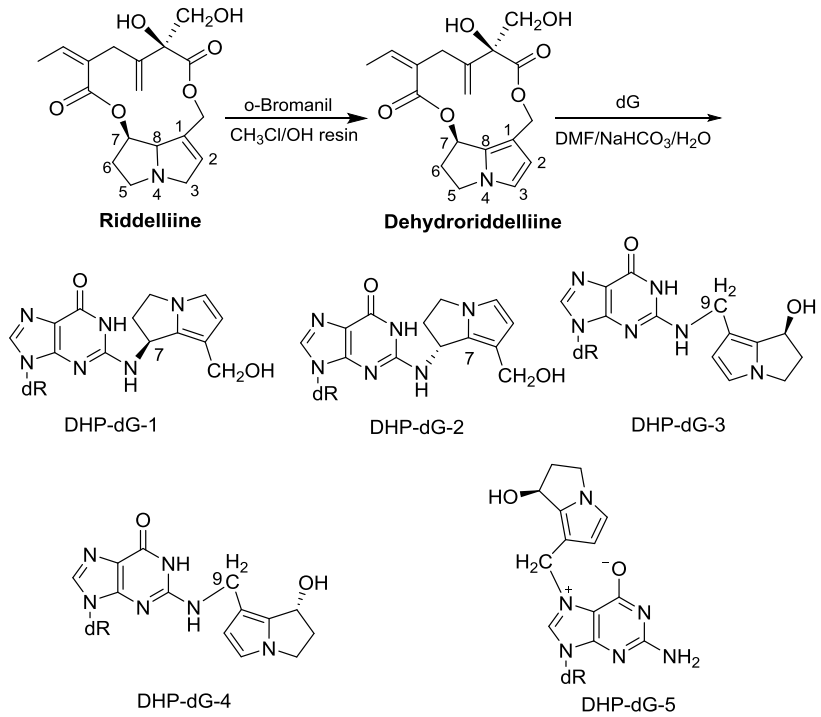

Figure 5. Synthesis of DHP-dG adducts from reaction of dehydroriddelliine and dG.

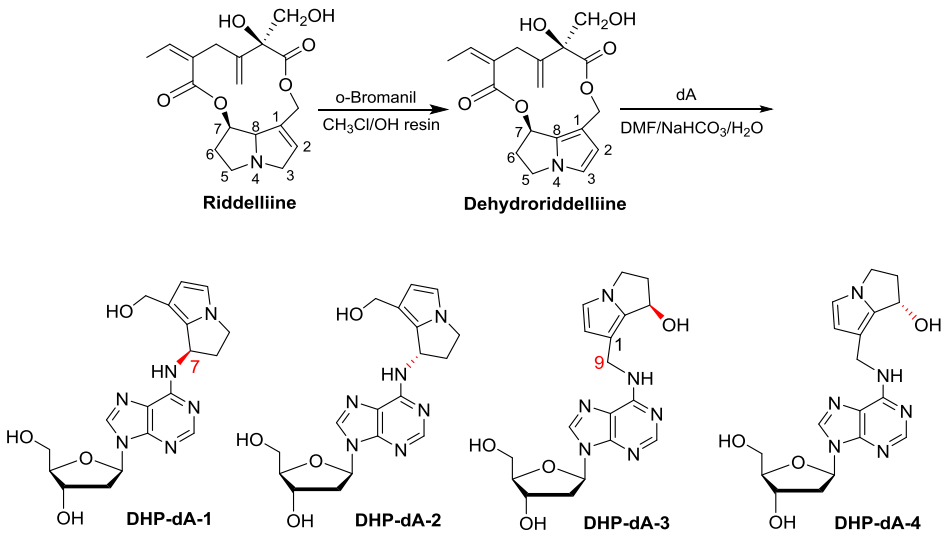

Figure 6. Synthesis of DHP-dA adducts from reaction of dehydroriddelliine and dA.

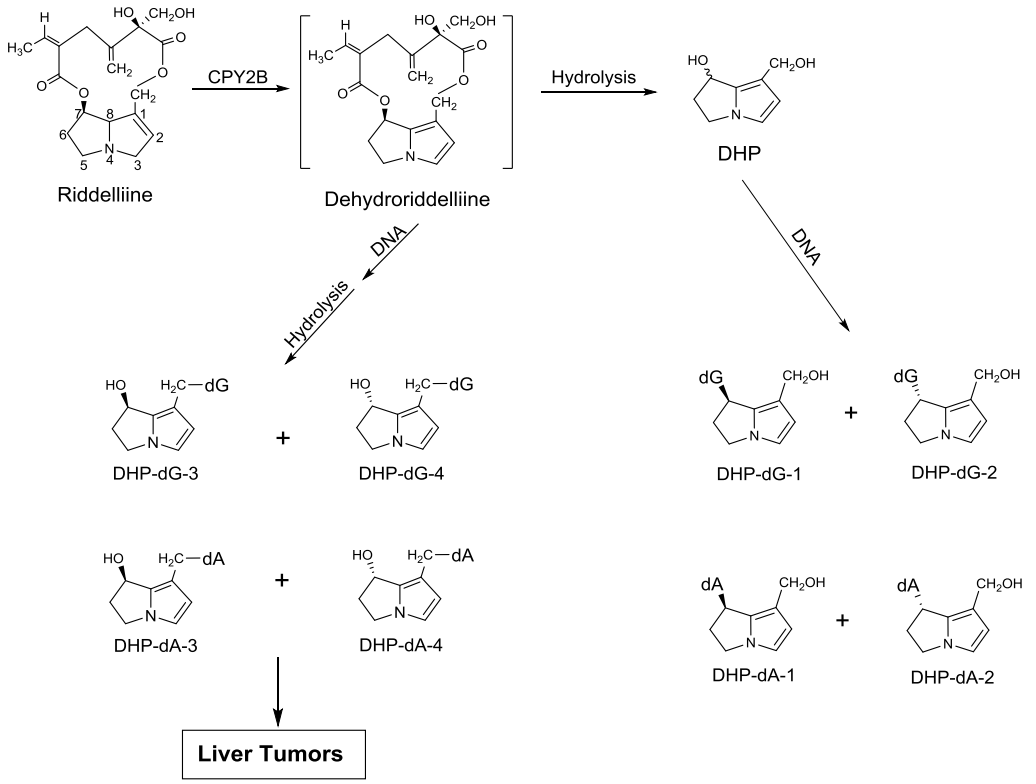

Figure 7. Proposed metabolic activation pathway of riddelliine leading to liver tumor formation.

The most recent study conducted by Xia et al. [187] was to use the HPLC-ES-MS/MS method for identification and quantitation. In this study, eleven pyrrolizidine alkaloids were each orally gavaged to female F344 rats for 3 consecutive days, and rats were sacrificed 24 hrs after the last dose. These pyrrolizidine alkaloids are: seven hepatocarcinogenic pyrrolizidine alkaloids (riddelliine, retrorsine, monocrotaline, lasiocarpine, heliotrine, clivorine, and senkirkine), two extrahepatocarcinogenic pyrrolizidine alkaloids (lycopsamine and retronecine), a non-tumorigenic pyrrolizidine alkaloid (platyphylliine), and a pyrrolizidine alkaloid N-oxide (riddelliine N-oxide). Similar to the results of riddelliine described earlier, DHP-dG-3, DHP-dG-4, DHP-dA-3, and DHP-dA-4 adducts were formed in the liver of rats treated with the individual seven hepatocarcinogenic pyrrolizidine alkaloids and riddelliine N-oxide, and that these DNA adducts were not formed in the liver of rats dosed lycopsamine, retronecine, platyphylliine, or the vehicle control.

Based on the levels of DNA adduct formation, there is a correlation between the order of liver tumor potency and the level of DNA adduct formation of high dose experiments (retrorsine > lasiocarpine > riddelliine ~ monocrotaline > riddelliine N-oxide > senkirkine > heliotrine ≥ clivorine > lycopsamine > retronecine > platyphylliine ~ control) [4].

These results indicate that this set of DNA adducts, DHP-dG-3, DHP-dG-4, DHP-dA-3, and DHP-dA-4, is a common biological biomarker of pyrrolizidine alkaloid-induced liver tumor formation. A general mechanism leading to DHP-derived DNA adduct formation from the metabolism of the three types of carcinogenic pyrrolizidine alkaloids and pyrrolizidine

alkaloid N-oxides was proposed (Figure 8) [4]. To date, this is the first finding that a set of exogenous DNA adducts is formed in common from a series of tumorigenic xenobiotics.

PERSPECTIVES

Pyrrolizidine alkaloid-containing plants are widespread in the world and are probably the most common type of poisonous plants affecting livestock, wildlife, and humans. Food poisoning caused by pyrrolizidine alkaloid-containing plants to humans is still a serious concern.

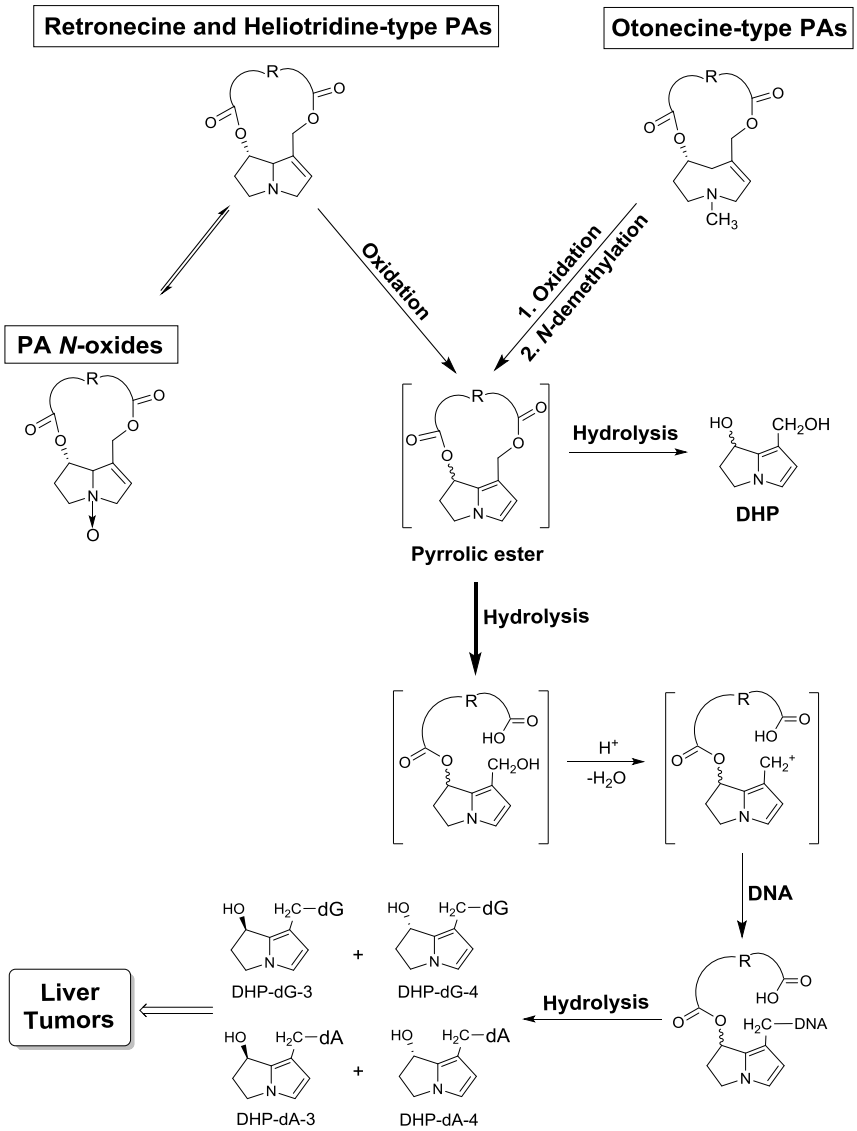

Figure 8. Proposed general mechanism leading to DHP-derived DNA adduct formation from the metabolism of the three types of carcinogenic pyrrolizidine alkaloids (PAs) and PA *N*-oxides.

During the last several decades, the use of dietary supplements and functional foods has grown rapidly in the United States and other countries. As such, it is important to ensure that commercial herbal plants and herbal products are free from pyrrolizidine alkaloids or contaminated at a level that is not toxic.

One major difficulty in preventing from pyrrolizidine alkaloid-associated poisoning is inability to detect and quantify the levels of toxic pyrrolizidine alkaloids contained in herbal plants and herbal products, and in contaminated food. In 1992, the Federal Health Department of Germany restricted the manufacture and use of pharmaceuticals containing toxic pyrrolizidine alkaloids. It stated that the herbal plants "may be sold and used only if daily external exposure to no more than 100 μg pyrrolizidine alkaloids and internal exposure to no more than 1 μg per day for no more than six weeks a year" [29]. Unfortunately, since there are more than 660 structurally different pyrrolizidine alkaloids present in over 6,000 plants worldwide and about half of those plants are hepatotoxic, there are currently no practical analytical methods that can be used to quantify the total quantity of toxic pyrrolizidine alkaloids present in herbal plants, herbal products, or in contaminated food. Therefore, mechanism-based analytical methods must be developed in order to assess the risk posed by pyrrolizidine alkaloids contained in herbal plants, herbal products, and contaminated food.

Due to the large number of pyrrolizidine alkaloid constituents in herbal plants, it is extremely difficult, if possible, to conduct mechanism determinations. This is because even though there are methods available for determining the mechanisms by which a pure chemical induces toxicity and tumorigenicity, none of these methods can be applicable to determine the mechanism of tumor induction posed by chemical mixtures, such as herbal plants, herbal dietary supplements, tobacco smoke condensates, and environmental pollution mixtures [101, 102, 192, 193]. As such, development of practical and liable methods for determining mechanisms by which chemical mixtures induce genotoxicity and tumorigenicity is timely and important.

ACKNOWLEDGMENTS

We thank Dr. Frederick A. Beland for critical review and comments. This article is not an official U.S. Food and Drug Administration guidance or policy statement. No official support or endorsement by the U.S. Food and Drug Administration is intended or should be inferred.

REFERENCES

[1] Fu, P. P.; Xia, Q.; Lin, G.; Chou, M. W. Pyrrolizidine alkaloids--genotoxicity, metabolism enzymes, metabolic activation, and mechanisms. *Drug Metab. Rev.*, 2004, 36, 1-55.

[2] Mattocks, A. R. Chemistry and toxicology of pyrrolizidine alkaloids. Academic Press: London, NY, 1986.

[3] Roeder, E. Medicinal plants in Europe containing pyrrolizidine alkaloids. *Pharmazie*, 1995, 50, 83-98.

[4] Xia, Q.; Zhao, Y.; Von Tungeln, L. S.; Doerge, D. R.; Lin, G.; Cai, L.; Fu, P. P. Pyrrolizidine alkaloid-derived DNA adducts as a common biological biomarker of pyrrolizidine alkaloid-induced tumorigenicity. *Chem. Res. Toxicol.*, 2013, 26, 1384-96.

[5] Bah, M.; Bye, R.; Pereda-Miranda, R. Hepatotoxic pyrrolizidine alkaloids in the Mexican medicinal plant Packera candidissima (Asteraceae: Senecioneae). *J. Ethnopharmacol.*, 1994, 43, 19-30.

[6] Creeper, J. H.; Mitchell, A. A.; Jubb, T. F.; Colegate, S. M. Pyrrolizidine alkaloid poisoning of horses grazing a native heliotrope (Heliotropium ovalifolium). *Aust Vet J.*, 1999, 77, 401-2.

[7] Hill, B. D.; Gaul, K. L.; Noble, J. W. Poisoning of feedlot cattle by seeds of Heliotropium europaeum. *Aust Vet. J.*, 1997, 75, 360-1.

[8] Mattocks, A. R. Toxicity of pyrrolizidine alkaloids. *Nature*, 1968, 217, 723-728.

[9] McLean, E. K. The toxic actions of pyrrolizidine (senecio) alkaloids. *Pharmacol. Rev.*, 1970, 22, 429-83.

[10] Noble, J. W.; Crossley, J.; Hill, B. D.; Pierce, R. J.; McKenzie, R. A.; Debritz, M.; Morley, A. A. Pyrrolizidine alkaloidosis of cattle associated with Senecio lautus. *Aust. Vet. J.*, 1994, 71, 196-200.

[11] Seaman, J. T. Pyrrolizidine alkaloid poisoning of sheep in New South Wales. *Aust. Vet. J.*, 1987, 64, 164-7.

[12] Seaman, J. T. Pyrrolizidine alkaloid poisoning of horses. *Aust. Vet. J.*, 1978, 54, 150.

[13] Araya, O.; Fuentealba, I. C. Chronic hepato-toxicity of Senecio erraticus in calves from two 50-day feeding periods in consecutive years. *Vet. Hum. Toxicol.*, 1990, 32, 555-7.

[14] Arzt, J.; Mount, M. E. Hepatotoxicity associated with pyrrolizidine alkaloid (Crotalaria spp) ingestion in a horse on Easter Island. *Vet. Hum. Toxicol.*, 1999, 41, 96-9.

[15] Baker, D. C.; Pfister, J. A.; Molyneux, R. J.; Kechele, P. Cynoglossum officinale toxicity in calves. *J. Comp. Pathol.*, 1991, 104, 403-10.

[16] Chung, W. G.; Buhler, D. R. Major factors for the susceptibility of guinea pig to the pyrrolizidine alkaloid jacobine. *Drug Metab. Dispos.*, 1995, 23, 1263-7.

[17] Curran, J. M.; Sutherland, R. J.; Peet, R. L. A screening test for subclinical liver disease in horses affected by pyrrolizidine alkaloid toxicosis. *Aust. Vet. J.*, 1996, 74, 236-40.

[18] Bull, L. B.; Culvenor, C. C.; Dick, A. J. The pyrrolizidine alkaloids. Their chemistry, pathogenicity and other biological properties. North-Holland, Amsterdam, 1968.

[19] Byron, J. Pyrrolizidine alkaloids in eggs; new alkaloid found in potatoes. *Food Chem. News*, 1998, 14, 6-7.

[20] Prakash, A. S.; Pereira, T. N.; Reilly, P. E.; Seawright, A. A. Pyrrolizidine alkaloids in human diet. *Mutat. Res.*, 1999, 443, 53-67.

[21] Rosberger, D. F.; Resch, J. F.; Meinwald, J. The occurrence of senecionine in Tussilago farfara. *Mitt. Gebiete Letensm. Hyg.*, 1981, 72, 432-436.

[22] Stegelmeier, B. L.; Edgar, J. A.; Colegate, S. M.; Gardner, D. R.; Schoch, T. K.; Coulombe, R. A.; Molyneux, R. J. Pyrrolizidine alkaloid plants, metabolism and toxicity. *J. Nat. Toxins*, 1999, 8, 95-116.

[23] Winship, K. A. Toxicity of comfrey. *Adverse Drug React. Toxicol. Rev.*, 1991, 10, 47-59.

[24] Woo, Y.-T.; Lai, D. Y.; Arcos, J. C.; Argus, M. F. *Chemical induction of cancer*. Academic Press Inc.: San Diego, 1988.

[25] IPCS. Pyrrolizidine Alkaloids Health and Safety Guides. In Health and Safety Criteria Guides 26., International Programme on Chemical Safety: WHO: Geneva, 1989.

[26] NTP. NTP 12th Report on Carcinogens (RoC). U.S. Department of Health and Human Services, 2011; Vol. 12, pp iii-499.

[27] Fu, P. P.; Chou, M. W.; Churchwell, M.; Wang, Y.; Zhao, Y.; Xia, Q.; Gamboa da Costa, G.; Marques, M. M.; Beland, F. A.; Doerge, D. R. High-performance liquid chromatography electrospray ionization tandem mass spectrometry for the detection and quantitation of pyrrolizidine alkaloid-derived DNA adducts in vitro and in vivo. *Chem. Res. Toxicol.*, 2010, 23, 637-652.

[28] Fu, P. P.; Xia, Q.; Lin, G.; Chou, M. W. Genotoxic Pyrrolizidine Alkaloids — Mechanisms Leading to DNA Adduct Formation and Tumorigenicity. *Int. J. Mol. Sci.*, 2002, 3, 948-964.

[29] Roeder, E. Medicinal plants in China containing pyrrolizidine alkaloids. *Pharmazie*, 2000, 55, 711-26.

[30] (COT), C. o. T. COT statement on pyrrolizidine alkaloids in food Committee on Toxicity of Chemicals in Food, C. P. a. t. E., Ed. UK, 2008; pp 1-24.

[31] (EFSA), E. F. S. A. Opinion of the Scientific Panel on Contaminants in the Food Chain on a request from the European Commission related to pyrrolizidine alkaloids as undesirable substances in animal feed. *EFSA J.*, 2007, 447, 1-51.

[32] Cheeke, P. R. Nutritional implications of pyrrolizidine alkaloids as contaminants of foodstuffs. In Poisonous plant contamination of edible plants, Rizk, A.-F. M., Ed. CRC Press: Boca Raton, FL, 1991; pp p. 157–175.

[33] Cheeke, P. R. Toxicity and metabolism of pyrrolizidine alkaloids. *J. Anim. Sci.*, 1988, 66, 2343-50.

[34] Coulombe, R. A., Jr. Pyrrolizidine alkaloids in foods. *Advances in food and nutrition research*, 2003, 45, 61-99.

[35] Crews, C.; Berthiller, F.; Krska, R. Update on analytical methods for toxic pyrrolizidine alkaloids. *Anal. Bioanal. Chem.*, 2010, 396, 327-38.

[36] Culvenor, C. C.; Edgar, J. A.; Jago, M. V.; Qutteridge, A.; Peterson, J. E.; Smith, L. W. Hepato- and pneumotoxicity of pyrrolizidine alkaloids and derivatives in relation to molecular structure. *Chem. Biol. Interact.*, 1976, 12, 299-324.

[37] Edgar, J. A.; Colegate, S. M.; Boppre, M.; Molyneux, R. J. Pyrrolizidine alkaloids in food: a spectrum of potential health consequences. *Food Addit Contam Part A Chem. Anal. Control. Expo. Risk Assess*, 2011, 28, 308-24.

[38] Frei, H.; Luthy, J.; Brauchli, J.; Zweifel, U.; Wurgler, F. E.; Schlatter, C. Structure/activity relationships of the genotoxic potencies of sixteen pyrrolizidine alkaloids assayed for the induction of somatic mutation and recombination in wing cells of Drosophila melanogaster. *Chem. Biol. Interact.*, 1992, 83, 1-22.

[39] Fu, P. P. Quality assurance and safety of herbal dietary supplements. *J. Food Drug Anal.*, 2007, 15, 333-334.

[40] Fu, P. P.; Chou, M. W.; Xia, Q.; Yang, Y. C.; Yan, J.; Doerge, D. R.; Chan, P. C. Genotoxic pyrrolizidine alkaloids and pyrrolizidine alkaloid N-oxides - mechanisms leading to DNA adduct formation and tumorigenicity. *J. Environ. Sci. Health, Part C: Environ. Carcinog. Ecotoxicol. Rev.*, 2001, 19, 353-386.

[41] Fu, P. P.; Xia, Q.; Chou, M. W.; Lin, G. Detection, hepatotoxicity, and tumorigenicity of pyrrolizidine alkaloids in Chinese herbal plants and herbal dietary supplements. *J. Food Drug Anal.*, 2007, 15, 400-415.

[42] Huxtable, R. J. Human health implications of pyrrolizidine alkaloids and herbs containing them. In: I. Alkaloids. CRC Press: Boca Raton, FL, 1989; p p. 41–86.

[43] IPCS. Pyrrolizidine alkaloids. In Environmental Health Criteria 80, International Programme on Chemical Safety WHO: Geneva, 1988.

[44] Kempf, M.; Reinhard, A.; Beuerle, T. Pyrrolizidine alkaloids (PAs) in honey and pollen-legal regulation of PA levels in food and animal feed required. *Mol. Nutr. Food Res.*, 2010, 54, 158-68.

[45] Molyneux, R. J.; Gardner, D. L.; Colegate, S. M.; Edgar, J. A. Pyrrolizidine alkaloid toxicity in livestock: a paradigm for human poisoning? *Food Addit Contam Part A Chem. Anal. Control. Expo. Risk Assess*, 2011, 28, 293-307.

[46] Schoental, R. Toxicology and carcinogenic action of pyrrolizidine alkaloids. *Cancer, Res* 1968, 28, 2237-46.

[47] Wiedenfeld, H. Plants containing pyrrolizidine alkaloids: toxicity and problems. *Food Addit. Contam. Part A Chem. Anal. Control. Expo. Risk Assess*, 2011, 28, 282-92.

[48] Beuerle, T.; Theuring, C.; Klewer, N.; Schulz, S.; Hartmann, T. Absolute configuration of the creatonotines and callimorphines, two classes of arctiid-specific pyrrolizidine alkaloids. *Insect. Biochem. Mol. Biol.*, 2007, 37, 80-9.

[49] Hartmann, T. Plant-derived secondary metabolites as defensive chemicals in herbivorous insects: a case study in chemical ecology. *Planta*, 2004, 219, 1-4.

[50] Kirk, H.; Macel, M.; Klinkhamer, P. G.; Vrieling, K. Natural hybridization between Senecio jacobaea and Senecio aquaticus: molecular and chemical evidence. *Mol. Ecol.*, 2004, 13, 2267-74.

[51] Macel, M.; Bruinsma, M.; Dijkstra, S. M.; Ooijendijk, T.; Niemeyer, H. M.; Klinkhamer, P. G. Differences in effects of pyrrolizidine alkaloids on five generalist insect herbivore species. *J. Chem. Ecol.*, 2005, 31, 1493-508.

[52] Molyneux, R. J.; Johnson, A. E.; Olsen, J. D.; Baker, D. C. Toxicity of pyrrolizidine alkaloids from Riddell groundsel (Senecio riddellii) to cattle. *Am. J. Vet. Res.*, 1991, 52, 146-51.

[53] Smith, L. W.; Culvenor, C. C. Plant sources of hepatotoxic pyrrolizidine alkaloids. *J. Nat. Prod.*, 1981, 44, 129-52.

[54] Roeder, E.; Wiedenfeld, H. Pyrrolizidine alkaloids in medicinal plants of Mongolia, Nepal and Tibet. *Pharmazie*, 2009, 64, 699-716.

[55] Steenkamp, V.; Stewart, M. J.; Zuckerman, M. Clinical and analytical aspects of pyrrolizidine poisoning caused by South African traditional medicines. *Ther. Drug Monit.*, 2000, 22, 302-6.

[56] Le Roux, J. J.; Wieczorek, A. M.; Tran, C. T.; Vorsino, A. Disentangling the dynamics of invasive fireweed (Senecio madagascariensis Poir. species complex) in the Hawaiian Islands. *Biological. Invasions*, 2010, 12, 2251-2264.

[57] Gardner, D. R.; Thorne, M. S.; Molyneux, R. J.; Pfister, J. A.; Seawright, A. A. Pyrrolizidine alkaloids in Senecio madagascariensis from Australia and Hawaii and assessment of possible livestock poisoning. *Biochem. Syst. Ecol.*, 2006, 34, 736-744.

[58] Gilruth, J. A. Hepatic cirrhosis affecting horses and cattle (so-called 'Winton disease'): a report on its nature, cause, treatment, distribution etc.; New Zealand Department of Agriculture: Wellington, New Zealand, 1903; pp p228-278.

[59] Nobre, V.; Dantas, A.; Riet-Correa, F.; Barbosa Filho, J.; Tabosa, I.; Vasconcelos, J. Acute intoxication by< i> Crotalaria retusa</i> in sheep. *Toxicon,* 2005, 45, 347-352.

[60] Betz, J. M.; Eppley, R. M.; Taylor, W. C.; Andrzejewski, D. Determination of pyrrolizidine alkaloids in commercial comfrey products (Symphytum sp.). *J. Pharm. Sci.*, 1994, 83, 649-53.

[61] Edgar, J. A.; Roeder, E.; Molyneux, R. J. Honey from plants containing pyrrolizidine alkaloids: a potential threat to health. *J. Agric. Food Chem.*, 2002, 50, 2719-30.

[62] Fu, P. P.; Yang, Y.-C.; Xia, Q.; Chou, M. W.; Cui, Y.; Lin, G. Pyrrolizidine alkaloids - tumorigenic components in Chinese herbal medicines and dietary supplements. *J. Food Drug Anal.*, 2002, 10, 198-211.

[63] IARC. Pyrrolizidine alkaloids. In IARC Monograph on the evaluation of carcinogenic risk of chemicals to man - Some naturally occurring substance, International Agency for Research in Cancer: Lyon, France, 1976; Vol. 10.

[64] Chan, P. C.; Mahler, J.; Bucher, J. R.; Travlos, G. S.; Reid, J. B. Toxicity and carcinogenicity of riddelliine following 13 weeks of treatment to rats and mice. *Toxicon.*, 1994, 32, 891-908.

[65] Huxtable, R. J. Herbal teas and toxins: novel aspects of pyrrolizidine poisoning in the United States. *Perspect. Biol. Med.*, 1980, 24, 1-14.

[66] Chauvin, P.; Dillon, J. C.; Moren, A. An outbreak of Heliotrope food poisoning, Tadjikistan, November 1992- March 1993. *Sante,* 1994, 4, 263-8.

[67] Steyn, D. Poisoning of human beings by weeds contained in cereals (bread poisoning). *Onderstepoort J. Vet Sci Anim. Ind.,* 1933, 1, 219-266.

[68] Willmot, F. C.; Robertson, G. W. Senecio disease, or cirrhosis of the liver due to senecio poisoning. *Lancet,* 1920, 2, 848-849.

[69] Mohabbat, O.; Younos, M. S.; Merzad, A. A.; Srivastava, R. N.; Sediq, G. G.; Aram, G. N. An outbreak of hepatic veno-occlusive disease in north-western Afghanistan. *Lancet,* 1976, 2, 269-71.

[70] Tandon, H. D.; Tandon, B. N.; Mattocks, A. R. An epidemic of veno-occlusive disease of the liver in Afghanistan. Pathologic features. *Am. J. Gastroenterol.,* 1978, 70, 607-13.

[71] (IRIN), I. R. I. N. Afghanistan: 'Charmak' still killing people, livestock in West Herat, 16 December 2008. Available from: http://www.irinnews.org/Report.aspx?ReportId= 81971/ 2008.

[72] (IRIN), I. R. I. N. Afghanistan: WHO confirms 'charmak' disease in Herat Province, Kabul; 15 May 2008. Available from: http://www.irinnews.org/Report.aspx?ReportId= 78218/ 2008.

[73] Kakar, F.; Akbarian, Z.; Leslie, T.; Mustafa, M. L.; Watson, J.; van Egmond, H. P.; Omar, M. F.; Mofleh, J. An outbreak of hepatic veno-occlusive disease in Western afghanistan associated with exposure to wheat flour contaminated with pyrrolizidine alkaloids. *J. Toxicol.,* 2010, 2010, 313280.

[74] Molyneux, R. J.; Johnson, A. E.; Roitman, J. N.; Benson, M. E. Chemistry of toxic range plants. Determination of pyrrolizidine alkaloid content and composition in

Senecio species by nuclear magnetic resonance spectroscopy. *J. Agric. Food Chem.,* 1979, 27, 494-9.

[75] Mayer, F.; Luthy, J. Heliotrope poisoning in Tadjikistan. *Lancet,* 1993, 342, 246-7.

[76] Tandon, B. N.; Tandon, H. D.; Tandon, R. K.; Narndranathan, M.; Joshi, Y. K. An epidemic of veno-occlusive disease of liver in central India. *Lancet,* 1976, 2, 271-2.

[77] Tandon, R. K.; Tandon, B. N.; Tandon, H. D.; Bhatia, M. L.; Bhargava, S.; Lal, P.; Arora, R. R. Study of an epidemic of venoocclusive disease in India. *Gut,* 1976, 17, 849-55.

[78] Mei, N.; Guo, L.; Fu, P. P.; Heflich, R. H.; Chen, T. Mutagenicity of comfrey (Symphytum Officinale) in rat liver. *Br. J. Cancer,* 2005, 92, 873-5.

[79] Hirono, I.; Ueno, I.; Aiso, S.; Yamaji, T.; Haga, M. Carcinogenic activity of Farfugium japonicum and Senecio cannabifolius. *Cancer Lett.,* 1983, 20, 191-8.

[80] Deinzer, M. L.; Thomson, P. A.; Burgett, D. M.; Isaacson, D. L. Pyrrolizidine alkaloids: their occurrence in honey from tansy ragwort (Senecio jacobaea L.). *Science,* 1977, 195, 497-9.

[81] Culvenor, C. C.; Edgar, J. A.; Smith, L. W. Pyrrolizidine alkaloids in honey from Echium plantagineum L. *J. Agric. Food Chem.,* 1981, 29, 958-60.

[82] Dubecke, A.; Beckh, G.; Lullmann, C. Pyrrolizidine alkaloids in honey and bee pollen. *Food Addit Contam. Part A Chem. Anal. Control. Expo. Risk Assess,* 2011, 28, 348-58.

[83] Edgar, J. A.; Smith, L. W. Transfer of pyrrolizidine alkaloids into eggs: food safety implications. American Chemical Society: Washington D.C., 2000; Vol. ACS Symposium Series 745, p 118-128.

[84] Molyneux, R. J.; James, L. F. Pyrrolizidine alkaloids in milk: thresholds of intoxication. *Vet. Hum. Toxicol.,* 1990, 32, 94-103.

[85] Beales, K. A.; Betteridge, K.; Colegate, S. M.; Edgar, J. A. Solid-phase extraction and LC-MS analysis of pyrrolizidine alkaloids in honeys. *J. Agric. Food Chem.,* 2004, 52, 6664-72.

[86] Kempf, M.; Wittig, M.; Schonfeld, K.; Cramer, L.; Schreier, P.; Beuerle, T. Pyrrolizidine alkaloids in food: downstream contamination in the food chain caused by honey and pollen. *Food Addit. Contam. Part A Chem Anal. Control. Expo. Risk Assess,* 2011, 28, 325-31.

[87] Edgar, J. A.; Lin, H. J.; Kumana, C. R.; Ng, M. M. Pyrrolizidine alkaloid composition of three Chinese medicinal herbs, Eupatorium cannabinum, E. japonicum and Crotalaria assamica. *Am. J. Chin. Med.,* 1992, 20, 281-8.

[88] Zhao, X. G.; Wang, Z. T.; Lin, G.; Cui, Y. Y.; Zhang, M.; Xu, L. S.; Xu, G. J.; Damani, L. A. Hepatotoxic pyrrolizidine alkaloids and tranitional Chinese medicines. *Chinese Traditional and Herbal Drugs,* 1998, 29, 115-119.

[89] Bras, G.; Brooks, S. E.; Watler, D. C. Cirrhosis of the liver in Jamaica. *The Journal of pathology and bacteriology,* 1961, 82, 503-12.

[90] Brooks, S. E.; Miller, C. G.; McKenzie, K. A.; Audretsch, J. J.; Bras, G. Acute veno-occlusive disease of the liver: Fine structure in Jamaican children. *Arch. Pathol.,* 1970, 89, 507-20.

[91] Freiman, I.; Schmaman, A.; Zamit, R.; Appleberg, M. Veno-occlusive disease of the liver--some new aspects. South African medical journal= Suid-Afrikaanse tydskrif vir geneeskunde 1968, 42, 126-129.

[92] Saint-Aimé, M. M.; Ponsar, C.; Lacombe, C.; Lacombe, W. Maladie Veino-Occlusive du Foie chez L'Enfant Martiniquais. *Bordeaux Médical.*, 1977, 10, 665-670.

[93] Lyford, C. L.; Vergara, G. G.; Moeller, D. D. Hepatic veno-occlusive disease originating in Ecuador. *Gastroenterology*, 1976, 70, 105-8.

[94] Culvenor, C. C.; Edgar, J. A.; Smith, L. W.; Kumana, C. R.; Lin, H. J. Heliotropium lasiocarpum Fisch and Mey identified as cause of veno- occlusive disease due to a herbal tea. *Lancet*, 1986, 1, 978.

[95] Margalith, D.; Heraief, C.; Schindler, A.; Birchler, R.; Mosimann, F.; Aladjem, D.; Gonvers, J. Veno-occlusive disease of the liver due to the use of tea made from Senecio plants. *J. Hepatol. Suppl.*, 1985, 204, 280.

[96] Roulet, M.; Laurini, R.; Rivier, L.; Calame, A. Hepatic veno-occlusive disease in newborn infant of a woman drinking herbal tea. *J. Pediatr.*, 1988, 112, 433-6.

[97] Weston, C. F.; Cooper, B. T.; Davies, J. D.; Levine, D. F. Veno-occlusive disease of the liver secondary to ingestion of comfrey. *Br. Med. J. (Clin Res Ed)*, 1987, 295, 183.

[98] Tomioka, M.; Calvo, F.; Siguas, A.; Sanchez, L.; Nava, E.; Garcia, U.; Valdivia, M.; Reategui, E. [Hepatic veno-occlusive disease associated with ingestion of Senecio tephrosioides]. *Rev. Gastroenterol. Peru*, 1995, 15, 299-302.

[99] Sperl, W.; Stuppner, H.; Gassner, I.; Judmaier, W.; Dietze, O.; Vogel, W. Reversible hepatic veno-occlusive disease in an infant after consumption of pyrrolizidine-containing herbal tea. *Eur. J. Pediatr.*, 1995, 154, 112-6.

[100] Vilar, J.; Garcia, M.; Cabrera, P. Enfermedad venooclusiva hepática de causa Tóxica por Senecio vulgaris. *Gastroenterología y hepatología*, 2000, 23, 285-286.

[101] Fu, P. P.; Xia, Q. Assessment of safety and quality assurance of herbal dietary supplements. In Nutraceutical and Functional Food Regulations in the United States and Around the World, 2nd ed.; Bagchi, D., Ed. Elsevier/Academic Press: New York, NY, 2014; Vol. 10, pp 151-168.

[102] Fu, P. P.; Xia, Q.; Zhao, Y.; Wang, S.; Yu, H.; Chiang, H. M. Phototoxicity of herbal plants and herbal products. *Journal of environmental science and health. Part C, Environmental carcinogenesis & ecotoxicology reviews*, 2013, 31, 213-55.

[103] Chou, M. W.; Fu, P. P. Formation of DHP-derived DNA adducts in vivo from dietary supplements and chinese herbal plant extracts containing carcinogenic pyrrolizidine alkaloids. *Toxicol. Ind. Health*, 2006, 22, 321-327.

[104] IARC. Some Traditional Herbal Medicines, Some Mycotoxins, Naphthalene and Styrene. In IARC Monographs on the evaluation of carcinogenic risks of chemicals to humans, International Agency for Research in Cancer: Lyon, France, 2002; Vol. 82, pp 153-168.

[105] Schoental, R. Carcinogens in plants and microorganisms. American Chemical Society: Washington, DC, 1976; Vol. ACS Monograph 173.

[106] Chen, T.; Mei, N.; Fu, P. P. Genotoxicity of pyrrolizidine alkaloids. *J. Appl. Toxicol.*, 2010, 30, 183-96.

[107] Huxtable, R. J. Human embryotoxicity of pyrrolizidine-containing drugs. *Hepatology*, 1989, 9, 510-1.

[108] Peterson, J. E.; Jago, M. V.; Reddy, J. K.; Jarrett, R. G. Neoplasia and chronic disease associated with the prolonged administration of dehydroheliotridine to rats. *J. Natl. Cancer Inst.*, 1983, 70, 381-6.

[109] (WHO), W. H. O. In Pyrrolizidine alkaloids. International programme on chemical safety, environmental health criteria, Geneva, World Health Organization: Geneva, 1988; p 337.

[110] Coulombe, R. A., Jr.; Drew, G. L.; Stermitz, F. R. Pyrrolizidine alkaloids crosslink DNA with actin. *Toxicol. Appl. Pharmacol.*, 1999, 154, 198-202.

[111] Hincks, J. R.; Kim, H. Y.; Segall, H. J.; Molyneux, R. J.; Stermitz, F. R.; Coulombe, R. A. DNA cross-linking in mammalian cells by pyrrolizidine alkaloids: structure-activity relationships. *Toxicol. Appl. Pharmacol.*, 1991, 111, 90-98.

[112] Kim, H. Y.; Stermitz, F. R.; Coulombe, R. A. Pyrrolizidine alkaloid-induced DNA-protein cross-links. *Carcinogenesis*, 1995, 16, 2691-2697.

[113] Hincks, J. R.; Coulombe, R. A., Jr. Rapid detection of DNA-interstrand and DNA-protein cross-links in mammalian cells by gravity-flow alkaline elution. *Environ Mol. Mutagen*, 1989, 13, 211-7.

[114] Mattocks, A. R.; Bird, I. Alkylation by dehydroretronecine, a cytotoxic metabolite of some pyrrolizidine alkaloids: an in vitro test. *Toxicol. Lett.*, 1983, 16, 1-8.

[115] Petry, T. W.; Bowden, G. T.; Huxtable, R. J.; Sipes, I. G. Characterization of hepatic DNA damage induced in rats by the pyrrolizidine alkaloid monocrotaline. *Cancer Res.*, 1984, 44, 1505-9.

[116] Bruggeman, I. M.; van der Hoeven, J. C. Induction of SCEs by some pyrrolizidine alkaloids in V79 Chinese hamster cells co-cultured with chick embryo hepatocytes. *Mutat. Res.*, 1985, 142, 209-12.

[117] Mirsalis, J. C.; Steinmetz, K. L.; Blazak, W. F.; Spalding, J. W. Evaluation of the potential of riddelliine to induce unscheduled DNA synthesis, S-phase synthesis, or micronuclei following in vivo treatment with multiple doses. *Environ. Mol. Mutagen*, 1993, 21, 265-71.

[118] MacGregor, J. T.; Wehr, C. M.; Henika, P. R.; Shelby, M. D. The in vivo erythrocyte micronucleus test: measurement at steady state increases assay efficiency and permits integration with toxicity studies. *Fundam Appl. Toxicol.*, 1990, 14, 513-22.

[119] Brink, N. G. The mutagenic activity of the pyrrolizidine alkaloid heliotrine in Drosophila melanogaster. II. Chromosome rearrangements. *Mutat. Res.*, 1969, 8, 139-46.

[120] Chan, P. C.; Haseman, J. K.; Prejean, J. D.; Nyska, A. Toxicity and carcinogenicity of riddelliine in rats and mice. *Toxicol. Lett.*, 2003, 144, 295-311.

[121] Galloway, S. M.; Armstrong, M. J.; Reuben, C.; Colman, S.; Brown, B.; Cannon, C.; Bloom, A. D.; Nakamura, F.; Ahmed, M.; Duk, S.; et al. Chromosome aberrations and sister chromatid exchanges in Chinese hamster ovary cells: evaluations of 108 chemicals. *Environ. Mol. Mutagen*, 1987, 10 Suppl 10, 1-175.

[122] Brink, N. G. Somatic and teratogenic effects induced by heliotrine in Drosophila. *Mutat. Res.*, 1982, 104, 105-11.

[123] Rubiolo, P.; Pieters, L.; Calomme, M.; Bicchi, C.; Vlietinck, A.; Vanden Berghe, D. Mutagenicity of pyrrolizidine alkaloids in the Salmonella typhimurium/mammalian microsome system. *Mutat. Res.*, 1992, 281, 143-7.

[124] Wehner, F. C.; Thiel, P. G.; van Rensburg, S. J. Mutagenicity of alkaloids in the Salmonella/microsome system. *Mutat. Res.*, 1979, 66, 187-90.

[125] Yamanaka, H.; Nagao, M.; Sugimura, T.; Furuya, T.; Shirai, A.; Matsushima, T. Mutagenicity of pyrrolizidine alkaloids in the Salmonella/mammalian- microsome test. *Mutat. Res.*, 1979, 68, 211-6.

[126] Zeiger, E.; Anderson, B.; Haworth, S.; Lawlor, T.; Mortelmans, K. Salmonella mutagenicity tests: IV. Results from the testing of 300 chemicals. *Environ. Mol. Mutagen.*, 1988, 11 Suppl 12, 1-157.

[127] Mei, N.; Heflich, R. H.; Chou, M. W.; Chen, T. Mutations induced by the carcinogenic pyrrolizidine alkaloid riddelliine in the liver cII gene of transgenic big blue rats. *Chem. Res. Toxicol.*, 2004, 17, 814-8.

[128] Kuhara, K.; Takanashi, H.; Hirono, I.; Furuya, T.; Asada, Y. Carcinogenic activity of clivorine, a pyrrolizidine alkaloid isolated from Ligularia dentata. *Cancer Lett.*, 1980, 10, 117-122.

[129] Mattocks, A. R.; Cabral, J. R. Carcinogenicity of some pyrrolic pyrrolizidine alkaloid metabolites and analogues. *Cancer Lett.*, 1982, 17, 61-6.

[130] Rao, M. S.; Reddy, J. K. Malignant neoplasms in rats fed lasiocarpine. *Br. J. Cancer*, 1978, 37, 289-93.

[131] Schoental, R. Pancreatic islet-cell and other tumors in rats given heliotrine, a monoester pyrrolizidine alkaloid, and nicotinamide. *Cancer Res.*, 1975, 35, 2020-4.

[132] Schoental, R.; Cavanagh, J. B. Brain and spinal cord tumors in rats treated with pyrrolizidine alkaloids. *J. Natl. Cancer Inst.*, 1972, 49, 665-71.

[133] Schoental, R.; Fowler, M. E.; Coady, A. Islet cell tumors of the pancreas found in rats given pyrrolizidine alkaloids from Amsinckia intermedia Fisch and Mey and from Heliotropium supinum L. *Cancer Res.*, 1970, 30, 2127-31.

[134] Schoental, R.; head, M. A.; Peacock, P. R. Senecio alkaloids: Primary liver tumours in rats as a result of treatment with (1) a mixture of alkaloids from S. jacobaea lin.; (2) retrorsine; (3) isatidine. *Br. J. Cancer*, 1954, 8, 458-465.

[135] Svoboda, D. J.; Reddy, J. K. Malignant tumors in rats given lasiocarpine. *Cancer Res.*, 1972, 32, 908-13.

[136] Harris, P. N.; Chen, K. K. Development of hepatic tumors in rats following ingestion of *senecio longilobus*. *Cancer Res.*, 1970, 30, 2881-2886.

[137] Schoental, R.; Hard, G. C.; Gibbard, S. Histopathology of renal lipomatous tumors in rats treated with the "natural" products, pyrrolizidine alkaloids and, -unsaturated aldehydes. *J. Natl. Cancer Inst.*, 1971, 47, 1037-44.

[138] Schoental, R.; head, M. A. Progression of liver lesions produced in rats by temporary treatment with pyrrolizidine (senecio) alkaloids, and the effecs of betaine and high casein diet. *Br. J. Cancer*, 1957, 11, 535-544.

[139] Brandange, S.; Luning, B.; Moberg, C.; Sjostrand, E. Studies on orchidaceae alkaloids. XXIV. A pyrrolizidine alkaloid from Phalaenopsis cornu-cervi Rchb. f. *Acta. Chem. Scand.*, 1970, 25, 349-50.

[140] Allen, J. R.; Hsu, I. C.; Carstens, L. A. Dehydroretronecine-induced rhabdomyosarcomas in rats. *Cancer Res.*, 1975, 35, 997-1002.

[141] Shumaker, R. C.; Robertson, K. A.; Hsu, I. C.; Allen, J. R. Neoplastic transformation in tissues of rats exposed to monocrotaline or dehydroretronecine. *J. Natl. Cancer Inst.*, 1976, 56, 787-90.

[142] Hirono, I.; Mori, H.; Culvenor, C. C. Carcinogenic activity of coltsfoot, Tussilago farfara L. *Gann*, 1976, 67, 125-129.

[143] Cook, J. W.; Duffy, E.; Schoental, R. Primary liver tumours in rats following feeding with alkaloids of Senecio jacobaea. *Br. J. Cancer*, 1950, 4, 405-10.

[144] Hirono, I.; Haga, M.; Fujii, M.; Matsuura, S.; Matsubara, N.; Nakayama, M.; Furuya, T.; Hikichi, M.; Takanashi, H.; Uchida, E.; Hosaka, S.; Ueno, I. Induction of hepatic tumors in rats by senkirkine and symphytine. *J. Natl. Cancer Inst.*, 1979, 63, 469-472.

[145] Hirono, I.; Mori, H.; Haga, M. Carcinogenic activity of symphytum officinale. *J. Natl. Cancer Inst.*, 1978, 61, 865-868.

[146] Rao, M. S.; Jago, M. V.; Reddy, J. K. Effect of calorie restriction on the fate of hyperplastic liver nodules induced by concurrent administration of lasiocarpine and thioacetamide. *Hum. Toxicol.*, 1983, 2, 15-26.

[147] Svoboda, D. J.; Reddy, J. K. Lasiocarpine-induced, transplantable squamous cell carcinoma of rat skin. *J. Natl. Cancer Inst.*, 1974, 53, 1415-8.

[148] Furuya, T.; Hikichi, M.; Iitaka, Y. Fukinotoxin, a new pyrrolizidine alkaloid from Petasites japonicus. *Chem. Pharm. Bull., (Tokyo)* 1976, 24, 1120-2.

[149] Hirono, I.; Mori, H.; Yamada, K.; Hirata, Y.; Haga, M. Carcinogenic activity of petasitenine, a new pyrrolizidine alkaloid isolated from Petasites japonicus Maxim. *J. Natl. Cancer Inst.*, 1977, 58, 1155-7.

[150] Crout, D. H. Pyrrolizidine and seco-pyrrolizidine alkaloids of Crotalaria laburnifolia L. subspecies eldomae. *J. Chem. Soc., [Perkin 1]* 1972, 13, 1602-7.

[151] Johnson, W. D.; Robertson, K. A.; Pounds, J. G.; Allen, J. R. Dehydroretronecine-induced skin tumors in mice. *J. Natl. Cancer Inst.*, 1978, 61, 85-9.

[152] Zhao, Y.; Xia, Q.; Gamboa da Costa, G.; Yu, H.; Cai, L.; Fu, P. P. Full structure assignments of pyrrolizidine alkaloid DNA adducts and mechanism of tumor initiation. *Chem. Res. Toxicol.*, 2012, 25, 1985-96.

[153] Buhler, D. R.; Kedzierski, B. Biological reactive intermediates of pyrrolizidine alkaloids. *Adv. Exp. Med. Biol.*, 1986, 197, 611-20.

[154] Chung, W. G.; Buhler, D. R. The effect of spironolactone treatment on the cytochrome P450-mediated metabolism of the pyrrolizidine alkaloid senecionine by hepatic microsomes from rats and guinea pigs. *Toxicol. Appl. Pharmacol.*, 1994, 127, 314-9.

[155] Kasahara, Y.; Kiyatake, K.; Tatsumi, K.; Sugito, K.; Kakusaka, I.; Yamagata, S.; Ohmori, S.; Kitada, M.; Kuriyama, T. Bioactivation of monocrotaline by P-450 3A in rat liver. *J. Cardiovasc. Pharmacol.*, 1997, 30, 124-9.

[156] Reid, M. J.; Lame, M. W.; Morin, D.; Wilson, D. W.; Segall, H. J. Involvement of cytochrome P450 3A in the metabolism and covalent binding of 14C-monocrotaline in rat liver microsomes. *J. Biochem. Mol. Toxicol.*, 1998, 12, 157-66.

[157] Cooper, R. A.; Huxtable, R. J. A simple procedure for determining the aqueous half-lives of pyrrolic metabolites of pyrrolizidine alkaloids. *Toxicon*, 1996, 34, 604-607.

[158] Kedzierski, B.; Buhler, D. R. The formation of 6,7-dihydro-7-hydroxy-1-hydroxy-methyl-5H-pyrrolizine, a metabolite of pyrrolizidine alkaloids. *Chem. Biol. Interact.*, 1986, 57, 217-22.

[159] Kedzierski, B.; Buhler, D. R. Configuration of necine pyrroles--toxic metabolites of pyrrolizidine alkaloids. *Toxicol. Lett.*, 1985, 25, 115-119.

[160] Xia, Q.; Yan, J.; Chou, M. W.; Fu, P. P. Formation of DHP-derived DNA adducts from metabolic activation of the prototype heliotridine-type pyrrolizidine alkaloid, heliotrine. *Toxicol. Lett.*, 2008, 178, 77-82.

[161] Dueker, S. R.; Lame, M. W.; Morin, D.; Wilson, D. W.; Segall, H. J. Guinea pig and rat hepatic microsomal metabolism of monocrotaline. *Drug Metab. Dispos,* 1992, 20, 275-80.

[162] Mattocks, A. R. Hydrolysis and hepatotoxicity of retronecine diesters. *Toxicol. Lett.,* 1982, 14, 111-6.

[163] Miranda, C. L.; Chung, W.; Reed, R. E.; Zhao, X.; Henderson, M. C.; Wang, J. L.; Williams, D. E.; Buhler, D. R. Flavin-containing monooxygenase: a major detoxifying enzyme for the pyrrolizidine alkaloid senecionine in guinea pig tissues. *Biochem. Biophys. Res. Commun,* 1991, 178, 546-52.

[164] Williams, D. E.; Reed, R. L.; Kedzierski, B.; Ziegler, D. M.; Buhler, D. R. The role of flavin-containing monooxygenase in the N-oxidation of the pyrrolizidine alkaloid senecionine. *Drug Metab. Dispos.,* 1989, 17, 380-6.

[165] Lin, G.; Cui, Y. Y.; Hawes, E. M. Characterization of rat liver microsomal metabolites of clivorine, an hepatotoxic otonecine-type pyrrolizidine alkaloid. *Drug Metab. Dispos.,* 2000, 28, 1475-1483.

[166] Lin, G.; Cui, Y. Y.; Liu, X. Q. Gender differences in microsomal metabolic activation of hepatotoxic clivorine in rat. *Chem. Res. Toxicol.,* 2003, 16, 768-74.

[167] Lin, G.; Cui, Y. Y.; Liu, X. Q.; Wang, Z. T. Species differences in the in vitro metabolic activation of the hepatotoxic pyrrolizidine alkaloid clivorine. *Chem. Res. Toxicol.,* 2002, 15, 1421-8.

[168] Liu, X. Q.; Lin, G.; Wang, G. G.; Qian, Z. Y. Involvement of human CYP3A in formation of hepatotoxic metabolites of clivorine. *Zhongguo Yaolixue Yu Dulixue Zazhi,* 2002, 16, 15-20.

[169] Mattocks, A. R.; White, I. N. The conversion of pyrrolizidine alkaloids to N-oxides and to dihydropyrrolizine derivatives by rat-liver microsomes in vitro. *Chem. Biol. Interact.,* 1971, 3, 383-96.

[170] Powis, G.; Ames, M. M.; Kovach, J. S. Metabolic conversion of indicine N-oxide to indicine in rabbits and humans. *Cancer Res.,* 1979, 39, 3564-70.

[171] Kim, H. Y.; Stermitz, F. R.; Molyneux, R. J.; Wilson, D. W.; Taylor, D.; Coulombe, R. A. Structural influences on pyrrolizidine alkaloid-induced cytopathology. *Toxicol. Appl. Pharmacol.,* 1993, 122, 61-69.

[172] Chou, M. W.; Wang, Y. P.; Yan, J.; Yang, Y. C.; Beger, R. D.; Williams, L. D.; Doerge, D. R.; Fu, P. P. Riddelliine N-oxide is a phytochemical and mammalian metabolite with genotoxic activity that is comparable to the parent pyrrolizidine alkaloid riddelliine. *Toxicol. Lett.,* 2003, 145, 239-47.

[173] Wang, Y. P.; Fu, P. P.; Chou, M. W. Metabolic activation of the tumorigenic pyrrolizidine alkaloid, retrorsine, leading to DNA adduct formation in vivo. *Int J Environ Res Public Health,* 2005, 2, 74-9.

[174] Wang, Y. P.; Yan, J.; Fu, P. P.; Chou, M. W. Human liver microsomal reduction of pyrrolizidine alkaloid N-oxides to form the corresponding carcinogenic parent alkaloid. *Toxicol Lett* 2005, 155, 411-20.

[175] Griffin, D. S.; Segall, H. J. Effects of the pyrrolizidine alkaloid senecionine and the alkenals trans-4-OH-hexenal and trans-2-hexenal on intracellular calcium compartmentation in isolated hepatocytes. *Biochem. Pharmacol.,* 1989, 38, 391-7.

[176] Griffin, D. S.; Segall, H. J. Genotoxicity and cytotoxicity of selected pyrrolizidine alkaloids, a possible alkenal metabolite of the alkaloids, and related alkenals. *Toxicol. Appl. Pharmacol.,* 1986, 86, 227-34.

[177] Segall, H. J.; Wilson, D. W.; Dallas, J. L.; Haddon, W. F. trans-4-Hydroxy-2-hexenal: a reactive metabolite from the macrocyclic pyrrolizidine alkaloid senecionine. *Science,* 1985, 229, 472-5.

[178] Tepe, J. J.; Williams, R. M. DNA cross-linking by phototriggered dehydromonocrotaline progenitor. *J. of the American Chemical. Society,* 1999, 121, 2951-2955.

[179] Winter, C. K.; Segall, H. J.; Haddon, W. F. Formation of cyclic adducts of deoxyguanosine with the aldehydes trans- 4-hydroxy-2-hexenal and trans-4-hydroxy-2-nonenal in vitro. *Cancer Res.,* 1986, 46, 5682-6.

[180] Kim, H. Y.; Stermitz, F. R.; Li, J. K.; Coulombe, R. A. Comparative DNA cross-linking by activated pyrrolizidine alkaloids. *Food Chem. Toxicol.,* 1999, 37, 619-625.

[181] Pereira, T. N.; Webb, R. I.; Reilly, P. E.; Seawright, A. A.; Prakash, A. S. Dehydromonocrotaline generates sequence-selective N-7 guanine alkylation and heat and alkali stable multiple fragment DNA crosslinks. *Nucleic Acids Res.,* 1998, 26, 5441-7.

[182] Reed, R. L.; Ahern, K. G.; Pearson, G. D.; Buhler, D. R. Crosslinking of DNA by dehydroretronecine, a metabolite of pyrrolizidine alkaloids. *Carcinogenesis* 1988, 9, 1355-61.

[183] Yang, Y. C.; Yan, J.; Doerge, D. R.; Chan, P. C.; Fu, P. P.; Chou, M. W. Metabolic activation of the tumorigenic pyrrolizidine alkaloid, riddelliine, leading to DNA adduct formation in vivo. *Chem. Res. Toxicol.,* 2001, 14, 101-9.

[184] Yang, Y.; Yan, J.; Churchwell, M.; Beger, R.; Chan, P.; Doerge, D. R.; Fu, P. P.; Chou, M. W. Development of a (32)P-postlabeling/HPLC method for detection of dehydroretronecine-derived DNA adducts in vivo and in vitro. *Chem. Res. Toxicol.,* 2001, 14, 91-100.

[185] Chou, M. W.; Yan, J.; Williams, L.; Xia, Q.; Churchwell, M.; Doerge, D. R.; Fu, P. P. Identification of DNA adducts derived from riddelliine, a carcinogenic pyrrolizidine alkaloid, in vitro and in vivo. *Chem. Res. Toxicol.,* 2003, 16, 1130-1137.

[186] Chou, M. W.; Yan, J.; Nichols, J.; Xia, Q.; Beland, F. A.; Chan, P. C.; Fu, P. P. Correlation of DNA adduct formation and riddelliine-induced liver tumorigenesis in F344 rats and B6C3F(1) mice. *Cancer Lett.,* 2003, 193, 119-125.

[187] Xia, Q.; Chou, M. W.; Kadlubar, F. F.; Chan, P. C.; Fu, P. P. Human liver microsomal metabolism and DNA adduct formation of the tumorigenic pyrrolizidine alkaloid, riddelliine. *Chem. Res. Toxicol.,* 2003, 16, 66-73.

[188] Wang, Y. H.; Li, Y.; Li, Y. H.; Yang, S. L.; Yang, L. Modeling K(m) values using electrotopological state: substrates for cytochrome P450 3A4-mediated metabolism. *Bioorg. Med. Chem. Lett.,* 2005, 15, 4076-84.

[189] Xia, Q.; Chou, M. W.; Edgar, J. A.; Doerge, D. R.; Fu, P. P. Formation of DHP-derived DNA adducts from metabolic activation of the prototype heliotridine-type pyrrolizidine alkaloid, lasiocarpine. *Cancer Lett.,* 2006, 231, 138-45.

[190] Xia, Q.; Chou, M. W.; Lin, G.; Fu, P. P. Metabolic formation of DHP-derived DNA adducts from a representative otonecine type pyrrolizidine alkaloid clivorine and the extract of Ligularia hodgsonnii hook. *Chem. Res. Toxicol.,* 2004, 17, 702-8.

[191] Yan, J.; Xia, Q.; Chou, M. W.; Fu, P. P. Metabolic activation of retronecine and retronecine N-oxide - formation of DHP-derived DNA adducts. *Toxicol. Ind. Health*, 2008, 24, 181-8.

[192] Fu, P. P.; Xia, Q.; Sun, X.; Yu, H. Phototoxicity and environmental transformation of polycyclic aromatic hydrocarbons (PAHs)-light-induced reactive oxygen species, lipid peroxidation, and DNA damage. *Journal of environmental science and health. Part C, Environmental carcinogenesis & ecotoxicology reviews*, 2012, 30, 1-41.

[193] Xia, Q.; Yin, J. J.; Zhao, Y.; Wu, Y. S.; Wang, Y. Q.; Ma, L.; Chen, S.; Sun, X.; Fu, P. P.; Yu, H. UVA photoirradiation of nitro-polycyclic aromatic hydrocarbons-induction of reactive oxygen species and formation of lipid peroxides. *Int. J. Environ. Res. Public Health*, 2013, 10, 1062-84.

In: Food Poisoning
Editor: Paresh C. Ray
ISBN: 978-1-63463-166-2

Chapter 2

NANOSILVER-BASED ANTIBACTERIAL AGENTS FOR FOOD SAFETY

Thabitha P. S. Dasari, Hua Deng, Danielle McShan and Hongtao Yu
Department of Chemistry and Biochemistry,
Jackson State University, Jackson, MS, US

ABSTRACT

The burden of foodborne diseases is a world-wide challenge. One in six Americans develops foodborne illnesses each year. Although, novel technologies for antibiotics are rapidly advancing, infectious diseases remain to be one of the significant health concerns worldwide. Especially, since bacterial pathogens are continuously developing drug-resistance, the advancement of new antibiotics or strategies for treatment must outpace drug-resistance. At present, bacterial infections are still mostly under control with antibiotics and proper treatment technologies. However, treatment of multiple drug resistance of bacteria demands high dose administration of antibiotics, significant economic, labor, and time investments, and often initiates elevated toxicity. Currently, nanosilver, an ancient antibiotic, is reconsidered for use as an antibiotic. One strategy is to use it in combination with some of the outdated antibiotics for treatment of infections. Many studies have reported on these studies including mechanism of antibiotic activity of nanosilver and its combined use with conventional antibiotics. This review summarizes bacteria-related food safety issues, mechanisms of antimicrobial/antiparasitic properties of nanosilver, and the use of nanosilver-based antimicrobials.

Keywords: Nanosilver, silver nanoparticle, microbial pathogens, food safety, antibiotics

1. INTRODUCTION

Infectious diseases caused by microorganisms and parasites are a worldwide problem [1-4]. The critical issue is not just the infectious diseases, but also the drug resistance developed by these pathogens [5-15]. Among these infectious diseases, foodborne illnesses are predominant as they are the leading cause of deaths and hospitalizations (Figure 1 and Table 1) [2, 4, 16-24]. Foodborne infections have affected millions and it is a worldwide challenge [24, 25]. Therefore, the ability to treat foodborne infections is essential to ensure human health [26].

Bacteria develop resistance to conventional antibiotics over time. These pathogens have the ability to undergo modifications due to their genetic and environmental factors [3, 6, 7, 9-14,27,28]. As a result, drug-resistances by pathogens have been ever growing and have become a serious threat to human health [1, 6-9, 11-14, 27-30]. The discovery of new antimicrobials has lessened some of the concerns [31-33]. However, there is no assurance that the development of new antimicrobial drugs can keep pace with the microbial pathogen's fast development of resistance.

Recent efforts to address this problem are the use of nanomaterials as novel antibiotics for which microbial pathogens may not develop resistance. The use of nanoparticles is gaining grounds because of their unique antibacterial, chemical, optical, and mechanical properties [33, 36-44]. One of the new approaches is to use the combination of antibiotics and nanoparticles [33, 45-49]. The combined use of nanoparticles with antibiotics makes it possible to reduce the toxicity of both agents towards humans due to lower dosages and synergistic enhancement of each others' antimicrobial activities [47, 50-52].

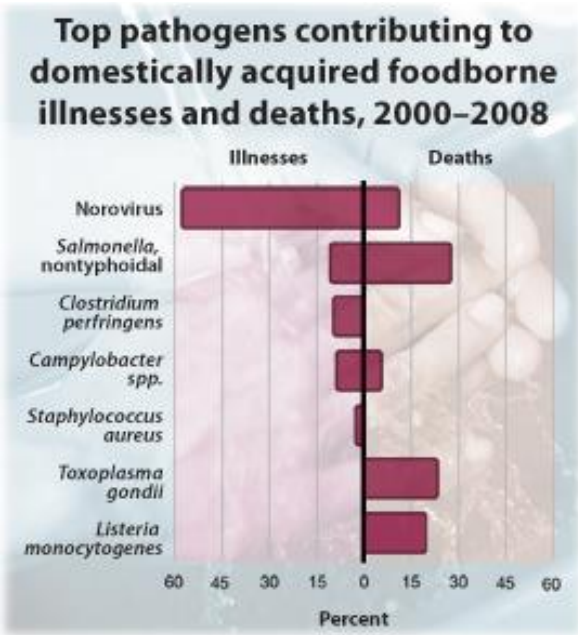

Figure 1. Top pathogens contributing to domestically acquired foodborne illnesses and deaths, 2000 - 2008 (Source: http://www.cdc.gov/Features/dsFoodborneEstimates/) [34].

Table 1. Estimated annual number of domestically acquired, foodborne illnesses, hospitalizations, and deaths due to 31 pathogens and unspecified agents transmitted through food in the United States [35]

Foodborne Agents	Estimated annual number of illnesses (90% credible interval)	%	Estimated annual number of hospitalizations (90% credible interval)	%	Estimated annual number of deaths (90% credible interval)	%
31 known pathogens	9.4 million (6.6–12.7 million)	20	55,961 (39,534–75,741)	44	1,351 (712–2,268)	44
Unspecified agents	38.4 million (19.8–61.2 million)	80	71,878 (9,924–157,340)	56	1,686 (369–3,338)	56
Total	47.8 million (28.7–71.1 million)	100	127,839 (62,529–215,562)	100	3,037 (1,492–4,983)	100

Source: http://www.cdc.gov/foodborneburden/2011-foodborne-estimates.html.

In order to make the combination of antibiotics and nanoparticles efficient antibiotic drugs, there must be a comprehensive understanding of the mechanistic pathways how antibiotics and nanoparticles work together [49, 52-61]. Kalan et al. [61] suggested that the following factors must be considered: synergism between antibiotics and nanoparticles, enzyme inhibition, blockage of antibiotics entry into cells, and physiological insensitivity of cells. Antimicrobial nanoparticles contribute to various factors such as mitigation of acute toxicity, overcoming resistance, and lowering cost when compared to antibiotics alone [26, 43, 60, 62-67]. Metallic nanoparticles, because of their larger surface to volume ratio, are usually used as antimicrobial agents [43, 68-72]. These antimicrobial metals are the most commonly used antimicrobial additives in food industry due to their temperature and mechanical stability [39, 41, 73-77]. Among them, silver nanoparticles, or nanosilver, have been widely used as a broad-spectrum antibacterial agent [45,68,78-86]. Actually, silver was used in ancient times for the treatment of burns and wounds [80,87-89]. Nanosilver is also used now as an additive in several food contact materials based on plastics, glass, or metal. Understanding of the mechanistic pathways of how nanosilver acts on microbial pathogens and parasites, will help to overcome the problem of antibiotic resistance. In this review, we will discuss the importance of food safety issues, the use of silver and nanosilver as antibacterial agents and the mechanism of action on microbial pathogens and parasites. Finally, we will explain the synergistic effects and mechanistic pathways of combined antibiotics and nanosilver on microbial pathogens and parasites.

2. FOOD SAFETY

Food safety has been a worldwide challenge in the past decades as it is an important concern for many countries [1, 2, 4, 5, 15, 16, 21-23, 38, 39, 76, 90-96]. Foodborne diseases are some of the most widespread health problems in the world. They have implications on both the health of individuals and the development of societies. The control and prevention of

foodborne illnesses is a major challenge to public health in the United States and in the world [2, 16, 18, 97, 98]. Each year, one in six Americans is affected by foodborne illnesses due to the consumption of contaminated foods and beverages [35]. Many countries now recognize that foodborne diseases continue to be a main public health issue [20-23, 95]. The major causative factors are microbial pathogens, which contaminates the food and beverages. These disease-causing pathogens include microbes, viruses, fungi, and parasites [2, 16, 18, 22, 23, 92, 93, 97, 99]. Generally, foodborne illnesses are categorized into foodborne infections and foodborne intoxications. A century ago, foodborne illnesses such as cholera, tuberculosis and typhoid were common. However, advancements in food safety have eradicated these diseases to some extent. Furthermore, the spectrum of the foodborne disease varies frequently and causes major outbreaks around the world. The U.S. Public Health Service has identified the least-wanted pathogens as major causes of foodborne illnesses. The list includes *Campylobacter*, *Clostridium botulinum*, *E. coli* 0157:H7, *Listeria monocytogenes*, *Norovirus*, *Salmonella*, *Staphylococcus aureus*, *Shigella*, *Toxoplasma gondii*, and *Vibrio vulnificus*. Velusamy et al. assembled a list of foodborne hazards and new emerging foodborne pathogens [100]. Below is an estimate of foodborne diseases outbreak in 2009-2010 in the United States [101].

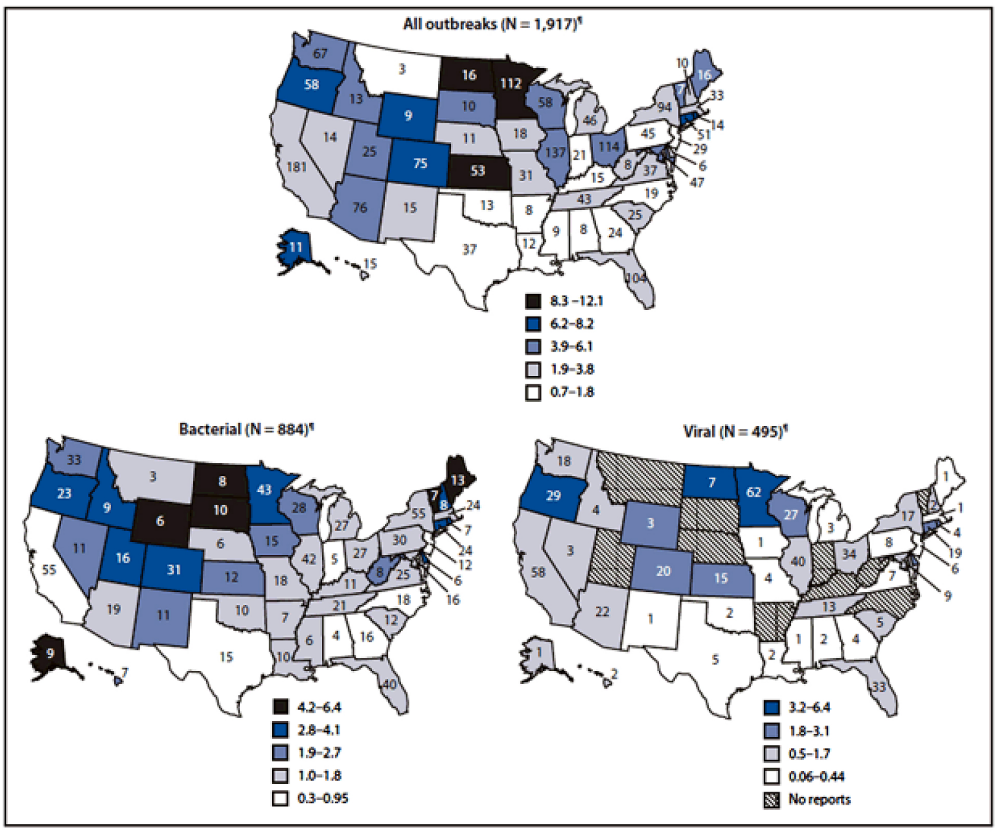

Source: http://www.cdc.gov/mmwr/preview/mmwrhtml/mm6203a1.htm [101].

Figure 2. Average annual rate of reported foodborne disease outbreaks per 1 million population and number of outbreaks by state and major etiology group.

Over the past years, the widespread of foodborne infections has changed significantly. Some established pathogens have been under control or are being eliminated, but new emerging microbial pathogens appear in foods [2, 3, 23, 91, 96]. Food processing companies cannot guarantee the absence of foodborne pathogens as they may get recontaminated during processing. Therefore, there is a need for new preventive methods to eradicate foodborne illnesses and diseases. The capability to manage and minimize higher risks of foodborne illnesses requires integrating the research data, control of food monitoring, epidemiological assessments, and disease surveillance [2, 16, 19, 20, 96, 97]. Pharmaceutical companies are inventing new antimicrobial and antiparasitic agents to reduce risks for both human and environmental health. In recent years, nanotechnology has been a major technology in which nanoparticles are used in the food industry to minimize emerging foodborne illnesses. There are five basic categories of nanotechnology applications and functionalities currently in the development of food sector: food processing, packaging, nutraceuticals delivery, food safety and functional food [76, 102, 103].

Silver is used as an additive in several food-contacting materials such as plastics, glass, or metal. In particular, silver compounds or nanosilver have already been used in many applications including food contact and food packaging materials and refrigerator inner liners [71, 74, 104-107].

Fast and precise detection of pathogenic bacteria is important for proper treatment, inhibition, and prevention of infectious diseases. Delay in diagnoses might cause deaths and side effects. Great advancements have been made in the past decade to detect and identify specific pathogens and toxins present in foods [91, 108-113]. Traditional methods for pathogen detection include microscopy, culture, and serology, which are inexpensive but time-consuming. Nanotechnology enables rapid detection and monitoring of pathogen and toxin contamination at various steps in food supply chains, thereby drastically reducing costly food recalls as well as human health costs [109, 114-116]. Number of studies summarized conventional methods, analytical methods, bacteriophage based methods and recent advancements in detection, identification and quantification of foodborne pathogens with biosensors [100, 108-111, 117, 118].

3. SILVER AND NANOSILVER AS ANTIBACTERIAL AGENTS

3.1. Silver as Antimicrobial and Antiparasitic Agent

Silver has been used for the treatment of burns and chronic wounds for centuries [87, 119-122]. As early as 1000 B.C., silver was used to make potable drinking water [80, 84]. In year 1700, silver nitrate was used for the treatment of various diseases [88,119]. In the 19th century, Lea reported that the synthesis of allotropic forms of silver [123]. During this period, colloidal silver was developed for medical applications [85, 86, 124, 125]. During the 20th century, silver in the form of silver nitrate was used for the treatment of burns as an antibacterial [80, 88, 121, 126]. In addition, silver was used to purify drinking and swimming pool waters [122, 127, 128]. In the late 20th century, United States FDA (Food Drug Administration) and EPA (Environmental Protection Agency) approved the use of silver in various consumer products [124]. Therefore, silver is known as a potent antibacterial,

antifungal, and antiviral agent used in many medical and consumer products [42, 78, 124, 129-133].

3.2. Nanosilver as Antimicrobial and Antiparasitic Agent

Nanosilver has many medical and nonmedical applications due to its unique physicochemical properties. Nanosilver plays a profound role in textile industry [68,134,135]. Several studies have shown the utility of coatings containing silver to prevent biofilm formation in different food-contacting surfaces and silver-based technologies [136,137]. They have also been used in aseptic surfaces with various applications, such as cutting boards, knifes, refrigerators, water filters, liquid soaps, working surfaces, and reusable food packaging [138,139].

Nanosilver is the most commonly used engineered nanomaterial in consumer goods [78, 85, 86, 124, 126, 128, 130, 157-162]. It is effective against numerous species of bacteria (Table 2). For centuries, nanosilver products have shown to be effective against bacteria via inhibition of bacterial growth and bactericidal effects. Nanosilver was evaluated for their antibacterial [131, 136, 163-170], anti-inflammatory [171], anti-viral [172], and antiparasitic [173] effects on various pathogenic microorganisms. Nanosilver inhibited the growth of *E. coli* [46, 78, 81, 140, 143, 144, 174], *E. faecalis* [175], *S. aureus* [176] and *B. subtilis* [174]. There are also studies on the antifungal activity of nanosilver [131, 136, 163-165, 167, 170, 177]. Additionally, nanosilver was proven to be efficient against resistant strains including MRSA (Methicillin-resistant *S. aureus*) [116, 176], MRSE (methicillin-resistant *S. epidermidis*) [176], vancomycin-resistant *Enterococcus* (VRE) [178], and extended spectrum β-lactamase (ESBL) producing *Klebsiella* [66, 179]. In addition, nanosilver is toxic to fungi *Candida albicans* [165], *Aspergillus niger* [180], *Trichophyton mentagrophytes* [164], and yeast isolated from *Bovine mastitis* [181].

4. MECHANISM OF ACTION FOR NANOSILVER ON MICROBIAL PATHOGENS

The antimicrobial activity can be defined as local killing of microbes or retardation of growth of the microbes. The antimicrobial agents are categorized either bactericidal or bacteriostatic. Various nanoparticles are used as antimicrobial and antifungal agents. In general, the antimicrobial activity of nanosilver is of significant interest because of their specificity towards various strains of bacteria [62]. There are various studies on the antimicrobial activities of nanosilver as well as on the mechanistic pathways [62, 63, 65, 130, 162, 182-187]. Various factors such as the cell wall properties, growth rate of bacteria, species of bacteria, composition of surface modifications, and large surface area of nanoparticles contribute to the antibacterial and antiparasitic activity of nanosilver. Some bacterial strains exhibit defense mechanisms to certain antimicrobial agents. Therefore, the specificity of different bacterial strains also plays an important role on the mechanism of

toxicity. In summary, the multiple mechanisms of toxicity of nanosilver on bacteria are elucidated in Figures 3 & 4. In Figure 3, Rai et al. listed eight different pathways for nanosilver action: Inhibition of cell wall formation, formation of free radicals, attachment to 30 S subunit of the ribosome, interaction with bacterial peptides that affect cell signaling, attaching to the surface of cell membrane, intercalate nucleic acid between DNA bases, preventing biofilm formation, and binding with thiol groups of enzymes [99].

Table 2. Activity of silver ions and nanosilver against broad spectrum of microbes (reproduced from Rai et al. (2012) [99]

No.	Forms of silver	Target organisms	References
1.	Silver ions	*S. aureus and E. coli*	[140]
2.	Silver nitrate	Periodontal pathogens	[141]
3.	Silver zeolite	*E. coli*	[142]
4.	Nanosilver	*E. coli*	[143,144]
5.	Silver ions	RNA viruses	[145]
6.	Nanosilver	*E. coli, V. cholerae, P. aeruginosa, S. typhi*	[79]
7.	Nanosilver	*E. coli* in liquid & solid medium	[81]
8.	Silver ions	*E. coli*	[146]
9.	Nanosilver	*S. aureus* and *E. coli*	[147]
10.	Super paramagnetic Nanosilver, bifunctional Fe_3O_4, @ Nanosilver	*S. epidermidis*	[148]
11.	Nanofibres impregnated Nanosilver	*E. coli* & *S. aureus*	[149]
12.	Nanosilver on cotton Fabrics	*S. aureus*	[63]
13.	Nanosilver impregnated on the wound dressing	*E. coli* & *S. aureus*	[150]
14.	Nanosilver	*E. coli, S. typhi, S. epidermidis, S. aureus*	[151]
15.	Nanosilver	*P. glomerata, P. herbarum, F. semitectum, Trichoderma sp*. and *C. albicans*	[58]
16.	Nanosilver	*E. coli, S. aureus* and *Ps. aeruginosa*	[83]
17.	Nanosilver	*E. coli* and *S. aureus*	[69]
18.	Nanosilver	*E. coli* and *Ps. aeruginosa*	[152]
19.	Nanosilver	*E. coli, S. aureus* and *Ps. aeruginosa*	[153]
20.	Nanosilver	*Ps. aeruginosa, S. aureus*, pathogenic fungi *A. flavus* and *A. niger*	[154]
21.	Nanosilver	*S. aureus, E. coli, K. pneumonia, B. subtilis, E. faecalis, Ps. aeruginosa*	[155]
22.	Nanosilver coated med. devices	*S. aureus* and *S. mutans*	[156]
23.	Cellulose-nanosilver complex	*E. coli* and *S. aureus*	[82]

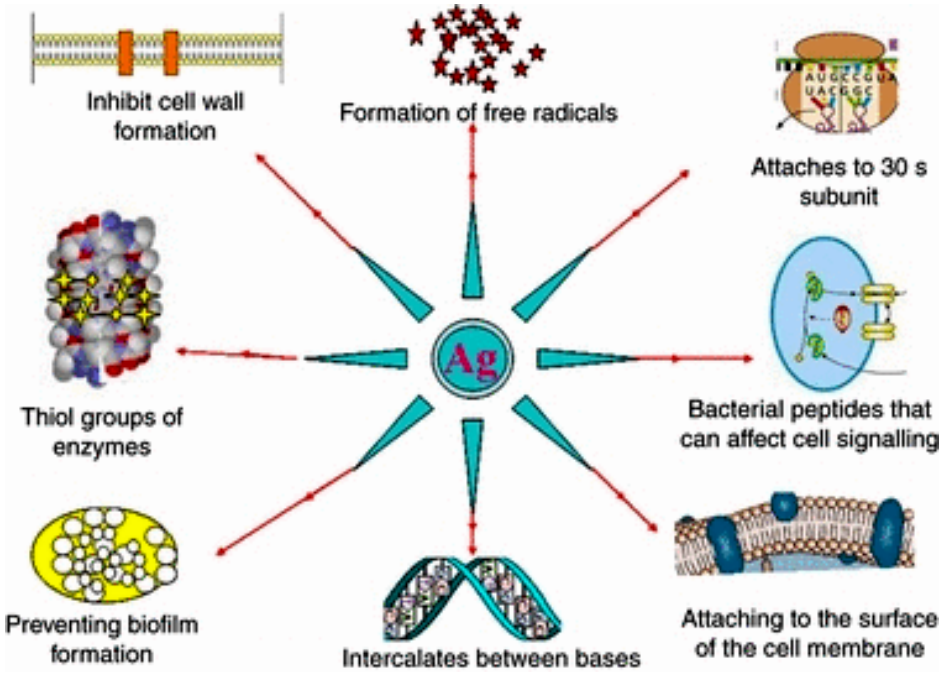

Figure 3. Multiple mechanisms of action for nanosilver on bacteria (reproduced with permission from Springer-Verlag [99]).

In Figure 4, Rizzello and Pompa presented a mechanism for Ag^+ ion release by nanosilver in biological media and its implication for toxicity [162]. Under anaerobic conditions, there may not be an ion release. But under aerobic conditions, due to oxidation of surface silver atoms to Ag_2O, there is always ion release. Ag^+ plays the key role for nanosilver's toxicity. They listed four modes of action: 1) Direct physical damage as a result of the interaction of Ag^+ or nanosilver with proteins of respiratory chain; 2) Production of ROS and subsequent lipid and DNA damages; 3) Ag^+ based DNA damages; and 4) Interaction of Ag^+ with intracellular proteins through electrostatic attractions.

Li et al. outlined three antibacterial mechanisms of toxicity of nanosilver [186]: 1). Nanosilver alters the cell membrane properties by adhering to the surface of bacteria. 2). Penetration of nanosilver inside the cell membrane causing DNA damage. 3). Release of silver ions from nanosilver particles interacts with sulfur containing proteins in the bacterial cell wall.

McShan et al. also pointed out that the toxicity of nanosilver is closely related to its transformation in biological and environmental media including surface oxidation, release of silver ions, and interaction with biological macromolecules [130]. They also summarized nanosilver's interaction with cell membrane proteins, ROS production, and the binding and damage to cellular proteins.

Lu et al. pointed out that environmental effect such as light and moisture also plays a role in nanosilver's toxicity in cells [188]. Using of a more robust coating agent can prevent surface oxidation and thus reduce the toxicity of released silver ions.

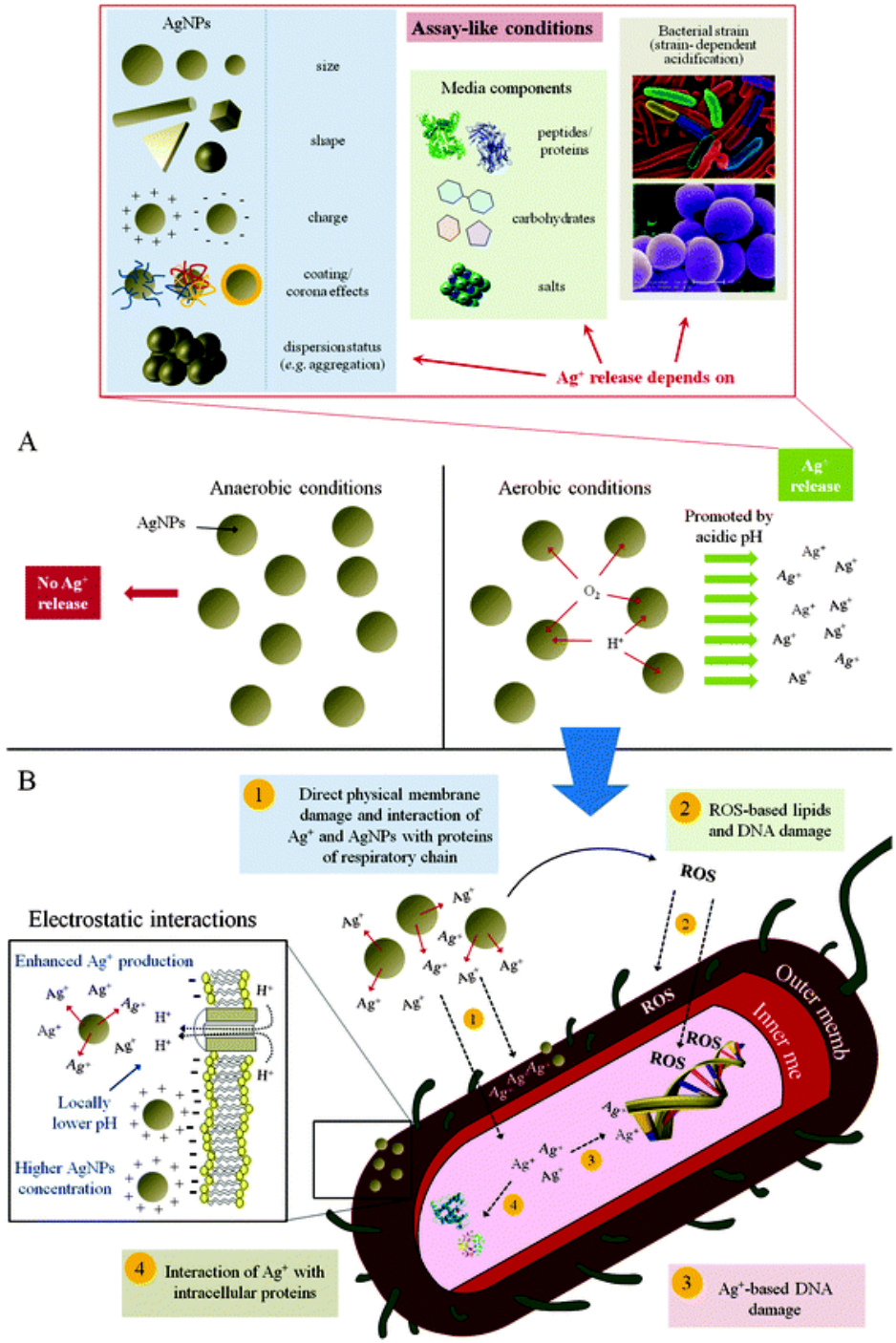

Figure 4. (A) Pictorial representation of factors influencing nanosilver inhibition on bacteria, silver ion release in acidic and aerobic environment. (B) Multiple mechanisms of nanosilver toxicity to gram-negative bacteria (Reproduced with permission from RSC Publishing [162]).

Due to the complexicity of the mechanisms, we use Table 3 to summarize recent research results on nanosilver's mechanisms of toxicity on different microorganisms. In the following sections (*a-d*), we will summarize in detail about nanosilver's mechanism of action.

Table 3. Summary of recently published reports on the mechanism of nanosilver toxicity on bacteria, fungi, and parasites

Microorganism	Nanosilver (nm)	Nanosilver Concentration	Mechanism of Toxicity	Ref.
E. coli	9.3 ± 2.8	0.4 nM	Target membrane and dissipate proton motive force	[189]
P. aeruginosa	1-10	25-100 mg/L	Disturb permeability, respiratory cell division, interact with cell membrane, sulfur and phosphorous compounds	[79]
E. coli		10 µg/mL	Bacterial cell membrane damage and deactivation of membranous enzymes	[186]
E. coli	18- 72		Ag^+ release	[190]
Enterococus	700-800	10 mg/L		[178]
P. aeruginosa *S. aureus* *S. aureus MRSA* *E. coli*	30 ± 7 9 ± 2 14 ± 5 24 ± 6	14.38-215.74 µg/mL	Antibacterial activity increased with decreasing particle size	[191
E. coli *P. fluorescens* *P. putida* *P. aeruginosa* *B. subtilis* *S. aureus*	10.5 – 85.7	0.71-0.74 mg/L	Additional dissolution of Ag^+ occurs at the particle-cell interface	[192]
B. subtilis	<100	10 mM	Significant inhibition on viability; Less toxic to Gram positive bacteria because of thicker layer	[193]
K. pneumonia	43	30 mg/L	Electrostatic interaction; Adsorption increases with increase of temperature from 20 to 37 ℃	[194]
E. coli	80 ± 38 18 ± 7	200 mg/L 50 mg/L	Significant influence on protein and metabolic processes of purine. Drastic change on protein, hypoxanthine adenosine, and guanosine	[182]
E. coli	9.1- 43.5	2.0 – 40.9 mg/L	Toxicity mediated by dissolved Ag^+, ROS production, and impairment of flagellar activity. Interaction between negatively and positively charged nanosilver with bacterial surface results in high concentration of dissolved and bioavailable Ag^+	[184]

a. **Silver ion release:** The nanosilver may attack the respiratory chain ultimately leading to cell death. Release of silver ions in the bacterial cells augments their bactericidal activity and plays a key role in exerting the antimicrobial activity of nanosilver [26, 79, 130, 140, 143]. Interaction between silver ions and thiol groups of enzymes results in the bacteria cell inactivation [26, 142, 195, 196]. Samberg et al. reported that the antibacterial activity of silver ions is the result of synergism between silver ions and the cell wall of bacteria [197]. Wong and Liu reported that silver ions interact with phosphorous containing compounds such as DNA and obstruct replication and cease cell proliferation [198]. Kim et al. reported that the positive charge on the silver ion plays a key role in exerting the antimicrobial activity via electrostatic attraction between negatively charged cell membrane of the microorganism and the positively charged nanoparticles [78]. Xiu et al. proposed a two-step process of silver ion release, metallic nanosilver particles oxidized to silver oxide and silver ions released through the reaction between Ag_2O and proton [190]. Silver ions also cause denaturation of the 30s subunit of the ribosome. It may suppress the expression of enzymes and proteins necessary for ATP production and hinder respiratory enzymes and thus destabilize and disrupt the outer membrane [142, 146, 158, 189].
b. **Membrane integrity disruption:** Bolla et al. reported that membrane permeability is part of the early bacterial defense [48]. Bacteria are categorized into Gram-positive and Gram-negative based on their membrane structures. Both Gram-positive (20-50 nm) and Gram-negative (2-3 nm) bacteria are made up of peptidoglycan layer. In the Gram-negative bacteria cell wall, there is an additional outer membrane composed of phospholipids, lipo-polysaccharides, and protein molecules. Understanding of the cell wall plays a significant role in elucidating the mechanism of toxicity. Shrivastava et al. discussed that Gram-positive bacteria contain high composition of negatively charged components such as lipopolysaccharides that attract the positively charged nanomaterials [159]. Amro et al. explained the irregular shaped pit on the outer membrane caused by metal depletion disturbs the membrane permeability with the release of lipopolysaccharides and membrane proteins [199]. Verma and Stellacci suggested that synthetic and natural chemical moieties on the nanoparticle surface (in addition to nanoparticle shape and size) impact their interaction with lipid bilayers and cells [200]. Sondi et al. pointed out that the similar mechanism might cause damage to membrane structure of *E. coli* [143]. There are two suggested pathways for disruption of membrane as described in the literature: i). Electrostatic interaction between positively charged nanoparticles and negatively charged cell membrane is the key mechanism for disruption of membrane integrity. The surface charge of nanosilver has a profound effect on how the nanoparticle interacts with the cell membrane [201]. ii). Interaction between nanosilver and the cell membrane of a bacterium might cause oxidative stress via generation of ROS [159]. Several studies reported that the disruption of bacterial cellular membrane is one of the causes of antibacterial activity of nanomaterials [159, 202-205]. Nanosilver has the ability to attach to the bacterial cell wall and thereby cause structural damages to the cell wall leading to cell death [78].

c. **Generation of reactive oxygen species (ROS)**: In general, when nanomaterials penetrate into the cell membrane, they trigger the generation of ROS. The metal ions released by nanomaterials also induce oxidative stress via direct interaction with cell organelles. The ROS might undergo breakage of DNA strand, inactivation of proteins, disruption of cellular metabolic processes, and finally leading to cell death [144]. Kim et al. [78] detected the formation of free radicals by nanosilver. Silver ion uptake in bacteria might also lead to the formation of ROS to disrupt cell membrane [206]. Xiu et al. supported the concept of silver ion toxicity by reporting that nanosilver shows no toxicity with the ceasing of silver ions [190].
d. **Electrochemical gradient Disruption:** Proton electrochemical gradient is essential for ATP synthesis in bacteria. Interruption of these processes leads to microbial cell death [26,189]. Cao et al. observed that the proton depleted regions around nanosilver particles may disrupt the electrochemical gradient in the bacteria's inter membrane space and interfere with adhesion and proliferation [26]. Shrivastava et al. reported that nanoparticles dephosphorylated peptide substances on tyrosine residues resulted in the inhibition of transduction and cessation of growth [159].

5. COMBINATION OF NANOSILVER WITH ANTIBIOTICS

Recently, the combination of nanosilver with traditional antibiotics has become a hot research topic. These findings are of great significance in two aspects in regards to the practical applications: i) A promising solution to the worldwide bacterial resistance to conventional antibiotics. The escalation of bacterial resistance to common medical antibiotics gradually appears to be a serious health problem. The presence of nanosilver can help conventional antibiotics restore antibacterial capability to destroy multidrug-resistant bacteria. ii) Combinational usage of nanosilver and antibiotics often lead to much lower minimal inhibitory concentration (MIC) than either nanosilver or antibiotics alone. This demonstrates a much higher efficiency of antibacterial effect, and decreases the potential toxicity of nanosilver and antibiotics to achieve the same treatment effectiveness.

There are a total of about 20 publications that tested the antibiotic activity of the combination of nanosilver and antibiotics. As listed in Table 3, one of the earliest publications is carried out by Li et al. [46], where the combined activity of nanosilver and amoxicillin was investigated against *E. coli*. Nanosilver was prepared by using freshly prepared ascorbic acid solution with an average size of 20 nm. MIC decreased greatly when nanosilver and amoxicillin were combined (5 μg/mL and 0.15 mg/mL, respectively), compared to separate use of either nanosilver (40 μg/mL) or amoxicillin (0.5 mg/mL). Dynamic tests showed that bacterial growth was decreased and delayed at exponential and stationary phases. Authors concluded that there was a synergistic effect of amoxicillin and silver nanoparticles and pre-incubation of a solution containing more nanosilver received better antimicrobial effects.

Kora et al. prepared nanosilver by reducing $AgNO_3$ solution with $NaBH_4$ [59]. Various sized nanosilver particles were formed when different stabilizing agents were used: citrate (38.3±13.5 nm), sodium dodecyl sulfate (SDS, 19.3±6.0 nm) and polyvinylpyrrolidone (PVP, 16.0 ±4.8 nm). These nanosilver particles were then combined with streptomycin (10 μg), ampicillin (10 μg), and tetracycline (30 μg) to inhibit the growth of *E. coli* and *S. aureus* as

models for Gram-negative and Gram-positive bacteria, respectively. The presence of the above three different sized nanosilver enhanced the antibacterial activity of the antibiotics, with percent of enhancement being different (Figure 5). As shown in Figure 5, the enhancement is the greatest with PVP-coated nanosilver, with the percents of enhancement being 45.4% and 50%, respectively, when PVP-stabilized nanosilver is combined with streptomycin against *S. aureus* or with ampicillin against *E. coli*.

Table 4. Summary of recent studies on antibacterial activity using the combination of nanosilver and conventional antibiotics

Nanosilver Synthesis	Antibiotics	Bacteria/fungi	Ref
Reduce $AgNO_3$ w. ascorbic acid, cubic shaped, 20 nm	Amoxicillin	*E. coli* (gram-negative)	[46]
Reduce $AgNO_3$ w. $NaBH_4$, capped by citrate (38.3±13.5 nm), SDS (19.3±6.0 nm), and PVP (16.0 ±4.8 nm)	Streptomycin, ampicillin tetracycline	*E. coli* and *S. aureus*	[59]
Reduce $AgNO_3$ in presence of *Klebsiella pneumonia*, 22.5 nm (5-32 nm)	Penicillin G amoxicillin erythromycin clindamycin vancomycin	*S. aureus* and *E. coli*	[147]
Photo-assisted reduction, 16.6 nm (7-20 nm)	Ceftazidime streptomycin kanamycin ampiclox polymyxin B chloramphenicol	Over 10 different kinds of bacteria	[125]
Fungus extracellular synthesis (60-80 nm)	Ampicillin gentamycin streptomycin vancomycin	*E. coli, S. aureus* and *Ps. aeruginosa*	[83]
Fungus-mediated synthesis (*Alternaria alternate*), 32.5 nm (20-60 nm)	Fluconazole	*P. glomerata, P. herbarum, F. semitectum, Trichoderma sp.*, and *C. albicans*	[58]
Fungus *Trichoderma viride*, 5-40 nm	Ampicillin kanamycin erythromycin chloramphenicol	*S. typhi* (Gram negative rods), *E. coli* (gram-negative rods), *S. aureus* (gram-positive cocci), *M. luteus* (gram-positive cocci)	[47]
Aspergillus terreus SP5, *Paecilomyces lilacinus* SF1 and *Fusarium sp.* MP5 (5-50 nm)	Erythromycin methicillin chloramphenicol ciprofloxacin	*S. aureus, S. pyogenes, S. enterica* and *E. faecalis*	[207]
Electrolytic, 10 nm (2-23 nm)	Ampicillin gentamicin	*S. typhi*	[60]
Dioscorea bulbifera tuber extract (8-20 nm)	Piperacillin erythromycin chloramphenicol, vancomycin, streptomycin	*A. baumannii, Ps. aeruginosa, E. coli*	[49]
Cryphonectria sp. (30-70 nm)	Streptomycin amphotericin	*S. aureus, E. coli, S. typhi, & C. albicans*	[57]

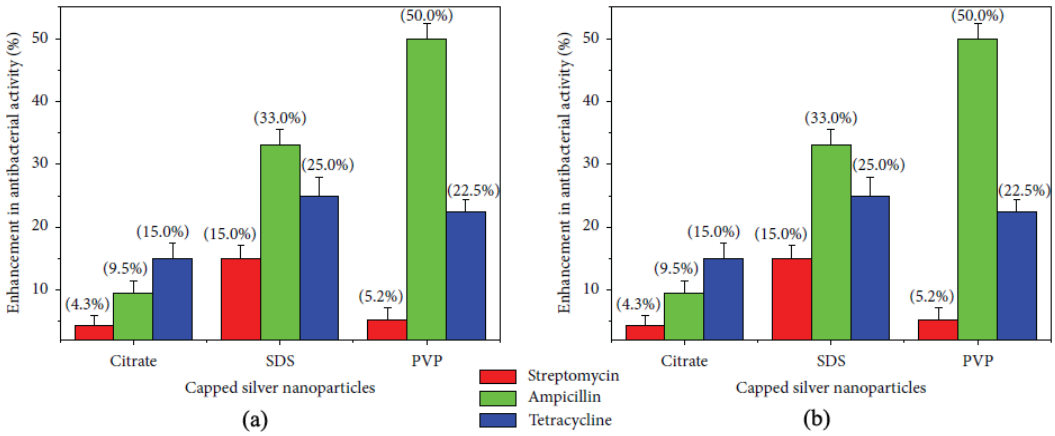

Figure 5. Percent of enhancement of antibacterial activity of antibiotics in combination with nanosilver, against *E. coli* (a) and *S. aureus* (b) (Reproduced with permission from Hindawi Publishing Corporation [59]).

It's well-known that nanosilver can be synthesized by reduction of silver ions using citrate, $NaBH_4$, or other reducing agents, and by applying various small molecules or polymers/biopolymers as coating agents. However, these traditional chemical methods involve many different kinds of chemicals that are potentially harmful and toxic to human cells [208]. This means that further purification process is required to get rid of remaining chemicals in nanosilver solution after the synthesis procedure. On the other hand, nanosilver is not stable without a coating agent and aggregate irreversibly to reduce their surface energy. Therefore, there is an underlying balance between purity and presence of coating agents, which is hard to achieve during operation. In this case, biosynthetic technology is developed using fungi [58, 83, 207,2 09] or natural extract [49]. As listed in Table 4, nanosilver ranged 2-70 nm have been synthesized by using many types of fungi or extract, including *Alternaria alternate* [58], *Trichoderma viride* [47], *Aspergillus terreus SP5*, *Paecilomyces lilacinus SF1* and *Fusarium sp. MP5* [207], *Cryphonectria sp.* [57] and *Dioscorea bulbifera* tuber extract [49].

These nanosilvers were then combined with various antibiotics to study the antimicrobial effects. In the presence of nanosilver, fluconazole showed the maximum inhibition against *C. albicans*, followed by *P. glomerata* and *Trichoderma viride* while no significant enhancement of activity was found against *P. herbarum* and *F. semitectum* [58]. Confirmed by Fayaz et al. [47], the antibacterial activities of ampicillin, kanamycin, erythromycin, and chloramphenicol were increased in the presence of nanosilver against both gram-negative (*S. typhi* and *E. coli*) and gram-positive (*S. aureus* and *M. luteus*) bacteria. The highest enhancement was observed for ampicillin. Devi et al. [207] also investigated the synergistic effect of nanosilver with erythromycin, methicillin, chloramphenicol and ciprofloxacin against *S. aureus*, *S. pyog*enes, *S. enterica* and *E. faecalis*.

Notably, Shahverdi et al. [147] synthesized nanosilver ranging from 5 to 30 nm (average size 22.5 nm) using the culture supernatants of *Klebsiella pneumoniae*. The nanosilver was then combined with 14 types of conventional antibiotics to investigate their antibacterial activity against *S. aureus* and *E. coli*. As reported in table 1 in their paper, antibacterial activities of penicillin G, amoxicillin, erythromycin, clindamycin and vancomycin are all

enhanced against both *S. aureus* and *E. coli*, while enhancements are the highest for vancomycin, amoxicillin, and penicillin G against *S. aureus*. There is no enhancement for all the other antibiotics.

Jain et al. reported antimicrobial effects of biostabilized nanosilver with the size range of 7-20 nm (average 16.6 nm) in combination with ceftazidime, streptomycin, kanamycin, ampiclox, polymyxin B and chloramphenicol against over 10 types of mirocorganisms [125]. Various MIC values were examined by utilizing Checkerboard Microdilution Studies. Interestingly, distinct effects are observed. Effect of nanosilver with ceftazidime is synergistic, while nanosilver with streptomycin, kanamycin, ampiclox and polymyxin B are additive, and nanosilver with chloramphenicol is antagonistic. Based on these results, authors developed an antimicrobial gel for topical treatment. Another study, carried out by Birla et al. [83], used synthesized nanosilver from *Phoma glomerata* with size ranged from 60-80 nm. The addition of nanosilver caused an increase of inhibition by ampicillin, streptomycin and vancomycin against *E. coli* and *Ps. aeruginosa*. The observed synergistic activity is better for *E. coli* and *Ps. aeruginosa* than for *S. aureus*.

Chopade et al. found that β-lactam (piperacillin) and macrolide (erythromycin) antibiotics showed a 3.6-fold and 3-fold increase, respectively, against multidrug-resistant *Acinetobacter baumannii*, in combination with nanosilver [49]. Chloramphenicol or vancomycin against *Pseudomonas aeruginosa* received a 4.9-fold and 4.2-fold increase, respectively, while a maximum 11.8-fold increase in zone diameter of streptomycin was observed when combined with nanosilver against *E. coli*. Dar et al. [57] also reported that streptomycin and amphotericin combined with nanosilver showed comparatively higher activity against both *S. aureus* and *E. coli* than against *S. typhi* and *C. albicans*. Rajawat et al. elctrolytically prepared nanosilver of average size 10 nm (2-23 nm) [60]. They found that the combination of synthesized nanosilver and ampicillin was more effective than the combination of nanosilver and gentamicin against *Salmonella typhi*.

6. MECHANISM OF ANTIBACTERIAL ACTIVITY OF COMBINED NANOSILVER WITH ANTIBIOTICS

Mechanisms of action for most of the conventional antibiotics have already been studied. β-Lactam antibiotics (penicillin class) can inhibit the formation of peptidoglycan cross-links in the bacterial cell wall by binding to the four-membered β-lactam ring of penicillin to the enzyme DD-transpeptidase [210]. Nanosilver is also widely investigated as potential antibacterial agents and how the antimicrobial effect is achieved [63].

Several hypotheses have been proposed to explain the synergistic effect of nanosilver-antibiotics complex for bacteria [46,51]. The two antimicrobial agents could function either separately or synergistically. Even one of the two is not effective due resistance by the bacterium, the other will still function to kill the bacteria. The synergistic effect may be caused by binding of the antibiotic molecules onto nanosilver. Antibiotics contain many functional groups including hydroxyl and amino groups which can bind to silver. Since the antibiotic usually has a strong affinity to the bacteria, the antibiotic-nanosilver complex can bind to the bacteria more easily than nanosilver alone, increasing the local concentration of

nanosilver and released Ag^{+}. Another possible mechanism is that nanosilver facilitates inter-membrane transportation of antibiotics (like amoxicillin) to the target cell surfaces.

Fayaz et al. proposed a four-step mechanism for the synergistic activity of ampicillin combined with nanosilver [47]. According to their mechanism, core nanosilver is formed with ampicillin based chelation. The nanosilver-ampicillin complex then interacts with bacteria cell wall and inhibits the formation of cross-links in the peptidoglycan layer, thus preventing cell wall formation. Finally, it leads to cell wall lysis. This is the same way in which β-lactam antibiotics (ampicillin) kill bacteria. Furthermore, silver-ampicillin complex can enter into bacterial cell and prevents the DNA unwinding.

Based on different results discussed here, it can be concluded that the antibacterial effect of nanosilver-antibiotic combination is greatly dependent on the size, stabilizer of nanosilver as well as the type of antibiotic molecules. Obviously, reactive functional groups, like sulfydryl, amino and hydroxyl groups, are responsible for the interactions between nanosilver and antibiotic molecules. If the binding between nanosilver and antibiotics is very weak van der Waals interaction, it dissociates easily when nanosilver-antibiotics complex is located in the bacterial environment. Nanosilver and antibiotic molecules will function separately. In contrast, when the binding is covalent or strong noncovalent interactions, nanosilver-antibiotics complexes are preferable to function as a unit. This indicates that the interaction between nanosilver and antibiotic molecules should be first studied. Then the changes of protein expression should be clarified to figure out the mechanistic pathway. These results will provide direct evidences for the mechanism of antimicrobial effect of nanosilver-antibiotics.

ACKNOWLEDGMENTS

Dr. Yu thanks NSF-PREM grant # DMR-1205194 grant for their generous funding.

REFERENCES

[1] Meng, J; Doyle, MP. Emerging and evolving microbial foodborne pathogens, *Bull. Inst. Pasteur*, 1998, 96, 151-163.

[2] Scallan, E; Hoekstra, RM; Angulo, FJ; Tauxe, RV; Widdowson, M.-A; Roy, SL; Jones, JL; Griffin, PM. Foodborne illness acquired in the United States - major pathogens, *Emerg. Infect. Dis.*, 2011, 17, 7-15.

[3] Skovgaard, N. New trends in emerging pathogens, *Int. J. Food. Microbiol.*, 2007, 120, 217-224.

[4] Tauxe, RV. Emerging foodborne pathogens, *Int. J. Food. Microbiol.*, 2002, 78, 31-41.

[5] Slifko, TR; Smith, HV; Rose, JB. Emerging parasite zoonoses associated with water and food, *Int. J. Parasitol.*, 2000, 30, 1379-1393.

[6] Byarugaba, DK. Antimicrobial resistance in developing countries and responsible risk factors, *Int. J. Antimicrob. Agents*, 2004, 24, 105-110.

[7] Mayrhofer, S; Paulsen, P; Smulders, FJ; Hilbert, F. Antimicrobial resistance profile of five major food-borne pathogens isolated from beef, pork and poultry, *Int. J. Food. Microbiol.*, 2004, 97, 23-29.

[8] Silbergeld, EK; Graham, J; Price, LB. Industrial food animal production, antimicrobial resistance, and human health, *Annu. Rev. Pub. Health*., 2008, 29, 151-169.

[9] Singer, RS; Finch, R; Wegener, HC; Bywater, R; Walters, J; Lipsitch, M. Antibiotic resistance - the interplay between antibiotic use in animals and human beings, *Lancet. Infect. Dis.*, 2003, 3, 47-51.

[10] Sorum, H; Labee Lund, TM. Antibiotic resistance in food-related bacteria: a result of interfering with the global web of bacterial genetics, *Int. J. Food. Microbiol.*, 2002, 78, 43-56.

[11] Su, L-H; Chiu, C-H; Chu, C; Ou, JT. Antimicrobial resistance in nontyphoid Salmonella serotypes: a global challenge, *Clin. Infect. Dis.*, 2004, 39, 546-551.

[12] Threlfall, E. J. Antimicrobial drug resistance in Salmonella: problems and perspectives in food - and water- borne infections, *FEMS Microbiol. Rev*., 2002, 26, 141-148.

[13] Threlfall, EJ; Ward, LR; Frost, JA; Willshaw, GA. The emergence and spread of antibiotic resistance in food-borne bacteria, *Int. J. Food. Microbiol.*, 2000, 62, 1-5.

[14] White, DG; Zhao, S; Simjee, S; Wagner, DD; McDermott, PF. Antimicrobial resistance of foodborne pathogens, *Microbe. Infect.*, 2002, 4, 405-412.

[15] Keiser, J; Utzinger, J. Emerging foodborne trematodiasis, *Emerg. Infect. Dis.*, 2005, 11, 1507-1517.

[16] Lynch, M; Painter, J; Woodruff, R; Braden, C. "Surveillance for Foodborne - Disease Outbreaks: United States, 1998-2002," Center for Disease Control and Prevention, 2006.

[17] Gorman, R; Bloomfield, S; Adley, CC. A study of cross-contamination of food-borne pathogens in the domestic kitchen in the Republic of Ireland, *Int. J. Food. Microbiol.*, 2002, 76, 143-150.

[18] Adak, GK; Long, SM; O'Brien, SJ. Trends in indigenous foodborne disease and deaths, England and Wales, 1992 to 2000, Gut, 2002, 51, 832-841.

[19] Ayers, LT; Williams, IT; Gray, S; Griffin, PM; Hall, AJ. Surveillance for foodborne disease outbreaks-United States, 2006, *Morbid. Mortal. Week. Rep*., 2009, 58, 609-615.

[20] Olsen, SJ; MacKinnon, LC; Goulding, JS; Bean, NH; Slutsker, L. "Surveillance for foodborne-disease outbreaks - United States, 1993-1997," CDC, 2000.

[21] Scharff, RL. Georgetown University: Washington, DC, 2010; Vol., 2014.

[22] Tauxe, RV. Emerging foodborne diseases: an evolving public health challenge, *Emerg. Infect. Dis.*, 1997, 3, 425-434.

[23] Tauxe, RV. Surveillance and investigation of foodborne diseases; roles for public health in meeting objectives for food safety, *Food Control*, 2002, 13, 363-369.

[24] Van de Venter, T. In Food, Nutrition, and Agriculture; Department of Health, Republic of South Africa: South Africa, 2000, Vol., 2014.

[25] Swaminathan, B; Gerner-Smidt, P; Ng, L-K; Lukinmaa, S; Kam, K-M; Rolando, S; Gutierrez, EP; Binsztein, N. Building PulseNet International: an interconnected system of laboratory networks to facilitate timely public health recognition and response to foodborne disease outbreaks and emerging foodborne diseases, *Foodborne Pathog. Dis.*, 2006, 3, 36-50.

[26] Cao, J; Kursten, D; Schneider, S; Knauer, A; Gunther, PM; Kohler, JM. Uncovering toxicological complexity by multi-dimensional screenings in microsegmented flow: modulation of antibiotic interference by nanoparticles, *Lab. Chip*, 2012, 12, 474-484.

[27] Chopra, I; Roberts, M. Tetracycline antibiotics: mode of action, applications, molecular biology, and epidemiology of bacterial resistance, *Microbiol. Mol. Biol. Rev.*, 2001, 65, 232-260.

[28] Engberg, J; Aarestrup, FM; Taylor, DE; Gerner-Smidt, P; Nachamkin, I. Quinolone and Macrolide Resistance in Campylobacter jejuni and C. coli: Resistance Mechanisms and Trends in Human Isolates, *Emerg. Infect. Dis.*, 2001, 7, 24-34.

[29] Cohen, ML. Changing patterns of infectious disease; Nature, 2000, 406, 762-767.

[30] Wilson, BA; Salyers, AA; Whitt, DD; Winkler, ME. Bacterial Pathogenesis: A Molecular Approach; American Society for Microbiology (ASM): Washington DC, 2011.

[31] Coates, A; Hu, Y; Bax, R; Page, C. The future challenges facing the development of new antimicrobial drugs, *Nat. Rev. Drug. Discov.*, 2002, 1, 895-910.

[32] Fischbach, MA; Walsh, CT. Antibiotics for Emerging Pathogens; Science, 2009, 325, 1089-1093.

[33] Huh, AJ; Kwon, YJ. Nanoantibiotics: A new paradigm for treating infectious diseases using nanomaterials in the antibiotics resistant era, J. Control. Release, 2011, 156, 128-45.

[34] CDC. Center for Disease Control and Prevention: Atlanta, GA, 2011, Vol., 2014.

[35] CDC In CDC, 2011 Estimates: Findings; Center for Disease Control and Prevention: Atlanta, GA, 2011, Vol., 2014.

[36] Kang, S; Pinault, M; Pfefferle, LD; Elimelech, M. Single-walled carbon nanotubes exhibit strong antimicrobial activity; Langmuir, 2007, 23, 8670-8673.

[37] Lines, M G. Nanomaterials for practical functional uses, *J. Alloy Compd.*, 2008, 449, 242-245.

[38] Dingman, J. Nanotechnology: Its Impact On Food Safety, *J. Environ. Health*, 2008, 70, 47-50.

[39] Sozer, N; Kokini, JL. Nanotechnology and its applications in the food sector, *Trend Biotechnol*., 2009, 27, 82-89.

[40] Magnuson, BA; Jonaitis, TS; Card, JW. A Brief Review of the Occurrence, Use, and Safety of Food - Related Nanomaterials, *J. Food. Sci.*, 2011, 76, R126-R133.

[41] Duncan, TV. Applications of nanotechnology in food packaging and food safety: Barrier materials, antimicrobials and sensors, *J. Colloid. Interface Sci.*, 2011, 363, 1-24.

[42] Marambio-Jones, C; Hoek, EMV. A review of the antibacterial effects of silver nanomaterials and potential implications for human health and the environment, *J. Nanopart. Res*., 2010, 12, 1531-1551.

[43] Azam, A; Ahmed, AS; Oves, M; Khan, MS; Habib, SS; Memic, A. Antimicrobial activity of metal oxide nanoparticles against Gram-positive and Gram-negative bacteria: a comparative study, *Int. J. Nanomed.*, 2012, 7, 6003-6009.

[44] Rai, M; Yadav, A; Cioffi, N. In Nano-Antimicrobials: Progress and Prospects, *Cioffi, N. Rai, M.*, Eds; Springer-Verlag: Berlin Heidelberg, 2012.

[45] Lara, HH; Ayala-Nunez, NV; Turrent, Ld CI; Padilla, CR. Bactericidal effect of silver nanoparticles against multidrug-resistant bacteria, *World J. Microbiol. Biotech*., 2010, 26, 615-621.

[46] Li, P; Li, J; Wu, C; Wu, Q; Li, J. Synergistic antibacterial effects of b-lactam antibiotic combined with silver nanoparticles, *Nanotechnology*, 2005, 16, 1912.

[47] Fayaz, AM; Balaji, K; Girilal, M; Yadav, R; Kalaichelvan, PT; Venketesan, R. Biogenic synthesis of silver nanoparticles and their synergistic effect with antibiotics: a study against gram-positive and gram-negative bacteria, *Nanomed. Nanotech. Biol. Med.*, 2010, 6, 103-109.

[48] Bolla, J-M; Alibert-Franco, S; Handzlik, J; Chevalier, J; Mahamoud, A; Boyer, G; Kieć-Kononowicz, K; Pagès, J-M. Strategies for bypassing the membrane barrier in multidrug resistant Gram-negative bacteria; *FEBS Lett.*, 2011, 585, 1682-1690.

[49] Ghosh, S; Patil, S; Ahire, M; Kitture, R; Kale, S; Pardesi, K; Cameotra, SS; Bellare, J; Dhavale, DD; Jabgunde, A; Chopade, B. Synthesis of silver nanoparticles using Dioscorea bulbifera tuber extract and evaluation of its synergistic potential in combination with antimicrobial agents, *Int. J. Nanomed.*, 2012, 7, 483-496.

[50] Chen, X; Niyonsaba, F; Ushio, H; Okuda, D; Nagaoka, I; Ikeda, S; Okumura, K; Ogawa, H. Synergistic effect of antibacterial agents human b-defensins, cathelicidin LL-37 and lysozyme against Staphylococcus aureus and Escherichia coli, *J. Dermatol. Sci.*, 2005, 40, 123-132.

[51] Allahverdiyev, AM; Kon, KV; Abamor, ES; Bagirova, M; Rafailovich, M. Coping with antibiotic resistance: combining nanoparticles with antibiotics and other antimicrobial agents, *Expert. Rev. Anti-Infect. Ther.*, 2011, 9, 1035-1052.

[52] Priya Dhas, S; Mukherjee, A; Chandrasekaran, N. Synergistic effect of biogenic silver nanocolloid in combination with antibiotics: A potent therapeutic agent, *Int. J. Pharm. Pharmaceut. Sci.*, 2013, 5, 292-295.

[53] Abeylath, SC; Turos, E. Drug delivery approaches to overcome bacterial resistance to beta-lactam antibiotics; *Expert. Opin. Drug. Deliv.*, 2008, 5, 931-949.

[54] Musee, N; Thwala, M; Nota, N. The antibacterial effects of engineered nanomaterials: implications for wastewater treatment plants, *J. Environ. Monit.*, 2011, 13, 1164-1183.

[55] Seil, JT; Webster, TJ. Antimicrobial applications of nanotechnology: methods and literature, *Int. J. Nanomed.*, 2012, 7, 2767-2781.

[56] Ramani, M; Ponnusamy, S; Muthamizhchelvan, C. Preliminary investigations on the antibacterial activity of zinc oxide nanostructures, *J. Nanopart. Res.*, 2013, 15, 1557.

[57] Dar, MA; Ingle, A; Rai, M. Enhanced antimicrobial activity of silver nanoparticles synthesized by Cryphonectria sp. evaluated singly and in combination with antibiotics, *Nanomed, Nanomed. Biol. Med.*, 2012, 9, 105-110.

[58] Gajbhiye, M; Kesharwani, J; Ingle, A; Gade, A; Rai, M. Fungus-mediated synthesis of silver nanoparticles and their activity against pathogenic fungi in combination with fluconazole, *Nanomed. Nanotechnol. Biol. Med.*, 2009, 5, 382-386.

[59] Kora, AJ; Rastogi, L. Enhancement of Antibacterial Activity of Capped Silver Nanoparticles in Combination with Antibiotics, on Model Gram-Negative and Gram-Positive Bacteria, *Bioinorgan. Chem. Appl.*, 2013, 2013, 1-7.

[60] Rajawat, S; Qureshi, MS. Study Comparative on Bactericidal Effect of Silver Nanoparticles, Synthesized Using Green Technology, in Combination with Antibiotics on Salmonella typhi, *J. Biomed. Nanotechnol.*, 2012, 3, 480-485.

[61] Kalan, L; Wright, GD. Antibiotic adjuvants: multicomponent anti-infective strategies, *Exp. Rev. Mol. Med.*, 2011, 13, e5.

[62] Reidy, B; Haase, A; Luch, A; Dawson, KA; Lynch, I. Mechanisms of silver nanoparticle release, transformation and toxicity: a critical review of current knowledge and recommendations for future studies and applications, *Materials*, 2013, 6, 2295-2350.

[63] Duran, N; Marcato, PD; Conti, RD; Alves, OL; Costa, F; Brocchi, M. Potential use of silver nanoparticles on pathogenic bacteria, their toxicity and possible mechanisms of action, *J. Brazil. Chem. Soc*., 2010, 21, 949-959.

[64] Hajipour, MJ; Fromm, KM; Akbar Ashkarran, A; Jimenez de Aberasturi, D; Larramendi, IRd; Rojo, T; Serpooshan, V; Parak, WJ; Mahmoudi, M. Antibacterial properties of nanoparticles, *Trends. Biotechnol*., 2012, 30, 499-511.

[65] Hwang, I-s; Hwang, JH; Choi, H; Kim, K-J; Lee, DG. Synergistic effects between silver nanoparticles and antibiotics and the mechanisms involved, *J. Med. Microbiol*., 2012, 61, 1719-1726.

[66] Leid, JG; Ditto, AJ; Knapp, A; Shah, PN; Wright, BD; Blust, R; Christensen, L; Clemons, CB; Wilber, JP; Young, GW; Kang, AG; Panzner, MJ; Cannon, CL; Yun, YH; Youngs, WJ; Seckinger, NM; Cope, EK. vitro antimicrobial studies of silver carbene complexes: activity of free and nanoparticle carbene formulations against clinical isolates of pathogenic bacteria, *J. Antimicrob. Chemother.*, 2011, 67, 138-148.

[67] Rai, RV; Bai, JA. In Science against microbial pathogens: Communicating current research and technological advances; Méndez-Vilas, A., Ed., Formatex Research Center: Spain, 2011, Vol. 3.

[68] Chernousova, S; Epple, M. Silver as antibacterial agent: ion, nanoparticle, and metal, *Angew. Chem*., 2012, 52, 1636-1653.

[69] Gade, A; Ingle, A; Whiteley, C; Rai, M. Mycogenic metal nanoparticles: progress and applications, *Biotechnol. Lett*., 2010, 32, 593-600.

[70] Height, MJ. In FIFRA scientific advisory panel (SAP) open consultation meeting; Silver Nanotechnology Working Group (SNWG), 2009, Vol., 2014.

[71] Llorens, A; Lloret, E; Picouet, PA; Trbojevich, R; Fernandez, A. Metallic-based micro and nanocomposites in food contact materials and active food packaging, *Trends. Food Sci. Tech*., 2012, 24, 19-29.

[72] Slawson, RM; Lee, H; Trevors, JT. Bacterial interactions with silver, *Biol. Metal*, 1990, 3, 151-154.

[73] Appendini, P; Hotchkiss, JH. Review of antimicrobial food packaging, *Innov. Food Sci. Emerg. Technol*., 2002, 3, 113-126.

[74] Azeredo, H. Nanocomposites for food packaging applications, *Food Res. Int.*, 2009, 42, 1240-1253.

[75] Bata-Vidács, I; Adányi, N; Beczner, J; Farkas, J; Székács, A. In Microbial pathogens and strategies for combating them: science, technology and education; Méndez-Vilas, A., Ed., Formatex: Spain, 2013.

[76] Bouwmeester, H; Dekkers, S; Noordam, MY; Hagens, WI; Bulder, AS; De Heer, C; Ten Voorde, SE; Wijnhoven, SW; Marvin, HJ; Sips, AJ. Review of health safety aspects of nanotechnologies in food production, *Regulat. Toxicol. Pharmacol*., 2009, 53, 52-62.

[77] de Azeredo, HMC. Antimicrobial nanostructures in food packaging, *Trends. Food. Sci. Tech*, 2009, 30, 56-69.

[78] Kim, JS; Kuk, E; Yu, KN; Kim, J-H; Park, SJ; Lee, HJ; Kim, SH; Park, YK; Park, YH; Hwang, C-Y; Kim, Y-K; Lee, Y-S; Jeong, DH. Antimicrobial effects of silver nanoparticles, *Nanomed. Nanotechnol. Biol. Med*., 2007, 3, 95-101.

[79] Morones, JR; Elechiguerra, JL; Camacho, A; Holt, K; Kouri, JB; Ramirez, JT; Yacaman, MJ. The bactericidal effect of silver nanoparticles, *Nanotechnology*, 2005, 16, 2346-2353.

[80] Atiyeh, BS; Costagliola, M; Hayek, SN; Dibo, SA. Effect of silver on burn wound infection control and healing: review of the literature, *Burns*, 2007, 33, 139-148.

[81] Baker, C; Pradhan, A; Pakstis, L; Pochan, DJ; Shah, SI. Synthesis and antibacterial properties of silver nanoparticles, *J. Nanosci. Nanotech*., 2005, 5, 244-249.

[82] Barud, HS; Regiani, T; Marques, RFC; Lustri, WR; Messaddeq, Y; Ribeiro, SJ L. Antimicrobial bacterial cellulose-silver nanoparticles composite membranes, *J. Nanomat*., 2011, 2011, 10.

[83] Birla, SS; Tiwari, VV; Gade, AK; Ingle, AP; Yadav, AP; Rai, MK. Fabrication of silver nanoparticles by Phoma glomerata and its combined effect against Escherichia coli, Pseudomonas aeruginosa and Staphylococcus aureus, *Lett. Appl. Microbiol*., 2009, 48, 173-179.

[84] Castellano, JJ; Shafii, SM; Ko, F; Donate, G; Wright, TE; Mannari, RJ; Payne, W G; Smith, DJ; Robson, MC. Comparative evaluation of silver-containing antimicrobial dressings and drugs, *Int. Wound J*., 2007, 4, 114-122.

[85] Chaloupka, K; Malam, Y; Seifalian, AM. Nanosilver as a new generation of nanoproduct in biomedical applications, *Trends Biotechnol*., 2010, 28, 580-588.

[86] Chen, X; Schluesener, H. Nanosilver: a nanoproduct in medical application, *Toxicol. Lett*., 2008, 176, 1-12.

[87] Silver, S; Phung, LT; Silver, G. Silver as biocides in burn and wound dressings and bacterial resistance to silver compounds, *J. Ind. Microbiol. Biotechnol*., 2006, 33, 627-634.

[88] Klasen, H. A historical review of the use of silver in the treatment of burns. II. Renewed interest for silver; Burns, 2000, 26, 131-138.

[89] Modak, SM; Sampath, L; Fox Jr, CL Combined topical use of silver sulfadiazine and antibiotics as a possible solution to bacterial resistance in burn wounds, *J. Burn. Care. Res*., 1988, 9, 359-363.

[90] Dorny, P; Praet, N; Deckers, N; Gabriel, S. Emerging food-borne parasites, *Vet. Parasitol*., 2009, 163, 196-206.

[91] Velusamy, V; Arshak, K; Korostynska, O; Oliwa, K; Adley, C. An overview of foodborne pathogen detection: in the perspective of biosensors, *Biotechnol. Adv*., 2010, 28, 232-254.

[92] Farber, JM; Peterkin, PI. Listeria monocytogenes, a Food-Borne Pathogen, *Microbiol. Rev*., 1991, 55, 476.

[93] Mead, PS; Slutsker, L; Dietz, V; McCaig, LF; Bresee, JS; Shapiro, C; Griffin, PM; Tauxe, RV. Food-related illness and death in the United States; *Emerg. Infect. Dis.*, 1999, 5, 607-625.

[94] Montville, TJ; Matthews, KR; Kniel, KE. *Food Microbiology: An Introduction*, 3rd ed; ASM Press, 2012.

[95] Newell, DG; Koopmans, M; Verhoef, L; Duizer, E; Aidara-Kane, A; Sprong, H; Opsteegh, M; Langelaar, M; Threfall, J; Scheutz, F; Giessen, Jvd; Kruse, H. Foodborne

diseases - the challenges of 20 years ago still persist while new ones continue to emerge, *Int. J. Food Microbiol*., 2010, 139, S3-S15.

[96] Schlundt, J. New directions in foodborne disease prevention, *Int. J. Food Microbiol*., 2002, 78, 3-17.

[97] Swaminathan, B; Barrett, TJ; Hunter, SB; Tauxe, RV. PulseNet: the molecular subtyping network for foodborne bacterial disease surveillance, United States; *Emerg. Infect. Dis.*, 2001, 7, 382.

[98] Rangel, JM; Sparling, PH; Crowe, C; Griffin, PM; Swerdlow, DL. Epidemiology of Escherichia coli O157: H7 outbreaks, United States, 1982-2002, *Emerg. Infect. Dis.*, 2005, 11, 603-609.

[99] Rai, MK; Deshmukh, SD; Ingle, AP; Gade, AK Silver nanoparticles: the powerful nanoweapon against multidrug-resistant bacteria, *J. Appl. Microbiol*., 2012, 112, 841-852.

[100] Velusamy, V; Arshak, K; Korostynska, O; Oliwa, K; Adley, C. An overview of foodborne pathogen detection: in the perspective of biosensors, *Biotech. Adv*., 2010, 28, 232-254.

[101] CDC In Morbidity and Mortality Weekly Report (MMWR); Center for Disease Control and Prevention: Atlanta, GA, 2013, Vol., 2014.

[102] Siegrist, M; Stampfli, N; Kastenholz, H; Keller, C. Perceived risks and perceived benefits of different nanotechnology foods and nanotechnology food packaging, *Appetite*, 2008, 51, 283-290.

[103] Kalpana, SR; Anshul, S; Rao, NH. Nanotechnology in food processing sector-An assessment of emerging trends, *J. Food Sci. Technol.*, 2013, 50, 831-841.

[104] Schierholz, JM; Yücel, N; Rump, AF; Beuth, J; Pulverer, G. Antiinfective and encrustation - inhibiting materials - myth and facts, *Int. J. Antimicrob. Agent*, 2002, 19, 511-516.

[105] Chau, C-F; Wu, S-H; Yen, G-C. The development of regulations for food nanotechnology, *Trends Food Sci. Tech.*, 2007, 18, 269-280.

[106] Mahalik, NP; Nambiar, AN. Trends in food packaging and manufacturing systems and technology; *Trends. Food. Sci. Tech*., 2010, 21, 117-128.

[107] Quintavalla, S; Vicini, L. Antimicrobial food packaging in meat industry, *Meat Sci*., 2002, 62, 373-380.

[108] Lazcka, O; Campo, F; Munoz, FX. Pathogen detection: a perspective of traditional methods and biosensors, *Biosensors and Bioelectronics*, 2007, 22, 1205-1217.

[109] Ge, B; Meng, J. Advanced Technologies for Pathogen and Toxin Detection in Foods: Current applications and Future Directions, *JALA*, 2009, 14, 235-241.

[110] Van Dorst, B; Mehta, J; Bekaert, K; Rouah-Martin, E; De Coen, W; Dubruel, P; Blust, R; Robbens, J. Recent advances in recognition elements of food and environmental biosensors: a review; Biosens., *Bioelectron*., 2010, 26, 1178-1194.

[111] Su, W; Lin, M; Lee, H; Cho, M; Choe, W-S; Lee, Y. Determination of endotoxin through an aptamer-based impedance biosensor, *Biosens. Bioelectron.*, 2012, 32, 32-36.

[112] Singh, S; Chaubey, A; Malhotra, B. D. Amperometric cholesterol biosensor based on immobilized cholesterol esterase and cholesterol oxidase on conducting polypyrrole films, *Anal. Chim. Acta*., 2004, 502, 229-234.

[113] Singh, A; Poshtiban, S; Evoy, S. Recent advances in bacteriophage based biosensors for food-borne pathogen detection, *Sensors*, 2013, 13, 1763-1786.

[114] Hughes, SI; Dasary, SSR; Singh, AK; Glenn, Z; Jamison, H; Ray, PC; Yu, H. Sensitive and selective detection of trivalent chromium using hyper Rayleigh scattering with 5, 5′-dithio-bis-(2-nitrobenzoic acid)-modified gold nanoparticles, *Sens. Actuat. B: Chem*., 2013, 178, 514-519.

[115] Ray, PC; Yu, H; Fu, PP. Nanogold-based sensing of environmental toxins: excitement and challenges, *J. Environ. Sci. Health C*, 2011, 29, 52-89.

[116] Fan, Z; Khan, SA; Dai, X; Tchounwou, C; Lu, Y; Ray, PC. Theranostic Nanoplatforms for MRSA Detection and Destruction from Whole Blood, *Part. Part. Sys. Character*., 2014, 31, 357-364.

[117] Singh, A; Poshtiban, S; Evoy, S. Recent advances in Bacteriophage based Biosensors for Food-borne Pathogen Detection, *Sensors*, 2012, 13, 1763-1786.

[118] Singh, R; Mukherjee, MD; Sumana, G; Gupta, RK; Sood, S; Malhotra, BD. Biosensors for pathogen detection: A smart approach towards clinical diagnosis, *Sensor. Actuat. B: Chem*., 2014, 197, 385-404.

[119] Lansdown, A; Williams, A; Chandler, S; Benfield, S. Silver absorption and antibacterial efficacy of silver dressings, *J. Wound Care*, 2005, 14, 155-60.

[120] Lansdown, ABG. A review of the use of silver in wound care: facts and fallacies, *Br. J. Nurs*., 2004, 13, S6-S19.

[121] Dowsett, C. The use of silver-based dressings in wound care, *Nurs. Stand*., 2004, 19, 56-60.

[122] Silvestry-Rodriguez, N; Sicairos-Ruelas, EE; Gerba, CP; Bright, KR. Silver as a disinfectant, *Rev. Environ. Contam. Toxicol*., 2007, 191, 23-45.

[123] Lea, MC. Allotropic forms of silver, *Am. J. Sci*., 1889, 37, 476-491.

[124] Height, MJ. In Presentation "Health Risk Assessment of Nanosilver" Workshop; Federal Institute for Risk Assessment (BfR): Berlin Marienfelde, 2011, Vol., 2014.

[125] Jain, J; Arora, S; Rajwade, JM; Omray, P; Khandelwal, S; Paknikar, KM. Silver nanoparticles in therapeutics: development of an antimicrobial gel formulation for topical use, *Mol. Pharm*., 2009, 6, 1388-1401.

[126] Seltenrich, N. Nanosilver: Weighing the Risks and Benefits; Environ. *Health Perspect*., 2013, 121, a220-225.

[127] ATSDR In Agency for toxic substances and disease registry, *ATSDR*, USA: Atlanta, GA, 1997, Vol., 2014.

[128] Nowack, B; Krug, HF; Height, M. 120 years of nanosilver history: implications for policy makers, *Environ. Sci. Technol*., 2011, 45, 1177-1183.

[129] Wijnhoven, SWP; Peijnenburg, WJGM; Herberts, CA; Hagens, WI; Oomen, AG; Heugens, EHW; Roszek, B; Bisschops, J; Gosens, I; Van De Meent, D; Dekkers, S; De Jong, WH; van Zijverden, M; Sips, AJAM; Geertsma, RE. Nanosilver: A review of available data and knowledge gaps in human and environmental risk assessment, *Nanotoxicology*, 2009, 3, 109-138.

[130] McShan, D; Ray, PC; Yu, H. Molecular toxicity mechanism of nanosilver, *J. Food. Drug. Anal*., 2014, 22, 116-127.

[131] Paladini, F; De Simone, S; Sannino, A; Pollini, M. Antibacterial and antifungal dressings obtained by photochemical deposition of silver nanoparticles, *J. Appl. Polym. Sci*., 2014, 131, Online Publication.

[132] Khaydarov, RR; Khaydarov, RA; Estrin, Y; Evgrafova, S; Scheper, T; Endres, C; Cho, S. In Nanomaterials: Risks and benefits; Springer, 2009.

[133] Lara, HH; Garza-Trevino, EN; Ixtepan-Turrent, L; Singh, DK. Silver nanoparticles are broad-spectrum bactericidal and virucidal compounds, *J. Nanobiotechnol*., 2011, 9, 30.
[134] Windler, L; Height, M; Nowack, B. Comparative evaluation of antimicrobials for textile applications, *Environ. Int.*, 2013, 53, 62-73.
[135] Zhang, F; Wu, X; Chen, Y; Lin, H. Application of silver nanoparticles to cotton fabric as an antibacterial textile finish, *Fiber. Polym*., 2009, 10, 496-501.
[136] Monteiro, DR; Gorup, LF; Silva, S; Negri, M; de Camargo, ER; Oliveira, R; Barbosa, DB; Henriques, M. Silver colloidal nanoparticles: antifungal effect against adhered cells and biofilms of Candida albicans and Candida glabrata, *Biofouling*, 2011, 27, 711-719.
[137] Choi, O; Yu, C-P; Esteban Fernández, G; Hu, Z. Interactions of nanosilver with Escherichia coli cells in planktonic and biofilm cultures, *Water Res*., 2010, 44, 6095-6103.
[138] Newsome, R. IFT International Food Nanoscience Conference: Proceedings, *Comp. Revs. Food Sci. Food Saf*., 2013, 13, 190-228.
[139] Costa, C; Conte, A; Buonocore, GG; Del Nobile, MA. Antimicrobial silver-montmorillonite nanoparticles to prolong the shelf life of fresh fruit salad, *Int. J. Food. Microbiol.*, 2011, 148, 164-167.
[140] Feng, QL; Wu, J; Chen, GQ; Cui, FZ; Kim, TN; Kim, JO. A mechanistic study of the antibacterial effect of silver ions on Escherichia coli and Staphylococcus aureus, *J. Biomed. Mater. Res*., 2000, 52, 662-668.
[141] Spacciapoli, P; Buxton, D; Rothstein, D; Friden, P. Antimicrobial activity of silver nitrate against periodontal pathogens, *J. Periodontal. Res*., 2001, 36, 108-113.
[142] Matsumura, Y; Yoshikata, K; Kunisaki, S-i; Tsuchido, T. Mode of bactericidal action of silver zeolite and its comparison with that of silver nitrate; *Appl. Environ. Microbiol*., 2003, 69, 4278-4281.
[143] Sondi, I; Salopek-Sondi, B. Silver nanoparticles as antimicrobial agent: a case study on E. coli as a model for Gram-negative bacteria, *J. Coll. Interf. Sci*., 2004, 275, 177-182.
[144] Pal, S; Tak, YK; Song, JM. Does the antibacterial activity of silver nanoparticles depend on the shape of the nanoparticle? A study of the gram-negative bacterium Escherichia coli, *Appl. Environ. Microbiol*., 2007, 73, 1712-1720.
[145] Butkus, MA; Labare, MP; Starke, JA; Moon, K; Talbot, M. Use of aqueous silver to enhance inactivation of coliphage MS-2 by UV disinfection, *Appl. Environ. Microbiol*., 2004, 70, 2848-2853.
[146] Yamanaka, M; Hara, K; Kudo, J. Bactericidal actions of a silver ion solution on Escherichia coli, studied by energy-filtering transmission electron microscopy and proteomic analysis, *Appl. Environ. Microb*., 2005, 71, 7589-7593.
[147] Shahverdi, AR; Fakhimi, A; Shahverdi, HR; Minaian, S. Synthesis and effect of silver nanoparticles on the antibacterial activity of different antibiotics against Staphylococcus aureus and Escherichia coli, *Nanomed. Nanotechnol.*, 2007, 3, 168-171.
[148] Gong, P; Li, H; He, X; Wang, K; Hu, J; Tan, W; Zhang, S; Yang, X. Preparation and antibacterial activity of Fe_3O_4@Ag nanoparticles, *Nanotechnology*, 2007, 18, 285604.
[149] Jia, J; Duan, Y-y; Wang, S-h; Zhang, S-f; Wang, Z-y. Preparation and Characterization of Antibacterial Silver-containing Nanofibers for Wound Dressing Applications, *J. US China Med. Sci. (美中医学)*, 2007, 4, 52-54.

[150] Maneerung, T; Tokura, S; Rujiravanit, R. Impregnation of silver nanoparticles into bacterial cellulose for antimicrobial wound dressing, *Carbohyd. Polym*., 2008, 72, 43-51.

[151] Ingle, A; Gade, A; Pierrat, S; Sonnichsen, C; Rai, M. Mycosynthesis of silver nanoparticles using the fungus Fusarium acuminatum and its activity against some human pathogenic bacteria, *Curr. Nanosci*., 2008, 4, 141-144.

[152] Geethalakshmi, R; Sarada, DVL. Synthesis of Plant-mediated Silver nanoparticles using Trianthema decandra Extract and Evaluation of their Anti microbial activities, *Int. J. Eng. Sci. Technol*., 2010, 2, 970-975.

[153] Bonde, SR; Rathod, DP; Ingle, AP; Ade, RB; Gade, AK; Rai, MK. Murraya koenigii-mediated synthesis of silver nanoparticles and its activity against three human pathogenic bacteria, *Nanosci. Meth*., 2011, 1, 25-36.

[154] Govindaraju, K; Tamilselvan, S; Kiruthiga, V; Singaravelu, G. Biogenic silver nanoparticles by Solanum torvum and their promising antimicrobial activity, *J. Biopest*., 2010, 3, 394-399.

[155] Namasivayam, S; Chitrakala, K. Ecotoxicological effect of Lecanicillium lecanii (Ascomycota: Hypocreales) based silver nanoparticles on growth parameters of economically important plants, *J. Biopest*., 2011, 4, 97-101.

[156] Nam, K-Y. In vitro antimicrobial effect of the tissue conditioner containing silver nanoparticles, *J. Adv. Prosthodont*., 2011, 3, 20-24.

[157] EI-Badawy, A; Feldhake, D; Venkatapathy, R. "State of the Science Literature Review: Everything Nanosilver and More," Environmental Protection Agency, Office of Research and Development, 2010.

[158] Rai, M; Yadav, A; Gade, A. Silver nanoparticles as a new generation of antimicrobials, *Biotech. Adv*., 2009, 27, 76-83.

[159] Shrivastava, S; Bera, T; Roy, A; Singh, G; Ramachandrarao, P; Dash, D. Characterization of enhanced antibacterial effects of novel silver nanoparticles, *Nanotechnology*, 2007, 18, 225103.

[160] Liang, Z; Das, A; Hu, Z. Bacterial response to a shock load of nanosilver in an activated sludge treatment system, *Water Res.*, 2010, 44, 5432-5438.

[161] Likus, W; Bajor, G; Siemianowicz, K. Nanosilver - does it have only one face?, *Acta Biochim. Pol.*, 2013, 60, 495.

[162] Rizzello, L; Pompa, PP. Nanosilver-based antibacterial drugs and devices: Mechanisms, methodological drawbacks, and guidelines, *Chem. Soc. Rev.*, 2014, 43, 1501-1518.

[163] Kim, SW; Kim, KS; Lamsal, K; Kim, Y-J; Kim, SB; Jung, M; Sim, S-J; Kim, H-S; Chang, S-J; Kim, JK; Lee, YS. An in vitro study of the antifungal Effect of Silver Nanoparticles on oak Wilt Pathogen Raffaelea sp, *J. Microbiol. Biotechnol*., 2009, 19, 760-764.

[164] Kim, K-J; Sung, W. S; Moon, S-K; Choi, J-S; Kim, J. G; Lee, D. G. Antifungal effect of silver nanoparticles on dermatophytes, *J. Microbiol. Biotechnol*., 2008, 18, 1482-4.

[165] Panacek, A; Kolar, M; Vecerova, R; Prucek, R; Soukupov, J; Krystof, V; Hamal, P; Zboril, R; Kvítek, L. Antifungal activity of silver nanoparticles against Candida spp, *Biomaterials*, 2009, 30, 6333-6340.

[166] Choi, O; Deng, KK; Kim, N-J; Ross Jr, L; Surampalli, RY; Hu, Z. The inhibitory effects of silver nanoparticles, silver ions, and silver chloride colloids on microbial growth, *Water Res*, 2008, 42, 3066-3074.

[167] Prucek, R; Tucek, J; Kilianova, M; Panacek, A; Kvitek, L; Filip, J; Kolar, M; Tomankova, K; Zboril, R. The targeted antibacterial and antifungal properties of magnetic nanocomposite of iron oxide and silver nanoparticles, *Biomaterials*, 2011, 32, 4704-4713.

[168] Jo, Y-K; Kim, BH; Jung, G. Antifungal activity of silver ions and nanoparticles on phytopathogenic fungi, *Plant Disease*, 2009, 93, 1037-1043.

[169] Nair, LS; Laurencin, CT. Silver nanoparticles: synthesis and therapeutic applications, *J. Biomed. Nanotechnol*., 2007, 3, 301-316.

[170] Nasrollahi, A; Pourshamsian, KH; Mansourkiaee, P. Antifungal activity of silver nanoparticles on some of fungi, *Int. J. Nano. Dimension*, 2011, 1, 233-239.

[171] Nadworny, PL; Wang, J; Tredget, EE; Burrell, RE. Anti-inflammatory activity of nanocrystalline silver in a porcine contact dermatitis model, *Nanomed. Nanotechnol.*, 2008, 4, 241-251.

[172] Elechiguerra, JL; Burt, JL; Morones, JR; Camacho-Bragado, A; Gao, X; Lara, HH; Yacaman, MJ. Interaction of silver nanoparticles with HIV-1, *J. Nanobiotechnol*., 2005, 3, 1-10.

[173] Marimuthu, S; Rahuman, AA; Rajakumar, G; Santhoshkumar, T; Kirthi, AV; Jayaseelan, C; Bagavan, A; Zahir, AA; Elango, G; Kamaraj, C. Evaluation of green synthesized silver nanoparticles against parasites, *Parasitol. Res*., 2011, 108, 1541-1549.

[174] Yoon, K-Y; Hoon Byeon, J; Park, J-H; Hwang, J. Susceptibility constants of Escherichia coli and Bacillus subtilis to silver and copper nanoparticles, *Sci. Tot. Environ*., 2007, 373, 572-575.

[175] Sadhasivam, S; Shanmugam, P; Yun, KS. Biosynthesis of silver nanoparticles by Streptomyces hygroscopicus and antimicrobial activity against medically important pathogenic microorganisms, *Coll. Surf. B: Biointerf*., 2010, 81, 358-362.

[176] Nanda, A; Saravanan, M. Biosynthesis of silver nanoparticles from Staphylococcus aureus and its antimicrobial activity against MRSA and MRSE, *Nanomed. Nanotechnol.*, 2009, 5, 452-456.

[177] Jo, Y-K; Kim, BH; Jung, G. Antifungal activity of silver ions and nanoparticles on phytopathogenic fungi, *Plant Dis*., 2009, 93, 1037-1043.

[178] Persing, T. A Multipronged Approach to Vancomycin-Resistant Enterococcus Control in an Acute-Care Setting, *AJIC*, 2004, 32, E19-E20.

[179] Kon, K. Coping with antibiotic resistance: combining nanoparticles with antibiotics and other antimicrobial agents, *Expert Rev. Anti Infect. Ther*., 2011, 9, 1035-1052.

[180] Kathiresan, K; Alikunhi, NM; Pathmanaban, S; Nabikhan, A; Kandasamy, S. Analysis of antimicrobial silver nanoparticles synthesized by coastal strains of Escherichia coli and Aspergillus niger, *Can. J. Microbiol.*, 2010, 56, 1050-1059.

[181] Dehkordi, SH; Hosseinpour, F; Kahrizangi, AE. An in vitro evaluation of antibacterial effect of silver nanoparticles on Staphylococcus aureus isolated from bovine subclinical mastitis, *Afr. J. Biotechnol*., 2011, 10, 10795-10797.

[182] Cui, L; Chen, P; Chen, S; Yuan, Z; Yu, C; Ren, B; Zhang, K. In Situ Study of the Antibacterial Activity and Mechanism of Action of Silver Nanoparticles by Surface-Enhanced Raman Spectroscopy, *Anal. Chem*., 2013, 85, 5436-5443.

[183] Hsin, Y-H; Chen, C-F; Huang, S; Shih, T-S; Lai, P-S; Chueh, P. J. The apoptotic effect of nanosilver is mediated by a ROS-and JNK-dependent mechanism involving the mitochondrial pathway in NIH3T3 cells, *Toxicol. Lett*., 2008, 179, 130-139.

[184] Ivask, A; ElBadawy, A; Kaweeteerawat, C; Boren, D; Fischer, H; Ji, Z; Chang, CH; Liu, R; Tolaymat, T; Telesca, D. Toxicity Mechanisms in Escherichia coli Vary for Silver Nanoparticles and Differ From Ionic Silver, *ACS nano*, 2014, 8, 374–386.

[185] Lansdown, ABG; Silver, I. its antibacterial properties and mechanism of action, *J. Wound Care*, 2002, 11, 125-131.

[186] Li, W-R; Xie, X-B; Shi, Q-S; Zeng, H-Y; You-Sheng, O-Y; Chen, Y-B. Antibacterial activity and mechanism of silver nanoparticles on Escherichia coli, *Appl. Microbiol. Biotech*., 2010, 85, 1115-1122.

[187] Prabhu, S; Poulose, EK. Silver nanoparticles: mechanism of antimicrobial action, synthesis, medical applications, and toxicity effects, *Int. Nano Lett*., 2012, 2, 1-10.

[188] Lu, W; Senapati, D; Wang, S; Tovmachenko, O; Singh, AK; Yu, H; Ray, PC. Effect of surface coating on the toxicity of silver nanomaterials on human skin keratinocytes, *Chem. Phys. Lett*., 2010, 487, 92-96.

[189] Lok, C-N; Ho, C-M; Chen, R; He, Q-Y; Yu, W-Y; Sun, H; Tam, PK-H; Chiu, J-F; Che, C-M. Proteomic analysis of the mode of antibacterial action of silver nanoparticles, *J. Proteome Res*., 2006, 5, 916-924.

[190] Xiu, Z-M; Zhang, Q-B; Puppala, HL; Colvin, VL; Alvarez, PJJ. Negligible particle-specific antibacterial activity of silver nanoparticles, *NanoLett*., 2012, 12, 4271-4275.

[191] Guzman, M; Dille, J; Godet, S. Synthesis and antibacterial activity of silver nanoparticles against gram-positive and gram-negative bacteria, *Nanomed. Nanotech. Biol. Med*, 2012, 8, 37-45.

[192] Bondarenko, O; Ivask, A; Käkinen, A; Kurvet, I; Kahru, A. Particle-cell contact enhances antibacterial activity of silver nanoparticles, *PloS One*, 2013, 8, e64060.

[193] Sinha, R; Karan, R; Sinha, A; Khare, SK. Interaction and nanotoxic effect of ZnO and Ag nanoparticles on mesophilic and halophilic bacterial cells, *Bioresource. Technol*., 2011, 102, 1516-1520.

[194] Khan, SS; Mukherjee, A; Chandrasekaran, N. Studies on interaction of colloidal silver nanoparticles (SNPs) with five different bacterial species, *Colloids Surf. B*, 2011, 87, 129-138.

[195] Sedlak, RH; Hnilova, M; Grosh, C; Fong, H; Baneyx, F; Schwartz, D; Sarikaya, M; Tamerler, C; Traxler, B. Engineered Escherichia coli silver-binding periplasmic protein that promotes silver tolerance; *Appl. Environ. Microbiol*., 2012, 78, 2289-2296.

[196] Lee, H-H; Chou, K-S; Huang, K-C. Inkjet printing of nanosized silver colloids, *Nanotechnology*, 2005, 16, 2436.

[197] Samberg, ME; Orndorff, PE; Monteiro-Riviere, NA. Antibacterial efficacy of silver nanoparticles of different sizes, surface conditions and synthesis methods, *Nanotoxicology*, 2011, 5, 244-253.

[198] Wong, KKY; Liu, X. Silver nanoparticles - The real "silver bullet" in clinical medicine?, *Med. Chem. Commun*., 2010, 1, 125-131.

[199] El Badawy, AM; Scheckel, KG; Suidan, M; Tolaymat, T. The impact of stabilization mechanism on the aggregation kinetics of silver nanoparticles, *Sci. Total. Environ.*, 2012, 429, 325-331.

[200] Verma, A; Stellacci, F. Effect of Surface Properties on Nanoparticle–Cell Interactions; Small, 2009, 6, 12-21.

[201] Badawy, AME; Silva, RG; Morris, B; Scheckel, KG; Suidan, MT; Tolaymat, TM. Surface charge-dependent toxicity of silver nanoparticles, *Environ. Sci. Technol*., 2013, 45, 283-287.

[202] Jang, J; Oh, JH. Facile Fabrication of Photochromic Dye- Conducting Polymer Core-Shell Nanomaterials and Their Photoluminescence, *Adv. Mater.*, 2003, 15, 977-980.

[203] Kang, S; Mauter, MS; Elimelech, M. Physicochemical determinants of multiwalled carbon nanotube bacterial cytotoxicity; *Environ. Sci. Technol*., 2008, 42, 7528-7534.

[204] Kang, S; Mauter, MS; Elimelech, M. Microbial cytotoxicity of carbon-based nanomaterials: implications for river water and wastewater effluent, *Environ. Sci. Technol*., 2009, 43, 2648-2653.

[205] Boxall, ABA; Tiede, K; Chaudhry, Q. Engineered nanomaterials in soils and water: how do they behave and could they pose a risk to human health?, *Nanomed*., 2007, 2, 919-927.

[206] Park, HJ; Kim, JY; Kim, J; Lee, JH; Hahn, JS; Gu, MB; Yoon, J. Silver-ion-mediated reactive oxygen species generation affecting bactericidal activity, *Water Res.*, 2008, 43, 1027-1032.

[207] Devi, LS; Joshi, S. Antimicrobial and synergistic effects of silver nanoparticles synthesized using soil fungi of high altitudes of eastern Himalaya, *Mycobiology*, 2012, 40, 27-34.

[208] Chen, JC; Lin, ZH; Ma, XX. Evidence of the production of silver nanoparticles via pretreatment of Phoma sp. 3.2883 with silver nitrate, *Lett. Appl. Microbiol.*, 2003, 37, 105-108.

[209] Muhsin, TM; Hachim, AK. Mycosynthesis and characterization of silver nanoparticles and their activity against some human pathogenic bacteria, *World J. Microb. Biotechnol*., 2014, [Epub ahead of print], 1-10.

[210] Kasten, B; Reski, R. b-Lactam antibiotics inhibit chloroplast division in a moss Physcomitrella patens but not in tomato Lycopersicon esculentum, *J. Plant. Physiol*., 1997, 150, 137-140.

In: Food Poisoning
Editor: Paresh C. Ray
ISBN: 978-1-63463-166-2

Chapter 3

LASER-INDUCED BREAKDOWN SPECTROSCOPY (LIBS) AS A POTENTIAL TOOL FOR FOOD SAFETY

Rosalie A. Multari* *and David A. Cremers*
Applied Research Associates, Incorporated, Albuquerque, New Mexico, US

ABSTRACT

Laser-Induced Breakdown Spectroscopy (LIBS) is a chemical analysis technique in which a laser pulse is focused onto a sample surface to generate a high density electric field resulting in a micro-plasma or "spark". The light emissions from the spark are collected and analyzed to determine sample composition or for the identification of complex materials. Advantages of a LIBS analysis are that results are provided rapidly (seconds to minutes) and often there is little or no sample preparation. For many years, LIBS was used purely as an elemental analysis technique. However, with the advent of advanced computing that has allowed application of more complex mathematical analysis to LIBS spectra, LIBS is being used for more complex chemical and biological analysis. In this chapter, the potential of LIBS as a tool for food safety applications will be explored through a review of published works.

INTRODUCTION

Laser-Induced Breakdown Spectroscopy (LIBS) is an analysis technique in which a laser pulse is focused onto a sample surface to generate a high density electric field resulting in a micro-plasma or "spark". This micro-plasma contains material from the sample surface and the atmosphere surrounding the sample that has been vaporized with the resulting atoms excited to emit light by the high plasma temperature (8000 K). The light emissions are subsequently collected and analyzed to determine the sample composition. LIBS is a form of atomic emission spectroscopy (AES). In the 1860's the first use of AES to determine elemental composition was demonstrated by introducing a sample into a flame and observing the resulting color changes. [1] With the advent of lasers in the 1960's the flame was replaced

* Corresponding author: E-Mail: rmultari@ara.com.

by a laser generated plasma produced by focusing powerful laser pulses onto the sample surface. Over the next 50 years, LIBS has been investigated and found to be useful across a wide variety of fields including, but not limited to, coal analysis; sorting of metals and plastics; cultural heritage studies; detection of toxic metals in liquids; explosive, biological, and chemical detection; rock & soil analysis; aerosol, water, and soil analysis; and detection of trace elements in fresh vegetables and food powders. [2,3] Each year hundreds of LIBS articles are published relating to various applications. There is even a LIBS instrument (ChemCam) currently deployed on the Mars rover Curiosity. [4]

LIBS is an attractive analytical technique because there is typically little to no sample preparation, data are collected in seconds and, with automated analysis, results can be available to the user of a LIBS-based instrument in seconds to minutes. LIBS instruments can be designed not only for laboratory use but made portable for field use or built into manufacturing facilities as needed. General LIBS instruments developed for elemental analysis are commercially available. In recent years, investigations into possible uses for LIBS have been expanded to the analysis of biological and chemical materials through the application of advanced mathematical modeling of the spectral data. Morel et al. demonstrated that LIBS could detect and sort six bacteria species and two pollens in pellet form. [5] Guyron et al. studied the differences in LIBS bacterial spectra. [6] Rehse et al. and Diedrich et al. have shown that both pathogenic and nonpathogenic *Escherichia coli* (*E. coli*) cultured strains grown in both nutrient-rich and nutrient-free media can be differentiated. [7–9] Gottfried et al. and Snyder et al. have shown that LIBS can be used to differentiate biological warfare simulants in a defined sample set. [10] The first blind study demonstrating that LIBS could be used to differentiate species and strains of live bacteria was done by Multari, et al. [11] Multari et al. were also the first to demonstrate that LIBS could be used to differentiate viruses. [12] Investigations continue to better understand the biological and chemical detection capabilities of LIBS when the LIBS spectrum is analyzed with advanced mathematical techniques as opposed to traditional elemental analysis methods. Recently, a number of investigations have been made into the use of LIBS for food safety applications. [13-18] Each of these investigations examined different food safety applications and a review of these will aid in a better understanding of the potential use of LIBS as a tool for ensuring food safety.

THE LIBS APPARATUS

The primary components of a LIBS apparatus include a pulsed laser, an optical assembly for focusing laser pulses onto the sample, a sample holder capable of translation (for measurements in which a fresh interrogation spot is desired for each measurement), a method of collecting the light emitted from the laser spark, a spectrometer, detector, and a computer for equipment control and data analysis. A typical LIBS apparatus is shown in Figure 1. Often, the detector is time gated to only record emissions from the laser plasma at a certain period after initiation. Depending on the complexity of the LIBS apparatus, a LIBS data collection system can cost as little $25,000 or as much as a hundred thousand dollars. Typical laser energies used for LIBS analysis range from a few mJ to hundreds of mJ. The spectrometer wavelength range used for analysis typically extends from 200 nm in the

ultraviolet spectral region to 1000 nm in the near infra-red region. The optical components chosen for focusing the laser pulses onto the sample are customized for an application and the laser path, focusing optics, and timing parameters are chosen to produce the best possible spectrum as defined by the intensity of the spectrum without introducing saturation of emission lines. Care must also be taken to ensure that the spark does not ablate completely through the sample to the underlying sample holder.

SAMPLE PREPARATION

Depending on the investigation, sample preparation for LIBS can be simple or complex. Martelli et al. [13] investigated the analysis of common wheat grains of different kernel sizes by first selecting grains according to their thickness as measured with a caliper, then conditioning them at constant humidity using a saturated solution for at least a week prior to the LIBS measurements. To investigate wheat tissues, tissues were selected by hand according to the radial grain orientation. A scalpel was used to separate tissues as desired for the planned investigations and samples were dried between microscope slides. The moisture content was adjusted using a constant relative humidity and a saturated solution. Figure 2 shows examples of LIBS spectra collected from these samples. Barnett et al. [14] investigated the detection of *Salmonella enterica* serovar from foods by analyzing pellets made from purchased bacterial strains which were first grown on an agar plate. Individual bacteria colonies were harvested from the agar plate and then placed in brain heart infusion growth media (BHI) and incubated for 16 hours. Serial dilutions of the grown bacteria were then made using milk or chicken broth to obtain different concentrations of contamination. Samples were then centrifuged three times with the supernatant being discarded after each centrifuge step. The cells were washed between centrifuge steps by immersion in phosphate buffered saline (PBS) to remove media debris. Before being applied to a Si substrate, the cells were re-suspended in PBS and mixed to ensure even cell distribution. The Si substrate was washed, the cells in PBS were applied and then the samples were subsequently dried prior to LIBS analysis. Kim et al. [15] investigated pesticides in spinach and rice by powdering the leaves of these materials. The samples were first dried and then ground. The ground samples were subsequently filtered to achieve similar particle sizes and these were pelletized. To create pesticide contaminated samples, the pesticide was mixed in the powders prior to making the pellets. In contrast, although Multari et al. [16] also started from individual bacterial colonies and incubated as in previous works, the grown samples bacterial were subsequently diluted in de-ionized water and applied directly to food and food processing surfaces for LIBS measurements. No drying step was used and data were collected over sample surfaces that included a plastic cutting board, a metal drain strainer, eggshell, raw chicken, bologna, and ground beef. For liquid milk, the bacterial contamination was mixed into the milk and the milk was applied directly to an agar plate for data collection. To investigate pesticides and dioxins in tissue fats and rendered oils, Multari et al. [17]used samples consisting of pesticides diluted into hexane and subsequently mixed into tissue fats and rendered oils which were then applied directly to filter paper for analysis without drying. To investigate pesticides on apples, Ma et al. [18] applied pesticide dilutions in deionized water directly to the surfaces of pieces of apples. The apple samples were air dried for a

period of time prior to LIBS analysis. As can be seen from these examples, sample preparation can be either complex or simple depending on the food and the type of the investigation.

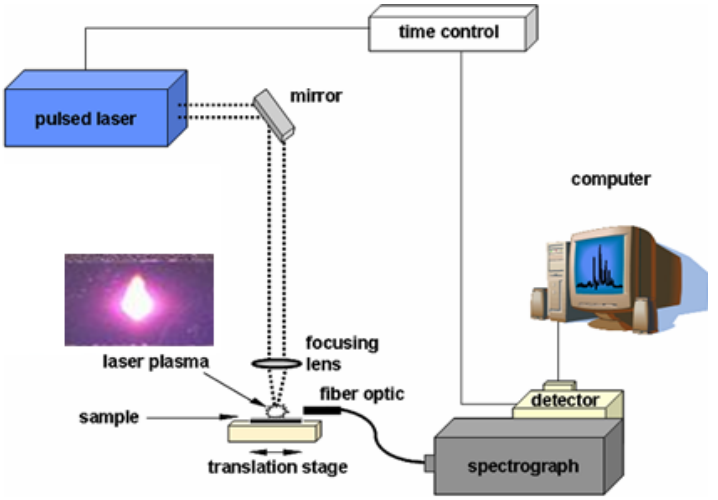

Figure 1. Typical equipment set-up for LIBS data collection and analysis. Insert is a photo of a laser spark on plastic.

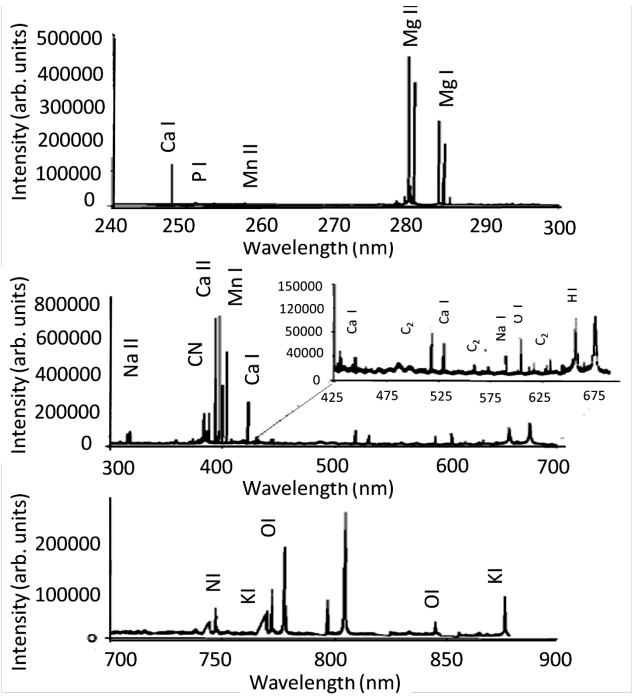

Figure 2. LIBS spectra obtained from wheat grains. A Nd:YAG laser was used to generate the laser pulses and data collection occurred 500 ns after spark generation. The results from ten successive. pulses were averaged to generate the LIBS spectra shown. Reprinted with permission (J. Agric. Food Chem., 2010, 58(12), pp. 7126–7134). Copyright 2010 American Chemical Society.

Because LIBS analysis is dependent on the emission spectrum which is a function of the coupling of the laser pulse energy with the sample and atmosphere surrounding the sample, sample preparation plays a key role in obtaining useful results. Results for an investigation are heavily dependent on the method chosen for sample preparation and care must be taken not to inadvertently introduce contaminations that may lead to erroneous results.

DATA ANALYSIS AND RESULTS

Once the spectral data have been collected, these must be analyzed for signals that can be correlated to the detection targets. For many years LIBS analysis was based entirely on elemental signatures as represented by individual emission peaks in the spectrum. For biological and complex chemical detection, more complicated mathematical analysis of the spectrum combined with statistical methods are often needed. Many different approaches have been taken to accomplish this.

Martelli et al. [13] pretreated collected spectra, prior to analysis, by baseline correcting and normalizing the spectral intensities to the C_2 Swan molecular band (516.52 nm) to compensate for any experimental fluctuations. The goal of the study was to drill into the sample to discriminate between wheat tissue layers (not to quantify elemental content) so this normalization was appropriate. Moving Window Two-Dimensional (MW2D) Correlation [19] was applied to a matrix consisting of the collected spectra arranged in pulse order. The spectral intensities from each individual spectrum were mean centered. The matrix was divided into subsets of data by a moving window of arbitrary fixed width. For a data subset, the autocorrelation was calculated and then plotted as a function of the local average value of the perturbation within the window. Window size was varied and the size yielding the lowest noise and highest peak resolution was chosen as the width for the new window. The window was moved and this process was repeated until all spectra were included in the analysis. 2D maps were then generated by plotting the autocorrelation intensities as a function of the window. Peaks could be observed in the 2D plot at the number of pulses where the largest spectral variations were found. By analyzing individual lines and tying these variations to changes in tissue layer, an understanding of the depth and chemistry of the tissue layers was obtained. As can be seen from Figure 3, Ca is found in the initial layers of the sample corresponding to pulses 1-40 and greater than 100 pulses whereas Mg is present for all pulse measurements. Next, Matlab 7.0[20] was used to perform Partial Least Squares - Discriminant Analysis (PLS-DA) on the data. [21] Results were validated by both calibration set cross-validation and external validation using a test set. It was found that it was possible to predict the wheat tissue layers that had been successfully modeled using PLS-DA. This work demonstrated the usefulness of LIBS for investigating wheat grain structure.

Barnett et al. [14] investigated *S. enterica* serovar *Typhimurium* concentrations in BHI, chicken broth, and milk using discriminate functional analysis (DFA) on selected emission lines. In this study, a number of elements known to provide identification and differentiation of bacteria based on relative intensities were selected to include in the analysis. A Gaussian curve was used to fit the emission line profile and determine the area under the curve which was used as the emission intensity. The data were then mean centered and normalized. DFA was then performed on the mean-centered normalized intensities of the selected emission

lines using SPSS 16 software [22]. From the analysis (Figure 3, reference 14), it is clear that *S. enterica* serovar *Typhimurium* in BHI can be distinguished from BHI.

Multari et al. [16] investigated detection of *S. enterica* and *E.coli* over a range of concentrations in a variety of foods (including milk) using multivariate regression applied to the entire LIBS spectrum and found bacteria could be differentiated over a much wider range of concentrations and to lower levels ($<10^3$ cells/mL) than that demonstrated using the analysis methods of Barnett et al. [14] To accomplish this, no wavelength regions were pre-selected and the entire spectrum was treated as a single variable set for which the x coordinates corresponded to the wavelength and the y coordinates to the intensity. Partial least square regression over the entire data set was performed to create differentiation models using the Unscrambler 9.7. [23] Spectral normalization such that the maximum peak intensity was set to unity was applied to all spectra prior to this analysis. Using this method, differentiation of *E.coli* and *Salmonella* (both live and dead) on plastic and metal food processing surfaces was demonstrated. Differentiation was also demonstrated for *Salmonella* in milk, raw chicken, eggshell, and swabs of eggshell surfaces and for *E.coli* on bologna, ground beef, eggshell and swabs of eggshell surfaces. In this work, the ability to differentiate live bacteria from dead bacteria was also demonstrated. Examples of prediction values obtained from test spectra input into various models are shown in Figure 4.

By employing the same methods of data analysis used to differentiate bacteria, Multari et al. [17] successfully demonstrated the differentiation of samples contaminated with pesticides and dioxins to low levels of contamination. In this study, tissue fat and rendering oil samples were contaminated with aldrin, 1,2,3,4,6,7,8-heptachlorodibenzo-p-dioxin, chlorpyrifos, and dieldrin for concentrations of 0.005 to 0.1 μg/g. In addition, the ability to build detection algorithms using individual differentiation models as building blocks for the overall detection capability was also demonstrated. An example of the algorithm flow for differentiating pesticides and dioxin in rendered oil deposited on filter paper is shown in Figure 5.

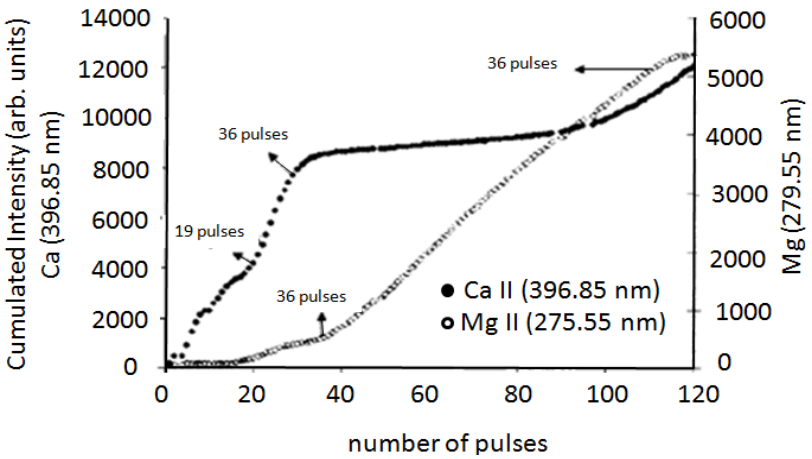

Figure 3. Cumulated intensities for Ca II (396.85 nm) and Mg II (279.55 nm) calculated from baseline corrected and normalized spectra during wheat ablation. Reprinted with permission (J. Agric. Food Chem., 2010, 58, (12), pp. 7126–7134). Copyright 2010 American Chemical Society.

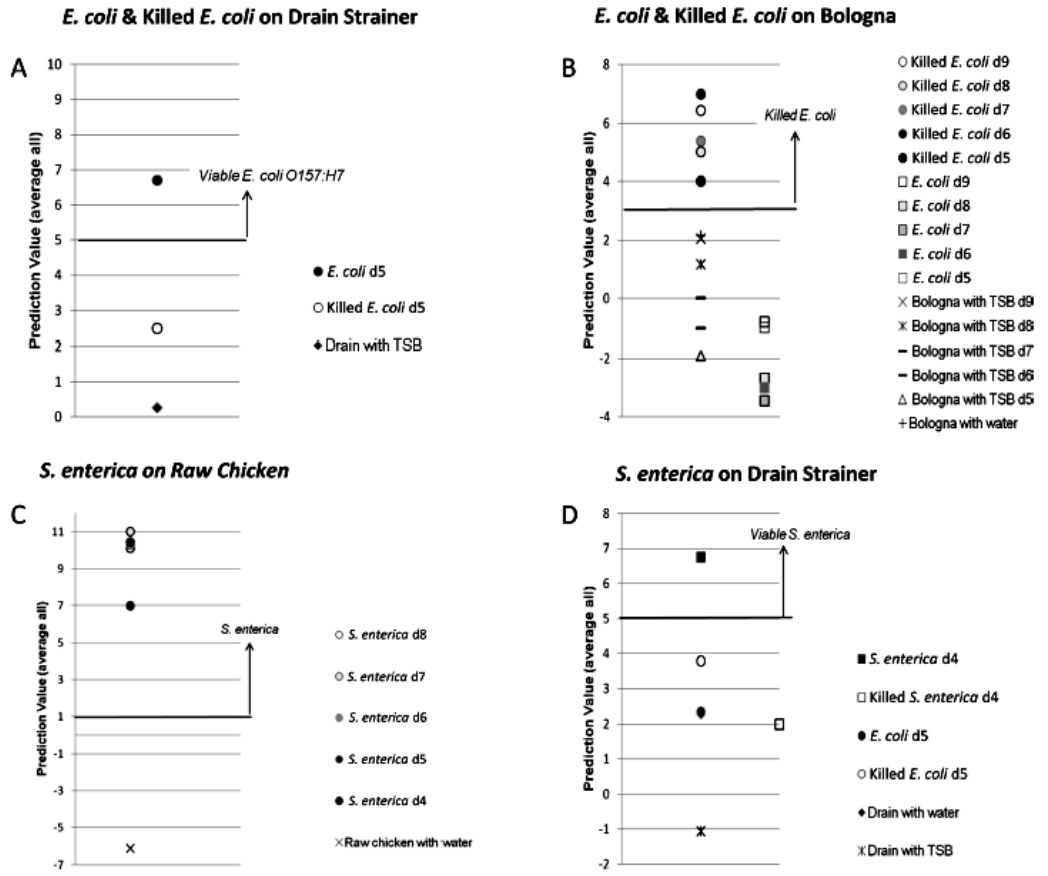

Figure 4. Prediction values obtained from test spectra for models designed to differentiate A) live from killed *E. coli* and a control on a metal drain strainer; B) killed *E. coli* dilutions from live *E. coli* dilutions and control dilutions on bologna, C) live *Salmonella* on raw chicken; and D) live *Salmonella* from dead *Salmonella*, live and dead *E. coli* and a control (Triptic soy broth, TSB) on a metal drain strainer. Reprinted with permission (J. Agric. Food Chem., 2013, 61 (36), pp 8687–8694). Copyright 2013 American Chemical Society.

Kim et al. [15] investigated the use of PLS-DA for the detection of pesticides in spinach and rice samples. In this work, key elements associated with the pesticides and the samples were identified and PLS-DA was performed on the spectral regions corresponding to emissions from these elements. From the score plots in the analysis, clean spinach could be differentiated from spinach spiked with parathion to 10 ppm; clean spinach could be differentiated from spinach spiked with forsetyl-aluminum; and clean rice could be differentiated from rice spiked with parathion (Figure 6).

Ma et al. [18] investigated the detection of pesticides on apples by identifying spectral emissions correlated with the presence of the pesticide and then performing principal component analysis (PCA) only on the spectral regions corresponding to these emissions. The Unscramber 9.7[23] was used to perform the PCA analysis and it was found that apples contaminated with chlorpyrifos could be differentiated from uncontaminated apples.

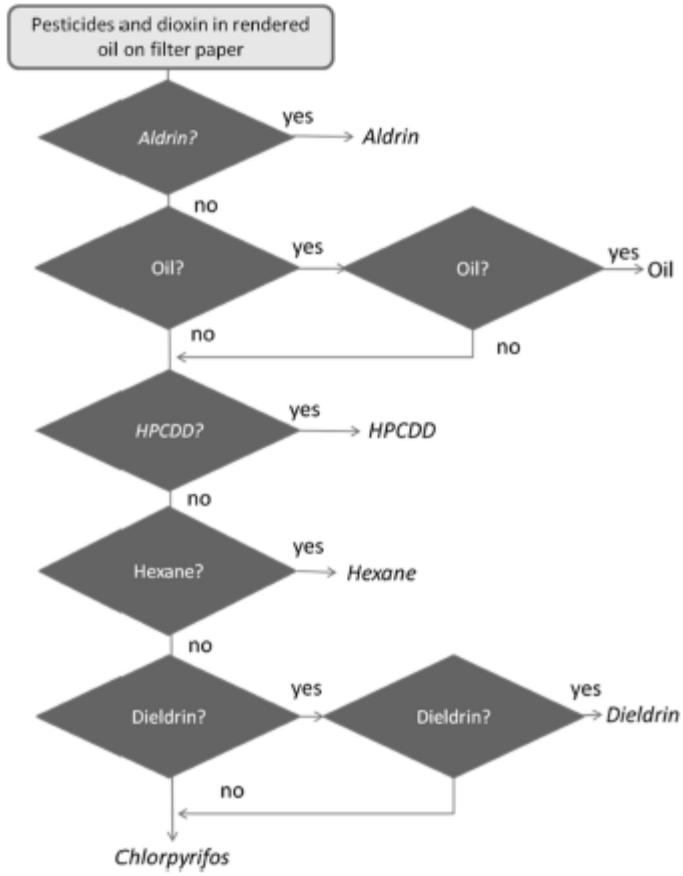

Figure 5. Algorithm flow for differentiating pesticides and dioxin in rendered oil on filter paper. Reprinted with permission (J. Agric. Food Chem., 2013, 61 (10), pp 2348 –2357). Copyright 2013 American Chemical Society.

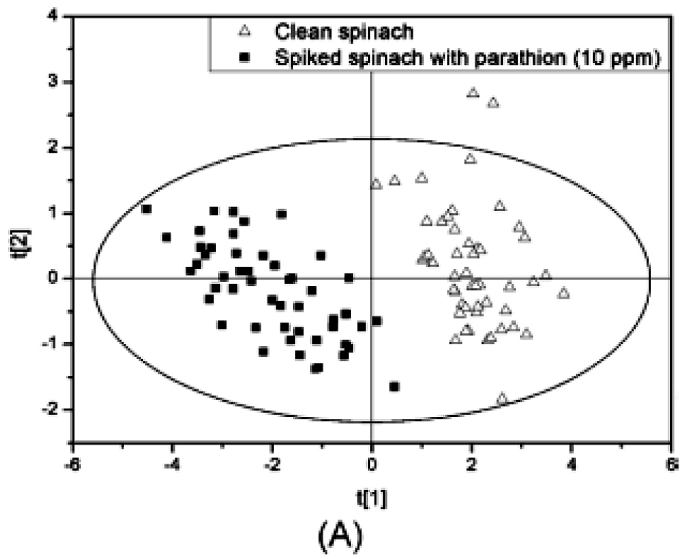

(A)

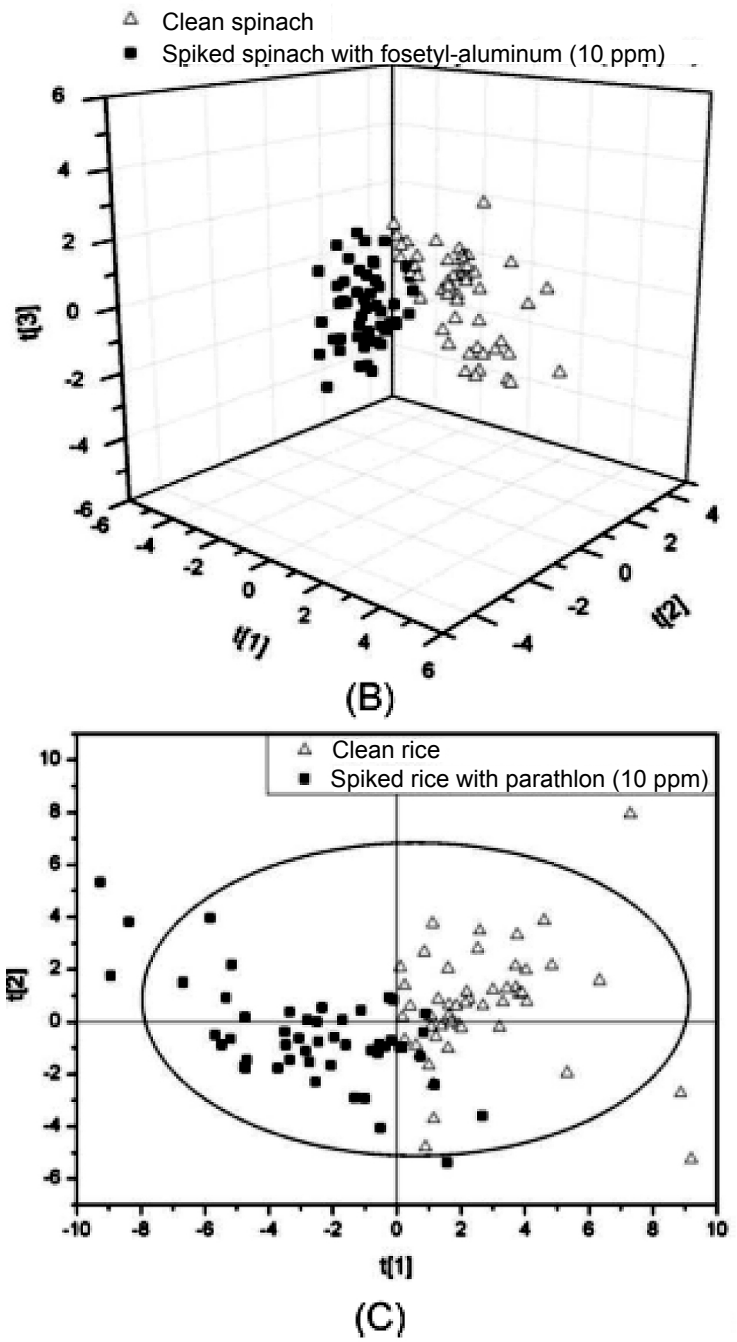

Figure 6. PLS-DA score plots for differentiating A) clean spinach from spinach spiked with parathion, B) clean spinach from spinach spiked with forsetyl-aluminum, and C) clean rice from rice spiked with parathion. Reprinted with permission (J. Agric. Food Chem., 2012, 60 (3), pp 718–724). Copyright 2012 American Chemical Society.

CONCLUSION

The use of LIBS as a diagnostic tool for certain food safety applications appears promising based on these initial studies. All studies to date have been carried out under controlled laboratory conditions using carefully prepared laboratory samples. To truly become useful as a food safety diagnostic, detection must be accomplished in the presence of unknown and varying background species in the uncontrolled environment of the "real world". To accomplish this, more investigation is needed into the robustness of the methods being used for data collection and analysis and "best" methods must be identified and further developed. If successfully developed, the use of LIBS for food safety would allow for near real-time detection of both chemical and bacterial contaminations thereby enhancing food safety.

REFERENCES

[1] Kirchhoff, G; Bunsen, R. Chemical analysis by observation of spectra, *Ann. Phys. Chem.*, 1860, 110, 161−189.

[2] Cremers, DA; Radziemski, LJ., *Handbook of Laser-Induced Breakdown Spectroscop*y 2nd ed., John Wiley, and Sons: Chichester, U.K., 2013.

[3] Musazzi, S; Perini, U. (Editors), *Laser-Induced Breakdown Spectroscopy: Theory, and Applications (Springer Series in Optical Sciences)*, Springer, U.S., 2014.

[4] Wiens, RC; et al. The ChemCam Instrument Suite on the Mars Science Laboratory (MSL) Rover: Body Unit, and Combined System Tests, *Space Sci. Rev.*, 2012, 170, 167-227.

[5] Morel, S; Leone, N; Adam, P; Amouroux, J. Detection of bacteria by time resolved laser-induced breakdown spectroscopy, *Appl. Opt*, 2003, 42, 6184-6191.

[6] Guyon, L; Baudelet, M; Amodeo, T; Fréjafon, E; Laloi, P; Yu, J; Wolf, JP. Laser-Induced Breakdown Spectroscopy analysis of Bacteria: What Femtosecond Lasers Make Possible, *International Conference on Ultrafast Phenomena* (UP) MH10 2006.

[7] Rehse, SJ; Diedrich, J; Palchaudhuri, S. Identification and discrimination of Pseudomonas aeruginosa bacteria grown in blood and bile by laser-induced breakdown spectroscopy, *Spectrochim. Acta*, 2007, Part B 62, 1169-1176.

[8] Diedrich, J; Rehse, SJ; Palchaudhuri, S. Escherichia coli identification and strain discrimination using nanosecond laser-induced breakdown spectroscopy, *Appl. Phys. Lett.*, 2007, 90, 163901 1-3.

[9] Rehse, SJ; Diedrich, J; Palchaudhuri, S. Pathogenic Escherichia coli strain discrimination using laser-induced breakdown spectroscopy, *J. Appl. Phys.*, 2007, 102, 014702.

[10] Gottfried, JL; De Lucia, FC; Jr. Munson, CA; Miziolek, A. W. Standoff Detection of Chemical, and Biological Threats Using Laser-Induced Breakdown Spectroscopy, *Appl. Spectrosc.*, 2008, 62, 353-363.

[11] Multari, RA; Cremers, DA; Dupre, JM; Gustafson, JE. The use of laser-induced breakdown spectroscopy for distinguishing between bacterial pathogen species and strains. *Appl. Spectrosc.* 2010, 64, 750−759.

[12] Multari, RA; Cremers, DA; Bostian, ML. Use of laser induced breakdown spectroscopy for the differentiation of pathogens and viruses on substrates. *Appl. Opt.* 2012, 51, B58−B64.

[13] Martelli, MR; Brygo, F; Sadoudi, A; Delaporte, P; Barron, C. Laser-Induced Breakdown Spectroscopy, and Chemometrics: A Novel Potential Method to Analyze Wheat Grains, *J. Agric. Food Chem.* 2010, 58, 7126-7134.

[14] Barnett, C; Bell, C; Vig, K; Akpovo, AC; Johnson, L; Pillai, S; Singh, S. Development of a LIBS assay for the detection of Salmonella enterica serovar Typhimurium from food, *Anal Bioanal Chem*, 2011, 400(10), 3323-3330.

[15] Kim, G; Kwak, J; Choi, J; Park, K. Detection of Nutrient Elements and Contamination by Pesticides in Spinach and Rice Samples Using Laser-Induced Breakdown Spectroscopy (LIBS), *J. Agric. Food Chem.* 2012, 60, 718-724.

[16] Multari, RA; Cremers, DA; Dupre, JM; Gustafson, JE. Detection of Biological Contaminants on Foods and Food Surfaces Using Laser-Induced Breakdown Spectroscopy (LIBS), *J. Agric. Food Chem.* 2013, 61, 8687−8694.

[17] Multari, RA; Cremers, DA; Scott, T; Kendrick, P. The detection of pesticides and dioxins in tissue fats and rendering oils using laser-induced breakdown spectroscopy (LIBS), *J. Agric. Food Chem.* 2013, 61, 2348−2357.

[18] Ma, F; Dong, D. A Measurement Method on Pesticide Residues of Apple Surface Based on Laser-Induced Breakdown Spectroscopy, *Food Anal. Methods*, 2014, DOI 10.1007/s12161-014-9828-4.

[19] 2D-Shige: https://sites.google.com/site/shigemorita/home/2dshige [Last accessed June 2014]

[20] Matlab 7.0: http://www.mathworks.com/products/matlab/ [Last accessed June 2014]

[21] Gottfried, JL. (Chemometric Analysis in LIBS) in D.A. Cremers and L. J. Radziemski, *Handbook of Laser-Induced Breakdown Spectroscopy* 2nd ed., John Wiley and Sons: Chichester, U.K., 2013.

[22] SPSS: http://www-01.ibm.com/software/analytics/spss/ [Last accessed June 2014]

[23] Unscrambler 9.7: http://www.camo.com/

In: Food Poisoning
Editor: Paresh C. Ray
ISBN: 978-1-63463-166-2

Chapter 4

TWO-DIMENSIONAL GRAPHENE MATERIAL FOR FOOD PATHOGEN DIAGNOSIS

Bhanu Priya Viraka Nellore, Rajashekhar Kanchanapally, Teresa Demeritte and Paresh C. Ray
Department of Chemistry and Biochemistry, Jackson State University, Jackson, MS, US

ABSTRACT

Contamination of food by pathogenic bacteria is very common in this world. Recent advancement in graphene, graphene oxide and hybrid graphene material has expanded our ability to design and construct platform with targeting and diagnostic functions. These multifunctional graphene oxide based materials have been demonstrated to be one of the most promising materials for selective pathogenic bacteria sensing. This book chapter discusses work from our and other groups on bio-conjugated graphene based nanomaterial based strategies for the selective and highly sensitive food pathogen detection. Current chapter is focused mainly on the basic concepts and critical properties of the hybrid graphene oxide platform that are useful for the food-pathogen sensing.

INTRODUCTION

Outbreaks of *Escherichia coli*, *Staphylococcus* and *Salmonella* food-borne pathogens occur regularly in the U.S and other developed countries [1–4]. According to the United States of America (USA) Centers for Disease Control and Prevention (CDC), an estimated 48 million food borne illnesses occur each year only in USA and on that around 3000 people die due to food borne diseases [3]. On the other hand, according to the European Food Safety Authority (EFSA), about 0.5 million of food borne illnesses occur each year in Europe [4]. Food recalls due to the presence of food-borne pathogens are the nightmare for world economical growth [1–9]. It is now well documented that due to the biological diversity and quite low infection dose, it is a continual challenge to prevent infectious disease outbreaks due to harmful pathogens [1–15]. Due to the lack of highly sensitive methods for the

identification of pathogenic bacteria and since current methods take several days to report the correct information, our society needs rapid, sensitive, and reliable assay to identify the harmful pathogens from food [1–15]. Nanomaterial-enabled detection strategies, though promising, is currently in its infancy, and may be able to help society to fulfill the demand in future. Since last ten years, several articles have demonstrated that very high selectivity can be achieved after the nanomaterials have been functionalized with targeting groups like antibody, aptamers, ligands. These recognition elements have the capability to recognize antigens or other epitopes on the exterior of a food-borne pathogen, and as a result, bio-conjugated nanomaterial can be used for selective capturing and detection of the food-borne pathogens. We and others have demonstrated that due to the presence of large surface area, nanomaterials enable attachment of large number of target-specific recognition elements. As a result, nanomaterial based techniques can be used for several pathogens simultaneously as well as selectively at the single bacterium level.

Graphene, a single sheet from graphite, has the ideal 2D structure and was produced in the laboratory in 2004 by Andre Geim and Konstantin Novoselov [16]. After that, in the last ten years it has revolutionized the scientific community due to the remarkable electronic and structural properties [17–24]. However, due to the presence of zero optical band gap, its device applications for food-borne pathogens are restricted. [16–24] Recently, we and others have shown that graphene oxide, which is chemically treated graphene, can be a potential alternative to graphene for the food-borne pathogen detection applications. [25–29] Recent articles have demonstrated that presence of oxygen moieties in the form of epoxy, hydroxyl, carbonyl or ether groups, opens up the band gap in graphene oxide, which helps it to be used for sensing applications. [25–33] Current book chapter intended to illustrate the current status of the use of graphene material for food-borne pathogen sensing and also to spur possible future research in this area for the next generation scientific community.

BIO-CONJUGATED GRAPHENE MATERIAL BASED SERS SENSOR FOR FOOD BORNE PATHOGEN DETECTION

Raman Spectroscopy is a powerful analytical tool for characterizing materials. The significant shortcoming of Raman spectroscopy is that it has a very week signal (low cross-section), requiring high concentrations of sample. However, in the presence of appropriate surfaces (rough surfaces, nanoparticles *etc*.) Raman cross section improves, hence called surface enhanced Raman scattering/spectroscopy (SERS). The two major factors contributing to the enhancement are electromagnetic enhancement (EM) and chemical enhancement (CM). SERS has been shown to be highly promising for biosensing applications due its ability to enhance Raman signals by $10^{6} - 10^{14}$ orders of magnitude with the potential for single-molecule detection and featuring the specificity due to its unique molecular fingerprinting information. [25–27] The major factor for enhancing the scattering is EM. Graphene cannot support EM, since the plasmon band is in the terahertz range. [28,29] However, CM is still possible, via charge transfer between the molecule and the substrate. Since charge transfer causes more separation of positive and negative charges, the polarizability of the molecule

increases resulting in the enhancement of Raman scattering cross-section. [30–32] Vast majority of biological molecules are aromatic and their structure is complementary to that of graphene. These aromatic molecules lie parallel to the surface of graphene, due to the π-π stacking, [33–35] resulting in minimal distance between graphene and the molecules. Possible position of the HOMO and LUMO of the molecules are all located on the two sides of the Fermi level of graphene which is an amicable situation for charge transfer between graphene and the molecules, causing chemical enhancement. Additionally, because of the similarity of the chemical structure between the molecules and graphene, the vibrational coupling [36] between them may be another factor contributing to the Raman enhancement. [28] The major drawback of chemical enhancement is that the enhancement factor is around $10 - 10^2$. This drawback can be overcome by modifying graphene substrate with metal nanostructures, which causes enhancement by EM mechanism, with surface plasmon which has enhancement factors more than 10^{10}. The advantage of using nanoparticles in conjunction with graphene is that, we can get a synergistic effect for Raman enhancement and graphene acts as stationary phase for nanoparticles, where immobilization is necessary.

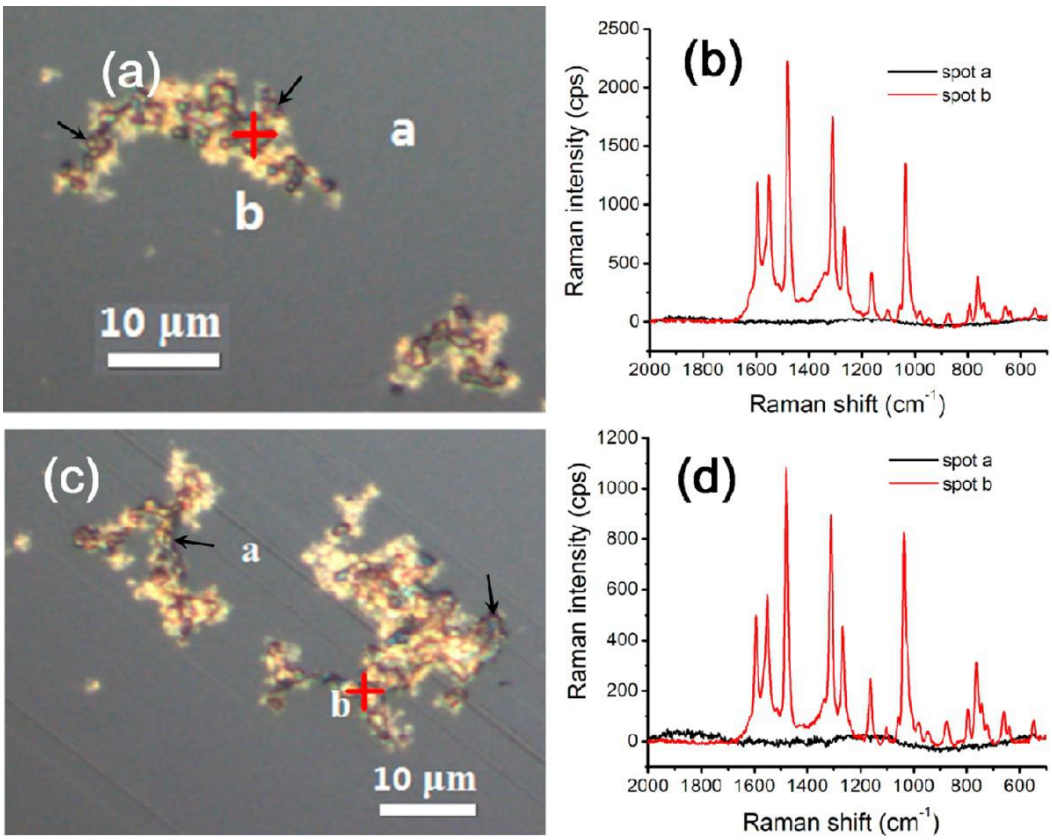

Figure 1. Dark-field microscopy images of (a) S. aureus (b) E. coli aggregated inside SERS tags. Corresponding SERS spectra are shown across the respective images. Black colored arrows indicate the bacteria and red colored crosses indicate the laser spot. (Reproduced with permission from ref. 37, copyright 2011, American Chemical Society).

Lin et al. [37] reported Graphene Oxide (GO) wrapped gold nanocluster SERS tags by using a glutaraldehyde (GA) modified poly (allylamine hydrochloride) labeled tris (2, 2′-bipyridyl) ruthenium - (II) chloride /GO nanohybrid as a complex Raman reporter for the detection of bacteria. Here the role of graphene is primarily a receptor for various aromatic compounds (dye in this case) which is a result of π−π stacking and electrostatic interaction between graphene and the dye molecule. Presence of graphene also resulted in several advantages like reproducibility, sensitivity, and colloidal signal stability. First, the morphology and optical property of tags are controllable. Au clusters with different aggregation extents can be obtained by using different-sized GO. The samples with near-infrared (NIR) absorption are easily attainable for further photothermal application. Second, high density of the Raman reporter can be enriched on GO sheets, rendering the high sensitivity of the tags. Third, GO forms an ultrathin (about 1 nm), transparent capping sheath of the tags, and thus the adsorbed Raman reporters "feel" the EM field with high efficiency for SERS enhancement, and the scattering signals export nearly without loss. [38] Fourth, the compact GO coating maintains the good water dispersibility and assures the tag's colloidal and signal stability in the biological matrix. Another interesting thermal property is also observed. Upon heating the SERS intensity decreases due to heat induced release of reporter molecules. [37] Both *S. aureus* and *Escherichia coli* bacteria were efficiently agglomerated by the tags owing to their unique sheet like coating structural properties combined with the cross-linking ability of GA, resulting in the enhancement of Raman signal. Using this method, we can also perform photothermal ablation by exposing agglomerated bacteria to LASER. Au cluster will generate the heat, which is required to destroy the cell wall of the microbes, upon exposure to light and as microbes are already agglomerated, heat transfer will be efficient resulting in better photothermal ablation.

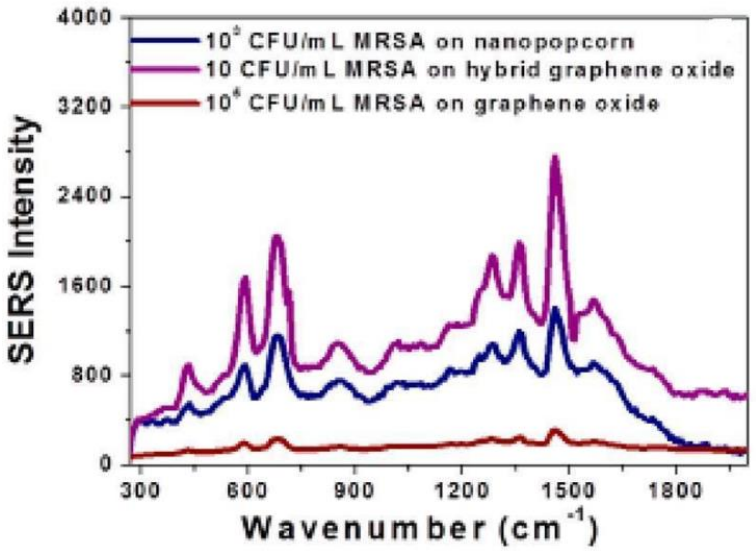

Figure 2. Plot showing SERS enhancement of the Raman signal from MRSA at 670 nm excitation, in the presence of nanoassemblies. SERS spectra from MRSA clearly show that the detection limit can be as low as 10 MRSA (reproduced with permission from ref. 12, copyright 2014, American Chemical Society).

Our group recently reported a label-free SERS probe for the detection of bacteria. [12] In this approach, a nano assembly is made of GO and popcorn shaped Gold Nano Particles. To understand whether the nano assembly is superior, Rhodamine 6G (Rh6G) SERS experiments were performed using graphene oxide alone and nanohybrid. The enhancement factor is calculated *by using following equation (1).*

$$G = \frac{[I_{SERS}]}{[I_{Raman}]} \times \frac{[M_{bulk}]}{[M_{ads}]} \quad (1)$$

where I_{SERS} is the intensity of a 1511 cm^{-1} vibrational mode in the *SERS* spectrum in the presence of graphene oxide, nanopopcorn, or hybrid graphene oxide and I_{Raman} is the intensity of the same mode in the bulk Raman spectrum from only Rh6G. M_{bulk} is the number of molecules used in the bulk, and M_{ads} is the number of molecules adsorbed on the nanosurface.

Experimental data show that the enhancement factor is about 1.2 x 10^9 in the case of gold nanopopcorn, and this huge SERS enhancement in the case of nanopopcorn is mainly due to the electromagnetic enhancement and a lightning rod effect. A SERS enhancement factor of 3.8×10^{11} is observed for the nano assembly, proving that hybrid is two orders of magnitude more sensitive. This huge eleven orders magnitude SERS enhancement of the hybrid material is mainly due to the CM by graphene oxide and very high plasmon enhancement (EM) by nanopopcorn. To specifically detect the *S. aureus*, nano assembly is modified with SEB1 aptamer *(APTSEB1)*, which is specific to *S. aureus*. After incubating with the nano assembly, *S. aureus* successfully aggregated inside the nano assembly. Since the cell wall of bacteria contains various proteins, carbohydrates and lipids, in the presence of nano assembly, we will be able to see vibrational modes of respective compounds. SERS data observed from MRSA show $\delta(CH_2)$ saturated lipids peak at 1460 cm^{-1} and that the ν(NH2) stretch for adenine and guanine peaks at 1320 cm^{-1}. Similarly, we have observed the ring breathing mode of the tyrosine protein peak at 855 cm^{-1}, C−O−C glycosidic ring deformation at 580 cm^{-1}, and the skeletal modes C-C peak at 420 cm^{-1}. We also see D and G bands of graphene oxide. Experimentally observed SERS bands using our SERS substrate are in good agreement with the Raman bands reported for different microorganisms in the literature. [39,40] Using this nano assembly, one can detect methicillin resistant *S. aureus* at the concentrations as low as 10 CFU/mL.

Table 1. Raman Modes Analysis Observed from MRSA (Reproduced with permission from ref. 12, copyright 2014, American Chemical Society)

Vibration mode Raman	Peak position [cm^{-1}]
graphene oxide G band and amide I 1603−1615δ	1603-1615
$\delta(CH_2)$ saturated lipids	1460
Graphene oxide D band	1350
$\nu(NH_2)$ Stretch for adenine and guanine	1320
Ring breathing Tyr protein	855
CH_2 rock	710
C−O−C glycosidic ring deformation	580
Skeletal modes C-C	420

BIO-CONJUGATED GRAPHENE MATERIAL BASED FIELD EFFECT TRANSISTOR (FET) SENSOR FOR FOOD BORNE PATHOGEN DETECTION

Field-effect sensors have several advantages over resistor sensors. First, the sensitivity can be dramatically enhanced by the modulation of the gate electrode when operating the devices in the sub-threshold regime. [41,42] Second, the current, the multiple parameters such as mobility, threshold voltage,and sub-threshold slope etc. can also be used for sensing. [42] The third advantage of the field-effect sensors is that the sensor response can be enhanced by combining them in oscillator and adaptive amplifier circuits. [41,42] Finally, the field-effect sensors can operate at room temperature, which has advantages of low power consumption, long device lifetime, and reduced explosion hazards. [42] Stimuli-responsive Field Effect Transistor (FET) devices are attractive due to their rapid response, real time monitoring and high sensitivity. [43] Integrating materials like graphene that has very low band gap in a FET device is more practical approach, since it reduces sensor to sensor variation improving the reproducibility. Due to zero-gap, graphene has exceptional electron mobility (~100 times greater than that of silicon) making it apposite for electronic applications. [44]

In a proof of concept example, Mohanty et al. reported the fabrication of Chemically modified graphene sheets (CMGs) based single bacterium resolution interfacial device, [45] which is fabricated by immobilizing graphene-amine on a silica substrate forming p-type chemically modified graphene device. CMGs can be valuable tool to develop versatile biohybrids. Since graphene contains huge surface area, they can strongly interfere with microscale biocomponents by the virtue of appropriate modification. These CMGs, which are p-type semiconducting nano sheets, upon interaction with biological cells, like bacteria, will experience highly sensitive charge carrier modulation that enables us to detect bacteria by an electrical signal. In this study, the CMGs and their biohybrids were synthesized using GO immobilized on heavily doped n-type silicon substrate and subsequently functionalized with a monolayer of (3-aminopropyl) to make the silica surface positively charged with tethered amine groups. The aminized GO scaffolds (GA), which are positively charged, can now be electrostatically attached to negatively surface charged bacteria forming CMG/bacteria biohybrids. The bacterial strain used in this experiment was *Bacillus cereus*, a gram positive strain with an abundance of polyteichoic acid molecules on their cell wall, making it negatively charged. To further enhance the specificity of biohybrids towards bacteria, it was modified with concanavalin, a biomolecule with highly specific affinity to the teichoic acid on the peptidoglycan membrane of the bacterial cell wall. The hybrid device's (GA based) hole and electron mobilities were compared to that of GO based device to determine the superiority. The hole mobilities for GO and GA were 0.0297 ± 0.0017 (cm^2/V)/s and 5.882 ± 0.098 (cm^2/V)/s, respectively, while the electron mobilities were ~0.00198 ± 0.0002 and 0.00747 ± 0.00178 (cm^2/V)/s, respectively. These carrier mobilities ($\mu_{carrier}$) were *calculated using Equation 2.*

$$\mu_{carrier} = \left(\Delta I_{DS}/\Delta V_G\right) \Big/ \left(C_G\left(l/w\right)V_{DS}\right) \qquad (2)$$

where ΔI_{DS} and V_{DS} are the source-drain current and voltage, C_G is the capacitance of the silica gate, and l and w are the length and width of the CMG sheets between electrodes. The increase in hole mobility can be attributed to the length between amine group end to graphene base, which is significantly higher than that of between carboxylic end to graphene base in case of GO. There is an increase of 42% in conductivity of GA device with the addition of single bacterium. Here attaching a bacterium, a negatively charged species, to GA device, a p-type device, is equivalent to negative potential gating that increases the hole density. The increase in hole density due to the bacterium attachment was calculated to be $3.53\times10^{10}cm^{-2}$. It is evident that on an average, there is an estimated ~1400 additional charge carriers generated with the addition of single bacterium to the device, resulting in the increase in conductivity, thereby confirming the presence of bacteria. The change in hole density (Δq) was *calculated using Equation 3.*

$$\Delta q = \left(R_2^{-1} - R_1^{-1}\right) \Big/ \left(\left(l/w\right)\mu_p\right) \tag{3}$$

where R2 and R1 are the final and initial resistances of the device.

Chang et al. reported a FET produced by thermally reduced monolayer GO (TRMGO), [46] which is able to detect *E. coli* selectively with a sensitivity of 10 CFU/mL. The electrodes were fabricated by solution process involving self assembly of monolayer graphene oxide sheets on to Au electrodes. The self assembly is a result of electrostatic interaction between oxygen groups on GO sheets and amine groups on the functionalized Au electrodes. Since the target (bacteria) is a charged species, sensing signals can be monitored directly by the change in FET electrical properties (e.g., current or conductance). To investigate the electrical properties of TRMGO FET devices, measurements were carried out in air at room temperature using the back-gated FET devices. While the gate bias was varied from -40 to +40 V, the current of the device decreased from 139 to 59 nA. The decrease in conductivity with increasing voltage indicates that the TRMGO sheets are p-type semiconducting materials. The sensing performance of TRMGO FET devices was investigated using anti-E. coli antibodies as probes. The device was exposed to various concentrations of *E. coli* cells in the cell culture grade water. The changes in transfer curves of the FET sensor after adding selected concentrations of *E. coli* cells (10, 10^2, 10^3 and 10^4 cfu/mL) have been investigated. It can be observed that the conductance of the devices continued to increase with increasing concentrations of *E. coli* cells. As the TRMGO FET was operated in the p-type region (*solution-gate voltage Vg = 0 V),* the device conductance increase is due to increased hole concentration, which is induced by the highly negatively charged bacteria. The conductance of the device with specific binding increased correspondingly with the addition of *E. coli* cell solution, and the current change of the device was around 1.1% with the introduction of 10 cfu/mL. For comparison, a control experiment was carried out on a device without modification of anti- E. coli antibody probes. In contrast, controlled injection of *E. coli* cells had almost no effect on the conductance of the TRMGO devices in the absence of probes. Therefore, it is confirmed that the conductance increase is solely attributed to the specific binding between probes and target materials. An increase in conductance of the device is observed with specific binding of *E. coli* and the current change

of the device was measured to be around 1.1% for 10 CFU/mL of *E. coli.* In the case of FET biosensor devices, proposed mechanisms include charge induced electrostatic gating and the Schottky barrier effect. Due to the high temperature (400 °C) during the annealing process, the Schottky barrier effect can be neglected. From the above discussion of sensor response from specific and non-specific bindings, it is believed that the gate modulation (FET performance) leads to the sensor signal by capturing negatively charged *E. coli* cells. And the device conductivity change is attributed to the direct electrostatic gating effect from the accumulation of negatively charged *E. coli* cells on the gate electrode.

Huang et al. demonstrated a high throughput nanoelectronic sensor based on antibody-modified graphene to detect bacteria (*E. coli*) with high sensitivity and selectivity. [47] To specifically detect bacteria *E. coli*, anti- E. coli antibodies were first immobilized onto graphene film via the linker molecules (1-pyrenebutanoic acid succinimidyl ester), whose pyrene group at one end binds to the graphene surface through strong π-π interaction and the succinimidyl ester group at the other end covalently reacts with the amino group on the antibody. To prevent nonspecific binding, ethanolamine was applied to quench the unreacted succinimidyl esters on the linker molecules and Tween 20 was used to passivate the uncoated graphene area. The CVD-grown graphene exhibited the characteristic ambipolar field-effect and each functionalization step led to shift in the transfer curve (drain-source current I_{ds} versus the solution-gate voltage V_g). The grapheme sensor was incubated with 10^5 *CFU/mL* of *E. coli* to determine kinetics of bacteria binding and the device response. The graphene conductance increases with time due to gradual increase in the number of *E. coli* caught by the antibodies on the graphene film. As the graphene FET was operated at the p-type region (V_g = 0 V), the increase in graphene conductance is due to increased hole density induced by the highly negatively charged bacterial wall. The device response reached the maximum in about an hour due to saturation of bacteria binding. The kinetic time constant of bacteria binding (time-dependent device response) was about 10 min. In control experiments, 1 hr incubation of 10^5 cfu/mL of E. coli did not cause any appreciable conductance change in the devices modified only with linker molecules, ethanolamine and Tween 20, suggesting the essential role of anti- E. coli antibodies in the detection. The functionalized graphene devices were incubated with different concentrations of *E. coli* for 30 min, rinsed thoroughly with PBS solution, and electrically characterized by measuring the I_{ds}–V_{ds} (I-V) characteristics while the solution-gate voltage V_g was held at 0 V. The increase in graphene conductance positively scaled with the concentration of bacteria. In comparison, 10^5 cfu/mL *Pseudomonas aeruginosa* did not cause significant response of anti- E. coli antibody functionalized graphene FET, indicating the high specificity of detection. The specificity is attributable to the fact that other bacterial strains are not able to bind with the anti- E. coli antibodies functionalized on the graphene, and non-specific binding to the graphene surface is prevented by Tween-20 passivation. Specifically, 10 cfu/mL caused 3.25 ± 0.43 % increase in graphene conductance (n = 6 devices) which corresponds to a current increase of ~1.17mA at V_{ds} = 0.2 V (significantly higher than the current noise of 0.02 mA). In contrast, high concentration of *P. aeruginosa* (10^5 cfu/mL) only produced 1.02 ± 0.81% increase (n = 6 devices). The transfer curves of graphene device measured before and after incubation with *E. coli* indicate the obvious right-shift of the Dirac point and a conductance increase at V_g = 0 V, agreeing with the notion that the negatively charged bacteria increase the hole density in graphene.

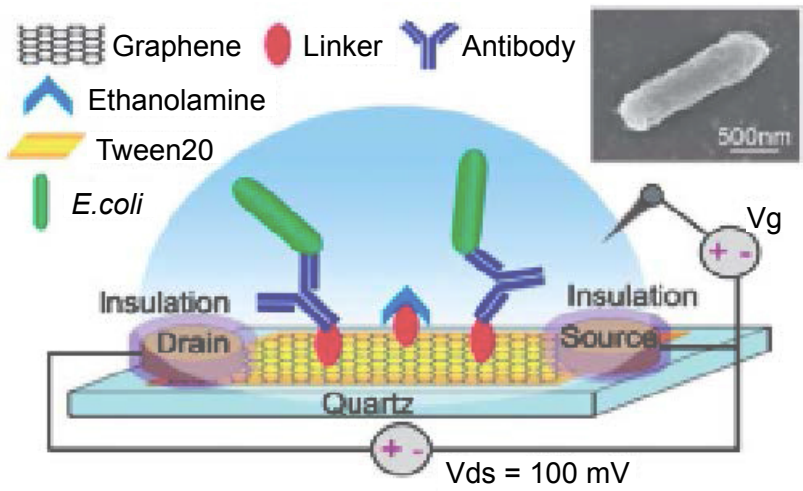

Figure 3. Illustration of anti- E. coli antibody functionalized graphene-FET for detection of *E. coli*. Inset: Scanning electron microscopy (SEM) image of an *E. coli* on antibody functionalized graphene (reproduced with permission from ref. 47, copyright 2011, Royal Society of Chemistry).

Basu et al. reported a low cost graphene based transparent flexible acetate substrate *E. coli* sensor, without using any linker or antibody. [48] The sensing study was done with different concentrations of *E. coli* along with the effect of acetate sheet and the media on impedance signal. It is observed that the impedance values obtained for the bare acetate substrate, with different concentration of *E. coli* is extremely high (MΩ), due to absence of graphene. The decrease in the impedance with increasing frequency can be attributed to capacitive component of the current. However, the impedance value does not change appreciably for different concentrations of *E. coli*. In order to assess the impact of media and its degradation, impedance spectroscopy was performed by taking different samples of LB broth stored over long time. The impedance did not change for different samples of LB broth in the absence of *E. coli*. However the impedance values are lower, which can be attributed to the presence of graphene channel. Finally, the impedance spectroscopy of graphene device was performed, with different concentrations of *E. coli* obtained from two different techniques. In the first technique, *E. coli* solution was collected after different times of incubation, with longer incubation time corresponding to higher concentration of *E. coli*. In the second technique, the master solution obtained after 2 hr of incubation was serially diluted. In both cases, the impedance decreases with increasing concentration of *E. coli*, clearly indicating the sensing capability of graphene device. The RC model can be applied in any graphene based sensor structure with interdigitated electrodes. Here the separation between two electrodes is 300 µm, so the capacitance (C_f) is very low and it can be neglected. The equivalent impedances at high frequency (Z_{eqH}) and low frequency (Z_{eqL}) are given by Equations 4 and 5.

$$Z_{eqH} = \frac{R_g \times R_s}{R_g + R_s} \tag{4}$$

$$Z_{eqL} = \frac{R_g(R_s + R_p)}{R_g + R_s + R_p} \tag{5}$$

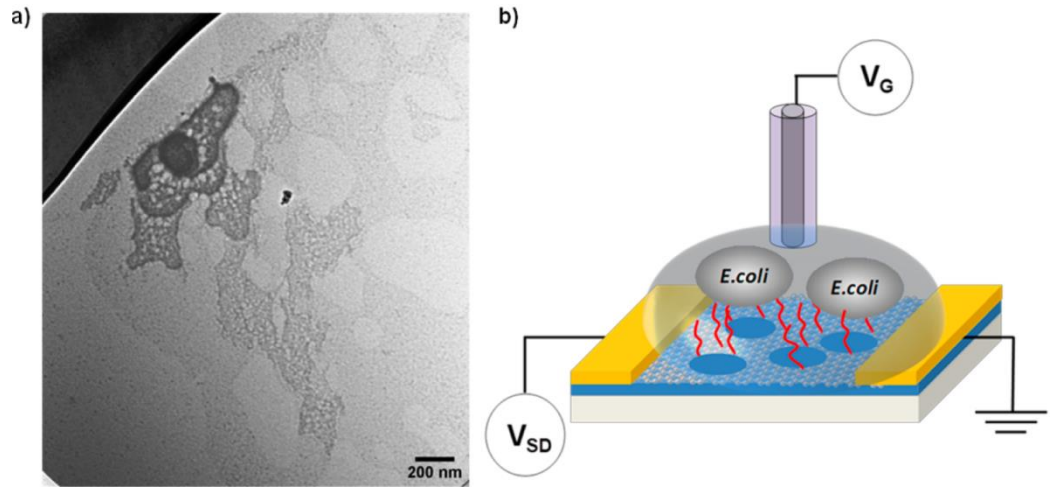

Figure 4. (a) TEM image of hRGO. (b) Schematic illustration of an AMP-functionalized hRGO FET for the selective detection of gram-negative (Reproduced with permission from ref. 51, copyright 2014, American Chemical Society).

Where R_p, R_s and R_g are polarization resistance, solution resistance and graphene resistance respectively. In this model, the observed impedance decrease with increasing concentrations of *E. coli* is attributed to increased hole doping in p-type graphene due to negatively charged *E. coli*. The sensitivity (S) of the model is calculated to be around 10^6 CFU/mL, by using the following Equation 6.

$$S = \frac{Z_0 - Z_e}{Z_0} \times 100 \qquad (6)$$

Where Z_0 is the impedance of media at 100 kHz and Z_e is the impedance after introducing *E. coli.*

Recently developed holey reduced graphene oxide (hRGO), [49] which demonstrates p-type semiconductor transfer characteristics and shown to be used as the transducer element in FET bacteria cell devices [50]. Chen et al. [51] recently reported a p-type FET device made up of holey reduced graphene oxide, modified with a positively charged anti microbial peptide (AMP), Magainin I (GIGKFLHSAGKFGKAFVGEIMKS), [52] specific for gram negative bacteria that operates by taking advantage of the electrostatic interaction between positively charged Magainin I and anionic lipopolysaccharides. AMPs, which are inherent to many organisms' immune systems, recognize target pathogens by interacting with surface components of microbial cells. [52–54] While the exact mechanism for their antimicrobial activities remains undetermined, the microbicidal or microbiostatic activity is generally postulated to occur via membrane disruption. [55]

hRGO was first synthesized via enzymatic oxidation [49] and then as-synthesized product was diluted in water to 0.01 mg/mL and deposited between interdigitated electrodes (Au/Ti, 100 nm/30 nm, 10μm spacing) using an alternating-current dielectrophoresis method with a bias voltage of 10 Vpp at 300 kHz for 60 s. Functionalization was accomplished by activating carboxylic groups on bare hRGO devices with 1-ethyl-3-[3-(dimethylamino)

propyl] carbodiimide/N-hydroxysuccinimide. After a thorough rinsing with PBS, activated devices were incubated overnight with AMP (1μM in PBS), resulting in the formation of amide bonds between Magainin I and activated hRGO. After incubation with a blocking buffer (BB; 0.1% Tween 20 in PBS) for 1 h, a further decrease in the conductance was detected as a result of Tween occupying nonspecific binding sites on hRGO. *The lack of a BB results in both* the allowance of nonspecific interactions and low response, possibly related to the conformation of AMP on the device surface. Upon subsequent exposure to heat-killed *E. coli* O157:H7 ($10^4 – 10^7$ cfu/mL in PBS) for 1 h at each concentration, *a time sufficient for cell capture*, the devices demonstrated a further response in the p-type region that was attributed to the specific interaction between the attached AMP and bacterial cells in the solution. Presumably, this interaction induces electron transfer with hRGO, which decreases the conductivity of the device by depleting the main carriers (i.e., holes); however, electrostatic gating may also contribute to the observed response, and so the overall mechanism is complex. The limit of detection for this sensor was calculated to be 803 *CFU*/mL. As a control experiment, functionalized devices were exposed to gram-positive *Listeria* cells, which do not interact with Magainin I. After incubation with *Listeria* ($10^4 - 10^7$ *CFU* /mL in PBS), the transfer characteristics changed negligibly comparable to a device treated equally with, thereby indicating minimal to no binding between AMP and the control bacterial cells. This instrument can be used in variety of bacterial species simply by choosing specific AMP from the library.

An impedimetric immuno sensor developed by electrodepositing reduced graphene oxide sheets (RGS) doped chitosan (CS) on to a glassy carbon electrode *(GCE)* to detect marine sulfate reducing pathogenic bacteria (SRB) is reported by Wan et al. [56] The electro deposited RGS-CS composite was further modified with anti-SRB antibody for specificity, then with bovine serum albumin to avoid any non-specific interaction. Upon immersing the electrode in a solution containing SRB, a significant change is observed in charge transfer resistance (over 90 Ω at a bacterial concentration of 1.8 x 10^7 CFU/mL) of redox couple, a similar change is not observed in case of counterpart gram negative pathogenic bacteria *Vibrio anguillarum* (less than 20 Ω at a bacterial concentration of 2.1 x 10^7 CFU/mL), owing to specificity. The sensitivity of the electrode mainly arises from graphene sheets, which is a very good conductor.

Another electrochemical impedimetric sensor for the detection of MRSA DNA is recently reported by Wang et al. *[*57] First *a GCE is* modified with aminopropyltriethoxysilane (APTES), then with RGS. A 30mer probe DNA adsorbed onto RGS through weak electrostatic/hydrogen bonding. As DNA is negatively charged, it will reduce the conductivity, that is increase in the resistance of charge transfer due to the repulsive interaction with redox mediator (in this case redox mediator is $[Fe(CN)_6]^{3-/4-}$). In the presence of complementary *DNA conductivity change is still higher, decrease by about 10 times*, which is measured by Nyquist plot. This method is able to detect DNA *even* at *a* concentration of 100 femto molar.

BIO-CONJUGATED GRAPHENE MATERIAL BASED FLUORESCENCE SENSOR FOR FOOD BORNE PATHOGEN DETECTION

According to Michael Kasha's rule, [58] the photoluminescence peak is independent of the wavelength of the excitation, as it is always observed for organic dyes and inorganic quantum dots fluorophores. Usually, the fluorophore is excited to the excited states in femto-second (10^{-15} s) time scale via the absorption of light and after that it undergoes non-radiative relaxation to the band edge in pico-second (10^{-12} s) time scale [59,60]. At the end, radiative recombination of the electron and hole to emit a photon as photoluminescence occurs at nano-second (10^{-9} s) time scale. As a result, all the excited electrons, independent of initial energy, have to relax to the band edge before it comes back to the ground state by releasing luminescence [59,60].

Recently our group demonstrated that two-photon photoluminescence imaging color and luminescence peak position can be tuned for graphene oxide, from deep blue to red simply by varying the excitation wavelength without changing its chemical composition and size. [61] The excitation energy dependent photoluminescence spectral shift for graphene oxide can be due to the several factors [62,63] and these are as follows: 1) possible excited-state protonation of the COOH group. In the excited state, intramolecular proton transfer occurs from hydroxy to carboxylate anions; 2) excitation wavelength dependent fluorescence from the OH moiety in the graphene oxide sheets; 3) Due to the local reorganization of photoexcited GO sheets in a polar solvent, the solvent relaxation time becomes comparable to the fluorescence lifetime. Though the GO photoluminescence can be tuned from the visible to the NIR region just by varying the excitation energy from 440–600 nm, we have not observed any clear fluorescence above 600 nm excitation, which clearly indicates that GO is not suitable for biological imaging applications using near-infrared (NIR) light within the biological transparency windows. [59,60,64,65] As a result, two-photon photoluminescence imaging at different excitation wavelengths with near-infrared light in two biological transparency windows has been used for MDRB imaging. As discussed earlier, the excitation wavelength dependent two-photon photoluminescence from freshly prepared graphene oxide can be tuned just by varying the NIR excitation energy from 760 to 1120 nm, without changing its chemical composition and size. Excitation wavelength power dependent two-photon intensity measurement experiments performed to know how 680 nm two-photon emission intensities from GO vary for 1120 nm fs laser excitation with various average powers show that the emission intensity is proportional to the square of the fs excitation intensity confirming the presence of the two-photon process. Continuous 1120 nm fs laser illumination experiment shows that two-photon luminescence signals remain unchanged till 40 minutes of illuminations, which indicates very good photo-stability of aptamer APT^{SEB1} - modified graphene oxide as a TPF material. Next, we have measured two-photon absorption cross-section values using the following Equation 7, which was then compared with literature reported values. [66,67]

$$\sigma_{GO} = \sigma_{FL} \cdot \left({}^{F_{GO}}/_{F_{FL}}\right) \cdot \left({}^{\Phi_{FL}}/_{\Phi_{GO}}\right) \cdot \left({}^{C_{FL}}/_{C_{GO}}\right) \qquad (7)$$

where the observed fluorescence intensity has been represented by F, the quantum yield is represented by Φ and C is the concentration. It was found that the two-photon absorption cross-section is 50840 Goeppert-Mayer units (GM), for -NH modified APT^{SEB1} attached graphene oxide at 760 nm excitation, which is higher than any other reported value in literature. Our measurement of σ_{2PA} for APT^{SEB1} attached graphene oxide is few orders of magnitude larger than that of organic molecules and even higher than that of the highest reported two-photon absorption cross-section for QDs. [68,69] Due to the very high two-photon absorption cross-section and good quantum yield, graphene oxide is a highly promising two-photon luminescence microscopy imaging contrast agent for bio-imaging. The purpose of using aptamer APT^{SEB1} is that it can be used for very selective detection of *Staphylococcus aureus*. [70] Next, we have incubated aptamer APT^{SEB1} -modified graphene oxide with different concentrations of MRSA for 30 minutes. To understand whether the two-photon luminescence of graphene oxide can be tuned just by varying the excitation energy from the first to the second biological transparency windows, we have performed two-photon photoluminescence experiments at 760, 880, 980 and 1120 nm excitation wavelength, which show that the two-photon luminescence of graphene oxide can be used for multi-color bio-imaging and it is due to the fact that two-photon photoluminescence from GO can be tuned just by varying the NIR excitation energy without changing its chemical composition and size, as we have discussed before. Due to the interaction of aptamer attached graphene oxide sheets and bacterial surface, GO density is much higher on the top of MRSA. As a result, we have observed much brighter two-photon fluorescence from graphene oxide on top of MRSA. Experimental data show that the fluorescence image becomes brighter due to the strong interaction between hybrid GO and aggregated MRSA. The above interaction helps to locate MRSA in the fluorescence image in the presence GO two-photon fluorescence background. To find out that whether aptamer APT^{SEB1} -modified graphene oxide based two-photon luminescence is selective for MRSA or not, *Salmonella* DT104 was incubated with aptamer APT^{SEB1} modified graphene oxide for 30 minutes. Two-photon fluorescence image and TEM image clearly show that *Salmonella* DT104 does not bind with aptamer APT^{SEB1} -modified graphene oxide sheet. The above experimental data clearly indicate that aptamer APT^{SEB1} modified graphene oxide based two-photon luminescence is highly selective for MRSA imaging and can be used selective and multi-color imaging of MRSA in the first and the second biological transparency windows.

Abdelhamid et al. reported a method to detect bacteria using multifunctional graphene magnetic nanosheet decorated with chitosan. [71] A graphene-magnetic nanoparticle-chitosan composite (GMCS) is prepared by synthesizing chitosan modified magnetic nanoparticles and chitosan modified graphene sheets separately, then incubating them together. The GMCS is used to develop an effective biosensor that can generate photoluminescence as a function of the bacterial concentration. Two kinds of bacteria were detected with detection limits of 5.0×10^2 for *P. aeruginosa and* 4.5×10^2 for *S. aureus* by using fluorescence. GMCS is also used to detect the bacteria by matrix assisted laser desorption/ionization mass spectrometry (MALDI). To detect bacteria by MALDI analysis, bacteria were pre-concentrated by magnetic separation and were analyzed. This approach is able to detect *P. aeruginosa* and *S. aureus* at concentrations similar to that of fluorescence analysis.

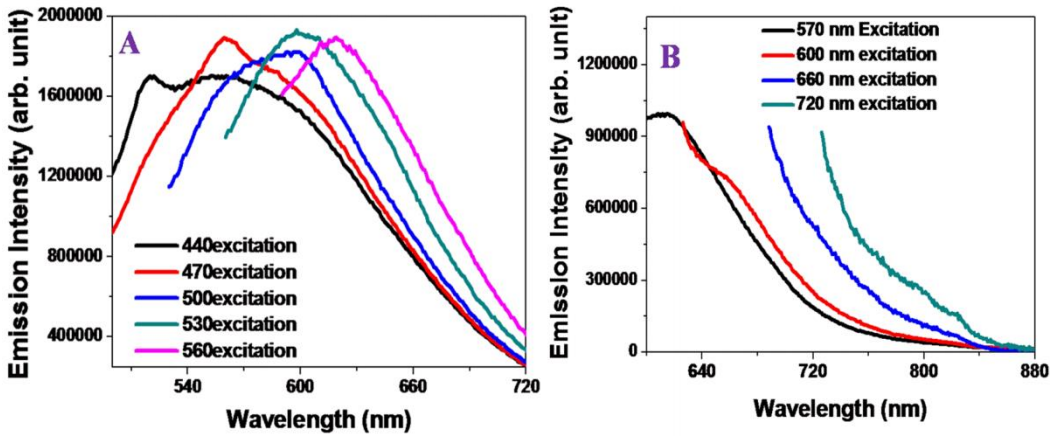

Figure 5. (A), (B) Excitation wavelength dependent single photon photoluminescence from freshly prepared graphene oxide. Plot clearly shows that water soluble GO photoluminescence can be tuned from the visible to near NIR region just by varying the excitation energy, without changing its chemical composition and size (reproduced with permission from ref. 61, copyright 2014, Nature Publishing Group).

Liao et al. proposed a novel multivariate testing strategy that depends on a QD and GO nanoplatform. [72] It aims at multiplex gene monitoring of *Listeria monocytogenes* that can overcome false negatives and reduce the false-dismissal probability in routine tests, based on the principles of probability statistics, the probability of independent random events occurring at the same time is far less than that of a single event occurring independently. In this approach, the linear-after-the-exponential polymerase chain reaction *(LATE-PCR), is* employed as the amplification system, and the *iap* and *hlyA* genes of *L. monocytogenes* are used as the target genes. This platform consists of three parts: multiplex LATE-PCR amplification, DNA hybridization, and GO−QD signal detection. When the genome of *L. monocytogenes* exists, the multiplex LATE-PCR amplification system can obtain ssDNA amplification products of the *iap* and *hlyA* genes at an efficiency between linear amplification and exponential amplification. Then, QD probes are added and incubated with the ssDNA amplification products to achieve sufficient hybridization of the ssDNA amplification products and QD probes. At the same time, helper probes are imported to constitute a longer double chain structure. Then, the single-stranded QD probes are quenched by GO. However, partial formation of double-stranded DNA (dsDNA) through the hybridization of QD probes and amplification products leads to sufficient resistance to the quenching effect induced by GO. Therefore, the nanoplatform can achieve characteristic signals corresponding to the target genes. The sensitivity of the model evaluated by varying the concentration of DNA from 10 to 10^7 fg/μL. After amplification, the products of target genes were mixed with pre prepared QD probes and helper probes. The mixture was incubated at 37°C for 30 min. Then, GO was added to the system, reaching a final concentration of 16μg/mL and leading to a quenching effect on the excess QD probes within 10 min. Finally, changes in the fluorescence intensity of the final mixture were observed and recorded. The fluorescence intensity synchronously decreased with the reduction of genomic DNA. When the concentration of genomic DNA decreased to 10 fg/μL, the fluorescence intensity tended to be coincident with that of the control group. It was demonstrated that the QD−GO multiplex gene monitoring

platform achieved a sensitivity of 100 fg/μL. We performed linear regression analysis of the fluorescence intensities with different genomic DNA concentrations for verification of the reliability and feasibility of this platform. This platform exhibited a good dynamic range from 10^2 to 10^6 fg/μL. To further evaluate the performance of the platform, samples of the genomic DNA of *Salmonella enterica*, *E. coli* O157:H7, and *L. monocytogenes* with an isometric concentration of 10^6 fg/μL were also analyzed using this platform. The fluorescence intensities of *Salmonella enteric* and *E. coli* O157:H7 exhibited no significant enhancements, where as *L. monocytogenes* gave a dramatic response, which confirms that this platform has highly responsive specificity to *L. monocytogenes.*

BIO-CONJUGATED GRAPHENE MATERIAL BASED FRET SENSOR FOR FOOD BORNE PATHOGEN DETECTION

Fluorescence resonance energy transfer (FRET) is the transfer of photoexcitation energy from a donor fluorophore to an acceptor molecule. According to the quantum physical model and the classical Coulombic dipole–dipole interactions, FRET occurs via radiationless transitions. [73,74] The energy transfer efficiency depends highly on the relative distance between the FRET pair. [75] Over the past few decades, single-molecule FRET has become a sensitive and powerful tool for determining conformational biomolecular changes and molecular interactions, and it has been used for inter- and intramolecular distance measurement for biochemical processes. [76] Since the FRET process originates from dipole–dipole interactions, the energy transfer between the donor and the acceptor is strongly dependent on the center-to-center separation distance. Due to the coupling requirement, the energy transfer efficiency is inversely proportional to the sixth power of the donor to acceptor distance. [77] As a result, the length scale of a FRET ruler is of the order of 10 nm maximum. Due to its nearly transparent, semimetallic nature, graphene is also a unique interface for fluorescence energy transfer. Graphene exhibits linear band dispersion around the corners of its Brillouin zone and also has a nearly constant optical absorption. [78–80] As a result, optically excited species can be quenched by resonant energy transfer via the excitation of electron–hole pairs in graphene. [78–82] Using theoretical calculations, Swathi and Sebastian [79,80] determined that graphene could act as a highly efficient quencher of fluorophores. They calculated that quenching of FRET fluorescence using graphene would be observable up to a distance of approximately 300 Å, whereas FRET is typically observable at about 20–60 Å. [83] In spite of being a disrupted lattice of sp^2-bonded carbon atoms, GO can exhibit similar behavior. Interestingly, in studies in which GO was used as the acceptor, quenching was observable at distances greater than 20 nm. [84] Graphene oxide has been reported to be a universal highly efficient long-range quencher of fluorescence. [85,86] *Morales-Narváez* reported a novel pathogen-detection system based on antibody quantum dot (Ab-QD) probes, in which GO is employed as a pathogen-revealing agent (based on its quenching performance). [87] The system uses Ab-QD microarrays for pathogen attachment. The pathogen is selectively captured onto the Ab-QD probes, which fluoresces when excited with a laser, and then GO is added. In the presence of the pathogen, the bound probes barely interact with GO; consequently, GO cannot quench their fluorescence. However, in the absence of the pathogen, the (free) probes extensively interact with GO through π-π stacking, and GO quenches their fluorescence. In FRET, the fraction of photons that are absorbed by

the donor and subsequently transferred to the acceptor can usually be increased by increasing the number of acceptor molecules. [88] Ab-QD complexes in microspots of approximately 140±10 µm were printed, and then assayed for quenching of their fluorescence by GO at different GO concentrations. As in microarray technology, the interaction of the spotted probes (in this system, Ab-QDs) and the molecule that is to be attached onto the probes (in this system, GO) strongly depends on both the concentration and the incubation time. [89] A calibration curve obtained from the quenching of the Ab-QD microarrays by GO at different concentrations (0 – 350 mg/mL) at an incubation time of 30 min yielded a linear response, however, at an incubation time of 75 min, the response was exponential. These results indicate that an increase in GO concentration and an increase in the incubation time can both induce an increase in quenching efficiency. This system, once optimized, would be able to display an ON/OFF (digital-like) response. When used a high concentration of GO (<110 mg/mL) as the pathogen-revealing agent (which led to a dense coating of GO platelets), distinguishing between the absence and presence of the pathogen is not possible, as the quenching levels were similarly high in the two cases. In contrast, when used a low concentration of GO (<40 mg/mL), the probes were scarcely quenched. This result indicates that the optimal conditions for the use of GO were an incubation time of 75 min and a GO concentration of approximately 70 mg/mL. Under optimal conditions, the system exhibits a transition at an *E. coli* concentration of approximately 10 CFU/mL and becomes saturated at an *E. coli* concentration of about 10^7 CFU/mL. When similar experiment performed with *Salmonella typhimurium* as a non-target pathogen, there was no much difference observed compared to the blank, indicating the specificity of the system.

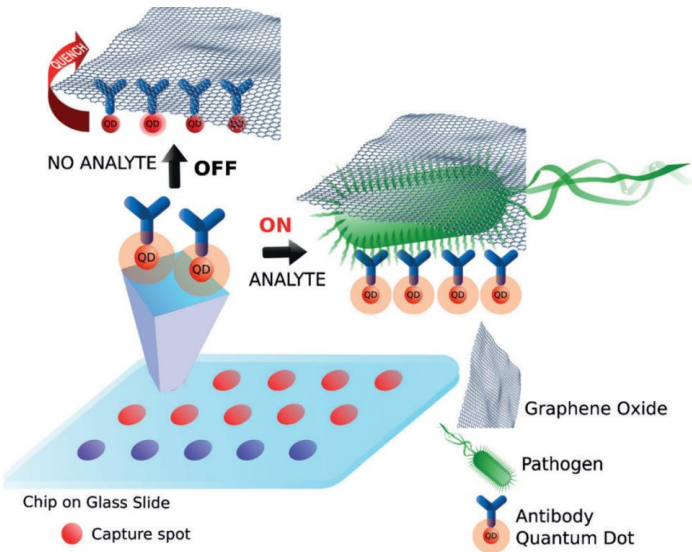

Figure 6. Operational concept of the nano-enabled system (illustration not to scale). The system relies on Ab-QD microarrays as a pathogen attachment mechanism. Once the pathogen is selectively captured onto the Ab-QD probes (which can be excited with a laser), they are coated with GO platelets that reveal the presence of the pathogen. In the presence of the pathogen, the quenching of the probes is minimal, as they barely interact with GO (ON state), whereas in the absence of the pathogen, the probes are quenched by electrostatic or π-π stacking interactions between the probes and GO (OFF state) (reproduced with permission from ref. 87, copyright 2013, John Wiley & Sons).

CONCLUSION AND OUTLOOKS

In conclusion, the current chapter discussed the great potential of graphene based materials for the possible application of food-pathogen diagnostics. Reported data from different groups have shown that outstanding electronic and plasmonic properties of hybrid graphene based materials are useful for food-pathogen labeling, imaging and diagnosis. Reported results clearly show that graphene based materials are going to make the essential tools that are necessary to face the food-pathogen infection challenges in 21st century. Though the use of graphene material for food-pathogen sensing is only just the beginning, scientists believe that it represents one of the highly promising areas of scientific inquiry into the food technology field. Though there are several advantages of using graphene based material for pathogen sensing, as we have discussed before, several challenges need to be solved before it will be useful for the society. Problems such as environmental stability, possible toxicity, nonspecific binding need to be addressed before it can be used for sensing in food technology field environments in presence of competing targets. We believe that after overcoming these issues, we can realize the dream of bringing graphene based technology to the real life food industry applications.

ACKNOWLEDGMENT

Dr. Ray thanks NSF-PREM grant # DMR-1205194, NSF-CREST grant # HRD-0833178 and NSF-RISE grant # HRD-1137763 for their generous funding

REFERENCES

[1] Vikesland, PJ; Wigginton, KR. Nanomaterial Enabled Biosensors for Pathogen Monitoring - A Review. *Environ. Sci. Technol*., 2010, 44, 3656–3669.
[2] http://fsrio.nal.usda.gov/pathogen-Biology.
[3] http://www.cdc.gov/foodsafety/investigations.html.
[4] http://www.efsa.europa.eu/en/topics/topic/foodbornezoonoticdiseases.htm.
[5] Singh, AK; Kanchanapally, R; Fan, Z; Senapati, D; Ray, PC. Synthesis of Highly Fluorescent Water-Soluble Silver Nanoparticles for Selective Detection of Pb(II) at the Parts per Quadrillion (PPQ) Level. *Chem. Commun*., 2012, 48, 9047–9049.
[6] Rosi, N. L; Mirkin, C. A. Nanostructures in Biodiagnostics. *Chem. Rev*., 2005, 105, 1547–1562.
[7] Shang, L; Dong, S; Nienhaus, GU. Ultra-Small Fluorescent Metal Nanoclusters: Synthesis and Biological Applications. *Nano Today*., 2011, 6, 401–418.
[8] Xie, P; Xiong, Q; Fang, Y; Qing, Q; Lieber, CM. Local Electrical Potential Detection of DNA by Nanowire-Nanopore Sensors. *Nat. Nanotechnol*., 2012, 7, 119–125.
[9] Alivisatos, P. The Use of Nanocrystals in Biological Detection. *Nat. Biotechnol*., 2004, 22, 47–52.
[10] Jain, KK. Nanotechnology in Clinical Laboratory Diagnostics. *Clin. Chim. Acta*., 2005, 358, 37–54.

[11] Daniel, MC; Astruc, D. Gold Nanoparticles: Assembly, Supramolecular Chemistry, Quantum-Size-Related Properties, and Applications toward Biology, Catalysis, and Nanotechnology. *Chem. Rev*., 2004, 104, 293–346.

[12] Fan, Z; Kanchanapally, R; Ray, PC. Hybrid Graphene Oxide Based Ultrasensitive SERS Probe for Label-Free Biosensing. *J. Phys. Chem. Lett*., 2013, 4, 3813–3818.

[13] Fan, Z; Senapati, D; Singh, AK; Ray, PC. Theranostic Magnetic Core–Plasmonic Shell Star Shape Nanoparticle for the Isolation of Targeted Rare Tumor Cells from Whole Blood, Fluorescence Imaging, and Photothermal Destruction of Cancer. *Mol. Pharm*., 2013, 10, 857–866.

[14] Kanchanapally, R; Fan, Z; Singh, AK; Sinha, SS; Ray, PC. Multifunctional Hybrid Graphene Oxide for Label-Free Detection of Malignant Melanoma from Infected Blood. *J. Mater. Chem. B*. 2014, 2, 1934–1937.

[15] Montet, X; Montet-Abou, K; Reynolds, F; Weissleder, R; Josephson, L. Nanoparticle Imaging of Integrins on Tumor Cells. *Neoplasia*., 2006, 8, 214–222.

[16] Kharat, DK; Muthurajan, H; Praveenkumar, B. Present and Futuristic Military Applications of Nanodevices. *Synth. React. Inorg. MetOrg. Nano-Met. Chem*., 2006, 36, 231–235.

[17] Thilagavathi, G; Raja, ASM; Kannaian, T. Nanotechnology and Protective Clothing for Defence Personnel. *Def. Sci. J*., 2008, 58, 451–459.

[18] Van de Groep, J; Spinelli, P; Polman, A. Transparent Conducting Silver Nanowire Networks. *Nano Lett*., 2012, 12, 3138–3144.

[19] Dean, CR; Young, AF; Meric, I; Lee, C; Wang, L; Sorgenfrei, S; Watanabe, K; Taniguchi, T; Kim, P; Shepard, KL; et al. Boron Nitride Substrates for High-Quality Graphene Electronics. *Nat. Nanotechnol*., 2010, 5, 722–726.

[20] Madaria, AR; Kumar, A; Zhou, C. Large Scale, Highly Conductive and Patterned Transparent Films of Silver Nanowires on Arbitrary Substrates and Their Application in Touch Screens. *Nanotechnology*., 2011, 22, 245201.

[21] Bae, S; Kim, H; Lee, Y; Xu, X; Park, JS; Zheng, Y; Balakrishnan, J; Lei, T; Ri Kim, H; Song, YI; et al. Roll-to-Roll Production of 30-Inch Graphene Films for Transparent Electrodes. *Nat. Nanotechnol*., 2010, 5, 574–578.

[22] Wang, ZL; García-Martínez, J. *Nanotechnology for the Energy Challenge*; John Wiley & Sons. 2013.

[23] Wang, ZL; Wu, W. Nanotechnology-Enabled Energy Harvesting for Self-Powered Micro-/Nanosystems. *Angew. Chem. Int. Ed*., 2012, 51, 11700–11721.

[24] Wu, ZS; Ren, W; Wen, L; Gao, L; Zhao, J; Chen, Z; Zhou, G; Li, F; Cheng, HM. Graphene Anchored with Co3O4 Nanoparticles as Anode of Lithium Ion Batteries with Enhanced Reversible Capacity and Cyclic Performance. *ACS Nano*., 2010, 4, 3187–3194.

[25] Inci, F; Tokel, O; Wang, S; Gurkan, UA; Tasoglu, S; Kuritzkes, DR; Demirci, U. Nanoplasmonic Quantitative Detection of Intact Viruses from Unprocessed Whole Blood. *ACS Nano*., 2013, 7, 4733–4745.

[26] Miranda, OR; Li, X; Garcia-Gonzalez, L; Zhu, ZJ; Yan, B; Bunz, UHF; Rotello, V. M. Colorimetric Bacteria Sensing Using a Supramolecular Enzyme–Nanoparticle Biosensor. *J. Am. Chem. Soc*., 2011, 133, 9650–9653.

[27] Saha, K; Agasti, SS; Kim, C; Li, X; Rotello, VM. Gold Nanoparticles in Chemical and Biological Sensing. *Chem. Rev*., 2012, 112, 2739–2779.

[28] Ling, X; Xie, L; Fang, Y; Xu, H; Zhang, H; Kong, J; Dresselhaus, M. S; Zhang, J; Liu, Z. Can Graphene Be Used as a Substrate for Raman Enhancement? *Nano Lett*., 2010, 10, 553–561.

[29] Murphy, S; Huang, L; Kamat, PV. Reduced Graphene Oxide–Silver Nanoparticle Composite as an Active SERS Material. *J. Phys. Chem. C*., 2013, 117, 4740–4747.

[30] Otto, A; Mrozek, I; Grabhorn, H; Akemann, W. Surface-Enhanced Raman Scattering. *J. Phys. Condens. Matter*., 1992, 4, 1143–1212.

[31] Persson, BNJ; Zhao, K; Zhang, Z. Chemical Contribution to Surface-Enhanced Raman Scattering. *Phys. Rev. Lett*., 2006, 96, 207401.

[32] Otto, A. The "chemical" (electronic) Contribution to Surface-Enhanced Raman Scattering. *J. Raman Spectrosc*., 2005, 36, 497–509.

[33] Ichii, T; Hosokawa, Y; Kobayashi, K; Matsushige, K; Yamada, H. Molecular-Resolution Imaging of Lead Phthalocyanine Molecules by Small Amplitude Frequency Modulation Atomic Force Microscopy Using Second Flexural Mode. *Appl. Phys. Lett*., 2009, 94, 133110.

[34] Uehara, Y; Ushioda, S. Single Molecule Spectrum of Rhodamine 6G on Highly Oriented Pyrolytic Graphite. *Appl. Phys. Lett*., 2005, 86, 181905.

[35] Humbert,. Molecular C; Volcke, C; Sartenaer, Y; Peremans, A; Thiry, PA; Dreesen, L. Conformation and Electronic Properties of Protoporphyrin-IX Self-Assembled Monolayers Adsorbed on a Pt(1 1 1) Surface. *Surf. Sci*., 2006, 600, 3702–3709.

[36] Sariciftci, NS; Heeger, AJ; Krasevec, V; Venturini, P; Mihailovic, D; Cao, Y; Libert, J; Brédas, JL. Symmetry-Specific Electron-Phonon Coupling for Electronic States near the Fermi Energy of Metallic Polyaniline: Resonant Raman Scattering. *Synth. Met*., 1994, 62, 107–112.

[37] Lin, D; Qin, T; Wang, Y; Sun, X; Chen, L. Graphene Oxide Wrapped SERS Tags: Multifunctional Platforms toward Optical Labeling, Photothermal Ablation of Bacteria, and the Monitoring of Killing Effect. *ACS Appl. Mater. Interfaces*. 2014, 6, 1320–1329.

[38] Xu, W; Xiao, J; Chen, Y; Chen, Y; Ling, X; Zhang, J. Graphene-Veiled Gold Substrate for Surface-Enhanced Raman Spectroscopy. *Adv. Mater*., 2013, 25, 928–933.

[39] Premasiri, WR; Moir, DT; Klempner, MS; Krieger, N; Jones, G; Ziegler, LD. Characterization of the Surface Enhanced Raman Scattering (SERS) of Bacteria. *J. Phys. Chem. B*., 2005, 109, 312–320.

[40] Wang, Y; Lee, K; Irudayaraj, J. Silver Nanosphere SERS Probes for Sensitive Identification of Pathogens. *J. Phys. Chem. C*., 2010, 114, 16122–16128.

[41] Shaymurat, T; Tang, Q; Tong, Y; Dong, L; Liu, Y. Gas Dielectric Transistor of CuPc Single Crystalline Nanowire for SO2 Detection Down to Sub-Ppm Levels at Room Temperature. *Adv. Mater*., 2013, 25, 2269–2273.

[42] Zhao, X; Cai, B; Tang, Q; Tong, Y; Liu, Y. One-Dimensional Nanostructure Field-Effect Sensors for Gas Detection. *Sensors*., 2014, 14, 13999–14020.

[43] Trung, TQ; Tien, NT; Kim, D; Jung, JH; Yoon, OJ; Lee, NE. High Thermal Responsiveness of a Reduced Graphene Oxide Field-Effect Transistor. *Adv. Mater*., 2012, 24, 5254–5260.

[44] Avouris, P. Graphene: Electronic and Photonic Properties and Devices. *Nano Lett*., 2010, 10, 4285–4294.

[45] Mohanty, N; Berry, V. Graphene-Based Single-Bacterium Resolution Biodevice and DNA Transistor: Interfacing Graphene Derivatives with Nanoscale and Microscale Biocomponents. *Nano Lett*., 2008, 8, 4469–4476.

[46] Chang, J; Mao, S; Zhang, Y; Cui, S; Zhou, G; Wu, X; Yang, CH; Chen, J. Ultrasonic-Assisted Self-Assembly of Monolayer Graphene Oxide for Rapid Detection of Escherichia Coli Bacteria. *Nanoscale*., 2013, 5, 3620.

[47] Huang, Y; Dong, X; Liu, Y; Li, LJ; Chen, P. Graphene-Based Biosensors for Detection of Bacteria and Their Metabolic Activities. *J. Mater. Chem*., 2011, 21, 12358.

[48] Basu, PK; Indukuri, D; Keshavan, S; Navratna, V; Vanjari, SRK; Raghavan, S; Bhat, N. Graphene Based E. Coli Sensor on Flexible Acetate Sheet. *Sens. Actuators B Chem*., 2014, 190, 342–347.

[49] Kotchey, GP; Allen, BL; Vedala, H; Yanamala, N; Kapralov, AA; Tyurina, YY; Klein-Seetharaman, J; Kagan, VE; Star, A. The Enzymatic Oxidation of Graphene Oxide. *ACS Nano*., 2011, 5, 2098–2108.

[50] Vedala, H; Sorescu, DC; Kotchey, GP; Star, A. Chemical Sensitivity of Graphene Edges Decorated with Metal Nanoparticles. *Nano Lett*., 2011, 11, 2342–2347.

[51] Chen, Y; Michael, ZP; Kotchey, GP; Zhao, Y; Star, A. Electronic Detection of Bacteria Using Holey Reduced Graphene Oxide. *ACS Appl. Mater. Interfaces*., 2014, 6, 3805–3810.

[52] Kulagina, NV; Shaffer, KM; Anderson, GP; Ligler, FS; Taitt, CR. Antimicrobial Peptide-Based Array for Escherichia Coli and Salmonella Screening. *Anal. Chim. Acta*., 2006, 575, 9–15.

[53] Kulagina, NV; Lassman, ME; Ligler, FS; Taitt, CR. Antimicrobial Peptides for Detection of Bacteria in Biosensor Assays. *Anal. Chem*., 2005, 77, 6504–6508.

[54] Zasloff, M. Antimicrobial Peptides of Multicellular Organisms. *Nature*., 2002, 415, 389–395.

[55] Strauss, J; Kadilak, A; Cronin, C; Mello, CM; Camesano, TA. Binding, Inactivation, and Adhesion Forces between Antimicrobial Peptide Cecropin P1 and Pathogenic E. Coli. *Colloids Surf. B Biointerfaces*., 2010, 75, 156–164.

[56] Wan, Y; Lin, Z; Zhang, D; Wang, Y; Hou, B. Impedimetric Immunosensor Doped with Reduced Graphene Sheets Fabricated by Controllable Electrodeposition for the Non-Labelled Detection of Bacteria. *Biosens. Bioelectron*., 2011, 26, 1959–1964.

[57] Wang, Z; Zhang, J; Chen, P; Zhou, X; Yang, Y; Wu, S; Niu, L; Han, Y; Wang, L; Chen, P; et al. Label-Free, Electrochemical Detection of Methicillin-Resistant Staphylococcus Aureus DNA with Reduced Graphene Oxide-Modified Electrodes. *Biosens. Bioelectron*., 2011, 26, 3881–3886.

[58] Kasha, M. Characterization of Electronic Transitions in Complex Molecules. *Discuss. Faraday Soc*., 1950, 9, 14–19.

[59] Loh, KP; Bao, Q; Eda, G; Chhowalla, M. Graphene Oxide as a Chemically Tunable Platform for Optical Applications. *Nat. Chem*., 2010, 2, 1015–1024.

[60] Eda, G; Lin, YY; Mattevi, C; Yamaguchi, H; Chen, HA; Chen, IS; Chen, CW; Chhowalla, M. Blue Photoluminescence from Chemically Derived Graphene Oxide. *Adv. Mater*., 2010, 22, 505–509.

[61] Pramanik, A; Fan, Z; Chavva, SR; Sinha, SS; Ray, PC. Highly Efficient and Excitation Tunable Two-Photon Luminescence Platform For Targeted Multi-Color MDRB Imaging Using Graphene Oxide. *Sci. Rep*., 2014, 4.

[62] Exarhos, AL; Turk, ME; Kikkawa, JM. Ultrafast Spectral Migration of Photoluminescence in Graphene Oxide. *Nano Lett*., 2013, 13, 344–349.
[63] Cushing, SK; Li, M; Huang, F; Wu, N. Origin of Strong Excitation Wavelength Dependent Fluorescence of Graphene Oxide. *ACS Nano*. 2014, 8, 1002–1013.
[64] Li, JL; Bao, HC; Hou, XL; Sun, L; Wang, XG; Gu, M. Graphene Oxide Nanoparticles as a Nonbleaching Optical Probe for Two-Photon Luminescence Imaging and Cell Therapy. *Angew. Chem. Int. Ed*., 2012, 51, 1830–1834.
[65] Shang, J; Ma, L; Li, J; Ai, W; Yu, T; Gurzadyan, G. G. The Origin of Fluorescence from Graphene Oxide. *Sci. Rep*., 2012, 2.
[66] Albota, MA; Xu, C; Webb, WW. Two-Photon Fluorescence Excitation Cross Sections of Biomolecular Probes from 690 to 960 Nm. *Appl. Opt*., 1998, 37, 7352–7356.
[67] Xu, C; Zipfel, W; Shear, JB; Williams, RM; Webb, WW. Multiphoton Fluorescence Excitation: New Spectral Windows for Biological Nonlinear Microscopy. *Proc. Natl. Acad. Sci*., 1996, 93, 10763–10768.
[68] Zipfel, WR; Williams, RM; Webb, WW. Nonlinear Magic: Multiphoton Microscopy in the Biosciences. *Nat. Biotechnol*., 2003, 21, 1369–1377.
[69] Larson, DR; Zipfel, WR; Williams, RM; Clark, SW; Bruchez, MP; Wise, FW; Webb, WW. Water-Soluble Quantum Dots for Multiphoton Fluorescence Imaging in Vivo. *Science*. 2003, 300, 1434–1436.
[70] Kim, J; Cote, LJ; Kim, F; Huang, J. Visualizing Graphene Based Sheets by Fluorescence Quenching Microscopy. *J. Am. Chem. Soc*., 2010, 132, 260–267.
[71] Abdelhamid, HN; Wu, HF. Multifunctional Graphene Magnetic Nanosheet Decorated with Chitosan for Highly Sensitive Detection of Pathogenic Bacteria. *J. Mater. Chem. B*. 2013, 1, 3950–3961.
[72] Liao, Y; Zhou, X; Xing, D. Quantum Dots and Graphene Oxide Fluorescent Switch Based Multivariate Testing Strategy for Reliable Detection of Listeria Monocytogenes. *ACS Appl. Mater. Interfaces*. 2014, 6, 9988–9996.
[73] Schuler, B; Lipman, EA; Steinbach, PJ; Kumke, M; Eaton, WA. Polyproline and the "spectroscopic Ruler" Revisited with Single-Molecule Fluorescence. *Proc. Natl. Acad. Sci. U. S. A*., 2005, 102, 2754–2759.
[74] Ray, PC; Fan, Z; Crouch, RA; Sinha, SS; Pramanik, A. Nanoscopic Optical Rulers beyond the FRET Distance Limit: Fundamentals and Applications. *Chem. Soc. Rev*., 2014, 43, 6370–6404.
[75] Vendrell, M; Zhai, D; Er, JC; Chang, YT. Combinatorial Strategies in Fluorescent Probe Development. *Chem. Rev*., 2012, 112, 4391–4420.
[76] Thomas, SW; Joly, GD; Swager, TM. Chemical Sensors Based on Amplifying Fluorescent Conjugated Polymers. *Chem. Rev*., 2007, 107, 1339–1386.
[77] Stryer, L. Fluorescence Energy Transfer as a Spectroscopic Ruler. *Annu. Rev. Biochem*., 1978, 47, 819–846.
[78] Georgakilas, V; Otyepka, M; Bourlinos, AB; Chandra, V; Kim, N; Kemp, KC; Hobza, P; Zboril, R; Kim, KS. Functionalization of Graphene: Covalent and Non-Covalent Approaches, Derivatives and Applications. *Chem. Rev*., 2012, 112, 6156–6214.
[79] Swathi, RS; Sebastian, KL. Resonance Energy Transfer from a Dye Molecule to Graphene. *J. Chem. Phys*., 2008, 129, 054703.

[80] Swathi, R. S; Sebastian, K. L. Long Range Resonance Energy Transfer from a Dye Molecule to Graphene Has (distance)−4 Dependence. *J. Chem. Phys*., 2009, 130, 086101.

[81] Huang, PJJ; Liu, J. DNA-Length-Dependent Fluorescence Signaling on Graphene Oxide Surface. *Small*. 2012, 8, 977–983.

[82] Wang, Y; Li, Z; Hu, D; Lin, CT; Li, J; Lin, Y. Aptamer/Graphene Oxide Nanocomplex for in Situ Molecular Probing in Living Cells. *J. Am. Chem. Soc*., 2010, 132, 9274–9276.

[83] Selvin, PR. The Renaissance of Fluorescence Resonance Energy Transfer. *Nat. Struct. Mol. Biol*., 2000, 7, 730–734.

[84] Lin, TN; Huang, LT; Shu, GW; Yuan, CT; Shen, JL; Lin, CAJ; Chang, WH; Chiu, CH; Lin, DW; Lin, CC; et al. Distance Dependence of Energy Transfer from InGaN Quantum Wells to Graphene Oxide. *Opt. Lett*., 2013, 38, 2897–2899.

[85] Morales-Narváez, E; Merkoçi, A. Graphene Oxide as an Optical Biosensing Platform. *Adv. Mater*., 2012, 24, 3298–3308.

[86] Morales-Narváez, E; Pérez-López, B; Pires, LB; Merkoçi, A. Simple Förster Resonance Energy Transfer Evidence for the Ultrahigh Quantum Dot Quenching Efficiency by Graphene Oxide Compared to Other Carbon Structures. *Carbon*. 2012, 50, 2987–2993.

[87] Morales-Narváez, E; Hassan, AR; Merkoçi, A. Graphene Oxide as a Pathogen-Revealing Agent: Sensing with a Digital-Like Response. *Angew. Chem. Int. Ed*., 2013, 52, 13779–13783.

[88] Somers, RC; Bawendi, MG; Nocera, DG. CdSe Nanocrystal Based Chem-/bio- Sensors. *Chem. Soc. Rev*., 2007, 36, 579–591.

[89] Kusnezow, W; Syagailo, YV; Rüffer, S; Klenin, K; Sebald, W; Hoheisel, JD; Gauer, C; Goychuk, I. Kinetics of Antigen Binding to Antibody Microspots: Strong Limitation by Mass Transport to the Surface. *PROTEOMICS*. 2006, 6, 794–803.

In: Food Poisoning
Editor: Paresh C. Ray
ISBN: 978-1-63463-166-2

Chapter 5

PLASMONIC NANO-PROBE AND NANO-MEDICINE FOR SELECTIVE DETECTION, ULTRASENSITIVE QUANTIFICATION, AND UNTRENDY TREATMENT FOR FOOD-BORNE BACTERIAL INFECTION

Dulal Senapati*
Nanophotonics Group, Chemical Sciences Division,
Saha Institute of Nuclear Physics, Bidhannagar, Kolkata, India

ABSTRACT

Food-borne bacterial infection is one of the most serious threats to public health and comprise a large part of the global mortality burden. Despite the tremendous development of standardized treatment protocols, food poisoning due to bacterial infection is still very common. Driven by the needs of the society, large scale production of processed food and associated bacterial infections sometimes create food-borne disease outbreaks. Along with this large scale food-born bacterial infections, several different strains of these bacterial pathogens are becoming resistant to drug, heat, and to pH. Due to this increasing resistance, usual medications for the destruction is no more suitable in the context of present scenario. Recent advancement in nanoscience and nanotechnology has expanded our ability to design and construct nanomaterials with selective targeting, effective therapeutic, and efficient diagnostic functions. With the emergence of nanoscience & nanotechnology and the ability to make tailored plasmonic nanomaterials suitable for efficient light harvest, we are now in a position to offer several plasmonic nano-probes for rapid and cost effective sensing of food-borne pathogens suitable for field application to beat the urgency and universality respectively. More interestingly, this advancement of nano-probes also gives the ray of hope to design nano-medicine for the future to destruct these pathogens not only in the large scale but will also be suitable for multi-resistant (drug, heat, pH, etc.) bacteria. This chapter describes different established plasmonic nanomaterials-based optical and spectroscopic techniques

* Corresponding author: Email: dulal.senapati@saha.ac.in.

for strain-specific detection, ultra-sensitive quantification, and efficient destruction of different food-borne bacteria.

1. INTRODUCTION

Bacterial infection is the major cause of food-borne diseases (FBD) throughout the world and is one of the most serious threats to public health for decades and remains a major public health challenge even in the 21st century. FBD comprise a large part of the global mortality burden, though the true extent of their impact is unknown due to innumerable unreported cases and inefficient health record system of the developing countries. Food-borne diseases have devastating health and economic impact in both developed and developing countries. World Health Organization (WHO)[1] estimates the full extent and cost of the disease burden associated with FBD and pointed it out as an important cause of morbidity and mortality worldwide. Diarrhoeal disease alone - a considerable proportion of which is food-borne, kills 1.9 million children globally every year. FBD in United states alone results 76 million illness, 325000 hospitalizations, and ~5000 deaths each year [2]. With every bite we eat, each drop we drink, and all breath we draw, we might expose ourselves to illness from either microbial or chemical contamination. Out of several microbial infections (bacteria, virus, amoeba, protozoa, etc.) bacterial infection is the most common cause for food poisoning and results outbreak and adverse health effects. Estimates of the economic cost of food-borne illness play an important role in guiding food safety policy. Two 2012 studies of the cost of food-borne illness in the United States-one conducted by researchers from Economic Research Service (ERS), US Department of Agriculture and the University of Florida and the other by a researcher from Ohio State University-agree on which food-borne pathogens are the costliest in terms of medical care, lost time from work, and losses due to premature death. The studies find that *Salmonella* (non-typhoidal) and *Toxoplasma gondii* are the first and second costliest food-borne pathogens, followed by *Listeria monocytogenes*, Norovirus, and *Campylobacter*. Out of these five pathogens, four of them are bacterial pathogens (except Norovirus). Together, these five pathogens account for over 85 percent of the estimated costs for illnesses caused by the 14 major food-borne pathogens. ERS estimates that the total food-borne costs by these 14 pathogens in US about $14.6 billion (updated to 2010 $ price)[3]. Other common bacteria thatcauses the most illness, hospitalization, and death are *E. coli, Clostridium perfringens, Clostridium botulinum, Streptococcus A, Sigella, and Staphylococcus aureus* [4]. The worldwide food-production industry is worth about US$578 billion and food recalls due to the presence of food-borne bacteria are becoming a nightmare for the food industry [5,6]. Currently there are several well established bacteria detection techniques are available in the market which include polymerase chain reaction (PCR) [7], enzyme-linked immunosorbent assay (ELISA)[8], Fourier transform infrared spectroscopy [9], mass spectrometry [10]. Their slow response, time consuming and labour intensive sample preparation, and initial establishment cost limit their ability to detect food-borne bacteria in a multiplex format [11-19]. As a consequence, the demand to develop a rapid, sensitive, and highly specific method capable of simultaneous detection of several food-borne bacteria is growing day-by-day. Most of the bacteria that are major cause of food-borne disease are generally transmitted to humans through consumption of contaminated food of animal origin, mainly meat, poultry, eggs, milk, etc. and minimum infection dose can harm badly which may become life-threatening.

To stop fast spreading of bacterial infection and rapid assessment of the outbreak data from the remote sites we urgently need a sustainable ultrasensitive sensing technology for global food safety which has a direct impact on the world economy [5]. These new technologies should work in a multiplex format capable of simultaneous detection of multiple bacteria of interest in a time saving and cost effective way [21]. To address this issue, multiplexed PCR, DNA microarray techniques, and array-based immuno-sensors have been developed to identify two to three food-borne pathogens in one assay [21-25]. Nanoparticle-based biosensors have also been developed using magnetic nanoparticles [26-29], silver nanoparticles [30-32], and silver nanoshells [33] to detect pathogens. However, these methods have a limited ability to detect multiple organisms. More recently, triple-dye-doped fluorescent silica nanoparticles [34] and quantum dots (QDs) [35] have been used for detecting multiple bacteria. However, the fluorescent detection modality requires the use of fluorescent probes and is typically susceptible to photo bleaching and careless handling, sometimes requiring specific excitations for sensitive detection, while QDs are difficult to synthesize, toxic, expensive, and surface modification is not trivial. Compared to these, there are several reports based on gold nanoparticle-based optical and spectroscopic techniques [20,36-39] developed in the last two decades or so for ultrasensitive, highly specific, rapid, and non toxic assay for accurate sensing and diagnosis of a specific bacteria in uniplex or multiplex pattern from environmental samples which has direct influence in the modern age food safety regulation, as well as world economy. Though the FBD being a overgrown concern in the modern days, clusters of cases reported which closely resemble to the known adverse effects of bacterial infection even in the 1940s and 1950s, much before their identification [8c]. There is an increase in new food-borne pathogens (toxin-producing strains) in the recent years, possibly due to improved bio analytical detection techniques or could be gene-swapping (or DNA-swapping) among bacteria for better resistance. Gene swapping could be due to several different conditions, which include (i) change in farming practice, (ii) multi-species farming, (iii) excessive use of preservation, or even (iv) change in environmental condition. There are increasing reports on drug resistant, thermal resistant, or even chemical resistant bacteria to increase our problem for our regulatory system. There is an urgent need for better understanding of the survival mechanism of bacteria than making their antidotes, otherwise "we could be storing up problems for ourself"[8c] as large number of these pathogens are now part of their normal flora.

In this article, I reviewed different types of food-borne bacterial species and their possible adverse health effect; existing nano-materials based optical and spectroscopic techniques for detection, diagnosis, and quantification; reliability of nano-probes against the standard kits; untrendy treatment for food-borne bacterial infection. More stress will be given on the recent development of new ultra sensitive optical and spectroscopic techniques for bacterial detection, principle of these detection techniques, and nanomaterials-based untrendy treatment for the future.

2. EMERGING FOOD-BORNE BACTERIA

The epidemiology of food-borne infections throughout the globe has remarkably changed during the past two decade and an increasing number of bacteria or genetic variant or subtype

of a bacteria have been associated with human infections. Several different practices of food processing or protocols for food preservation in the past known to be safe from bacterial infection is no more secure for intake in the present day. This is due to their continual mutation or gene swapping to make them resistant over those protecting conditions. These protecting conditions could be (i) antibiotics: force them to transform into drug resistant bacteria (e.g., salmonella DT104)[37,8c], (ii) heating: forces them to transform into temperature resistant bacteria (e.g., E. *coli* 0111 and strains of Salmonella entrica)[8c], (iii) pH: acid resistant bacteria (O157:H7 strain of E. *coli* now can survive in acidic condition which supposed to be a condition for safe food. The marked acidic and environmental resistance of *E. coli* O157[40,41] also allowed the organism to survive in apple cider and dried venison jerky.). Internal contamination of intact eggs by *Salmonella enteritidis* is a peculiar ecological niche of Salmonella serotype in egg-laying flocks [42]. Though most bacterial outbreaks related to minced meat products, mincing allows bacteria being transferred to the interior of such products where they can survive even after cooking. Not only meat product, bacterial food infection can occur through egg, fish, milk, fruit juice, vegetables, or even through water. Along with the food-borne bacterial infection from individual food products, untreated animal dejections as fertilizer can cause serious bacterial contamination in vegetable items from large farms [43,44]. Fresh products like lettuce, tomatoes, coleslaw, and berries are established or potential vehicles of Shiga-toxin producing E. *coli* (STEC) infection [43,44]. Although most strains of E. *coli* are harmless, others can make serious outbreaks. There are six pathogenic E. *coli* associated with diarrhoea while others can cause urinary tract infections, respiratory illness, pneumonia, and other infections [45]. Six diarrheal E. *coli* strains are: (i) Shiga toxin-producing *E. coli* (STEC))—STEC may also be referred to as Verocytotoxin-producing *E. coli* (VTEC) or enterohemorrhagic *E. coli* (EHEC) or E. *coli* O157:H7, (ii) Enterotoxigenic *E. coli* (ETEC), (iii) Enteropathogenic *E. coli* (EPEC), (iv) Enteroaggregative *E. coli* (EAEC), (v) Enteroinvasive *E. coli* (EIEC), and (vi) Diffusely adherent *E. coli* (DAEC).

Similar to *E.coli*, *Salmonella* is another group of bacteria that causes most common food poisoning throughout the world especially for older adults, infants, and persons with chronic disease [46]. Proper cooking and pasteurization can remove *Salmonella* completely from food. Common symptoms are diarrhoea, fever, abdominal cramps, and vomiting. It is estimated that tens of millions of human cases occur worldwide every year and the disease results in more than hundred thousand deaths. For *salmonella* species, over 2500 different strains (called "serotypes" or "serovars") have been identified to date. *Salmonella* is a ubiquitous and can survive several weeks in a dry environment and several months in water [5]. Different strains of *Salmonella* are categorized based on the presence of specific antigen set. There are five most common *Salmonella* strains in food-borne illness outbreaks [47] and these are:

(i) *SalmonellaEnteritidis*: This specific serotype most often associated with poultry. *Salmonella Enteritidis* infects the gastrointestinal tract of poultry. *Salmonella* is passed from bird to bird in several ways, most commonly through fecal matter. Based on U.S. Centers for Disease Control and Prevention (CDC) data, *Enteritidis* outbreaks since 2010 were linked to shell eggs, alfalfa sprouts, pine nuts and ground beef.

(ii) *SalmonellaTyphimurium*: *Typhimurium* is the second most common serotype associated with food-borne illness and the third most frequently identified with chicken. This serotype is also linked to ground beef, pork and other poultry products. *Typhimurium* has proven to be antibiotic-resistant, which makes eliminating the pathogen from food products very challenging. Discussion on drug resistance bacteria will be provided in the later sections of this chapter. Unlike other serotypes that populated the intestinal tract of animals, *Typhimurium* might be in the lymph system of cattle. Research is ongoing. The CDC list of outbreaks associated with *Typhimurium* since 2006 show the following as sources: ground beef, hedge hogs, cantaloupes, peanut butter, tomatoes and African dwarf and water frogs.

(iii) *SalmonellaNewport*: *Newport* is currently the third most common *Salmonella* serotype associated with food-borne illness. This strain is most often associated with turkey products. Like *Typhimurium*, it has been determined to be antibiotic-resistant. In the fall of 2012, *Salmonella Newport* and *Typhimurium* were found in cantaloupe. The outbreak led to three deaths and more than 250 illnesses in 24 states of USA. In addition to cantaloupe, live poultry and alfalfa sprouts have been linked to Newport outbreaks since 2010.

(iv) *SalmonellaJaviana*: *Javiana* is the fourth most common serotype associated with food-borne illness. This serotype is associated with exposure to amphibians in the Southeast U.S. It has also been linked to contaminated mozzarella cheese, watermelon, bass, poultry, lettuce and tomatoes. CDC has not reported a multistate outbreak associated with *Javiana* since 2006.

(v) *SalmonellaHeidelberg*: *Heidelberg* is the fifth most common *Salmonella* serotype associated with food-borne illness and the second most frequently associated with human health issues and poultry, according to a recent report from Food Safety and Inspection Service (FSIS). *Salmonella Heidelberg* has caused recent poultry recalls and food-borne illness outbreaks. In March 2013, 128 illnesses in USA were linked to *Heidelberg* in chicken meat. It is also found in shell eggs.

Listeria is another class of food-borne bacteria which can cause serious outbreaks most commonly found in soil and water and in some animals which includes cattle and poultry. This causes common infection in raw milk, milk products, and processed meats. Main concern of *Listeria* outbreak is its ability to grow even in the cold refrigerated temperature. Like *Salmonella*, *Listeria* can be removed by cooking and pasteurization. Common symptoms of *Listeria* infection are Fever, stiff neck, confusion, weakness, vomiting, sometimes preceded by diarrhea and mostly affected to older adults, pregnent women, persons with immune deficiency, organ transplant patients, or people with certain disease, like HIV/AIDS, cancer, end-stage-renal disease, liver disease, alcoholism, diabetes, etc. Though there are several strains of *Listeria* have been isolated, few of them been reported to cause human *Listeriosis* outbreak. Most common stains to cause food-borne outbreaks are as follows:

(i) *ListeriaJ0161, FSL R2-499*: caused human listeriosis outbreak in 2000 linked to consumption of sliced turkey [48].

(ii) *Listeria10403S*: 10403S is a streptomycin resistant strain of *Listeria*. This strain causes unusual bacterial disease, listeriosis, a serious infection caused by eating food contaminated with the bacteria and affects primarily to pregnant women, newborn, adults with weak immune system [49,50].
(iii) *Listeria FSL J1-194*: This strain has been linked to two human listeriosis outbreaks and is also responsible for a number of sporadic human listeriosis outbreaks.
(iv) *Listeria FSL R2-503*: Particular strain was responsible for a gastrointestinal listeriosis outbreak in the US in 1994. Analysis of this strain will provide insight into the differences between strains causing systemic versus diarrheal disease.
(v) *ListeriaJ2818*: Human listeriosis outbreak in 2000 was linked to consumption of sliced turkey with J2818 infection [48].

Campilobacter is another most common bacterium for food poisoning. The vast majority of cases occurs as isolated events, not as part of recognized outbreaks [5]. Most common sources of contamination are raw and undercooked poultry, unpasteurized milk, and contaminated water. Common symptoms are diarrhoea, cramps, fever, and vomiting; diarrhoea could be bloody. Frequency of infection is ~14/100,000 persons in the population. Many more cases go undiagnosed or unreported, and campylobacteriosis is estimated to affect over 1.3 million persons every year. Campylobacteriosis occurs much more frequently in the summer months than in the winter and affects more to infant and young males. Although *Campylobacter* infection does not commonly cause death, it has been estimated that approximately 76 persons with *Campylobacter* infections die each year. Though *Campylobacter* has several species, most human illness is caused by one species, called *Campylobacter Jejuni*. *Campylobacter jejuni* grows best at 37°C to 42°C, the approximate body temperature of a bird (41°C to 42°C), and seems to be well adapted to birds, who carry it without becoming ill. These bacteria are spiral-shaped and fragile. They cannot tolerate drying and can be killed by oxygen. They grow only in places with less oxygen than the amount in the atmosphere. Freezing reduces the number of *Campylobacter* bacteria on raw meat [51].

Clostridium perfringens or C. perfringens is also a common bacterium to cause food poisoning throughout the world and causes nearly a million illness every year. Cooking kills the growing *C. perfringens* cells that cause food poisoning, but not necessarily the spores that can grow into new cells. If cooked food is not promptly served or refrigerated, the spores can grow and produce new cells. These bacteria thrive between 40-140˚F (the "Danger Zone"). This means that they grow quickly at room temperature, but they cannot grow at refrigerator or freezer temperatures. It prefers to grow in conditions with very little or no oxygen, and under ideal conditions can multiply very rapidly. *C. perfringens* infections often occur when the food is prepared in large quantities and then is kept warm for a long time before serving. That's why outbreaks of these infections are usually linked to institutions (such as hospitals, school cafeterias, prisons, and nursing homes) or events with catered food. Common sources of infection are beef, poultry, and gravies and the general symptoms of infection are diarrhoea and abdominal pain but without fever and vomiting. The illness usually begins suddenly and lasts for less than 24 hours and most affected the very young and the elderly people. Some strains of *C. perfringens* produce a toxin in the intestine that causes illness [52].

3. PLASMONIC NANO-MATERIALS BASED OPTICAL AND SPECTROSCOPIC TECHNIQUES FOR DETECTION, DIAGNOSIS, AND QUANTIFICATION OF BACTERIA

Various different techniques are available in laboratories for pathogenic bacteria detection and identification, including (i) plating and culturing [53], (ii) luminescence [54], (iii) immunological approaches [53b-c], (iv) nucleic acid probe-based methods [7] (PCR, LCR), (v) mass spectrometry [10], (vi) microarrays [53f], and (vii) biosensors [53g-h]. Each of these systems has its advantages; however the utility of these methods is generally limited by their high cost for use and the requirement of trained operators. Compared to these techniques, recent advancement in the field of nanoscience and nanotechnology offers a rapid and cost effective sensing of food-borne pathogen suitable for field application to beat the urgency and universality respectively. It is the proven fact that there is an increased interaction between nanoscience & nanotechnology and biological science in the last couple of decades. Though there is a broad spectrum of diverse nanomaterials, noble metal (mainly Au, Ag, and Cu) nanostructures especially attract much interest because of their unique properties, including large optical field enhancements resulting in the strong scattering and absorption of light [20,39f-i,55-76]. In the last 15 years, the field of biosensors using nanomaterial has witnessed an explosion of interest for small analytes, DNA/RNA, and pathogen detection [20,39f-i,55-76]. In terms of sensing, the use of nanotechnology has led to the production of numerous, rapid, sensitive multianalyte assays which are useful not only in the laboratory but also in the field as portable instruments [20,39f-i,55-76]. Due to the increased availability of nanostructures with highly controlled optical properties, nanosystems are attractive in their use in technological systems for diagnostic applications. Gold and silver nanosystems attract much interest because of their unique properties, including their shape and size-dependent optical properties. Due to the lack of toxicity [20,39f-i,55-79], scientists have shown great interest in using gold nanosystems for sensing and imaging. Besides plasmonic nanomaterials, semiconductor materials which generally used for macroscopic optical and electrical sensor, can now be made on the size scale of individual biological macromolecules. In the last few decades, extensive research in the field of nanomaterials synthesis has allowed us to make many tailored nanomaterials that could be size variable or shape variable. Due to this size and shape variation ability, we can now either decorate the surface of a pathogen (e.g. bacteria) by nanomaterials or pathogens (e.g. virus) can be decorated on the surface of a nanomaterial to utilize the near-field-electromagnetic field enhancement technology for optical and spectroscopic diagnosis of pathogens. The dimension of bacteria can vary a lot in the range of 0.5μm to even 750μm depending on their types. Not only size but also bacteria have a variable shape like most common cocci have round shape with dimension 0.5-1μm, second most common bacilli have rod shape with 0.5-1μm in breadth and 1-4μm in length, and third most common are spiral bacteria with 1-100μm in length. Besides that there are several giant bacteria, like *Epulopiscium fishelsoni* which has a bacillus shape and measures 80 micrometers in diameter while the length of the organism can measure from 200 to 600 micrometers, and the *Thiomargarita namibiensis*, a coccus that measures from 100 to 750 micrometers in diameter. These bacteria can sometimes be seen by the naked eye when in their largest sizes. Due to their large size we can decorate the bacteria

surface by thousands to millions of nanoparticles. Along with the inorganic nanomaterials, considerable advances have been observed in the field of polymeric, dendritic [80], and organic nanostructures. Although all these nanomaterials can influence the enhanced sensing of specific food-borne bacteria, this discussion will be limited to the plasmonic nanomaterials only. In physics, a plasmon is a quanta of plasma oscillation. The plasmon can be considered a quasiparticle since it arises from the quantization of plasma oscillations, just like phonons are quantization of mechanical vibrations. Thus, plasmons are collective oscillations of the free electron gas density and the nanomaterials which show plasma oscillation are called plasmonic nanomaterials. For plasmonic nanomaterials, incident light can couple to the plasmon excitation of the metal, which involves the light-induced motion of all the valance electrons [81]. As a result of this, the cross-section for absorption and scattering from a nanoparticle increases several orders compared to organic chromophores. Along with this, nanomaterial's size and shape dependent properties [82-86], hyper quenching activities [59,66,87-96], extra ordinary nonlinear activity [38d,97], and ease of surface modification [20,36-37, 38d] make them versatile tool kit for biological detection. Electromagnetic field in the near-field region around a plasmonic nanoparticle is greatly enhanced and provides important new ways of sensitive detection. In this chapter, we will focus mainly on different nanomaterials-based optical and spectroscopic detection of food-borne bacteria which include colorimetric method, surface enhancer Raman scattering (SERS) technique, localized surface plasmon (LSP) based sensing, fluorescence-based quenching (or nano-surface energy transfer, NSET), and non-linear-optics based techniques.

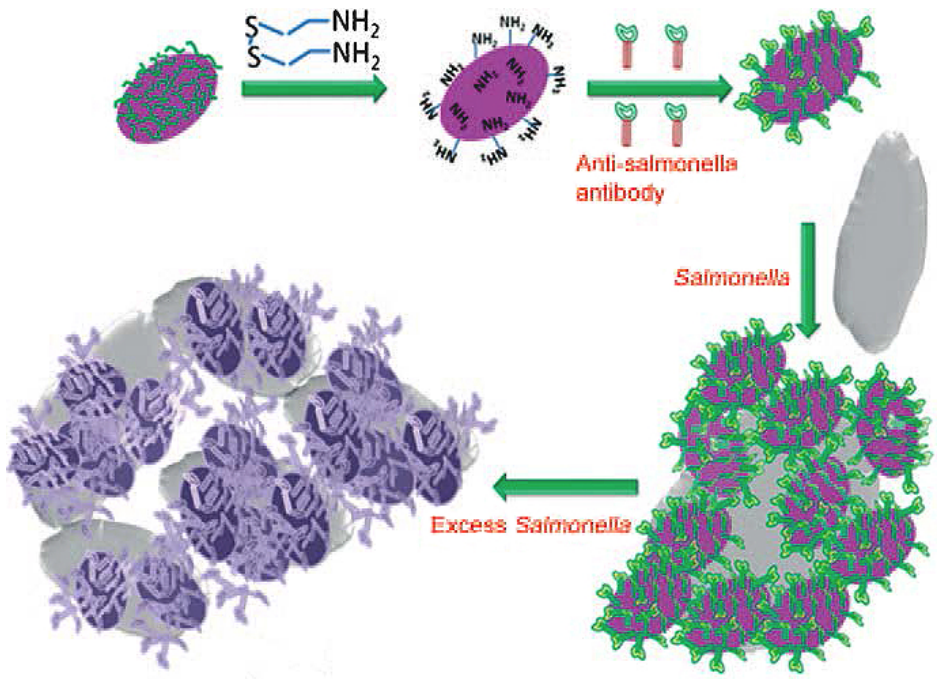

Figure 1. Schematic representation showing the nanotechnology-driven approach for selective targeting pathogenic Salmonella bacteria by antibody-conjugated oval-shaped gold nanoparticles (reprinted with permission from ref. 36, Copyright 2010, Wiley-VCH).

3.1. Colorimetric Identification and Sensing

3.1.1. Principle

Plasmonic nanoparticles are now known to be very good materials for colorimetric bioassays due to their attractive bright colours [6,98-99]. Bright colour of the plasmonic nanomaterials originated from their strong localized surface plasmon resonance. The working principle for the nanoparticle-based colorimetric sensor is based on the fact that the color of the nanoparticle solution is highly dependent on the interparticle distance of nanoparticles. When individual nanoparticles come into close proximity and the center-to-center distance is normally smaller for effective surface electron cloud overlap, due to the interparticle plasmon coupling, a distinct color change occurs depending on the extent of plasmon coupling [6,98-99]. Since the extinction coefficient of each gold nanoparticle is several orders of magnitude higher than that of common organic dyes, the inter particle distance dependent AuNP color change phenomenon has been extensively applied in solution phase for colorimetric bio-detection [6,98-99] including detection of bacteria.

3.1.2. Research and Development

Out of different optical and spectroscopic techniques, colorimeric detection technique is the simplest and most cost effective, does not require any instrumentation, and can be handled by any untrained person and hence securing its potential application for field detection to control any food-borne bacterial outbreak. Due to its simplicity, since the last fifteen years we and other groups have used this colorimetric technique for ultrasensitive biological sensing. Conventional methods are selective and sensitive too, but since they rely on a series of enrichment steps, they are too slow from the perspective of industrial needs. Driven by this need, we reported a rapid colorimetric identification of *Salmonella* bacteria by using bio-conjugated oval-shaped gold nanoparticles [36]. In this colorimetric assay, we have conjugated anti-salmonella antibody to biocompatible oval-shaped gold nanoparticle for label-free detection of *Salmonella typhimurium* (Figure 1). The obtained detection limit is 10^4 bacteria/L with excellent discrimination over other bacteria and pathogens ensures our nanotechnology-based assay as potential new-age sensor for rapid, on-site pathogen detection to avoid the distribution of contaminated foods. Our *Salmonella* bacteria identification is based on the fact that 1) anti-salmonella-antibody-conjugated oval-shaped gold nanoparticles can readily and specifically identify *Salmonella typhimurium* bacteria, through antibody–antigen recognition (as illustrated in Figures 1 and 2) when anti-salmonella-antibody-conjugated oval-shaped gold nanoparticles were mixed with various concentrations of Salmonella typhimurium bacteria, a nice calorimetric change was observed (Figure 2a). This color change is due to the fact that the Salmonella bacteria are more than an order of magnitude larger in size (1–3 μm) than the anti-salmonella-antibody conjugated oval-shaped gold nanoparticles. In the presence of Salmonella bacteria, several oval-shaped gold nanoparticles conjugate with one Salmonella bacterium, and nanoparticle aggregates are thereby produced. Our TEM image (Figure 2d) shows clear aggregation of anti-salmonella-antibody-conjugated oval-shaped gold nanoparticles on the surface of *Salmonella typhimurium* bacteria and results a colorimetric change from pink to a bluish color (Figure 2a). As shown in Figure 2i, the absorption maximum for the plasmon-absorption band of anti-salmonella-antibody-conjugated oval-shaped gold nanoparticles at 550 nm decreases with the

increase in the concentration of Salmonella bacteria, and a new broad band appears at around 700 nm confirms the binding of gold nanoparticles on individual bacteria surface or acts as bridge between two bacterium to form bacterial assembly. This bioassay is rapid, takes less than 5 min from bacterium binding to detection and analysis, and is also convenient and highly selective.

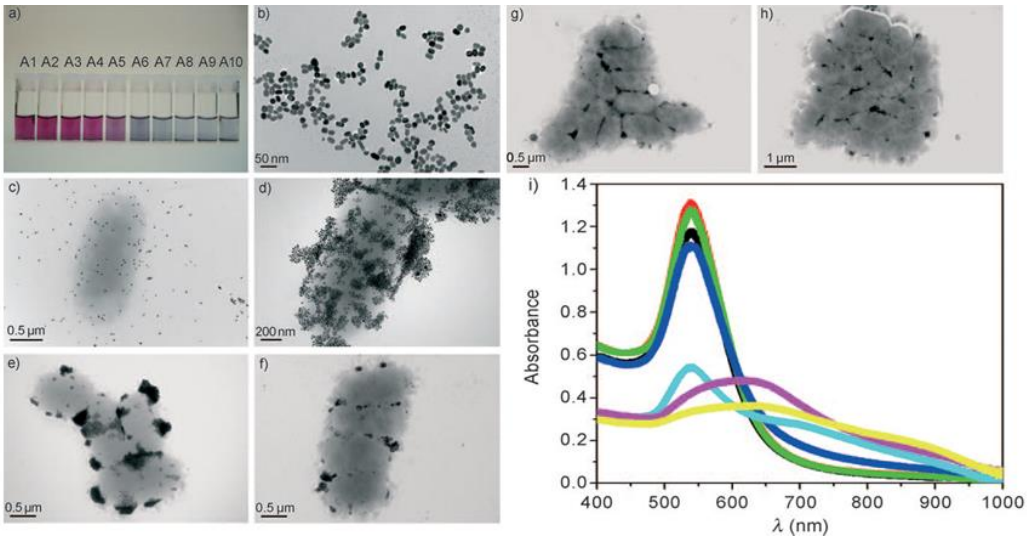

Figure 2.a) Photograph showing colorimetric change upon the addition of A1) 10, A2) 50, A3) 100, A4) 500, A5) 1000, A6) 5000, A7) 10000, A8) 50000, A9) 100 000, and A10) 500 000 *Salmonella*bacteria. b) TEM image showing anti-salmonella-antibody-conjugated oval-shaped gold nanoparticles before the addition of *Salmonella* bacteria. c) TEM image of *Salmonella* bacteria in the presence of oval-shaped gold nanoparticles conjugated with anti-E. coli antibody. The TEM image clearly illustrates that the *Salmonella typhimurium* bacterium cells are poorly labelled by the gold nanoparticles coated with anti-E. coli antibody. d) TEM image demonstrating aggregation of oval-shaped gold nanoparticles after the addition of 10^3 CFU mL^{-1}*Salmonella* bacteria. e) TEM image illustrating the aggregation of oval-shaped gold nanoparticles and the formation of microbial clusters in presence of 10^4 CFU mL^{-1}*Salmonella* bacteria. f–h) TEM images illustrating the formation of bigger microbial clusters in the presence 10^5, 5×10^5, and 10^6 CFU mL^{-1}*Salmonella* bacteria, respectively. i) Absorption-profile variation of anti-salmonella-antibody-conjugated oval-shaped gold nanoparticles in the absence of bacteria (red) due to the addition of 10^6 CFU mL^{-1} E. coli bacteria (green) or different concentrations of *Salmonella* bacteria (10 (black), 50 (dark blue), 10^3 (light blue), 10^4 (pink), and 10^5 bacteria (yellow)). The strong long-wavelength band in the visible region (λ_{PR}=550 nm) is due to the oscillation of the conduction-band electrons. The new band appearing at around 680 nm, due to the addition of *Salmonella* bacteria indicates the aggregation of the gold nanoparticles (reprinted with permission from ref. 36, Copyright 2010, Wiley-VCH).

Selectivity of our gold-nanoparticle-based colorimetric assay was tested on E. *coli* bacteria or by using anti-E. *coli* antibody conjugated oval shaped gold nanoparticles. In both the cases we have not observed any color change. However, distinct color changes were observed when we added 10^6 E. coli bacteria to the nanoparticles conjugated with anti-E. *coli* antibodies (Figure 3a) or when we added 10^6 Salmonella typhimurium bacteria to anti-salmonella-antibody-conjugated oval-shaped gold nanoparticles (Figure 2a). Corresponding

TEM image shows the selectivity of our assy. Figure 2i shows that absorption profile for the anti-salmonella-antibody-conjugated oval-shaped gold nanoparticles remains unchanged after the addition of 10^6 CFU mL^{-1} *E. coli* bacteria, whereas the plasmon-band absorption profile changed abruptly and shifted by about 100-150 nm when 10^6 CFU mL^{-1} of *Salmonella* bacteria were added. This difference clearly demonstrates that our colorimetric assay based on antibody-coated oval shaped gold nanoparticles is highly specific for *Salmonella typhimurium* bacteria and even can distinguish between different bacteria. Sensitivity of our colorimetric assay is 10^4 bacteria cells, which is comparable with the detection limit of enzyme-linked immunosorbent assays or ELISA (10^4–10^5 CFU mL^{-1})[8b], antibody-microarray biochip techniques [8c], and biofunctionalized magnetic-nanoparticle assays [38f]. As discussed before, we used the absorption coefficient of the 550 nm band for quantifying the concentration of Salmonella bacteria. As shown in Figure 3c, the plasmon-band intensity is highly sensitive to the concentration of Salmonella bacteria. Our experimental results clearly demonstrate that our assay based on anti-salmonella-antibody- conjugated oval-shaped gold nanoparticles can quantify the amount of Salmonella bacteria over the range of 10^3–10^7 bacteria.

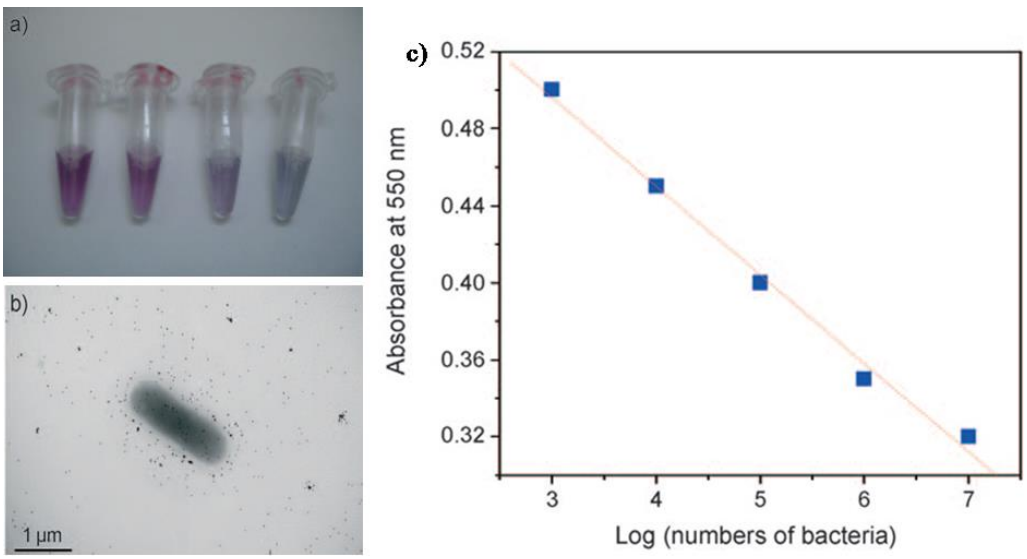

Figure 3. a) Photograph showing colorimetric change upon addition of A1) 10^6 *E. coli* bacteria to anti-salmonella-antibody-conjugated ovalshaped gold nanoparticles, A2) 10^6 *Salmonella* bacteria to oval-shaped gold nanoparticles conjugated with anti-E. coli antibody, A3) 10^3 *E. coli* bacteria to oval-shaped gold nanoparticles conjugated with anti-E. coli antibody, and A4) 10^6 *E. coli* bacteria to oval-shaped gold nanoparticles conjugated with anti-E. coli antibody. b) TEM image showing anti-salmonella-antibody-conjugated oval-shaped gold nanoparticles after addition of *E. coli* bacteria. c) Plot illustrating how the plasmon-band intensity of the anti-salmonella-antibody-conjugated oval-shaped gold nanoparticles at 550 nm changes upon addition of different concentrations of *Salmonella typhimurium*. Squares indicate the experimental data and the line shows the linear fit obtained with R=0.99 (reprinted with permission from ref. 36, Copyright 2010, Wiley-VCH).

To evaluate whether our assay can be used for the detection of Salmonella bacteria in environmental samples, spiking experiments were performed and recovery values were

determined. In this spiking experiment, we used 1×10^5 *S. typhimurium* per mL and a mixtureof 5×10^4 *E. coli* O157:H7 and 5×10^4 *S. typhimurium* per mL. In Table 1, the supplied concentration and determined concentrations are compared. Our data show that the recovery values are quite good, even for the mixture and confirm the capability of our assay to detect a low concentration of one type of bacteria in the presence of another kind of bacteria.

Along with our original research work, several other groups throughout the world have contributed significantly in the field of colorometric detection of bacteria. Recently, Sundaram Gunasekaran [100] and co-workers reported a switchable linker (SL)-attached nanoparticle-based visible detection of E. *coli* at a concentration fewer than 100 CFU/mL. Colorimetric detection based on nanoparticle aggregation is highly advantageous for rapid on-site detection of bacterial infection as this methodology does not seek a trained person and any specialized instrument for successful execution. For bacteria, key feature for designing SL is based on the concept that a target has thousands of receptor molecules. In fact, immunogenic attachment of NPs on the cell surface using functionalized antibody (f-AB) has been reported to produce an optical signal for selective detection of bacteria [20,38d,101-103]. Recently, V. M. Rotello and co-workers [104] have reported a hybrid colorimetric enzymatic nanocomposite biosensor that uses enzyme amplification to provide high sensitivity for the detection of pathogens in aqueous solution. They have mentioned two key issues in designing an effective pathogen sensor to find application in field detection. First, the limit of detection (LOD) required for application in either environmental testing [105-107] or clinical applications [106-108] is 10^4-10^2 pathogen/mL. Second, the readout should not require expensive instrumentation. Their colorimetric sensor design features three maincomponents: (a) β-galactosidase (β-Gal), an anionic enzyme (pI 4.6), to provide signal amplification; (b) chlorophenol red β-D-galactopyranoside (CPRG), a chromogenic substrate, toprovide a color readout; and (c) a cationic NP that bindsreversibly to β-Gal, inhibiting the enzyme without denaturation(Figure 4a). The AuNPs used here were functionalized withquaternary ammonium ligands to provide high stability, biocompatibility, and a head group for tuning surface interactions, all of which are critical requirements for stable and sensitive biosensors (Figure 4b). Binding of the anionic surface of analyte bacteria [107] (Figure 4b) to the cationic particle surface displaces the β-Gal, with concomitant restoration of activity. The active enzyme converts the pale-yellow substrate into the red product, providing a colorimetric readout (Figure 4a). They have checked the effectiveness of their assay by using E. *coli* (XL1) as a model analyte and they could successfully and reproducibly differentiate bacterial levels by visible color change as low as 100 cells/mL within 10min of load. They observed similar changes by using gram positive bacteria like *Streptomyces griseus* and *Bacillus subtilis*, indicating the generality of their assay. V. M. Rotello and co-workers
[104] also designed a test strip suitable for field application by using GF/B binder free microfiber filter paper as the platform because of its high wet strength, high loading capacity, and rapid response. By using this assy they have proven the effectiveness of this chromogenic platform, demonstrating that 1×10^4 bacteria/mL can be distinguished using this method. Similar electrostatic interaction between CTAB-based cationic gold nanorod or nanosphere and *Bacillus cereus* has been reported by Berry et al. [5k].

Though colorimetric detection is fundamentally simple, aggregation based methods can be quite difficult to be developed into daily life quantitative bacteria sensing methods. One needs to determine the strategy of how to control the aggregation size. Otherwise it may be

challenging to reproduce, particularly in the presence of several bacteria contaminants, which will be true in daily life samples. In future, there should be greater focus on how to control the nanoparticle aggregation size, so that it can be expanded to the detection of microorganisms in environmental and clinical samples.

3.2. Surface Enhance Raman Scattering (SERS) Based Identification and Sensing

3.2.1. Principle

SERS is a nanoparticle-based Raman spectroscopic technique has been studied extensively in the last few decades [109-113] and promised to be one of the most powerful techniques for the future applications in diagnosis and sensing [114-115]. The usefulness of this technique lies in its ability to provide the chemical signature along with its signal amplification (10^8–10^{14} order) leads to state-of-the-art highly specific and sensitive assay for diagnosis, detection and monitoring [114-115]. Though bulk SERS enhancements have been understood as largely plasmon-based [116,117] since the first experimental demonstrations [118], resonance [119-120] and chemical contributions [121,122]can also be quite large under certain conditions. The Raman enhancement, G, is measured experimentally by direct comparison as shown in Equation (1) [109,113, 123-124].

$$G = \left({}^{I_{SERS}}\!/_{I_{Raman}}\right) \times \left({}^{[M_{Bulk}]}\!/_{[M_{Ads}]} \right) \quad (1)$$

In which I_{SERS} is the intensity of a particular vibrational mode in the observed SERS spectrum of the analyte in presence of nanoparticle, and I_{Raman} is the intensity of the same mode in the bulk Raman spectrum from the same analyte in absence of nanosurface. M_{Bulk} is the number of molecules used in the bulk, M_{Ads} is the number of molecules adsorbed and sampled on the SERS-active substrate. The possibility of observing Raman signals, which are normally very weak, with enhancements of the order of 10^8–10^{14} and the unique ability to obtain molecular recognition of bacteria at very low concentrations allow SERS to be unique for ultrasensitive pathogen sensing [109, 125-127]. Very high selectivity and sensitivity offered by SERS, along with the highly informative spectral characteristics of Raman spectroscopy, allows an SERS-based method to be a feasible alternative to detect bacteria [32,37,109, 125-130] than more commonly used optical sensing methods.

Table 1. Comparison of supplied and found concentrations of S. typhimurium in water samples (reprinted with permission from ref. 36, Copyright 2010, Wiley-VCH)

Water Sample	Bacteria supplied	S. typhimurium found
tap water	1×10^5 S. typhimurium	1.5×10^5
tap water	5×10^4 S. typhimurium and 5×10^4 E. coli	8.9×10^4
drinking water	1×10^5 S. typhimurium	1.3×10^5
drinking water	5×10^4 S. typhimurium and 5×10^4 E. coli	7.7×10^4

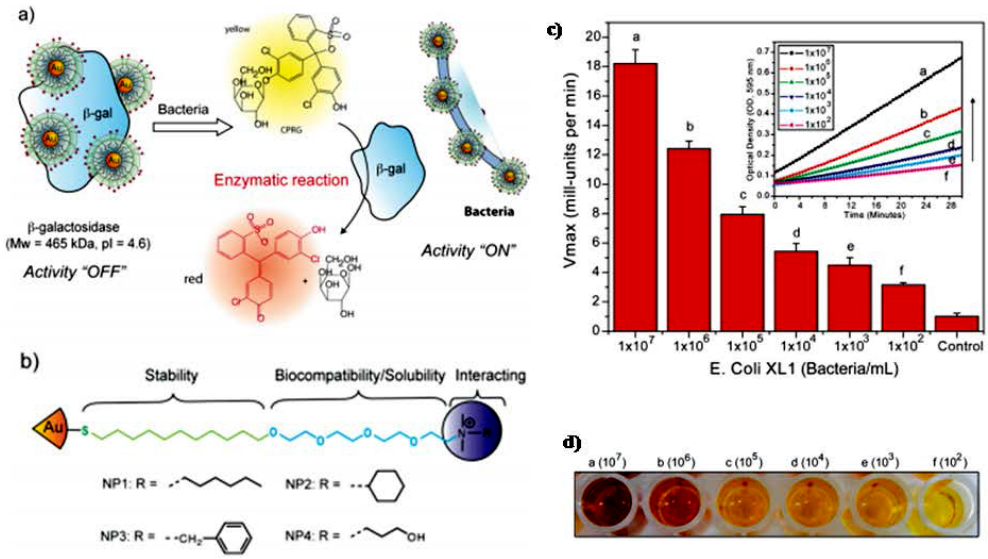

Figure 4. (a) Enzyme-amplified sensing of bacteria, showing the relative sizes of the 2 nm core diameter NPs and β-Gal. (b) Structures of ligands used for sensing studies. (c) LOD of E. coli using the β-GalNP2nanocomposite. Kinetic absorbance responses upon addition of different bacteria concentrations are shown; the β-Gal-NP2 nanocomposite without bacteria was used as the control. (d) Microplate wells showing the color change upon variation of the bacteria concentration (reprinted with permission from ref. 104, Copyright 2011, American Chemical Society).

3.2.2. Research and Development

Since last one decade, we and other groups have used SERS-based technique for ultrasensitive biological sensing motivated by both applications in clinical diagnostic microbiology and potential bioterrorist attack [131-146]. Though the colorimetric sensing is the easiest technique for field detection to control any food-borne bacterial outbreak, lack of noticeable color change at low concentration of pathogen does not make colorimetric method as an ultrasensitive methodology for low level diagnosis. Contrary to that, the ability to provide chemical signature of bacteria species at low concentration illustrates the potential applications of SERS-based techniques as valuable analytical and structural spectroscopic tool. Limited literature of bulk Raman (non-SERS) spectra of whole-cell bacteria are available over the last couple of decades and their vibrational fingerprint can serve as the basis for classification and identification of different bacterial pathogens with species and, in some case, strain specifically. Though the diagnosis and sensing efficiency of bacterial pathogens by bulk Raman is almost comparable to the current methodologies, like polymerage chain reaction (PCR), and enzyme linked immunosorbent assay (ELISA), SERS offers several advantages over bulk Raman observation. Enhanced Raman cross-section in SERS reduces data accumulation time, excitation laser power, and easy accessible visible line over UV lines for Raman excitation make the SERS-based detection a rapid, cost effective venture for bacteria sensing and diagnosis [147-157].

SERS spectra have been previously reported for bacteria in silver and gold colloid solutions [140-144], bacteria placed on electrochemically roughened metal surfaces [143-145], bacteria coated by silver metal deposits [141-142], and bacteria co-deposited with silver colloid aggregates on inert substrates [146]. Though the relative band intensity and absolute

enhancement vary from sample to sample of nanomaterials, their vibational signature remain constant for a specific bacterial pathogen. It was Jarvis et al. who first shown that SERS could be an useful and powerful tool in pathogen identification and discrimination because of its ability to generate whole organism fingerprints [128, 146]. Premasiri et al. [32] reported an aggregated gold nanoparticle covered SiO_2 chips based SERS probe for the detection of Gram-positive bacteria *Bacillus cereus*, *Bacillus subtilis* (YS11 and 3610), *Bacillus anthracis Sterne* (a nonvirulent strain), and *Bacillus thuringiensis* and Gram-negative bacteria *Escherichia coli* K12 and *Salmonella typhimurium*.

They have also reported the Raman cross-section enhancement for E. *coli* and *B. anthracis* by a factor of 2×10^4 and 5×10^4 per bacterium respectively on gold nanoparticle covered SERS substrate. The difference per bacterium enhancement factor was explained on the basis of different Gram-positive and Gram-negative cell surface structures of these two bacterial species. They have acquired SERS spectra of six closely related species of bacteria in the 400-1700 cm^{-1} range on the gold nanoparticle covered chip as shown in Figure 5. Spectral differences between the SERS spectra of closely related bacteria species indicate that the bacterial SERS fingerprints can be used to clearly distinguish different species. They have also demonstrated the ability to quickly obtain high quality Raman spectra of bacterial single cells, which may be useful for distinguishing dangerous pathogens in a mixture more specifically.

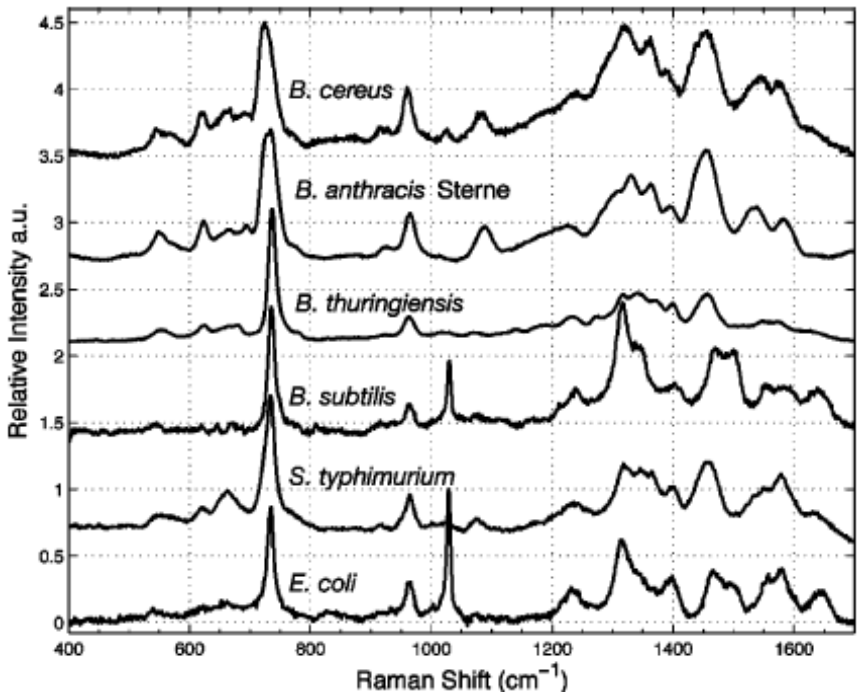

Figure 5. SERS spectra of six bacterial species obtained on gold aggregate coated SiO_2 chips. Spectra are offset vertically for display purposes and top-to-bottom ordered according to their phylogenetic relationship (reprinted with permission from ref. 32, Copyright 2005, American Chemical Society).

Very recently, Joseph Irudayaraj and co-workers have developed a novel SERS active substrate of 60-80nm diameter through the assembly of silver nanocrystals (AgNCs) into Ag

nanospheres (AgNSs) and used them for ultrasensitive identification of pathogens [158]. Interestingly, by using this SERS active substrate they could ultrasensitively detect different pathogenic bacteria as low as 10 colony forming units/mL (CFU/mL). In their experiment, they have taken three different species of bacteria, E. *coli*, *S. typhimurium, and S. aureus* respectively, and recorded their Raman fingerprint as shown in Figure 6.

Fingerprint Raman spectra of *S. Aureus* obtained from their study show typical Raman bands of adenine, amine, membrane proteins, phospholipids, and polysacharides consistent with the existing literature [159-160]. Furthermore, their study also demonstrates that the SERS spectra from two different bacteria species of the same type (e.g. gran-negative or gram-positive) although share many common spectral features, differences in vibrational bands and the relative intensity are clearly observable. In addition to the detection and differentiation of live bacteria, the versatility of their assay to distinguish between live and dead species, a critical area in food safety as dead bacteria, can alter the test of a food but is no more can act as a toxin. A considerable difference in the spectra of dead and live cells were obtained possibly due to the rupture of the outer layer of the bacterial cell wall with a possible change in the membrane proteins resulting in the release of carbohydrates from these cells [161]. All of these changes contribute to inducing a significant difference in the SERS signal between the live and dead samples. Since SERS fingerprint is sensitive to the membrane protein composition, we could possibly use SERS sensing technique to distinguish between normal and drug resistant bacteria. For the detailed understanding on the bacteria membrane permeability and drug resistance, readers can go through the review by Anne H. Delcour [162].

Along with these results, we have also recently reported a Rh-6G modified antibody-conjugated popcorn shaped gold nanoparticle-based SERS technique for the detection of multiple drug resistant bacteria (MDRB) Salmonella DT104 [37]. In this report, the central sphere of the nanopopcorn acts as an electron reservoir while the tips are capable of focusing the field at their apexes, which provides huge field enhancement of the scattering signal [37, 129]. Our result indicates that in the presence of drug resistant MDRB Salmonella DT104, antibody-conjugated gold nanoparticles undergo aggregation, which helped to form several hot spots and provided ~10^9 order of magnitude SERS signal enhancement through mainly an electromagnetic field enhancement mechanism. As shown in Figure 7, the SERS intensity change was negligible in the presence of 10^6 *Salmonella ser. Agona* bacteria per mL or E. *coli* bacteria, whereas a good enhancement has been observed even in the presence of only 10 CFU g^{-1} MDRB *S. typhimurium* DT104.

Though SERS is rapidly evolving as a practical analytical tool that can be simultaneously applied to multiple bacteria sensing, SERS has its own challenges. There are several factors that can change the SERS signal and these are (1) slight changes in the SERS substrate, (2) variation of the extent of aggregation of nanoparticle based on the physical parameters of the analyte, (3) substrate surface chemistry, (4) analytes orientation, etc. Although simultaneous detection of multiple pathogens has been reported, it is not always straightforward to apply the SERS assay to a mixture of pathogens with a similar structure, polarity, or molecular weight. As a result, in future, the SERS experimental parameters must be carefully designed so that the SERS results can be reproduced from one lab to the other lab and SERS can be used for the real-life sample.

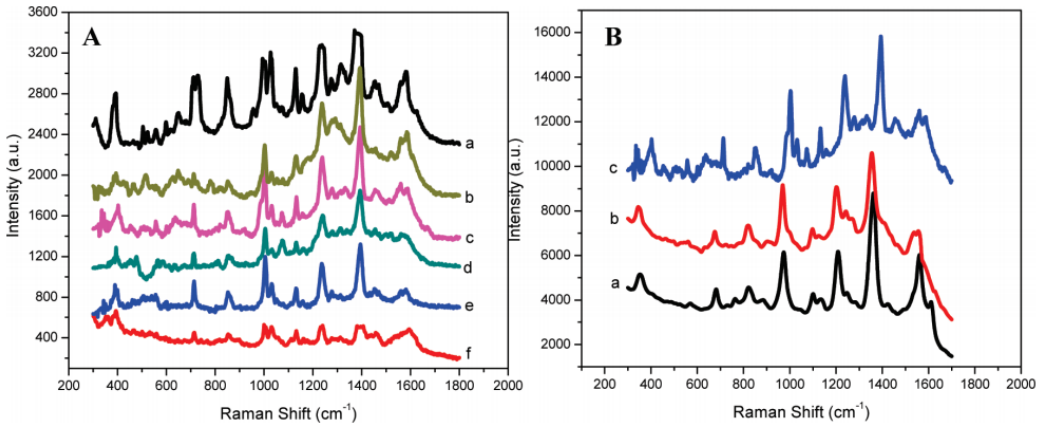

Figure 6. (A) SERS spectra of *S. aureus* on the as-prepared AgNSs at concentrations of a, 10^6; b, 10^5 ; c, 10^4 ; d, 10^3 ; e, 10^2 ; and f, 10 CFU/mL. (B) Comparison of SERS spectra of *E. coli* O157 (a), S. typhimurium (b), and *S. aureus* (c) at 785 nm excitation (reprinted with permission from ref. 158, Copyright 2010, American Chemical Society).

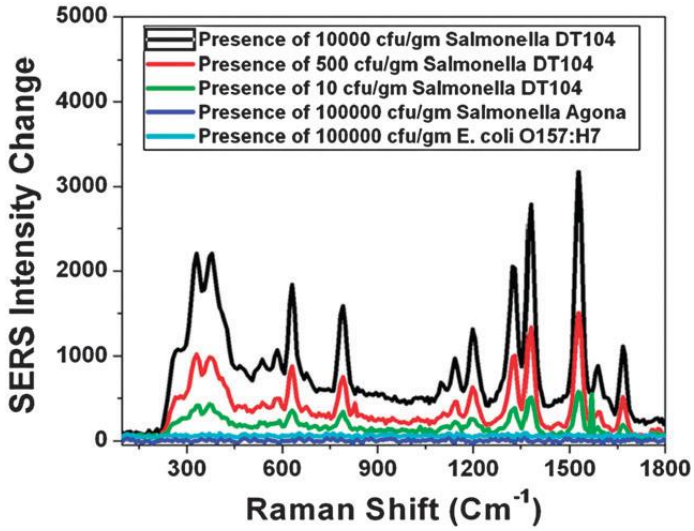

Figure 7. Plot demonstrating SERS enhancement (SERS intensity change before and after addition of bacteria) due to the addition of different kinds of bacteria to monoclonal M3038 antibody-conjugated popcorn shaped gold nanoparticles (reprinted with permission from ref. 37, Copyright 2011, Royal Society of Chemistry).

3.3. Localized Surface Plasmon (LSP)-Based Identification and Sensing

3.3.1. Principle

When a small spherical metallic nanoparticle is irradiated by light, the oscillating electric field causes the conduction electrons to oscillate coherently which can be depicted by Figure 8 [86].

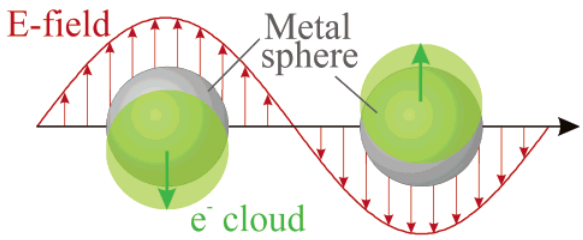

Figure 8. Schematic representation of plasmon oscillation for a sphere, showing the displacement of the conduction electron charge cloud relative to the nuclei (reprinted with permission from ref. 86, Copyright 2003, American Chemical Society).

When the electron cloud is displaced relative to the nuclei, a restoring force arises from Coulomb attraction between electrons and nuclei that results in oscillation of the electron cloud relative to the nuclear framework. This electron oscillation frequency depends on six factors: (i) the density of electrons, (ii) the effective electron mass, (iii) the shape and (iv) size of the charge distribution, (v) dielectric constant of the material, and (vi) dielectric constant of the surrounding medium [125,163-175]. This collective oscillation of the nanostructure's conduction electrons in resonance with the incident electromagnetic field is called the dipole plasmon resonance of the particle or dipolar Localized Surface Plasmon Resonance (dipolar-LSPR). Higher modes of plasmon excitation can occur, such as the quadrupole mode where half of the electron cloud moves parallel to the applied field and half moves antiparallel. The contribution of the different parameters to the total extinction of the metal nanoparticles is described by the Mie theory. Due to the presence of LSPR, electromagnetic fields near the particle's surface are greatly enhanced and the particle's optical extinction (scattering + absorption) reaches maximum at the plasmon resonant frequency at visible and NIR wavelengths depending on the size and shape of nanoparticles [20, 36, 37,38i,98,128, 129, 171, 176-188]. Due to this enormous surface plasmon enhancement, absorption cross-section of plasmonic nanomaterials increases 5-7 orders more compared to the available dye molecule depending on their size and shape and results in the intense development of noble metal nanostructures for various biomedical applications such as biosensor assay for food-borne bacterial pathogen detection. Depending on the origin of the LSPR change, we can make two different LSPR sensors. In both the cases we observe a change in absorption spectral position (λ_{max}) of the nanoparticle. Two different LSPR sensors are aggregation-based LSPR sensing and refractive index based LSPR sensing.

3.3.1.1. Aggregation-based LSPR sensing

In the presence of an analyte (which have specific tendency to bind with the nanoparticle surface) when the nanoparticles come close to each other and make aggregates, it results in a distinct color change which is obviously associated with an absorption spectral position (λ_{max}) change of the surface plasmon. Due to the association of the nanoparticles through specific analyte, the diameter of the particle increases and results a red-shift of the LSPR [175]. In the early 1990's, aggregation-based LSPR sensing of biomolecules was first reported by Mirkin et al. to detect femtomolar levels of ssDNA using this technology [189]. The same methodology has been applied for the technological development of pregnancy testing kit in which gold

nanoparticle micro-latex beads are used with specific antibodies to β-hCG, a hormone released by pregnant women. Upon mixing these particles with urine containing the hormone, pink aggregates could be clearly observed [190]. Though aggregation-based LSPR sensing is a label-free solution based assay technique which offers low cost for universal application and rapid sensing for urgency, it suffers from several drawbacks too which include low sensitivity; and the change of physical parameters (e.g. pH, temperature, ionic strength) can also bring the change of nanomaterial-assay color. Therefore, one needs to determine the strategy before performing the LSPR sensing.

3.3.1.2. Refractive index based LSPR sensing

The LSPR of plasmonic nanoparticle is highly dependent on the local refractive index at the nanoparticle surface. The relationship between the change in LSPR spectral position ($\Delta\lambda_{LSPR}$) and the change in local refractive index (Δn) induced by the adsorbents can be expressed by equation (2).

$$\Delta\lambda_{LSPR} = m\Delta_n\left[1 - exp\left(\frac{-2d}{l_d}\right)\right] \quad (2)$$

where m is the bulk refractive index response of the nanoparticle, d is the adsorbent thickness on nanoparticle surface, and l_d is the characteristic electromagnetic-field-decay length. As such, when molecules bind to a AuNP, the refractive index will change giving rise to a shift of the LSPR. Though the sensitivity of this assay towards refractive index change is distance dependent, refractive index change at close proximity of nanoparticle (localization) will result a LSPR shift. Englebienne et al. have used antibody-coated AuNP probes to monitor changes in protein conformation using this technology [191,192]. Recently, PharmaDiagnostics has commercialized this LSPR-based biosensing. This technology is named SoPRano-technology and it has diverse applications in basic research and therapeutic R&D, including bio-kinetics, antibody screening, protein-protein interaction, etc.

3.3.2. Research and Development

The most exciting application of LSPR phenomenon for food-borne bacterial pathogen sensing was studied by Joseseph Irudayaraj [20]. In their report they have used cystamine modified gold nanorod, synthesized by using CTAB as a active surfactant. The resulting amine modified gold nanorods then have immobilized to pathogen-specific antibodies to make gold nanorod bioprobes by activating the ranorods with glutaraldehyde. They have investigated the use of different gold nanorod bioprobes with different aspect ratios, conjugated to anti-E. coli and anti-S. typhimurium antibodies, as novel optical labels based on changes in SPR band for rapid (less than 30 min) and sensitive detection of two major species of food-borne pathogenic bacteria, *E. coli O157: H7* and *S. typhimurium*, used as model pathogens in one solution simultaneously at concentrations lower than 10^2 CFU mL^{-1}. Figure 9 shows the procedure for attaching nanorods to antibody and its assay detection concept.

Upon the addition of bacteria, they could easily observe the decrease in LSPR intensity associate with red shifting of the LSPR peak and they could simply detect the bacteria concentration as low as 10 CFU mL^{-1} as shown in Figure 10.

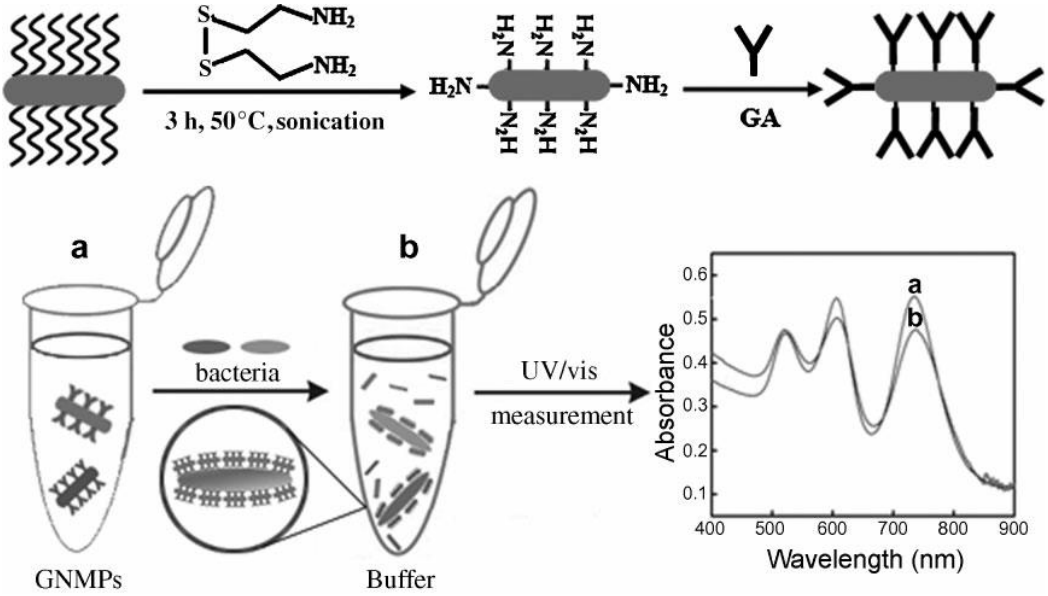

Figure 9. Schematic representation of (top) the synthesis of pathogen-antibody-conjugated gold nanorods and (bottom) the simultaneous detection of two species of pathogens in an assay based on gold nanorod probes (GNPs). CTAB. Cetyltrimethylammmonium bromide, GA. glutaraldehyde (reprinted with permission from ref. 20, Copyright 2008, Wiley-VCH).

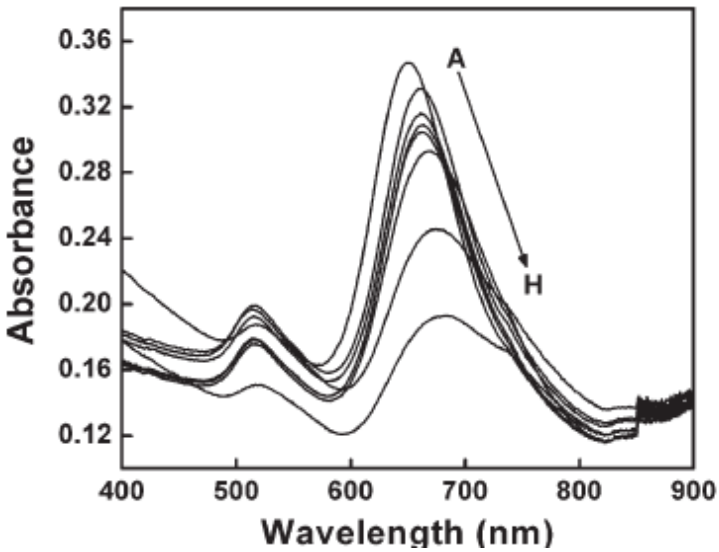

Figure 10. UV/Vis absorbance spectra of A) amine-modified gold nanorods, B) anti-E.coli-antibody conjugates, and C)–H) after the addition of *E. coli* at different concentrations (1–10, 10^3, 10^2, 10^4, 10^5, 10^6 CFU mL^{-1}) to antibody-conjugated amine-modified gold-nanorod bioprobes (reprinted with permission from ref. 20, Copyright 2008, Wiley-VCH).

More interestingly, they could simultaneously monitor two species of bacterial pathogens in a multiplex format by using two different gold nanorods (for separated LSPR) with two different antibodies specific for E. *coli* and *S. typhimurium*. Figure 11 shows the visible/NIR

absorption spectra of sample that contains both E. *coli* and *S. typhimurium* at concentrations in the range of 1-10 to 10^8 CFU mL^{-1}. As seen from the spectra, the LP bands present changes in intensity when the concentration is less than 10^4 CFU mL^{-1}, and both intensity decrease and red shift were observed at higher concentrations (10^6–10^8 CFU mL^{-1}). These results indicate that the gold-nanorod bioprobes of each aspect ratio could bind to their respective bacterial target in a mixture of the two species to produce changes in the LP bands of the nanorods.

Fu et al. [193] demonstrated a LSPR sensor for *Salmonella* detection using Au NPs fabricated by oblique angle deposition setup. Their anti-Salmonella coated gold nanosurface can successfully capture Salmonella and the plasmon peak shifts due to the antigen-antibody reaction, but their report also indicates that this shift is not sensitive to the concentration of the bacteria. This clearly indicates that the detection ability of the LSPR sensor has a limitation for whole bacteria cells, which needs further investigation for improvement. Yu-bin Lan and co-workers [194] have reported a SPR biosensor for rapid detection of Salmonella typhemurium in chicken carcass by using a commercial Spreeta SPR biosensor purchased from Texas Instruments. For the detail of the instrumentation, readers are requested to go through the specific paper. In brief, incident light interacts with gold sensor film on which the sample is placed and the analytes in the sample generate a specific refractive index. This refractive index is plotted against time and provides the necessary information for determining whether a pathogen is present in the sample or not. By using this SPR biosensor, they could successfully detect *S. typhemurium* at the concentration of 10^6 CFU mL^{-1}.

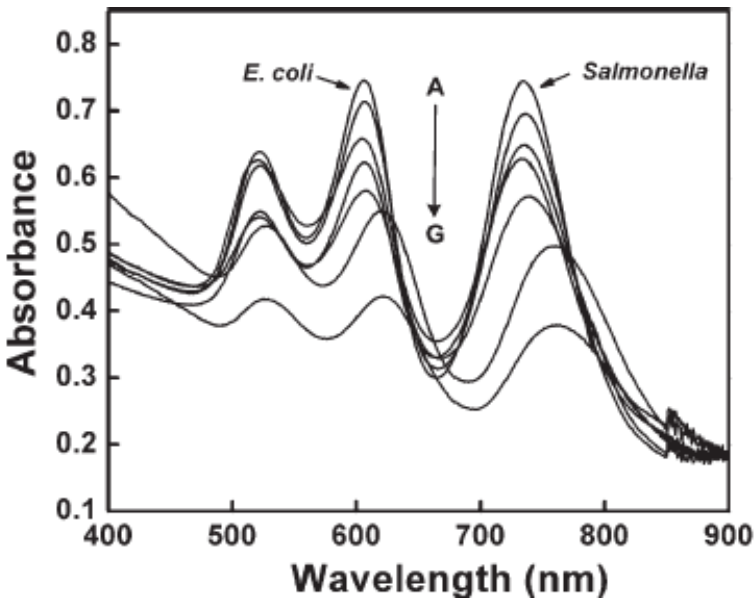

Figure 11. UV/Vis absorbance spectra after the addition of a mixture of *E. coli* and *S. typhimurium* to anti- E. coli- and S. typhimurium-antibody conjugated amine-modified gold nanorods with aspect ratios of 2.0 and 3.2, respectively. The concentrations of *E. coli* and *S. typhimurium* were 1–10 to 10^8 CFU mL^{-1} (A–G) (reprinted with permission from ref. 20, Copyright 2008, Wiley-VCH).

Besides these noted research activities, there are several reports where researchers have used LSPR-based biosensor for the detection of different food-borne bacterial pathogens. Like, Datta Mazumdar [195] and co-workers used SPR method to detect *Salmonella* in milk and the detection limit of their assay is 1.25×10^5 cells/mL within 1h. Nanduri et al. have reported a SPR-based biosensor for the detection of *L. monocytogenes* using phase-displayed scFv antibody. The detection limit for *L. monocytogenes* whole cells was estimated to be 2×10^6 CFU/mL. Recently, Zhang et al. [196] reported a new method based on SPR DNA biosensor for the rapid detection of the *invA* gene which is highly conserved gene present in all *Salmonella* serovars. This DNA biosensor can detect as low as 10^2 CFU of Salmonella cells form 1 mL sample within 4.5 h, and excellent regeneration of sensor surface could reduces the cost of the approach greatly. The strategy proposed in this report performs the advantages of rapid detection, free label, high sensitivity and specificity, and general applicability to almost all *Salmonella* serotypes, which has potential application in *Salmonella* detection. Waswa et al. [197] reported a SPR biosensor for the detection of *Salmonella enterica* serovar *Enteritidis* and *Escherichia coli* in spiked skim milk using specific antibodies. In their report, they have shown that the SPR sensor registers changes in the refractive index during binding of the bacteria to the antibody, which was immobilized on the gold-coated sensor chip surface. They have shown that the SPR sensor is highly specific, and the limits of detection of the assay were found to be 25 CFU mL^{-1} for E. coli and 23 CFU mL^{-1} for Salmonella.

Although there is a considerable advancement of the LSPR technique which offers a rapid and cost effective absorption spectroscopy based technique for food-borne bacteria detection, we need careful assessment before we use this technique as a standard tool kit. Main challenges it face at present are: reproducibility, specificity, and sensitivity. Also, for the detection of bacteria from blood, serum, urine samples, the main challenge is the optical transparency where we could think about a solid state LSPR biosensor to avoid this problem. To overcome these problems and to use this technique as standard tool for quantification and scaling in a clinical environment, we need intense further research to develop optimum LSPR substrates.

3.4. Non-Linear-Optics-based Identification and Sensing

3.4.1. Principle

Non-linear-optics describes the behaviour of light in nonlinear media, media in which the dielectric polarization (P) responds nonlinearly to the electric field (E) of the light. This nonlinearity is typically only observed at very high light intensities such as those provided by laser. Nonlinear optics gives rise to a host of optical phenomena and this discussion will only be limited to the application of hyper-Rayleigh scattering (HRS) for the identification and sensing of bacteria. The HRS or two-photon Rayleigh scattering (TPRS) is a nonlinear optical effect observed in isotropic solutions due to the fluctuations in symmetry, caused by rotational fluctuations, where incoherent scattering by a fundamental laser beam can be detected at the second-harmonic wavelength. This technique can be readily applied to study a very wide range of materials because electrostatic fields and phase matching are not required.

NLO properties of nanostructured materials, which are drastically influenced by quantum confinement effect, can be promising for applications in photonics and bio-imaging [38d,97,198-201]. Plasmonic nanostructures are particularly interesting, due to the presence of surface plasmon resonances (SPR), which generally significantly enhances (~10^4-10^6) weak nonlinear effects via strong electromagnetic (plasmon) fields at the surfaces of metallic nanostructures [39h, 39i, 164, 189, 202]. Nanostructured geometries offer its own unique near-field properties: plasmon resonant frequency, spatial distribution of the near-field amplitude across the surface of the nanostructure and orientation dependence on polarization of the incident light wave. The intensity of two-photon scattering signal from gold nanoparticle solution can be expressed as [39h-i,60,64,203-207]

$$I_{TPS} = G\langle N_W \beta_W^2 + N_{nano}\beta_{nano}^2\rangle I_\omega^2 e^{-N_{nano}\varepsilon_{2\omega}l} \qquad (3)$$

where G is a geometric factor, N_w and N_{nano} are the number of water molecules and gold nanoparticles per unit volume, β_w and β_{nano} are the quadratic hyperpolarizabilities of a single water molecule and a single gold nanoparticle, $\varepsilon_{2\omega}$ is the molar extinction coefficient of the gold nanoparticle at 2ω, l is the path length, and $I_\omega$is the fundamental intensity. The exponential factor accounts for the losses through absorption at the harmonic frequency. It is obvious that for non-geometric structures (non-centro-symmetric), main contribution of TPS intensity arises from electric dipole contribution where as for centro-symmetric nano structures the enhanced nonlinearity originates from multipolar (like electric quadrupole, octupole, etc.) contribution of the harmonic energy of the excited dipole. Multipolar contribution is very important when the size of the particle is no longer negligible [38d,208] compared to the harmonic wavelength.

3.4.2. Research and Development

Compared to colorimetric or LSPR and SERS-based identification and sensing of food-borne bacteria, nanomaterials-based two-photon Rayleigh scattering assay for bacteria sensing is relatively a new detection scheme with enormous potential. Last one decade we have applied extensively this technique for selective and sensitive detection of bacterial pathogens along with other chemical and biological toxins [38d,199,209]. Using the unique optical properties of gold nanorods, we reported [38d] the first time that two-photon Rayleigh scattering properties of gold nanorods can be used for rapid, highly sensitive, and selective detection of *E. coli* O157:H7 bacteria from aqueous solution. This nanotechnology method could be adapted for the detection of a wide variety of bacterial pathogens used as bioterrorism agents in food and environmental samples.

Our detection is based on the fact that (1) anti-*E. coli*O157:H7 antibody-conjugated nanorods can readily and specifically identify *Escherichia coli* O157:H7 bacterium, through antibody-antigen recognition (as shown in Figure 12), and (2) when anti-*E. coli* antibody-conjugated nanorods (as shown in Figure 13) were mixed with various concentrations of *Escherichia coli* O157:H7 bacterium, two-photon scattering intensity increases by about 40 times (4-times increment after the addition of only 50 CFU mL^{-1} E. *coli* bacteria). This increment is due to the fact that *E. coli* bacteria are more than an order of magnitude larger in

size (1-3 μm) than the anti-*E. coli*antibody-conjugated gold nanorods. In the presence of *E. coli* bacteria, several gold nanorods binds with one *E. coli* bacterium surface, and as a result, anti-*E. coli*antibody-conjugated gold nanorods undergo aggregation (as shown in Figure 12D). Due to this aggregation, a new broad band appears around 200 nm far from their longitudinal plasmon absorption band, and color change takes place (as shown in Figure 12C). This bioassay is rapid, takes less than 15 min from bacterium binding to detection and analysis, and is convenient and highly selective.

Observed change in the two-photon Rayleigh scattering (TPRS) intensity after the addition of *E. coli* bacteria to anti-*E. coli* in our assay can be due to several factors:

(i) Due to the apparent centro-symmetric structure of nanorod, the TPRS intensity cannot be due to electric dipole contribution from individual nanorods, unless it posses any nanoscale defects. The very high total nonlinear polarization could originates from multipolar contribution like electric quadrupole contribution as I have discussed in the previous section. Due to the aggregation of nanorods in presence of *E. coli* bacteria, nanorods lose the centre of symmetry, and as a result, one can expect a significant amount of electric dipole contribution to the two-photon scattering intensity. Since electric dipole contributes several times higher than that of multipolar moments, we expect two-photon scattering intensity to increase with aggregation.

(ii) Due to the binding of antibody-conjugated gold nanorods on bacteria surface, longitudinal absorption band at 680nm shifts to 950nm due to the formation of nanorod aggregates. According to the two-state model [210]

$$\beta_{TwoState} = \left[\frac{3\mu_{eg}^2 \Delta\mu_{eg}}{E_{eg}^2}\right] \times \left[\frac{\omega_{eg}^4}{(\omega_{eg}^2 - 4\omega^2)(\omega_{eg}^2 - \omega^2)}\right] \qquad (4)$$

where ω is the fundamental energy of the incident light, μ_{eg} is the transition dipole moment, and ω_{eg} is the transition energy between the ground state $|g\rangle$ and the charge-transfer excited state $|e\rangle$, $\Delta\mu_{eg}$ is the difference in dipole moment between $|e\rangle$ and $|g\rangle$ states. Since $\omega_{eg} \propto 1/\lambda_{max}$, and λ_{max} shifted 270 nm toward red upon the addition of bacteria (Figure 13B), β and associated TPRS intensity should change tremendously upon the addition of bacteria.

(iii) In the present set of experiment, the fundamental excitation wavelength (mode-locked Ti:sapphire laser delivering at the fundamental wavelength of 860 nm with a pulse duration of about 150 *fs* at a repetition rate of 80 MHz.) matches well with the LSPR of gold nanorod and fulfil the resonance condition for the enhanced TPRS.

Interestingly, though we could observe increment of the TPRS by four times, after the addition of 50 CFU/ mL of bacteria to our assay, we need at least 10^4 CFU/mL bacteria concentration for any visible color change to originate from nanorod aggregation. This indicates that our two-photon scattering-based gold nanorod assay is more than 2-orders of magnitude more sensitive than the usual colorimetric technique. Besides its ultra-sensitivity,

our assay is very selective over other pathogenic bacteria like *S. typhemurium*. As shown in Figure 13, there is only 6% change in TPRS signal in presence of *S. typhemurium* compared to 4000% for *E. coli*. Similarly, when we added *E. coli* bacteria to anti-Salmonella-antibody-conjugated gold nanorods, two-photon scattering intensity changes only 5%. So the above data demonstrate that our assay is highly selective. Moreover, this assay can not only distinguish two different species of bacteria (*E. coli* and *Salmonella*) but also can discriminate different strains of a single species of bacteria. In a more recent publication [211], we have also shown that gold-nanoparticle-based TPRS assay is capable of label-free detection of *Salmonella typhimurium* (*S. typhimurium*) with excellent detection limit (10^3 bacteria/mL) and high selectivity over other pathogens.

As it is clear from the above discussion that, though TPRS is a highly sensitive technique for ultrasensitive (50 CFU/mL) and selective (over different species or even different strains of same species) detection of food-borne pathogenic bacteria, research activity in this field is very limited. This could be due to the initial cost of establishment for performing the experiment or not so much knowledge is available in this field to readout the information from the experiment and apply them for efficient bacteria sensing. Hence, we need extensive research in this field to establish the TPRS technique as one of the most efficient optical methods for sensitive food-borne bacteria detection.

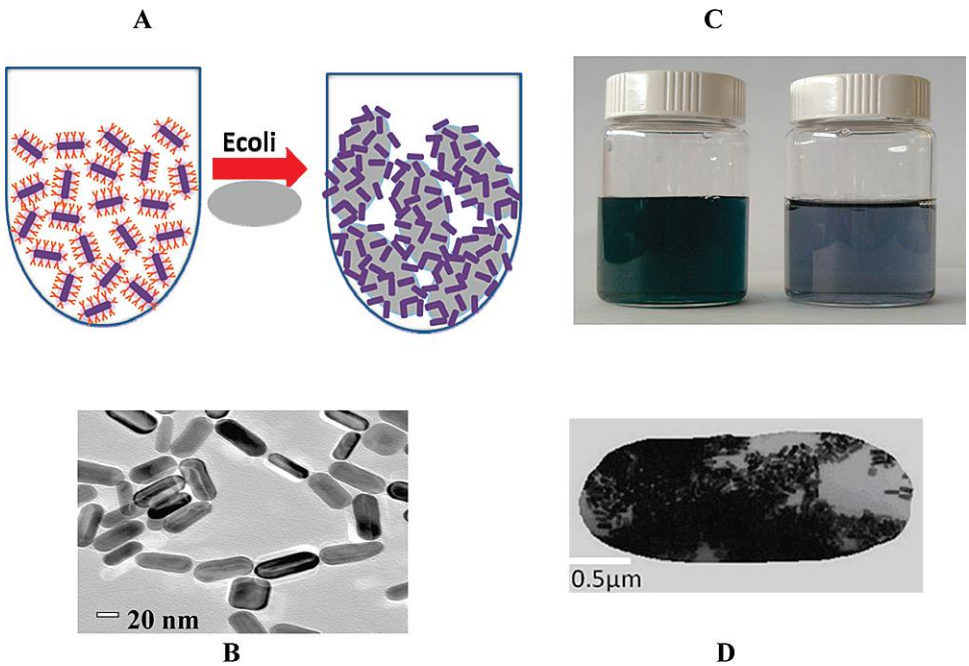

Figure 12. (A) Schematic representation of anti-*E. coli*-antibody-conjugated nanorod-based sensing of *E. coli* bacteria. (B) TEM image of anti-*E. coli*-antibody-conjugated nanorods before addition of *E. coli* bacteria. (C) Photograph showing colorimetric change upon addition of *E. coli* bacteria (10^4 CFU/mL), and (D) TEM image demonstrating aggregation of gold nanorods after the addition of *E. coli* bacteria (10^3 CFU/mL) (reprinted with permission from ref. 38d, Copyright 2009, American Chemical Society).

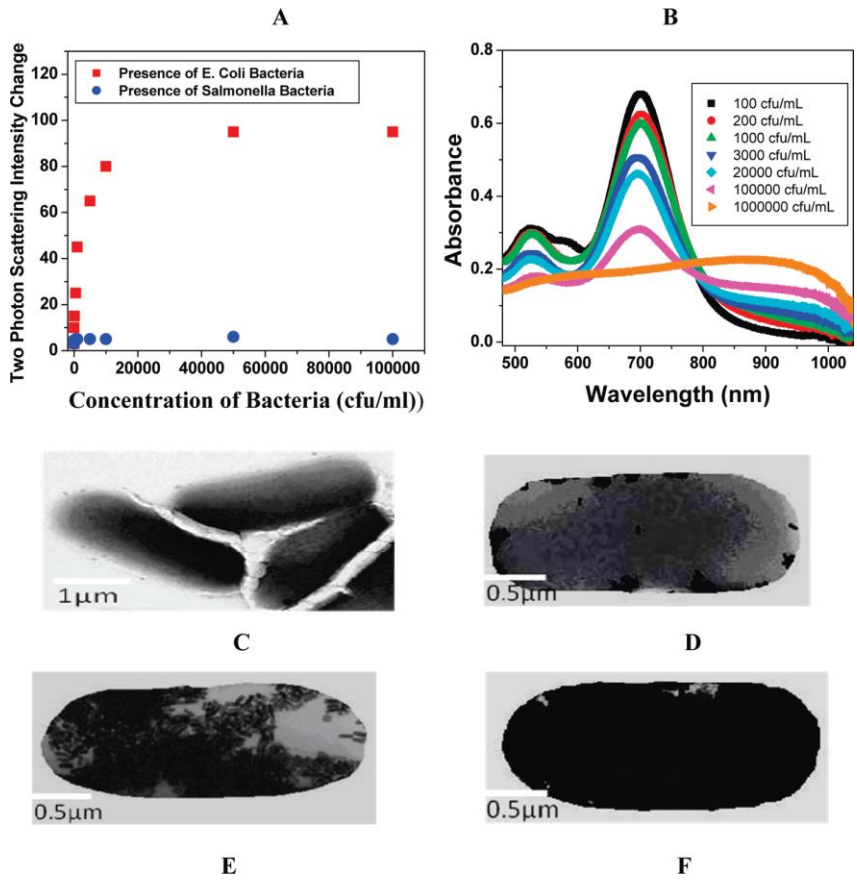

Figure 13. (A) Plot demonstrating two-photon scattering intensity changes upon the addition of *E. coli* and *Salmonella* bacteria to anti-*E. coli*-antibody-conjugated gold nanorods. (B) Absorption profile variation of anti-*E. coli*-antibody-conjugated Au nanorods due to the addition of different concentrations of *E. coli* bacteria (10^2 to 10^7 CFU/mL) (C) TEM image of *E. coli* bacteria before the addition of nanorod. (D) TEM image after the addition of 10^2 CFU/mL *E. coli* bacteria. (E) TEM image demonstrating aggregation of gold nanorods after the addition of 8×10^4 CFU/mL *E. coli* bacteria. (F) TEM image demonstrating aggregation of gold nanorods after the addition of 10^7 CFU/mL *E. coli* bacteria (reprinted with permission from ref. 38d, Copyright 2009, American Chemical Society).

3.5. Fluorescence-based Identification and Sensing

3.5.1. Principle

Plasmonic nanomaterials can serve as an excellent fluorescence quencher for Förster resonance energy transfer (NSET)-based assay [39f,212-213] due to their extraordinary high molar extinction coefficients and broad energy bandwidth [214]. Recently, there have been many reports on the development of fluorescence-based assay for the detection of bacteria [215 and the references]. These assays are based on FRET [216] or non-FRET quenching mechanisms. FRET is a spectroscopic technique in which excitation energy of the donor is transferred to an acceptor through an induced-dipole/induced-dipole interaction. The efficiency of energy transfer (E) is given by equation (5) as:

$$E = \frac{1}{1+\left(\frac{R}{R_0}\right)^6} \quad (5)$$

in which R is the distance between the donor and an acceptor and R_0 is the distance at which 50% of the energy is transferred and is a function of the spectral overlap of the donor emission and acceptor absorption, refractive index of the medium, quantum yield of the donor, and a factor κ [2] that depends on the relative orientation in space between the transition dipoles of donor and acceptor. In case of plasmonic nanoparticle-based FRET, the interaction is still dipole–dipole in nature, but is geometrically different because an acceptor nanoparticle has a surface and an isotropic distribution of dipole vectors to accept energy from the donor [56,59,91,217-218]. This arrangement increases the probability of energy transfer and accounts for the enhanced efficiency of nanoparticle-based FRET. In the case of resonant surface plasmon excitation, a small dipole in the excited fluorophore induces a large dipole in the particle, leading to an enhancement in the energy-transfer efficiencies [56,59,91,217-218].

3.5.2. Research and Development

Recently, Phillips et al. [215] have developed a bacteria sensor using chemical nose technology. The prototype sensor array was generated using three cationic gold nanoparticles and one anionic poly (*p*-Phenyleneethynylene) (PPE) polymer. As illustrated in Figure 14, presence of bacteria disrupts the initially quenched assemblies leading to fluorescence restoration of PPE. From the distinct fluorescence response patterns, the sensor array was capable of identifying 12 bacteria including both Gram-positive (e.g., *A. azurea, B. subtilis*) and Gram-negative (e.g., *E. coli, P. putida*) species, as well as three different strains of *E. coli* (Figure 14). Utilizing surface plasmon effects, Huang et al. developed a method that relies on carbohydrate-protected Au nanoparticles for bacterial detection. The method is relatively simple and capable of sensing bacteria [220]. In their assay, they have synthesized a water-soluble, luminescent, α-D-mannose-conjugated Au nanodots (Man-Au NDs) and demonstrate their applications for the detection of *Escherichia coli* (*E. coli*) through multivalent cooperative interactions between Man-Au NDs and proteins as shown in the following scheme (Scheme 1).

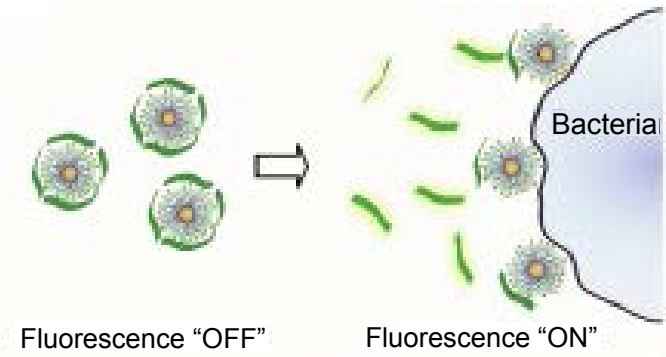

Figure 14. Displacement assay between bacteria and the AuNP-PPE complex which shows fluorescence ON-OFF for the array-based sensing of bacteria (reprinted with permission from ref. 215, Copyright 2008, Wiley-VCH).

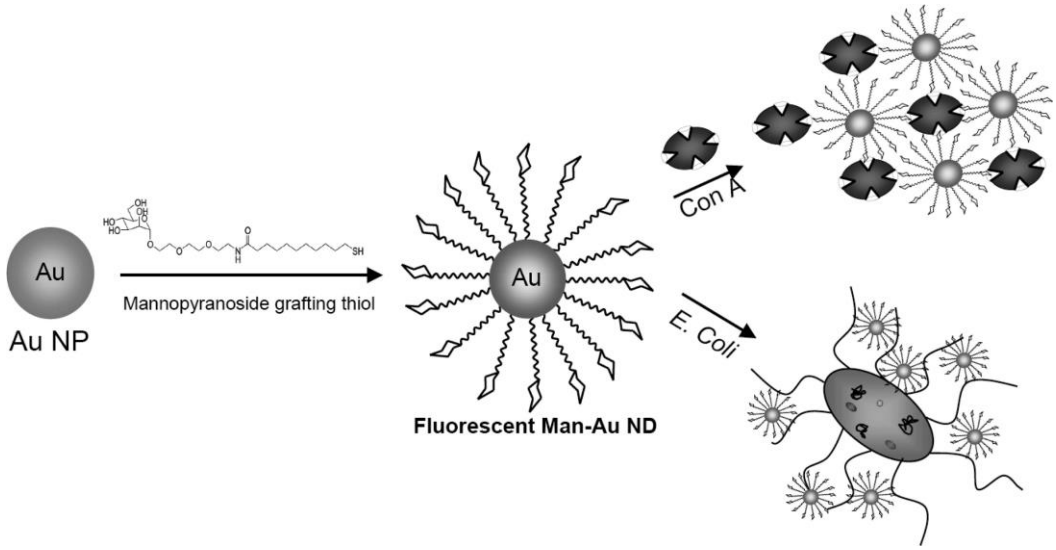

Scheme 1. Schematic Representation of the Preparation of Fluorescent Man-Au NDs for the Detection of Con A and *E. coli* (reprinted with permission from ref. 220, Copyright 2009, American Chemical Society).

Type 1 fimbriae present on the surface of Enterobacteriaceae, such as *E. coli*, are responsible for their mannose- and mannoside-binding activities [221-222]. Due to this specific affinity between mannose and fimbriae, Man-Au NDs shows mannose-specific adhesin FimH of type 1 pili in *E. coli* and could easily detect *E. coli* in a fluorescence turn-on mode. Type 1 pili are filamentous proteinaceous appendages that extend from the surface of many Gram-negative organisms; they are composed of FimA, FimF, FimG, and FimH proteins [221]. FimA accounts for more than 98% of the pilus protein; FimH is uniquely responsible for the binding to D-mannose [222]. In this study, they tested an *E. coli* strain K12 (ATCC 25404) that expresses wild-type 1 pili. After incubation of the bacterial suspensions ((1.0×10^6)-(2.5×10^8) cells/mL, 1.0 mL) with the Man-Au NDs (25 nM) in phosphate-buffered saline (PBS, pH 7.4) at 25 °C for 60 min. Incubation with *E. coli* (2.50×10^8 cells/mL) revealed that the Man-Au NDs (25 nM) bind to the bacteria, yielding brightly fluorescent cell clusters as shown in Figure 15.

Figure 15 indicates that the fluorescence increased upon increasing the concentration of *E. coli*. This assay shows a linear relationship between the fluorescence signal and the *E. coli* concentration (necessary requirement for an effective sensor) in the concentration range between 1.0×10^6 to 5.0×10^7 cells/mL ($R^2 = 0.96$), with the LOD (at a S/N ratio of 3) of *E. coli* being 7.2×10^5 cells/mL.

Though there is a considerable development in making plasmonic nanomaterials-based fluorescence sensor for bacteria detection, detection limit which ranges between 10^4-10^5 limiting its application for highly sensitive detection platform to regulate food-borne bacterial pathogens. We need to focus to design efficient fluorescent plasmonic nanomaterials for its high throughput applications in different bacteria detection in the future to compete with the QD-based assay. Due to their non toxic nature and easy surface modification, fluorescent plasmonic nanomaterials have enormous potential for the bacteria detection in a safe mode.

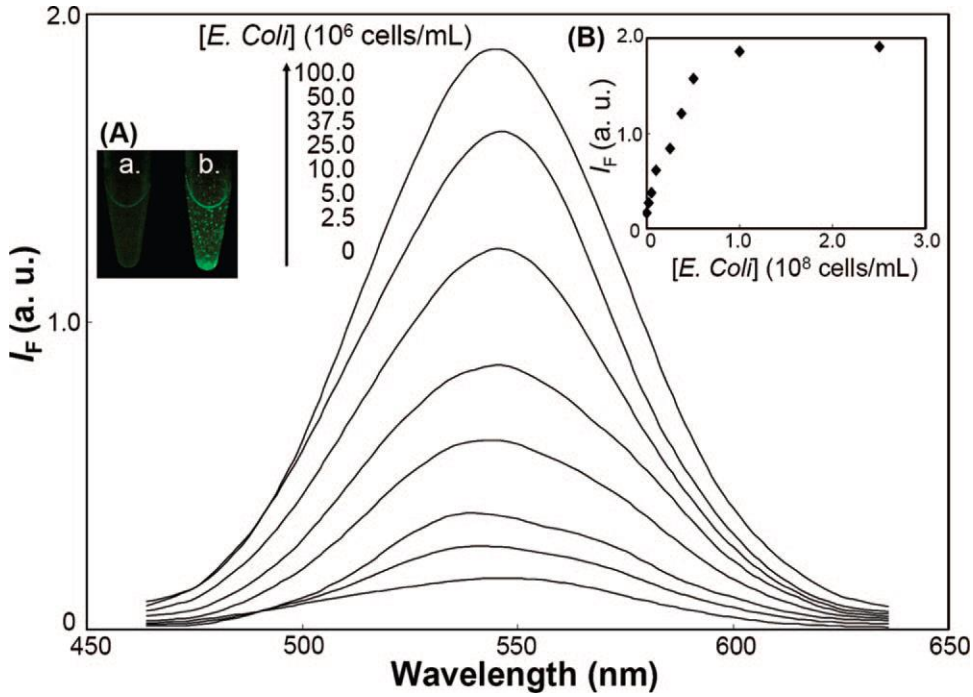

Figure 15. Fluorescence spectra of Man-Au NDs (25 nM) used as probes for the detection of *E. coli* ((2.5×10^6)-(1.0×10^8) cells/ mL). (Inset A). Visualization of Man-Au NDs (25 nM) in the (a) absence and (b) presence of *E. coli* (2.50 × 108 cells/mL) upon excitation (365 nm) under a hand-held UV lamp. (Inset B). Plot of fluorescence intensity (545 nm) versus *E. coli* concentration (reprinted with permission from ref. 220, Copyright 2009, American Chemical Society).

4. RESISTANT-BACTERIA AGAINST DRUG, HEAT, AND PH

Due to their continual mutation or gene swapping, make these bacteria resistant over the protecting conditions. These protecting conditions could be (i) antibiotics: force them to transform into drug resistant bacteria (e.g., salmonella DT104) [37, 8c], (ii) heating: forces them to transform into temperature resistant bacteria (e.g., E. *coli* 0111 and strains of Salmonella entrica) [8c], (iii) pH: acid resistant bacteria (O157:H7 strain of E. *coli* now can survive in acidic condition which supposed to be a condition for safe food. The marked acidic and environmental resistance of *E. coli* O157 [40-41] also allowed the organism to survive in apple cider and dried venison jerky). There are high proportions of antibiotic resistance (ABR) in bacteria that cause common infections (e.g. urinary tract infections, pneumonia, bloodstream infections) in all regions of the world. A high percentage of hospital-acquired infections are caused by highly resistant bacteria such as methicillin-resistant *Staphylococcus aureus* (MRSA) or multidrug-resistant Gram-negative bacteria. Antibiotic resistance (ABR) is resistance of a microorganism (e.g. bacteria) to an antibiotic drug that was originally effective for the treatment of infections caused by it. Drug resistant bacteria are able to withstand attack by antibiotics. Since the last few decades, antibiotics have been used extensively to treat pathogenic bacterial infections. Introduction of antibiotics in the medical field is one of the

most important interventions for reducing human morbidity and mortality [223-225]. After the development of penicillin in the 1940s, antibiotics became responsible for saving countless human and other lives, as well as enabling modern medical procedures. As a result, antibiotics are the economic powerhouses of our society and in the USA. There were roughly 42 billion US dollars worth of sales of antibiotics in 2009, which is almost 15–30% of drug expenditure among all therapeutic groups of drugs [223-225]. However, due to the intensive use of antibiotics, 100000 tons annually worldwide, human pathogens have become resistant to many antibiotics [171,176,223-226]. Multidrug resistance (MDR) in bacteria occurs by the accumulation of resistant plasmids or transposons of genes, with each coding for resistance to a specific drug type [223-225]. Due to the presence of multiple antimicrobial resistance genes like (1) *pse* for ampicillin resistance, (2) *floR* for chloramphenicol resistance, (3) *str* for streptomycin resistance, (4) *sulI* for sulfonamide resistance, and (5) *tetR* or tetG for tetracycline resistance, MDR bacteria are resistant to five mostly used ampicillin, chloramphenicol, streptomycin, sulfonamides, and tetracycline antibiotics and it is a cause for a major source of hospital acquired infections [223-225]. It is now estimated that multiple drug resistant bacteria cause approximately 60% of nosocomial infections [223-225]. The Infectious Diseases Society of America has already proposed a 10×20 challenge, which indicates that we must deliver 10 new antibiotics by the year 2020 [223-225]. Developing completely new antibiotics will not be easy in the present world economic condition. Since, unlike any other type of drugs, antibiotics have a limited lifespan of utility, soon we will reach a point when we will not be able to confidently treat bacterial infections by using available antibiotics. According to World Health Organization (WHO) [225] there may be another 1–2 decades left for people to use the existing antibiotics and after that multiple drug resistant bacteria (MDRB) infectious diseases cannot be cured using current antibiotics. This clearly indicates that the new approaches for the treatment of infectious bacterial pathogens that do not rely on traditional therapeutic regimes are very urgent. One promising method, still in its infancy, is to use a nanomaterial-based photothermal process for selective treatment of bacterial infections [36-37,38g-i,20,128-129,171,176-185,226].

Like drug-resitant bacteria, society is going to face the next threat from heat-resistant bacteria in everyday public health. Men's respiratory passage, skin, and superficial wounds are common sources of *S. aureus*. When *S. aureus* is allowed to grow in food, it can produce a toxin that causes illness. Although cooking destroys *S.aureus*, the toxin produced is heat stable and may not be destroyed. *Clostridium perfringens* is another bacteria that can exist as a heat-resistant spore and hence it may survive cooking and grow to large numbers if the cooked food is kept for an extensive time period. Relatively more lethal *Clostridium botulinum* bacteria can also exist as a heat-resistant spore, and can grow and produce a neurotoxin in the food. Besides these, other heat-resistant bacterium is *Bacillus cereus* whose common source is starchy food. A detailed report on the assessment of heat resistance of bacterial spores from food products by fluorescence monitoring of dipicolinic acid release was studied by Kort et al. [227]. Dipicolinic acid was first identified in bacterial spores by Powell [228] which is not indispensable for full heat-resistance. The high sensitivity, selectivity, and rapidity of this fluorescent DPA assay are of crucial importance to a direct assessment of the heat resistance of spores occurring in food samples. They have monitored fluorescence of released DPA upon heat inactivation of three different spores, Bacillus

subtilis 168, Bacillus subtilis A163, and Bacillus sporothermodurans IC4, based on the enhancement of the fluorescence emission (at 545nm) of the terbium ion (Tb^{3+}) upon binding to DPA [229]. The critical DPA release temperature (T_c), the temperature at which half the DPA content has been released within a fixed incubation time, from three different Bacillus strains 168, A163, and IC4 are of 108°C, 121°C, and 131°C, respectively.

Like heat-resistant bacteria, there are several acid-resistance bacteria available which can create a serious concern for the resistant bacterial infection. For more study on acid resistant bacteria, readers can go through the review article by Cotter and Hill [230]. Most common acid-resistant bacteria are: *L. monocytogenes* (Listeria not only survives in extreme acid stress but also requires a drop in pH in order to activate hemolysin, the toxin that permits its escape from the phagosome), *Rhodococcus equi* (stable at pH~4.0), *Mycobacterium tuberculosis* (causative agent of tuberculosis), *Mycobacterium avium* (causes one of the most common opportunistic infections in AIDS patients), *Mycobacterium avium* subsp. *paratuberculosis* (causative agent of para-tuberculosis), *Staphylococcus aureus* (resistant at pH 2.0), and *B. cereus* (resistant at pH 4.6). Out of all these different acid-resistant bacteria, only *B. cereus* causes serious food poisoning.

5. BIO-CONJUGATED PLASMONIC NANOMATERIALS FOR SELECTIVE DESTRUCTION OF FOOD-BORNE BACTERIA

Since last one decade, we have exploited bio-conjugated plasmonic nanomaterials for the selective destruction of pathogens, multidrug-resistant bacteria, and cancer cells. For this purpose, bio-conjugated nanomaterials of different sizes and shapes have been designed for diagnostics, capture and photothermal killing of normal and MDR bacteria. For the selective sensing and therapy, nanomaterials have been modified with different recognition elements to target antigen-presenting cells as epitopes present on the pathogen surface [36-37,38i,128-129,171,176-185,226]. Antibodies, aptamers, organic ligands and antimicrobial peptides are the most common recognition elements that have been used to modify nanomaterials for selective sensing and therapy [6,36-37,38i,128-129,171,176-185,226] (as shown in Scheme 2). Once we specifically target the bacterium by bio-conjugated plasmonic nanomaterials, optical radiation can be used to destruct the targeted bacteria. The basic principle of this destruction is based on the hyperthermic effect of plasmonic nanomaterials, i.e., the energy funneling of nanomaterials' plasmon excitation (electronic excitation) as thermal energy [231-232]. In this case, gold nanoparticles serve as ‘‘light-directed nanoheaters’’, which are very useful in biomedicine, such as selective laser photothermolysis of pathogens [20,36,38g,129,184-185]. Gold nanoparticles are known to absorb light several million times stronger than organic dye molecules and also there is a possibility that most of the absorbed light will be converted to heat via the nonradiative properties [20,36,38g,109,129,182,184-185].

From earlier dynamics studies [233-245] it is clear that the entire process starting from electronic excitation of the nanomaterial to finally thermal releasing of the input energy to the surroundings occurs in the sub nano second time scale through stepwise dynamic process. From the solid state thermalization knowledge, the probable mechanism of nanomaterials energy relaxation process (Scheme 3) starts with very fast electronic excitation of the

nanomaterials' surface electron cloud in the *fs* time scale (~100*fs*), followed by relatively fast electron-phonon coupling between surface electron energy and nanocrystals' phonons in the *sub-ps* time scale (<10*ps*). Once the energy tunnels to the crystal lattice, phonon-phonon coupling starts heating up the nanocrystals in *ps* time scale (>30*ps*) and finally the generated heat transports site-specifically to the surface-adsorbed entity through surrounding medium in the sub-ns time scale (>100*ps*) [234] depending on the thermal conductivity of the surrounding medium, heat capacity of the exciting nanocrystals, size and shape of the nanoparticles, dimension of the surface-adsorbed molecule, nature of bonding (chemisorbed Vs. physisorbed) between nanosurface and surface-adsorbed entity [232].

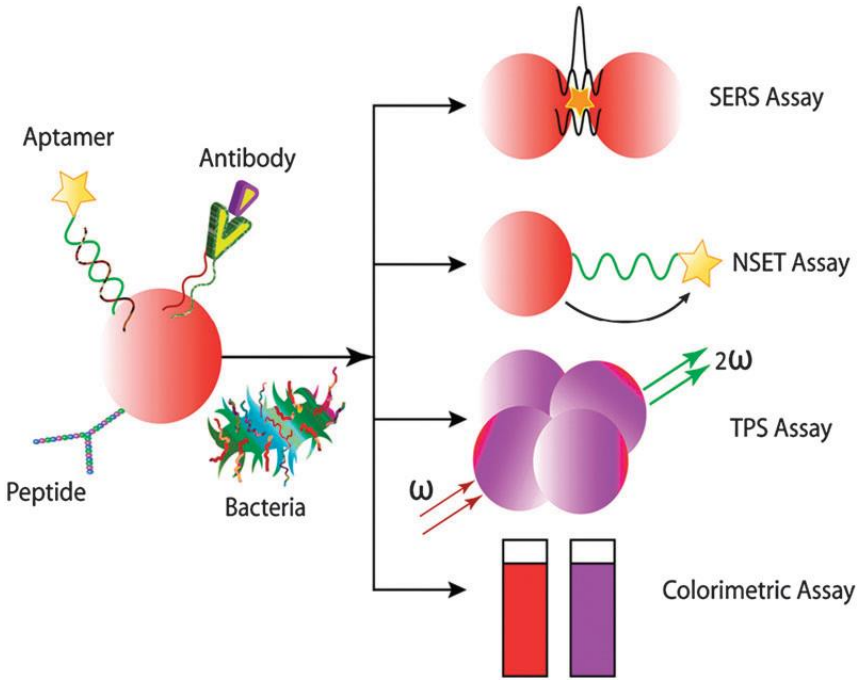

Scheme 2. Schematic representation showing different plasmon based optical techniques for selective sensing of pathogens (reprinted with permission from ref. 6, Copyright 2012, Royal Society of Chemistry).

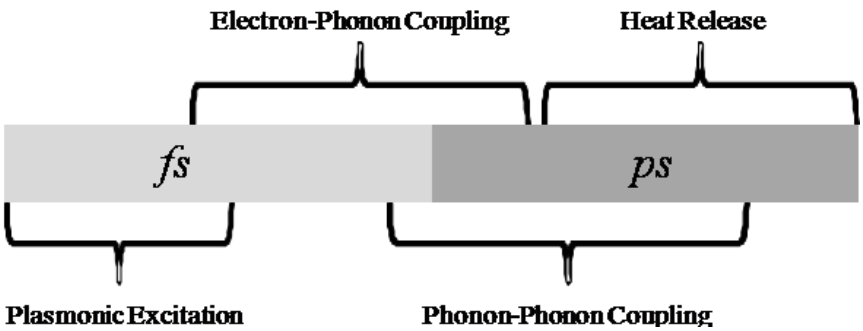

Scheme 3. Energy relaxation dynamics of Plasmonic nanomaterials.

As a result of this, temperature rises on the order of a few tens of degrees on the surface nanoscopically, which produces sufficient heat for the destruction of bacteria attached with these nanomaterials *via* cell damage using different thermal effects, such as denaturation of proteins/enzymes, induction of heat-shock proteins, metabolic signaling disruption, endothelial swelling, microthrombosis, etc. Since the previously discussed multidrug-resistant bacteria can't be killed by applying the existing antibiotics, we can adopt this hyperthermic method for MDRB destruction too [20,36,38g,129,184-185]. Moreover, bio-conjugated plasmonic nanomaterials can selectively bind with the bacteria surface and hence by proper tuning the laser wavelength to match with the LSPR of the nanomaterials we can destroy MDRB completely. Destruction of MDRB via cell damage can happen through different thermal effect, such as denaturation of proteins/enzymes, induction of heat-shock proteins, metabolic signaling disruption, endothelial swelling, microthrombosis, etc [20,36,38,129,184-185,246].

In the last few years, due to the availability of established synthetic protocols for the controlled preparation of gold nanostructures and their unique photothermal properties in the presence of IR light, several groups including ours have been developing suitable nanomaterials for photothermal therapy of pathogenic bacteria and cancer [20,36,66,109,182,185,212,247-250]. Among several MDRB, *Salmonella DT104* and *E. coli* are the two major food-borne pathogens which can cause serious food poisoning and mortality of human life. Recently we have reported targeted photothermal killing of MDRB *Salmonella DT104* by using antibody-conjugated popcorn shaped gold nanoparticles [129]. For selective killing, we have modified the popcorn shaped gold nanoparticle surface by monoclonal M3038 antibody, as shown in Scheme 4.

For photothermal therapy we have used a portable continuous wavelength OEM laser operating at 670 nm, with 200 mW cm^{-2} power as an excitation light source. Our selective MDRB *Salmonella typhimurium DT104* photothermal lysis is based on the fact that monoclonal M3038 antibody-conjugated popcorn shaped gold nanoparticles can readily and specifically bind with *Salmonella typhimurium DT104* bacterium O-antigen [251], through antibody–antigen recognition. In presence of M3038 antibody-conjugated popcorn shaped gold nanoparticle, gold nanoparticle not only undergoes aggregation on *Salmonella typhimurium DT104* bacteria surface but also form a microbial cluster with absorption maxima ~650nm and fulfil the suitable condition for the resonance excitation of SPR to generate light induced heating and subsequent killing of MDRB through irreversible cell membrane destruction. Photothermal lysis of MDRB *Salmonella typhimurium DT104* was confirmed by colony counting on the tryptic agar plate. Figure 16 shows the number of colonies after 0, 6, 11, and 17 minutes of NIR exposure, when the initial concentration of MDRB was 4×10^5 CFU mL^{-1}. Figure 16B shows that after 20 minutes of NIR exposure, 100% of bacteria were killed.

To demonstrate that our gold nanotechnology based assay can kill MDRB from a food sample, we have reported [129] a photothermal assay to kill MDRB using MDRB *Salmonella DT104* infected romaine lettuce. Table 2 shows how the laser irradiation time varies with the concentration of bacteria (CFU g^{-1}) to kill 100% MDRB, from an MDRB infected lettuce sample. As shown in Table 2, 100% of bacteria can be destroyed by 6 to 30 minutes laser irradiation treatment, depending on the initial MDRB concentration (10^2–10^7 CFU g^{-1}).

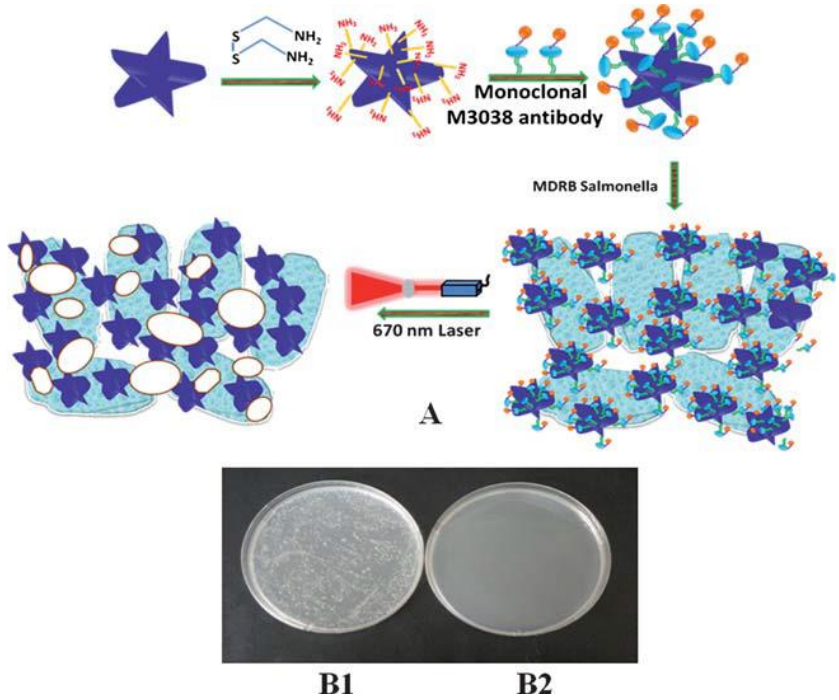

Scheme 4. (A) Schematic representation showing the monoclonal M3038 antibody conjugated popcorn shaped gold nanotechnology-driven approach to selective photothermal killing of MDRB Salmonella. (B) Colonies of MDRB Salmonella DT104 (B1) before and (B2) after exposing to 670 nm light with 200 mW cm^{-2} power for 20 minutes in the presence of monoclonal M3038 antibody-conjugated popcorn shaped gold nanoparticles (reprinted with permission from ref. 129, Copyright 2011, Royal Society of Chemistry).

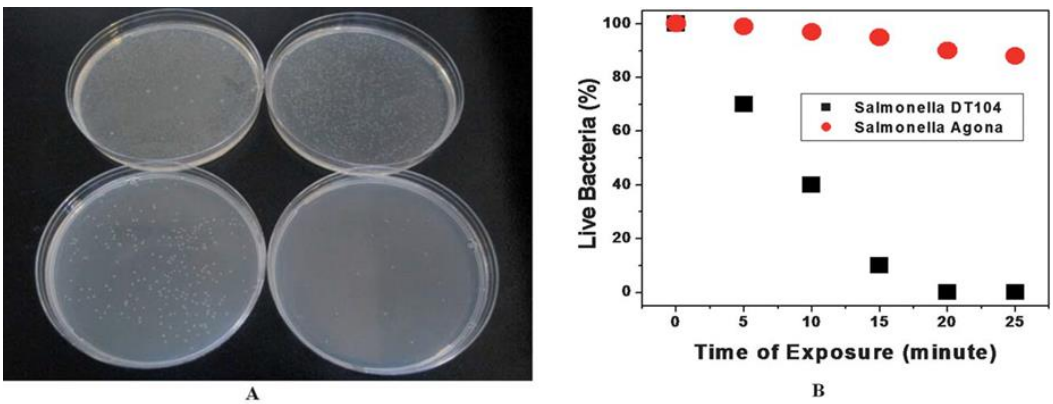

Figure 16. (A) Colonies of MDRB *Salmonella* DT104 after exposing to monoclonal M3038 antibody-conjugated popcorn shaped gold nanoparticles using 200 $mWcm^{-2}$ 670 nm light for 0, 6, 11 and 17 minutes. (B) Plot showing time dependent effect of photothermal lysis when antibody attached popcorn shaped gold nanoparticle conjugated *Salmonella* DT104, *Salmonella Agona* bacteria were treated using 200 mW/cm^2 670 nm light (reprinted with permission from ref. 129, Copyright 2011, Royal Society of Chemistry).

Table 2. Laser irradiation time to kill 100% MDRB in lettuce samples (reprinted with permission from ref. 129, Copyright 2011, Royal Society of Chemistry)

Concentration of MDRB (CFU g^{-1}) in lettuce samples	Laser irradiation time (minutes) to kill 100% bacteria
10^2	6
10^3	9
10^4	14
10^5	20
10^6	25
10^7	30

Our photothermal therapy result is encouraging to find the alternative medication to treat the food-borne multidrug-resistant Salmonella typhimurium DT104 bacteria. Similar technology we can apply for the destruction of drug-resistant *E. coli* bacteria too, which is the leading cause of gastrointestinal infections. Multidrug-resistant *E. coli* is simultaneously resistant to a third generation cephalosporin, aminoglycoside, and fluoroquinolone. In a recent study by J. A. Karlowsky and co-workers [252] revealed that out of 38,835 urinary isolates of *E. coli* which have been tested against ampicillin, cephalothin, ciprofloxacin, nitrofurantoin, and trimethoprim-sulfamethoxazole, 7.1% (2,763 of 38,835) were resistant to three or more agents and considered multidrug resistant. Among the multidrug-resistant isolates, 97.8% were resistant to ampicillin, 92.8% were resistant to trimethoprim-sulfamethoxazole, 86.6% were resistant to cephalothin, 38.8% were resistant to ciprofloxacin, and 7.7% were resistant to nitrofurantoin. Still there is no definitive medication to treat multidrug-resistant *E. coli* and in this respect our nanoparticle-based photothermal therapy could lead the road for the treatment of multidrug-resistant *Salmonella* and *E. coli*.

CONCLUSION

The current chapter gives a brief review about the food-borne pathogenic bacteria, consequence of their infections, different plasmonic nanomaterials developed for their selective and sensitive detection, and possible roots for their complete destructions. By utilizing nanomaterial's size and shape dependent plasmonic properties, development of different optical and spectroscopic techniques for selective and sensitive bacteria detection has been accounted. Each technique has some advantages and disadvantages over the others to formulate our ultimate target of making a sensor for universal application. Properly chosen bio-functionalized plasmonic nanostructured materials enable us to develop Nano-Medicine for selective detection and ultrasensitive quantification. A special section of this chapter review, the cause and consequences of resistant-Bacteria against drug, heat, and pH. Nanomaterials-based hyperthermic or photothermal therapeutic method has been described in details where the nanomaterials act as a nano-antena to absorb light several million times stronger than the organic dye molecules and then finally release this input light energy as thermal energy on to the surface of bacteria to destroy them via cell damage through different thermal effects, such as denaturation of proteins/enzymes, induction of heat-shock

proteins, metabolic signaling disruption, endothelial swelling, and microthrombosis. This nanomaterials-based untrendy therapy is most suitable for MDRB as multidrug-resistant bacteria can't be killed by applying the existing antibiotics.

ACKNOWLEDGMENT

Special thanks to BARD project (PIC No. 12-R&D-SIN-5.04-0103), Department of Atomic Energy, Government of India, for their generous laboratory establishment funding.

REFERENCES

[1] Estimation of the global burden of foodborne disease, http://www.who.int/foodsafety/ foodborne_disease/ferg/en/

[2] Mead, PS; Slutsker, L; Dietz, V; McCaig, LF; Bresee, JS; Shapiro, C; Griffin, PM; Tauxe, RV. Food-related illness and death in the United States, *Emerg. Infec. Dis.* 1999, 5, 607-625.

[3] United States Department of Agriculture, http://www.usda.gov/ wps/portal/usda /usdahome

[4] Bacteria and Viruses. http://www.foodsafety.gov/poisoning/causes/bacteriaviruses/

[5] (a) National Antimicrobial Resistance Monitoring System for Enteric Bacteria (NARMS), http://www.cdc.gov/NARMS; (b) Salmonella, http://www. who.int/topics/ salmonella/en; (c) Escherichia coli infections, http://www.who.int/topics/escherichia _coli_infections/en/; (d) Listeria infections, http://www.who.int/topics/listeria_ infections/en/; (e) Campylobacter, http://www.who. int/ topics/campylobacter/en/; (f) Parasites-Toxoplasmosis (*Toxoplasma* Infection) http://www.cdc.gov/parasites/ toxoplasmosis/gen_ info/faqs.html; (g) Xu, C; Li, ZS; Du, YQ; Gong, YF; Yang, H; Sun, B; Jin, J. Construction of recombinant attenuated Salmonella typhimurium DNA vaccine expressing H pylori ureB and IL-2, *World J. Gastroenterol.* 2007, 13, 939 – 944; (h) Strassert, CA; Otter, M; Albuquerque, RQ; Hçne, A; Vida, Y; Maier, B; De Cola, L. Photoactive Hybrid Nanomaterialfor Targeting, Labeling, and Killing Antibiotic-Resistant Bacteria, *Angew. Chem.* 2009, 121, 8070 – 8073, Angew. Chem. Int. Ed. 2009, 48, 7928 –7931; (i) Delibato, E; Volpe, G; Romanazzo, D; De Medici, D; Toti, L; Moscone, D; Palleschi.G. Development and Application of an Electrochemical Plate Coupled with Immunomagnetic Beads (ELIME) Array for *Salmonella enterica* Detection in Meat Samples, *J. Agric. Food Chem.* 2009, 57, 7200 – 7204; (j) Zelada-Guillen, GA; Riu, J ;Duzgun, A; Rius, FX. Immediate Detection of Living Bacteria at Ultralow Concentrations Using a Carbon Nanotube Based Potentiometric Aptasensor, *Angew. Chem.* 2009, 121, 7470 – 7473; *Angew. Chem. Int. Ed.* 2009, 48, 7334 – 7337; (k) Berry, V; Gole, A; Kundu, S; Murphy, CJ; Saraf, RF. Deposition of CTAB-Terminated Nanorods on Bacteria to Form Highly Conducting Hybrid System, *J. Am. Chem. Soc.* 2005, 127, 17600 –17601.

[6] Ray, PC; Khan, SA; Singh, AK; Senapati, D; Fan, Z. Nanomaterials for targeted detection and photothermal killing of bacteria, *Chem. Soc. Rev.*, 2012, 41, 3193–3209.

[7] Yang, H; Qu, LW; Lin, Y; Jiang, XP;Sun,YP. Detection of Listeria monocytogenes in Biofilms Using Immunonanoparticles, *J. Biomed. Nanotechnol.*, 2007, 3, 131–138.

[8] a) Ram, S;Vajpayee, P;Shanker, R. Rapid Culture-Independent Quantitative Detection of Enterotoxigenic *Escherichia coli* in Surface Waters by Real-Time PCR with Molecular Beacon, *Environ. Sci. Technol.*, 2008, 42, 4577 – 4582; b) Phillips,CA. The epidemiology, detection and control of *Escherichia coli* O157 *J. Sci. Food Agric.*, 1999, 79, 1367 –1381; c) Butler, D. Novel pathogens beat food safety checks, *Nature*, 1996, 384, 397; d) Wyatt, A;Langley, MN;Lee, HA;Morgan, MRA. Further Studies on the Feasibility of One-Day *Salmonella* Detection by Enzyme-Linked Immunosorbent Assay, *Appl. Environ. Micobiol.*, 1993, 59, 1383 – 1390; e) Rivas, LA;Villadangos, MG;Paz, MM;Gil, PC;Elvira, JG;Parro, V. A 200-Antibody Microarray Biochip for Environmental Monitoring: Searching for Universal Microbial Biomarkers through Immunoprofiling, *Anal. Chem.*, 2008, 80, 7970 –7979.

[9] Naumann, D;Helm, D;Labischinski, H. Microbiological characterization by FT-IR spectroscopy, *Nature*, 1991, 351, 81-82.

[10] Lay, JOJ. MALDI-TOF mass spectrometry and bacterial taxonomy, *Trends Anal. Chem.*, 2000, 19, 507-516.

[11] Zhou, X;Jiao, X. Polymerasechain reaction detection of *Listeria monocytogenes*using oligonucleotide primers targeting *actA* gene, *Food Control*, 2005, 16, 125-130.

[12] Hawkes, JJ; Long, MJ;Coakley, WT;McDonnell, MB. Ultrasonic deposition of cells on a surface, *Biosens. Bioelectron.* 2004, 19, 1021-1028.

[13] Dubosson, CR;Conzelmann, C;Miserez, R;Boerlin, P;Frey, J;Zimmermann, W. Development of two real-time PCR assays for the detection of Mycoplasma hyopneumoniae in clinical samples, *Vet. Microbiol.*, 2004, 102, 55-65.

[14] Kox, LF;Rhienthong, D;Miranda, AM;Udomsantisuk, N;Ellis, K;van Leeuwen, J;van Heusden, S;Kuijper, S;Kolk, AH. A more reliable PCR for detection of Mycobacterium tuberculosis in clinical samples, *J. Clin. Microbiol.*, 1994, 32, 672-678.

[15] Subramanian, A; Irudayaraj, J;Ryan, T. A mixed self-assembled monolayer-based surface plasmon immunosensor for detection of E coli O157:H7, *Biosens. Bioelectron.*, 2006, 21, 998-1006.

[16] Prior, JL; Titball, RW. Monoclonal antibodies against Yersinia pestis lipopolysaccharide detect bacteria cultured at 28 degrees C or 37 degree C, *Mol. Cell. Probes*, 2002, 16, 251-256.

[17] Maalouf, R;Wirth, CF;Coste, J;Chebib, H;Saikali, Y;Vittori, O;Errachid, A;Cloarec, JP;Martelet, C;Renault, NJ. Label-free detection of bacteria by electrochemical impedance spectroscopy: comparision to surface plasmon resonance, *Anal. Chem.*, 2007, 79, 4879-4886.

[18] Subramanian, A; Irudayaraj, J;Ryan, T. Mono and dithiol surfaces on surface plasmon resonance biosensors for detection of *Staphylococcus aureus*, *Sens. ActuatorsB*, 2006, 114, 192-198.

[19] Møller, K;Nielsen, R;Andersen, LV;Kilian, M. Clonal analysis of the *Actinobacillus pleuropneumoniae* population in a geographically restricted area by multilocus enzyme electrophoresis, *J. Clin. Microbiol.* 1992, 30, 623-627.

[20] Wang,C;Irudayaraj, J. Gold Nanorod Probes for the Detection of Multiple Pathogens, *small*, 2008, 4, 2204–2208.

[21] Jofre, A; Martin, B; Garriga, M;Hugas, M; Pla, M; Rodriguez-Lazaro, D; Aymerich, T. Simultaneous detection of Listeria monocytogenes and Salmonella multiplex PCR in cooked ham,*Food Microbiol.*, 2005, 22, 109-115.

[22] Gonzalez, SF;Krug, MJ;Nielsen, ME;Santos, Y;Call, DR. Simultaneous Detection of Marine Fish Pathogens by Using Multiplex PCR and a DNA Microarray, *J. Clin. Microbiol.*, 2004, 42, 1414-1419.

[23] Wang, D; Coscoy, L; Zylberberg, M; Avila, PC; Boushey, HA; Ganem, D; DeRisi, JL. Microarray-based detection and genotyping of viral pathogens, *Proc. Natl. Acad. Sci. USA*, 2002, 99, 15687-15692.

[24] Sapsford, KE; Rasooly, A; Taitt, CR; Ligler, FS. Detection of campylobacter and Shigella species in food samples using an array biosensor, *Anal. Chem.*, 2004, 76, 433-440.

[25] Taitt, CR; Golden, JP; Shubin, YS; Shriver-Lake, LC; Sapsford, KE; Rasooly, A; Ligler, FS. A portable array biosensor for detection multiple analytes in complex samples, *Microb. Ecol.*, 2004, 47, 175-185.

[26] El-Boubbou, K; Gruden, C; Huang, XF. Magnetic Glyco-nanoparticles: A Unique Tool for Rapid Pathogen Detection, Decontamination, and Strain Differentiation, *J. Am. Chem. Soc.*, 2007, 129, 13392-13393.

[27] Gu, HW;Ho, PL;Tsang, KWT;Wang, L;Xu, B. Using Biofunctional Magnetic Nanoparticles to Capture Vancomycin-Resistant Enterococci and Other Gram-Positive Bacteria at Ultralow Concentration, *J. Am. Chem. Soc.*, 2003, 125, 15702-15703.

[28] Ho, KC; Tsai, PJ; Lin, YS; Chen, YC. Using biofunctionalized nanoparticles to probe pathogenic bacteria, *Anal. Chem.*, 2004, 76, 7162-7168.

[29] Lin, YS; Tsai, PJ; Weng, MF; Chen, YC. Affinity capture using vancomycin-bound magnetic nanoparticles for the MALDI-MS analysis of bacteria, *Anal. Chem.*, 2005, 77,1753-1760.

[30] Varshney, M; Li, YB. Inter digitated array microelectrode based impedance biosensor coupled with magnetic nanoparticle–antibody conjugates for detection of *Escherichia coli* O157:H7 in food samples, *Biosens. Bioelectron.*, 2007, 22, 2408-2414.

[31] Naja, G; Bouvrette, P; Hrapovic, S; Luong, JHT. Raman-based detection of bacteria using silver nanoparticles conjugated with antibodies, *Analyst*, 2007, 132, 679-686.

[32] Premasiri, WR;Moir, DT;Klempner, MS;Krieger, N;Jones, G II; Ziegler, LD. Characterization of the Surface Enhanced Raman Scattering (SERS) of Bacteria, *J. Phys. Chem. B*, 2005, 109, 312-320.

[33] Kalele, SA;Kundu, AA;Gosavi, SW;Deobagkar, DN;Deobagkar, DD;Kulkarni, SK. Rapid Detection of *Escherichia coli* by Using Antibody-Conjugated Silver Nanoshells, *Small*, 2006, 2, 335-338.

[34] Wang, L;Zhao, WJ; O'Donoghue, MB;Tan, WH. Fluorescent Nanoparticles for Multiplexed Bacteria Monitoring, *Bioconjugate Chem.*, 2007, 18, 297-301.

[35] Yang, L;Li, YB. Simultaneous detection of Escherichia coli O157:H7 and Salmonella Typhimurium using quantum dots as fluorescence labels, *Analyst*, 2006, 131, 394-401.

[36] Wang, S;Singh, AK;Senapati, D;Neely, A;Yu, H;Ray, PC. Rapid Colorimetric Identification and Targeted Photothermal Lysis of *Salmonella* Bacteria by Using Bioconjugated Oval-Shaped Gold Nanoparticles, *Chem. Eur. J.*, 2010, 16, 5600 – 5606.

[37] Khan, SA;Singh, AK;Senapati, D;Fan, Z;Ray, PC. Targated highly sensitive detection of multi-drug resistant salmonella DT104 using gold nanoparticles, *Chem. Commun.*, 2011, 47, 9444–9446.

[38] a) Lee, H;Yoon, TJ;Weissleder, R. Ultrasensitive detection of bacteria using core-shell nanoparticles and an NMR-filter system, *Angew. Chem.*, 2009, 121, 5767 – 5770; *Angew. Chem. Int. Ed.*, 2009, 48, 5657 –5660; b) Zheng, X;Sallum, UW;Verma, S;Athar, H;Evans, CL;Hasan, T. Exploiting a Bacterial Drug-Resistance Mechanism: A Light-Activated Construct for the Destruction of MRSA, *Angew. Chem.*, 2009, 121, 2182 –2185; *Angew. Chem. Int. Ed.*, 2009, 48, 2148 –2151; c) Sean, NR;John, SW;Murphy, CJ;Attwood, S. Targated Photothermal Lysis of the Pathogenic Bacteria, *Pseudomonas aeruginosa*, with Gold Nanorods, *Nano Lett.*, 2008, 8, 302 –306; d) Singh, AK;Senapati, D;Wang, S;Griffin, J;Neely, A;Candice, P;Naylor, KM;Varisli, B;Kalluri, JR;Ray, PC. Gold nanorod Based Selective Identification of *Escherichia coli* Bacteria Using Two-Photon Rayleigh Scattering Spectroscopy, *ACS Nano*, 2009, 3, 1906 – 1912; f) Ravindranath, SP;Mauer, LJ;Deb-Roy, C;Irudayaraj, J. Biofunctionalized Magnetic Nanoparticle Integrated Mid-Infrared Pathogen Sensor for Food Matrixes, *Anal. Chem.*, 2009, 81, 2840 – 2846; g) Zharov, VP;Mercer, KE;Galitovskaya, EN;Smeltzer, MS. Photothermal Nanotherapeutics and Nanodiagnostics for Selective Killing of Bacteria Targeted with Gold Nanoparticles, *Biophys. J.*, 2006, 90, 619 –627; h) Kim, CB;Yi, DK;Kim, PS;Lee, W;Kim, MJ. Rapid photothermal lysis of the pathogenic bacteria, Escherichia coli using synthesis of gold nanorods, *J. Nanosci. Nanotechnol.*, 2009, 9, 2841 –2845; i) Huang, WC;Tsai, PJ;Chen, YC. Functional gold nanoparticles as photothermal agents for selective-killing of pathogenic bacteria, *Nanomedicine*, 2007, 2, 777 – 787.

[39] a) Kalluri, JR;Arbneshi, T;Khan, SA;Neely, A;Candice, P;Varisli, B;Washington, M;McAfee, S;Robinson, B;Banerjee, S;Singh, AK;Senapati, D;Ray, PC. Use of Gold Nanoparticles in a Simple Colorimetric and Ultrasensitive Dynamic Light Scattering Assay: Selective Detection of Arsenic in Groundwater, *Angew. Chem.*, 2009, 121, 9848 –9851; *Angew. Chem. Int. Ed.*, 2009, 48, 9668 –9671; b) Dasary, SSR;Singh, AK;Senapati, D;Yu, H;Ray, PC. Gold Nanoparticle Based Label-Free SERS Probe for Ultrasensitive and Selective Detection of Trinitrotoluene, *J. Am. Chem. Soc.*, 2009, 131, 13806 – 13812; c) Mulvihill, M;Tao, A;Benjauthrit, K;Arnold, J;Yang, P. Surface-Enhanced Raman Spectroscopy for Trace Arsenic Detection in Contaminated Water, *Angew. Chem.*, 2008, 120, 6556 –6560; *Angew. Chem. Int. Ed.*, 2008, 47, 6456 – 6460; d) Marbella, L;Mitasev, BS;Basu, P. Development of a Fluorescent Pb^{2+} Sensor, *Angew. Chem.*, 2009, 121, 4056 –4058; *Angew. Chem. Int. Ed.*, 2009, 48, 3996 –3998; e) Chen, X;Braunschweig, AB;Wiester, MJ;Yeganeh, S;Ratner, MA;Mirkin, CA. Spectroscopic Tracking of Molecular Transport Junctions Generated by Using Click Chemistry, *Angew. Chem.*, 2009, 121, 5280 – 5283; *Angew. Chem. Int. Ed.*, 2009, 48, 5178 – 5181; f) Griffin, J;Singh, AK;Senapati, D;Rhodes, P;Mitchell, K;Robinson, B;Yu, E;Ray, PC.. Size- and Distance-Dependent Nanoparticle Surface-Energy Transfer (NSET) Method for Selective Sensing of Hepatitis C Virus RNA, *Chem.-Eur. J.*, 2009, 15, 342 –351; g) Du, BA;Li, ZP;Liu, CH. One-Step Homogeneous Detection of DNA Hybridization with Gold Nanoparticle Probes by Using a Linear Light-Scattering Technique, *Angew. Chem. Int. Ed.*, 2006, 45, 8022 – 8025; h) Darbha, GK;Rai, US;Singh, AK;Ray, PC. Selective Detection of Mercury (II) Ion Using

Nonlinear Optical Properties of Gold Nanoparticles, *J. Am. Chem. Soc.*, 2008, 130, 8038 –8043; i) Ray, PC. Diagnostics of Single Base-Mismatch DNA Hybridization on Gold Nanoparticles by Using the Hyper-Rayleigh Scattering Technique, *Angew. Chem.*, 2006, 118, 1169 –1172; *Angew. Chem. Int. Ed.*, 2006, 45, 1151 – 1154.

[40] Armstrong, GL; Hollingsworth, J; Morris, JG jr. Emerging foodborne pathogens: Escherichia coli O157:H7 as a model of entry of a new pathogen into the food supply of the developed world, *Epidemiol Rev.*, 1996, 18, 29-51.

[41] Busani, L; Scavia, G; Luzzi, I; Caprioli, A. Laboratory surveillance for prevention and control of foodborne zoonoses, *Ann. Ist. Super Sanità.*, 2006, 42, 401-404

[42] StLouis, ME; Morse, DL; Potter, ME; DeMelfi, TM; Guzewich, JJ; Tauxe, RV. The emergence of grade A eggs as a major source of Salmonella enteritidis infections, *JAMA* 1988, 259, 2103-2107.

[43] Caprioli, A; Morabito, S; Brugere, H; Oswald, E. Enterohaemorrhagic Escherichia coli: emerging issues on virulence and modes of transmission,*Vet. Res.*, 2005, 36, 289-311.

[44] Tozzi, AE; Gorietti, S; Caprioli, A. In: Duffy G, Garvey P, McDowell D (Ed.) *Verocytotoxigenic Escherichia coli*. Trumbull: Food & Nutrition Press; 2001. 161-79.

[45] *E. coli (Escherichia coli)*,http://www.cdc.gov/ecoli/general/

[46] Salmonella.http://www.foodsafety.gov/poisoning/causes/bacteriaviruses/salmonella/index.html

[47] Robinson, S. The big five: Most common Salmonella strains in food-borne illness outbreaks, August 19, 2013

[48] Olsen, SJ; Patrick, M; Hunter, SB; Reddy, V; Kornstein, L; MacKenzie, WR; Lane, K; Bidol, S; Stoltman, GA; Frye, DM; Lee, I; Hurd, S; Jones, TF; LaPorte, TN; Dewitt, W; Graves, L; Wiedmann, M; Schoonmaker-Bopp, DJ; Huang, AJ; Vincent, C; Bugenhagen, A; Corby, J; Carloni, ER; Holcomb, ME; Woron, RF; Zansky, SM; Dowdle, G; Smith, F; Ahrabi-Fard, S; Ong, AR; Tucker, N; Hynes, NA; Mead, P. Multistate Outbreak of *Listeria monocytogenes* Infection Linked to Delicatessen Turkey Meat, *Clin. Infect. Dis.*, 2005, 40, 962-967.

[49] Edman, DC; Pollock, MB; Hall, ER. *Listeria monocytogenes* L Forms I. Induction, Maintenance, and Biological Characteristics, *J. Bacteriology*, 1968, 96, 352-357.

[50] Bishop, DK; Hinrichs, DJ. Adoptive transfer of immunity to Listeria monocytogenes. The influence of in vitro stimulation on lymphocyte subset requirements, *J. Immunol.*, 1987, 139, 2005-2009.

[51] National Center for Emerging and Zoonotic Infectious Disease, http://www.cdc.gov/nczved/divisions/dfbmd/diseases/campylobacter/

[52] Food safety, Clostridium perfingens. http://www.cdc.gov/foodsafety/clostridium-perfingens.html

[53] (a) Hugo, WB; Russell, AD. Pharmaceutical Microbiology, 6th ed.; Blackwell: Oxford, U.K., 1998; (b) Safarik, I; Safarikova, M; Forsythe, SJ. The application of magnetic separations in applied microbiology, *J. Appl. Bacteriol.*, 1995, 78, 575-585; (c) Harrigan, HF. Laboratory Methods in Food Microbiology, 3rd ed.; Academic Press: San Diego, CA, 1998; (d) Eeles, RA;Stamps, AC. Polymerase Chain Reaction (PCR): The Technique and Its Applications; R. G. Landes: Austin, TX, 1993; (e) Strachan, NJC;Nicholson, FJ;Ogden, ID. An automated sampling system using ion mobility spectrometry for the rapid detection of bacteria, *Anal. Chim. Acta*, 1995, 313, 63-67; (f)

Maughan, NJ; Lewis, FA; Smith, V. An introduction to arrays, *J. Pathol.*, 2001, 195, 3-6; (g) Aitman, TJ. DNA microarrays in medical practice, *Br. Med. J.*, 2001, 323, 611-615; (h) Ivnitski,D;Abdel-Hamid, I; Atanasov, P;Wilkins, E. Biosensors for detection of pathogenic bacteria, *Biosens. Bioelectron.*, 1999, 14, 599-624.

[54] Hilpert, K; Hancock, REW. Use of luminescent bacteria for rapid screening and characterization of short cationic antimicrobial peptides synthesized on cellulose using peptide array technology, *Nat. Protoc.*, 2007, 2, 1652-1660.

[55] Stewart, ME;Anderton, CR;Thompson, LB;Maria, J;Gray, SK;Rogers, JA;Nuzzo, RG. Nanostructured Plasmonic Sensors, *Chem. Rev.*, 2008, 108, 494–521.

[56] Durr, NJ;Larson, T;Smith, DK;Korgel, BA;Sokolov, K;Yakar, AB. Two-Photon Luminescence Imaging of Cancer Cells Using Molecularly Targeted Gold nanorods, *Nano Lett.*,2007, 7, 941–945.

[57] Ni, W;Yang, Z;Chen, H;Li, L;Wang, J. Coupling between Molecular and Plasmonic Resonances in Freestanding Dye-Gold Nanorod Hybrid Nanostructures, *J. Am. Chem. Soc.*,2008, 130, 6692–6693.

[58] Kell, AJ;Stewart, G;Ryan, S;Peytavi, R;Boissinot, B;Huletsky, A;Bergeron, MG;Simard, B. Vancomycin-Modified Nanoparticles for Efficient Targeting and Preconcentration of Gram-Positive and Gram-Negative Bacteria, *ACS Nano*,2008, 2, 1777–1788.

[59] Darbha, GK; Ray, A;Ray, PC. Gold Nanoparticle-Based Miniaturized Nanomaterial Surface Energy Transfer Probe for Rapid and Ultrasensitive Detection of Mercury in Soil, Water, and Fish, *ACS Nano*,2007, 1, 208–214.

[60] Griffin, J;Singh, AK;Senapati, D;Lee, E;Gaylor, K;Jones-Boone, J;Ray, PC.. Sequence-Specific HCV RNA Quantification Using the Size-Dependent Nonlinear Optical Properties of Gold Nanoparticles, *Small*, 2009, 5, 839–845.

[61] Ni, W;Kou, X;Yang, Z;Wang, J. Tailoring Longitudinal Surface Plasmon Wavelengths, Scattering and Absorption Cross Section of Gold Nanorods,*ACS Nano*,2008, 2, 677–686.

[62] Mayer, KM; Lee, S; Liao, H; Rostro, BC; Fuentes, A; Scully, PT; Nehl, CL; Hafner, JH. A Label-Free Immunoassay Based Upon Localized Surface Plasmon Resonance of Gold Nanorods, *ACS Nano*, 2008, 2, 687–692.

[63] Wijaya, A; Schaffer, SB; Pallares, IG; Kimberly, HS. Selective Release of Multiple DNA Oligonucleotides from Gold Nanorods, *ACS Nano*, 2009, 3, 80–86.

[64] Darbha, GK; Rai, US; Singh, AK; Ray, PC. Gold Nanorod-Based Sensing of Sequence Specific HCV-1 Virus DNA by Using Hyper-Rayleigh Scattering Spectroscopy, *Chem.-Eur. J.* 2008, *14*, 3896–3903.

[65] Liao, H; Hafner, JH. Gold Nanorod Bioconjugates, *Chem. Mater.*, 2005, 17, 4636–4641.

[66] Huang, X;El-Sayed, IH;Qian, W;El-Sayed, MA. Cancer Cell Imaging and Photothermal Therapy in the Near-Infrared Region by Using Gold Nanorods, *J. Am. Chem. Soc.*, 2006, 128, 2115–2120.

[67] Berry, V;Gole, A;Kundu, S;Murphy, CJ;Saraf, RF. Deposition of CTAB-terminated nanorods on bacteria to form highly conducting hybrid systems, *J. Am. Chem. Soc.*,2005, 127, 17600-17601.

[68] Murphy, CJ;Sau, TK;Gole, AM;Orendroff, CJ;Gao, J;Gou, L;Hunyadi, SE;Li, T. Anisotropic netal nanoparticles: Synthesis, assembly, and optical applications, *J. Phys. Chem. B*,2005, 109, 13857–13870.

[69] Pietrobon, B;McEachran, M;Kitaev, V. Synthesis of Size-Controlled Faceted Pentagonal Silver Nanorods with Tunable Plasmonic Properties and Self-Assembly of theses Nanorods, *ACS Nano*,2009, 3, 21–26.

[70] Chen, Y;Munteanu, CA;Huang, YF;Phillips, J;Zhu, Z;Mavros, M;Tan, W.Mapping Receptor Density on Live Cells by Using Fluorescence Correlation Spectroscopy, *Chem.-Eur. J.*,2009, 21, 5327–5336.

[71] Tang, B;Cao, L;Xu, K;Zhuo, L;Ge, J;Li, Q;Yu, L. A New Biosensor for Glucose with High Sensitivity and Selectivity in Serum Based on Fluorescence Resonance Energy Transfer (FRET) between CdTe Quantum Dots and Gold Nanoparticles, *Chem.-Eur. J.*,2008, 14, 3637-3644.

[72] Satyabrata, S; Mandal, TK. Tryptophan Based Peptides to Synthesize Gold and silver Nanoparticles: A Mechanistic and Kinetics Study, *Chem.-Eur. J.*, 2007, 27, 3160–3168.

[73] Alivisatos, P. The use of nanocrystals in biological detection, *Nat. Biotechnol.*, 2004, 22, 47–52.

[74] Xiang, J; Lu, W; Hu, Y; Wu, Y; Yan, H; Lieber, CM. Ge/Si nanowire heterostructures as high-performance field-effect transistors, *Nature*,2006, 441, 489-493.

[75] Cao, YWC; Jin, RC; Mirkin, CA. Nanoparticles with Raman Spectroscopic Fingerprints for DNA and RNA Detection, *Science*,2002, 297, 1536–1540.

[76] Donath, E. Biosensors: Viruses for ultrasensitive assays, *Nat. Nanotechnol.*, 2009, 4, 215–216.

[77] Zhang, J; Langille, MR; Mirkin, CA. Synthesis of silver nanorods by low energy excitation of spherical plasmonic seeds, Nano Lett., 2011, 11, 2495–2498.

[78] Jana, NR; Gearheart, L; Murphy, CJ. Wet chemical synthesis of silver nanorods and nanowires of controllable aspect ratio, *Chem. Comm.*, 2001, 617-618.

[79] Jin, R;Cao, Y;Mirkin, C.A;Kelly, KL;Schatz, GC;Zheng, JG. Photoinduced Conversion of Silver Nanospheres to Nanoprisms, Science, 2001, 294, 1901-1903.

[80] Stiriba, SE; Frey, H; Haag, R. Dendritic Polymers in Biomedical Applications: From Potential to Clinical Use in Diagnostics and Therapy, *Ange. Chem. Int. Ed.*, 2002, 41, 1329-1334.

[81] Kreibig, U; Vollmer, M. Optical properties of metal clusters, Springer Verlag, Berlin, 1995.

[82] Zeng, J;Zheng, Y;Rycenga, M;Tao, J;Li, ZY;Zhang, Q;Zhu, Y;Xia, Y. Controlling the Shapes of Silver Nanocrystals with Different Capping Agents, *J. Am. Chem. Soc.*, 2010, 132, 8552-8553.

[83] Cheetham, AK; Rao, CNR;Feller, RK. Structural diversity and chemical trends in hybrid inorganic-organic framework materials, *Chem. ommun.* 2006, 4780-4795.

[84] Mock, JJ; Barbic, M;Smith, DR;Schultz, DA;Schultz, S. Shape effects in plasmon resonance of individual colloidal silver nanoparticles, *J. Chem. Phys.* 2002, 116, 6755-6759.

[85] Link, S; Mohamed, MB;El-Sayed, MA. Simulation of the Optical Absorption Spectra of Gold Nanorods as a Function of Their Aspect Ratio and the Effect of the Medium Dielectric Constant, *J. Phys. Chem. B* 1999, 103, 3073-3077.

[86] Kelly, KL;Coronado, E;Zhao, LL;Schatz, GC. The Optical Properties of Metal Nanoparticles: The Influence of Size, Shape, and Dielectric Environment, *J. Phys. Chem. B*, 2003,107, 668-677.

[87] Battistini, G;Cozzi, PG;Jalkanen, J;Montalti, M;Prodi, L;Zaccheroni, N;Zerbetto, F. The Erratic Emission of Pyrene on Gold Nanoparticles, *ACS Nano*, 2008, 2, 77-84.

[88] Tiwari, VS;Oleg, T;Darbha, GK;Hardy, W;Singh, JP;Ray, PC. Non-resonance SERS effect of silver colloids with different shapes, *Chem. Phys. Lett.*, 2007, 446, 77-82.

[89] Ray, PC;Darbha, GK;Ray, A;Hardy, W. A gold-nanoparticle-based fluorescence resonance energy transfer probe for multiplexed hybridization detection: accurate identification of bio-agents DNA, *Nanotechnology*, 2007, 18, 375504.

[90] Ray, PC;Fortner, A;Darbha, GK. Gold Nanoparticle Based FRET assay for the Detection of DNA Cleavage, *J. Phys. Chem. B*, 2006, 110, 20745-20748.

[91] Jennings, TL;Singh, MP;Strouse, GF. Fluorescent Lifetime Quenching near *d*=1.5 nm Gold Nanoparticle: Probing NSET Validity, *J. Am. Chem. Soc.*, 2006, 128, 5462-5467.

[92] Wu, W;Zhou, T;Aiello, M;Zhou, S. Construction of optical glucose nanobiosensor with high sensitivity and selectivity at physiological pH on the basis of organic-inorganic hybrid microgels, *Biosens. Bioelectron.* 2010, 25, 2603-2610.

[93] Jenning, TL;Schlatterer, JC;Singh, MP;Greenbaum, NL;Strouse, GF. NSET Molecular Beacon Analysis of Hammerhead RNA Substrate Binding and Catalysis, *Nano Lett.*, 2006, 6, 1318-1324.

[94] Chu, LQ;Fçrch, R;Knoll, W. Surface-Plasmon-Enhanced Fluorescence Spectroscopy for DNA Detection Using Fluorescently Labelled PNA as ""DNA Indicator", *Angew. Chem.*, 2007, 119, 5032; *Angew. Chem. Int. Ed.*, 2007, 46, 4944-4947.

[95] Grossmann, TN;Rçglin, L;Seitz, O. Triplex molecular beacons as modular probes for DNA detection, *Angew. Chem.*, 2007, 119, 5315-5318; *Angew. Chem. Int. Ed.*, 2007, 46, 5223-5225.

[96] Huang, X;El-Sayed, IH;Qian, W;El-Sayed, MA. Cancer Cells Assembles and Align Gold Nanorods Conjugated to Antibodies to Produce Highly Enhanced, Sharp, and Polarized Surface Raman Spectra: A Potential Cancer Diagnostic Marker, *Nano Lett.*, 2007, 7, 1591-1597.

[97] Senapati, D;Singh, AK;Khan, SA;Senapati, T;Ray, PC. Probing real time gold nanostar formation process using two-photon scattering spectroscopy, *Chem. Phys. Lett.*, 2011, 504, 46-51.

[98] Kuo, WS;Chang, CN;Chang,YT;Yeh, CS. Antimicrobial gold nanorods with dual-modality photodynamic inactivation and hyperthermis, *Chem. Commun.*, 2009, 4853–4855.

[99] Fortin, JP;Wilhelm, C;Servais, J;Me´nager, C;Bacri, JC; Gazeau, F. Size-Sorted Anionic Iron Oxide Nanomagnets as Colloidal Mediators for Magnetic Hyperthermia, *J. Am. Chem. Soc.*, 2007, 129, 2628–2635.

[100] Lim, S;Koo, OK;You, YS;Lee, YE;Kim, MS;Chang, PS;Kang, DH;Yu, JH;Choi, YJ;Gunasekaran, S. Enhancing Nanoparticle-Based Visible Detection by Controlling the Extent of Aggregation, *Scientific Reports*, 2012, 2, Art. No. 456, 1-6.

[101] Lin, CC;Yeh, YC;Yang, CY;Chen, CL;Chen, GF;Chen, CC;Wu,YC. Selective Binding of Mannose-Encapsulated Gold Nanoparticles to Type 1 Pili in *Escherichia coli*, *J. Am. Chem. Soc.*, 2002, 124, 3508-3509.

[102] Zhao, X;Hilliard, LR;Mechery, SJ;Wang, Y;Bagwe, RP;Jin, S;Tan, W. A rapid bioassay for single bacteria cell quantitation using bioconjugated nanoparticles, *Proc. Natl. Acad. Sci. USA.*, 2004, 101, 15027-15032.

[103] Kalele, SA;Kundu, AA;Gosavi, SW;Deobagkar, DN;Deobagkar, DD;Kulkarni, SK. Rapid Detection of *Escherichia coli* by Using Antibody-Conjugated Silver Nanoshells, *Small*, 2006, 2, 335-338.

[104] Miranda, OR;Li, X;Garcia-Gonzalez, L;Zhu, ZJ;Yan, B; Bunz, WHF;Rotello, VM. Colorimetric Bacteria Sensing Using a Supramolecular Enzyme-Nanoparticle Biosensor, *J. Am. Chem. Soc.* 2011, 133, 9650-9653.

[105] Deisingh, AK;Thompson, M. Detection of infectious and toxigenic bacteria, *Analyst*, 2002, 127, 567-581.

[106] (a) Guidelines for Drinking-water Quality, 3rd ed.; World Health Organization: Geneva, 2004. (b) Gerba, CP. Pathogens in the Environment; Academic Press: New York, 1996; pp 279299. (c) Straub, TM;Chandler, DP. Towards a unified system for detecting waterborne pathogens, *J. Microbiol. Methods*, 2003, 53, 185-197.(d) McFeters,GA. Drinking Water Microbiology; Springer: New York, 1990.

[107] (a) Kates, M. Handbook of lipid research: Glycolipids, phospho-glycolipids, and sulfoglycolipids; Plenum: Oxford, U. K., 1990; pp 123-234. (b) Dmitriev, B;Toukach, F;Ehlers, S. Towards a comprehensive view of the bacterial cell wall, *Trends Microbiol.*, 2005, 13, 569-574. (c) Koch, AL. Bacterial Wall as Target for Attack Past, Present and Future Research, *Clin. Microbiol. Rev.*, 2003, 16, 673-687. (d) Schaffer,C;Messner, P. The structure of secondary cell wall polymers: how Gram-positive bacteria stick their cell walls together, *Microbiology*, 2005, 151, 643-651. (e) Bos, MP;Tefsen, B;Geurtsen, J;Tommassen, J. Identification of an outer membrane protein required for the transport of lipopolysaccharide to the bacterial cell surface, *Proc. Natl. Acad. Sci. U.S.A.*, 2004, 101, 9417-9422.

[108] (a) Holme, S;McAlister, MB;Ortolano, GA;Chong, C;Cortus, MA;Jacobs, MR;Yomtovian, R;Freundlich, LF;Wenz, B. Enhancement of a culture-based bacterial detection system (eBDS) for platelet products based on measurementof oxygen consumption, *Transfusion*, 2005, 45, 984-993. (b) Hoffmann, O;Keilwerth, N;Bille, M;Reuter, U;Angstwurm, K;Schumann, RR;Dirnagl, U;Weber, JR. Triptans Reduce the Inflammatory Response in Bacterial Meningitis, *J. Cereb. Blood Flow Metab.*, 2002, 22, 988-996. (c) Wagner, SJ. Transfusion-transmitted bacterial infection: risks, sources and interventions, *Vox Sang.*, 2004, 86, 157-163. (d) Wu, YD;Chen, LH;Wu, XJ;Shang, SQ;Lou, JT;Du, LZ;Zhao, ZY. Gram Stain-Specific-Probe-Based Real-Time PCR for Diagnosis and Discrimination of Bacterial Neonatal Sepsis, *J. Clin. Microbiol.*, 2008, 46, 2613-2619.

[109] Lu, W;Singh, AK;Khan, SA;Senapati, D;Yu, H;Ray, PC. Gold nano-popcorn-based targeted diagnosis, nanotherapy treatment, and in situ monitoring of photothermal therapy response of prostate cancer cells using surface-enhanced Raman spectroscopy, *J. Am. Chem. Soc.*, 2010, 132, 18103-18114.

[110] Haynes, CL;Yonzon, CR;Zhang, X;Van Duyne, RP. Surface-enhanced Raman sensors: early history and the development of sensors for quantitative biowarfare agent and glucose detection, *J. Ram.Spec.*,2005, 36, 471-484.

[111] Quang, LX;Lim, C;Seong, GH;Choo, J;Do, KJ;Yoo, SK. A portable surface-enhanced Raman scattering sensor integrated with a lab-on-a-chip for field analysis, *Lab Chip*,2008, 8, 2214-2219.

[112] Vo-Dinh, T;Yan, F;Wabuyele, MB. Surface-enhanced Raman scattering for medical diagnostics and biological imaging, *J. Ram. Spec.*,2005, 36, 640-647.

[113] Senapati, D;Dasary, SSR;Singh, AK;Senapati, T;Yu, H;Ray, PC. A Label-Free Gold-Nanoparticle-Based SERS Assay for Direct Cyanide Detection at the Parts-per-Trillion Level, *Chem. Eur. J.*,2011, 17, 8445-8451.

[114] Alvarez-Puebla, RA;Liz-Marzan, LM. SERS-based diagnosis and biodetection, *Small*,2010, 6, 604-610.

[115] Vikesland, PJ;Wigginton, KR. Nanomaterial enabled biosensors for pathogen monitoring- a review, *Environ. Sci. Technol.*,2010, 44, 3656-3669.

[116] Moskovits, MM. Surface-enhanced spectroscopy, *Rev. Mod. Phys.*,1985, 57, 783-826.

[117] Zou, S;Schatz, GC. Silver nanoparticle array structures that produce giant enhancements in electromagnetic fields, *Chem. Phys. Lett.*,2005, 403, 62-67.

[118] Fleischmann, M;Hendra, PJ;McQuillan, AJ. Raman spectra of pyridine adsorbed at a silver electrode, *Chem. Phys. Lett.*,1974, 26, 163-166.

[119] Myers, AB; Mathies, RA. In *Biological applications of Ramanspectroscopy*; Spiro, T. G., Ed.; Wiley and Sons: New York, 1987; pp 1.

[120] Myers, AB. Resonance Raman Intensity Analysis of Excited-State Dynamics, *Acc. Chem. Res.*, 1997, 30, 519-527.

[121] Otto, A. In *Light Scattering in Solids IV*; Cardona, M. G., G., Ed.; Springer-Verlag: Berlin, 1984; Vol. 4, 289-418.

[122] Persson, BNJ. On the theory of surface-enhanced Raman scattering, *Chem. Phys. Lett.*, 1981, 82, 561-565.

[123] Brus, L. Noble Metal Nanocrystals: Plasmon Electron Transfer Photochemistry and Single-Molecule Raman Spectroscopy, *Acc. Chem. Res.*,2008, 41, 1742-1749.

[124] Casadio, F;Leona, M;Lombardi, JR;Van Duyne, R. Identification of organic colorants in fibers, paints, and glazes by surface enhanced Raman spectroscopy, *Acc. Chem. Res.*,2010, 43, 782-791.

[125] Willets, KA; Van Duyne, RP. Localized Surface Plasmon Resonance Spectroscopy and Sensing, *Annu. Rev. Phys. Chem.*, 2007, 58, 267–297.

[126] Larmour, IA;Graham, D. Surface enhanced optical spectroscopies for bioanalysis, *Analyst*, 2011, 136, 3831–3853.

[127] Alvarez-Puebla, RA;Liz-Marzan, LM. Traps and cages of universal SERS detection, *Chem. Soc. Rev.*, 2012, 41, 43–51.

[128] Jarvis, RM;Brooker, A;Goodacre, R. Surface-enhanced Raman scattering for the rapid discrimination of bacteria, *Faraday Discuss.*, 2006, 132, 281–292.

[129] Khan, SA;Singh, AK;Senapati, D;Fan, Z;Ray, PC. Bio-conjugated popcorn shaped gold nanoparticles for targeted photothermal killing of multiple drug resistant Salmonella DT104, *J. Mater. Chem.*, 2011, 21, 17705–17709.

[130] Premasiri, WR;Moir, DT;Klempner, MS;Krieger, N;Jones, II G;Ziegler, LD. Characterization of the Surface Enhanced Raman Scattering (SERS) of Bacteria, *J. Phys. Chem. B*, 2005, 109, 312–320.

[131] Cotton, TM.; Kim, JM.; Chumanov, GD. Application of surface-enhanced Raman spectroscopy to biological systems, *J. Raman Spectrosc.*,1991, 22, 729-742.
[132] Herne, TM;Ahern, AM;Garrrell, RL. Surface-enhanced Raman spectroscopy of peptides: preferential N-terminal adsorption on colloidal silver, *J. Am. Chem. Soc.*,1989, 113, 846-854.
[133] Grabb, ES;Buck, RP. Surface-enhanced Raman spectroscopic investigation of human immunoglobulin G adsorbed on a silver electrode, *J. Am. Chem. Soc.*,1989, 111, 8362-8366.
[134] Wantanabe, T;Maeda, H. Adsoption-controlled redox activity. Surface-enhanced Raman investigation of cystine versus cysteine on silver electrodes, *J. Phys. Chem.*,1989, 93, 3258-3260.
[135] Chumanov, GD;Efremov, RG;Nabiev, IR. Surface-enhanced Raman spectroscopy of biomolecules. Part I. – water-soluble proteins, dipeptides and amino acids, *J. Raman Spectrosc.*,1990, 21, 43-48.
[136] Vo-Dinh, T;Houck, K;Stokes, DL. Surface-Enhanced Raman Gene Probes, *Anal. Chem.*,1994, 66, 3379-3383.
[137] Kneipp, K;Kneipp, H;Manoharan, H;Hanlon, EB;Itzkan, I;Desari, RR;Feld, MS. Detection and identification of a single DNA base molecule using surface enhance Raman scattering (SERS), *Phys. Rev. E*,1998, 57, R6281.
[138] Weldon, MK;Morris, MD. Surface-Enhanced Raman Spectroscopic Investigation of Bacterial Lipolysis in a Skin Pore Phantom, *Appl. Spectrosc.*,2000, 54, 20-23.
[139] Cavalu, S;Cinta-Pinzaru, S;Leopold, N;Kieffer, W. Raman and surface enhanced Raman spectroscopy of 2,2,5,5-tetramethyl-3-pyrrolin-1-yloxy-3-carboxamide labelled proteins: Bovine serum albumin and cytochrome c, *Biopolymers* (*Biospectrosc.*), 2001, 62, 341-348.
[140] Sockalinham, GD;Lamfarraj, H;Beljebbar, A;Pina, P;Allouch, P;Manfeit,M. *Proceedings of the European Conference on the Spectroscopy of Biological Molecules*; Kluwer Academic: Boston, 1999, p 599.
[141] Efrima, S;Bronk, BV;Czege,J. Surface-enhanced Raman spectroscopy of bacteria coated by silver, *Proc. SPIE*,1999, 3602, 164-171.
[142] Zeiri, L;Bronk, BV;Shabtai, Y;Czege, J;Efrima, S. Silver metal induced surface enhanced Raman of bacteria, *Colloids Surf. A*,2002, 208, 357-362.
[143] Guzelian, AA;Sylvia, JM;Janni, JA;Clauson, SL;Spencer, KM. SERS of Whole Cell Bacteria and Trace Levels of Biological Molecules, *Proc. SPIE*,2002, 4577, 182-192.
[144] Fell, NF Jr.; Smith, AGB;Vellone, M;Fountain, AW. Optimization of substrates for surface-enhanced Raman spectroscopy of bacteria, *Proc. SPIE*,2002, 4577, 174-181.
[145] Grow, AE;Wood, LL;Claycomb, JL;Thompson, PA. New biochip technology for label-free detection of pathogens and their toxins, *J. Microbiol. Methods*,2003, 53, 221-233.
[146] Jarvis, RM;Goodacre, R. Discrimination of bacteria using surface-enhanced Raman spectroscopy, *Anal. Chem.*,2004, 76, 40-47.
[147] Puppels, GJ;de Mul, FFM;Otto, C;Greve, J;Robert-Nicoud, M;Arndt-Jovin, DJ;Jovin, TM. Studying single living cells and chromosomes by confocal Raman microscopy, *Nature*,1990, 347, 301-303.
[148] Puppels, GJ;Colier, W;Olminkhof, JHF;Otto, C;de Mul, FFM;Greve, JDescription and performance of a highly sensitive confocal Raman microspectrometer, *J. Raman Spectrosc.*,1991, 22, 217-225.

[149] Schuster, KC; Urlaubb, E; Gapesa, JR. Single-cell analysis of bacteria by Raman microscopy: spectral information on the chemical composition of cells and on the heterogeneity in a culture, *J. Microbiol. Methods*, 2000, 42, 29-38.

[150] Schuster, K; Reese, I; Urlaub, E; Gapes, JR; Lendl, B. Multidimensional Information on the Chemical Composition of Single Bacterial Cells by Confocal Raman Microscopy, *Anal. Chem.*, 2000, 72, 5529-5534.

[151] Maquelin, K; Choo-Smith, LP; van Vreeswijk, T; Endtz, H; Smith, B; Bennett, R; Bruining, HA; Puppels, GJ. Raman Spectroscopic Method for Identification of Clinically Relevant Microorganisms Growing on Solid Culture Medium, *Anal. Chem.*, 2000, 72, 12-19.

[152] Kirschner, C; Maquelin, K; Pina, P; Ngo-Thi, NA; Choo-Smith, LP; Sockalingum, GD; Sandt, C; Ami, D; Orsini, F; Doglia, SM; Allouch, P; Manfait, M; Puppels, GJ; Naumann, D. Classification and identification of enterococci: a comparative phenotypic, genotypic, and vibrational spectroscopic study, *J. Clin. Microbiol.*, 2001, 39, 1763-1770.

[153] Maquelin, K; Choo-Smith, LP; Endtz, HP; Bruining, HA; Puppels, GJ. Rapid Identification of *Candida* Species by Confocal Raman Microscopy, *J. Clin. Microbiol.*, 2002, 40, 594-800.

[154] Maquelin, K; Kirschner, C; Choo-Smith, LP; van den Braak, N; Endtz, HP; Naumann, D; Puppels, GJ. Identification of medically relevant microorganisms by vibrational spectroscopy, *J. Microbiol. Methods*, 2002, 51, 255-271.

[155] Maquelin, K; Kirschner, C; Choo-Smith, LP;Ngo-Thi, NA; van Vreeswijk, T; Stammler, M; Endtz, HP; Bruining, HA; Naumann, D; Puppels, GJ. Prospective study of the performance of vibrational spectroscopies for rapid identification of bacterial and fungal pathogens recovered from blood cultures, *J. Clin. Microbiol.*, 2003, 41, 324-329.

[156] Choo-Smith, LP; Edwards, HGM; Endta, HP; Kros, JM; Heule, F; Barr, H; Robinson, JS; Bruing, HA; Puppels, GJ. Medical applications of Raman spectroscopy: From proof of principle to clinical implementation, *Biopolymers* (*Biospectrosc.*), 2002, 67, 1-9.

[157] Belgrader, P; Benett, W; Hadley, D; Richards, J; Stratton, P; Mariella, R; Jr. Milanovich, F. PCR Detectin of Bacteria in Seven Minutes, *Science*, 1999, 284, 449-450.

[158] Wang, Y; Lee, K;Irudayaraj, J. Silver Nanosphere SERS Probes for Sensitive Identification of Pathogens, *J. Phys. Chem. C*, 2010, 114, 16122–16128.

[159] Kao, P; Malvadkar, NA; Cetinkaya, M; Wang, H; Allara, DL; Demirel, MC. Surface-Enhanced Raman Detection on Metalized Nanostructured Poly(*p*-xylylene) Films, *Adv. Mater.*, 2008, 20, 3562-3565.

[160] (a) Williams, AC; Edwards, HGM. Fourier transform Raman spectroscopy of bacterial cell walls, *J. Raman Spectrosc.*, 1994, 25, 673-677. (b) Edwards, HGM; Russell, NC; Weinstein, R; Wynn-Williams, DD. Fourier transform Raman spectroscopic study of fungi, *J. Raman Spectrosc.*, 1995, 26, 911-916. (c) Britton, KA; Dalterio, RA; Nelson, WH; Britt, D; Sperry, JF. Ultraviolet Resonance Raman Spectra of *Escherichia coli* with 222.5-251.0 nm Pulsed Laser Excitation, *Appl. Spectrosc.*, 1988, 42, 782-788. (d) Keir, R; Sadler, D; Smith, WE. Preparation of Stable, Reproducible Silver Colloids for use as Surface-Enhanced Raman Scattering Substrates, *Appl. Spectrosc.*, 2002, 56, 551-559.

[161] Chu, H; Huang, Y; Zhao, YP. Silver Nanorod Arrays as a Surface-Enhanced Raman Scattering Substrate for Foodborne Pathogenic Bacteria Detection, *Appl. Spectrosc.*, 2008, 62, 922-931.

[162] Delcour, AH. Outer Membrane Permeability and Antibiotic Resistance, *Biochim Biophys Acta*, 2009, 1794, 808–816.

[163] Yguerabide, J; Yguerabide, EE. Light –scattering submicroscopic particles as highly fluorescent analogs and their use as tracer labels in clinical and biological applications, *Anal. Biochem.*, 1998, 262, 137–156.

[164] Jain, PK; Lee, KS; El-Sayed, IH; El-Sayed, MA. Calculated Absorption and Scattering Properties of Gold Nanoparticles of Different Size, Shape, and Composition: Applications in Biological Imaging and Biomedicine, *J. Phys. Chem. B*, 2006, 110, 7238–7248.

[165] Storhoff, JJ; Lazarides, AA; Mucic, RC; Mirkin, CA; Letsinger, RL; Schatz, GC. What Controls the Optical Properties of DNA-Linked Gold Nanoparticle Assemblies? *J. Am. Chem. Soc.*, 2000, 122, 4640–4650.

[166] Hu, M; Chen, J; Li, Z; Au, L; Hartland, GV; Li, X; Marquez, M; Xia, Y. Gold Nanostructures: engineering their plasmonic properties for biomedical applications, *Chem. Soc. Rev.*, 2006, 35, 1084–1094.

[167] Sun, Y; Xia, Y. Gold and silver nanoparticles: A class of chromophores with colors tunable in the range from 400 to 750nm, *Analyst*, 2003, 128, 686–691.

[168] Wang, H; Brandl, D; Nordlander, P; Halas, NJ. Plasmonic Nanostructures: Artificial Molecules, *Acc. Chem. Res.*, 2006, 40, 53–62.

[169] Luk'yanchuk, B;Zheludev, NI;Maier, SA;Halas, NJ;Nordlander, P;Giessen, H;Chong, CT. The Fano resonance in plasmonic nanostructures and metamaterials, *Nat. Mater.*, 2010, 9, 707–715.

[170] Halas, NJ;Lal, S;Chang, W;Link, S;Nordlander, P. Plasmons in strongly coupled metallic nanostructures, *Chem. Rev.*, 2011, 111, 3913–3961.

[171] Jones, MR;Osberg, KD;Macfarlane, RJ;Langille, MR;Mirkin, CA. Templated Techniques for the Synthesis and Assembly of Plasmonic Nanostructures, *Chem. Rev.*, 2011, 111, 3736–3827.

[172] Sepu´lveda, B; Angelome´, PC;Lechuga, LM;Liz-Marza´n, LM. LSPR-based nanobiosensors, *Nano Today*, 2009, 4, 244–251.

[173] Englebienne, P; VanHoonacker, A;Verhas, M. Surface Plasmon resonance: principles, methods and applications in biomedical sciences, *Spectroscopy*, 2003, 17, 255–273.

[174] Aslan, K; Lakowicz, JR;Geddes, CD. Plasmon light scattering in biology and medicine: new sensing approaches, visions and perspectives, *Curr. Opin. Chem. Biol.*, 2005, 9, 538–544.

[175] Ghosh, SK; Pal, T. Interparticle Coupling Effect on the Surface Plasmon Resonance of Gold Nanoparticles: From Theory to Applications, *Chem. Rev.*, 2007, 107, 4797–4862.

[176] Gao, J;Gu, H;Xu, B. Multifunctional magnetic nanoparticles: design, synthesis, and biomedical applications, *Acc. Chem. Res.*, 2009, 42, 1097–1107.

[177] Cheon, J;Lee, JH. Synergistically integrated nanoparticles as multimodal probes for nanobiotechnology, *Acc. Chem. Res.*, 2008, 41, 1630–1640.

[178] Nel, AE;Mädler, L;Velegol, D;Xia, T;Hoek, EMV;Somasundaran, P;Klaessig, F;Castranova, V;Thompson, M. Understanding biophisicochemical interactions at the nano-bio interface, *Nat. Mater.*, 2009, 8, 543–557.

[179] Boisselier, E;Astruc, D. Gold nanoparticles in nanomedicine: preparations, imaging, diagnostics, therapies, and toxicity, *Chem. Soc. Rev.*, 2009, 38, 1759–1782.

[180] Yuan, J;Xu, Y;Müller, AHE. One-dimensional magnetic inorganic-organic hybrid nanomaterials, *Chem. Soc. Rev.*, 2011, 40, 640–655.

[181] Li, YF;Chen, C. Fate and Toxicity of Metallic and Metal-Containing Nanoparticles for Biomedical Applications, *Small*, 2011, 7, 2965–2980.

[182] Dreaden, EC;Mackey, MA;Huang, X;Kangy, BEl-Sayed, MA. Beating cancer in multiple ways using nanogold, *Chem. Soc. Rev.*, 2011, 40, 3391–3404.

[183] Kuo, WS;Wu, CM;Yang, ZS;Chen, SY;Chen, CY;Huang, CC;Li, WM;Sun, C.-K;Yeh, CS. Biocompatible bacteria@Au composites for application in the photothermal destruction of cancer cells, *Chem. Commun.*, 2008, 4430–4432.

[184] Huang, WC;Tsai, PJ;Chen, YC. Multifunctional Fe_2O_3@Au Nanoeggs as Photothermal Agents for Selective Killing of Nosocomial and Antibiotic-Resistant Bacteria, *Small*, 2009, 5, 51–56.

[185] Norman, RS;Stone, JW;Gole, A;Murphy, CJ;Sabo-Attwood, TL. Targeted photothermal lysis of the pathogenic bacteria, Pseudomonas aeruginosa, with gold nanorods, *Nano Lett.*, 2008, 8, 302–306.

[186] Mayer, KM;Hafner, JH. Localized Surface Plasmon Resonance Sensors, *Chem. Rev.*, 2011, 111, 3828–3857.

[187] Abeylath, SC;Turos, E. Drug delivery approaches to overcome bacterial resistance to β-lactam antibiotics, *Expert Opin. Drug Delivery*, 2008, 5, 931–949.

[188] Lal, S;Grady, NK;Kundu, J;Levin, CS;Lassiter, JB;Halas, NJ. Tailoring plasmonic substrates for surface enhanced spectroscopies, *Chem. Soc. Rev.*, 2008, 37, 898–911.

[189] Mirkin, CA;Letsinger, RL;Mucic, RC;Storhoff, JJ. A DNA-based method for rationally assembling nanoparticles into macroscopic materials, *Nature*, 1996, 382, 607–609.

[190] Lee, TMH. Over-the-Counter Biosensors: Past, Present, and Future, *Sensors*, 2008, 8, 5535–5559.

[191] Englebienne, P;Van Hoonacker, A;Verhas, M. High-throughput screening using the surface Plasmon resonance effect of colloidal gold nanoparticles, *Analyst*, 2001, 126, 1645–1651.

[192] Englebienne, P. Use of colloidal gold surface Plasmon resonance peak shift to infer affinity constants from the interactions between protein antigens and antibodies specific for single or multiple epitopes, *Analyst*, 1998, 123, 1599–1603.

[193] Fu, J;Park, B;Zhao, Y. Limitation of a localized surface Plasmon resonance sensor for *Salmonella*detection, *Sensors and Actuators B*, 2009, 141, 276–283.

[194] Lan, YB;Wang, SZ;Yin, YG;Hoffmann, WC;Zhen, XZ. Using a Surface Plasmon Resonance Biosensor for Rapid Detection of *Salmonella Typhimurium* in Chicken Carcass, *J. Bionic Eng.*, 2008, 5, 239–246.

[195] Mazumdar, SD;Hartmann, M;K¨ampfer,P;Keusgen, MRapid method for detection of *Salmonella* in milk by surface Plasmon resonance (SPR), *Biosensors and Bioelectronics* 2007, 22,2040–2046.

[196] Zhang, D;Yan, Y;Li, Q;Yu, T;Cheng, W;Wang, L;Ju, H;Ding, S. Label-free high-sensitive detection of *Salmonella* using a surface Plasmon resonance DNA-based biosensor, *J. Biotechnology*, *2012*, 160, 123– 128.

[197] Waswa, JW;Debroy, C;Irudayaraj, J. Rapid Detection of *Salmonella* Enteritidis and *Escherichia coli* Using Surface Plasmon Resonance Biosensor, *J. Food Process Eng.*, 2006, 29, 373–385.

[198] Duboisset, J;Russier-Antoine, I;Benichou, E;Bachelier, G;Jonin, C;Brevet, P.F.Single Metallic Nanoparticle Sensitivity with Hyper Rayleigh Scattering, *J. Phys. Chem. C* 2009, 113, 13477-13481.

[199] Neely, A;Perry, C;Varisli, B;Singh, AK;Arbneshi, T;Senapati, D;Kalluri, JR;Ray, PC. Ultrasensitive and highly selective detection of Alzheimer's disease biomarker using two-photon Rayleigh scattering properties of gold nanoparticles, *ACS Nano*, 2009, 3, 2834-2840.

[200] Zhang, CX;Zhang, Y;Wang, X;Ming, T.Z;Lu, Z.H. Hyper-Rayleigh scattering of protein-modified gold nanoparticles, *Anal. Biochem.* 2003, 320, 136-140.

[201] Russier-Antoine, I;Huang, J;Benichou, E;Bachelier, G;Jonin, C;Brevet, P.F. Hyper Rayleigh scattering of protein-mediated gold nanoparticles aggregates, *Chem. Phys. Lett.*, 2008, 450, 345-349.

[202] Seferos, DS;Giljohann, D.A;Hill, D.H;Progodich, A.E;Markin, C.A. Nano-Flares: Probes for Transfection and mRNA Detection in Living Cells, *J. Am. Chem. Soc.*, 2007, 129, 15477-15479.

[203] Chandra, M;Das, P.K. "Small-particle limit" in the second harmonic generation from noble metal nanoparticles, *Chem. Phys.*, 2009, 358, 203-208.

[204] Novak, JP; Brousseau, LC; Vance, FW; Johnson, RC; Lemon, BI; Hupp, JT; Feldheim, DL. Nonlinear Optical Properties of Molecularly Bridged Gold Nanoparticle Arrays, *J. Am. Chem. Soc.*, 2000, 122, 12029-12030.

[205] Russier-Antoine, I; Benichou, E; Bachelier, G; Jonin, C; Brevet, PF. Multipolar Contributions of the Second Harmonic Generation from Silver and Gold Nanoparticles, *J. Phys. Chem. C*, 2007, 111, 9044-9048.

[206] Clays, K;Persoons, A. Hyper-Rayleigh scattering in solution, *Phys. Rev. Lett.*,1991, 66, 2980–2983.

[207] Russier-Antoine, I;Jonin, C;Nappa, J;Benichou, E;Brevet, PF. Wavelength dependence of the hyper Rayleigh scattering response from gold nanoparticles, *Chem. Phys.*,2004, 120, 10748-10752.

[208] Singh, AK;Senapati, D;Neely, A;Kolawole, G;Hawker, C;Ray, PC. Nonlinear optical properties of triangular silver nanomaterials, *Chem. Phys. Lett.*, 2009, 481, 94–98.

[209] Lu, W;Arumugam, SR;Senapati, D;Singh, AK;Arbneshi, T;Khan, SA;Yu, H;Ray, PC. Multifunctional Oval-Shaped Gold-Nanoparticle-Based Selective Detection of Breast Cancer Cells Using Simple Colorimetric and Highly Sensitive Two-Photon Scattering Assay, *ACS Nano*, 2010, 4, 1739-1749.

[210] Oudar, JL. Optical nonlinearities of conjugated molecules. Stilbene derivatives and highly polar aromatic compounds, *J. Chem. Phys.*,1977, 67, 446–457.

[211] Neeley, A;Khan, SA;Beqa, L;Fan, Z;Singh, AK;Lu, W;Senapati, D;Arbneshi, T;Lee, E;Anderson, Y;Banerjee, S;Mao, J;Dubey, M;Amritharaj, P;Ray. P. Selective detection of chemical and biological toxins using gold-nanoparticle-based two-photon scattering assay, *Nanotechnology, IEEE Transaction on*, 2011, 10, 26-34.

[212] Singh, AK;Lu, W;Senapati, D;Khan, SA;Fan, Z;Senapati, T;Demeritte, T;Beqa, L;Ray, PC. Long-Range Nanoparticle Surface-Energy-Transfer Ruler for Monitoring Photothermal Therapy Response, *Small*, 2011, 7, 2517-2525.

[213] Sapsford, KE;Berti, L;Medintz, IL. Materials for fluorescence resonance energy transfer analysis: beyond traditional donor-acceptor combinations, *Angew. Chem., Int. Ed.*, 2006, *45*, 4562-4589.

[214] Jain, PK;El-Sayed, IH;El-Sayed, MA. Au nanoparticles target cancer, *Nano Today*, 2007, 2, 18-29.

[215] Phillips, RL;Miranda, OR;You, CC;Rotello, VM;Bunz, UHF. Rapid and Efficient Identification of Bacteria Using Gold-Nanoparticle-Poly(*para*-phenyleneethynylene) Constructs, *Angew. Chem. Int. Ed.*, 2008, 47, 2590-2594.

[216] Förster, T. Zwischenmolekulare Energiewanderung und Fluoreszenz, *Ann. Phys.*, 1948, 437, 55-75.

[217] Pons, T;Medintz, IL;Sapsford, KE;Higashiya, S;Grimes, AF;English, DS;Mattoussi, H. On the Quenching of Semiconductor Quantum Dot Photoluminescence by Proximal Gold Nanoparticles, *Nano Lett.*, 2007, 7, 3157-3164.

[218] Skewis, LR;Reinhard, BM. Spermidine modulated ribonuclease activity probed by RNA Plasmon rulers, *Nano Lett.* 2008, 8, 214-220.

[219] You, CC;Miranda, OR;Gider, B;Ghosh, PS;Kim, IB;Erdogan, B;Krovi, SA;Bunz, UHF;Rotello, VM. Detection and identification of proteins using nanoparticle-fluorescent polymer 'chemical nose' sensors, *Nat. Nanotechnol.*, 2007, 2, 318-323.

[220] Huang, CC;Chen, CT;Shiang, YC;Lin, ZH;Chang, HT. Synthesis of Fluorescent Carbohydrate-Protected Au Nanodots for Detection of Concanavalin A and *Escherichia coli*, *Anal. Chem.*, 2009, 81, 875-882.

[221] Soto, GE;Hultgren,SJ. Bacterial Adhesions: Common Themes and Variations in Architecture and Assembly, *J. Bacteriol.*,1999, 181, 1059–1071.

[222] (a) Harris, SL;Spears, PA;Havell, EA;Hamrick, TS;Horton, JR;Orndorff, PE. Characterization of *Escherichia coli* Type 1 Pilus Mutants with Altered Binding Specificities, *J. Bacteriol.*,2001, 183, 4099–4102. (b) Krogfelt, KA;Bergmans, H;Klemm, P. Direct evidence that the FimH protein is the mannose-specific adhesion of Escherichia coli type 1 fimbriae, *Infect. Immun.*,1990, 58, 1995–1998.

[223] Andersson, DI;Hughes, D. Antibiotic resistance and its cost: is it possible to reverse resistance? *Nat. Rev.*, 2010, 8, 260–271.

[224] Wright, GD. Molecular mechanism of antibiotic resistance, *Chem. Commun.*, 2011, 47, 4055–4061.

[225] Multidrug-resistant tuberculosis (MDR-TB) http://www.who.int/tb/challenges /mdr/en/index.html.

[226] Ray, PC. Size and Shape Dependent Second Order Nonlinear Optical Properties of nanomaterials and their Applications in Biological and Chemical Sensing, *Chem. Rev.*, 2010, 110, 5332–5365.

[227] Kort, R;O'Brien, AC;van Stokkum, IHM;Oomes, SJCM;Crielaard, W;Hellingwerf, KJ;Brul, S. Assessment of Heat Resistance of Bacterial Spores from Food Product Isolated by Fluorescence Monitoring of Dipicolinic Acid Release, *App. Environ. Microbiol.*, 2005, 71, 3556-3564.

[228] Powell, JF. Isolation of dipicolinic acid (pyridine-2:6-dicarboxilic acid) from spores of *Bacillus megatherium*, *Megaterium. Biochem.J.*, 1953, 54, 210–211.

[229] Rosen, DL;Sharpless, C;McGown, LB. Bacterial Spore Detection and Determination by Use of Terbium Dipicolinate Photoluminescence, *Anal. Chem.*, 1997, 69, 1082–1085.

[230] Cotter, PD;Hill, C. Surviving the Acid Test: Responses of Gram-Positive Bacteria to Low pH, *Microbiol. mol. Biol. Rev.*, 2009, 67, 429-453.

[231] Hone, J;Batlogg, B;Benes, Z;Johnson, AT;Fischer, JE. Quantized Photon Spectrum of Single-Wall Carbon Nanotube, *Science*,2000, 289, 1730-1733.

[232] Huschka, R;Zuloaga, J;Knight, MW;Brown, LV;Nordlander, P;Halas, NJ. Light-Induced Release of DNA from Gold Nanoparticles: Nanoshells and Nanorods, *J. Am. Chem. Soc.*,2011, 133, 12247-12255.

[233] Mohammed, OF;Samartzis, PC;Zewail, AH. Heating and Cooling Dynamics of Carbon Nanotubes Observed by Temperature-Jump Spectroscopy and Electron Microscopy, *J. Am. Chem. Soc.*,2009, 131, 16010-16011.

[234] Link, S;Burda, C;Nikoobakht, B;El-Sayed, MA. Laser-Induced Shape Changes of Colloidal Gold Nanorods Using Femtosecond and Nanosecond Laser Pulses, *J. Phys. Chem. B*,2000, 104, 6152-6163.

[235] Grinolds, MS;Lobastov, VA;Weissenrieder, J;Zewail, AH. Four-dimensional ultrafast electron microscopy of phase transitions, *Proc. Nat. Ac. Sci.*,2006, 103, 18427-18431.

[236] Hodak, JK;Martini, I;Hartland, GV. Spectroscopy and Dynamics of Nanometer-Sized Noble Metal Particles, *J. Phys. Chem. B*,1998, 102, 6958-6967.

[237] Hodak, JK;Henglein, A;Hartland, GV. Size dependent properties of Au particles: Coherent excitation and dephasing of acoustic vibrational modes, *J. Chem. Phys.*,1999, 111, 8613-8621.

[238] Perner, M;Bost, P;Plessen, GV;Feldmann, J;Becker, U;Mennig, M;Schmidt,H. Optically Induced Damping of the Surface Plasmon Resonance in Gold Colloids, *Phys. Rev. Lett.*,1997, 78, 2192-2195.

[239] Ahmadi, TS;Logunov, SL;El-Sayed, MA. Picosecond Dynamics of Colloidal Gold Nanoparticles, *J. Phys. Chem.*,1996, 100, 8053-8056.

[240] Link, S;Burda, C;Wang, ZL;El-Sayed, MA. Electron dynamics in gold and gold-silver alloy nanoparticles: The influence of a nonequilibrium electron distribution and the size dependence of the electron-phonon relaxation, *J. Chem. Phys.*,1999, 111, 1255-1264.

[241] Link, S;Burda, C;Mohamed, MB;Nikoobakht, B; El-Sayed, MA. Femtoseconf transient-absorption dynamics of colloidal gold nanorods: Shape independence of the electron-phonon relaxation time, *Phys. Rev. B*,2000, 61, 6086-6090.

[242] Roberti, TW;Smith, BA;Zhang, JZ. Ultrafast electron dynamics at the liquid-metal interface-femtosecond studies using surface plasmons in aqueous silver colloid, *J. Chem. Phys.*,1995, 102, 3860-3866.

[243] Smith, BA;Zhang, JZ;Giebel, U;Schmid, G. Direct probe of size-dependent electronic relazation in single-sized Au and nearly monodisperse Pt colloidal nano-particles, *Chem. Phys. Lett.*,1997, 270, 139-144.

[244] Averitt, RD;Westcott, SL;Halas, NJ. Ultrafast electron dynamics in gold nanoshells, *Phys. Rev. B*,1998, 58, 10203-10206.

[245] Heilweil, EJ;Hochstrasser, RM. Nonlinear spectroscopy and picoseconds transient grating study of colloidal gold, *J. Chem. Phys.*,1985, 82, 4762-4770.

[246] Chen, WJ;Tsai, PJ;Chen, YC. Functional Fe_3O_4/TiO_2 Core/Shell Magnetic Nanoparticles as Photokilling Agents for Pathogenic Bacteria, *Small*, 2008, 4, 485–491.

[247] Spangenberg, T;Kishi, Y. Highly sensitive, operationally simple, cost/time effective detection of the mycolactones from the human pathogen *Mycobacterium Ulcerans*, *Chem. Commun.*, 2010, 46, 1410–1412.

[248] Sharma, P;Brown, SC;Singh, A;Iwakuma, N;Pyrgiotakis, G;Krishna, V;Knapik, JA;Barr, K;Moudgil, BM;Grobmyer, SR. Near-Infrared Absorbing and Luminescent Gold Speckled Silica Nanoparticles for Photothermal Therapy, *J. Mater. Chem.*, 2010, 20, 5182-5185.

[249] Yong, KT; Roy, I; Swihart, MT; Prasad, PN. Multifunctional nanoparticles as biocompatible targeted probes for human cancer diagnosis and therapy, *J. Mater. Chem.*, 2009, 19, 4655–4672.

[250] Bunz, UHF;Rotello, VM. Gold nanoparticle-fluorophore complexes: Sensitive and discerning "noses" for biosystems sensing, *Angew. Chem., Int. Ed.*, 2010, 49, 3268–3279.

[251] Ronholm, J; Zhang, Z; Cao, X; Lin, M. Monoclonal Antibodies to Lipopolysaccharide Antigenes of *Salmonella enteric* serotype Typhimurium, *Hybridoma*, 2011, 30, 43–52.

[252] Sahm, DF; Thornsberry, C; Mayfield, DC; Jones, ME; Karlowsky, JA; Multidrug-Resistant Urinary Tract Isolates of *Escherichia coli:* Prevalence and Patient Demographics in the United States in 2000, *Antimicrob Agents Chemother*, 2001, 45, 1402–1406.

In: Food Poisoning
Editor: Paresh C. Ray
ISBN: 978-1-63463-166-2

Chapter 6

PSEUDOMONAS AND ARSENIC MEDIATED ENDEMIC OUTBREAKS OF FOOD AND WATER

Debashis Chatterjee[1], Shilajit Barua[2], Jishnu Adhikari[2] Debankur Chatterjee[3] and Parna Choudhury[2]

[1]Department of Chemistry, University of Kalyani, Kalyani, Nadia, West Bengal, India
[2]Department of Microbiology and Research & Development Centre, Vijaygarh Jyotish Ray College, Bejoygarh, Jadavpur. Kolkata, West Bengal, India
[3]Heritage Institute of Technology East Kolkata Township, Chowbaga Rd, Anandapur, Kolkata, West Bengal, West Bengal, India

ABSTRACT

Hygienic food and water is essential for sustenance of a healthy and safe lifestyle, most significantly for woman, children and the elderly. Shortage of food due to spoilage is common both in developed and developing countries. Currently, one third of the food produced worldwide is lost due to spoilage. This is often governed by several factors and necessary management practices should be undertaken to overcome the problem. Major factors are the lack of food storage and transport facilities which is ubiquitous in developing countries with hot and humid climate. For example, products with high protein content and vegetables are mostly affected due to contamination by several microorganisms such as proteolytic, lipolytic, pectinolytic and cellulolytic bacteria. In this context, *Psudomonas* is one of the most important group of bacteria related to food spoilage both in closed and open environment. Post-harvest rot of fresh produce is mostly predominant in low income countries and the main causal organisms are *P. viridiflava* and by *P. fluorescens* (40%). In 2004 about 96 million cases of food borne diseases have been reported in India, which resulted in nearly 3000 deaths. Another important concern is that of contaminated drinking water. Supply of safe water needs adequate treatment strategies to ensure quality. Around 1.1 billion people of low income group do not have access to safe water sources and about 2.4 billion have no basic sanitation. Diarrheal infections are widespread throughout the developing world. In Southeast Asia and Africa around 8.5% and 7.7% of all deaths respectively are due to diarrheal infections. Access of contaminated water into food materials causes food borne infections. Endemic diarrheal

infection is often caused by *Pseudomonas*, important episode occurred (1947) through milk. Apart from bacterial contamination of food it has been reported that the global phenomenon of environmental exposure to arsenic (As) from groundwater is now reported to be "The Largest Case of Mass Poisoning" in the world. Groundwater samples are often known to exceed WHO guideline values (> 10 ppb) from natural shallow aquifers (>50m) in more than 40 countries. The immense risks of this bane on mankind are represented by 150 million people at health risk from Arsenicosis in India and Bangladesh. This chapter mainly deals with the subject of little studied food spoilage by *Pseudomonas* and As which not only affects food but also the groundwater, fresh water source of life for millions. Finally, attempts have been made to highlight issues and concerns on public health of food spoilage by genus *Pseudomonas* and groundwater contamination of arsenic as well as their management.

INTRODUCTION

Food-the most essential requirement for maintenance of life, is to be produced by every country in sufficient quantity and with right nutrient content to meet the needs of an ever increasing population. Such food has to be safe, such that on consumption, it should not give rise to any food borne disease whether from infection, intoxication, contamination, adulteration or other sources. Food spoilage is a complex process where excessive amounts of foods are lost due to microbial activities even with modern day preservation techniques [1], while food borne diseases cause morbidity and mortality in the general population and they have emerged as a growing public health and economic problem in many countries during the last two decades [2].

Health disorder is also caused by contamination of food and water with high levels of heavy metals notably arsenic. Among the chemical elements, metals are the largest group. Simultaneously, the characteristics and distribution of metals vary greatly in the biosphere. Out of the ten most abundant elements in this Earth's crust, seven are metals such as Al (7.5 %wt), Fe (4.7 % wt), Ca (3.4 % wt), Na and K (2.6 and 2.8 % wt), Mg (1.9 % wt) and Ti (0.6 % wt). It is now clearly evident that many metals produce some form of an effect (positive and or negative) on various organisms and depends on the specific chemical forms that conclusively influences the toxic effect of an element.

In 2009, FAO estimated an overall 32% loss of food produced worldwide. Food spoilage during post-harvest storage and post-production handling contributes considerably to global food loss [3]. The estimate was based on weight in tons for all types of food, thereby erroneously overlooking the energy in food products that could have been consumed by people. Using FAO balance sheet, Lipinski et al., 2013 converted FAO's loss and waste estimates into calories and inferred a lower but substantially significant 24% percent of all food produced. Table 1 depicts the comparative estimation of loss in weight and in calorific value of different food materials.

Regionally, more food loss and waste (kg/year/capita) occurred in developed regions (Europe, North America, Oceania and Industrial Asia) than developing countries (Africa and Southeast Asia) both at consumer and production to retail stages (Figure 1).

However this food loss and waste varies significantly between developed and developing regions with developed countries seeing more at consumption and developing countries seeing more during production, handling and storage (Table2).

Table 1. Approximate loss of foods in Kcal and weight (100% = 1.48 quadrillion kcal of energy and 1.35 billion tonnes off weight)

TYPES OF FOOD	LOSS IN PERCENTAGE	
	Approximate Loss and Waste (kCal)	Approximate Loss and Waste (Weight)
Cereals	53%	19%
Roots and Tubers	19%	15%
Fruits and Vegetables	14%	44%
Oilseed and Pulses	10%	04%
Meat	10%	06%
Milk	11%	10%
Fish and Sea food	2%	4%

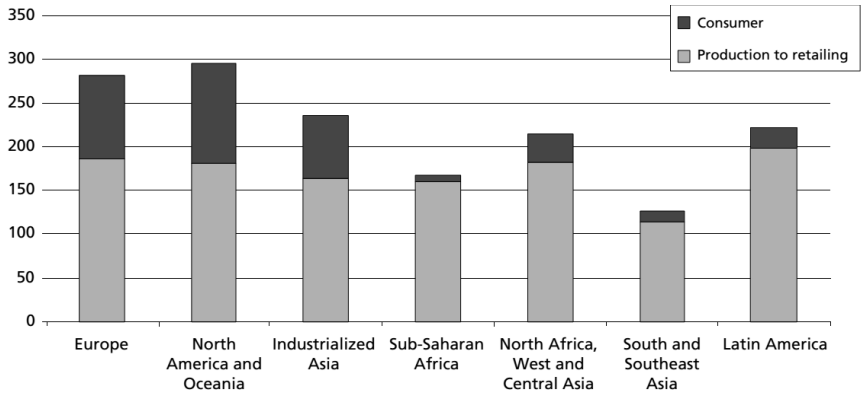

Figure 1. Per capita food losses and waste (kg/year) (Reprinted with permission from FAO, 2011 [3]).

Table 2. Comparative analysis of total food loss and waste (2009) in various stages in the value chain (100% = 1.5 quadrillion kcal)

Stages in which food is lost	Approximate loss of food in Developing Countries(%)	Approximate loss of food in Developed countries(%)
Production	14	10
Handling and Storage	15	11
Processing and Packaging	1	3
Distribution and Market	9	4
Consumption	7	28
Total loss of food	***46%***	***56%***

Food spoilage is a change in food, making it unsafe, less acceptable or unacceptable to the consumer for its original purpose. Thus, food may be spoiled by being contaminated with disease-causing microorganisms, or by the growth of microorganisms that may become manifest in a variety of ways [4]. In contrast, Food-borne infection or disease is defined as any illness resulting from ingestion of contaminated food [5]. Pathogenic bacteria, fungi, parasites, viruses, marine phytoplankton, and cyanobacteria cause microbial food-borne

diseases. Food-borne illnesses are among the most widespread diseases of the contemporary world. In most cases, severity of these diseases ranges from infections without apparent clinical manifestations, to mild illness, to severe illness, to death.

According to food safety experts and enforcement agencies, microbiological spoilage and contamination of food with pathogens represent the most severe and costly health hazards in connection with food. Microbial pathogens in food are responsible for an estimated 6.5–33 million cases of human illness and considerable degree of mortality every year. Over 40 different food-borne microbial pathogens, including fungi, viruses, parasites, and bacteria are believed to cause human illnesses. Effective preventive measures by enforcing hygiene along the whole food chain must be implemented in the most rigorous manner [6]. Factors involved in food-borne diseases represent four main groups of contributing points, related to contamination, survival of microorganisms, microbial growth that can contribute to outbreaks and other factors, mostly of unknown sources (Figure 2).

Food-borne diseases can be classified as infections, toxicoinfections, or intoxications. The characteristics of these three classes are now briefly described [5] (Figure 3).

A food-borne infection occurs when pathogenic microorganisms in ingested food establish themselves in the human host's body. They are able to grow or colonize the intestines, often invading the mucosa or other tissues and thereby causing invasive infections. All classes of food-borne pathogens (viruses, bacteria, parasitic protozoa, and other parasites) include infectious agents. Pathogenic bacteria that are not obligate intracellular parasites, e.g. *Salmonella spp.* and *Shigella spp.*, invade intestinal cells and multiply, thereby causing salmonellosis and shigellosis respectively.

Food-borne toxicoinfections result when a microorganism from contaminated ingested food grows in the intestinal tract and produces a toxin or toxins that damage the tissues or interfere with normal organ or tissue function. Examples of toxicoinfective bacteria include *Vibrio cholera, Bacillus cereus, Clostridium perfringens, C. botulinum*, (infant botulism), and enterotoxigenic *Escherichia coli*. The onset times for toxicoinfections are frequently, but not necessarily, longer than those for intoxications but shorter than those for infections. The predominant clinical manifestation of food-borne toxicoinfections is diarrhea.

Food-borne intoxications, the most common cause of food poisoning outbreaks, occur when during their growth, specific pathogenic bacteria release toxins into food that is subsequently consumed. The time in which symptoms develop after consumption of foods containing microbial toxins often is useful in differentiating intoxications from infections. Generally, intoxications are manifested more rapidly after consumption of contaminated food than are infections because time for growth and invasion or elaboration of the toxin in vivo is not required [7-8]. Bacteria capable of causing food-borne intoxications include *Staphylococcus aureus, Bacillus cereus, and Clostridium botulinum*.

Progression of human civilization has been catalyzed by the cultural and social evolution of mankind and the need to solve specific societal issues. One such issue is the necessity to free people from foraging for food, and the need for adequate nutrition via consistent food supply round the year. This has led to development of the food industry, which has contributed immensely to the basis for a healthy human civilization and helped society prosper and flourish [9]. Historical records revealed that there was clear understanding and recognition for the need to control food quality to protect consumers. Early Chinese and Hindu literature and the laws of ancient Egypt, Greece and Rome had described protective

measures principally related to fraudulent trade practices, many of which did have an impact on food quality, particularly those measures governing food adulteration and cleanliness [10].

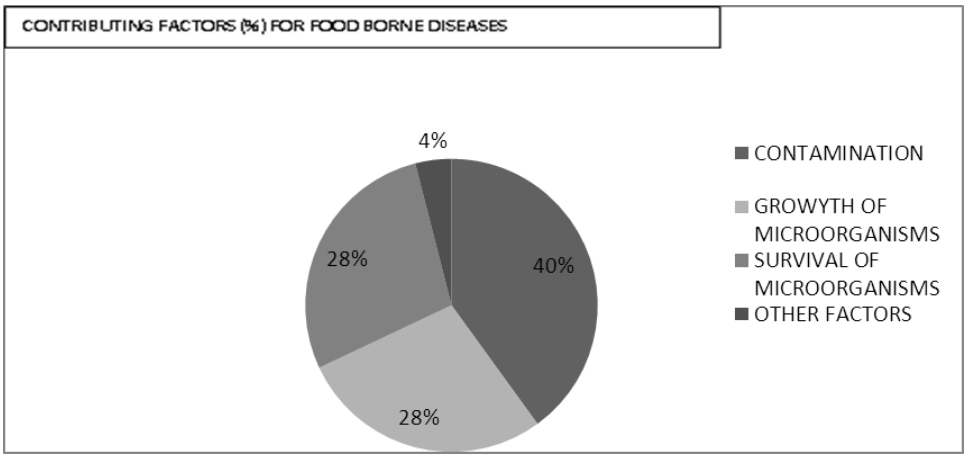

Figure 2. Contributing factors for food borne disease.

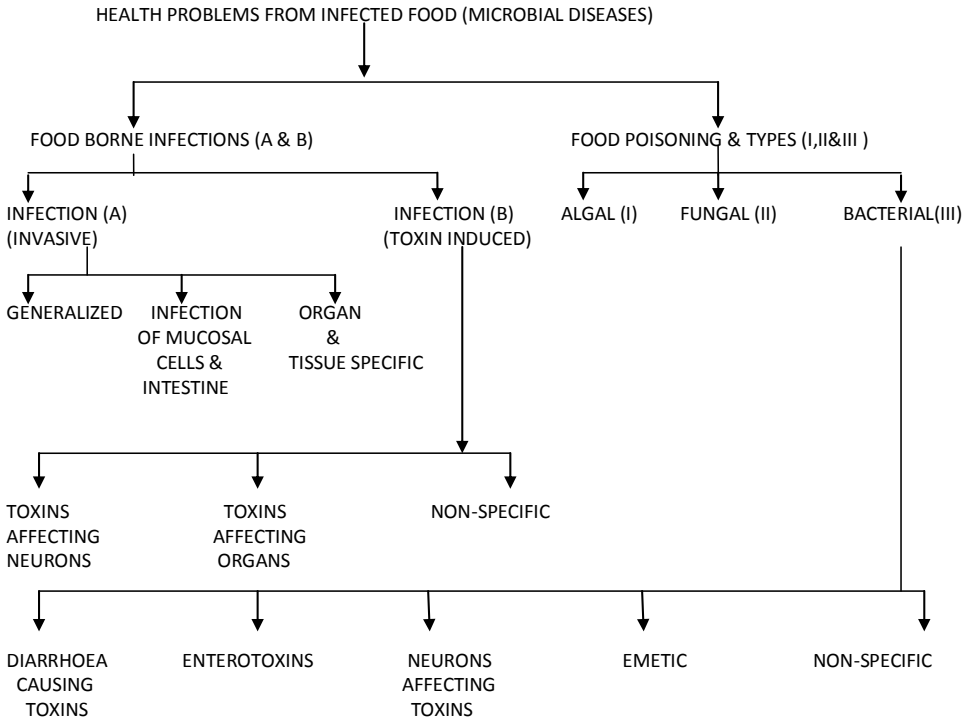

Figure 3. Health problems from infected food (microbial disease).

It has been estimated that around 30% of world population suffers from food borne disease. Under these circumstances, governments recognize a responsibility to establish an effective national food control system. This usually involves the integration of a mandatory regulatory approach with preventive and educational strategies that ensures food safety from farm to table. Effective national food control systems are not only necessary to maintain the

safety of food so as to protect domestic consumers, but also to ensure the safety and quality of exported and imported food. Food safety in Asia-Pacific region is a matter of grave concern. Factors affecting food safety are improper use of chemicals such as pesticides, hormones, additives, and preservatives in food production and processing and improper handling of food during storage and consumption, especially amongst poor households living in unhygienic environments. Food safety related hazards severely affects population in countries of Asia pacific region. Reports of more than one million food contamination reports in Bangladesh alone in the year 1998 with 2064 related deaths depicts the severity of situation. Food safety related hazards has also been reported in India (> 1000 fatalities), Thailand (~1,20,000 food intoxication annually), China and Korea [11].

In a survey carried out, diarrheal disease was found to be the primary cause of mortality in South East Asiatic regions, (2008) (Table 3).

Table 3. Mortality (%) due to major diseases in relation to diarrhoea in S. E. Asia (2008)

Major diseases other than diarrhoea afflicting populations in S.E. Asia	Percentage of deaths due to diarrhoea in relation to other major diseases
Tuberculosis	244
HIV/AIDS	491
Childhood Cluster diseases	490
Malaria	2352

In India, food-borne diseases are not categorized separately in the Health Information of India. In 2004, 9575112 cases of acute diarrheal diseases including gastroenteritis with 2855 deaths have been recorded, necessitating implication of rigorous food borne disease surveillance for estimating the burden of food borne diseases and monitoring trends, identifying priorities, and setting policy in the control and prevention of food borne diseases and their outbreaks, detection, and evaluation of control strategies.

To carry out food borne disease investigation epidemiological, environmental and laboratory components should integrate closely at the beginning, during the course, and at the end of an investigation. This type of investigation system is lacking in India [12]. Various initiatives with respect to toxicological and microbiological aspects of food safety have been taken to improve product safety during commercial food production. “Microbiologically safe food” is ensured by control measures based on processes that kill pathogenic organisms and the utilization of intrinsic factors to stabilize microbial populations or even kill organisms present in the food. Standards are used to guide the food industry in controlling food hazards and preventing food borne illnesses. These standards also assist food safety professionals in determining whether or not food products are deemed "safe." Food safety standards vary in degree of complexity and enforceability, from federal regulations that mandate specific standards for a particular food product to general advice for the consumer on safe food handling practices at home. Over the past several decades, greater emphasis has been placed on the use of scientific and factual information in the prioritization and setting of food safety standards. The preferred approach of incorporating scientific information into setting food safety standards is called risk analysis [13]. Approaches such as the Hazard Analysis Critical Control Point (HACCP) system have been developed and elements of these approaches are

increasingly being applied to both toxicological and microbiological food safety [14]. Good manufacturing practices with strict attention to sanitation and hygiene can prevent colonization by many, but not all, microbes and are the most important first step in delaying the spoilage process [15].

Along with the curse of the intoxication of food by microorganisms, contamination by metals and metalloids are becoming source of increasing menace. Metals such as arsenic, manganese etc., which are present in groundwater in high concentrations find their way into crops by means of irrigation water. These crops are causing mass poisoning by heavy metals. The modus operandi by which these metals act in environment is that they have several properties, physical and chemical which reveal periodicity for eg. conductivity (electrical and thermal), density, atomic and ionic radii, electronegativity and oxidation number. These properties are important for studying them in the environment. Importantly the abundance of these metals in the lithosphere usually decreases with increasing atomic mass barring Ti and Mn (0.1%) where tail enders (trace elements) lack in the natural occurrence (<0.1%). Metal densities are usually higher than non-metals and when they exceed 5 gm/cm^{3}the metal is designated as heavy metals. Metals readily liberate electrons unlike non metals and they tend to form positive ions (electrpositivity) in contrast to non-mettallic behaviour (electronegativity). This characteristic of the metals are important to bind the metals to various entities. Oxidation number of the metals are important in most environmental research because individual metal impact particularly trace metal is largely dependent on their combined capacity.

1. SPOILAGE AND INTOXICATION OF FOOD BY GENUS *PSEUDOMONAS*

1.1. *Pseudomonas*: An Ubiquitously Opportunistic Pathogen

The genus *Pseudomonas* encompasses arguably the most diverse and ecologically significant group of bacteria on the planet. Members of the genus are found in large numbers in all of the major natural environments (terrestrial, freshwater and marine) and also form intimate associations with plants and animals. They are capable of utilizing a wide range of organic and inorganic compounds and of living under diverse environmental conditions, making them ubiquitous in soil and water ecosystems and are important as plant, animal and human pathogens [16]. The bacterial genus *Pseudomonas* comprises a group of gram-negative and non-spore-forming rods, which are mostly aerobic and motile by polar flagella. They have simple nutritional requirement and can utilize a wide array of C sources, thus making *Pseudomonas* truly ubiquitous. Any habitat with pH 4–8, temperature 4–42°C and containing simple or complex organic compounds can be used by *Pseudomonas.* They are parasitic or saprophytic microbes. *Pseudomonas* are also obligate aerobeic, neutrophilic microbes inhabiting mesophilic terrestrial and aquatic habitats.

Though most *Pseudomonas spp*. are obligate aerobes, they are capable of growing in the absence of oxygen provided that NO_3 is available as a respiratory electron acceptor in the environment. *Pseudomonas spp*. produce acid from glucose or other carbohydrates only in the presence of oxygen. They are usually catalase and oxidase positive, but lactose negative on MacConkey agar. Another unique feature of *Pseudomonas spp* is its ability to form biofilms.

Model study system for biofilm production is *P. putida*, which have a remarkable ability to secrete exopolysaccharides [17]. They carry out cell to cell communication by a subtle strategy called quorum sensing via the production of small molecules called acyl homoserine lactones. This mechanism is believed to play a vital role in the biofilm development, and is being investigated further as a therapeutic target for control of chronic infections by *Pseudomonas*. Biofilm facilitates the bacterium to survive through adverse environmental changes. The glycocalyx biofilm formation by *P. pseudomallei* and transformation into several phenotypic variants protect the bacterium from the hostile environment and aid in its survival. They also have the unique ability to produce certain diffusible pigments. Many *Pseudomonas* species secrete a fluorescent yellow-green siderophore called pyoverdine (fluorescein) under conditions of iron limitation. *Pseudomonas aeruginosa* is capable of producing a blue phenazine pigment pyocyanin, a reddish brown pigment pyorubin, and a brown to black pigment pyomelanin which help to differentiate this species from others of the genus. *Pseudomonas fluorescens* also has been reported to synthesize a secondary siderophore quinolobactin, which results due to the hydrolysis of the unstable molecule 8-hydroxy-4-methoxy-2-quinoline thiocarboxylic acid (thioquinolobactin) and is yellow, dark green in the presence of iron [17].

Extensive metabolic diversity and genetic plasticity of the genus *Pseudomonas* enables them to grow rapidly and metabolize substrates, including toxic organic chemicals, such as aliphatic and aromatic hydrocarbons. Strains of *Pseudomonas* species are often resistant to antibiotics, disinfectants, detergents, heavy metals, and organic solvents. Some strains have been confirmed to produce metabolites, that stimulate plant growth or inhibit plant pests. All these properties make them ecologically significant. The heterogenous collection of large number of species in the genus *Pseudomonas* dated way back, when Stanier [18] surveyed 267 strains of aerobic pseudomonads, which revealed the extensive catabolic and phylogenetic diversity of the species. However, systemic reorganization of bacteria in general and *Pseudomonas* in particular, based on their natural relationship lead to the development of a new genera. Phylogenetic heterogeneity of *Pseudomonas* has initiated re-evaluations of the phenotypic characteristics, metabolic activities, genetics, ecology and other characteristics, in light of the inter- and intrageneric phylogenetic relationships. Recent advances in molecular characterization based on genome sequencing, genomics and proteomics have presented researchers, a wealth of data to understand all facets of these bacteria [19].

Members of the genus *Pseudomonas* was differentiated from the phenotypically similar bacteria and the distinct intergenic groupings among the genus *Pseudomonas* was established by DNA-rRNA hybridization [20-21], which are based on the DNA-rRNA homology study. This resulted in the inclusion of *Pseudomonas* in Gammaproteobacteria [22]. In *Bergeys Manual of Determinative Bacteriology*, 29 well characterized species of *Pseudomonas* was listed. This was based on their G+C content of genomic DNA along with another 206 less well-described species included as addenda [23]. Later, development of polymerase chain reaction [24], combined with advances in DNA sequencing [25], of 16S rRNA gene [26]resulted in enrichment of *Pseudomonas* genomic sequences in public databases. Taxonomically, the genus *Pseudomonas* comprises Genus I of the family Pseudomonaceae, which also included *Azotobacter*, *Azomonas*, *Azorhizophilus* and *Cellvibrio*. All members of the family Pseudomonaceae have certain common physiological properties, such as they are aerobic, chemoorganotrophic metabolism, absence of fermentation capacity and absence of photosynthetic capacity to grow by metabolizing a large variety of organic substrates [27].

Pseudomonadaceae have come to be regarded as "pseudomonads" and, by association, related to *Pseudomonas*. However, it is to be clarified that "*Pseudomonas*" (capitalized and written in italics) is the validly published (i.e. with nomenclature standing) name of a bacterial genus comprising species of defined collective phenotypic characteristics. On the other hand, "pseudomonad" (not capitalized and not italicized) is a descriptive term (i.e., *Pseudomonas* like) with no formal nomenclatural status, accorded to a nonexclusive collection of bacteria exhibiting various levels of similarity to species of the genus *Pseudomonas* [19].

1.2. Food Spoilage by Members of the Genera *Pseudomonas*

Pseudomonas mediated food spoilage is associated with both stored food as well as fresh produce. However, the former is of immense importance keeping in mind post production process and its economy required in keeping off such spoilage.

Pseudomonas fluorescens represents a very large and heterogeneous group, comprised of 5 Biovars, each associated with various fresh produce (Table 1.1)

Three major species of *Pseudomonas* (*P. fragi*, *P. fluorescens* and *P. lundensis*) has been reported to be associated with animal food products (Table 1.2).

Table 1.1. Members of genera *Pseudomonas* affecting fresh produce [28-41]

Fresh Produce	*Pseudomonas* Biovars associated	Reference
Spinach	*Pseudomonas fluorescens* Biovar III	Medina et al., 2012 [28]
Lettuce	*Pseudomonas fluorescence*	Takeuchi, 2000 [29]
Cabbage	*Pseudomonas cichorii*	Lazzaroni et al., 2003 [30]
Potato	Unclassified *Pseudomonas spp.*	Masum et al., 2013 [31]
Tomatoes	*Pseudomonas stutzer*	Mbajiuka et al., 2014 [32]
Salad vegetables	*Pseudomonas cichorii*	Marchetti et al., 1992 [33]
Baby carrot	*Pseudomonas marginalis*	Liao, 2007 [34]

Table 1.2. Members of genera *Pseudomonas* affecting animal food products

Food Product	Members of genus *Pseudomonas* associated	Reference
Raw & pasteurized milk	*P. aeruginosa*, *P. jessenii*	BCCDC [35]; Franzetti and Scarpelini, 2007[36]
Fish	*Pseudomonas fragi*	García-López et al.,2004 [37]
Sea bream fish	**Pseudomonas** *lundensis*	Tryfinopoulou et al., 2002 [38]
Beef, pork, lamb	*P. fragi, P. fluorescens, P. putida*	Shaw & Latty (1984) [39]
Meat	*P. fragi, P. fluorescens, P. aureofaciens P. putida*	Molin & Ternström (1982) [40]
Poultry products	*P. fragi, P. fluorescens, P. lundensis*	Russell et al. (1995) [41]

Pseudomonas fluorescens, *P. viridiflava*, *P. fragi* and *P. lundensis*, are four species mainly responsible for a large portion of the food spoilage. Soft rot of fresh fruits and vegetables are caused by pectolytic strains of *P. fluorescens* and *P. Viridiflava*. Proteolytic and lipolytic *P. fluorescens*, *P. fragi*, *P. lundensis* and *S. putrefaciens* are responsible for

spoilage of animal-derived foods including meat, poultry, milk and fish. Spoilage by these bacteria results in a slimy or mushy appearance along with the production of mal-odours, and partial or complete degradation of plant or animal tissues [42].

A major causative agent of soft rot in fresh produce is *Pseudomonas marginalis*, a Biovar of *Pseudomonas fluorescence* [43]. Over 40% of post-harvest rot of fresh produce is caused by oxidase-negative *P. viridiflava* and by at least three *P. fluorescens biovars* (I, II and IV) [44]. Part from the pectinolytic activity of spoilage bacteria, outbreak of onion bulbs *P. aeruginosa* [45], mushroom blight by *P. tolaasii* [46] and spoilage in specific types of produce such as lettuce by *P. cichorii* [47], has been reported.

A major type of spoilage of food material is often associated with storage at low temperature by psychrotrophic bacteria that grows at (0-7)°C, but their temperature optimum is in the range 20-40°C [48]. Several studies have been concerned with effects of temperature and other environmental conditions on growth of psychrotrophic or psychrophilic *Pseudomonas* species characteristic of spoilage of meats and other foods [49]. Earlier study by Duncan and Nickerson, 1963 [50], revealed increase in growth rate of *Pseudomonas fragi* with an increase in incubation temperature of the culture from 0 to 20°C, without any effect of physiological age and incubation temperature of the culture. Study on the effect of temperature cycling on *Pseudomonas fluorescence* [51] revealed their versatility for growth at either low or moderate temperatures.

Pseudomonas aeruginosa and *Pseudomonas fluorescence* are included among the major psychrotrophic food spoilage bacteria [52]. *P. fluorescens, P. fragi and P. lundensis*, cause spoilage of animal-derived foods (meat, fish, milk) by secreting lipases and proteases that cause formation of sulfides and trimethylamine (off-odors) and by forming biofilms (slime) on surfaces [53-54]. Different *Pseudomonas spp.* are responsible for limiting the shelf life of processed fluid milk at 4°C [55]. Detailed study to assess the genetic diversity of *Pseudomonas spp.* in milk and dairy processing environments and determine the association between genetic types (ribotypes) of *Pseudomonas spp.* and their potentials to cause spoilage (i.e., production of proteolytic and lipolytic enzymes), was carried out by Dogan and Boor, 2003 [56]. They identified majority of the ribotypes as *Pseudomonas fluorescence*, while the remaining were *Pseudomonas putida*. Of them, 69% of the *P. fluorescens* strains were positive for protease, lecithinase and lipase, while 87% of the *Pseudomonas putida* strains were negative for all enzyme activities, which revealed the dominance of the former group as the major mediators of spoilage in dairy industry.

Members of the genus *Pseudomonas* has been reported to be one of the major mediators of spoilage of fish and fish products [57]. *Pseudomonas putrifaciens*, a group IV pseudomonads [58] have been identified to cause spoilage of fish, stored under aerobic condition [59-60]. *Pseudomonas fragi*, another common fish spoilage bacterium [61], has been reported to be the spoilage mediators of high salt surimi, a finfish based seafood [62]. ‘Sweet’ and ‘fruity’ off-odors that frequently develop during the early stages in spoilage of refrigeratedfillets, is due to the non proteolytic *Pseudomonas fragi* which has been characterized as producing a "sweet, ester-like odor resembling that of the flower of the May apple". Isolates of *P. fragi* from seafood are characterized as being nonfluorescent, non proteolytic, do not produce TMA, or H_2S, but are capable of producing ammonia from amino acids, are lipolytic and are isolated from both fresh and spoiled fillets [63].

Pseudomonas bacteria are responsible for more than 80% of the egg spoilage [64]. Green fluorescent rots produced by *Pseudomonas fluorescens* are the most common as an early type of spoilage. Green fluorescent rots may be detected by the "black light" (long-wave ultraviolet) candler when populations of the pseudomonads have reached large numbers. Fluorescent pigment-producing strains of *P. fluorescens* are motile, and the pyoverdine that they produce binds metals in competition with conalbumin. They also are not susceptible to the antimicrobial factors in the egg white. *P. fluorescens* can grow and produce pyoverdine in ovalbumin substrates that have only trace amounts of essential ions [49].

One of the unique features of *Pseudomonas* mediated food spoilage is formation of slimy biofilm on the food surface. Highly chemi-synthetic and frequently psychrotrophic nature of these organisms, makes them ubiquitously responsible for spoilage of proteinaceous foods stored aerobically at chilled temperatures [65]. Spoilage in foods of animal origin by these organisms occurs first by utilization of the non-protein nitrogen fraction, followed by the production of lipases and proteases which liberate fatty and amino acid from the substrate commonly causing off-odors, off-flavors and rancidity [66]. Advanced stages of food spoilage by pseudomonads are characterized by pigmentation and the production of extra-cellular slime [67].

1.3. Food Borne Infection and Intoxication by the Genera *Pseudomonas*

Illness caused by the consumption of contaminated foods has a wide economic and public health impact worldwide [68]. Members of the genus *Pseudomonas* have been reported as one of the major causal agents of foodborne diseases [69]. Several members of the genus *Pseudomonas* are related to different gastrointestinal and associated disease (Table 1.3)

Table 1.3. Food bourn infection by genera *Pseudomonas*

Name of the disease	Causative agent	Reference
Necrotizing enterocolitis	*Pseudomonas aeruginosa*	Motarjemi, 2013 [17]
Perirectal infection		Agger and Mardan, 1995 [70]
Pediatric diarrhea		Amisano et al., 2011 [71]
Typical gastroenteritis		Lawley et al., 2012 [72]
Necrotizing enterocolitis		Doyle, 1989 [73]
Shanghai fever		O'Connor, 2005 [74]
Gastroenteritis	*Pseudomonas aeruginosa*	Cliver and Riemann, 2002 [75]
Gastroenteritis	*Pseudomonas michiganii*	Doyle, 1989 [73]
Melioidosis	*Pseudomonas mallei and Pseudomonas pseudomallei*	CSFPH,2007 [76]

Pseudomonas aeruginosa, an emerging opportunistic pathogen of clinical relevance worldwide, is the causative agent of Pseudomonal infection, which generally accounts for gastroenteritis [75]. *P. aeruginosa* may spread among particularly immunocompromised individuals by direct contact with or by the ingestion of contaminated foods and water.

Reports suggest that *Pseudomonas* is associated with typhlitis (also termed as neutropenic enterocolitis) in neutropenic patients, who suffer a sudden onset of fever, abdominal distension and worsening abdominal pain as a result of this disease [77].

Reports regarding epidemic diarrhea by *Pseudomonas*, accounts way back to 1947, in the new-born nursery St. Rose Hospital at Great Bend, Kans. 24 new-born were found to be affected of which there were 9 deaths. Investigations revealed that the infecting organism was *Pseudomonas aeruginosa* which gained entrance to the milk supply accidentally through contaminated water. *Pseudomonas aeruginosa* was isolated from both stool and autopsy materials of infected patients [78]. In 1974 an outbreak of *P. aeruginosa* food-borne illness was reported in a school. The probable source of infection was a kitchen worker who was an asymptomatic carrier of the same *P. aeruginosa* serotype isolated from the patients. Only 41 (7.75%) of 529 persons who ate a common lunch of fish developed symptoms, which included weakness, dizziness, and painful joints (arthralgia), but without diarrhea [79]. *Pseudomonas* has been identified as one of the several communicable agents of diarrheal disease epidemic [80]. While some infecting strains of *Pseudomonas aeruginosa* appear to be endemic within the hospital environment, others are traced to a common source associated with a specific outbreak or epidemic [74].

Community-acquired *P aeruginosa* sepsis infection can trigger a diarrheal disease known as 'Shanghai fever', which involves high fever, prostration, headache, and diarrhea, and is associated with high mortality primarily in Taiwan, Hong Kong and China [74,81]. *P. aeruginosa* is pathogenic only when introduced into areas lacking normal defenses, such as tissue damage of mucous membranes and skin, severe burns, and intravenous or urinary catheters. Also, this bacterium can potentially cause bacteremia or septicemia by the invasion of GI tissues leading to its lethal entry into the bloodstream. In a study carried out on twenty-seven consecutive children who met criteria for Shanghai fever in Chang Gung Children's Hospital in Taiwan from July 2003 to June 2012 were evaluated [81]. Based on the observations of Chuang et al., 2014 [81], the proportion of different clinical manifestations has been depicted in Figure 1.1.

Twenty-three patients had severe necrotizing enteritis and nine had bowel perforation requiring immediate surgical intervention. Intraoperative findings showed widespread patchy necrosis with fibrin coating of the small intestine or colon. Of patients with ecthyma gangrenosum, 10 had multiple sites affected.

Pseudomonas michiganii (later reclassified and named as *Pleisomonas shigelloides*) [73], a representative pseudomonads, that is responsible for gastroenteric [82] and extraintestinal disease in human. Outbreaks of *P. michiganii* associated gastroenteritis have been attributed to contaminated oysters and also to fish (salt mackerel and cuttlefish salad), crab, shrimp, scallops, and sushi consumption (Kirov, 1997). In the USA, infection with *P. shigelloides* has been strongly associated with eating raw or undercooked shellfish, usually raw oysters, and with travelling to high-risk areas (i.e., Mexico or Southeast Asia). The high incidence in Japan has been linked with dietary habits and also with trips to other Asian countries [83-84].

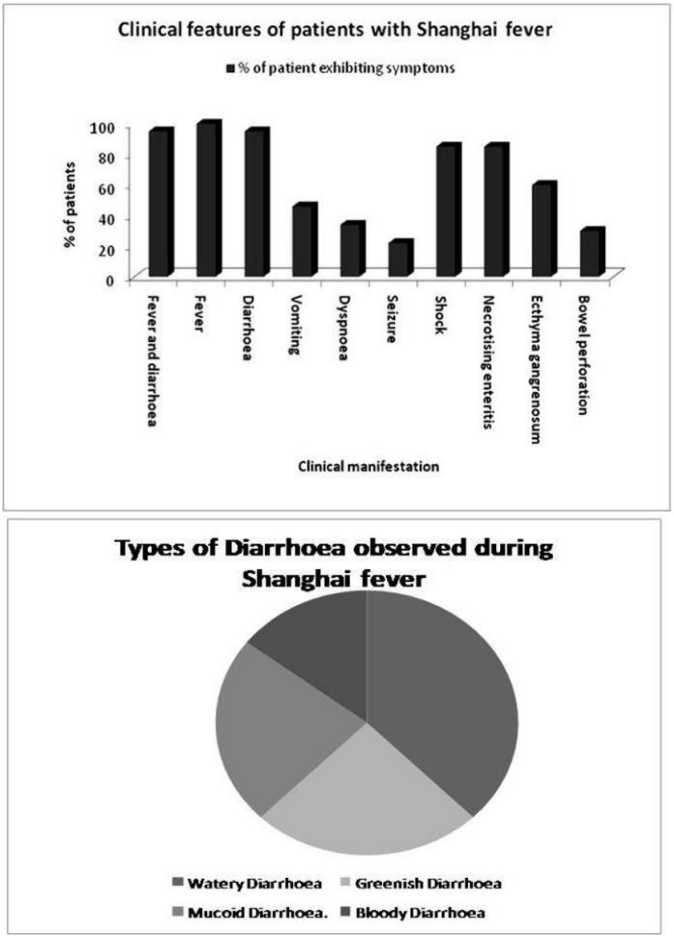

Figure 1.1. Shanghai fever symptoms.

Three major clinical presentations of *P. michiganii* associated gastroenteritis have been reported. A secretory (watery) type of diarrhea, a more invasive disease resembling shigellosis and a subacute or chronic disease lasting between 2 weeks and 2–3 months [85]. It is often secretory in nature [85], but the dysenteric form (enteroinvasiveness) of diarrhea is the most common presentation of this gastroenteritis [86]. The infective dose is unknown but is presumed to be very high. On average, symptoms may begin between 24 and 50 h after consumption of contaminated food or water although shorter incubation times of 1–1.5 h have been also reported. Diarrhea is the predominant symptom occurring in 94% of cases. Accompanying symptoms vary, but severe abdominal pain or cramping, nausea and/or vomiting and low grade fever, are most common. Less frequent symptoms include chills, headache, and some degree of dehydration [87].

Reported epidemic cases of *P. michiganii* associated gastroenteritis is by ingestion of contaminated water and raw or undercooked fish and shellfish, the risk of infection can be reduced by avoiding the use of untreated water for drinking and food preparation, by maintaining appropriate heating temperatures for fishery products and by avoiding contamination of cooked or processed foods. Appropriate chill storage, salting conditions and CO_2 will prevent growth of the organism [87]. Treatment of *P. michiganii* associated

diarrhea, involves use of tetracycline or trimethoprim-sulfamethoxazole. It should be noted that *P. michiganii* strains exhibits natural resistance to penicillin, roxithromycin, clarithromycin, lincosamides, streptogramins, glycopeptides, and fusidic acid [88].

Pseudomonas mallei and *P. pseudomallei*, the causative agents of Melioidosis are animal pathogens that can cause zoonoses. Humans are highly susceptible to this disease. Zoonotic transmission, often occur after contamination of skin lesions by exposure to infected animals, tissues including meat, or milk. Infection by ingestion has been noted in several occasions in humans, with an Australian having microabscesses of the gastric wall with seeding of the peritoneum from a ruptured gastric ulcer [89]. Melioidosis is endemic in Southeast Asia, China, the Indian subcontinent and parts of Australia. It has also been reported from the Caribbean, the Middle East, South America, Singapore and Taiwan. However, the bacterium is not associated with any gastrointestinal disease. [76]. Pulmonary disease either as a primary syndrome or as a component of septicemia is the most common form of melioidosis. The symptoms usually include fever, coughing, pleuritic chest pain and, in some cases, hemoptysis. Ulcerative lesions and nodules are sometimes found in the nose, and the septum may perforate. Severe weight loss may be seen. Pulmonary signs can develop suddenly, or may occur gradually after a prodromal syndrome characterized by headache, anorexia and generalized myalgia. In some patients septicemia may develop more gradually, with a fluctuating fever often associated with severe weight loss. Pulmonary signs including dyspnea are common, and arthritis or meningitis may be seen. Some patients have a disseminated pustular rash with regional lymphadenopathy, cellulitis or lymphangitis. Septic shock is common, and it is usually fatal once it develops. Chronic Melioidosis is characterized by abscesses and supportive lesions in liver, spleen, skeletal muscle and prostate gland in majority of the cases. Rarely, Melioidosis can result in brain abscesses, encephalomyelitis (often accompanied by flaccid paralysis) or meningitis. Fever may or may not be present in chronic Melioidosis [76].

Several prospective randomized comparisons of antimicrobial therapy for Melioidosis have been undertaken over the past 20 years, resulting in a good evidence base for treatment. The standard approach to chemotherapy of severe disease is to use at least 2 weeks of parenteral treatment initially, followed by 12-20 weeks of oral 'eradication' therapy to reduce the risk of relapse. The former involves combinatorial therapy with Imipenem or meropenem and Ceftazidime for 2 weeks, while the later uses a combination of Co-trimoxazole + Doxycycline and Amoxicillin-clavulanate. Mild cases may be treated with oral drugs alone. Co-amoxiclav and cefoperazone-sulbactam have also been used for parenteral treatment, but experience is more limited [90].

1.4. Food Borne Intoxication by the Genera *Pseudomonas*

Bacterial food intoxication refers to food-borne illness caused by the ingestion of food containing preformed bacterial toxins [91]. Majority of *Pseudomonas* infections are both invasive and toxicogenic. They invades tissues by the production and subsequent release of extracellular enzymes and toxins that break down physical barriers and damage host cells. Different *Pseudomonas* associated toxins and their producer strains are listed here in (Table 1.4).

Pseudomonas has been reported to produce three soluble proteins that have implications in invasion: a pore-forming cytotoxin and two hemolysins. *Pseudomonas* endotoxin lipopolysaccharide (LPS) may contribute to resistance to phagocytosis and the serum bactericidal response. The lipid A moiety of LPS mediates typical pathogenesis of Gram-negative septicemia. *Pseudomonas aeruginosa* have been reported to produce a pore-forming protein cytotoxin [96]. Isolated from bacterial autolysates, the cytotoxin has been characterized as a protein of 25,000 to 29,000 Mr which acts primarily on the plasma membranes of mammalian cells by binding to high affinity binding sites [98]. As a consequence, pores of about 2 nm diameter are formed resulting in a breakdown of the cellular gradient for low molecular substances [99]. Orlik et al., 1990 [100], studied the toxicity effect and binding property of the cytotoxin to plasma membrane preparations from Ehrlich ascites cells. The cytotoxin gene was pinned down and was cloned in *E. coli*. It was observed that, trypsin treated (removes short peptide sequence thereby activating the cytotoxin) cytotoxin exhibited rapid increase in cytotoxicity than non-processed toxin, as evident from granulocyte lysis assay.

Binding studies of the in vitro synthesized cytotoxin derivative and iodinated cytotoxin as derived from *Pseudomonas aeruginosa* autolysates to membrane preparations from Ehrlich ascites cells was assessed by co-sedimentation of the radiolabeled cytotoxin with the membranes through a sucrose cushion of neutral pH. No difference was detected in the binding properties of in vitro synthesized full-size cytotoxin and the processed cytotoxin. In both instances binding was reversible by the addition of a 100-fold excess of unlabeled cytotoxin. They inferred that binding to peripheral acceptor sites on membrane does not require proteolytic processing and also does not involve the N-terminal sequences [100]. The toxin was opined to be a phage encoded 31.7-kDa procytotoxin, which is processed by removal of the C terminus during bacterial autolysis. This water soluble, acidic 29-kDa protein attacks plasma membranes of a great variety of eukaryotic cells resulting in a channel of ~1-2 nm in diameter [101]and forms ion channels in planar lipid bilayers [102]. In a study, regarding oligomerization process of the toxin during maturity, the secondary structure composition, the changes in cytotoxin tertiary structure during the intoxication process justifies the classification of cytotoxin as a member of the bacterial pore-forming toxins that contain a high percentage of β-sheet structure and must oligomerize in order to insert into target cell. However, in comparison to other cytotoxins, the *P. aeruginosa* cytotoxin forms functional pentamers instead of heptamers [103].

Pseudomonas aeruginosa exotoxin A (PA toxin) is considered the most toxic substance produced by this organism and as such may have a significant role in its pathogenicity [97]. *P. aeruginosa* is a highly potent protein synthesis inhibitor [104] and thus acts as a cytotoxic agent on a whole range of mammalian cells, including cells of the immune system. *P. aeruginosa* toxin inhibits mammalian protein synthesis by the same mechanism as diphtherial toxin. Both toxins catalyze the transfer of the adenosine 5'-diphosphate-ribosyl moiety of nicotinamide adenine dinucleotide onto the same amino acid of elongation factor 2 in a stereochemically identical fashion [105]. This AB type toxin [106] could be related to death due to *Pseudomonas* bacteremia [107].

Table 1.4. Food contaminating toxins produced by members of the genera *Pseudomonas*

Name of toxin	Producer *Pseudomonas* species	Reference
Enterotoxin	*Pseudomonas aeruginosa*	Kubota and Liu, 1971 [92]
	Pseudomonas enteritis (Takigawa)	Aiso and Matsuno, 1961 [93]
Bongkrek Acid	*Pseudomonas cocovenenans*	Jiao et al., 2003 [94]
Toxoflavin	*Pseudomonas cocovenenans*	Cliver et al., 2011 [95]
Tetrodotoxin	*Pseudomonas putida*	Motarjemi, 2013 [17]
Cytotoxin	*Pseudomonas aeruginosa*	Kluftinger et al., 1989 [96]
PA toxin	*Pseudomonas aeruginosa*	Liu, 1974 [97]

In 1971 the production of an enterotoxin by *P. aeruginosa* was demonstrated by its capacity to cause fluid accumulation in rabbit ileal loops following the injection of live organisms [92]. The amount of fluid accumulated was less than observed with *Vibrio cholerae*, heat-sensitive and could be destroyed by the action of trypsin [92]. It appears to be distinct from any of the other toxic materials produced by *Pseudomonas* such as exotoxin A, haemolysin, or phospholipase [108]. In a laboratory culture base study, it was found that *Pseudomonas aeruginosa* produces maximum amount of enterotoxin at pH 7.0 and an incubation temperature of 37°C, optimally in Brain-Heart infusion and Trypticase Soy Broth. The enterotoxin could be detected after 6h of growth, but maximum amount was produced around 28h. Extended incubation, however, decreased the amount of enterotoxin and at 96h it was only 30 per cent of the maximum amount [109]. *Pseudomonas aeruginosa* has been shown to be capable of producing enterotoxins and has infrequently been linked with food poisoning [110].

In 1982 and 1985, Zhao and co-workers [111-112] studied 17 strains of the bacteria isolated in Heilongjiang Province, that were found to be similar to the genus *Pseudomonas*, and named them "*Pseudomonas farinofermentans*". Later, "*P. farinofermentans*" was found to be responsible for cases of food poisoning caused by consumption of deteriorated *Tremella fuciformis* (white fungus) in Shandong, Hopei, and Honan Provinces. They produce two toxins, bongkrekic acid (Figure 1.2A) and toxoflavin (Figure 1.2B), which were similar to the toxins of *Pseudomonas cocovenenans* [113].

Pseudomonas cocovenenans is a typical *Pseudomonas* in terms of morphology and biochemical characteristics. The word 'cocovenenans' came from Cocos, the genus name for coconut, and veneno, which means poison. Thus, cocovenenans means coconut poisoning. *P. cocovenenans* produces a yellow, poisonous compound "toxoflavin" [95]. Toxoflavin functions under aerobic conditions as an active electron carrier between reduced nicotinamide-adenine dinucleotide (NADH) and oxygen, leading to production of hydrogen peroxide and bypass of the cytochrome system. This is the basis of the strong poisoning properties associated with the toxin [114].

In Indonesia, bongkrek and tempeh bongkrek is made by fermenting a mixture of soybeans, peanut and coconut with Rhizopus. In unusual conditions the mold may grow abnormally slowly, and *P. cocovenenans*, and yeast may overgrow and spoil the product by producing toxoflavin and bongkrekic acid [94]. Bongkrekic acid is the major toxin. It is a substituted heat stable glutaconic acid derivative of aconitic acid with a molecular weight of 486. The production of bongkrekic acid appears to be specific to coconut pressed cake, and is

produced only in the presence of fatty acids. The simple lowering of pH during fermentation to below pH 5.5 can prevent toxin production. Below this pH, the toxigenic bacteria do not grow; however, the growth of the mold in bongkrek is in fact stimulated at these lower pH values [115]. Bongkrekic acid is the more toxic of the two. The main symptoms of poisoning include an initial hyperglycemia quickly followed by a marked hypoglycemia, which exhausts the glycogen reserves in many tissues, particularly the liver and heart. The acid interferes with mitochondrial oxidative phosphorylation, as well as with the citric acid cycle in heart muscle [116]. It reacts with ADP and ATP in the mitochondria and inhibits the enzyme adenine nucleotide translocase [117]. Bongkrekic acid is very toxic, and can result in spasms, hypoglycemia and the death of patients. Consumption of toxic tempe bongkrek has led to numerous human fatalities. The onset of symptoms occurs within a few hours of ingestion of contaminated food. The patient complains of malaise, abdominal pains, dizziness, extensive sweating, fatigue, and eventually, coma. Death can occur within 20 hrs of the onset of symptoms. Both bongkrekic acid and toxoflavin may play a role in poisonings. However, bongkrekic acid is likely to be the more important toxin. In addition to being more toxic, the concentration of bongkrekic acid is typically ten times higher than toxoflavin [118-119].

Pseudomonas enteritis (Takigawa) was reported to be associated with several outbreaks of enteritis-type food poisoning along the Pacific Ocean and the Sea of Japan. Inshore cuttlefish from Sea of Japan were considered to be the causes of these diseases. The microorganism was found to be resistant against 0.1% bile and grow at 37°C. Primary manifestations includes violent epigastric pain, which was accompanied by nausea, vomiting and diarrhea. Diarrhea was evident in all cases taken ill, and the stools were watery; however, no tenesmus followed. In several cases, mucus and blood could be observed in the feces. Fever occurred in 60 to 70 per cent of all patients, and temperatures were recorded up to 37.5-38.5°C. Headache and chills in few cases, but no nervous symptoms such as paralysis and excitement were observed [94].

Certain *Pseudomonas spp.* are capable of producing a lethal toxin called tetrodotoxin (TTX) harbored by a variety of marine animals. *P. putida* are capable of producing a potent neurotoxin called tetrodotoxin (TTX) primarily found in marine puffer fish. The toxin is believed to potentially exist in the gonads, liver, intestine, and skin of these fish at levels sufficient to cause rapid and violent death. Bioaccumulation of the toxin is thought to contribute to its high concentrations in the food-chain. Mortality due to consumption of infected puffer fish is often reported [17]. TTX is a sodium channel blocker that causes nerve conduction failure which manifests as paralysis. TTX poisoning manifests itself as a sensorimotor neuropathy which may be associated with mild gastrointestinal effects. Poisoning develops over hours and more rapidly with severe cases. Neurological effects include perioral paresthesia and numbness, ataxia, progressive distal to proximal muscle weakness. Severe poisoning is characterized by respiratory muscle paralysis and rarely cardiovascular toxicity (bradycardia, arrhythmias and hypotension) [120].

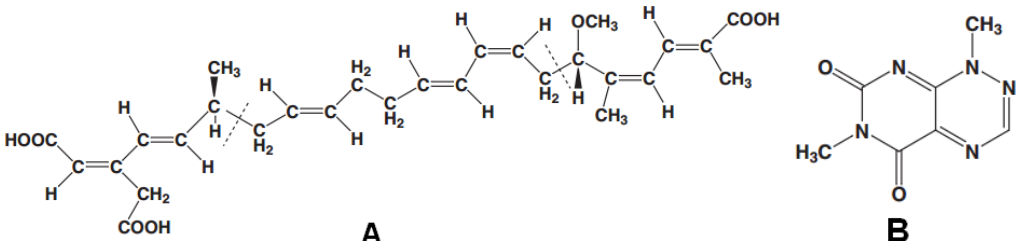

Figure 1.2. Structures of (A) bongkrekic acid and (B) toxoflavin.

1.5. Detection and Enumeration of *Pseudomonas*Contamination in Food

Current Food Safety Inspection Service (FSIS) regulations for the food-processing industry include mandatory testing programs *Salmonella*, *Listeria monocytogenes*, *Campylobacter*, and *Escherichia coli* O157:H7 while low attention is paid for *P. aeruginosa*. Pathogen-specific tests can be divided into the categories of metabolic-based and genome-based methods [87]

Principal metabolic based technique involves extensive use of agarized selective media for detection and enumeration of *Pseudomonas spp.* As per Liao et al., 2006 [42], several selective agents are used in each of these media. This involves use of antibiotics (nalidixic acid, fucidin, erythromycin, cephaloridine, nitrofluration, novobiocin, penicillin, ampicillin and chloramphenicol), dyes (crystal violet, phenol red and fuschin) and other chemical additives (cetrimide, cycloheximide, Irgasan and triphenyl tetrazolium chloride). In some instances, several physiological groups among the genus Pseudomonas can also be selected out. For example King A, King B and Cetrimide Agar media are used to promote growth of non-fluorescent, fluorescent Pseudomonas and *P aeruginosa* respectively. The selective agents inhibit the growth of non-*Pseudomonas* flora while antimicrobials are usually added at a concentration just sufficient to suppress the growth of non-*Pseudomonas* flora [42].

Presence of *Pseudomonas* is diagonosed by its ability to produce fluorescent and non-fluorescent pigments (fluorescin, pyocyanin and pyomelanin) on King's medium B and medium A [120]. *Pseudomonas* CFC agar [121] prevents the growth of the vast majority of non-*Pseudomonas* flora, including *Enterobacteriaceae* and Gram-positive *Bacillus* and *Lactobacillus spp.*, and shows minimal effect on the growth of spoilage related pseudomonads, including *P. fluorescens, P. fragi, P. lundensis, P. aerugionos, and P. putida.* Liao, 2006 [42] opined that King's media B and A and other *Pseudomonas* base media (Oxoid) can be supplemented with cetrimide, Irgasanor nalidixic acid to improve the detection of *P.* fluorescens, *P. aeruginosa* and other pseudomonads in water, soil, foods and clinical specimens. Identification and enumeration of *Pseudomonas spp.* in dairy products were obtained by plating onto *Pseudomonas* selective media, e.g., cetrimide, fucidin, cephaloridine (CFC) agar, followed by confirmation of well-isolated colonies by biochemical methods. [122]. However, culture and identification assay require time to produce results, and underestimation of bacterial numbers sometimes occurs because the conventional techniques could not recover sublethally injured cells that may occur in heat-treated products such as pasteurized milk [123].

Amendment of cetrimide and nalidixic acid to *Pseudomonas* agar base favoured selective isolation of *Pseudomonas aeruginosa* [124]. Based on this fact, Corry et al., 2012 [125], reported use of cetrimide and nalidixic acid amended *Pseudomonas* agar base for selective isolation as confirmed by enhanced pigment production of *Pseudomonas aeruginosa*. *Pseudomonas aeruginosa* WDCM 00114 and *Pseudomonas putida* WDCM 00117 was used as productivity test strains, while *Escherichia coli* WDCM 00090 and *Staphylococcus aureus* WDCM 00033 was used as selectivity test strain. *Pseudomonas aeruginosa* exhibited round colonies 2–3 mm in diameter with the presence of blue-green or brown pigmentation. The medium also got pigmented. *Pseudomonas putida* has similar sized colonies but does not produce any pigment, while *Staphylococcus aureus* and *Escherichia coli* were inhibited. The time required for the detection of *P. aeruginosa* by direct enumeration of bacteria is ~20 hrs but is not expansive and does not require any specific equipment. Another media dependent metabolic based technique involves rapid detection of metabolic end-products of bacteria grown on specific media, generally referred to as direct impedance measurement [126]. Rapid detection of *Pseudomonas* within 2–6 to 11–14 hrs was carried out in specific highly selective media named as Z-broth. The test relies on the ability of *P. aeruginosa* to grow on ammonia and acetate as the sole sources of nitrogen and carbon. Acetamide, a compound containing ammonia and acetate in an amide linkage, has been included as the main component of Z-broth that is dissociated by *P. aeruginosa* leading to the change in the impedance [127].

More sensitive metabolic based techniques involves magnetoelastic immunosensor based direct, real-time quantification of *P. aeruginosa* in growth media [128], fourier transform infrared spectroscopy (FT-IR) based identification of *P. aeruginosa* in bottled drinking water [129] and electroimmunoassay technology available [87]. Genome-based culture independent methods were much more sensitive and involves the identification conserved regions of bacterial genomes use more stable genotypic characteristics of the microorganism [130]. Direct hybridization assay involves hybridization of species-specific oligonucleotides immobilized on a nylon membrane to PCR amplicons of 16S–23S rDNA intergenic regions obtained by amplification using universal primers [131]. This technique has been efficiently used for the direct detection of organisms including *P. aeruginosa* in food samples [132]. PCR screening using primers 5'-ATGGATGAGCGCTTCCGTG-3'and 5'-TCATCCTTCGCCTCCCTG-3' is highly reliable, giving PCR products of the expected size for all *P. aeruginosa* strains tested and not amplifying DNA from any of the other *Pseudomonas* species tested [133]. In advanced fluorescent *in situ* hybridization (FISH) technique, standard linear oligonucleotide probes has been replaced by molecular beacons. DNA molecular beacons for flow cytometric detection of *P. putida* have doubled signal-to-noise ratio demonstrated improved detection [134]. Using TaqMan real-time quantitative PCR, *P. aeruginosa* has been successfully detected in municipal and wastewater treatment together with another 13 foodborne pathogens [135].

Metagenomic approach to detect spoilage bacteria in food by directly detecting species-specific sequences using next-generation sequencing (NGS) technologies has been developed and validated for meat samples [136]. Heterogeneous mixture of amplicons bearing sequences specific to *Pseudomonas spp.* in meat samples have been validated by bacterial 16S tag-encoded FLX Titanium amplicon pyrosequencing (bTEFAP), and the possibility of bar-coding samples by most NGS platforms revealed that amplicons generated from several food samples could by analyzed in a single run [137]. Matsuda et al., 2007 [138] used total RNA based reverse-transcriptase quantitative PGR (RT-qPCR) using primers specific to *P.*

aeruginosa 16S rRNA to quantify microbial count of *P. aeruginosa*. Standard real-time quantitative PCR to determine copy number, and thus it can infer equivalent $cfug^{-1}$ in the sample.

1.6. Management of Food Contamination and Food Borne Disease by Genus *Pseudomonas*

Several physical, chemical and biological treatment processes are adopted or practiced to control spoilage of food by *Pseudomonas*. Though they are effective, yet they don't ensure complete elimination, without affecting the physical appearance of the food. In addition, the bacteria itself got resistant to disinfectants like quaternary ammonium compounds following prolong treatment [139] or it had adapted several escape strategies like formation of biofilm [140] and strategically positioning itself in remote pockets in food to avoid exposure to disinfectants [29]. Both chemical and physical treatment of food has been adapted to prevent *Pseudomonas* mediated spoilage.

Treatment of food materials with ozonated water has been found to be effective against *P. aeruginosa* [141] and *P. fluorescens* [142]. *Pseudomonas spp*. were also reported to be sensitive to ClO_2 treatment [143], that efficiently reduced the microbial count on fresh produce of fruits and vegetables [144]. Application of H_2O_2 has been has been shown to reduce the number of fluorescent *Pseudomonas* on the surfaces of fruits by 90% [145]. The inhibitory effects of potassium sorbate and sodium benzoate against food spoilage bacteria *Pseudomonas fragi* has been established [146]. Pulsed electric fields (PEF) either alone or in combination with acetic or propionic acid has been reported to reduce counts of *Pseudomonas fluorescens* in skim milk [147]. In a recent study, mixture of organic acids, commercially available by the name Citrosteril (citric acid 21%, lactic acid 2%, malic acid 2%) and Rena X (citric acid 22%, lactic acid 3%, malic acid 2%) has been proved to be efficient disinfectant against *Pseudomonas aeruginosa* [148].

"Modified atmosphere" (MA) storage, i. e., storage of food in atmospheres containing increased amounts of CO_2 has been proved throughout the world to be an efficient technology of preventing food spoilage. The principle of MA storage is to replace the air surrounding the foodstuff with a mixture of CO_2, O_2 and N_2. CO_2 is used to inhibit the growth of aerobic bacteria and molds and N_2 used to inhibit the oxidation of fats [42]. Tudela et al., 2013 [149], studied the effect of 3 different MA conditions, low O_2 + CO_2, low O_2 and moderate O_2 + CO_2 and subsequently observed that the first treatment condition maximally reduced *Pseudomonas* population of baby spinach. Irradiation by ionizing radiation (^{60}Co or ^{137}Cs) has also been proved to be an effective means of reducing the load of *Pseudomonas fluorescens* on beef steaks [150]. Other non-thermal treatment methods like pulsed electric field (PEF) of milk [151], and synergestic application of high-pressure and the lactoperoxidase system has been proved to be efficient in preventing spoilage of dairy products [152]. Due to its ubiquitous nature, infection with *Pseudomonas aeruginosa* is difficult to control. Hence, immuno-compromised patients must be more precautious about any possible incidence caused by this pathogen. Hence, patients particularly with neutropenia should not consume foods like raw fruits and vegetables (surface principally harboured by *Pseudomonas*) because of the risk of subsequent GI colonization and bacteremia. Appropriate heat sterilization of the

milk should be applied before consumption considering the potential for pathogenicity of this bacterium [17].

2. METALS AND ADVERSE HEALTH EFFECTS

2.1. Metal's Behavior

Metals can accept a pair of electrons (Lewis acids) from an electron donor (Lewis base) that may be generalized as follows:

$$A+:B \rightarrow A:B\ (AB) \qquad \text{(eqn.2.1)}$$

The resulting pair may be termed as ion pair, a metal complex, a co-ordination compound or a donor- acceptor complex depending upon the donor-acceptor response. The stability of the resulting species (AB) can be classified with respect to hard, intermediate and soft acceptor as well as donor concept because hard acceptors prefer to bind hard donors. Similarly soft acceptors prefer to bind to soft donors. These hard to hard and soft to soft binding happens to form stable compounds (Table 2.1). In the abiotic and biotic systems, the chemistry of metals often play an important role in the chemical stability processes viz. electron mobility, electronegetivity, charge density, oxidation numbers etc. For example, hard acceptors are more likely to have low electron mobility, electronegetivity and ionic radii along with high oxidation numbers and the reverse is true for soft acceptors. The hard donors also have similar/dissimilar chemical properties such as low electron mobility with high electronegetivity, high negative charge density and the converse holds good for a soft donor. This suggests that the hard acid soft base and the reverse combination do not form strong bonds and their chemical products are easily leachable in the various environmental compartments.

As a result, several metals, notably heavy metals, are widely and dynamically distributed in the environment and the striking example is the heavy metals that pollute the waters which subsequently the living organisms uptake in their systems. These metals are often natural and/or anthropogenic. Major sources are rocks, soils and minerals and their anthropogenic uses such as industries, municipal wastes, transportation etc.

Table 2.1. Donor-acceptor concept and response

ACCEPTORS		
HARD	**SOFT**	**MIDDLE**
Na^+, K^+, Mg^{2+}, Ca^{2+},Be^{2+}, Mn^{2+}, Cr^{3+}, Al^{3+}, Co^{3+}, Fe^{3+}, As^{3+}	Au^+, Ag^+, Cu^+, Hg^{2+}, Cd^{2+}, Pd^{2+}, CH_3Hg^+	Ni^{2+},Co^{2+}, Fe^{2+}, Zn^{2+}, Cu^{2+}, Pb^{2+}
DONORS		
HARD	**SOFT**	**MIDDLE**
OH^-, Cl^-, F^-, SO_4^{2-}, CO_3^{2-},PO_4^{3-}, O^{2-}	S^-, RS^-, SH^-, CN^-, SCN^-, RSH, CO	NO_2^-, Br^-, SO_3^{2-}

Metals in the environment occur in different forms (both chemical and physical). It could be in various physical forms such as suspended, non-suspended (even as colloids) and dissolved. In environment, metals can be in various chemical forms such as hydroxides, carbonates, silicates, sulphides and even bind to organic matter and the options are different such as adsorbent, ion-exchanger and complex/chelate. Soluble metal species can be single or complex and/or unionized organo-metallic compounds. Metal species and their various chemical forms often change from one form to the other by physical, chemical or biological interplays or interactions.

2.2. Speciation of Metals

The metal speciation generally relates to the particular chemical and physical forms that element occurs in. It is important to note that the importance of metals in environment, notably heavy metals, is often based on measurement of concentration (Total). It has now become evident that the environmental impact and bioavailability of metals, significantly heavy metals, are greatly influenced by their species than their usual total concentration [153]. The distribution, mobility, toxicity, bioaccumulation and biodegradability of heavy metals depend largely on the concentration of their species in the natural environment. This is important both in terms of inorganic and organic substances bearing soluble heavy metal species for their long term environmental occurrence.

Table 2.2. Physico-chemical forms of metal in air, water, soil/sediment systems

Physico-chemical form	Potential examples	Abiotic /Biotic Compartments
1)Gaseous emission	Hg^0, Zn^0	Air / Atmosphere
2)Dissolved		
a)Free acquired ions	$Fe(H_2O)_6^{3+}$,$Co(H_2O)_6^{2+}$	Water /Hydrosphere, Soil/Sediment systems/lithosphere,Meteorological water
b)Inorganic complexes	$Cu(OH)_3^-$, $Fe(OH)_2^+$	Do
c)Organic complexes	HgR_2, Copper fulvate	Do
d)Colloidal		Do
i)Metals sorbed	Clays, Amorphous substances (e.g FeOOH), Organics etc.	water/soil/sediment
3)Solid		
a)Precipitated	CdS, $ZnSiO_3$	Soil/sediment, water, air borne particulates, biologicalmaterials
b)Organics		Metals in algae, fish andMammals

Metals, mostly heavy metals, occur in different physico-chemical forms which varies in different environmental abiotic compartments e.g air, water, soil/sediment (Table 2.2). Several heavy metals (Hg, Pb, As, Se) have major gaseous forms and are also soluble in water /biological fluids even in various form e.g particulates, colloidal, colloid-adsorbed and

dissolved. Soluble species are often in hydrated ions, inorganic and organic complexes and their stability depend on physico-chemical affinity of the metal species. NO_3, Cl, CO^3, OH, SO^4 and even occasionally F and PO_4 are common inorganic ligands present to hold the metals in environment. Organic ligands are numerous depending on their structure/functional sites (electron releasing strength), molecular weight, concentration, thermodynamic stability and kinetic lability.

Metals (mostly trace elements) are present in different types of chemical forms in living systems (Table 2.3) and often strongly/weekly bound to biological molecules. Notably, they can form essential biological compounds (metalloenzymes) within the human body and take part in large number of chemical interactions even in the cellular levels. Important redox species are many such as As(V)/(III), Se(IV)/(VI), Cr(III)/(VI), Fe(II)/(III), Cu(I)/(II), Mn(II)/(IV), Mo(V)/(VI) amongst which some are toxic and others are non-toxic but essential. However, some of these are again toxic when concentration levels exceed over required levels (over supply). Nevertheless, metals can be potentially hazardous to living organisms at large and at prolonged exposure levels. The metal ions required for biological systems should be readily available (soluble species notably in aqueous environment) and abundant (commonly restricted to At. no. <40 as well as their solubility). The toxicity and availability play an important role in controlling metal toxicity and bioavailability and speciation influences not only toxicity and but also bioavailability, mobility, eutrophication, flocculation and adsorbabiliy notably in aqueous environment [154].

Ionic strength, pH and electron activity are the central environmental factors that can regulate the metal speciation as well as availability and toxicity. Transport, biogeochemical cycling and biological impact of metals are also dependent on several physico–chemical factors such as interaction of dissolved/ suspended metal species with solid/colloids particles, particulate size, oxidation status, electronic configuration and nature of coordination etc. Metal species, notably heavy metals, play an important role in controlling toxicity and bioavailability of living systems. For example, As and Cr are much more toxic in their different oxidation state, As (III) has greater reactivity and toxicity than As (V) whereas Cr (VI) has been classified in Group 1 for human carcinogen. Additionally, Mn and Fe are more toxic in reduced form whereas Hg is significantly more toxic in methyl form and often heavy metals (hydrated metal ions) are toxic in free ionic form to fish and other aquatic life [155].

2.3. Toxic Heavy Metals

Environmental exposure of heavy metals is now a key issue both in terms of toxicity (poisonous) to humans and widespread distribution /availability. Occurrence of heavy metals is now omnipresent in groundwater, air, soil, food, biological fluids even in umbilical cord (contamination of stem cell). The impact of heavy metals and their geological factors on human health has now emerged as a new branch of science “Medical Geology” and recently is receiving increased attention by the researchers due to the knowledge gap for the protection of human health from adverse consequences related to exposure to heavy metals [156].

Inorganic heavy metals are a group of metals because their densities (273K,1. atm pressure, kg/m^3) are higher than common metals. Few of them are amongst the greatest environmental hazards and are poisonous to humans such as Cadmium (Cd, density- 8650), Arsenic (As, density – 5727), Chromium (Cr, density-7200), Lead (Pb, density -11340) and

Mercury –(Hg, density- 13546) etc. Each one of these have widespread occurrence in several parts of the world both in terms of geographical area coverage and human exposure [157]. Among these toxic heavy metals, As is a metalloid and historically employed as common poison, notably in several parts of S.E. Asia, as well as its compounds have also been used therapeutically for more than 2000 years [158]. The weird property of the king of poison is that it is harmful yet useful. This uncommon chemical property of As in abiotic and biotic systems has helped it in creating a niche with a class of its own. This has provided the inspiration for us to choose As among all the toxic heavy metals.

2.4. As in Environment

The environmental human exposure of As has been recognized in several parts of the world and is now a global public health issue. Elevated levels of As is found in anthropogenic as well as natural geogenic sources. Nevertheless, the prolonged elevated levels of As from several sources (groundwater and food, notably rice) is commonly recognized as the primary route of iAs exposure to human health [159]. It has also been reported that groundwater samples often exceed WHO guideline values (> 10 ppb) from natural useable aquifers of more than 40 countries of both developed and developing nations. Nearly 100 million people, worldwide, are now exposed to geogenic As and mortality rate from As –bearing diseases are relatively high in As "Hot Spots"areas. [160].

Arsenic is a natural component of the earth's crust (2-3 mg As/kg) and often found in all the abiotic components of the earth (where it is also found in nearly 200 mineral forms). Bedrock iAs enter into the environment, potentially in soil, depending on parent material characteristics and human interaction and activities. Chemical form of As, climate and redox condition are important factors towards contribution of As in soil/sediment. The interactions among various compartment (sediment-soil-water) and environmental accumulation have trigged recycling of the metal in the biosphere.

Table 2.3. Elements availability and toxicity as well as biological impacts

Relatively non-toxic	Toxic and insoluble	Toxic and soluble
Readily not available in elemental form but available as compound	Poor availability	Readily available
H, Li,C,N,O,F,Na,Mg, Al Si,P,S, Cl, K, Ca, Fe, Br, Rb, Sr.	Ti, Zr, Nb, Mo, Ru, Rh, Ba, La-Lu (series), Hf, Ta, W, Re, Os, Ir, Ac-Lr (series)	Be, Co, Ni, Cu, Zn, As, Se, Pd, Ag, Cd, Sn, Sb, Te, Pt, Au, Hg, Tl, Pb, Bi, Mn, V, Cr, U (relatively less available)

2.5. As Exposure

2.5.1. Air

Mean concentration of airborne inorganic arsenic varies largely depending on location (urban upto 100ng/$m^3$and remote areas - upto 3 ng/m^3) and sources (both natural and anthropogenic). Major natural sources are air blown dust, volcanic ashes, forest fires, sea salt spray. Smelting, fossil fuel burning and combustion, use of arsenical plant protecting agents are principal anthropogenic sources of airborne As. Inhaled As undergoes deposition mostly in the upper respiratory tract depending upon solubility and chemical form of iAs. Deposition in the nasopharyngeal region followed by muco –clearance may be swallowed (upto 60 – 70 %) and the rest is absorbed in the gastrointestinal tract. However, absorption may be lower if the inhaled As is in highly insoluble form [161].

2.5.2. Water

Drinking water, notably groundwater of potential aquifers is a major source of natural iAs contamination for millions of people. iAs presence in groundwater has been reported from almost the entire globe, notably Asia, Europe, Africa, North America, South America and Australia. WHO designated the unprecedented high levels of iAs in groundwater as the "largest mass poisoning of population in the history" [162]. The scale of the problem is of utmost severity in the countries of South and Southeast Asia, predominantly in Bangladesh and adjoining part of West Bengal where hundreds of thousands are suffering from Arsenicosis and millions more are at risk. The region (~20×10^5 km^2) is the most densely populated (~ 2% of the total population of world) areas where millions of drinking water wells are contaminated (> 10 ppb) with natural iAs. The area, Bengal Delta Plains, (BDP also called Bengal Basin), is the 4^{th} largest riverine drainage (River Ganges, Brahmaputra and Meghna) of the world. These regional rivers headsinto the Bay of Bengal where the world's largest delta has developed. These low land delta plains are often contaminated with As. The hydrostratigraphic framework and hydrogeochemical factors under local redox condition of the deltaic plains are the key players in the spatial distribution of several redox elements (As, Fe and Mn) in groundwater of shallow aquifers of BDP. The low redox condition in the BDP aquifer is delineated to be metal oxyhydroxides reducing conditions, thereby helping in As mobilization in groundwater. The enrichments of NH_4^+, PO_4^{3-}, Fe and As in groundwater along with high reducing conditions of BDP aquifer reflect reductive dissolution of Fe oxyhydroxides where the oxidation of organic matter is important to maintain the prevailing redox process causing high As mobilization into groundwater. The sediment geochemistry indicates that As is mainly bound to the amorphous Fe oxyhydroxides in the aquifer sediment and readily exchangeable with PO_4^{3-}. The determination of isotopic composition of δ^2H and $\delta^{18}O$ in groundwater of two sites indicate the recharge of evaporative surface water to the As rich aquifer. It is revealed that the vertical distribution of As and other aqueous redox parameters is related to the redox zonation within aquifer. Hand operated tube well platform colors can be used as a rapid screening tool for As and Mn in drinking water wells to prioritize As mitigation management [163]. The current situation reveals newer As hotspots, along with increasing iAs concentration in deeper aquifers which are emerging, thusshifting our attention to the question that maybe anthropogenic factors are aiding the geogenic factors.

This concept has necessitated research to determine the degree of importance of the loop between the anthropogenic and geogenic factors.

2.5.3. Food Chain

Use of iAs rich groundwater for irrigation and agriculture is another important issue both in terms of contamination in food chain and livelihood security due to prolonged exposure. The scale of the problem is much serious and wide distribution of contaminated food articles also causes exposure to virgin areas. The complexity of the food exposure and their uncontrolled tradeoff practice are multi-dimensional and needs intensive attention and debate than drinking water iAs exposure. Among the diet, rice (staple food, ~ 2/3rd world's supply from Asia and SE Asia, production rate ~4T/hec.) has been often identified to be contaminated with iAs. Self-sufficiency (Green Revolution) in rice production in As "Hot Spot "areas of SE Asia have resulted in rice production to become solely dependent on iAs rich groundwater irrigation. Studies on sustainable agricultural production with iAs rich groundwater and the impacts on food security at the regional and global levels should be intensified to regulate further policies to protect human health from iAs exposure. The most important message is that only the supply of As free drinking water is not sufficient to protect populations afflicted with groundwater As contamination.

2.6. Metabolism

Ingested As is readily absorbed (~ 70- 95%) by the gastrointestinal tract. Absorbed As, irrespective of forms, is widely distributed in the body. Clearance of iAs, mainly As (III), from skin, gastrointestinal tract, skeleton, thyroid gland and soft tissues are relatively slow than other organs. The highest level of iAs is deposited in the root of hair (20-200 µg/kg), nails (30-500 µg/kg) and skin (upto 600µg/kg) due to high bound capacity of SH groups. The main route of excretion is completed by the kidneys in the methylated forms [164]. Methylation acts in the usual detoxification process to protect biotransformation of iAs. Once ingested in drinking water as oxyanion (iAs III/V, ratio), iAs is metabolized along several pathways in several methylated species. Among the metabolites, the AsIII (both inorganic and organic forms) often show more cytoxicity and acts as a potent inhibitor of several enzymes and as a powerful promoter of oxidative DNA damage. When conjugated with SH (glutathione forms) the divalent As may act as a potential metabolite in the blood [165].

The major route of excretion of As metabolites is via the kidneys. Methylation efficiency varies on relative amounts of different metabolites in urine. A considerable variation has been observed for iAs as well as between the species. It has also been found that patients with skin lesions notably in the acute stages (skin cancer) have large variations in the methylation processes and are often susceptible to higher iAs than organic Arsenic.

2.7. Health Effects

As, mostly as As (III) induces identifiable skin manifestations (pigmentation, keratosis, leukodermal hyperkeratosis) that are common in the different As-affected countries where the

As levels are elevated (> 50 ppb) in the drinking water. These skin lesions often lead to the development of skin cancer and Bowen's disease where the magnitude of the iAs dose and the time frame of exposure are relatively high and prolonged. The possible manifestations of chronic As toxicity(arsenicosis) are many such as respiratory problems, gastrointestinal disorders, liver disease, peripheral vascular and neuropathy disturbances and hematological changes including internal cancers (lungs, bladder, kidney and liver).

2.8. Mitigation

Supply of As safe water is the most important step to rescue As-affected community and patients. Treatment of contaminated groundwater is done by using filters and devices. A variety of technologies are practiced such as oxidation, co-precipitation, adsorption, ion-exchange and membrane process. The efficiency, applicability and field application of the As removal technologies are usuallyfound to beconflicting. This is because there is low success in these operations under field conditions. The basic problem is the management of toxic sludge, construction of unit and management to overcome regular O & M difficulties. Their sustainability (economic viability and social acceptability) needs to be proven under field conditions in several parts of the globe. Presently, exploitation of deeper aquifers is the feasible alternative and should be under skillful management.

Research will be useful for the development of affordable and user friendly technologies to alleviate the problems of the As contaminated drinking water mostly afflicting the poor in the villages and in remote areas. The need of the day is a sustainable technology to be whole heartedly welcomed by those affected by this menace and mostly inhabiting areas of tremendous poverty.

REFERENCES

[1] Gram, L., Ravn, L., Rasch, M., Bruhn, J. B., Christensen, A. B. & Givskov, M. (2002). Food spoilage—interactions between food spoilage bacteria. *International journal of food microbiology*, *78*, 79-97.

[2] Adams M. R. &Moss M. O. (2003). Significance of food borne diseases. In Food Microbiology. 2, 160–164.

[3] FAO. (2011). Global food losses and food waste—extent, causes and prevention. Rome: UN FAO,

[4] Harrigan, W. F. and Park, R. W. A. (1991). Making Safe Food: A management guide for microbiological quality, London: Academic Press. 36

[5] Deshpande, S. S. (2002). Handbook of food toxicology. CRC Press. 457-459

[6] Anklam, E. & Battaglia, R. (2001). Food analysis and consumer protection. *Trends in Food Science & Technology*, *2*, 197-202.

[7] Concon,J. (1998). Food Toxicology. New York: Marcel Dekker. 511-603.

[8] CAST. (1994). Labeling of food-plant biotechnology products, paper from Center for Agricultural Science and Technology Issue, 4.

[9] Lund, D. (1989). Food processing: from art to engineering. *Food Technology*, 43, 242–308.

[10] Whitehead, A. J. (1995). Elements of an effective national food control system. *Food Control*, *6*, 247-251.

[11] Prabhakar, S. V. R. K., Sano, D. & Srivastava, N. (2010). Food safety in the Asia-Pacific region: Current status, policy perspectives, and a way forward. *Sustainable consumption and production in the Asia-Pacific region: Effective responses in a resource constrained world*, 215-238.

[12] Sudershan, R. V., Naveen Kumar, R., Kashinath, L., Bhaskar, V. & Polasa, K. (2014). Foodborne Infections and Intoxications in Hyderabad India. *Epidemiology Research International*.

[13] Knechtges, P. L. (2011). *Food safety: Theory and practice*. Jones & Bartlett Publishers.

[14] Notermans, S., Mead, G. C. & Jouve, J. L. (1996). Food products and consumer protection: a conceptual approach and a glossary of terms. *International journal of food microbiology*, *30*, 175-185.

[15] Davidson, P. M., Taylor, T. M., Doyle, M. P. & Beuchat, L. R. (2007). Chemical peservatives and natural antimicrobial compounds. *Food microbiology: Fundamentals and frontiers*, (Edn. 3), 713-745.

[16] Hendson, M., Hildebrand, D. C. & Schroth, M. N. (1992). Relatedness of *Pseudomonas syringae*pv. tomato, *Pseudomonas syringaepv. maculicola* and *Pseudomonas syringae pv. antirrhini*. *Journal of applied bacteriology*, *73*, 455-464.

[17] Motarjemi, Y. (2013). *Encyclopedia of Food Safety*. Academic Press.

[18] Stanier, R. Y., Ingraham, J. L., Wheelis, M. L. & Painter, P. R. (1987). *General microbiology* (No. Ed. 5). MacMillan Education Ltd. 517

[19] Moore, E. R., Tindall, B. J., Dos Santos, V. A. M., Pieper, D. H., Ramos, J. L. & Palleroni, N. J. (2006). Nonmedical: *Pseudomonas*. In *The Prokaryotes*. Springer New York. pp. 646-703.

[20] Palleroni, N. J., Kunisawa, R., Contopoulou, R. & Doudoroff, M. (1973). Nucleic acid homologies in the genus *Pseudomonas*. *International Journal of Systematic Bacteriology*, *23*, 333-339.

[21] De Vos, P., Van Landschoot, A., Segers, P., Tytgat, R., Gillis, M., Bauwens, M. & De Ley, J. (1989). Genotypic relationships and taxonomic localization of unclassified *Pseudomonas* and *Pseudomonas*-like strains by deoxyribonucleic acid: ribosomal ribonucleic acid hybridizations. *International journal of systematic bacteriology*,*39*, 35-49.

[22] Krieg, N. R. & Garrity, G. M. (2001). On using the Manual. In Bergey's Manual of Systematic Bacteriology, Vol. 1, 2nd edn. ed. Boone, D. R., Castenholz, R. W. and Garrity, G. M. 15–19. New York: Springer.

[23] Douderoff, M.,& Palleroni, N. J. (1974). Genus I: *Pseudomonas migula* 1894. In: R. E. Buchanan and N. E. Gibbons (Eds.) Bergey's Manual of Determinative Bacteriology, 8th ed. Williams and Wilkins. Baltimore, MD. 217–243.

[24] Mullis, K. B. & Faloona, F. A. (1987). Specific synthesis of DNA in vitro via a polymerase-catalyzed chain reaction. Methods in enzymology, 155, 335.

[25] Hunkapiller, T., Kaiser, R. J., Koop, B. F. & Hood, L. (2991). Large-scale and automated DNA sequence determination. *Science*, *254*, 59-67.

[26] Kersters, K., Ludwig, W., Vancanneyt, M., De Vos, P., Gillis, M. & Schleifer, K. H. (1996). Recent changes in the classification of the pseudomonads: an overview. Systematic and Applied Microbiology, 19, 465-477.

[27] Anzai, Y., Kim, H., Park, J. Y., Wakabayashi, H. & Oyaizu, H. (2000). Phylogenetic affiliation of the pseudomonads based on 16S rRNA sequence. *International Journal of Systematic and Evolutionary Microbiology*,*50*, 1563-1589.

[28] Medina, M. S., Tudela, J. A., Marín, A., Allende, A. & Gil, M. I. (2012). Short postharvest storage under low relative humidity improves quality and shelf life of minimally processed baby spinach (Spinacia oleracea. L.). *Postharvest Biology and Technology*,*67*, 1-9.

[29] Takeuchi, K., Matute, C. M., Hassan, A. N. & Frank, J. F. (2000). Comparison of the attachment of *Escherichia coli* O157: H7, *Listeria monocytogenes*, *Salmonella typhimurium*, and *Pseudomonas fluorescens* to lettuce leaves. *Journal of Food Protection®*, *63*, 1433-1437.

[30] Lazzaroni, S., Evidente, A. & Surico, G. (2003). Toxic metabolites and lipopolysaccharides from *Pseudomonas cichorii*. In *Pseudomonas syringae and related pathogens*. Springer Netherlands. 233-243.

[31] Masum, M. M. I., Islam, S. M. M., Islam, M. S. & Kabir, M. H. (2013). Estimation of loss due to post harvest diseases of potato in markets of different districts in Bangladesh. *African Journal of Biotechnology*, *10*, 11892-118902.

[32] Mbajiuka, S, Chinedu, Enya & Emmanuel. (2014). Isolation of Microorganisms associated with Deterioration of Tomato (*Lycopersicon esculentum*) and Pawpaw (*Carica papaya*) Fruits. International Journal of Current Microbiology and Applied Sciences, 3, 501-512.

[33] Marchetti, R., Casadei, M. A. & Guerzoni, M. E. (1992). Microbial population dynamics in ready-to-use vegetable salads. *Italian journal of food science*, *4*(2), 97-108.

[34] Liao, C. H. (2007). Inhibition of foodborne pathogens by native microflora recovered from fresh peeled baby carrot and propagated in cultures. Journal of food science, 72, M134-M139.

[35] BCCDC:http://www.bccdc.ca/NR/rdonlyres/3A2C5D87-5615-4B4B-9279-F28BE80E7764/0/RawMilk Pathogens.pdf

[36] Franzetti, L. & Scarpellini, M. (2007). Characterisation of *Pseudomonas* spp. isolated from foods. *Annals of microbiology*,*57*, 39-47.

[37] García-López, I., Otero, A., García-López, M. L. & Santos, J. A. (2004). Molecular and phenotypic characterization of nonmotile Gram-negative bacteria associated with spoilage of freshwater fish. *Journal of applied microbiology*, *96*, 878-886.

[38] Tryfinopoulou, P., Tsakalidou, E. & Nychas, G. J. (2002). Characterization of Pseudomonas spp. associated with spoilage of gilt-head sea bream stored under various conditions. *Applied and environmental microbiology*, *68*, 65-72.

[39] Shaw, B. G. & Latty, J. B. (1984). A study of the relative incidence of different *Pseudomonas* groups on meat using a computer-assisted identification technique employing only carbon source tests. *Journal of Applied Bacteriology*, *57*, 59-67.

[40] Molin, G. & Ternström, A. (1982). Numerical taxonomy of psychrotrophic pseudomonads. *Journal of General Microbiology*,*128*, 1249-1264

[41] Russell, S. M., Fletcher, D. L. & Cox, N. A. (1995). Spoilage bacteria of fresh broiler chicken carcasses. *Poultry science*, *74*, 2041-2047.

[42] Liao, C. H. & Blackburn, C. D. W. (2006). *Pseudomonas* and related genera. *Food spoilage microorganisms*, 507-540.

[43] Lelliott, R. A., Billing, E. & Hayward, A. C. (1996). A determinative scheme for the fluorescent plant pathogenic pseudomonads. *Journal of applied bacteriology*,*29*, 470-489.

[44] Liao, C. H. & Wells, J. M. (1987). Diversity of pectolytic, fluorescent pseudomonads causing soft rots of fresh vegetables at produce markets. *Phytopathology*,*77*, 673-677.

[45] Cother, E. J. (1976). *Pseudomonas aeruginosa*: Cause Of Internal Brown Rot Of Onion 66.

[46] Wong, W. C. & Preece, T. (1979). FIdentification of *Pseudomonas tolaasi*: the white line in agar and mushroom tissue block rapid pitting tests. *Journal of Applied Bacteriology*, *47*, 401-407.

[47] Ceponis, M. J. (1970). Diseases of California head lettuce on the New York market during the spring and summer months. *Plant Disease Reporter*, 964-966.

[48] Hamad, S. H. (2012). Factors Affecting the Growth of Microorganisms in Food. *Progress in Food Preservation* 418.

[49] Kraft, A. A. (1992). *Psychotropic Bacteria in Foods Disease and Spoilage*. CRC Press.

[50] Duncan, D. W. & Nickerson, J. T. R. (1963). Effect of Environmental and Physiological Conditions on the Phase of Adjustment of *Pseudomonas fragi*. *Applied microbiology*, 179-183.

[51] Howell, A. J., Saffle, R. L. & Powers, J. J. (1971). Temperature cycling effects on bacterial growth. 1. *Pseudomonas fluorescens*. *Journal of Food Science*, *36*, 778-780.

[52] Jay, J. M., Loessner, M. J. & Golden, D. A. (2005). *Modern food microbiology*. Springer.

[53] Vogel, B. F., Jørgensen, K. I. R. S. T. E. N., Christensen, H., Olsen, J. E. & Gram, L. (1997). Differentiation of *Shewanella putrefaciens* and *Shewanella alga* on the basis of whole-cell protein profiles, ribotyping, phenotypic characterization, and 16S rRNA gene sequence analysis. *Applied and environmental microbiology*, *63*, 2189-2199.

[54] Hozbor, M. C., Saiz, A. I., Yeannes, M. I. & Fritz, R. (2006). Microbiological changes and its correlation with quality indices during aerobic iced storage of sea salmon (*Pseudopercis semifasciata*). *LWT-Food Science and Technology*, *39*, 99-104.

[55] Ternström, A., Lindberg, A. M. & Molin, G. (1993). Classification of the spoilage flora of raw and pasteurized bovine milk, with special reference to *Pseudomonas* and Bacillus. *Journal of Applied Bacteriology*, *75*, 25-34.

[56] Dogan, B. & Boor, K. J. (2003). Genetic diversity and spoilage potentials among *Pseudomonas spp*. isolated from fluid milk products and dairy processing plants. *Applied and environmental microbiology*, *69*, 130-138.

[57] Shewan, J. M. (1961). The microbiology of sea-water fish. *Fish as food*,*1*, 487-560.

[58] Shewan, J. M., Hobbs, G. & Hodgkiss, W. (1960). A determinative scheme for the identification of certain genera of Gram-negative bacteria, with special reference to the *Pseudomonadaceae*. *Journal of Applied Bacteriology*, *23*, 379-390.

[59] Levin, R. E. (1968). Detection and incidence of specific species of spoilage bacteria on fish I. Methodology. *Applied microbiology*, *16*, 1734-1737.

[60] Robertson, G. L. (2012). *Food packaging: principles and practice*. CRC press, 353-354

[61] Duncan Jr, D. W. & Nickerson, J. T. R. (1962). Effect of environmental and physiological conditions on the exponential phase growth of *Pseudomonas fragi* (ATCC 4973). In *Proc. Low Temp. Microbiol. Symp., Campbell Soup Comp., Camden, New Jersey* 253-262.

[62] Ingham, S. C. & Potter, N. N. (1988). Growth of *Aeromonas hydrophila* and *Pseudomonas fragi* on mince and surimis made from Atlantic pollock and stored under air or modified atmosphere. *Journal of food protection (USA)*.

[63] Levin, R. E. (2010). Assessment of seafood spoilage and the microorganisms involved. In: *Safety Analysis of Foods of Animal Origin*, 469.

[64] Vieira, E. R. (1999).*Elementary food science*. Springer.

[65] Fratamico, P. M., Annous, B. A. & Guenther, N. W. (2009). (Eds.). *Biofilms in the food and beverage industries*. Elsevier. 175

[66] Huis in't Veld, J. H. (1996). Microbial and biochemical spoilage of foods: an overview. *International Journal of Food Microbiology*,*33*, 1-18.

[67] Dainty, R. H. (1996). Chemical/biochemical detection of spoilage. *International Journal of Food Microbiology*,*33*, 19-33.

[68] Mead, P. S., Slutsker, L., Dietz, V., McCaig, L. F., Bresee, J. S., Shapiro, C. & Tauxe, R. V. (1999). Food-related illness and death in the United States. *Emerging infectious diseases*, *5*, 607.

[69] Rahman, A. & Kang, S. C. (2009). Inhibition of foodborne pathogens and spoiling bacteria by essential oil and extracts of *Erigeron ramosus* (Walt.) BSP. *Journal of food safety*, *29*(2), 176-189.

[70] Agger, W. A. & Mardan, A. (1995). *Pseudomonas aeruginosa* infections of intact skin. *Clinical infectious diseases*, *20*, 302-308.

[71] Amisano, G., Fornasero, S., Migliaretti, G., Caramello, S., Tarasco, V. & Savino, F. (2011). Diarrheagenic *Escherichia coli* in acute gastroenteritis in infants in North-West Italy. *New Microbiologica*, *34*, 45-51.

[72] Lawley, R., Curtis, L. & Davis, J. (2012). *The food safety hazard guidebook*. Royal Society of Chemistry. 81.

[73] Doyle, M. (Ed.). (1989). *Foodborne bacterial pathogens*. CRC Press.

[74] O'Connor, P.http://bacteriainfections.blogspot.in/2005/12/psuedomona-bacterial-infections.html

[75] Cliver, D. O. & Riemann, H. (Eds.). (2002). *Foodborne diseases*. Gulf Professional Publishing. 155.

[76] CSFPH Melioidosis. (2007).http://www.cfsph.iastate.edu/Factsheets/pdfs/melioidosis.pdf.

[77] Cheifetz, A. S., Brown, A., Curry, M. & Moss, A. C. (2011). *Oxford American Handbook of Gastroenterology and Hepatology*. Oxford University Press.

[78] Hunter, C. A. & Ensign, P. R. (1947). An Epidemic of Diarrhea in a New-Born Nursery Caused by *Pseudomonas aeruginosa*. American Journal of Public Health and the Nations Health*, *37*, 1166-1169.

[79] Meitert, E., Vlad, A. & Sima, F. (1983). Food poisoning associated with *Pseudomonas aeruginosa*. *Archives roumaines de pathologie experimentales et de microbiologie*, *43*, 115-119.

[80] Coetzer, P. W. W. & Kroukamp, L. M. (1989). Diarrhoeal disease intervention. *SAMJ*, *76*, 465.

[81] Chuang, C. H., Wang, Y. H., Chang, H. J., Chen, H. L., Huang, Y. C., Lin, T. Y. & Chiu, C. H. (2014). Shanghai fever: a distinct *Pseudomonas aeruginosa* enteric disease. *Gut*, *63*, 736-743.

[82] Clark, R. B. & Michael Janda, J. (1991). *Plesiomonas* and human disease. *Clinical Microbiology Newsletter*, *13*, 49-52.

[83] Kirov, S. M. (1997).*Aeromonas and Plesiomonas species*. In Food Microbiology: Fundamentals and Frontiers, Doyle. M. P. Bcuchat. L. R., and Montvillc. T. J. Eds. ASM Press. Washington. DC.

[84] Shigematsu, M., Kaufmann, M. E., Charlett, A., Niho, Y. & Pitt, T. L. (2000).An epidemiological study of *Plesiomonas shigelloides* diarrhoea among Japanese travellers. Epidemiology and infection, 125, 523-530.

[85] Brenden, R. A., Miller, M. A. & Janda, J. M. (1988). Clinical disease spectrum and pathogenic factors associated with *Plesiomonas shigelloides* infections in humans. *Review of Infectious Diseases*,*10*, 303-316.

[86] Kain, K. C. & Kelly, M. T. (1989). Antimicrobial susceptibility of *Plesiomonas shigelloides* from patients with diarrhea. *Antimicrobial agents and chemotherapy*, *33*, 1609-1610.

[87] Liu, D. (Ed.). (2009). *Molecular detection of foodborne pathogens*. CRC Press.

[88] Stock, I. & Wiedemann, B. (2001). Natural antimicrobial susceptibilities of *Plesiomonas shigelloides* strains. *Journal of Antimicrobial Chemotherapy*, *48*, 803-811.

[89] Currie, B. J., Fisher, D. A., Howard, D. M., Burrow, J. N., Selvanayagam, S., Snelling, P. L. & Mayo, M. J. (2000). The epidemiology of melioidosis in Australia and Papua New Guinea. *Acta tropica*, *74*, 121-127.

[90] Cook, G. C. & Zumla, A. (2008). *Manson's tropical diseases*. Elsevier Health Sciences. 66.

[91] Singh, S. K., Pandey, V. D. & Verma, V. C. (2012). Bacterial Food Intoxication. In Microbial Toxins and Toxigenic Microbes, Studium Press. 216.

[92] Kubota, Y. & Liu, P. V. (1971). An enterotoxin of *Pseudomonas aeruginosa*. *Journal of Infectious Diseases*, *123*, 97-98.

[93] Aiso, K. & Matsuno, M. (1961). The outbreaks of enteritis-type food poisoning due to fish in Japan and its causative bacteria. *Japanese journal of microbiology*, *5*, 337-346.

[94] Jiao, Z., Kawamura, Y., Mishima, N., Yang, R., Li, N., Liu, X. & Ezaki, T. (2003). Need to Differentiate Lethal Toxin-Producing Strains of *Burkholderia gladioli*, Which Cause Severe Food Poisoning: Description of *B. gladioli Pathovar cocovenenans* and an Emended Description of *B. gladioli*. *Microbiology and immunology*, *47*, 915-925.

[95] Cliver, D. O., Potter, M. & Riemann, H. P. (2011). *Foodborne infections and intoxications*. Academic Press.

[96] Kluftinger, J. L., Lutz, F. & Hancock, R. E. (1989). *Pseudomonas aeruginosa* cytotoxin: periplasmic localization and inhibition of macrophages. *Infection and immunity*, *57*, 882-886.

[97] Liu, P. V. (1974). Extracellular toxins of *Pseudomonas aeruginosa*. *Journal of Infectious Diseases*, *130* (Supplement), S 94-S 99.

[98] Lutz, F. (1986). Interaction of *Pseudomonas aeruginosa* cytotoxin with plasma membranes from Ehrlich ascites tumor cells. *Naunyn-Schmiedeberg's archives of pharmacology*, *332*, 103-110.

[99] Lutz, F., Maurer, M. & Failing, K. (1987). Cytotoxic protein from *Pseudomonas aeruginosa*: formation of hydrophilic pores in Ehrlich ascites tumor cells and effect on cell viability. *Toxicon*, *25*, 293-305.

[100] Orlik-Eisel, G., Lutz, F., Henschen, A., Eisel, U., Struckmeier, M., Kräuter, J. & Niemann, H. (1990). The cytotoxin of *Pseudomonas aeruginosa*: Cytotoxicity requires proteolytic activation. *Archives of microbiology*, *153*, 561-568.

[101] Xiong, G., Struckmeier, M. & Lutz, F. (1994). Pore-forming *Pseudomonas aeruginosa* cytotoxin. *Toxicology*, 87, 69-83.

[102] Weiner, R. N., Schneider, E., Haest, C. W. M., Deuticke, B., Benz, R. & Frimmer, M. (1985). Properties of the leak permeability induced by a cytotoxic protein from *Pseudomonas aeruginosa* (PACT) in rat erythrocytes and black lipid membranes. *Biochimica et Biophysica Acta (BBA)-Biomembranes*, *820*, 173-182.

[103] Sliwinski-Korell, A., Engelhardt, H., Kampka, M. & Lutz, F. (1999). Oligomerization and structural changes of the pore-forming *Pseudomonas aeruginosa* cytotoxin. *European Journal of Biochemistry*, *265*, 221-230.

[104] Pavlovskis, O. R., Iglewski, B. H. & Pollack, M. (1978). Mechanism of action of *Pseudomonas aeruginosa* exotoxin A in experimental mouse infections: adenosine diphosphate ribosylation of elongation factor 2. *Infection and immunity*, *19*, 29-33.

[105] Iglewski, B. H., Liu, P. V. & Kabat, D. (1977). Mechanism of action of *Pseudomonas aeruginosa* exotoxin Aiadenosine diphosphate-ribosylation of mammalian elongation factor 2 in vitro and in vivo. *Infection and immunity*,*15*, 138-144.

[106] Vasil, M. L., Kabat, D. & Iglewski, B. H. (1977).Structure-activity relationships of an exotoxin of *Pseudomonas aeruginosa*. *Infection and immunity*,*16*, 353-361.

[107] Cross, A. S., Sadoff, J. C., Iglewski, B. H. & Sokol, P. A. (1980). Evidence for the role of toxin A in the pathogenesis of infection with *Pseudomonas aeruginosa* in humans. *Journal of Infectious Diseases*, *142*, 538-546.

[108] Pavlovskis, O. R. & Wretlind, B. (1982). *Pseudomonas aeruginosa toxins* (No. NMRI-82-66). Naval Medical Research Inst Bethesda MD.

[109] Saxena, M., Sehgal, S. C., Chhibber, S. & Vadehra, D. V. (1988). *Pseudomonas aeruginosa* enterotoxin optimization of environmental conditions and comparison of assay procedures. *Indian Journal of Comparative Microbiology, Immunology and Infectious Diseases*, 9, 229-234.

[110] Wareing, P., Fernandes, R. & Stuart, F. (2010). *Micro-facts: The working companion for food microbiologists.* Royal Society of Chemistry.

[111] Xu, D. C., N. X. Zhao, Z. C. Zhao, D. Y. Zhang, Z. J. Sun, & Wang, X. Y.(1982). *Further study on the classificatory position of Flavobacterium farinofermentans. Journal of Harbin Medical University, 2:69-73. (In Chinese.)*

[112] Zhao, N. X., D. C. Xu,D. Y. Zhang, Z. C. Zhao, C. L. Chin, & Jiang, L. R. (1985). Study on the fermented corn flour poisoning bacteria. *Microbiology Journal*. 1, 152-162.

[113] Van Damme, P. A., Johannes, A. G., Cox, H. C. & Berends, W. (1960). On toxoflavin, the yellow poison of *Pseudomonas cocovenenans*. *Recueil des Travaux Chimiques des Pays-Bas*,*79*, 255-267.

[114] Cox, J., Kartadarma, E. & Buckle, K. *Burkholderia cocovenenans*. (1997). In Foodborne Microorganisms of Public Health Significance. Food Microbiology Group (NSW Branch), Australian Institute of Food Science and Technology, Sydney, 521–524

[115] van Veen, A. G. (1967). The bongkrek toxins. *Biochemistry of Some Foodborne Microbial Toxins*, 43-50.

[116] Welling, W., Cohen, J. A. & Berends, W. (1960). Disturbance of oxidative phosphorylation by an antibioticum produced by *Pseudomonas cocovenenans*. *Biochemical pharmacology*,*3*, 122-135

[117] Henderson, P. J. & Lardy, H. A. (1970). Bongkrekic acid an inhibitor of the adenine nucleotide translocase of mitochondria. *Journal of Biological Chemistry*, *245*, 1319-1326.

[118] Garcia, R. A. (1999). The effect of lipids on bongkrekic (Bongkrek) acid toxin production by *Burkholderia cocovenenans* in coconut media. *Food Additives & Contaminants*,*16*, 63-69.

[119] Bateman, N., Jefferson, R., Thomas, S., Thompson, J. & Vale, A. (Eds.). (2014). Oxford Desk Reference: Toxicology. Oxford University Press. 331.

[120] King, E. O., Ward, M. K. & Raney, D. E. (1954). Two simple media for the demonstration of pyocyanin and fluorescin. *Journal of laboratory and clinical medicine*, *44*, 301-307.

[121] Mead, G. C. & Adams, B. W. (1977). A selective medium for the rapid isolation of pseudomonads associated with poultry meat spoilage. *British Poultry Science*, *18*, 661-670.

[122] Flint, S., Hartley, N. (1996). A modified selective medium for the detection of *Pseudomonas* species that cause spoilage of milk and dairy plants. *International Dairy Journal*, 6: 223–230.

[123] Nollet, L. M. & Toldrá, F. (Eds.). (2009). *Handbook of dairy foods analysis*. CRC Press.

[124] Goto, S. & Enomoto, S. (1970). Nalidixic acid cetrimide agar. *Japanese journal of microbiology*,*14*, 65-72.

[125] Corry, J. E., Curtis, G. D. & Baird, R. M. (Eds). (2012).*Pseudomonas* agar base with cetrimide and nalidixic acid. In: *Handbook of Culture Media for Food and Water Microbiology*. Royal Society of Chemistry.

[126] Chang, T. C. & Huang, A. H. (2000). Rapid differentiation of fermentative from non fermentative gram-negative bacilli in positive blood cultures by an impedance method. *Journal of clinical microbiology*, *38*, 3589-3594.

[127] Szita, G., Gyenes, M., Soos, L., Retfalvi, T., Bekesi, L., Csikó, G. & Bernáth, S. (2007). Detection of *Pseudomonas aeruginosa* in water samples using a novel synthetic medium and impedimetric technology. *Letters in applied microbiology*, *45*, 42-46.

[128] Pang, P., Huang, S., Cai, Q., Yao, S., Zeng, K. & Grimes, C. A. (2007). Detection of *Pseudomonas aeruginosa* using a wireless magnetoelastic sensing device. *Biosensors and Bioelectronics*, *23*, 295-299.

[129] Al-Qadiri, H. M., Al-Holy, M. A., Lin, M., Alami, N. I., Cavinato, A. G. & Rasco, B. A. (2006). Rapid detection and identification of *Pseudomonas aeruginosa* and *Escherichia coli* as pure and mixed cultures in bottled drinking water using Fourier transform infrared spectroscopy and multivariate analysis. *Journal of agricultural and food chemistry*,*54*, 5749-5754.

[130] Jannes, G. & De Vos, D. (2006). A review of current and future molecular diagnostic tests for use in the microbiology laboratory. In *Diagnostic Bacteriology Protocols* (pp. 1-21). Humana Press.

[131] Hong, B. X., Jiang, L. F., Hu, Y. S., Fang, D. Y. & Guo, H. Y. (2004). Application of oligonucleotide array technology for the rapid detection of pathogenic bacteria of foodborne infections. *Journal of microbiological methods*, *58*, 403-411.

[132] Lin, M. C., Huang, A. H., Tsen, H. Y., Wong, H. C. & Chang, T. C. (2005). Use of oligonucleotide array for identification of six foodborne pathogens *and Pseudomonas aeruginosa* grown on selective media. *Journal of Food Protection®*, *68*, 2278-2286.

[133] Lavenir, R., Jocktane, D., Laurent, F., Nazaret, S. & Cournoyer, B. (2007).Improved reliability of *Pseudomonas aeruginosa* PCR detection by the use of the species-specific *ecfX* gene target. *Journal of microbiological methods*, *70*, 20-29.

[134] Lenaerts, J., Lappin-Scott, H. M. & Porter, J. (2007). Improved fluorescent in situ hybridization method for detection of bacteria from activated sludge and river water by using DNA molecular beacons and flow cytometry. *Applied and environmental microbiology*, *73*, 2020-2023.

[135] Shannon, K. E., Lee, D. Y., Trevors, J. T. & Beaudette, L. A. (2007). Application of real-time quantitative PCR for the detection of selected bacterial pathogens during municipal wastewater treatment. *Science of the total environment*, *382*, 121-129.

[136] Reynisson, E., Lauzon, H. L., Magnusson, H., Hreggvidsson, G. Ó. & Marteinsson, V. (2008). T. Rapid quantitative monitoring method for the fish spoilage bacteria Pseudomonas. *Journal of Environmental Monitoring*, *10*, 1357-1362.

[137] Ercolini, D., Ferrocino, I., Nasi, A., Ndagijimana, M., Vernocchi, P., La Storia, A. & Villani, F. (2011). Monitoring of microbial metabolites and bacterial diversity in beef stored under different packaging conditions. *Applied and environmental microbiology*, *77*, 7372-7381.

[138] Matsuda, K., Tsuji, H., Asahara, T., Kado, Y. & Nomoto, K. (2007). Sensitive quantitative detection of commensal bacteria by rRNA-targeted reverse transcription-PCR. *Applied and environmental microbiology*, *73*, 32-39.

[139] Langsrud, S., Sidhu, M. S., Heir, E. & Holck, A. L. (2003). Bacterial disinfectant resistance—a challenge for the food industry. *International biodeterioration & biodegradation*, *51*, 283-290.

[140] Wirtanen, G., Salo, S., Helander, I. M. & Mattila-Sandholm, T. (2001). Microbiological methods for testing disinfectant efficiency on *Pseudomonas* biofilm. *Colloids and Surfaces B: Biointerfaces*, *20*, 37-50.

[141] Sheldon, B. W. & Brown, A. L. (1986). Efficacy of ozone as a disinfectant for poultry carcasses and chill water. *Journal of Food Science*, *51*, 305-309.

[142] Kim, J. G. & Yousef, A. E. (2000). Inactivation kinetics of foodborne spoilage and pathogenic bacteria by ozone. *Journal of Food Science*, 65, 521-528.

[143] Wu, V. C. & Kim, B. (20007).Effect of a simple chlorine dioxide method for controlling five foodborne pathogens, yeasts and molds on blueberries. *Food microbiology*, *24*, 794-800.

[144] Beuchat, L. (1998). Surface decontamination of fruits and vegetables eaten raw: a review. In *Surface decontamination of fruits and vegetables eaten raw: a review*. OMS.

[145] Sapers, G. M. & Simmons, G. F. (1998). Hydrogen peroxide disinfection of minimally processed fruits and vegetables. *Food Technology*, *52*, 48-52.

[146] Moustafa, H. H. & Collins, E. B. (1969). Effects of Selected Food Additives on Growth of *Pseudomonas fragi*. *Journal of dairy science*, *52*, 335-340.

[147] Fernández-Molina, J. J., Altunakar, B., Bermúdez-Aguirre, D., Swanson, B. G. & Barbosa-CáNovas, G. V. (2005).Inactivation of *Pseudomonas fluorescens* in skim milk by combinations of pulsed electric fields and organic acids. *Journal of Food Protection®*, *68*, 1232-1235.

[148] Quadir, A. M. & Ahmed, M. (2013). Organic acids effective antimicrobial agents against *Escherichia coli*, *Staphylococcus aureus* and *Pseudomonas aeruginosa* at ambient temperature. Journal of Pharmacy Research. 1, 983-987

[149] Tudela, J. A., Marín, A., Garrido, Y., Cantwell, M., Medina-Martínez, M. S. & Gil, M. I. (2013). Off-odour development in modified atmosphere packaged baby spinach is an unresolved problem. *Post harvest Biology and Technology*, *75*, 75-85.

[150] Chung, M. S.,Ko, Y. T. & Kim, W. S. (2000). Survival of *Pseudomonas fluorescens* and *Salmonella typhimurium* after electron beam and gamma irradiation of refrigerated beef. *Journal of Food Protection®*, *63*, 162-166.

[151] Michalac, S., Alvarez, V., Ji, T. & Zhang, Q. (2003). HInactivation of selected microorganisms and properties of pulsed electric field processed milk. *Journal of food processing and preservation*,*27*, 137-151.

[152] García-Graells, C., Van Opstal, I., Vanmuysen, S. & Michiels, C. W. (2003). The lactoperoxidase system increases efficacy of high-pressure inactivation of foodborne bacteria. *International journal of food microbiology*,*81*, 211-221

[153] Ure, A. & Davidson, C. (Eds.). (2008). Chemical speciation in the environment. John Wiley & Sons.

[154] De Silva, J. J. R. F. & Williams, R. J. P. (1991). The biological chemistry of the elements. Inorganic Chemistry of Life, Clarendon Press, Oxford, NY, 541.

[155] ARC, I. & International Agency for Research on Cancer. (1982). I ARC Monographs on the Evaluation of the Carcinogenic Risk of Chemicals to Humans. Hexachlorobenzene, 20, 155-178

[156] Fuge, R. (2005). Soils and iodine deficiency. In 'Essentials of medical geology–Impacts of the natural environment on public health'(Eds O Selinus, B Alloway, JA Centeno, RB Finkelman, R Fuge, U Lindh, P Smedley) 417-433.

[157] Williams, R. J. P. & Silva, J. J. R. (1996). The natural selection of the chemical elements: the environment and life's chemistry. Clarendon Press; Oxford University Press.

[158] Adriano, D. C. (2001). Chapter 1 Introduction. Trace elements in terrestrial environment: biogeochemistry, bioavailability, and risks of metals, 22-23.

[159] World Health Organization. (2001). Environmental health criteria 224: arsenic and arsenic compounds. World Health Organization, Geneva, 1-108.

[160] NRC, National Academy Press, US. (1999).

[161] ATSDR Toxicology Profile of Arsenic. Draft for public comment. Agency for Toxic Substances and Disease Registry Atlanta, GA. 29-290. 2005.

[162] Report, WHO Guidelines for Drinking Water Quality, 3rd ed. 2004

[163] BISWAS, A. (2013).Arsenic Geochemistry in the Alluvial Aquifers of West Bengal, India: Implications for targeting safe aquifers for sustainable drinking water supply. KTH, Sweden.

[164] Abernathy, C. O., Calderon, R. L. & Chappell, W. R. (Eds). (1997).Arsenic: exposure and health effects. Springer Netherlands,

[165] Handbook on the toxicology of Metals 3rd edition, Gunnar F., Bruse F., Nordberg M. (AP) 1978.

In: Food Poisoning
Editor: Paresh C. Ray
ISBN: 978-1-63463-166-2

Chapter 7

HYBRID MULTIFUNCTIONAL NANOPARTICLES AS PLATFORMS FOR TARGETED DETECTION, SEPARATION, AND PHOTOTHERMAL DESTRUCTION OF FOOD PATHOGENS

Brian G. Yust[1*], Dhiraj K. Sardar[2] and Paresh C. Ray[3]
[1]Department of Physics & Geology, University of Texas-Pan American, Edinburg, TX, US
[2]Department of Physics & Astronomy, University of Texas at San Antonio, San Antonio, TX, US
[3]Department of Chemistry, Jackson State University, Jackson, Mississippi, US

ABSTRACT

Recently, one of the most important and complex problems facing our global society is treating or preventing infectious diseases caused by multi drug resistant bacteria (MDRB) which have developed from overuse of existing antibiotics. The increase in the presence of MDRB in food supplies has created an urgent need for new approaches to early stage detection of MDRB and highly specific destruction of MDRB which do not rely on traditional regimes. Driven by this need, we explore herein, the development of a multifunctional popcorn shape iron magnetic core- gold plasmonic shell nanotechnology-driven approach for targeted magnetic separation & enrichment, label free surface enhanced Raman spectroscopy (SERS) detection, and selective photothermal destruction of MDR *Salmonella* DT104. The experimental data shows that M308 antibody-conjugated popcorn shape magnetic core – plasmonic shell nanoparticles can be used for targeted separation & SERS imaging of MDR *Salmonella* DT104. A targeted photothermal lysis experiment, using 670-nm light at 1.5 W/cm^2 for 10 minutes, resulted in selective irreparable cellular damage to most of MDR *Salmonella*. We discuss the possible mechanisms and operating principle for the targeted separation, imaging, and photothermal destruction of MDRB using popcorn shape magnetic/plasmonic nanotechnology and expound upon the implications to such technology in the food safety industry.

* Corresponding author: e-mail: bribriwork@gmail.com.

INTRODUCTION

Infectious disease outbreaks due to multidrug-resistant bacteria (MDRB) infections are one of the leading causes of death worldwide totaling to about one-third of global mortality. [1-5]Due to the biological diversity of the deadly bacteria and quite low infectious dose, there is an urgent need for reliable, quick approaches to identify harmful bacterium with sufficient specificity and sensitivity. [5-9] Since the development of penicillin in 1940, antibiotics have become economic powerhouses for our society and are the most life saving drugs in modern medical procedures. [1-4] Annually in the USA, antibiotics generate sales of about 42 billion USD per year and account for between 15–30% of total drug expenditures for therapeutic drugs. [5-9]However, due to the heavy use of antibiotics worldwide, deadly human pathogens such as Tuberculosis, Staphylococcus, and Salmonella bacteria have developed a resistance to many antibiotics. [1-4] Due to the presence of multiple antimicrobial-resistance genes, such as 1) pse for ampicillin resistance, 2) rpoB for rifampicin resistance, 3) floR for chloramphenicol resistance, 4) str for streptomycin resistance, 5) catG for isoniazid resistance, 6) sulI for sulfonamide resistance, and 7) tetR or tetG for tetracycline resistance, several strains of deadly bacteria are now highly resistant to many commonly used antibiotics. [1-4, 10]According to the World Health Organization (WHO), [6] within 10 – 20 years, the currently available antibiotics will fail to cure infectious diseases caused by MDRB. There are numerous pathways through which MDRB can enter the body and cause serious infection. Some of the most common areas of exposure to MDRB include public transit, contaminated water supplies, contaminated hospital and medical equipment, and contaminated food supplies and preparation areas. In particular, MDRB infection is extremely dangerous for those with a suppressed or compromised immune system such as burn patients, patients on immunosuppressive medication, patients with autoimmune diseases, and the elderly. In the case of burn patients, there is an extreme danger of MDRB colonization and infection of the open would area which can lead to MDRB directly getting into the bloodstream and causing sepsis. [11] Sterilization of catheters and other medical equipment including surgical and implanted devices is another major concern with MDRB as these all provide a direct way of the invading bacteria to bypass the body's first line of defense, the skin. Furthermore, there has been a major increase in MDRB within hospital care and recovery facilities themselves causing illness and even death in many patients through secondary infections during recovery. [12-15] In the food industry, it is possible for MDRB to contaminate products along the entire product processing line. From contamination in fields, as was seen recently in spinach [16] and peanuts [17], or from slaughterhouses to packaging plants, factory conveyor belts, and even food preparation stations, our food is constantly at risk of contamination, and with bacteria developing resistance to current antibiotics, it is crucial to develop new strategies for maintaining food safety standards. [18-21] This potential crisis demands the development of a new approach for the treatment of infectious bacterial pathogens which does not rely on the traditional therapeutic action. Driven by this need, we have developed a hybrid plasmonic shell–magnetic core multifunctional nanotechnology-driven approach for the targeted separation, label-free surface-enhanced Raman spectroscopy (SERS) detection, and selective photothermal destruction of MDR Salmonella DT104.

While there are many research efforts towards preventing MDRB contamination including new antimicrobial materials which incorporate silver (Ag) nanoparticles [22-24], oxide nanoparticles [25-27], or metallopolymers [28], they each have their own drawbacks. For instance, silver nanoparticles which have already been incorporated into commercially available antimicrobial clothing, food packaging, and kitchenware, are known to be very effective at passively preventing bacterial colonization and growth on surfaces. [29-34] However, these nanoparticles are known to be quite toxic to certain types of cells within the body and are known to break down by releasing Ag ions which can cause DNA damage. [35-38] Therefore, although they are already used in commercial products, they can pose a risk to consumers mainly through the non-specificity and passive nature of their antimicrobial properties. Once MDRB have either infected a person or colonized a food surface or liquid, the options for treatment are limited. Current therapeutic and bactericidal avenues include combinatorial therapy with antibiotic cocktails [39-41], utilizing "old" antibiotics such as fosfomyacin with known but acceptably low toxic effects to the patient [42-45], targeted Ag nanoparticles [22-24], photodynamic inactivation of MDRB through photoactivation of compounds such as porphyrins [46, 47], and using bacterial viruses [48]. Of these approaches, all except the photodynamic inactivation would affect a patient or consumer systemically, further reducing the colonies of "good bacteria" which can aid in preventing MDRB from spreading. While the photodynamic inactivation has been shown to effectively sterilize hospital water supplies [46], this is done under UV or visible excitation which is not ideal for any internal therapeutic procedure. Our own approach addresses many of the shortcomings of other proposed solutions to the MDRB problem since the hybrid plasmonic shell–magnetic core nanoparticles do not involve Ag with its known ion leaching and toxicity issues, would not kill or prohibit growth of beneficial bacteria since it is targeted to specific bacteria and activated by NIR illumination, and should be safe to use on foods or in water supplies since they would not affect a patient or consumer systemically the way that traditional antibiotics do.

Our approach to solving the complex MDRB infection problem is to develop new materials with multifunctional capabilities that satisfy the critical needs of early-stage detection and therapeutic action. [49-54] As reported by the authors as well as other groups in the last decade, plasmonic gold nanoparticles with optical properties that are tunable in the near-infrared (NIR) region are very useful for biological imaging due to their high transmission rate of NIR photons through biological tissues. [54-59] In addition, the exhibited biocompatibility, lack of toxicity, and their ability to generate high temperatures at a desired site make plasmonic gold nanotechnology a promising solution to the greatest health safety challenges of society, selective destruction of MDRB infection. [60-75] On the other hand, iron-based magnetic nanoparticles have been shown to be a very attractive material for use as contrast agents in magnetic resonance imaging (MRI) and biological separation. [76-88] Building off of our previous work, we have developed core–shell popcorn-shaped nanoparticles and demonstrate herein their capability for magnetic separation and SERS imaging of MDRB. Very high sensitivity, along with the highly informative spectra characteristics of Raman spectroscopy, [89-98] enables us to use the SERS- based method as a fingerprint for the label-free detection of MDRB. In the case of nano-popcorn, the central

sphere acts as an electron reservoir while the tips are capable of focusing the field at their apexes. As a result, the characteristic sharp tips provide a huge field enhancement of the SERS-scattering signal. We also report that the same core–shell popcorn- shaped nanoparticle can be used as "light-directed nanoheaters" for the hyperthermic destruction of MDRB under NIR light exposure. This will be extremely useful for killing MDRB in cases of patient infection as well as in cases of food or food packaging contamination. In these popcorn-shaped hybrid nanoparticles, the plasmonic gold coating also serves to stabilize the high-magnetic-moment nanoparticles and protect the core from corrosive biological conditions. The gold coating also help to eliminate the known toxicity of iron nanoparticles since it will allow easy bio-conjugation through the well-understood chemistry of Au−S. Finally, the plasmonic shell can also be used as photothermal material for the hyperthermic destruction of MDRB by using NIR light. As such, our hybrid nanoparticles are unique in providing a single, multifunctional platform for detection, separation, destruction of MDRB.

MATERIALS AND METHODS

Nanoparticles with a popcorn-shaped plasmonic gold shell and an iron magnetic core were synthesized through a two-step process, using seed-mediated growth, as shown in Figure 1 A. In the first step, very small spherical iron nanoparticles were synthesized by using trisodium citrate as a stabilizer and sodium borohydride as a strong reducing agent. Hydrogen tetrachloroaurate ($HAuCl_4 \cdot 3\ H_2O$), $NaBH_4$, sodium citrate, and iron chloride, were purchased from Sigma–Aldrich and used without further purification. For this purpose, an aqueous solution of $NaBH_4$ (2.5m) was added drop-wise into $FeCl_3$ deionized (DI) water. Next, an aqueous solution of trisodium citrate (TSC, 0.25 mm) was added at room temperature with vigorous stirring. TSC helps the formation of iron nanocrystals through the nucleation-growth pathway, and a black powder was produced immediately. After stirring for one hour, the iron nanoparticles were separated by magnet and washed with DI water and ethanol. After that, the black powder was dried in an N_2 atmosphere at room temperature. Figure 1 B show the JEM-2100F transmission electron microscope (TEM) image of the iron nanoparticle with a size of about 20 nm. Figure 1 D shows the absorption spectra of ferric chloride and the iron nanoparticle.

In the second step, the popcorn-shaped magnetic gold shell was synthesized by using the seed-mediated growth procedure in the presence of CTAB. The above prepared Fe nanoparticle (10 mg) was suspended in CTAB (10 mg) in DI water (50 mL). $HAuCl_4$ (2 mL 10^{-2} m) was added into the solution and stirred for 1 min. After that, CTAB acts as a shape-templating surfactant so that the seeds can grow into the larger particles with the particular morphology we desired. After continued stirring for 24 h, the hybrid magnetic nanoparticles were separated by using a magnet and washed with DI water and ethanol. A TEM and Hitachi 5500 Ultra-high resolution SEM microscope and UV–visible absorption spectrum were used to characterize the core–shell nanoparticles (as shown in Figure 2 A–C). A plasmon band around 580 nm, as shown in Figure 1 D, clearly shows the formation of gold shell. The TEM and SEM images show clear spikes, which indicate the formation of popcorn-shaped

nanoparticle. As shown in Figure 2 C-D, energy dispersion X-ray (EDX) spectra and mapping also indicate the presence of both iron and gold. The observed Cu and Al peak in the EDX data originate from the support grid and holder, respectively.

For selective sensing and killing of MDR DT104, we modified the surface of the popcorn-shaped magnetic core–gold shell nanoparticle by using the monoclonal M3038 antibody, [99]as shown in Figure 3. As was previously mentioned, the popcorn-shaped magnetic core–gold shell nanoparticles were synthesized by using seed-mediated growth procedure in the presence of CTAB. As a result, the as-synthesized core–shell nanoparticles have a CTAB coating. However, CTAB is known to be cytotoxic, and as a result, is not ideal for in vivo applications. Furthermore, CTAB is positively charged at physiological pH, and therefore it will be able to attract negatively charged bacteria easily to its surface. [50-54] At this point, the CTAB-coated popcorn-shaped magnetic core–gold shell nanoparticles will face severe non-specific binding problems. To overcome this problem, we modified the surface of the gold-shell nanoparticle with amine groups (as shown in Figure 3). For this purpose, we added cystamine dihydrochloride (30 mm) to the popcorn-shaped magnetic core–gold shell nanoparticles (50 mL) and the solution was kept at 50°C for several hours under constant sonication. After that, the excess cystamine dihydrochloride was removed by centrifugation at 4000 rpm for several minutes. For covalent immobilization of the monoclonal M3038 antibody onto the now-amine-coated popcorn- shaped magnetic core–gold shell nanoparticle, the highly established glutaraldehyde-spacer method was used. [55, 58-60]To remove the excess antibody afterwards, the antibody-conjugated popcorn-shaped magnetic core–gold shell nanoparticles were washed several times with PBS. The number of M3038 antibody molecules in each core–shell nanoparticle was measured by performing a KCN dissolution procedure, as reported previously. [80, 89]In this case, we used an Rh-6G-modified antibody. We estimated that there were about 100–120 Rh-6G-modified M3038 antibodies per popcorn-shaped magnetic core–gold shell nanoparticle. This experiment has been performed 5 to 6 times, and the average values are reported in this manuscript. During immobilization of the antibody, we did not note any aggregation of popcorn-shaped magnetic core–gold shell nanoparticle as examined by TEM or UV–visible absorption spectroscopy.

For the SERS experiment, we designed and used a SERS probe, which we have reported recently. [85] In short, a continuous wavelength DPSS laser from laser glow technology (LUD-670) operating at 670 nm is used as an excitation light source. For excitation and data collection, an InPhotonics 670 nm Raman fiber optic probe was used which has a combination of 90 μm excitation fiber and 200 μm collection fiber with filtering and steering micro-optics. For Raman signal collection, a miniaturized QE65000 Scientific-grade Spectrometer from Ocean Optics was used as a Raman detector. The spectral response range of this mini Raman spectrometer is 220–3600 cm^{-1}. It is equipped with a TE cooled 2048 pixel CCD and interfaced to computer through a USB port. The Hamamatsu FFT-CCD detector used in the QE65000 provides 90% quantum efficiency with high signal-to-noise and rapid signal processing speed as well as remarkable sensitivity for low-light level applications. The Raman spectrum was collected with Ocean Optics data acquisition SpectraSuite spectroscopy software.

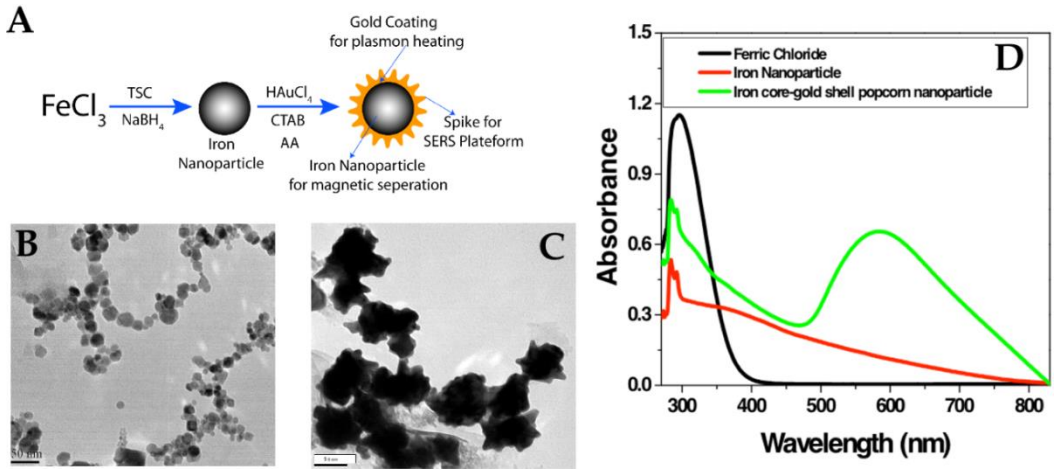

Figure 1. A) A schematic representation of the synthetic procedure of multifunctional magnetic core–gold shell popcorn-shaped nanoparticles. B) TEM image of freshly prepared iron nanoparticle; scale bar, 50 nm. C) TEM image of freshly prepared magnetic core-gold shell popcorn-shaped nanoparticle; scale bar, 50 nm. D) Absorption spectra of ferric chloride, iron nanoparticle, magnetic core–gold shell popcorn-shaped nanoparticle. The strong, long wavelength band in the visible region (l_{PR} = 580 nm) is due to the oscillation of the conduction band electrons of gold.

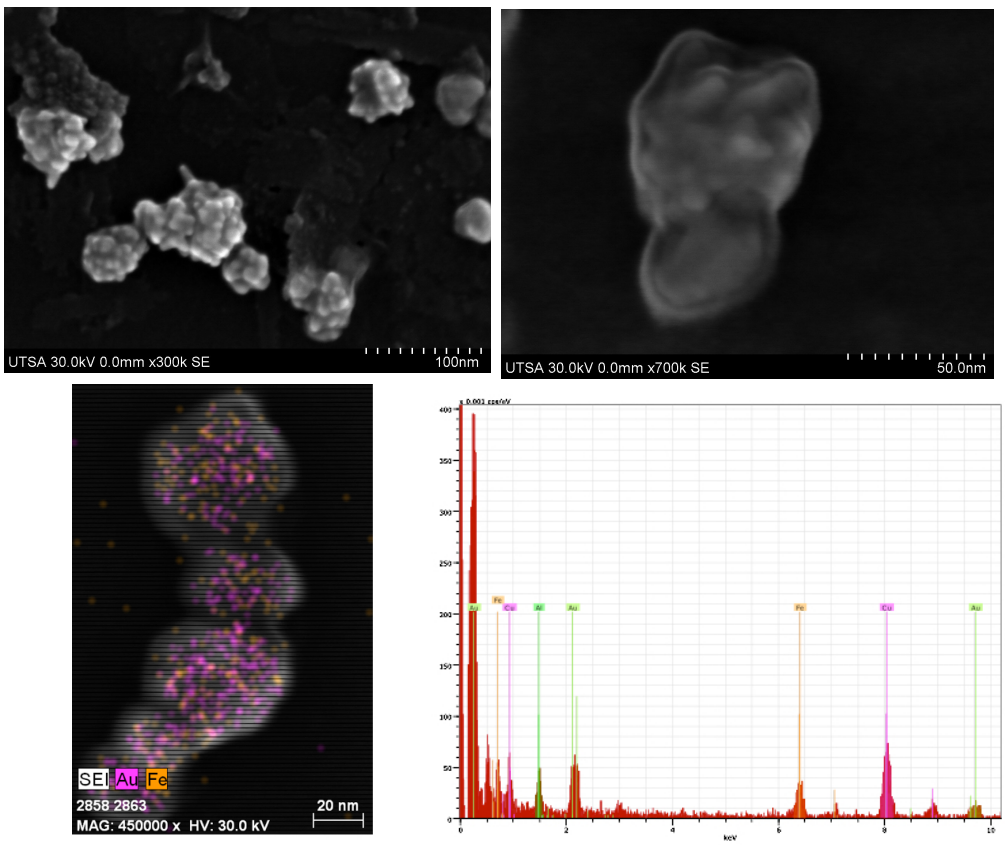

Figure 2. A - B) SEM images of freshly prepared magnetic core–gold shell popcorn-shaped nanoparticles. The SEM image clearly demonstrates that the synthesized nanoparticles are popcorn-

shaped. C) EDX elemental mapping overlayed on SEM image of nanoparticles. D) EDX data of freshly prepared magnetic core-gold shell popcorn-shaped nanoparticles. The Cu and Al peak in the EDX data originate from the support grid.

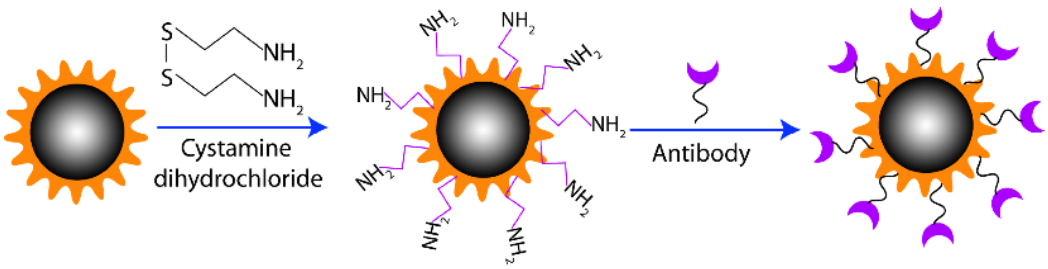

Figure 3. A schematic representation showing the synthetic protocol of monoclonal antibody and A9 conjugated popcorn shape magnetic core– gold shell nanoparticle for the selective sensing and killing of Salmonella DT104.

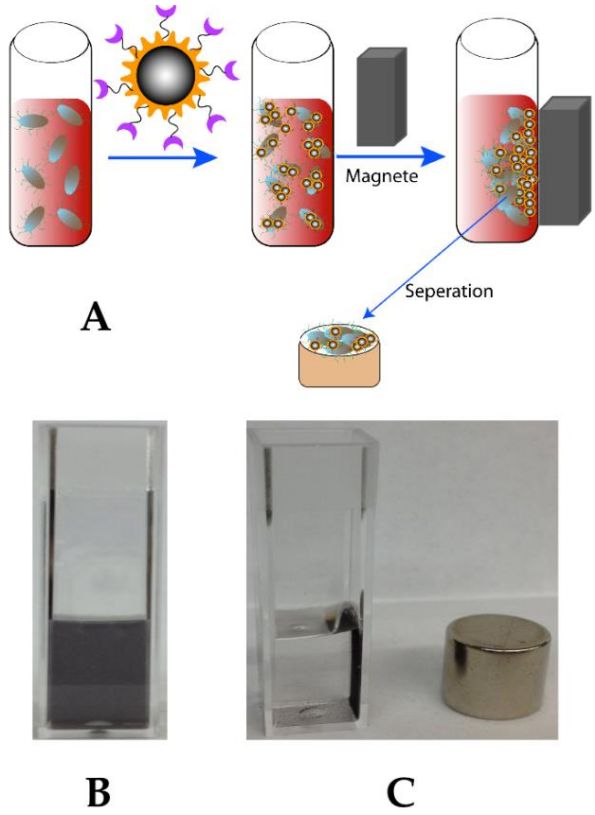

Figure 4. A) A schematic representation showing the separation procedure for Salmonella DT104 by using M3038 antibody-conjugated core- shell nanoparticles. B) The separation of Salmonella DT104-attached magnetic/plasmonic nanoparticles by using a magnet. Salmonella DT104-attached core–shell nanoparticle in the absence of a bar magnet and C) Salmonella DT104-attached core–shell nanoparticle in the presence of bar magnet.

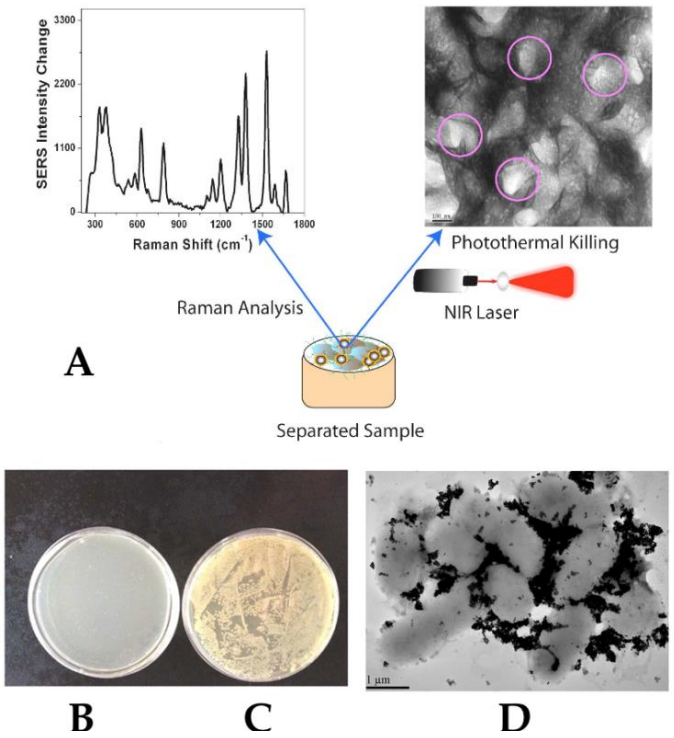

Figure 5. A) A schematic representation showing the selective SERS imaging and targeted photothermal destruction of Salmonella DT104 after magnetic separation. B) Colonies of MDR Salmonella DT104 shows absence of bacteria in the supernatant solution after magnetic capture and C) Colonies of MDR Salmonella DT104 show the presence of bacteria in the suspension of magnetic/plasmonic nanoparticle-conjugated-MDR Salmonella DT104 after magnetic capture and resuspension in PBS. The initial number of MDR was 1.2 x 10^5 CFU mL^{-1}. D) TEM image demonstrating the aggregation of antibody-conjugated nanoparticles after the addition of 1.2 x 10^5 CFU mL^{-1} MDR Salmonella DT104 bacteria. The TEM image also shows the formation of bigger microbial clusters in presence of 6.2 x 10^4 CFU mL^{-1} MDR Salmonella DT104 bacteria; scale bar, 1 μm.

Salmonella typhimurium DT104, which is resistant to five different antibiotics including Ampicillin, chloramphenicol, streptomycin, sulfonamides, and tetracycline, was purchased from the ATCC (ATCC 700408) and then cultured in our laboratory. The MDR bacteria were cultured by following the ATCC protocol as instructed. Initially, the supplied pellet of DT104 was rehydrated on bactotryptic soy broth (BD; 5 to 6 mL) and incubated at 37°C for 24 h. Next, from the growth culture, a loop of bacteria were streaked on tryptic agar plate and incubated for 24 h at 37°C, as instructed by ATCC. A tryptic agar plate was made with Difcotryptic soy agar (BD). A single colony from tryptic agar plate was inoculated into the tryptic soy broth (TSB; 10 mL) and incubated (37°C for 16 h) in a shaker at 150 rpm, which have an inoculum of 10^8CFU mL^{-1}. We then diluted the stock bacteria several times to vary the concentration of Salmonella DT104 from 10–10^7CFUmL^{-1}. All the growth medium and Agar were autoclaved at 121°C for 15 min at high pressure (0.1 MPa) before the experiment. Different amounts of bacteria were then immersed into the antibody-conjugated magnetic core–plasmonic shell popcorn-shaped nanoparticle solution at room temperature before performing the magnetic separation experiment. After magnetic separation, we performed TEM and colony counting (Figure 4). The absorption data show that Salmonella DT104

bound to the magnetic/plasmonic pop- corn-shaped nanoparticles have quite broad absorption (Figure 6 A); this may be due to the aggregation of nanoparticles on Salmonella DT104 bacteria surfaces as shown in the TEM picture in Figure 5.

To induce photothermal lysis, a portable continuous wavelength OEM laser operating at 670 nm, with a power of 1 W $cm^{-2}$was used as an excitation light source for 10–20 min. After that, the bacteria were transferred to tryptic agar plate, which was incubated for 24h at 37°C, and colony number for each plate was counted with a colony counter.

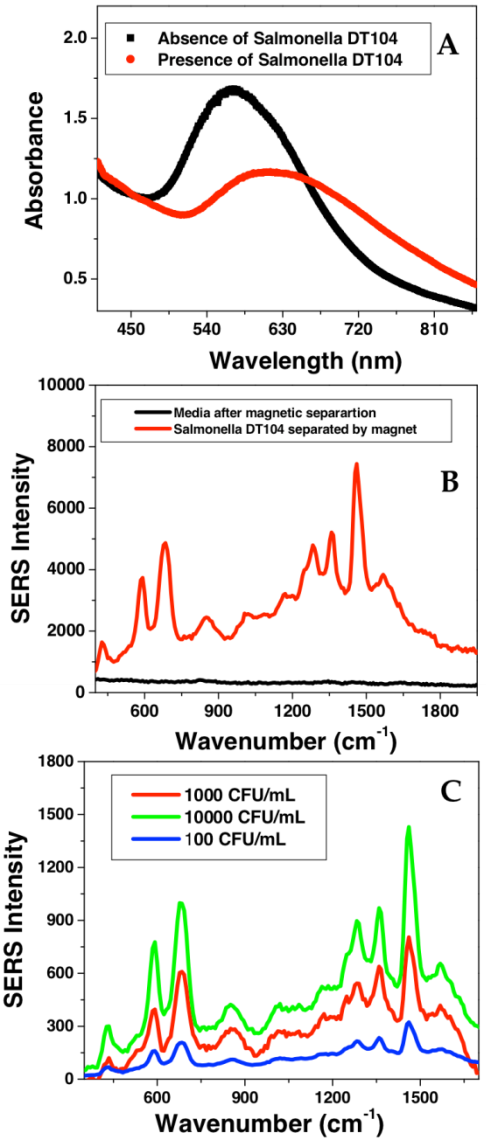

Figure 6. A) Absorption profile variation of antibody-conjugated nanoparticles due to the addition of 1.2 x 10^5 CFU mL^{-1} MDR Salmonella DT104 bacteria. B) Plot shows SERS intensity from a bacteria-conjugated nanoparticle after magnetic separation and resuspension with PBS. All observed Raman signal is directly from Salmonella DT104. No SERS signal has been observed from supernatant that is mainly PBS. C) The plot shows the variation in the SERS intensity from different concentrations of MDR Salmonella DT104. All the reported concentrations are before magnetic separation.

RESULTS AND DISCUSSIONS

To demonstrate the ability to separate MDR Salmonella DT104 from a sample, M3038 antibody-conjugated popcorn-shaped hybrid nanoparticles (100 μL) were incubated with a MDR Salmonella DT104 suspension (2 mL) containing 1.2 $x10^5$ colony forming units (CFU) mL^{-1}. After 20 min of incubation at room temperature under gentle shaking, the suspension was washed three times to remove un-conjugated nanoparticles. Next, a bar magnet was used to separate and enrich the MDR Salmonella DT104-attached nanoparticles (Figure 4 B-C). During the 10 min magnetic-separation process, the nanoparticle–MDR bacteria conjugates were confined, and as a result, the MDRB concentration was enriched. In the next step, the supernatant was carefully removed with a pipette. Then, the nanoparticle–MDR bacteria conjugates were re-suspended with autoclaved PBS to 100 mL; since we started with a volume of 2 mL and the final volume was100 mL, the concentration was enriched 20 times during the magnetic separation. Next, suspensions of the nanoparticle–MDR bacteria conjugates and supernatants were characterized by using bacteria colony counting, TEM and SERS techniques, as shown in Figure 5. In Figure 5 B, it is clear that no bacteria are visible in the supernatant which clearly indicates that most of the bacteria are conjugated withM3038 antibody-conjugated popcorn-shaped plasmonic gold shell–iron magnetic core nanoparticles. To ensure that most of the bacteria were attached to the hybrid nanoparticles, we counted the amount of bacteria from the suspension and compared this value with the original concentration of bacteria. The amount of bacteria in the suspension was 1.15 $x10^5$, whereas the initial concentration of the bacteria was 1.2 x 10^5, which indicates that the capture efficiency is about 96 %. As shown in Figure 5 D, in the presence of MDR Salmonella DT104 bacteria, several M3038 antibody-conjugated popcorn-shaped core–shell nanoparticles conjugate with one MDR bacteria, thereby producing nanoparticle aggregates. Since the MDR Salmonella DT104 bacteria is more than an order of magnitude larger in size (1–2 μm) than the antibody-conjugated core–shell nanoparticles, in the presence of MDR Salmonella bacteria, several nanoparticles conjugate with one Salmonella bacteria through an antigen–antibody interaction. As a result, the absorption maximum for the plasmon absorption band of the popcorn-shaped core–shell gold nanoparticles at 580nm was red shifted to about 650nm and became much broader (Figure 6 A). This red shift might be due to two factors: one is the change in the local refractive index on the nanoparticle surface caused by the specific binding of the antibody-conjugated core–shell nanoparticles on the MDR bacterium cell surface; the other is the interparticle interaction resulting from the assembly of nanoparticles on the cell surface. [64-68]As shown in Figure 6 A, our experimental results also show the formation of MDR microbial clusters in the presence of the M3038 antibody-conjugated nanoparticles. MDR microbial clusters form because the M3038 antibody-conjugated popcorn-shaped core– shell nanoparticles act as binding agents between the cells to give a sort of extracellular network. There are multiple antibodies present on the surface of each nanoparticle; therefore, when an M3038 antibody from one side of the core–shell nanoparticle binds to a specific binding-site on the surface of the target MDR Salmonella DT104 bacterium, there are other M3038 antibodies on the other side of nanoparticle that could be unoccupied, which enables each nanoparticle to bind to more than one MDR Salmonella bacteria cell. As a result, the distance between the nanoparticles in such a cellular

network is expected to be much smaller than the distance between nanoparticles that are not conjugated with bacteria, and an intense red shift in the absorption spectra is observed.

The optical properties of the multifunctional popcorn-shaped magnetic–plasmonic gold nanoparticles also depend on the refractive index near the nanoparticle surface. As the refractive index near the nanoparticle surface increases, the nanoparticle extinction spectrum shifts to longer wavelengths. [90-97, 100, 101] The refractive index near surface of the nanostructure is readily influenced by analyte binding. It is known that the plasmonic properties of a metal nanostructure functionalized with a chemical receptor change when a molecule binds to the receptor and significantly alters the refractive index of the medium directly surrounding the metal nanostructure. [90-97, 100, 101] In our case, when the antibody-attached nanoparticles conjugate with one Salmonella bacteria through an antigen–antibody interaction, the local refractive index on the nanoparticle surface is expected to increase as a result of a red shift in the plasmon mode.

As we have discussed before, the high sensitivity afforded by the SERS detection enables the detection of bacteria by using SERS without the use of a tagged dye. Also, as reported before by several groups, the largest Raman scattering enhancements are observed when molecules are residing in the fractal space between aggregated colloidal nanoparticles. [90-94] As shown in Figure 5 D, it is evident that the MDR Salmonella DT104 help to generate "hot spots" by aggregation of the multifunctional M3038-antibody nanoparticles through an antigen–antibody interaction. These are the perfect conditions in which to use the SERS spectra as "fingerprint" for the whole MDR organism. Figure 6 B shows the SERS spectra from the suspensions of the nanoparticle–Salmonella conjugates after magnetic separation. Since the bacterial cell wall consists of proteins, lipids, and carbohydrates, one can expect to see the SERS spectra from the vibrational mode of the above compositions. Table 1 shows the vibrational assignments of the observed SERS peak as shown in Figure 6 B. Our observed SERS bands are in good agreement with the Raman bands reported for different microorganisms in the literature. [81-83]

The Raman enhancement, G, was measured experimentally by direct comparison with normal and SERS spectra as shown in Equation (1):[90-93]

$$G = [I_{SERS}]/[I_{Raman}] \times [M_{bulk}]/[M_{ads}]$$

in which *I*SERS is the intensity of a 1460 cm^{-1} vibrational mode in the surface-enhanced spectrum in the presence of Salmonella DT104, and *I*Raman is the intensity of the same mode in the bulk Raman spectrum from only bacteria. *M*bulk is the number of bacteria used in the bulk, *M*ads is the number of bacteria adsorbed and sampled on the SERS- active substrate. *M*bulk was calculated by counting colonies. For the *M*ads calculation, we also counted the colonies after magnetic separation. All spectra were normalized for the integration time. The resultant enhancement factor estimated from the SERS signal and normal Raman signal ratio for 1460 cm^{-1} band is approximately 8.5×10^7. No significant changes in Raman frequencies were observed by comparison to the corresponding SERS and Raman bands. To evaluate the sensitivity of our SERS probe, different concentrations of MDR Salmonella DT104 from one stock-solution were evaluated. As shown in Figure 6 C, the SERS intensity is quite sensitive to the concentration of MDR Salmonella DT104. The MDR concentration mentioned in Figure 4 C is the concentration before separation and enrichment. Our experimental results

clearly demonstrate that the sensitivity of our popcorn- shaped magnetic–plasmonic nanoparticle-based label-free SERS probe is as low as 100 CFU mL^{-1} for MDR bacteria.

To understand whether our antibody-conjugated nanoparticle-based assay is highly selective for magnetic separation and Raman imaging, we also investigated how our assay responds to the addition of E. coli bacteria to the M3038 antibody-conjugated popcorn-shaped magnetic core–plasmonic shell gold nanoparticles. For this experiment, M3038 antibody-conjugated nanoparticles (100 μL) were incubated with an E. coli suspension (2 mL) containing 1.2 x 105 CFU mL^{-1}. After incubating for 20 min at room temperature with gentle shaking, a bar magnet was used to separate and enrich the sample. As shown in Figure 7, no E. coli bacteria were captured by the magnetic nanoparticles. As shown in Figure 7 C, our colony-counting results indicate that the bacteria-capture efficiency for E. coli was less than 1%; on the other hand, the bacteria-capture efficiency was 96% for MDR Salmonella DT104. This result clearly shows that our bio-conjugated popcorn-shaped magnetic core–plasmonic shell nanoparticle can be used for selective separation, enrichment and imaging of the MDR bacteria. The novelty of our approach is the simplicity of the methodology used to capture, separate, and enrich the MDR Salmonella DT104 bacterium by using a bio-conjugated popcorn-shaped magnetic core–plasmonic shell nanoparticle.

Table 1. Analysis for the observed SERS vibrational modes from *Salmonetta* DT104

Vibration mode	Raman peak position [cm^{-1}]
$\nu(COO^-)$ anti-symmetric	1585
$\delta(CH_2)$ saturated lipids	1460
$\nu(COO^-)$ symmetric	1380
$\nu(NH_2)$ Stretch for adenine and guanine	1340
ν(CC) ring stretch, *n*-alkanes	1150
δ(CCH), aliphatic	830
$\rho(CH_2)$	720
δ(CCC) ring deformation	590

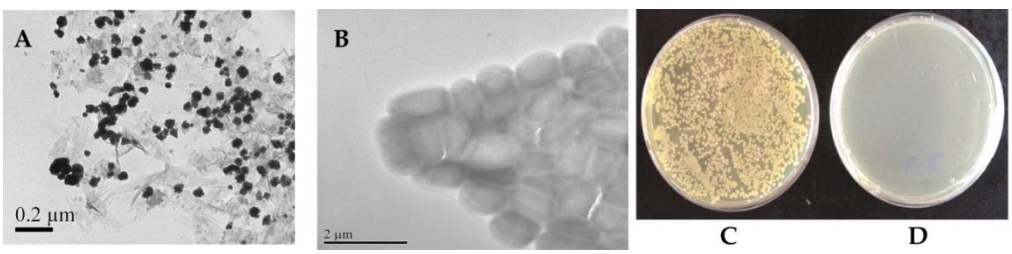

Figure 7. A) TEM image showing lack of the presence of E. coli bacteria in the part captured by the magnetic field when 6 x 10^5 E. Coli bacteria were initially incubated with M308 antibody conjugated nanoparticles. B) TEM image showing an extensive amount of bacteria present in the supernatant solution after the magnetic capture, when 1.2 x 10^5 E. coli were incubated with M3038 antibody conjugated magnetic core-plasmonic shell popcorn-shaped gold nanoparticles ; scale bar, 2 μm. B) Colonies of E. coli bacteria. C) Colonies showing a huge amount of bacteria presence in the supernatant solution after magnetic capture and D) Colonies show no bacteria in the suspension in the presence of the magnetic/plasmonic nanoparticle after magnetic separation and resuspension in PBS. The initial number of E. coli was 1.2 x 10^5 CFU mL^{-1}.

After successful targeted magnetic separation and imaging, we performed NIR irradiation experiments to determine whether the popcorn-shaped core–shell magnetic/plasmonic nanoparticles can also be used for selective photothermal destruction of MDRB through heating the gold shell. Gold nanoparticles are known to be capable of converting NIR light to vibrational energy and can generate sufficient heat to kill microorganisms and cancer cells. [54-56, 58, 59, 64, 66] For the photothermal destruction of MDR bacteria, the samples were exposed to red light (670 nm OEM laser at 1–2 W cm^{-2}) for 10 min. When the MDR Salmonella DT104-conjugated with M3038 antibody-attached nanoparticles are excited with 670 nm light, photoexcitation of the electron gas of the gold shell occurs and results in rapid non-equilibrium heating, which is due to the strong absorption at this wavelength seen in Figure 6 A. As reported by several articles, [64-66, 89]the initial electronic excitation followed by relaxation will give rise to a rapid increase in the surface temperature of the metal. This initial rapid-heating will be cooled to equilibrium by energy exchange between the electrons and the lattice. Finally, the lattice will cool through phonons, resulting in local heating of the surrounding the nanostructure. [54, 56, 64, 65] This local temperature increase produces sufficient heat for the destruction of MDRB which could therefore be the perfect solution to kill MDR bacteria without the use of antibiotics. Following photothermal lysis, the amount of MDR Salmonella DT104 bacteria that was destroyed was confirmed by colony plating. Figure 8 C-D shows the number of colonies after 10 min exposure to 670 nm light for MDR Salmonella DT104 with and without magnetic/plasmonic nanoconjugation. As shown in Figure 8, our experimental results clearly demonstrate that the localized heating that occurs during NIR irradiation is able to perform irreparable cellular damage. Therefore, our study demonstrates that bioconjugated core–shell magnetic/plasmonic nanoparticles could be the next avenue for exploration to selectively target and destroy MDR microbial cells.

Since SERS is capable of determining the fine structures of the bacterial cell wall, we wanted to understand whether SERS could be used to monitor any change in the cell wall during the photothermal destruction of bacteria. For this purpose, SERS spectra were also collected after the photothermal lysis experiment. As can be seen in Figure 8 A, there was no appreciable change in the SERS vibrational modes even after 20 min of laser exposure (670 nm). This may indicate that during the photothermal destruction of bacteria, there may not be any occurrence of significant changes in the MDR cell wall. The mechanism of MDR Salmonella DT104 death could be due to numerous factors including thermal stresses, shock waves, bubble formation and nanoparticle explosion. [54-56, 58-60]Next, to understand whether the antibody- conjugated hybrid nanoparticle-based magnetic separation and photothermal destruction is highly selective, the same experiment was performed with E. coli colonies. For this purpose, we incubated M3038 antibody-conjugated hybrid nanoparticles (100 μL) with of E. coli suspension (2 mL) containing 1.2 x 10^5 CFU mL^{-1}. After 20 min of incubation at room temperature with gentle shaking, a bar magnet was used to separate and enrich the sample. As we have discussed before, because almost all the E. coli remained in the supernatant solution; therefore, after separation we treated the supernatant with light (670 nm at 1.5 W cm^{-2}) for 10 min. As shown in Figure 8 B, during photothermal lysis, the time-interval live-bacteria test indicated that within 10 min, all the MDR Salmonella DT104 were killed when exposed to light (670 nm at a power of 1.5Wcm-2); however, almost 97% of the *E.coli* bacteria were still alive even after 20 min of treatment with the same exposure conditions. These results clearly demonstrate that the conjugation of nanoparticles with bacteria is necessary for photothermal destruction by using light (670 nm). As was seen in

Figure 7, the M3038 antibody-conjugated nanoparticles do not bind with E. coli, so the bacteria in the supernatant do not have significant absorption at 670 nm. Therefore, during exposure under 670 nm light, the effective temperature increase in bacteria will be very little and will be insufficient to kill these cells. Next, to understand how the temperature increases during photothermal destruction, thermal imaging was performed at one-minute intervals during the therapy process by using a MikroShot Camera. We found that the temperature increased to about 48°C when nanoparticle-conjugated MDR Salmonella DT104 were exposed to a 670 nm laser at 1.5 W cm^{-2} power for 10 min. Conversely, under the same conditions, the temperature increased to only 30°C for E. coli bacteria without any nanoparticles.

DISCUSSION

Herein, we have demonstrated that our hybrid nanoparticles can be used as a multifunctional platform for separation and enrichment, SERS imaging, and photothermal destruction of MDR Salmonella DT104. This satisfies the critical need in areas such as the food and medical industries for early detection, specificity, and non-traditional antimicrobial action to combat MDRB contamination and prevent infections. As MDRB are expected to become more common and new resistances are continually developing in microbes, it is now more important than ever to develop new strategies towards maintaining safety standard since a wide range of applications including hospital and medical equipment [11-15], food processing [18-21], and food packaging and kitchenware [29-34]. As was previously mentioned, there have been other proposals for either preventing MDRB contamination or for killing MDRB including antibiotic cocktails [39-41], older antibiotics with known harmful side-effects [42-44], bacterial viruses [48], photodynamic inactivation [46, 47], metallopolymers [28], and Ag or oxide nanoparticles [22-27]. Using conventional or older known antibiotics have a major drawback since they will also affect beneficial bacteria and can lead to further mutations and resistances in organisms which are already difficult to kill. Furthermore, when these approaches are used in the instances of medical or food safety, they can also affect a patient or someone who consumes a food with antibiotics on or in it systemically. Undue exposure to these harsh antibiotics could throw off the balance of their own microbiome and suppress their immune system as well as cause toxicity in the liver or kidneys. Likewise, engineering bacterial viruses to be more effective could have unintended consequences in consumers and patients, and there are still many questions which need to be addressed for this approach to be seen as a viable option to dealing with MDRB. As we discussed earlier, Ag nanoparticles, while a very effective bactericidal agent can also be quite toxic and are known to leach Ag ions which can cause further damage. [35-38] Since all of these proposed approaches to killing MDRB are passive by nature, it is much more difficult to target them to specific organisms. Through requiring activation of our hybrid nanoparticles with NIR light combined with the specific binding of the M3038 antibody, we have shown that the killing of MDR Salmonella is highly selective and site specific. Finally, our multifunctional platform also allows for sensing and confirmation of MDRB presence through the large SERS enhancement. This will allow for serial detection and destruction of MDRB in field environments such as food packaging and processing plants. In fact, with such

a large SERS signal from our hybrid nanoparticles, it would be possible to image and map out areas of infection with a handheld Raman spectrometer.

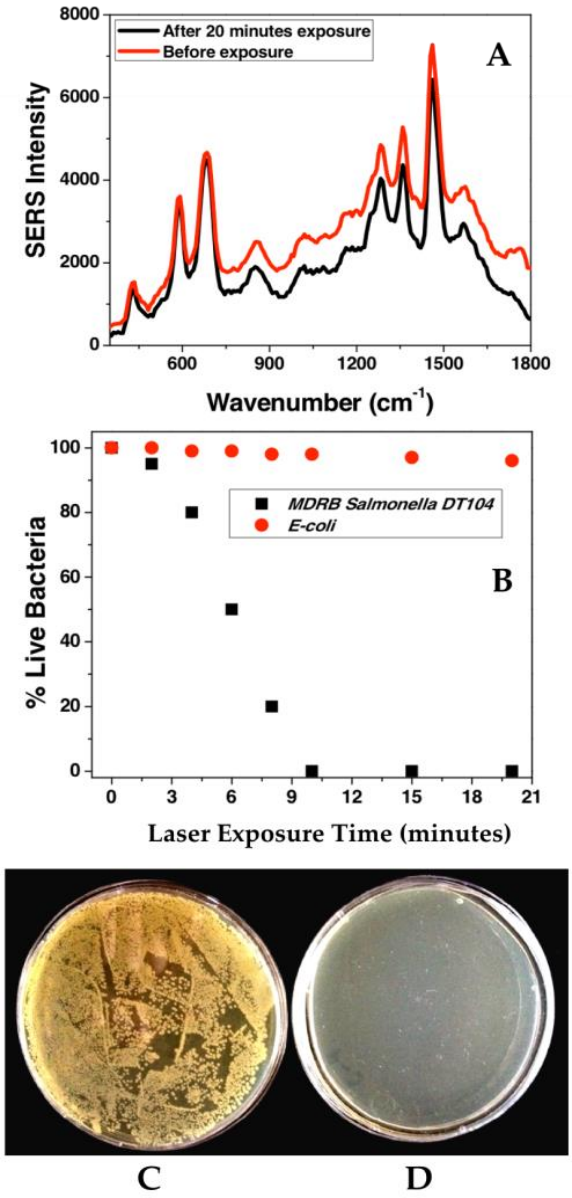

Figure 8. A) Plot shows SERS intensity variation from MDR Salmonella DT104, before and after photothermal lysis. We did not observe any significance change. B) Plot demonstrating the percent- age of live bacteria during the time-dependent photothermal lysis by using 670 nm light at a power of 1.5 W cm^{-2}. An amount of 1.2 $x10^{5}$ CFU mL^{-1} bacteria was used for each case. C) Colonies of MDR Salmonella DT104 bacteria (1.2$x10^{5}$ CFUmL^{-1}) demonstrating the amount of live bacteria after exposure to 670 nm light for 10 min without NPs. D) Colonies of MDR Salmonella DT104 bacteria (1.2 x 10^{5} CFU mL^{-1}) demonstrating the amount of live bacteria after exposure to 670 nm light for 10 min in the presence of M3038 antibody-conjugated magnetic core–plasmonic shell popcorn- shaped gold nanoparticles.

CONCLUSION

We have reported the synthesis and characterization of a multifunctional popcorn-shaped iron magnetic core–shell gold nanoparticle and demonstrated the use of M3038 anti-body-conjugated popcorn-shaped core–shell nanoparticles for the targeted magnetic separation and enrichment, SERS imaging, and the photothermal destruction of MDR Salmonella DT104. Our experimental results show that the M3038 antibody-conjugated hybrid nanoparticles are capable of selective label-free SERS detection of MDR Salmonella DT104 with an excellent detection limit (102 $CFUmL^{-1}$). Our experimental results shown that when the antibody-conjugated core–shell nanoparticles are attached to MDR Salmonella DT104 bacterial cells, the localized heating that occurs during 670 nm light irradiation is able to cause irreparable cellular-damage and kill approximately 100% of MDR Salmonella bacteria within 10 min of exposure even at a power of 1.5 Wcm^{-2}. The reported bioassay by using the popcorn-shaped magnetic core–plasmonic shell nanoparticles is rapid, takes about 30 min from bacterium binding to separation and enrichment, selective detection, and photo- thermal cell death. With the prevalence of multidrug-resistant bacteria is on the rise, our results demonstrated that the bioconjugated multifunctional hybrid-nanoparticle approach to selectively target and destroy MDRB is an extremely promising and important avenue for exploration. Even though our experimental observation have demonstrated promising results for MDRB separation and enrichment, followed by SERS imaging and therapy, it is fair to admit that we are still at a relatively early stage of developing this technology. After the optimization of different parameters, we believe that this multifunctional popcorn-shaped hybrid nanotechnology-driven assay could have enormous potential for applications in the rapid detection and photothermal destruction of MDRB in the food supply chain and the medical supply and device chain.

ACKNOWLEDGMENT

P.C.R. thanks the NSF-PREM grant ## DMR-1205194 for their generous funding. D.S. thanks the NSF- PREM grant DMR-0934218 for their generous funding.

REFERENCES

[1] Nikaido, H. Multidrug resistance in bacteria. *Annual review of biochemistry*, 2009, 78, 119.

[2] Andersson, DI; Hughes, D. Antibiotic resistance and its cost: is it possible to reverse resistance? *Nature Reviews Microbiology*, 2010, 8, 260-271.

[3] Hartmann, M; Betz, P; Sun, Y; Gorb, SN; Lindhorst, TK; Krueger, A., Saccharide-Modified Nanodiamond Conjugates for the Efficient Detection and Removal of Pathogenic Bacteria. *Chemistry-A European Journal*, 2012, 18, 6485-6492.

[4] Allen, HK; Donato, J; Wang, HH; Cloud-Hansen, KA; Davies, J; Handelsman, J., Call of the wild: antibiotic resistance genes in natural environments. *Nature Reviews Microbiology*, 2010, 8, 251-259.

[5] http://www.cdc.gov/eid/content/15/4/623.htm.
[6] WHO http://www.who.int/tb/challenges/mdr/en/index.html.
[7] Ram, S; Vajpayee, P; Shanker, R. Prevalence of multi-antimicrobial-agent resistant, shiga toxin and enterotoxin producing Escherichia coli in surface waters of river Ganga. *Environmental science & technology*, 2007, 41, 7383-7388.
[8] DeRussy, BM; Aylward, MA; Fan, Z; Ray, PC; Tandonm, R. Inhibition of cytomegalovirus infection and photothermolysis of infected cells using bioconjugated gold nanoparticles, *Scientific Reports*, 2014, 4, srep05550
[9] Andersson, DI. The biological cost of mutational antibiotic resistance: any practical conclusions? *Current opinion in microbiology*, 2006, 9, 461-465.
[10] Magiorakos, AP; Srinivasan, A; Carey, RB; Carmeli, Y; Falagas, ME; Giske, CG; Harbarth, S; Hindler, JF; Kahlmeter, G; Olsson-Liljequist, B; Paterson, DL; Rice, LB; Stelling, J; Struelens, MJ; Vatopoulos, A; Weber, JT; Monnet, DL., Multidrug-resistant, extensively drug-resistant and pandrug-resistant bacteria: an international expert proposal for interim standard definitions for acquired resistance. *Clinical Microbiology and Infection*, 2012, 18, 268-281.
[11] Glasser, JS; Guymon, CH; Mende, K; Wolf, SE; Hospenthal, DR; Murray, CK. Activity of topical antimicrobial agents against multidrug-resistant bacteria recovered from burn patients. *Burns*, 2010, 36, 1172-1184.
[12] Xumei; D; Fan, Z; Yuefeng; L; Ray, PC., Multifunctional Nanoplatforms For Targeted MDRB Theranostic Applications, *ACS Applied Mater. Sci.*, 2013, 5, 11348-11354.
[13] Susy Hota, MD; Zahir Hirji, M; Karen Stockton, M; Camille Lemieux, ML; Helen Dedier, MLT; Gideon Wolfaardt, P; Michael A. Gardam, MDM. Outbreak of Multidrug-Resistant Pseudomonas aeruginosa Colonization and Infection Secondary to Imperfect Intensive Care Unit Room Design • *Infection Control and Hospital Epidemiology*, 2009, 30, 25-33.
[14] Peleg, AY; Hooper, DCHospital-Acquired Infections Due to Gram-Negative Bacteria. *New England Journal of Medicine*, 2010, 362, 1804-1813.
[15] Arias, CA; Murray, BEAntibiotic-Resistant Bugs in the 21st Century — A Clinical Super-Challenge. *New England Journal of Medicine*, 2009, 360, 439-443.
[16] Cooley, M; Carychao, D; Crawford-Miksza, L; Jay, MT; Myers, C; Rose, C; Keys, C; Farrar, J; Mandrell, REIncidence and Tracking of <italic>Escherichia coli</italic> O157:H7 in a Major Produce Production Region in California. *PLoS ONE*, 2007, 2, e1159.
[17] Sheth, AN; Hoekstra, M; Patel, N; Ewald, G; Lord, C; Clarke, C; Villamil, E; Niksich, K; Bopp, C; Nguyen, T.-A; Zink, D; Lynch, MA National Outbreak of Salmonella Serotype Tennessee Infections From Contaminated Peanut Butter: A New Food Vehicle for Salmonellosis in the United States. *Clinical Infectious Diseases*, 2011, 53, 356-362.
[18] Luning, PA; Bango, L; Kussaga, J; Rovira, J; Marcelis, WJComprehensive analysis and differentiated assessment of food safety control systems: a diagnostic instrument. *Trends in Food Science & Technology*, 2008, 19, 522-534.
[19] Waters, AE; Contente-Cuomo, T; Buchhagen, J; Liu, CM; Watson, L; Pearce, K; Foster, JT; Bowers, J; Driebe, EM; Engelthaler, DM; Keim, PS; Price, LBMultidrug-Resistant Staphylococcus aureus in US Meat and Poultry. *Clinical Infectious Diseases*, 2011.

[20] Pavithra, M; Ghosh, ARMultidrug-Resistant stx1 Harboring Escherichia coli from Meat Shop and Fast Food. *Journal of Food Safety*, 2013, 33, 453-460.

[21] Lu, Y; Zhao, H; Sun, J; Liu, Y; Zhou, X; Beier, RC; Wu, G; Hou, XCharacterization of Multidrug-Resistant <italic>Salmonella enterica</italic> Serovars Indiana and Enteritidis from Chickens in Eastern China. *PLoS ONE*, 2014, 9, e96050.

[22] Rai, MK; Deshmukh, SD; Ingle, AP; Gade, AKSilver nanoparticles: the powerful nanoweapon against multidrug-resistant bacteria. *Journal of Applied Microbiology*, 2012, 112, 841-852.

[23] Lara, H; Ayala-Núñez, N; Ixtepan Turrent, L; Rodríguez Padilla, CBactericidal effect of silver nanoparticles against multidrug-resistant bacteria. *World J Microbiol Biotechnol*, 2010, 26, 615-621.

[24] Vishnupriya, S; Chaudhari, K; Jagannathan, R; Pradeep, TSingle-Cell Investigations of Silver Nanoparticle–Bacteria Interactions. *Particle & Particle Systems Characterization*, 2013, 30, 1056-1062.

[25] Kunkalekar, RK; Naik, MM; Dubey, SK; Salker, AVAntibacterial activity of silver-doped manganese dioxide nanoparticles on multidrug-resistant bacteria. *Journal of Chemical Technology & Biotechnology*, 2013, 88, 873-877.

[26] Xing, R; Bhirde, A; Wang, S; Sun, X; Liu, G; Hou, Y; Chen, XHollow iron oxide nanoparticles as multidrug resistant drug delivery and imaging vehicles. *Nano Research*, 2013, 6, 1-9.

[27] Li, L.-H; Yen, M.-Y; Ho, C.-C; Wu, P; Wang, C.-C; Maurya, PK; Chen, P.-S; Chen, W; Hsieh, W.-Y; Chen, H.-WNon-Cytotoxic Nanomaterials Enhance Antimicrobial Activities of Cefmetazole against Multidrug-Resistant <italic>Neisseria gonorrhoeae</italic>. *PLoS ONE*, 2013, 8, e64794.

[28] Zhang, J; Chen, YP; Miller, KP; Ganewatta, MS; Bam, M; Yan, Y; Nagarkatti, M; Decho, AW; Tang, CAntimicrobial Metallopolymers and Their Bioconjugates with Conventional Antibiotics against Multidrug-Resistant Bacteria. *Journal of the American Chemical Society*, 2014, 136, 4873-4876.

[29] Appendini, P; Hotchkiss, JH. Review of antimicrobial food packaging. *Innovative Food Science & Emerging Technologies*, 2002, 3, 113-126.

[30] Fernández, A; Soriano, E; López-Carballo, G; Picouet, P; Lloret, E; Gavara, R; Hernández-Muñoz, P. Preservation of aseptic conditions in absorbent pads by using silver nanotechnology. *Food Research International*, 2009, 42, 1105-1112.

[31] Matsumura, Y; Yoshikata, K; Kunisaki, S.-i; Tsuchido, T. Mode of Bactericidal Action of Silver Zeolite and Its Comparison with That of Silver Nitrate. *Applied and Environmental Microbiology*, 2003, 69, 4278-4281.

[32] An, J; Zhang, M; Wang, S; Tang, J. Physical, chemical and microbiological changes in stored green asparagus spears as affected by coating of silver nanoparticles-PVP. *LWT - Food Science and Technology*, 2008, 41, 1100-1107.

[33] Pinto, RJB; Marques, PAAP; Neto, CP; Trindade, T; Daina, S; Sadocco, P. Antibacterial activity of nanocomposites of silver and bacterial or vegetable cellulosic fibers. *Acta biomaterialia*, 2009, 5, 2279-2289.

[34] Rhim, J-W; Hong, S-I; Park, H-M; Ng, PK. W. Preparation and Characterization of Chitosan-Based Nanocomposite Films with Antimicrobial Activity. *Journal of Agricultural and Food Chemistry*, 2006, 54, 5814-5822.

[35] Kim, S; Ryu, D-Y. Silver nanoparticle-induced oxidative stress, genotoxicity and apoptosis in cultured cells and animal tissues. *Journal of Applied Toxicology*, 2013, 33, 78-89.

[36] Sahu, SC; Zheng, J; Graham, L; Chen, L; Ihrie, J; Yourick, JJ; Sprando, RL. Comparative cytotoxicity of nanosilver in human liver HepG2 and colon Caco2 cells in culture. *Journal of Applied Toxicology*, 2014, ASAP Article.

[37] Gliga, A; Skoglund, S; Odnevall Wallinder, I; Fadeel, B; Karlsson, H. Size-dependent cytotoxicity of silver nanoparticles in human lung cells: the role of cellular uptake, agglomeration and Ag release. *Particle and Fibre Toxicology*, 2014, 11, 11.

[38] Greulich, C; Braun, D; Peetsch, A; Diendorf, J; Siebers, B; Epple, M; Koller, M. The toxic effect of silver ions and silver nanoparticles towards bacteria and human cells occurs in the same concentration range. *RSC Advances*, 2012, 2, 6981-6987.

[39] Worthington, RJ; Melander, C. Combination approaches to combat multidrug-resistant bacteria. *Trends in Biotechnology*, 2013, 31, 177-184.

[40] López-Cortés, LE; Cisneros, JM; Fernández-Cuenca, F; Bou, G; Tomás, M; Garnacho-Montero, J; Pascual, A; Martínez-Martínez, L; Vila, J; Pachón, J; Rodríguez Baño, J. Monotherapy versus combination therapy for sepsis due to multidrug-resistant Acinetobacter baumannii: analysis of a multicentre prospective cohort. *Journal of Antimicrobial Chemotherapy*, 2014, ASAP Article

[41] Lee, HJ; Bergen, PJ; Bulitta, JB; Tsuji, B; Forrest, A; Nation, RL; Li, J. Synergistic Activity of Colistin and Rifampin Combination against Multidrug-Resistant Acinetobacter baumannii in an In Vitro Pharmacokinetic/Pharmacodynamic Model. *Antimicrobial Agents and Chemotherapy*, 2013, 57, 3738-3745.

[42] Bergen, PJ; Landersdorfer, CB; Lee, HJ; Li, J; Nation, RL. 'Old' antibiotics for emerging multidrug-resistant bacteria. *Current Opinion in Infectious Diseases*, 2012, 25, 626-633 10.1097/QCO.0b013e328358afe5.

[43] Dinh, A; Salomon, J; Bru, JP; Bernard, L. Fosfomycin: Efficacy against infections caused by multidrug-resistant bacteria. *Scandinavian Journal of Infectious Diseases*, 2012, 44, 182-189.

[44] Reffert, JL; Smith, WJ. Fosfomycin for the Treatment of Resistant Gram-Negative Bacterial Infections. *Pharmacotherapy: The Journal of Human Pharmacology and Drug Therapy*, 2014, ASAP Article

[45] Karaiskos, I; Giamarellou, H. Multidrug-resistant and extensively drug-resistant Gram-negative pathogens: current and emerging therapeutic approaches. *Expert Opinion on Pharmacotherapy*, 2014, 15, 1351-1370.

[46] Almeida, J; Tome, JPC; Neves, MGPMS; Tome, AC; Cavaleiro, JAS; Cunha, A; Costa, L; Faustino, MAF; Almeida, A. Photodynamic inactivation of multidrug-resistant bacteria in hospital wastewaters: influence of residual antibiotics. *Photochemical & Photobiological Sciences*, 2014, 13, 626-633.

[47] Zhao, Y; Jiang, X. Multiple strategies to activate gold nanoparticles as antibiotics. *Nanoscale*, 2013, 5, 8340-8350.

[48] Viertel, TM; Ritter, K; Horz, H-P. Viruses versus bacteria—novel approaches to phage therapy as a tool against multidrug-resistant pathogens. *Journal of Antimicrobial Chemotherapy*, 2014, ASAP Article

[49] Liu, T-Y; Tsai, K-T; Wang, H-H; Chen, Y; Chen, Y-H; Chao, Y-C; Chang, H-H; Lin, C-H; Wang, J-K; Wang, Y-L. Functionalized arrays of Raman-enhancing nanoparticles

for capture and culture-free analysis of bacteria in human blood. *Nature communications*, 2011, 2, 538.

[50] Berry, V; Gole, A; Kundu, S; Murphy, CJ; Saraf, RF. Deposition of CTAB-terminated nanorods on bacteria to form highly conducting hybrid systems. *Journal of the American Chemical Society*, 2005, 127, 17600-17601.

[51] Norman, RS; Stone, JW; Gole, A; Murphy, CJ; Sabo-Attwood, TL. Targeted photothermal lysis of the pathogenic bacteria, Pseudomonas aeruginosa, with gold nanorods. *Nano letters*, 2008, 8, 302-306.

[52] Miranda, OR; Li, X; Garcia-Gonzalez, L; Zhu, Z-J; Yan, B; Bunz, UH; Rotello, VM. Colorimetric bacteria sensing using a supramolecular enzyme–nanoparticle biosensor. *Journal of the American Chemical Society*, 2011, 133, 9650-9653.

[53] Hayden, SC; Zhao, G; Saha, K; Phillips, RL; Li, X; Miranda, OR; Rotello, VM; El-Sayed, MA; Schmidt-Krey, I; Bunz, UH. Aggregation and interaction of cationic nanoparticles on bacterial surfaces. *Journal of the American Chemical Society*, 2012, 134, 6920-6923.

[54] Ray, PC; Khan, SA; Singh, AK; Senapati, D; Fan, ZNanomaterials for targeted detection and photothermal killing of bacteria*Chemical Society reviews*, 2012, 41, 3193-3209.

[55] Wang, C; Irudayaraj, J. Gold nanorod probes for the detection of multiple pathogens. *Small*, 2008, 4, 2204-2208.

[56] Zharov, VP; Mercer, KE; Galitovskaya, EN; Smeltzer, MSPhotothermal nanotherapeutics and nanodiagnostics for selective killing of bacteria targeted with gold nanoparticles. *Biophysical journal*, 2006, 90, 619-627.

[57] Singh, AK; Senapati, D; Wang, S; Griffin, J; Neely, A; Candice, P; Naylor, KM; Varisli, B; Kalluri, JR; Ray, PC. Gold nanorod based selective identification of Escherichia coli bacteria using two-photon Rayleigh scattering spectroscopy. *Acs Nano*, 2009, 3, 1906-1912.

[58] Wang, S; Singh, AK; Senapati, D; Neely, A; Yu, H; Ray, PCRapid Colorimetric Identification and Targeted Photothermal Lysis of Salmonella Bacteria by Using Bioconjugated Oval-Shaped Gold Nanoparticles. *Chemistry-A European Journal*, 2010, 16, 5600-5606.

[59] Singh, AK; Kanchanapally, R; Fan, Z; Senapati, D; Ray, PC. Synthesis of highly fluorescent water-soluble silver nanoparticles for selective detection of Pb (II) at the parts per quadrillion (PPQ) level. *Chemical communications*, 2012, 48, 9047-9049.

[60] Yang, P; Xu, QZ; Jin, SY; Zhao, Y; Lu, Y; Xu, XW; Yu, SH. Synthesis of Fe3O4@ Phenol Formaldehyde Resin Core–Shell Nanospheres Loaded with Au Nanoparticles as Magnetic FRET Nanoprobes for Detection of Thiols in Living Cells. *Chemistry-A European Journal*, 2012, 18, 1154-1160.

[61] Jin, Y; Jia, C; Huang, S-W; O'Donnell, M; Gao, X. Multifunctional nanoparticles as coupled contrast agents. *Nature communications*, 2010, 1, 41.

[62] Kell, AJ; Stewart, G; Ryan, S; Peytavi, R; Boissinot, M; Huletsky, A; Bergeron, MG; Simard, B. Vancomycin-modified nanoparticles for efficient targeting and preconcentration of Gram-positive and Gram-negative bacteria. *Acs Nano*, 2008, 2, 1777-1788.

[63] Ray, PC. Size and shape dependent second order nonlinear optical properties of nanomaterials and their application in biological and chemical sensing. *Chemical reviews*, 2010, 110, 5332-5365.

[64] Huang, X; El-Sayed, IH; Qian, W; El-Sayed, MA. Cancer cell imaging and photothermal therapy in the near-infrared region by using gold nanorods. *Journal of the American Chemical Society*, 2006, 128, 2115-2120.

[65] Kaittanis, C; Santra, S; Perez, JM. Role of nanoparticle valency in the nondestructive magnetic-relaxation-mediated detection and magnetic isolation of cells in complex media. *Journal of the American Chemical Society*, 2009, 131, 12780-12791.

[66] Guo, S; Dong, S; Wang, E. A general route to construct diverse multifunctional Fe3O4/metal hybrid nanostructures. *Chemistry-a European Journal*, 2009, 15, 2416-2424.

[67] Bardhan, R; Lal, S; Joshi, A; Halas, NJTheranostic nanoshells: from probe design to imaging and treatment of cancer. *Accounts of chemical research*, 2011, 44, 936-946.

[68] Chen, WJ; Tsai, PJ; Chen, YC. Functional Fe3O4/TiO2 core/shell magnetic nanoparticles as photokilling agents for pathogenic bacteria. *Small*, 2008, 4, 485-491.

[69] Chung, HJ; Reiner, T; Budin, G; Min, C; Liong, M; Issadore, D; Lee, H; Weissleder, R. Ubiquitous detection of Gram-positive bacteria with bioorthogonal magnetofluorescent nanoparticles. *ACS nano*, 2011, 5, 8834-8841.

[70] Kievit, FM; Zhang, M. Surface engineering of iron oxide nanoparticles for targeted cancer therapy. *Accounts of chemical research*, 2011, 44, 853-862.

[71] Taylor, EN; Kummer, KM; Durmus, NG; Leuba, K; Tarquinio, KM; Webster, TJ. Superparamagnetic Iron Oxide Nanoparticles (SPION) for the Treatment of Antibiotic-Resistant Biofilms. *Small*, 2012, 8, 3016-3027.

[72] Wang, Y; Chen, L; Liu, P. Biocompatible Triplex Ag@ SiO2@ mTiO2 Core–Shell Nanoparticles for Simultaneous Fluorescence-SERS Bimodal Imaging and Drug Delivery. *Chemistry-A European Journal*, 2012, 18, 5935-5943.

[73] Ruiz-Hernandez, E; Baeza, A; Vallet-Regí, M. a. Smart drug delivery through DNA/magnetic nanoparticle gates. *ACS nano*, 2011, 5, 1259-1266.

[74] Xu, Z; Hou, Y; Sun, S. Magnetic core/shell Fe3O4/Au and Fe3O4/Au/Ag nanoparticles with tunable plasmonic properties. *Journal of the American Chemical Society*, 2007, 129, 8698-8699.

[75] Qu, Y; Cheng, R; Su, Q; Duan, X. Plasmonic enhancements of photocatalytic activity of Pt/n-Si/Ag photodiodes using Au/Ag core/shell nanorods. *Journal of the American Chemical Society*, 2011, 133, 16730-16733.

[76] Levin, CS; Hofmann, C; Ali, TA; Kelly, AT; Morosan, E; Nordlander, P; Whitmire, KH; Halas, NJ. Magnetic− plasmonic core− shell nanoparticles. *Acs Nano*, 2009, 3, 1379-1388.

[77] Zhang, Q; Ge, J; Goebl, J; Hu, Y; Sun, Y; Yin, Y. Tailored synthesis of superparamagnetic gold nanoshells with tunable optical properties. *Advanced materials*, 2010, 22, 1905-1909.

[78] Shi, D; Bedford, NM; Cho, HS. Engineered multifunctional nanocarriers for cancer diagnosis and therapeutics. *Small*, 2011, 7, 2549-2567.

[79] Croissant, J; Zink, JI. Nanovalve-controlled cargo release activated by plasmonic heating. *Journal of the American Chemical Society*, 2012, 134, 7628-7631.

[80] Fan, Z; Shelton, M; Singh, AK; Senapati, D; Khan, SA; Ray, PC. Multifunctional plasmonic shell–magnetic core nanoparticles for targeted diagnostics, isolation, and photothermal destruction of tumor cells. *ACS nano*, 2012, 6, 1065-1073.

[81] Jarvis, RM; Brooker, A; Goodacre, R. Surface-enhanced Raman spectroscopy for bacterial discrimination utilizing a scanning electron microscope with a Raman spectroscopy interface. *Analytical chemistry*, 2004, 76, 5198-5202.

[82] Premasiri, W; Moir, D; Klempner, M; Krieger, N; Jones, G; Ziegler, L. Characterization of the surface enhanced Raman scattering (SERS) of bacteria. *The Journal of Physical Chemistry B*, 2005, 109, 312-320.

[83] Wang, Y; Lee, K; Irudayaraj, J. Silver nanosphere SERS probes for sensitive identification of pathogens. *The Journal of Physical Chemistry C*, 2010, 114, 16122-16128.

[84] Lu, W; Arumugam, SR; Senapati, D; Singh, AK; Arbneshi, T; Khan, SA; Yu, H; Ray, PC. Multifunctional oval-shaped gold-nanoparticle-based selective detection of breast cancer cells using simple colorimetric and highly sensitive two-photon scattering assay. *ACS nano*, 2010, 4, 1739-1749.

[85] Dasary, SS; Singh, AK; Senapati, D; Yu, H; Ray, PC. Gold nanoparticle based label-free SERS probe for ultrasensitive and selective detection of trinitrotoluene. *Journal of the American Chemical Society*, 2009, 131, 13806-13812.

[86] Senapati, D; Dasary, SS; Singh, AK; Senapati, T; Yu, H; Ray, PC. A Label-Free Gold-Nanoparticle-Based SERS Assay for Direct Cyanide Detection at the Parts-per-Trillion Level. *Chemistry-A European Journal*, 2011, 17, 8445-8451.

[87] Papadopoulou, E; Bell, S. E. Label-Free Detection of Nanomolar Unmodified Single- and Double-Stranded DNA by Using Surface-Enhanced Raman Spectroscopy on Ag and Au Colloids. *Chemistry-A European Journal*, 2012, 18, 5394-5400.

[88] Fan, K; Cao, C; Pan, Y; Lu, D; Yang, D; Feng, J; Song, L; Liang, M; Yan, X. Magnetoferritin nanoparticles for targeting and visualizing tumour tissues. *Nature nanotechnology*, 2012, 7, 459-464.

[89] Lu, W; Singh, AK; Khan, SA; Senapati, D; Yu, H; Ray, PC. Gold nano-popcorn-based targeted diagnosis, nanotherapy treatment, and in situ monitoring of photothermal therapy response of prostate cancer cells using surface-enhanced Raman spectroscopy. *Journal of the American Chemical Society*, 2010, 132, 18103-18114.

[90] Casadio, F; Leona, M; Lombardi, JR; Van Duyne, R. Identification of organic colorants in fibers, paints, and glazes by surface enhanced Raman spectroscopy. *Accounts of chemical research*, 2010, 43, 782-791.

[91] Brus, L. Noble metal nanocrystals: plasmon electron transfer photochemistry and single-molecule Raman spectroscopy. *Accounts of chemical research*, 2008, 41, 1742-1749.

[92] Pallaoro, A; Braun, GB; Reich, N; Moskovits, M. Mapping local pH in live cells using encapsulated fluorescent SERS nanotags. *Small*, 2010, 6, 618-622.

[93] Baik, JM; Lee, SJ; Moskovits, M. Polarized surface-enhanced Raman spectroscopy from molecules adsorbed in nano-gaps produced by electromigration in silver nanowires. *Nano letters*, 2009, 9, 672-676.

[94] Yang, L; Ma, L; Chen, G; Liu, J; Tian, ZQ. Ultrasensitive SERS detection of TNT by imprinting molecular recognition using a new type of stable substrate. *Chemistry-A European Journal*, 2010, 16, 12683-12693.

[95] Singh, AK; Khan, SA; Fan, Z; Demeritte, T; Senapati, D; Kanchanapally, R; Ray, P. C. Development of a Long-Range Surface-Enhanced Raman Spectroscopy Ruler. *Journal of the American Chemical Society*, 2012, 134, 8662-8669.

[96] Wustholz, KL; Henry, A-I; McMahon, JM; Freeman, RG; Valley, N; Piotti, ME; Natan, MJ; Schatz, GC; Duyne, RPV. Structure− Activity Relationships in Gold Nanoparticle Dimers and Trimers for Surface-Enhanced Raman Spectroscopy. *Journal of the American Chemical Society*, 2010, 132, 10903-10910.

[97] Liang, H; Li, Z; Wang, Z; Wang, W; Rosei, F; Ma, D; Xu, H. Enormous Surface-Enhanced Raman Scattering from Dimers of Flower-Like Silver Mesoparticles. *Small*, 2012, 8, 3400-3405.

[98] Majetich, S; Wen, T; Booth, R. Functional magnetic nanoparticle assemblies: formation, collective behavior, and future directions. *ACS nano*, 2011, 5, 6081-6084.

[99] Ronholm, J; Zhang, Z; Cao, X; Lin, M. Monoclonal antibodies to lipopolysaccharide antigens of Salmonella enterica serotype Typhimurium DT104. *Hybridoma*, 2011, 30, 43-52.

[100] Beeram, SR; Zamborini, FP. Effect of protein binding coverage, location, and distance on the localized surface plasmon resonance response of purified Au nanoplates grown directly on surfaces. *The Journal of Physical Chemistry C*, 2011, 115, 7364-7371.

[101] Novo, C; Funston, AM; Pastoriza-Santos, I; Liz-Marzan, L. M; Mulvaney, P. Influence of the medium refractive index on the optical properties of single gold triangular prisms on a substrate. *The Journal of Physical Chemistry C*, 2008, 112, 3-7.

In: Food Poisoning
Editor: Paresh C. Ray
ISBN: 978-1-63463-166-2

Chapter 8

MULTIFUNCTIONAL SERS-BASED SWCNT & GOLD NANOSTRUCTURES FOR TARGETED DETECTION AND PHOTOTHERMAL DESTRUCTION OF FOODBORNE PATHOGENS

Ashton T. Hamme II*, Yunfeng Lin and Thomas J. Ondera
Department of Chemistry, Jackson State University,
Jackson, Mississippi, US

ABSTRACT

Contamination of food such as lettuce, eggs, peanut butter by pathogenic bacteria has lead to food safety becoming one of the biggest consumer issues in recent years. A number of organisms such as *Salmonella DT104*, *E. coli O157*, *Cryptosporidium*, and *Listeria* have recently caused significant outbreaks of food poisoning in the USA. [1] This has led to an upsurge of "superbugs" that are insusceptible to even the most powerful antibiotics and has emerged as one of the biggest modern threats to public health. In this regard, efforts aimed at modernizing public health microbiology and bioinformatics capacities to speed microbial detection, eradication and monitoring are very urgently needed. This book chapter will summarize the work of our research group on the antibody-conjugated SWCNT hybrid nanostructures used for the detection and photo thermal destruction of foodborne pathogens. The book chapter will also present a summary of the development of plasmonic nanotechnology-based bioassays used for detection and photothermal destruction of foodborne pathogens. The fundamental concepts and novel properties of the nanomaterials that are useful for the detection and killing of the pathogens will also be discussed.

* Corresponding author: E-mail: ashton.t.hamme@jsums.edu. Fax: 601-979-3674.

1. INTRODUCTION

Foodborne pathogenic bacteria have always been a major threat to human health. Contamination of food by pathogenic bacteria such as *Salmonella* and *E. coli* has been a threat to human health throughout human history. [2-4] This problem was temporary solved in the 1940's through the discovery and use of penicillin. Since then, antibiotics have been utilized as the most effective antibacterial drugs for modern medical procedures. [5-8] However, due to the world wide abuse of antibiotics within last 50 years, bacterial pathogens are becoming drug resistant. [9,10] Recently, these multiple drug resistant bacteria (MDRB) present an even greater challenge to today's public health care. [11] A recent Centers for Disease Control and Prevention (CDC) report shows that an estimated 48 million illnesses, 128,000 hospitalizations, and 3,000 deaths of Americans occur each year caused by pathogens in contaminated food. [12] Every year, *Salmonella* is estimated to cause about 1.2 million illnesses in the United States, with about 23,000 hospitalizations and 450 deaths. [13] Furthermore, *Escherichia coli (E. coli)* are members of a large group of bacterial germs that inhabit the intestinal tract of humans and other warm blooded animals, and as few as 10 cells can cause serious human illness and even death. [14] The presence of *E. coli* in foodstuffs and drinking water is a chronic worldwide problem. [15] The worldwide food production industry is worth about 578 billion US dollars and food recalls due to the presence of pathogenic bacteria contamination are becoming an economical challenge for the food industry. [16] Traditional detection methods such as plating and culture usually involve time-consuming steps such as pre-concentration. Conventional techniques such as enzyme-linked immunosorbent assay (ELISA) and polymerase chain reaction are limited with regards to cost and versatility. [17-19] In this regard, the CDC/FDA (Food and Drug Administration) is encouraging efforts aimed at modernizing public health microbiology and bioinformatics capabilities to quicken microbial detection and response.

To help protect consumers by reducing or preventing illnesses and deaths related to food borne pathogens, and to minimize market disruptions and economic losses inflicted by food recalls, illness outbreaks and significant contamination incidents, highly sensitive, rapid, onsite, and low cost molecular detection and monitoring techniques are much needed. Various technologies have been developed for MDRB detection using optical, electrochemical, biochemical, and physical properties of microorganisms. [20,21] Although these methods are selective and sensitive, they still rely on a series of enrichment steps, which are so time-consuming and labor intensive that require days to week for completion. [22-24] As a result, scientists have been searching for alternative methods for decades, and nanotechnology based biosensors are emerging as such devices capable of overcoming the limitations of conventional techniques for bacterial detection. [11,14,25-34] Recently, several groups, including us, have reported the development of gold and SWCNT-gold hybrid nanomaterials as highly sensitive assays for the detection of a variety of pathogens. [14,30,35-37] Due to the presence of their large surface area, the surface of gold nanoparticles (GNPs) can attach to a large number of target-specific recognition elements such as antibodies, aptamers, and peptides, which allows selective and sensitive sensing of different pathogens. [38] Since GNPs possess unique shape and size-dependent optical properties, gold nanotechnology has become very attractive in their incorporation as diagnostic tools. [39,40] Also, GNPs have been of great interest for sensing and imaging due to lack of toxicity. [41] Furthermore, the

SWCNT-GNP hybrids even display some unique properties, [42,43] and as a result, bio-conjugated GNPs or SWCNT-GNPs can be used for selective detection of several pathogens simultaneously even at the single bacterium level. [11,44]

As for the destruction of MDRB, although human pathogens are becoming resistant to many available antibiotics, antibiotics are still the most efficient method currently. However, according to the World Health Organization (WHO), there may be only another 1-2 decades left for people to use the existing antibiotics. [16,45] Thus, new approaches for the treatment of infectious bacterial pathogens that do not rely on traditional antibiotics, is very urgent for our society's health care. Recently, several groups, including us, have reported that GNPs of different sizes and shapes with tunable optical properties in the near-infrared (NIR) region can be exploited for the hyperthermic destruction of bacteria, and because of their unique structure SWCNTs have the potential to be used as a photothermal therapy treatment option. [31,35,46-48] When irradiated at the proper laser power and wavelength, GNPs and SWCNTs have the ability to generate high temperatures at the desired site for the photothermal destruction of MDRB. [35,49] Through using hybrid nanomaterials, higher temperatures should be generated, and the photothermal process should be faster and more effective. [49,50] In this chapter, we will provide an overview of recently promising reports, suggest future strategies to apply SWCNT and gold nanotechnology to detect and destroy MDRB for food safety.

2. A CURRENT SWCNT AND GOLD NANOTECHNOLOGY

2.1. SWCNT

Due to the presence of strong Van der Waals interactions that tightly hold them together, SWCNTs are insoluble in a variety of solvents. [51,52] However, once the sidewall functionalization has been accomplished, the solubility of sidewall functionalized SWCNTs in organic solvents or water is usually improved because the functionalization breaks the nanotube bundles, [53] which is essential for solubility. Furthermore, new optical properties will be introduced. The carbon atoms on the sidewalls of SWCNTs that react with functional groups are converted from sp^2 into sp^3 hybridized carbons, and the functionalization of the p-network leads to a significant change in the electronic band structure of SWCNTs, which can be monitored by optical spectroscopy. Also, the presence of sp^3-hybridized carbon atoms in the SWCNT framework can be detected by Raman spectroscopy and is reflected by an increase in the relative intensity of the disorder mode of the SWCNTs after sidewall functionalization. Current chemical methods of SWCNT modification (Figure 1) include carboxylation, acid oxidation, halogenation, cycloadditions, radical additions, electrophilic additions, nucleophilic additions, ozonolysis, etc. [54] The reaction conditions may also include conventional or microwave assisted heating. These reactions may roughly be divided into two categories: a direct attachment of functional groups to the graphitic surface and the use of the SWCNT-bound carboxylic acids [53].

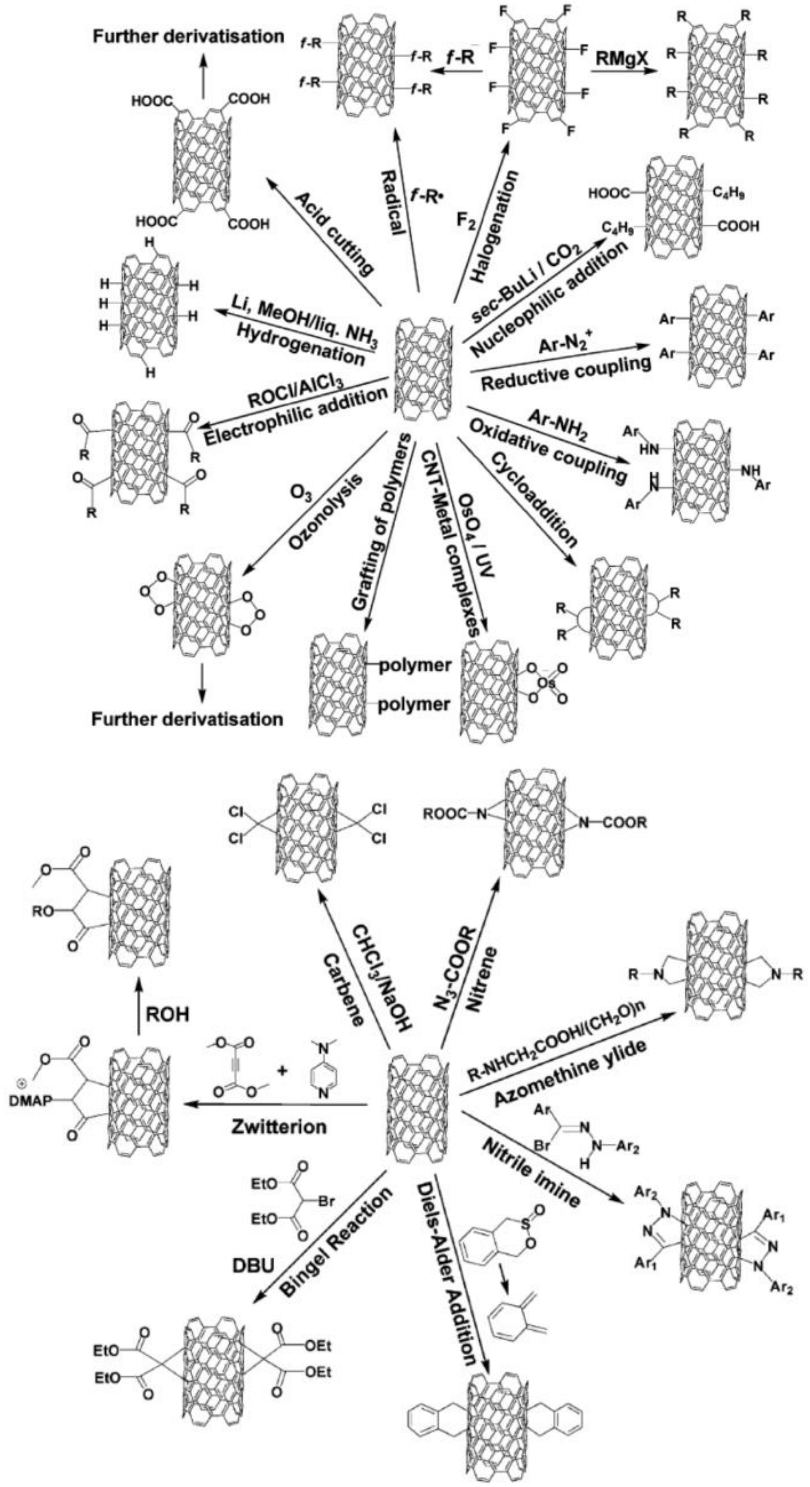

Figure 1. (A) Surface functionalization of carbon nanotubes. (B) Functionalization of carbon nanotubes by cycloaddition reactions.*(Reprinted with permission from Ref. (54), Copyright 2010, Royal Society of Chemistry.)*

2.2. GNP

GNPs have attracted considerable attention recently because of their many interesting properties and potential technological applications. Due to the presence of strong localized surface plasmon resonance (LSPR), GNP based colorimetric sensors can be used for the detection of several bacteria. Since GNPs have strong interactions with visible light through the resonant excitations of the collective oscillations of the conduction electrons within the particles, GNPs are widely used as a SERS based assay for the detection of a variety of analytes. When molecules are adsorbed onto roughened surfaces of GNPs, the Raman signal can be enhanced by several orders of magnitude. [49,55] Also, by photo exciting conduction electrons which oscillate at the surfaces of gold plasmons, highly efficient local heating can be achieved by non-radiative relaxation through electron–phonon and subsequent phonon–phonon coupling processes, [55] which makes GNPs suitable for the photothermal destruction of MDRB. Based on their shape and size-dependent optical properties, the potential uses of GNPs have been published using a variety of noble metal nanostructures, including gold nanoball, [35] gold nanoshells, [56] gold nanorods, [57,58] gold nanopopcorn [25,31] and gold nanocages etc. [50]

3. MDRB TARGET DETECTION

Considering the low infectious dose and high health risks of many bacterial pathogens (e.g., infective dosage for *Salmonella* and *E.coli* O157:H7 are as low as 10 cells), [13] a convenient, rapid, sensitive, and reliable detection method is essential for minimizing or eliminating potential infections. However, conventional methods, such as culture-based techniques and enzyme-linked immunosorbent assays (ELISA), suffer from the disadvantages of being time-consuming, having low sensitivity, being a laborious process, [59,60] and polymerase chain reaction (PCR) analyses often require intensive and careful sample pre-purification and skilled technical staff. [61]

Since the discovery of SWCNTs in 1991, their unique physical and chemical properties make them very promising materials for their use in nanotechnology. [62,63] SWCNTs have a tubular structure composed by monomers of graphene that can be disposed in either a single sheet or in multiple sheets of graphene concentrically grown, [64] which typically possess a diameter of a few nanometers, displaying a one dimension structure with a high surface area-to-volume ratio and providing an enhanced signal-to-noise ratio than the planar structures. Theoretically, this property is translated into a lower number of target molecules that are necessary to elicit a response to be detected by the biosensor. Based on this theory, as shown in Figure 2, Cristina Garcia-Aljaro et al. have developed a simple chemistry resistive based sensing platform for the detection of *E. coli* bacteria, based on a network of parallel aligned SWCNTs bridging two gold electrodes acting as a source and drain as the transducer element. [36] A significant increase in the resistance of the device was observed when the biosensor was exposed to target bacteria with a limit of detection of 10^3 CFU/mL.

Although the chemistry resistive based sensing platform reported by Cristina Garcia-Aljaro et al. has greatly improved the detection efficiency, this technique still relies on skilled technical staff. Recently, many research groups including us have reported newer MDRB

detection methods based on SWCNT & gold technology, such as label-free colorimetric sensing, [25,65] SERS, [66-68] and ICP-MS [69] etc.

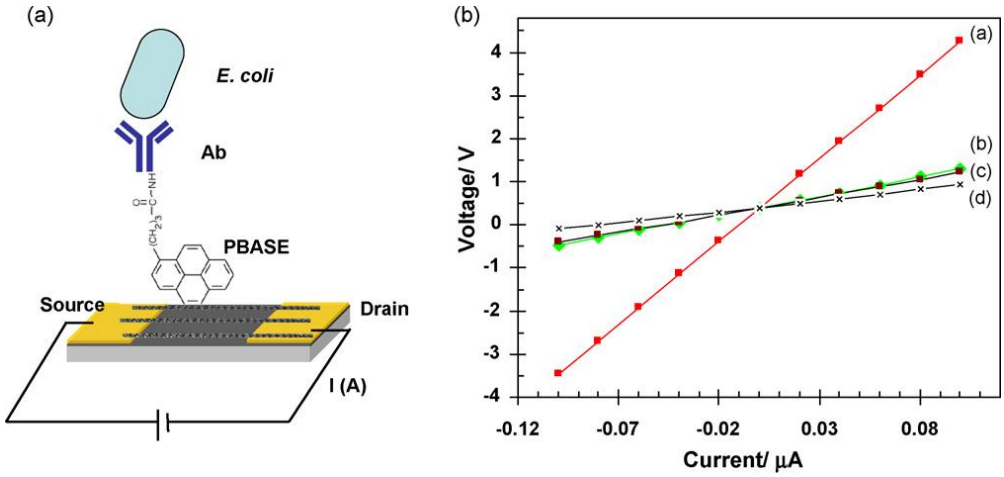

Figure 2. Schematic representation of the CNT-biosensor used for *E. coli* detection (A) and typical current changes observed after each functionalization step (B). A decrease in the current was observed after fuctionalization of the CNTs with (a) PBASE (1-pyrene butanoic acid succinimidyl ester) followed by (b) coupling of antibody (Ab) to PBASE. Blocking of the biosensor with ethanolamine (c) was used to prevent unspecific binding onto the CNTs causing a slight decrease in the current. In the example capture of *E.coli O157* is shown (d). *(Reprinted with permission from Ref. (36), Copyright 2010, ScienceDirect)*

3.1. SERS

Surface enhanced Raman scattering (SERS) has overcome the problem of conventional detection methods. SERS is a surface sensitive technique that enhances Raman scattering by molecules adsorbed on rough metal surfaces. It is known that metal nanoparticles, especially gold and silver nanoparticles, exhibit great SERS properties, which make them very attractive for the development of biosensors and biocatalysts. [70]

Table 1. Analysis for the observed SERS vibrational modes from *Salmonella DT104* [46]

Vibration mode	Raman peak position (cm^{-1})
$\upsilon(COO^-)$ anti-symmetric	1585
$\delta(CH_2)$saturated lipids	1460
τ(COO-) symmetric	1380
$\tau(NH_2)$ stretch for adenine and guanine	1340
τ(CC) ring stretch, n-alkanes	1150
δ(CCH) aliphatic	830
$P(CH_2)$	720
δ(CCC) ring deformation	590

(Reprinted with permission from Ref. (46), Copyright 2013, Wiley-VCH.)

3.1.1. Label-Free SERS-Based Biosensors

In the intrinsic (label-free) detection, the analyte is identified directly using its inherent fingerprint spectrum peaks. The analyte is immobilized directly onto the nanostructured surfaces, and the inherent Raman spectrum of the biomolecule directly measured to identify the specimen. To facilitate capture, and to aid specificity of detection, antibodies, enzymes or aptamers are conjugated onto nanostructured surfaces and the Raman spectral differences before and after capture of the analyte can be used to identify the species. [71]

Ray et al. have reported the development of iron core-gold shell popcorn shaped nanoparticles and showed their capability for magnetic separation, followed by the SERS imaging of MDRB. [46] In the magnetic core-gold shell nanoparticles, the central sphere will act as an electron reservoir, whereas the tips are capable of focusing the field at their apexes. As a result, the sharp tips will provide a huge field enhancement of the SERS scattering signal. [46] This very high sensitivity, along with the highly informative spectral characteristics of Raman spectroscopy, will enable scientists to use the SERS based method as a fingerprint for the label-free detection of MDRB. Since the bacteria cell wall consists of proteins, lipids, and carbohydrates, one can expect to see the SERS spectra from the vibrational mode of the aforementioned compositions. Vibrational assignments of the observed SERS peak are shown in Table 1.

3.1.2. Raman tagged SERS-based biosensors

In extrinsic detection strategy, a Raman reporter molecule (referred to as Raman tag) is used to generate a known SERS spectrum which is indirectly used to detect the pathogen. The strongly Raman scattering molecules are rationally attached on or near the surface of the plasmonic noble metal nanostructures. The biosensor specificity is integrated through the use of recognition biomolecules such as antibodies, aptamers, enzymes, or bacteriophages which will target specific epitopes on the exterior of the pathogens.

Different sizes [72] and shapes of noble metal nanostructures [73-75] can amplify the Raman signals with different enhancement factors. Sharp tip and edge metal nanostructures give better enhancement due to 'lightning rod effect'. [76,77] For stronger enhancement to take place, the Raman reporter molecules should be attached on or near (less than 15 nm) the metal nanostructure to generate SERS fingerprint signatures. The interparticle distance between the metal nanostructures should also be kept at a minimum. [78,79]

However, for the physically adsorbed Raman reporter molecules, the Raman signal from these Raman tagged metal nanostructures may lack stability due to possible leaching effects, and/or the signal may be easily disturbed by non-specific adsorption of surrounding interfering molecules. Hence it is important to use an appropriate encapsulating material that will enhance the signal stability and biocompatibility of the Raman tagged nanostructures. [80] Therefore, a careful choice of the noble substrate nanostructures, control over interparticle distances, Raman reporter molecule attachment, and appropriate coating materials are essential to yield strong stable enhancements.

Ray et al. recently reported applications of a Raman tagged SERS-based assay to detect low levels of bacteria, as well as to discriminate between types and strains of pathogens. They demonstrated selective detection of *Salmonella typhimurium* DT104 by using Rh-6G modified monoclonal M3038 antibody-conjugated popcorn-shaped gold tags, and achieved an impressive limit of detection (LOD) of 10 CFU mL^{-1}. [25] (See Figure 4 below).

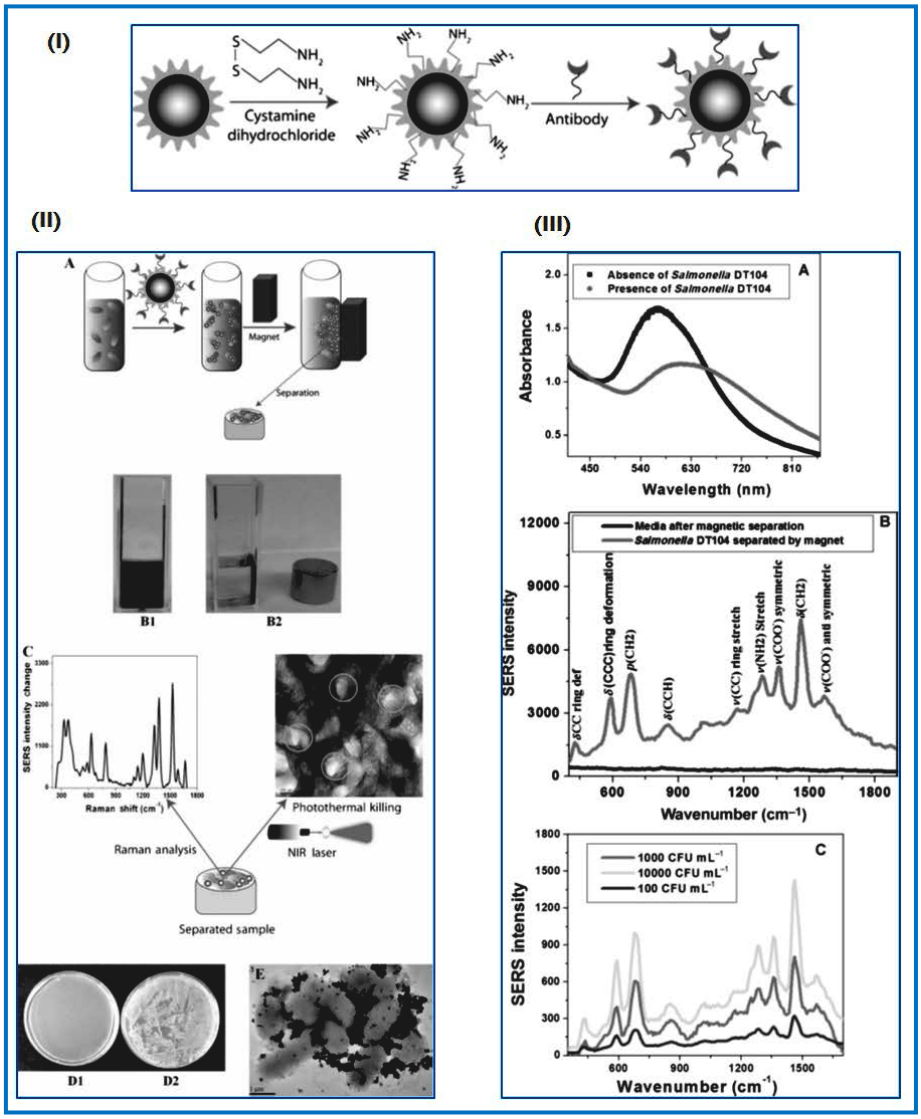

Figure 3. (I) A schematic representation showing the synthetic protocol of monoclonal antibody and A9 conjugated popcorn shape magnetic core–gold shell nanoparticle for the selective sensing and killing of Salmonella DT104.

(II) A) A schematic representation showing the separation procedure for *Salmonella DT104* by using M3038 antibody-conjugated core-shell nanoparticles. B) The separation of Salmonella DT104-attached magnetic/plasmonic nanoparticles by using a magnet. B) 1) *Salmonella DT104*-attached core–shell nanoparticle in the absence of a bar magnet and 2) Salmonella DT104-attached core–shell nanoparticle in the presence of bar magnet. C) A schematic representation showing the selective SERS imaging and targeted photothermal destruction of *Salmonella DT104* after magnetic separation. D) Colonies of MDR *Salmonella DT104*: 1) Colonies shows absence of bacteria in the supernatant solution after magnetic capture and 2) colonies show the presence of bacteria in the suspension of magnetic/plasmonic nanoparticle-conjugated-MDR *Salmonella DT104* after magnetic capture and re-suspension in PBS. The initial number of MDR was $1.2x10^5$ $CFUmL^{-1}$. E) TEM image demonstrating the aggregation of antibody-conjugated nanoparticles after the addition of $1.2x10^5$ $CFUmL^{-1}$ MDR

Salmonella DT104 bacteria. The TEM image also shows the formation of bigger microbial clusters in presence of $6.2x10^4$ $CFUmL^{-1}$ MDR *Salmonella DT104* bacteria; scale bar, 1 µm.

(III) A) Absorption profile variation of antibody-conjugated nanoparticles due to the addition of $1.2x10^5$ $CFUmL^{-1}$ MDR *Salmonella DT104* bacteria. B) Plot shows SERS intensity from a bacteria-conjugated nanoparticle after magnetic separation and re-suspension with PBS. All observed Raman signal is directly from *Salmonella DT104*. No SERS signal has been observed from supernatant that is mainly PBS. C) The plot shows the variation in the SERS intensity from different concentrations of MDR *Salmonella DT104*. All the reported concentrations are before magnetic separation. *(Reprinted with permission from Ref. (46), Copyright 2013, Wiley-VCH.*)

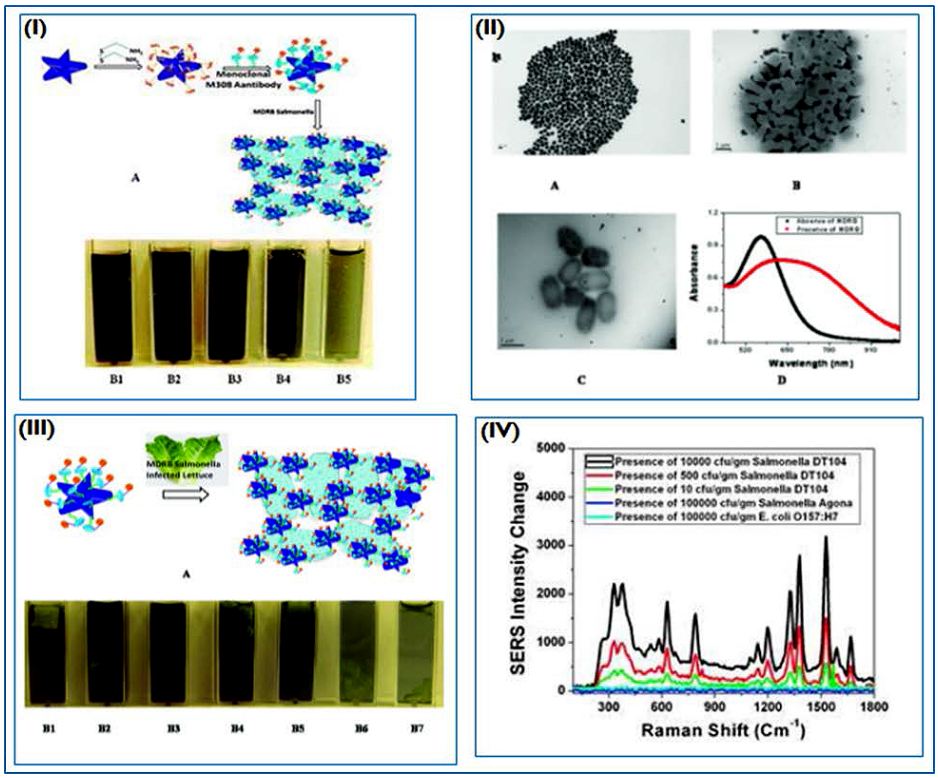

Figure 4. (I) Schematic representation showing monoclonal M3038 antibody conjugated popcorn-shape gold nanotechnology-driven approach to selectively detect MDRB *Salmonella*. (B) Photograph showing colorimetric change from purple to gray, upon the addition of different bacteria on antibody-conjugated gold nanoparticle, (B1) 10^2 CFU/mL MDRB *Salmonella* (B2) 10^6 CFU/mL *Salmonella ser. Agona* bacteria. (B3) 10^6 CFU/g *E. coli* bacteria, (B4) 10^3 CFU/mL MDRB *Salmonella* and (B5) 10^4 CFU/mL MDRB *Salmonella*.(II) TEM image showing (A) monoclonal M3038 antibody-conjugated popcorn-shape gold nanoparticles before the addition of MDRB. (B) Aggregation of gold nanoparticles as well as formation of microbial clusters in presence of 10^5 CFU/mL MDRB *Salmonella*. (C) Very little binding in the presence of 10^6 CFU/mL *Salmonella ser. Agona* bacteria. (D) Plot demonstrating absorption spectral change in the presence of 10^5 CFU/mL MDRB *Salmonella DT104*. (III) Schematic representation showing the gold nanotechnology-driven colorimetric approach for rapid selective screening of MDRB *Salmonella* bacteria from infected lettuce, (B) Photograph showing colorimetric change from purple to gray, upon the addition of infected lettuce on antibody-conjugated gold nanoparticles. Lettuce was infected by (B1) 10^2 CFU/g MDRB *Salmonella*, (B2) 10^6 CFU/g *Salmonella ser. Agona* bacteria. (B3) 10^6 CFU/g *E. coli* bacteria, (B4) mixture of 10^6 CFU/g *Salmonella ser. Agona*

and 10^6 CFU/g *E. coli*, (B5) mixture of 10^6 CFU/g *Salmonella ser. Agona* and 10^2 CFU/g MDRB *Salmonella*, (B6) mixture of 10^6 CFU/g *Salmonella ser. Agona* and 10^3 CFU/g MDRB *Salmonella*, (B7) 10^3 CFU/g MDRB *Salmonella*. (IV) Plot demonstrating SERS enhancement (SERS intensity change before and after addition of bacteria) due to the addition of different kinds of bacteria to monoclonal M3038 antibody-conjugated popcorn-shape gold nanoparticle. *(Reprinted with permission from Ref. (25), Copyright 2011, Royal Society of Chemistry.)*

Selectivity was achieved through covalent conjugation of monoclonal M3038 antibody which is highly selective for *Salmonella typhimurium DT104*. This assay was highly specific for MDRB *Salmonella typhimurium DT104*, and could distinguish between different *Salmonella* strains and other bacteria. Their results show that antibodies or related capture moieties can be used to provide selectivity to SERS biosensing. Their bioassay was rapid, taking less than 5 min from bacteria binding to detection and analysis. To improve the sensitivity of the popcorn-shape gold nanoparticle assay, they have employed Rh-6G modified monoclonal M3038 antibody-conjugated popcorn-shaped gold nanoparticle-based SERS platform. Their result shows that SERS tag-based strategy could readily be used to rapidly and selectively detect foodborne pathogens.

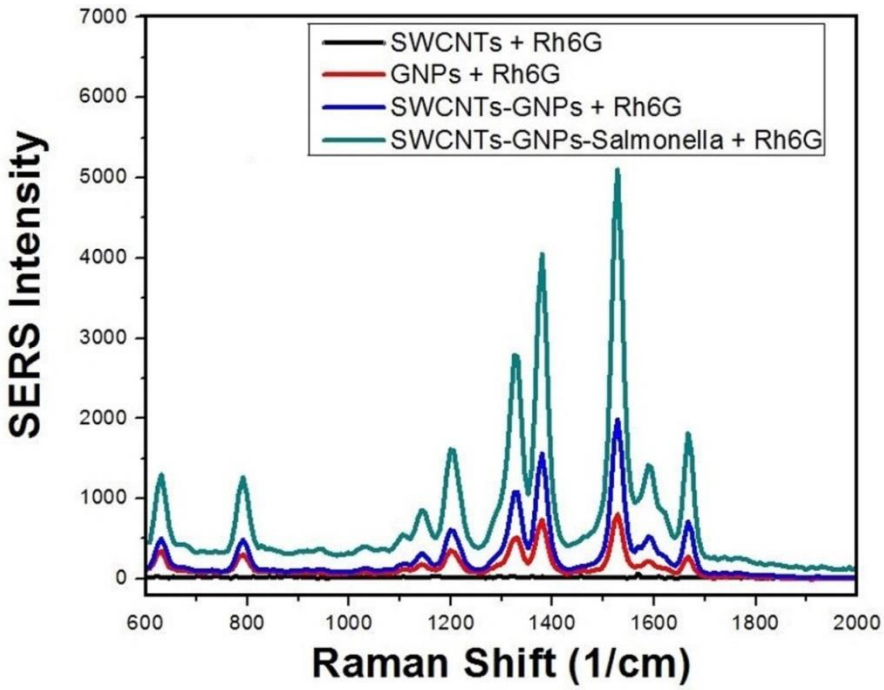

Figure 5. SERS enhancement (SERS intensity change before and after addition of bacteria) due to the addition of Salmonella to monoclonal AC04 antibody-conjugated, GNPs-decorated SWCNTs. *(Reprinted with permission from Ref. (35), Copyright 2014, Royal Society of Chemistry.)*

Gu, R.A. et al. used Ag core-Au shell nanoparticles labeled with monoclonal antibodies and SERS probes for the selective detection of pathogens. [81] In the proposed system, antibodies immobilized on a solid substrate can interact with the corresponding antigens to form a composite substrate, which can capture reporter-labeled Ag core-Au shell nanoparticles modified with the same antibodies. The immuno-reaction between the

antibodies and antigens was demonstrated by the detection of characteristic Raman bands of the probe molecules. Ag core-Au-shell bimetallic nanoparticles, as a new SERS active and biocompatible substrate, will be expected to improve the detection sensitivity of immunoassay because of the better SERS properties of the Ag core. [81]

Table 2. Summary of the different nanoparticles used for ultrasensitive diagnosis of pathogens

Bacteria	Nanomaterial	Method	Detection limit /CFU mL^{-1}	Ref
E. coli O157:H7	GNP	SERS	10	14
	QDs	Fluorescence	10^3	84
	Dye with magnetic NPs	Luminescence	20	85
	Dye with silica NPs	Fluorescence	16	86
Salmonella	GNP	SERS	10	25
	QDs	Fluorescence	10^3	87
	Dye with magnetic NPs	IR	10^4	88
	CNT	Potentiometric	10^4	89
S. aureus	GNP	SPR	10^4	90
	QDs	Fluorescence	10^3	91
	Magnetic	MALDI-MS	10^5	92
Listeria	TiO2 nanowire	Impedance	10^2	93
	Magnetic	PCR	500	94
M. tuberculosis	Dye-doped silica NPs	Fluorescence	---	95

(Adapted with permission from Ref. (11), Copyright 2012, Royal Society of Chemistry.)

Recently, we also report a highly sensitive detection of MDR *Salmonella DT104* through SWCNTs–GNPs bioconjugated nanohybrids, which offers an even stronger Raman enhancement due to the addition of SWCNTs. Since the antibody conjugated SWCNTs-GNPs aggregate in the presence of MDR *Salmonella*, as shown in Figure 5, the nanohybrid forms several hot spots and provided a significant enhancement of Raman signal intensity by several orders of magnitude from the Rh-6G. [35]

3.2. ICP-MS

Protection of food safety against bacterial contamination requires assays for fast and precise quantification detection of bacterial pathogens. Lan et al. have reported an localized surface plasmon resonance (LSPR) biosensor that can detect *Salmonella typhimurium* in chicken carcasses. [82] Their result shows that the detection limit of their LSPR biosensor is 1×10^6 CFU mL^{-1}. Wang et al. have improved the detection limit. They have reported amine-modified gold nanorods with different aspect ratios, for simultaneous detection of *Salmonella* and *E. coli* pathogens, [30] at concentrations less than 10^2 CFU mL^{-1}. Waswa et al. reported an LSPR biosensor for the detection of *Salmonella* and *E.coli* in spiked skim milk using

specific antibodies. [83] In their report, they have shown that the LSPR sensor registers changes in the refractive index during binding of the bacteria to the antibody, which was immobilized on the gold-coated sensor chip surface. They have shown that the LSPR sensor is highly specific, and the limits of detection of the assay were found to be 23 CFU/mL for *Salmonella* and 25 CFU/mL for *E. coli*. Ray et al. [11] (and the references cited therein) [14,25,84-95] have summarized the detection limit of different pathogenic bacteria sensing techniques using different nanomaterials (Table 2).

However, conventional methods mentioned above cannot detect the concentration of bacteria precisely. In 2010, Feng Li et al. have reported a rapid and sensitive assay for the *E. coli O157:H7* bacteria by using antibody affinity binding, GNP labeling, and inductively coupled plasma mass spectrometry (ICP-MS) detection, as shown in Figure 6. [69] Taking advantage of the signal amplification property of GNPs and the high sensitivity of ICP-MS, the assay was able to detect as few as 500 CFU/mL *E.coli O157:H7* and can precisely detect up to 5×10^6 CFU/mL. Their assay showed high specificity of the assay for *E. coli O157:H7* due to the antibody-antigen interaction.

4. PHOTOTHERMAL DESTRUCTION OF MDRB

Photothermal therapy is a minimally invasive treatment method in which photon energy is converted to thermal energy sufficient to induce cellular hyperthermia. Selectivity is achieved by focused directional control or invasive positioning of the incident radiation, often pulsed or continuous wave laser, and is typically accompanied by preferential administration of photoactive molecules or nanoscale particles. [96]

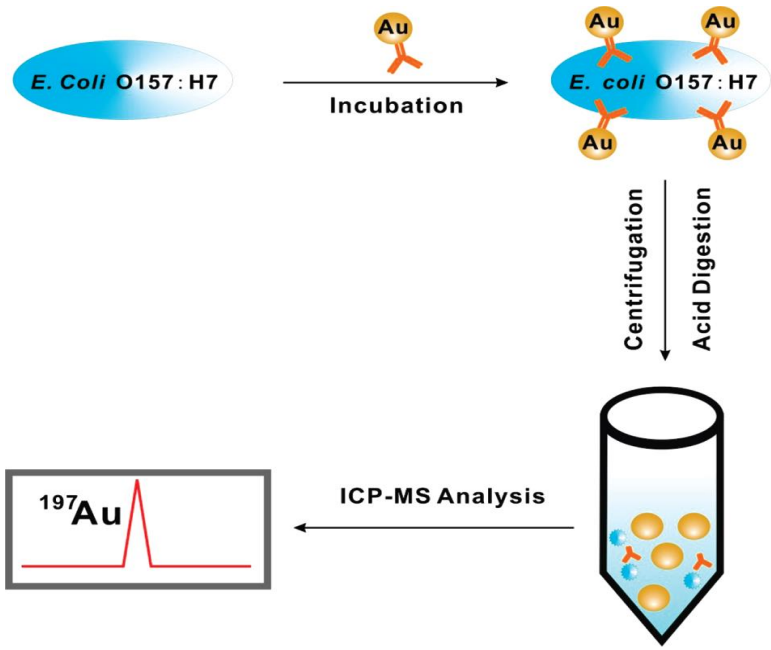

Figure 6. Schematic diagram showing the principle of the assay. The *E. coli O157:H7* cell was incubated with antibody-conjugated GNPs. The unbound GNPs were separated from the cell complex by centrifugation. The cell pellets containing GNPs were digested with 1% nitric acid after washing,

and the solution was analyzed by ICP-MS. The intensity of the ICP-MS measurement of Au at m/z 197 corresponds to the concentration of *E. coli O157:H7* cells in the original sample. *(Reprinted with permission from Ref. (69), Copyright 2010, American Chemical Society.)*

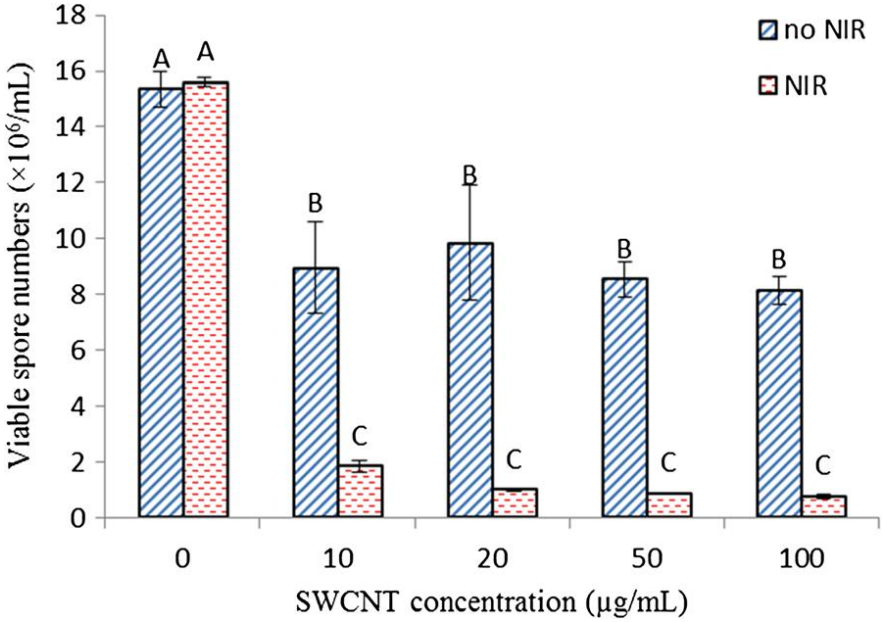

Figure 7. Viable spore numbers after being treated with SWCNTs at various concentrations and coupled with or without 20-min NIR radiation. *(Reprinted with permission from Ref. (99), Copyright 2013, BioMed Central journals.)*

SWCNTs are not only strong antimicrobial agents, but are also efficient photothermal agents. Kang et al. reported the first direct evidence of SWCNTs' strong antimicrobial activity based upon the following related influence factors, including CNT diameter, length, aggregation, concentration, CNT surface groups, buffer solution, bacterial species, contact time, and intensity. [97] Dong et al. reported that SWCNTs might be an effective alternative to antibiotics in dealing with drug-resistant and multidrug-resistant bacterial strains because of the physical mode of bactericidal action that SWCNTs display. [98] The mechanisms of SWCNT's antimicrobial activity to bacterial cells depended essentially on the direct contact resulting in cell membrane damage, but also included oxidative stresses due to direct oxidation of cellular components, and secondary oxidation of cellular lipid bilayer by reactive oxygen species. Under the treatment of NIR, SWCNTs show an even stronger antimicrobial activity. Recently, Dong et al. [99] has reported that the treatment of 10 μg/mL SWCNTs coupled with 20 min NIR significantly improved the antimicrobial effect by doubling the viable spore number reduction percentage when compared with SWCNTs without NIR irradiation (88% vs. 42%), as shown in Figure 7.

GNPs of different sizes and shapes with optical properties tunable in the visible to NIR region can be used for the photothermal destruction of MDRB by using NIR light. When the light of the appropriate wavelength is absorbed by bacteria conjugated GNPs, absorbed light will be converted into heat by rapid electron-phonon relaxation followed by phonon-phonon relaxation. This highly localized heat generated by the GNPs can be used to destroy MDRB selectively by disrupting the cell membrane. If the incident laser frequency overlapped with

the plasmon absorption maximum of the GNPs conjugated pathogens, the selective heating and destruction of MDRB can be achieved at a much lower laser power than that required to destroy healthy bacteria to which bio-conjugated nanoparticles do not bind specifically. The photothermal destruction process normally destroys MDRB via cell damage through thermal effects, such as denaturation of proteins/enzymes, induction of heat-shock proteins, metabolic signaling disruption, endothelial swelling, micro thrombosis, and other pathways. [16]

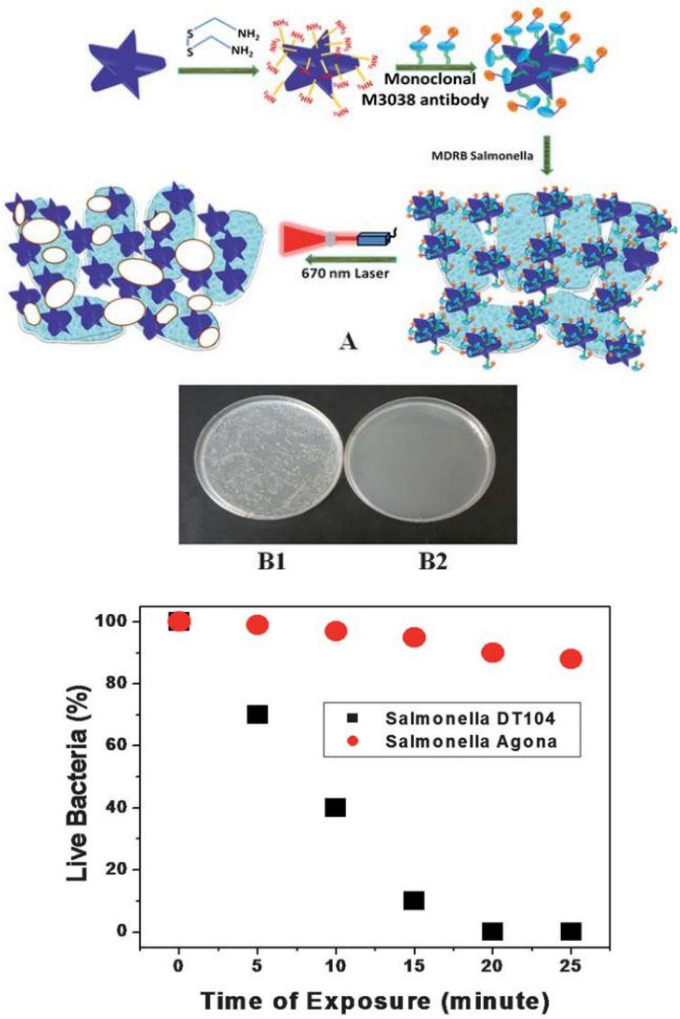

Figure 8. (A) Schematic representation showing the monoclonal M3038 antibody conjugated popcorn shaped gold nanotechnology-driven approach to selective photo thermal killing of MDRB *Salmonella*. (B) Colonies of MDRB *Salmonella* DT104 (B1) before and (B2) after exposing to 670 nm light with 200 mW/cm^2 power for 20 minutesin the presence of monoclonal M3038 antibody-conjugated popcorn shaped gold nanoparticles. (C) Plot showing time dependent effect of photothermal lysis when antibody attached popcorn shaped gold nanoparticle conjugated *Salmonella DT104, Salmonella Agonabacteria* were treated using 200 mW/cm^2 670 nm light. *(Reprinted with permission from Ref. (31). Copyright 2011, Royal Society of Chemistry.)*

Table 3. Laser irradiation time to kill 100% MDRB in lettuce samples

Concentration of MDRB in lettuce samples/CFU g^{-1}	Laser irradiation time to kill 100% bacteria/min
10^2	6
10^3	9
10^4	14
10^5	20
10^6	25
10^7	30

(Adapted with permission from Ref. (31). Copyright 2011, Royal Society of Chemistry.)

Zharov et al. reported localized killing of *Staphylococcus aureus in vitro* by combining laser and photothermal techniques. [100] Later, Norman et al. reported photothermal killing using gold nanorods that have been covalently linked with antibodies to selectively destroy *Pseudomonas aeruginosa*, [101] which was obtained from the upper respiratory tract of sinusitis patients. However, both of the studies did not demonstrate the selectivity of their assay with respect to other pathogens, which is very important before this technique can be used for food and real life samples.

For the selectively killing of pathogens, Sadia et al. has report bio-conjugated popcorn shaped GNPs for targeted photothermal killing of MDR *Salmonella DT104*, [31] as shown in Figure 8. They showed a monoclonal antibody-conjugated popcorn shaped GNP driven approach to selectively destroy ampicillin, chloramphenicol, streptomycin, sulfonamides, and tetracycline drug resistant *Salmonella DT104* bacteria from MDRB infected romaine lettuce. Their selectivity is based on the fact that monoclonal M3038 antibody-conjugated popcorn shaped GNPs can readily and specifically bind with *Salmonella DT104* bacterium O-antigen, through antibody–antigen recognition. They demonstrated that when antibody modified popcorn shaped GNP conjugated bacteria sample was exposed to 670 nm laser radiation, almost 100% of drug resistant bacteria were killed due to photothermal lysis. They demonstrated that the gold nanotechnology based assay is capable of destroying MDRB in food samples. Figure 8C shows the time dependent photo thermal killing of MDRB *Salmonella* DT104, which clearly shows that 100% of bacteria can be killed within 20 minutes of exposure to 670 nm light. Table 3 shows that 100% of bacteria can be destroyed from MDRB infected lettuce sample by 6 to 30 minutes of laser irradiation treatment, [31] depending on the MDRB concentration (10^2–10^7 CFU g^{-1}).

For selectively detecting and killing MDRB in lower concentration, in 2013, Fan et al. reported a popcorn-shaped magnetic core-plasmonic shell multifunctional GNPs for the targeted magnetic separation and enrichment, label-free SERS imaging, and photothermal destruction of multidrug-resistant bacteria, [46] as shown in Figure 9. According to them, the iron core is responsible for selective magnetic separation of MDRB, while the gold coating can be used as "light-directed nanoheaters" for the hyperthermic destruction of MDRB by using NIR light. Also, the plasmonic gold coating will be very useful for stabilizing the high-magnetic-moment nanoparticles in corrosive biological conditions, which also eliminates the possible toxicity of iron nanoparticles and aid in easy bioconjugation through the well-understood chemistry of Au-S. A targeted photothermal-lysis experiment, by using 670 nm

light at 1.5 Wcm^{-2} for 10 min, will result in selective and irreparable cellular-damage to MDR *Salmonella*, while almost no *E. coli* was killed in the same situation.

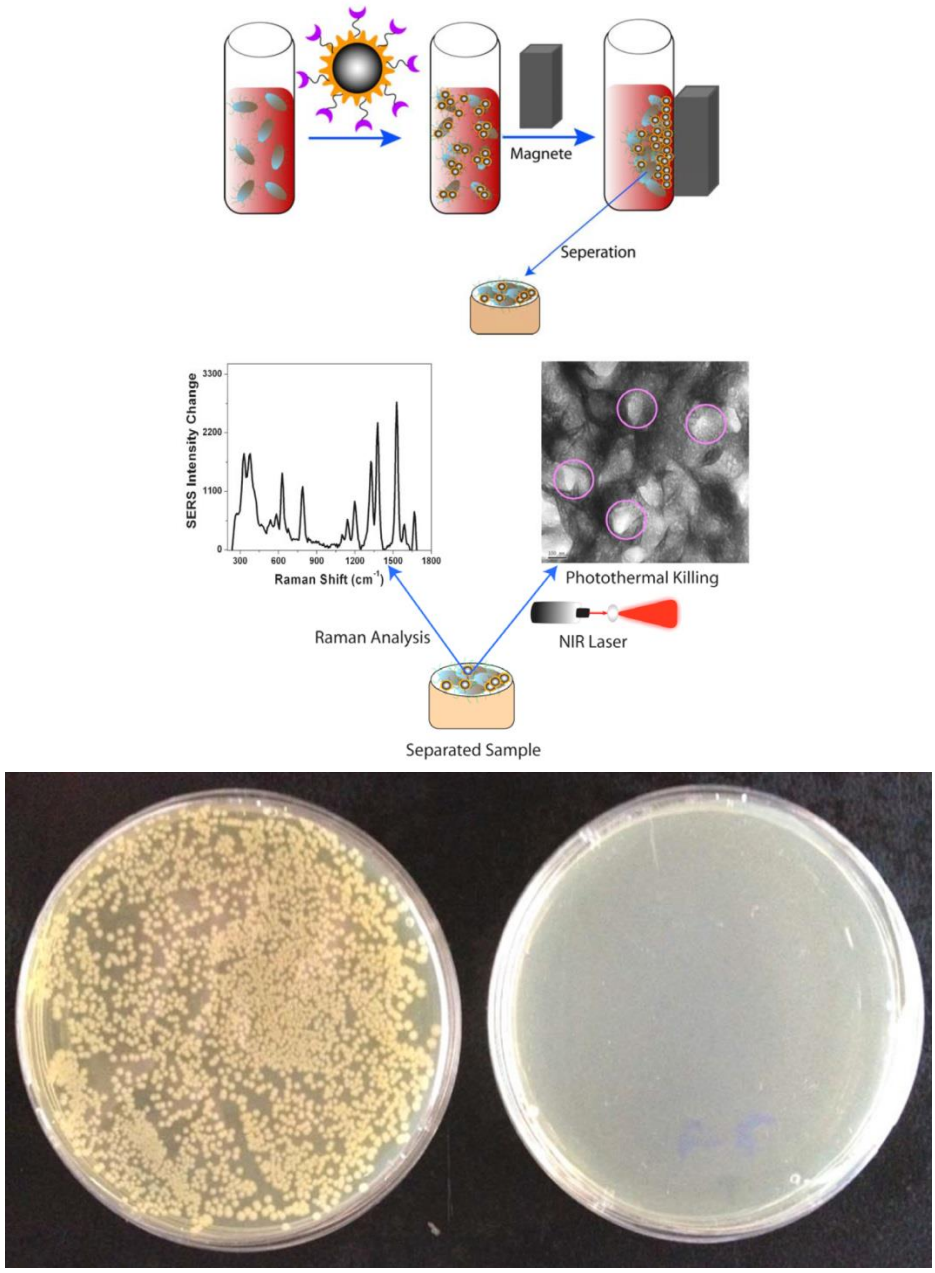

Figure 9. (A) Schematic representation showing the separation procedure for *Salmonella DT104* using-M3038 antibody conjugated popcorn shape plasmonic gold shell iron magnetic core nanoparticles. (B) Schematic representation showing the selective SERS imaging and targeted photothermal destruction of *Salmonella DT104* after magnetic separartion. (C) Colonies of bacteria demonstrating the selectivity of our photothermal lysis process. C1) 10^6/ml *E.coli* bacteria in the presence of anti–*Salmonella* antibody coated GNP. C2) 10^6/ml *Salmonella* bacteria in the presence of anti–*Salmonella* antibody coated GNP. *(Reprinted with permission from Ref. (46), Copyright 2013, Wiley-VCH.*)

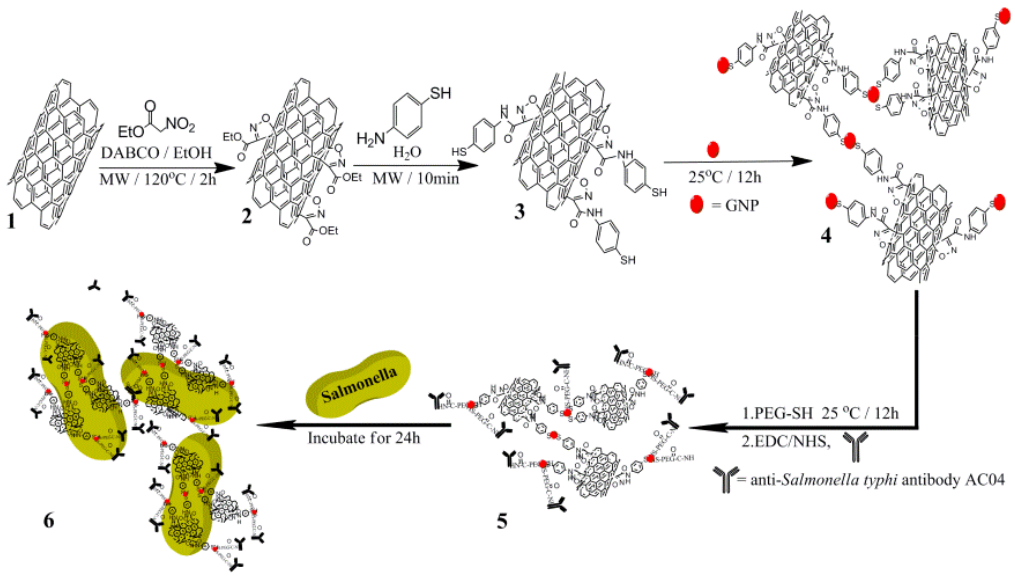

Figure 10. Schematic representation shows the synthetic protocol for the functionalization of SWCNTs, the formation of GNP attached SWCNTs, and SWCNTs–GNPs-antibody-*Salmonella*. *(Reprinted with permission from Ref. (35), Copyright 2014, Royal Society of Chemistry.)*

Huang et al. have reported that multifunctional Van-Fe_3O_4@Au nanoeggs are effective photothermal agents for the selective killing of MDRB bacteria under irradiation with 808 nm light. [102] They have shown that Van-Fe_3O_4@Au nanoeggs can be used for photo thermal killing of *A. baumannii, E. coli O157:H7, S. pyogenes, S. saprophyticus* and other bacteria, using 808 nm light. They have also shown that the photothermal approach can be used for effectively inhibiting the cell growth of nosocomial and antibiotic-resistant bacterial strains. Their results show that more bacteria were killed when aggregated under the magnetic field. [11]

By using certain hybrid nanomaterials, higher temperatures and a faster more effective photothermal process is expected. Also, SWCNT-GNP hybrids are expected to have good biocompatibility and low toxicity. [49] As a result, SWCNT-GNP hybrids may have greater promise for society for the therapeutic challenges of MDRB. Recently, we have reported a targeted highly sensitive detection/eradication of multi-drug resistant *Salmonella DT104* through SWCNT–GNP bioconjugated nanohybrids, [35] as shown in Figure 10. In our report, we combined monoclonal antibody-conjugated sphere-shaped GNPs with SWCNTs to create a nanohybrid system to selectively detect and eradicate MDR *Salmonella typhimurium DT104* bacteria. The localized heating that occurs during a targeted photothermolysis experiment using 670 nm light at 2W cm-2 for 15 min of light exposure, resulted in selective and irreparable damage to more than 99% *Salmonella DT104* at the concentration of 10^5 CFU mL^{-1}. In comparison to solely SWCNTs or GNPs, our SWCNT–GNPs nanohybrids have shown better photo thermal efficiency.

To verify the role of the laser and the hybrid SWCNTs–GNPs toward killing *Salmonella*, we performed 5 comparative photo thermal experiments. Based on the results shown in Figure 11A, after laser irradiation (2 W cm^{-2} power of 670 nm light, 15 min exposure) of the MDR *Salmonella* in the presence of the AC04 *Salmonella* antibody hybrid nanomaterial, more than 99% of the MDR *Salmonella* at the concentration of 10^5 CFU mL^{-1} were

eradicated, while the hybrid nanomaterial without laser irradiation (Figure 11D) and MDR *Salmonella* with laser irradiation (no hybrid nanomaterial, Figure 10E) killed a negligible amount of MDR *Salmonella*. This data confirmed that both hybrid SWCNTs–GNPs and laser irradiation play a vital role in the photo thermal destruction of *Salmonella* DT104, which validates the mechanism whereby laser irradiated hybrid nanomaterials composed of SWCNTs–GNPs produce enough heat to destroy the MDRS. [35]

To understand the advantages of using hybrid SWCNTs–GNPs instead of only GNPs or only SWCNTs, we have also performed photothermal experiments using antibody-conjugated GNPs and antibody conjugated SWCNTs separately. As shown in Figure 11 B and C, at the same power and exposure time, in the case of only GNPs or SWCNTs, they kill 10 to 40 percent less of MDRS than using hybrid SWCNTs–GNPs. On the other hand, the laser power had to be doubled (4 W cm^{-2}) and 20 minutes were required to eradicate the same amount of MDRS when SWCNTs and GNPs were used separately. Our experimental results depicted that the photo thermal effect with the SWCNTs–GNPs hybrid is much more than either SWCNTs or GNPs alone. This effect is mainly because of two reasons: (1) in the case of the hybrid SWCNTs–GNPs, both SWCNTs and GNPs can generate heat when exposed to laser irradiation, and the amount of heat generated is expected to be higher than only SWCNTs or GNPs alone, and (2) after the attachment of SWCNTs–GNPs hybrids with *Salmonella*, the hybrids have a very strong absorption peak at around 590 nm, near to the 670 nm laser source compared with GNPs attached MDRS and SWCNTs attached MDRS, as shown in Figure 12.

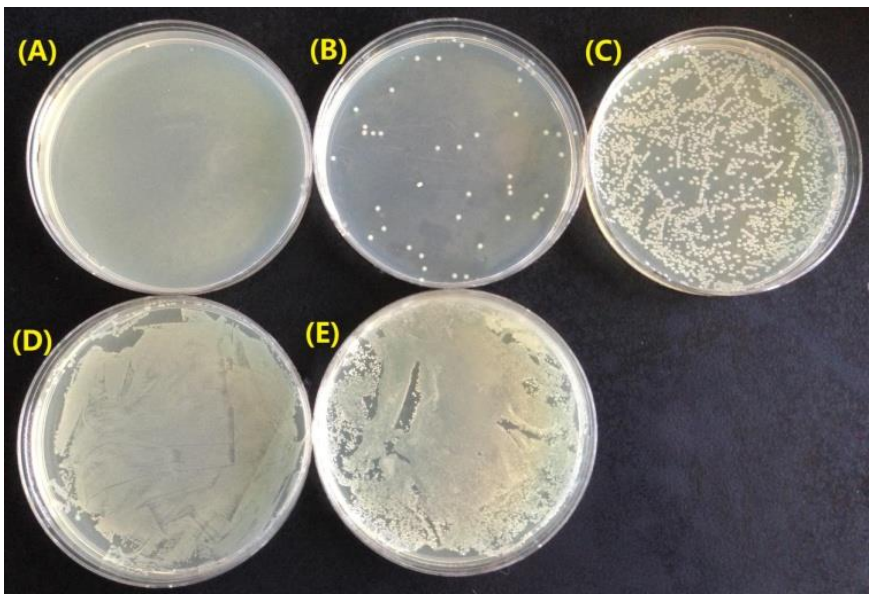

Figure 11. Photothermal killing of *Salmonella*. (A) SWCNTs–GNPs-antibody-*Salmonella* under laser irradiation for 15 min. (B) GNPs-antibody-*Salmonella* under laser irradiation for 15 min. (C) SWCNTs-antibody-*Salmonella* under laser irradiation for 15 min. (D) SWCNTs–GNPs-antibody-*Salmonella* before laser irradiation. (E) Only *Salmonella* under laser irradiation for 15 min. *(Reprinted with permission from Ref. (35), Copyright 2014, Royal Society of Chemistry.)*

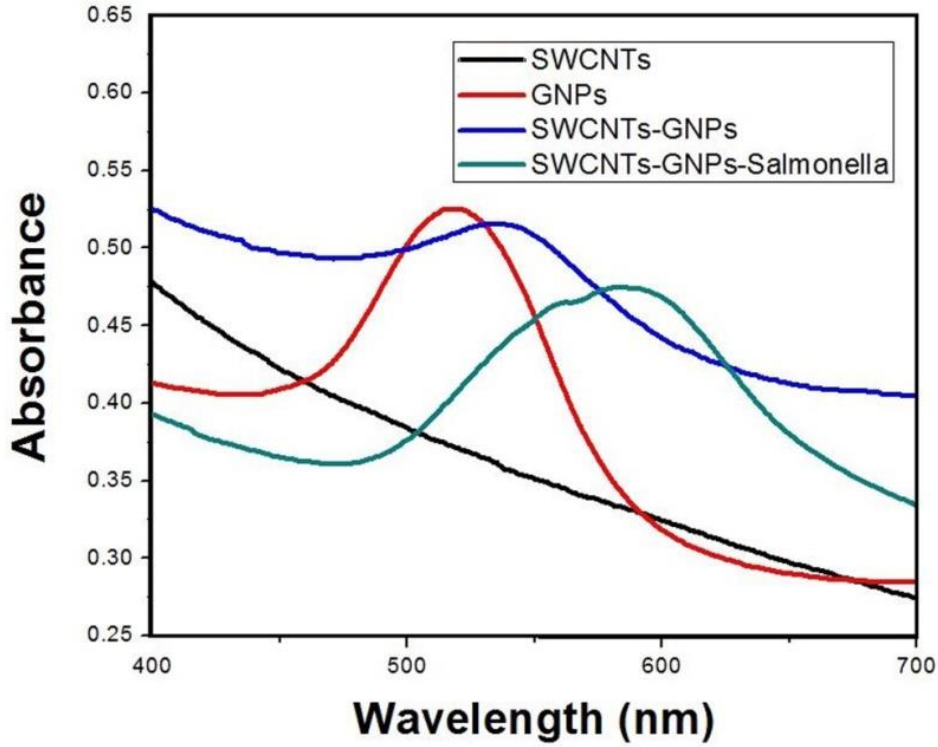

Figure 12. UV Absorption spectra for only SWCNTs, 0.3 nM GNPs, 0.3 nM GNPs attached SWCNTs, and SWCNTs–GNPs-*Salmonella*. *(Reprinted with permission from Ref. (35), Copyright 2014, Royal Society of Chemistry.)*

CONCLUSION AND OUTLOOKS

In this chapter, we have discussed the great potential of bio-conjugated GNPs and SWCNTs-GNPs hybrids for the possible application of MDRB diagnostics from food samples and photothermal destruction of MDRB. We have summarized a review that after conjugation of bacteria with specific antibodies, several shapes of GNPs and SWCNTs-GNPs hybrids are useful for bacteria detection with highly selective label-free colorimetric sensing, SERS, and several other methods, due to their size-dependent physical properties. Through ICP-MS, the concentration of MDRB can be precisely detected under a wide range of concentrations. We have also discussed that these SWCNT & gold based nanotechnologies can serve as "nanoscopic heaters" in the presence of a suitable wavelength light, which can be very useful for the selective photothermal destruction of MDRB without antibiotics. Even though this technology is only at the beginning stages, this technology has shown highly promising applications for MDRB detection and destruction from food samples.

Compared to current methods of MDRB detection and destruction from food samples, the aforementioned SWCNT and gold based assays have several advantages. However, a number of opportunities and challenges still exist. For example, to synthesize SERS-based biosensors with higher sensitivity and reproducibility, researchers must be able to assemble highly stable SERS-based substrates, precisely control the size and shape of the noble metal nanoparticle,

control the interparticle placement onto the supporting templates, and generate highly stable Raman tagged SERS substrates for molecular detection and monitoring. Many researchers have demonstrated exceptional sensitivity, selectivity, and rapidity of SERS-based biosensors as novel optical biosensors for detection and photothermal destruction of microorganisms. However, future efforts toward integrating the advantages of the conventional methods with those of SERS techniques are warranted. Furthermore, toxicity and side effects need to be addressed in a meticulous and systematic way as a function of nanoparticle size, shape, and surface coating. As a result, an understanding of biological response and environmental remediation is necessary before the aforesaid assays can be fully utilized in food processing technology. We believe that with properly chosen combinations of plasmonic and shape of GNPs, these SWCNT & gold based technology will enable us to develop multifunctional nanomedical platforms for multimodal diagnosis and therapy.

ACKNOWLEDGMENTS

The project described was supported by the National Science Foundation (HBCU-RISE: HRD-1137763 and PREM: DMR- 633156). The TEM CORE Facilities were supported by the National Institutes of Health/National Center for Research Resources (Award Number: G12RR013459) and the National Institutes of Health/National Institute on Minority Health and Health Disparities (Award Number: G12MD007581).

REFERENCES

[1] Foodborne Outbreaks. http://www.cdc.gov/foodsafety/outbreaks/.

[2] Newell, DG; Koopmans, M; Verhoef, L; Duizer, E; Aidara-Kane, A; Sprong, H; Opsteegh, M; Langelaar, M; Threfall, J; Scheutz, F; Van der Giessen, J; Kruse, H. Food-borne Diseases - the Challenges of 20 Years Ago Still Persist While New Ones Continue to Emerge. *Int J Food Microbiol*, 2010, 139 Suppl 1, S3.

[3] Salyers, AA; Gupta, A; Wang, Y. Human Intestinal Bacteria as Reservoirs for Antibiotic Resistance Genes. *Trends Microbiol*, 2004, 12, 412.

[4] Oliver, P; Jayarao, M; Almeida, RA. Foodborne Pathogens in Milk and the Dairy Farm. *Foodborne Pathogens and Disease*, 2005, 2, 115.

[5] Industrial Bulletin of Arthur D. Little, Inc. Penicillin. *J. Chem. Educ*., 1943, 20, 326.

[6] Fogel, R. Penicillin: First of the Miracle Drugs. *Chem. Eng. News*, 1983, 61, 44.

[7] Kauffman, G. B. The Discovery of Penicillin: Twentieth Century Wonder Drug. *J. Chem. Educ*., 1979, 56, 454.

[8] Strominger, JTP. Mode of Action of Penicillin. *Science*, 1957, 125, 99.

[9] Hartman, BJ; Tomasz, BJA. Low-affinity Penicillin-binding Protein Associated with Beta-lactam Resistance in Staphylococcus Aureus. *Journal of Bacteriology*, 1984, 158, 513.

[10] Pallares, R; Liñares, J; Vadillo, M; Cabellos, C; Manresa, F; Viladrich, PF; Martin, R; Gudiol, F. Resistance to Penicillin and Cephalosporin and Mortality from Severe

Pneumococcal Pneumonia in Barcelona, Spain. *New England Journal of Medicine*, 1995, 333, 474.

[11] Ray, PC; Khan, SA; Singh, AK; Senapati, D; Fan, Z. Nanomaterials for Targeted Detection and Photothermal Killing of Bacteria. *Chem Soc Rev*, 2012, 41, 3193.

[12] Budget Request Summary—Fiscal Year 2015. http://www.cdc.gov/budget.

[13] Salmonella Syndicated Content. http://www.cdc.gov/media/releases/2014/p0326-salmonella-data.html.

[14] Singh, AK; Senapati, D; Wang, S; Griffin, J; Neely, A; Candice, P; Naylor, KM; Varisli, B; Kalluri, JR; Ray, PC. Gold Nanorod Based Selective Identification of Escherichia coli Bacteria Using Two-Photon Rayleigh Scattering Spectroscopy. *ACS Nano*, 2009, 3, 1906.

[15] Boken, J; Dalela, S; Sharma, CK; Kumar, D. Detection of Pathogenic Escherichia coli (E. coli) Using Robust Silver and Gold Nanoparticles. *Journal of Chemical Engineering & Process Technology*, 2013, 04.

[16] Ray, PC; Khan, SA; Fan, Z; Senapati, D. Gold Nanotechnology for Targeted Detection and Killing of Multiple Drug Resistant Bacteria from Food Samples. *In Advances in Applied Nanotechnology for Agriculture*., 2013, 1143, 1.

[17] Pignato, S; Coniglio, MA; Faro, G; Lefevre, M; Weill, FX; Giammanco, G. Molecular Epidemiology of Ampicillin Resistance in Salmonella spp. and Escherichia coli from Wastewater and Clinical Specimens. *Foodborne Pathog. Dis*., 2010, 7, 945.

[18] Allen, HKDJ; Wang, HH; Cloud-Hansen, KA; Davies, J. Call of the Wild: Antibiotic Resistance Genes in Natural Environments. *Nat. Rev. Microbiol*., 2010, 8, 251.

[19] Chiu, CH; Chu, CH; Wang, MH; Yeh, CM; Weill, FX; Chu, C. Detection of Multidrug-Resistant Salmonella Enterica Serovar Typhimurium Phage Types DT102, DT104, and U302 by Multiplex PCR. *J. Clin. Microbiol*, 2006, 44, 2354.

[20] Noble, RT; Weisberg, SB. A Review of Technologies for Rapid Detection of Bacteria in Recreational Waters. IWA Publishing, 2005, 381.

[21] Lim, DV; Simpson, JM; Kearns, EA; Kramer, MF. Current and Developing Technologies for Monitoring Agents of Bioterrorism and Biowarfare. *Clin Microbiol Rev*, 2005, 18, 583.

[22] Yamamoto, Y. PCR in Diagnosis of Infection: Detection of Bacteria in Cerebrospinal Fluids. *Clinical and Vaccine Immunology*, 2002, 9, 508.

[23] Belgrader, P; Benett, W; Hadley, D; Richards, J; Stratton, P; Mariella, R; Milanovich, F. PCR Detection of Bacteria in Seven Minutes. *Science*, 1999, 284, 449.

[24] Zemanick, ET; Wagner, BD; Sagel, SD; Stevens, MJ; Accurso, FJ; Harris, JK. Reliability of Quantitative Real-time PCR for Bacterial Detection in Cystic Fibrosis Airway Specimens. *PLoS One*, 2010, 5, e15101.

[25] Khan, SA; Singh, AK; Senapati, D; Fan, Z; Ray, PC. Targeted Highly Sensitive Detection of Multi-drug Resistant Salmonella DT104 Using Gold Nanoparticles. *Chem Commun*, 2011, 47, 9444.

[26] Rule, KLVP. Surface-Enhanced Resonance Raman Spectroscopy for the Rapid Detection of Cryptosporidium Parvum and Giardia Lamblia. *J. Environ. Sci. Technol*., 2009, 1147.

[27] Wang, YRS; Irudayaraj. Separation and Detection of Multiple Pathogens in a Food Matrix by Magnetic SERS Nanoprobes. *J. Anal. Bioanal. Chem*., 2011, 399, 1271.

[28] Guven, B; Temur, E; Tamer, U; Boyaci, IH. SERS-Based Sandwich Immunoassay Using Antibody Coated Magnetic Nanoparticles for Escherichia coli Enumeration. *Analyst*, 2011, 136, 740.

[29] Vikesland, JW; Wigginton, KR. Nanomaterial Enabled Biosensors for Pathogen Monitoring-A Review. *Environ. Sci. Technol*, 2010, 44, 3656.

[30] Wang, C; Irudayaraj, J. Gold Nanorod Probes for the Detection of Multiple Pathogens. *Small*, 2008, 4, 2204.

[31] Khan, SA; Singh, AK; Senapati, D; Fan, Z; Ray, PC. Bio-conjugated Popcorn Shaped Gold Nanoparticles for Targeted Photothermal Killing of Multiple Drug Resistant Salmonella DT104. *Journal of Materials Chemistry*, 2011, 21, 17705.

[32] Ray, PC. Size and Shape Dependent Second Order Nonlinear Optical Properties of Nanomaterials and Their Application in Biological and Chemical Sensing. *Chem. Rev*., 2010, 110, 5332.

[33] Huang, X; El-Sayed, IH; Qian, W; El-Sayed, MA. Cancer Cell Imaging and Photothermal Therapy in the Near-Infrared Region by Using Gold Nanorods. J. Am. Chem. Soc., 2006, 128, 2115.

[34] Singh, AKLW; Senapati, D; Khan, SA; Fan, Z; Senapati, T; Demeritte, T; Beqa, L; Ray, PC. Long-Range Nanoparticle Surface-Energy-Transfer Ruler for Monitoring Photothermal Therapy Response. *Small*, 2011, 7, 2517.

[35] Lin, Y; Hamme II, AT. Targeted Highly Sensitive Detection/Eradication of Multi-drug Resistant Salmonella DT104 through Gold Nanoparticle-SWCNT Bioconjugated Nanohybrids. Analyst, 2014, 139, 3702.

[36] Garcia-Aljaro, C; Cella, LN; Shirale, DJ; Park, M; Munoz, FJ; Yates, MV; Mulchandani, A. Carbon Nanotubes-based Chemiresistive Biosensors for Detection of Microorganisms. *Biosens Bioelectron*, 2010, 26, 1437.

[37] Wang, S; Li, L; Jin, H; Yang, T; Bao, W; Huang, S; Wang, J. Electrochemical Detection of Hepatitis B and Papilloma Virus DNAs Using SWCNT Array Coated with Gold Nanoparticles. *Biosens Bioelectron*, 2013, 41, 205.

[38] D'Orazio, P. Biosensors in Clinical Chemistry - 2011 Update. *Clin Chim Acta*, 2011, 412, 1749.

[39] Kumar Jena, B; Retna Raj, C. Morphology Dependent Electrocatalytic Activity of Au Nanoparticles. *Electrochemistry Communications*, 2008, 10, 951.

[40] Ali, MR; Snyder, B; El-Sayed, MA. Synthesis and Optical Properties of Small Au Nanorods Using a Seedless Growth Technique. *Langmuir*, 2012, 28, 9807.

[41] Boisselier, E; Astruc, D. Gold Nanoparticles in Nanomedicine: Preparations, Imaging, Diagnostics, Therapies and Toxicity. *Chem Soc Rev*, 2009, 38, 1759.

[42] Huang, TS; Tzeng, Y; Liu, YK; Chen, YC; Walker, KR; Guntupalli, R; Liu, C. Immobilization of Antibodies and Bacterial Binding on Nanodiamond and Carbon Nanotubes for Biosensor Applications. *Diamond and Related Materials*, 2004, 13, 1098.

[43] Jain, S. Development of an Antibody Functionalized Carbon Nanotube Biosensor for Foodborne Bacterial Pathogens. *Journal of Biosensors & Bioelectronics*, 2012, 01.

[44] Heo, J; Hua, SZ. An Overview of Recent Strategies in Pathogen Sensing. Sensors (Basel), 2009, 9, 4483.

[45] Friedman, M. Properties of Wines and Winery Byproducts in Relation to Their Flavonoid Content. *J Agric Food Chem*, 2014.

[46] Fan, Z; Senapati, D; Khan, SA; Singh, AK; Hamme, A; Yust, B; Sardar, D; Ray, PC. Popcorn-shaped Magnetic Core-plasmonic Shell Multifunctional Nanoparticles for the Targeted Magnetic Separation and Enrichment, Label-free SERS Imaging, and Photothermal Destruction of Multidrug-resistant Bacteria. *Chemistry*, 2013, 19, 2839.

[47] DeRussy, BM; Aylward, MA; Fan, Z; Ray, PC; Tandon, R. Inhibition of Cytomegalovirus Infection and Photothermolysis of Infected Cells Using Bioconjugated Gold Nanoparticles. *Sci Rep*, 2014, 4, 5550.

[48] Liu, S; Lin, H; Fang, N; Chang, MW; Xu, R; Yang, YH; Chen, Y. Sharper and Faster "Nano Darts" Kill More Bacteria: a Study of Antibacterial Activity of Individually Dispersed Pristine Single Walled Carbon Nanotube. *ACS Nano*, 2009, 3, 3891.

[49] Beqa, L; Fan, Z; Singh, AK; Senapati, D; Ray, PC. Gold Nano-popcorn Attached SWCNT Hybrid Nanomaterial for Targeted Diagnosis and Photothermal Therapy of Human Breast Cancer Cells. *ACS Appl Mater Interfaces*, 2011, 3, 3316.

[50] Khan, SA; Kanchanapally, R; Fan, Z; Beqa, L; Singh, AK; Senapati, D; Ray, PC. A Gold Nanocage-CNT Hybrid for Targeted Imaging and Photothermal Destruction of Cancer Cells. *Chem Commun (Camb)*, 2012, 48, 6711.

[51] Ag, D; Seleci, M; Bongartz, R; Can, M; Yurteri, S; Cianga, I; Stahl, F; Timur, S; Scheper, T; Yagci, Y. From Invisible Structures of SWCNTs toward Fluorescent and Targeting Architectures for Cell Imaging. *Biomacromolecules*, 2013, 14, 3532.

[52] Wörle-Knirsch, JM; Pulskamp, K; Krug, HF. Oops They Did It Again! Carbon Nanotubes Hoax Scientists in Viability Assays. *Nano Letters*, 2006, 6, 1261.

[53] Sun, Y; Lin, Y; Huang, W. Functionalized Carbon Nanotubes Properties and Applications. *Acc. Chem. Res*., 2002, 35, 1096.

[54] Wu, HC; Chang, X; Liu, L; Zhao, F; Zhao, Y. Chemistry of Carbon Nanotubes in Biomedical Applications. *Journal of Materials Chemistry*, 2010, 20, 1036.

[55] Pal, SKG. Interparticle Coupling Effect on the Surface Plasmon Resonance of Gold Nanoparticles: From Theory to Applications. *Chem. Rev*, 2007, 107, 4797.

[56] Sanchez-Gaytan, BL; Qian, Z; Hastings, SP; Reca, ML; Fakhraai, Z; Park, SJ. Controlling the Topography and Surface Plasmon Resonance of Gold Nanoshells by a Templated Surfactant-Assisted Seed Growth Method. *The Journal of Physical Chemistry C*, 2013, 117, 8916.

[57] Shiotani, A; Akiyama, Y; Kawano, T; Niidome, Y; Mori, T; Katayama, Y; Niidome, T. Active Accumulation of Gold Nanorods in Tumor in Response to Near-Infrared Laser Irradiation. *Bioconjugate Chemistry*, 2010, 21, 2049.

[58] Yamashita, S; Fukushima, H; Niidome, Y; Mori, T; Katayama, Y; Niidome, T. Controlled-release System Mediated by a Retro Diels-Alder Reaction Induced by the Photothermal Effect of Gold Nanorods. *Langmuir*, 2011, 27, 14621.

[59] Dupont, D; Lugand, D; Rolet-Repecaud, O; Degelaen, J. LISA To Detect Proteolysis of Ultrahigh-Temperature Milk upon Storage. *Journal of Agricultural and Food Chemistry*, 2007, 55, 6857.

[60] Lotierzo, M; Abuknesha, R; Davis, F; Tothill, IE. A Membrane-Based ELISA Assay and Electrochemical Immunosensor for Microcystin-LR in Water Samples. *Environmental Science & Technology*, 2012, 46, 5504.

[61] Wen, CY; Hu, J; Zhang, ZL; Tian, ZQ; Ou, GP; Liao, YL; Li, Y; Xie, M; Sun, ZY; Pang, DW. One-step Sensitive Detection of Salmonella Typhimurium by Coupling

Magnetic Capture and Fluorescence Identification with Functional Nanospheres. *Anal Chem*, 2013, 85, 1223.

[62] Rossouw, D; Botton, GA; Najafi, E; Lee, V; Hitchcock, AP. Metallic and Semiconducting Single-Walled Carbon Nanotubes: Differentiating Individual SWCNTs by Their Carbon 1s Spectra. *ACS Nano*, 2012, 6, 10965.

[63] Hirano, A; Tanaka, T; Urabe, Y; Kataura, H. pH- and Solute-Dependent Adsorption of Single-Wall Carbon Nanotubes onto Hydrogels: Mechanistic Insights into the Metal/Semiconductor Separation. *ACS Nano*, 2013, 7, 10285.

[64] Hirano, A; Tanaka, T; Kataura, H. Thermodynamic Determination of the Metal/Semiconductor Separation of Carbon Nanotubes Using Hydrogels. *ACS Nano*, 2012, 6, 10195.

[65] Wang, S; Singh, AK; Senapati, D; Neely, A; Yu, H; Ray, PC. Rapid Colorimetric Identification and Targeted Photothermal Lysis of Salmonella Bacteria by Using Bioconjugated Oval-shaped Gold Nanoparticles. *Chemistry*, 2010, 16, 5600.

[66] Halvorson, RA; Vikesland, PJ. Surface-Enhanced Raman Spectroscopy (SERS) for Environmental Analyses. *Environmental Science & Technology*, 2010, 44, 7749.

[67] Shaw, CP; Fan, M; Lane, C; Barry, G; Jirasek, AI.; Brolo, AG. Statistical Correlation Between SERS Intensity and Nanoparticle Cluster Size. *The Journal of Physical Chemistry C*, 2013, 117, 16596.

[68] Wang, Y; Yan, B; Chen, L. SERS Tags: Novel Optical Nanoprobes for Bioanalysis. Chemical Reviews, 2012, 113, 1391.

[69] Feng, L; Wang, C; Lu, X; Li, XF; Chris, LX. Detection of Escherichia coli O157:H7 Using Gold Nanoparticle Labeling and ICPMS. *Anal. Chem*. 2010, 82, 3399.

[70] Katrin, Q; Alfredo, RV; Marco, AC; Ernestina, CL. SERS Properties of Different Sized and Shaped Gold Nanoparticles Biosynthesized under Different Environmental Conditions by Neurospora crassa Extract. *Plos One*, 2013, 8, 1.

[71] Knauer, M; Ivleva, PN; Liu, XJ; Niessner, R; Haisch, C. Surface-Enhanced Raman Scattering-Based Label-free Microarray Readout for the Detection of Microorganisms. *Anal. Chem*, 2010, 82, 2766.

[72] Moskovits, M. Surface-Enhanced Raman Spectroscopy: A Brief Retrospective. *J. Raman Spectrosc*, 2005, 36, 485.

[73] Schütz, MSD; Salehi, M; Kömpe, K; Schlücker, S. Hydrophilically Stabilized Gold Nanostars as SERS Labels for Tissue Imaging of the Tumor Suppressor p63 by Immuno-SERS Microscopy. *Chem. Com*, 2011, 47, 4216.

[74] Pazos-Pérez, NBS; Rodríguez-Lorenzo, L; Aldeanueva-Potel, P; Pérez-Juste, J; Pastoriza-Santos, I; Alvarez- Puebla, RA; Liz-Marzán, LM. Growth of Sharp Tips on Gold Nanowires Leads to Increased SERS Activity. *J. Phys. Chem. Lett.*, 2010, 1, 24.

[75] Rodríguez-Lorenzo, LAP; Pastoriza-Santos, I; Mazzucco, S; Stéphan, O; Kociak, M; Liz-Marzán, LM; Garcia de Abajo, FJ. Zeptomol Detection Through Controlled Ultrasensitive Surface-Enhanced Raman Scattering. *J. Am. Chem. Soc.*, 2009, 131, 4616.

[76] Guerrero-Martinez, ABS; Pastoriza-Santos, I; Liz- Marzán, LM. Nanostars Shine Bright for You: Colloidal Synthesis, Properties and Applications of Branched Metallic Nanoparticles. *Curr. Opin. Colloid Interface Sci*, 2011, 16, 118.

[77] Barbosa, SA; Rodríguez-Lorenzo, L; Pastoriza- Santos, I; Alvarez-Puebla, RA; Kornowski, A; Weller, H; Tuning Size and Sensing Properties in Colloidal Gold Nanostars. Liz- Marzán, L. M. Langmuir, 2010, 14943.

[78] Huang, YS; Bishnoi, SW. Rapid Raman Imaging of Stable, Functionalized Nanoshells in Mammalian Cell Cultures. *Nano Lett*, 2009, 9, 2914.

[79] Bosnick, KAJJ; Brus, LE. Fluctuations and Local Symmetry in Single-Molecule Rhodamine 6G Raman Scattering on Silver Nanocrystal Aggregates. *J. Phys. Chem. B*, 2002, 106, 8096.

[80] Wang, YB; Chen, L. SERS Tags: Novel Optical Nanoprobes for Bioanalysis. *Chem. Rev*., 2013, 113, 1391.

[81] Cui, YRB; Yao, JL; Gu, RA; Tian, ZQ. Synthesis of Ag core Au shell Bimetallic Nanoparticles for Immunoassay Based on Surface-Enhanced Raman Spectroscopy *J. Phys. Chem. B*, 2006, 110, 4002.

[82] Lan, Y; Wang, S; Yin, Y; Hoffmann, WC; Zheng, X. Using a Surface Plasmon Resonance Biosensor for Rapid Detection of Salmonella Typhimurium in Chicken Carcass. *Journal of Bionic Engineering*, 2008, 5, 239.

[83] Waswa, JW; Irudayara, CD. Rapid Detection of Salmonella enteritidis and Escherichia coli Using Surface Plasmon Resonance Biosensor. *Journal of Food Process Engineering*, 2006, 29, 373.

[84] Leevy,WM; Johnson, JR; Morris. J; Smith, BD. Quantum Dot Probes for Bacteria Distinguish Escherichia coli Mutants and Permit in Vivo Imaging. *Chem. Commun*., 2008, 2331.

[85] Cheng, Y; Huang, YL; Li, K; Zhang, W; Xian, Y; Jin, L. Combining Biofunctional Magnetic Nanoparticles and ATP Bioluminescence for Rapid Detection of Escherichia coli. *Talanta*, 2009, 1332.

[86] Zhao, LR; Mechery, YP; Wang, RP; Bagwe, SG; Jin, SG; Tan, WH. A Rapid Bioassay for Single Bacterial Cell Quantitation Using Bioconjugated Nanoparticles. *Proc. Natl. Acad. Sci. U. S. A*., 2004, 101, 15027.

[87] Zhao, Y; Cao, MY; Jia, N; Yu, G; Shen, HJ. Simultaneous Detection of Multifood-borne Pathogenic Bacteria Based on Functionalized Quantum Dots Coupled with Immunomagnetic Separation in Food Samples. *Agric. Food Chem*., 2009, 57, 517.

[88] Yu, C; Jain, H; Pantano, CG; Irudayaraj, J. Biofunctionalized Magnetic Nanoparticle Integrated Mid-infrared Pathogen Sensor for Food Matrixes. *Anal. Chem*., 2009, 81, 2840.

[89] Zelada-Guille, GA; Rius, FX. Immediate Detection of Living Bacteria at Ultralow Concentrations Using a Carbon Nanotube Based Potentiometric Aptasensor. *Angew. Chem., Int. Ed*., 2009, 48, 7334.

[90] Lin, YS; Weng, MF; Chen, YC. Affinity Capture Using Vancomycin-Bound Magnetic Nanoparticles for the MALDI-MS Analysis of Bacteria. *Anal. Chem*., 2005, 77, 1753.

[91] Huang, S. H. Gold Nanoparticle-based Immunochromatographic Test for Identification of Staphylococcus aureus from Clinical Specimens. *Clin. Chim. Acta*, 2006, 373, 139.

[92] Wang, YD; Li, Y; Li, D; Sun, R. Fluorescent Identification and Detection of Staphylococcus aureus with Carboxymethyl Chitosan/CdS Quantum Dots Bioconjugates. *J. Biomater. Sci., Polym. Ed.*, 2011, 22, 1881.

[93] Wang, R; Kanayeva, D; Lassiter, K; Li, Y. TiO2 Nanowire Bundle Microelectrode Based Impedance Immunosensor for Rapid and Sensitive Detection of Listeria monocytogenes. *Nano Lett*., 2008, 8.

[94] Yang, H; Lin, Y; Jiang, XP; Sun, YP. Detection of Listeria monocytogenes in Biofilms Using Immunonanoparticles. *J. Biomed. Nanotechnol.*, 2007, 3, 131.

[95] Abeylath, SC; Turos, E. Drug Delivery Approaches to Overcome Bacterial Resistance to Beta-lactam Antibiotics. Expert Opin. *Drug Delivery*, 2008, 5, 931.

[96] Dickerson, EB; Dreaden, EC; Huang, X; El-Sayed, IH; Chu, H; Pushpanketh, S; McDonald, JF; El-Sayed, MA. Gold Nanorod Assisted Near-infrared Plasmonic Photothermal Therapy (PPTT) of Squamous Cell Carcinoma in Mice. *Cancer Lett*, 2008, 269, 57.

[97] Kang, S; Pinault, M; Pfefferle, LD; Elimelech, M. Single-Walled Carbon Nanotubes Exhibit Strong Antimicrobial Activity. Langmuir, 2007, 23, 8670.

[98] Dong, L; Henderson, A; Field, C. Antimicrobial Activity of Single-Walled Carbon Nanotubes Suspended in Different Surfactants. *Journal of Nanotechnology*, 2012, 2012, 1.

[99] Dong, X; Tang, Y; Wu, M; Vlahovic, B; Yang, L. Dual Effects of Single-walled Carbon Nanotubes Coupled with Near-infrared Radiation on Bacillus anthracis Spores: Inactivates Spores and Stimulates the Germination of Surviving Spores. *Journal of Biological Engineering*, 2013, 7, 1754.

[100] Zharov, VP; Mercer, KE; Galitovskaya, EN; Smeltzer, MS. Photothermal Nanotherapeutics and Nanodiagnostics for Selective Killing of Bacteria Targeted with Gold Nanoparticles. *Biophys J*, 2006, 90, 619.

[101] Sean, NR; Anand, GJ; Catherine, J; Tara, LS. Targeted Photothermal Lysis of the Pathogenic Bacteria, Pseudomonas aeruginosa, with Gold Nanorods. *Nano Letters*, 2008, 8, 302.

[102] Huang WC; Chen, YC. Multifunctional Fe_3O_4@Au Nanoeggs as Photothermal Agents for Selective Killing of Nosocomial and Antibiotic-resistant Bacteria. *Small*, 2009, 5, 51.

In: Food Poisoning
Editor: Paresh C. Ray
ISBN: 978-1-63463-166-2

Chapter 9

DETECTION OF MELAMINE FROM FOOD IN PARTS PER QUADRILLION LEVEL USING FUNCTIONALIZED GRAPHENE OXIDE- GOLD NANOPARTICLE HYBRID SERS PLATFORM

Rajashekhar Kanchanapally, Zhen Fan, Willie Wesley, Bhanu Priya Viraka Nellore, Rebecca A. Crouch, Sudarson Sekhar Sinha, Avijit Pramanik, Suhash Reddy Chavva and Paresh C. Ray*

Department of Chemistry and Biochemistry, Jackson State University, Jackson, MS, US

ABSTRACT

Excellent SERS platform has the ability for ultra-sensitive chemical toxin sensing and providing its fingerprint. Melamine can form insoluble crystals in the kidney, which may cause renal failure and even death of the child. As a result, it is very important to develop a reliable and highly sensitive sensor that can provide on-site and real-time detection of melamine. Driven by the need, in the current chapter we report the chemically stable highly efficient SERS platform using functionalized graphene oxide-plasmonic gold nanoparticle hybrid. Experimental data with melamine show that the SERS enhancement factor for the hybrid platform is about two orders of magnitude higher than only nanoparticle. Our results demonstrate that in hybrid SERS platform, graphene oxide will enhance the SERS signal via chemical enhancement and the nano-popcorn will enhance the SERS signal via electromagnetic enhancement. We show that hybrid SERS platform can be used for highly selective and ultra-sensitive detection of melamine in parts per quadrillion level. Our reported results provide a good approach for developing ultra-sensitive SERS platform for toxin chemical detection and analysis.

* Corresponding author: E-mail:paresh.c.ray@jsums.edu; Fax: +16019793674.

1. INTRODUCTION

Graphene oxide (GO) is chemically treated graphene, which has emerged as a potential alternative to grapheme for sensing applications [1-6]. Functional groups such as −OH, −COOH, and epoxide along with structural defects serve as anchoring points for developing hybrid GO with selective functionality [7-16]. GO can be further modified with plasmonic metal nanoparticles to form hybrid graphene oxide for sensing applications [17-22]. Recently it has been reported that graphene can provide a surface-enhanced Raman spectroscopy (SERS) platform for studying the chemical enhancement [23-35]. SERS has the ability to detect single molecule and can be used as chemical fingerprint [36-50]. It is commonly believed that two primary mechanisms which are long-range electromagnetic (EM) enhancement and short-range chemical (CM) enhancement are very important for the SERS enhancement [14-16,45-51]. Since the surface plasmon on graphene is in the range of terahertz rather than in the visible range, scientists believe that graphene or graphene oxide does not support electromagnetic enhancement for SERS [26-41]. On the other hand, graphene has the ability to undergo π–π stacking with aromatic molecules due to the interconnected sp^2 network [5-10]. As a result, graphene oxide can be used as an excellent substrate for the SERS chemical enhancement. As we and other groups have reported that the main contribution of SERS enhancement is the electromagnetic enhancement, excellent SERS platform should possess strong EM and CE enhancement capability for providing enough sensitivity [14-23]. In this book chapter we report functionalized graphene oxide-gold nanoparticle hybrid SERS plastform, as shown in Scheme 1, with ultar-sensitive melamine sensing capability. In our design, due to the presence of large surface area and very high aspect ratio, graphene oxide will be useful as a flat SERS substrate. It will enhance the Raman signal via CE mechanism. On the other hand, nanoparticle provides several orders of magnitude enhancement of the electromagnetic field via electromagnetic enhancement [44-49]. Also, metal nanoparticles are in close contact on graphene oxide surafec, which generates "hot" sites to enhance the local E-fields. Nanoparticle also has capability to be used as reactive sites for the binding with cysteamine for selective detection of melamine.

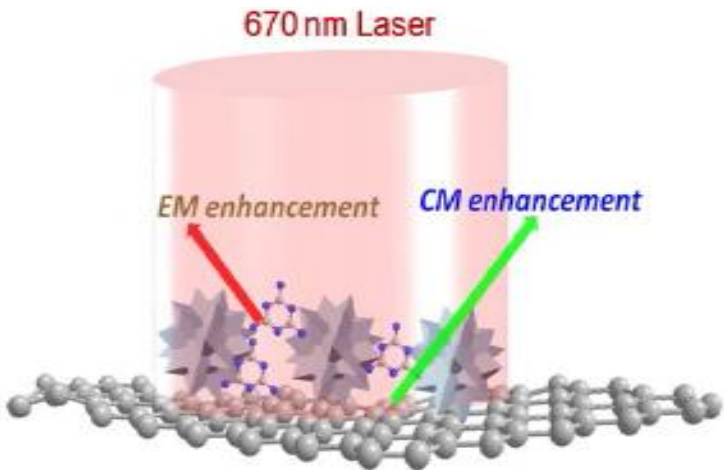

Scheme 1. The schematic representation shows plasmonic grapheme oxide based SERS platform for tuning electromagnetic and chemical enhancement simultaneously.

1,3,5-triazine-2,4,6-triamine, known as melamine, can facilitate polymerization through reaction with formaldehyde to form a heat-tolerant, fire-resistant resin [52-57]. As a result, melamine has been used extensively for the manufacturing of tableware, kitchen utensils, flame retardants and laminated surfaces. Due to its very high proportion of nitrogen, since last few years, unfortunately, melamine has been illegally used in milk, infant formulas, frozen yogurt and animal foods to increase the measured protein content [52-57]. Since melamine can form insoluble crystals in the kidney, which may cause renal failure and even death of the child, recently Food and Drug Administration (FDA) implement that baby foods should not contain any dose of melamine [55-57]. Driven by the need, here we report for the first time hybrid graphene oxide based SERS platform for the detection of melamine in parts per quadrillion (PPQ) level. As per our knowledge, our assay represents the most sensitive reported assay for melamine detection. To demonstrate that plasmonic graphene oxide based SERS assay developed by us can be used for the detection of melamine from food sample, we have tested melamine contaminated milk and baby formula.

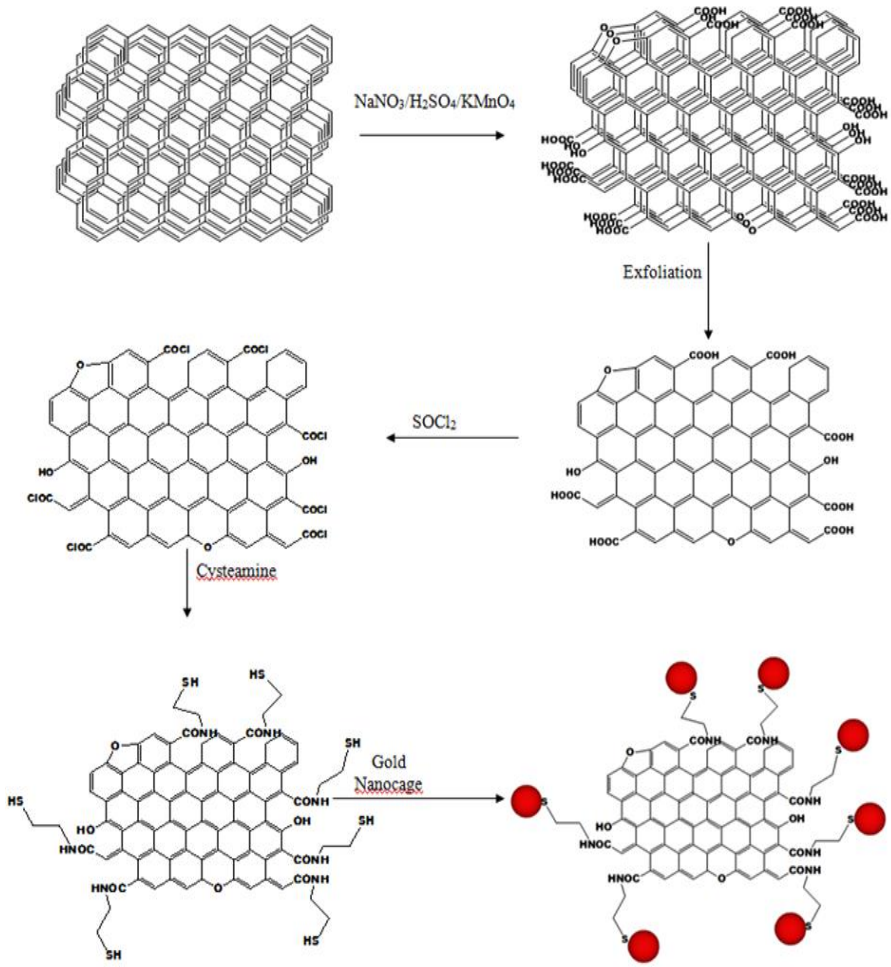

Scheme 2. Schematic representation showing our synthesis procedure to develop functionalized graphene oxide-gold nanoparticle hybrid SERS platform.

2. MATERIALS AND EXPERIMENTS

Hydrogen tetrachloroaurate ($HAuCl_4 \cdot 3H_2O$), $NaBH_4$, sodium citrate, cystamine dihydrochloride, melamine, graphite, and cetyl trimethylammonium bromide (CTAB) were purchased from Sigma-Aldrich and used without further purification.

2.1. Synthesis and Characterization of the Hybrid SERS Platform

Graphene oxide attached gold nanoparticle was synthesized via a four-step process, as shown in Scheme 2. In the first step, we have used graphite exfoliation by strong oxidizing agents to yield graphene oxide. For this purpose, we have used modified Hummers reported the method [14-16]. In brief, 1g of graphite powder was added to 1g of $NaNO_3$ in 45 mL of H_2SO_4 and was stirred in an ice bath. Then 3g of $KMnO_4$ was added very carefully, without changing the temperature. Then we have kept the reaction mixture container in a water bath, which is at 35 °C and then it was stirred for 30 minutes. A thick paste was obtained. After that, we have added 45 mL of water very carefully, drop by drop. During addition of water, the temperature increased to around 95 to 98 ° C. We have added another 140 mL of water. Then we waited for 30 more minutes. Then we filtered and re-dispersed the obtained graphene oxide in 100 mL of water. At the end, we have done sonication for 1 hr for exfoliation.

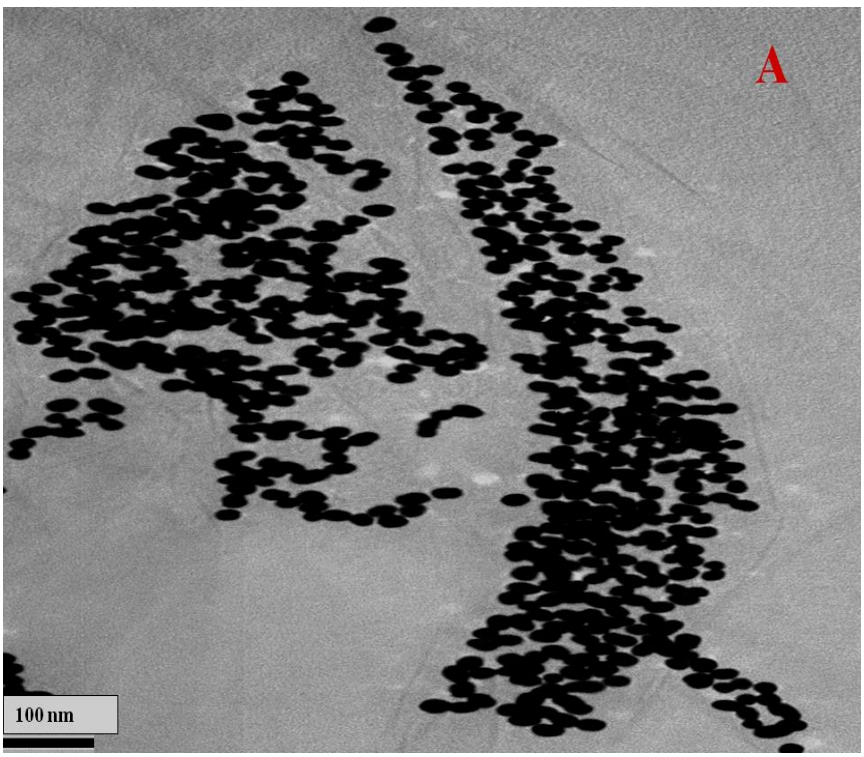

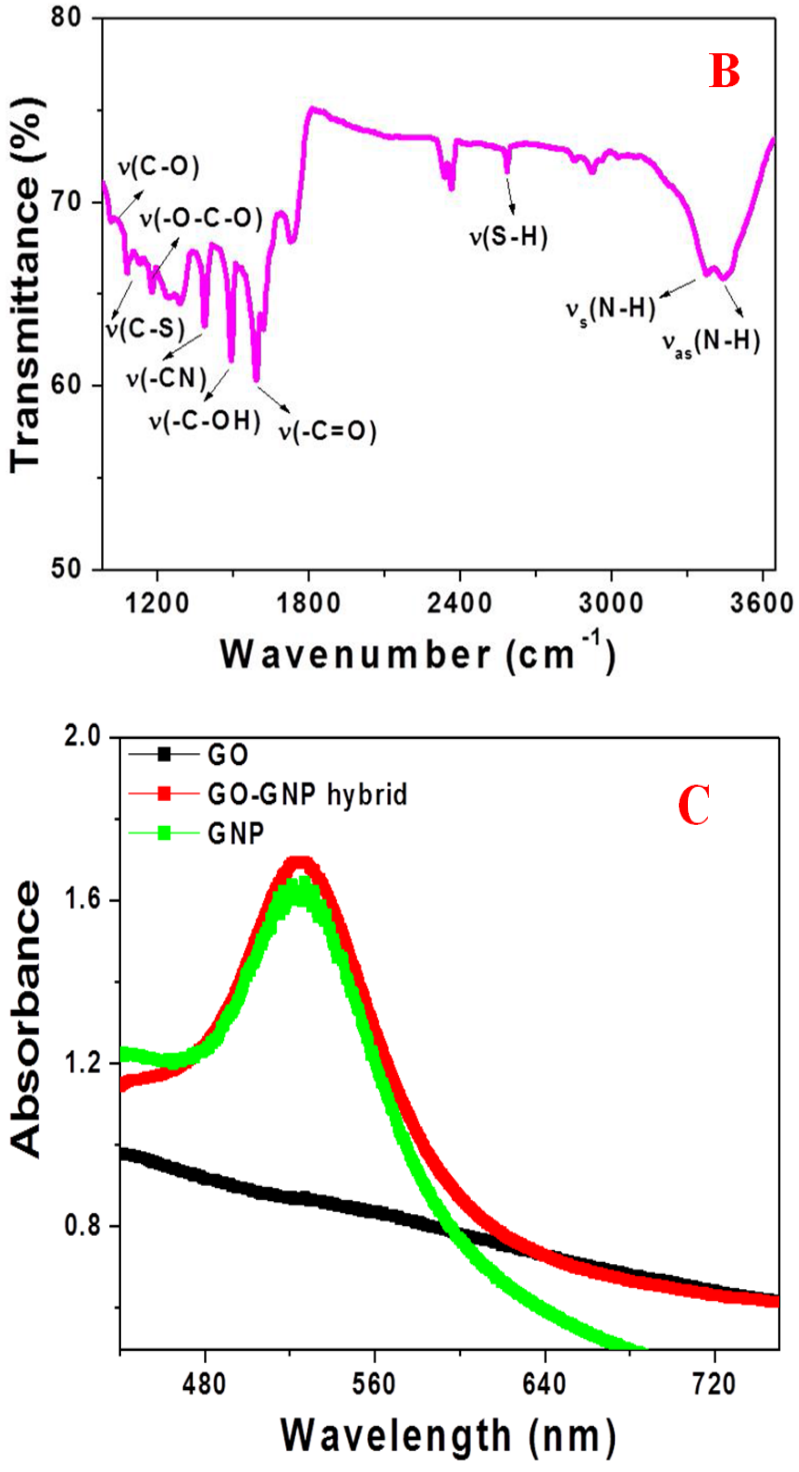

Figure 1. (Continued)

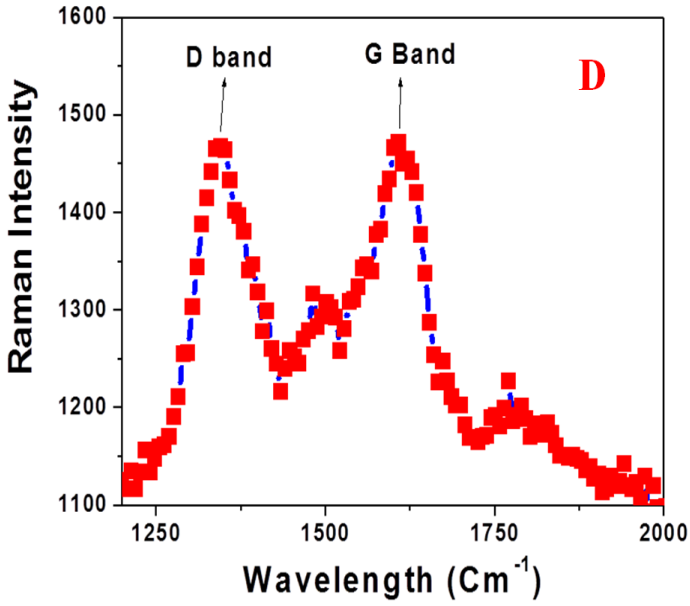

Figure 1. A) TEM picture shows the morphology of hybride graphene oxide, where graphene oxide has been attached with nanopoparticle. B) FTIR spectra of cysteamine modified grapheme oxide. Our FTIR spectra verifies the existence of epoxy groups, -OH and –COOH group. It also verifies the existence of –SH, -CS, -CN and –NH, group due to the formation of the bond between graphene oxide and cysteamine. C) Extinction spectra of gold nanoparticle, graphene oxide and hybrid graphene oxide. D) SERS spectra showing graphene oxide D-band at ~1350 cm^{-1} and G-band at ~1598 cm^{-1} in the presence of nanoparticle.

Then we have performed FTIR experiment to characterize grapheme oxide. Our FT-IR data, as shown in the Figure 1, verified the existence of epoxy groups in grapheme oxide at 1040 cm^{-1} for $\nu_{C\text{-}O}$ and 1250 cm^{-1} for $\nu_{O\text{-}C\text{-}O}$. The FT-IR spectra also demonstrates the formation of –OH and –COOH group and as a result, we observed clear peak at 1380 cm^{-1} which can be assigned to C-OH vibrational mode, the next peak at 1680 cm^{-1} corresponds to the vibrational mode of the ketone (-C=O) group. Next, we have attached spherical gold nanoparticle with graphene oxide. For this purpose, at first we have synthesized gold nanoparticles of 30 nm in size were by using HAuCl4, 3H2O and ascorbic acid as we have reported before [14-16]. In the next step, graphene oxide was attached with gold nanoparticle via p-amino thiophenol. For this purpose, acid chloride functionalized graphene oxide were prepared by treating –COOH functionalized graphene oxide with thionyl chloride in the presence of DMF catalyst under an argon medium. And then, the acid chloride group was used as a chemical anchor for further derivatization with cysteamine. As shown in the Figure 1B, the FTIR spectra of cysteamine modified graphene oxide shows the clear characteristic peaks for aminothiophenol and these are -SH and -CS stretching vibrations at 2524 cm^{-1} and 1088 cm^{-1} respectively. The absorption peak at 1306 cm^{-1} is a -CN stretching vibration. The 3448 cm^{-1} peak is an -NH asymmetrical stretching vibration and the one at 3359 cm^{-1} is the symmetrical stretching vibration of -NH. Since free thiol group is available for linkage with gold nanoparticle though Au-S bond, at the end, gold nanoparticles were attached to graphene oxide via –SH linkage. Transmission electron microscopy (TEM, JEM-2100F instrument),

UV-visible absorption spectroscopy and SERS spectroscopy were used to characterize the hybrid graphene oxide.

Figure 1A shows the TEM picture of gold nanoparticle conjugated graphene oxide. Our data show that the gold nanoparticles are nicely decorated on graphene oxide sheet. Figure 1C shows the absorption spectra of only graphene oxide, only gold nanoparticle and nanoparticles attached graphene oxide. Broad and structureless absorption spectrum for graphene oxide from near-infrared and visible region from 420 to 750 nm is mainly due to the E_{11} and E_{22} transition [1-8]. As shown in Figure 1C, gold nanoparticle exhibits a strong long wavelength plasmon band around 520 nm and it is due to the oscillation of the conduction band electrons [10-16]. When we attached the gold nanoparticle with graphene oxide, the absorption spectrum seems like from the mixture of both, as shown in Figure 1C. As shown in the Figure 1D, there was no significant structural change of the carbon framework during the chemical processing from grapheme oxide to gold nanoparticle attached grapheme oxide. The Raman spectrum of graphene oxide displays a D-band at ~1350 cm^{-1} and a G-band at ~ 1598 cm^{-1}.

2.2. SERS Measurement

For the SERS experiment, we have portable SERS probe, as we have reported recently [36-38]. In brief, we have used a continuous wavelength DPSS laser from laser glow technology (LUD-670) operating at 670 nm, as an excitation light source. InPhotonics 670 nm Raman fiber optic probe was used for excitation and data collection. It is a combination of 90 µm excitation fiber and 200 µm collection fiber with filtering and steering micro-optics. To collect SERS data, we have used miniaturized QE65000 scientific-grade spectrometer from Ocean Optics and Ocean Optics data acquisition Spectra Suite spectroscopy software. For the SERS measurement, at first, different concentrations of analyte were added to hybrid gaphene oxide solution and then it was transferred into a small eppendorf cap. After that, the sample inside the eppendorf cap was exposed to the 670 nm laser light and the scattering signal was collected with 10 sec acquisition time and 5 scan averaging. Laser power was kept at 2 mW for the entire experiment.

3. RESULTS AND DISCUSSION

For the selective detection of melamine we have modified the nanoparticle attached graphene oxide with cysteamine. It is well known that melamine forms molecular self-assembly using strong hydrogen bonding with cysteamine via $–NH_2$ groups. As a result, in the presence of melamine, cysteamine modified gold nanoparticle attached graphene oxide will form self assembly with melamine. As shown in Figure 1, our experimental data clearly show strong melamine SERS peak even at 300 parts per quadrillion (ppq) melamine level. All the observed melamine SERS peaks can be characterized using reported Raman data [55-57]. The most intense peak in our SERS spectrum is observed at 725 cm^{-1} and it can be assigned to the in-plane ring breathing II mode. The peak around 1040 cm^{-1} can be attributed due to the enhanced ring breathing mode of the pyridinium head group. The second SERS peak is at

1626 cm^{-1} and is identified with the ring stretching vibration. The CH_2 twisting vibration at 1338 cm^{-1} has combined with 1349 cm^{-1} D band of grapheme oxide. Our SERS spectra also show strong CH_2-scissoring vibration at 1450 cm^{-1}. We have also observed ring stretching band at 1620 cm^{-1}, which has also combines with 1603 cm^{-1} G band of grapheme oxide. The Raman enhancement, *G*, is measured experimentally by direct comparison as shown below [26-40].

$$G=[I_{SERS}]/[I_{Raman}]\times[M_{bulk}]/[M_{ads}] \quad (1)$$

Where I_{SERS} is the intensity of a 725 cm^{-1} vibrational mode in the surface-enhanced spectrum in the presence of hybrid graphene oxide, and I_{Raman} is the intensity of the same mode in the bulk Raman spectrum from only melamine. M_{bulk} is the number of molecules used in the bulk, M_{ads} is the number of molecules adsorbed and sampled on the SERS-active substrate. All spectra were normalized for the integration time. An enhancement factor estimated from the SERS signal and normal Raman signal ratio for 725 cm^{-1} band is approximately 4.8×10^{10} in case of hybrid material and 2.3×10^{8} for gold nanoparticle. We have not observed any melamine Raman spectra in the presence of graphene oxide. Figure 2A clearly shows that hybrid graphene oxide based SERS platform is about two orders of magnitude more sensitive than only gold nanoparticle. This extremely high sensitivity is due to the fact that, in our hybrid SERS platform, graphene oxide enhances the SERS signal via chemical enhancement and the gold nanoparticles enhance the SERS signal via electromagnetic enhancement.

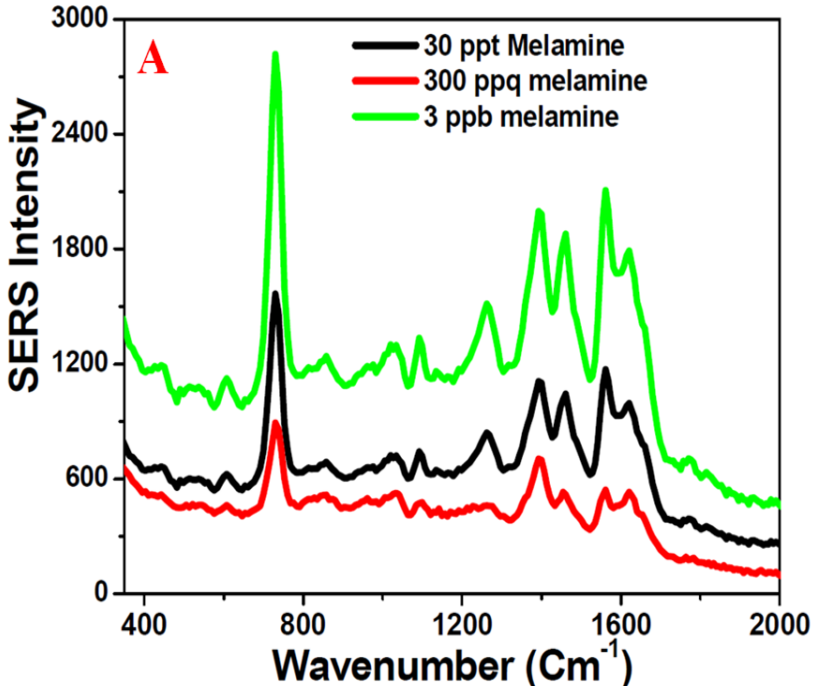

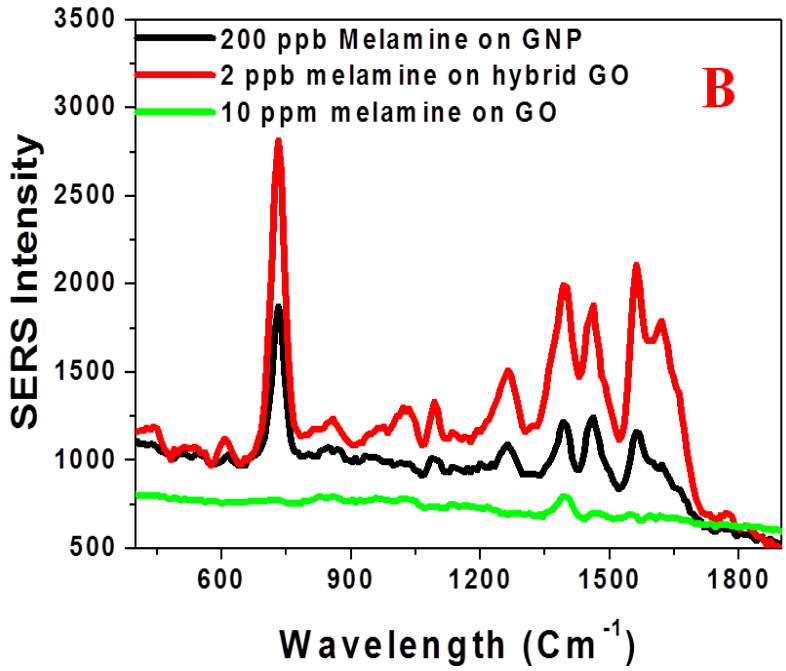

Figure 2. A) Plot showing SERS enhancement of the Raman signal at 670 nm excitation from melamine at different concentrations, in the presence of hybrid graphene oxide based SERS platform. Our SERS spectra show that one can detect melamine even at 300 ppq level. B) Plot showing SERS enhancement of the Raman signal from melamine, in the presence of graphene oxide, gold nanoparticle and hybrid graphene oxide.

Also, in hybrid graphene oxide metal nanoparticles are in close contact as shown in Figure 1A, which generates "hot" sites to enhance the local E-fields tremendously. When two nanoparticles are in close to each other, the polarization direction of the E-field is along the axis of the two particles. As a result, the local E-field in the gap can be further enhanced under the resonance condition. As we all know, reproducibility and stability of SERS signals from a SERS-active probe are highly important properties for sensor application. To monitor reproducibility, we have performed SERS spectra from melamine with hybrid SERS probe made in different batches. Figure 3A clearly shows that SERS reproducibility using our probe is excellent.

To evaluate the sensitivity of our plasmonic graphene oxide SERS substrate based assay, different concentrations of melamine from one stock solution were evaluated. As shown in Figure 2A, our experimental data indicate that plasmonic graphene oxide based SERS assay is highly sensitive for the detection of melamine and the sensitivity can be as low as 300 ppq melamine, which is the most sensitive reported SERS assay for the label-free detection of melamine.

Next, to determine whether our SERS assay can be used for the detection of melamine from real life sample, we have performed melamine detection from melamine contaminated milk and infant formula powder. Before testing the milk powder, we have tested the presence of possible interference such as Ca^{2+}, K^{+}, Na^{+}, Mg^{2+}, methionine, serine, vitamins B and C. For this purpose, we have performed the SERS experiment in the presence 1 ppb of each

interference together. As shown in the Figure 2B, SERS signal change is very little (<5%) in the presence of interferences. For the detection of melamine from melamine contaminated infant formula, at first 1% trichloroacetic acid and 10 mL of acetonitrile were added to melamine contaminated milk to precipitate proteins. After that we have performed 15 min of sonication and then heated at 100 °C by a water bath to promote the coagulation of proteins. Then we have filtered using PTFE membrane. At the end, the residue was dissolved and the SERS experiment was performed. As shown in Figure 3C, our results clearly show that one can detect melamine from melamine contaminated milk product even at the concentration of 50 ppt. We have also tested the detection limit and our experimental data indicate that the detection limit can be as low as 800 ppq from the milk product.

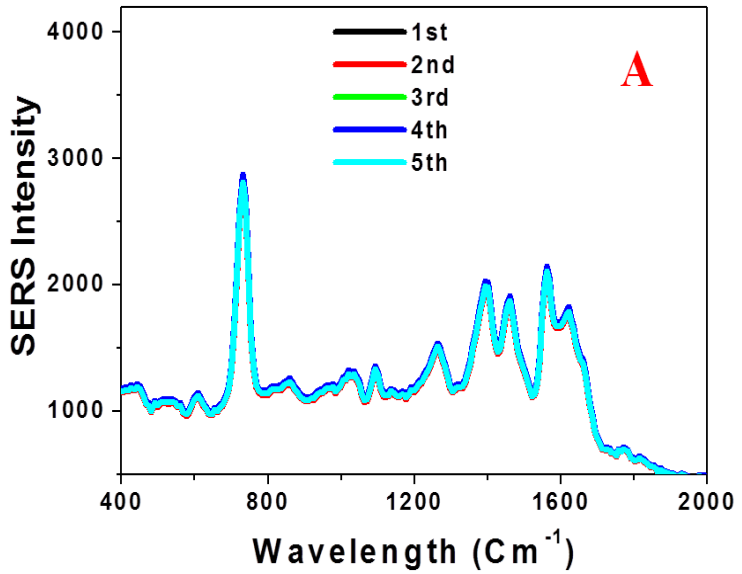

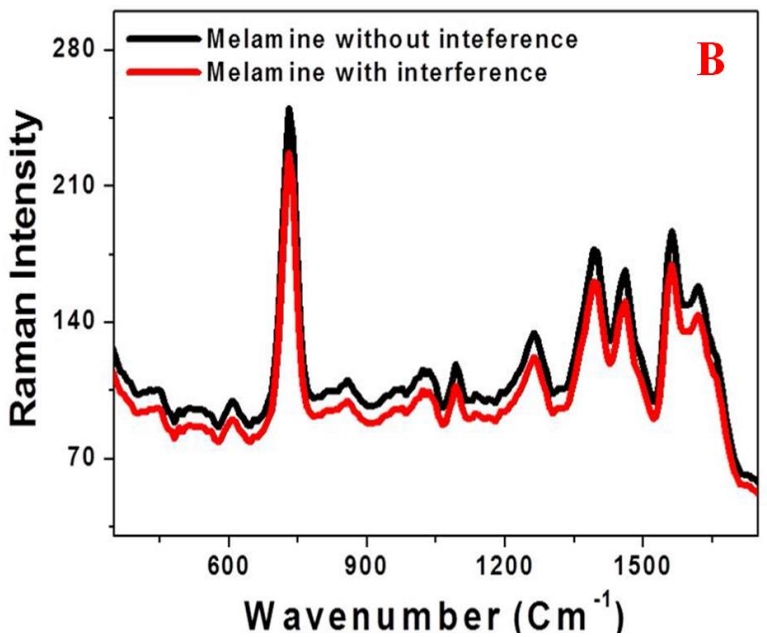

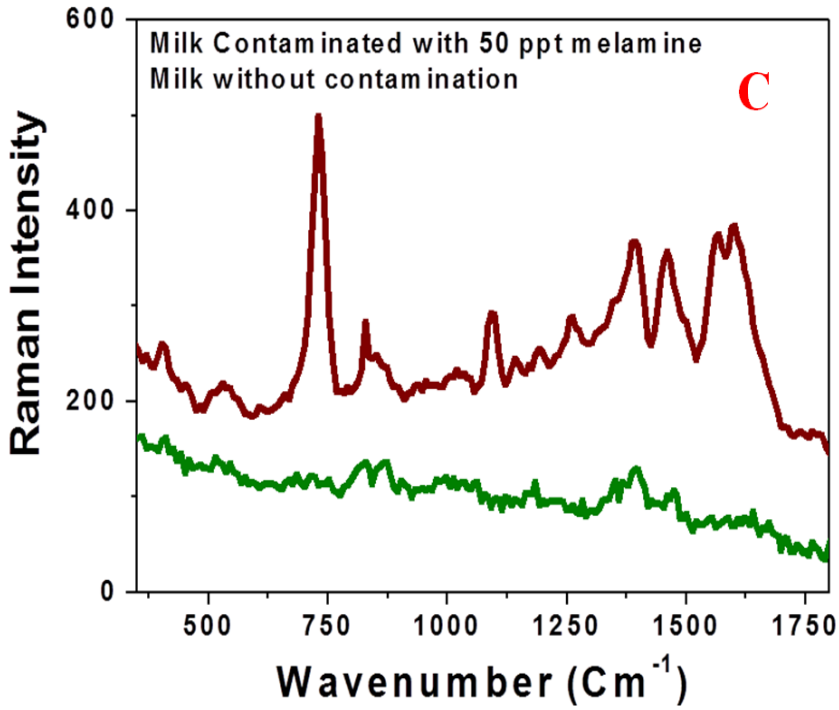

Figure 3. A) SERS spectra from melamine on hybrid graphene oxide based SERS platform made in different batches. SERS spectra show excellent reproducibility. B) Plot shows how SERS intensity varies in the presence of interferences. C) Melamine SERS signal from melamine contaminated infant formula.

CONCLUSION

In conclusion, in this manuscript, we have reported hybrid garphene oxide based SERS platform for the ultra-sensitive detection of melamine and the sensitivity of the assay can be as low as 300 ppq. In the reported SERS platform, graphene oxide enhances the SERS signal via chemical enhancement and the gold nanoparticles enhance via electromagnetic enhancement, by forming 'hot sites". Our result using melamine demonstrated that the SERS enhancement factor for hybrid graphene oxide is about two orders of magnitude higher than only nanoparticle. We have also shown that it can be used as an excellent SERS substrate for the ultra-sensitive melamine detection from melamine contaminated milk product. We believe that, ultimately this plasmonic graphene based assay could have enormous potential applications in rapid on-site screening of melamine in food samples.

ACKNOWLEDGMENTS

Dr. Ray thanks NSF-PREM grant # DMR-1205194 grant for their generous funding.

REFERENCES

[1] Geim, AK; Novoselov, KS. The Rise of Graphene, *Nat. Mater*., 2007, 6, 183– 191.

[2] Lightcap, IV; Kamat PV. Graphitic Design: Prospects of Graphene-Based Nanocomposites for Solar Energy Conversion, Storage, and Sensing, *Acc. Chem. Res.*, 2013, Articles ASAP.

[3] Kamat, PV. Graphene-Based Nanoarchitectures. Anchoring Semiconductor and Metal Nanoparticles on a Two-Dimensional Carbon Support, *J. Phys. Chem. Lett.*, 2010, 1, 520–527.

[4] Li, X; Wang, X; Zhang, L; Lee, S; Dai, H. Chemically Derived, Ultrasmooth Graphene Nanoribbon Semiconductors, *Science*., 2008, 319, 1229– 1232.

[5] Gao, W; Alemany, LB; Ci, L; Ajayan, PM. New Insights into the Structure and Reduction of Graphite Oxide, *Nat. Chem*., 2009, 1, 403– 408.

[6] Hossain, MZ; Johns, JE; Bevan, KH; Karmel, HJ; Liang, YT; Yoshimoto, S; Mukai, K; Koitaya, T; Yoshinobu, J; Kawai, M; Lear, AM; Kesmodel, LL; Tait, SL; Hersham, MC. Chemically Homogeneous and Thermally Reversible Oxidation of Epitaxial Graphene *Nat. Chem.*, 2012, 4, 305– 309.

[7] Dreyer, DR; Park, S; Bielawski, CW; Ruoff, RS. The Chemistry of Graphene Oxide *Chem. Soc. Rev.*, 2010, 39, 228–240.

[8] Lightcap, IV; Kosel, TH; Kamat, PV. Anchoring Semiconductor and Metal Nanoparticles on a 2-Dimensional Catalyst Mat. Storing and Shuttling Electrons with Reduced Graphene Oxide, *Nano Lett.*, 2010, 10, 577– 583.

[9] Bagri, A; Mattevi, C; Acik, M; Chabal, YJ; Chhowalla, M; Shenoy, VB. Structural Evolution During the Reduction of Chemically Derived Graphene Oxide *Nat. Chem.*, 2010, 2, 581– 587.

[10] Zhu, Y; Sun, Z; Yan, Z; Jin, Z; Tour, JM. Rational Design of Hybrid Graphene Films for High Performance Transparent Electrodes, *ACS Nano.*, 2011, 5, 6472– 6479.

[11] Robinson, JT; Tabakman, SM; Liang, Y; Wang, H; Casalongue, SH; Vinh, D; Dai, H. Ultrasmall Reduced Graphene Oxide with High Near-Infrared Absorbance for Photothermal Therapy, *J. Am. Chem. Soc.*, 2011, 133, 6825– 6831.

[12] Liu, Z; Robinson, JT; Sun, X; Dai, H; Wang, Y; Li, Z; Hu, D; Lin, C.T; Li, J; Lin, Y. Aptamer/Graphene Oxide Nanocomplex for *in Situ* Molecular Probing in Living Cells, *J. Am. Chem. Soc.*, 2010, 132, 9274– 9276.

[13] Hummers, WS; Offeman, R.E. Preparation of Graphitic Oxide, *J. Am. Chem. Soc.* 1958, 80, 1339– 1339.

[14] Fan, Z; Kanchanapally R; Ray, PC; Hybrid Graphene Oxide Based Ultrasensitive SERS Probe for Label-Free Biosensing, *J. Phys. Chem. Lett.*, 2013, 4, 3813.

[15] Kanchanapally, R; Sinha SS; Fan, Z; Dubey, M; Zakar, E; Ray, PC. Graphene Oxide-Gold Nanocage Hybrid for Trace Level Identification of Nitro Explosives Using Raman Fingerprint. *J. Phys. Chem. C.*, 2014, 4, 7070-7075.

[16] Pramanik, A; Chavva, SR; Fan, Z; Sinha, S; Nellore, BP; Ray, PC. Extremely High Two-Photon Absorbing Graphene Oxide for Imaging of Tumor Cells in the Second Biological Window, *J. Phys. Chem. Lett.*, 2014, *5*, 2150–2154.

[17] Castro Neto, AH; Guinea, F; Peres, NMR; Novoselov, KS; Geim, AK. The electronic properties of graphene, *Rev. Mod. Phys.*, 2009, *81*, 109.

[18] Kim, DW; Kim, YH; Jeong, HS; Jung, HT. Direct visualization of large-area graphene domains and boundaries by optical birefringency. *Nature Nanotech.*, 2012, *7*, 29–34.

[19] Wu, ZS; Yang, S; Sun, Y; Parvez, K; Feng, X; Müllen, K. 3D nitrogen-doped graphene aerogel-supported Fe 3O 4 nanoparticles as efficient electrocatalysts for the oxygen reduction reaction., *J. Am. Chem. Soc.*, 2012, 134, 9082–9085.

[20] Wu, XL; Wen, T; Guo, HL; Yang, S; Wang, X; Xu, AW. Biomass-Derived Sponge-like Carbonaceous Hydrogels and Aerogels for Supercapacitors, *ACS Nano*, 2013, 7, 3589-3597.

[21] Estevez, L; Kelarakis, A; Gong, Q; Husni Da'as E, Giannelis, EP. Multifunctional Graphene/Platinum/Nafion Hybrids via Ice Templating *J. Am. Chem. Soc.*, 2011, 133, 6122–6125.

[22] Yan, Z; Ma, L; Zhu, Y; Lahiri, I; Myung Hahm, G; Liu, Z; Yang, S; Xiang, C; Lu, W; Peng, Z; Sun, Z; Kittrell, C; Lou, J; Choi, W; Ajayan, PM; Tour, JM. Three-Dimensional Metal Graphene Nanotube Multifunctional Hybrid Materials. *ACS Nano*, 2013, 7, 58–64.

[23] Qian, X; Peng, XH; Ansari, DO; Yin-Goen, Q; Chen, GZ; Shin, DM; Yang, L; Young, AN; Wang, MD; Nie, S. In Vivo Tumor Targeting and Spectroscopic Detection with Surface-Enhanced Raman Nanoparticle Tags *Nat. Biotechnol.*, 2008, 26, 83– 90.

[24] Frontiera, RR; Henry, AI; Gruenke, NL; Van Duyne, RP. Surface-Enhanced Femtosecond Stimulated Raman Spectroscopy *J. Phys. Chem. Lett.*, 2011, 2, 1199–1203.

[25] Kleinman, SL; Ringe, E; Valley, N; Wustholz, KL; Phillips, E; Scheidt, KA; Schatz, GC; Van Duyne, RP. Single-Molecule Surface-Enhanced Raman Spectroscopy of Crystal Violet Isotopologues: Theory and Experiment, *J. Am. Chem. Soc.*, 2011, 133, 4115–4122.

[26] Kim, NH; Lee, SJ; Moskovits, M. Aptamer-Mediated Surface-Enhanced Raman Spectroscopy Intensity Amplification *Nano Lett.*, 2010, 10, 4181– 4185.

[27] Laurence, TA; Braun, G; Talley, C; Schwartzberg, A; Moskovits, M; Reich, N; Huser, T. Rapid, Solution-Based Characterization of Optimized SERS Nanoparticle Substrates *J. Am. Chem. Soc.*, 2008, 131, 162– 169.

[28] Barhoumi, A; Halas, NJ. Label-Free Detection of DNA Hybridization Using Surface Enhanced Raman Spectroscopy, *J. Am. Chem. Soc.*, 2010, 132, 12792– 12793.

[29] Barhoumi, A; Halas, NJ. Detecting Chemically Modified DNA Bases Using Surface-Enhanced Raman Spectroscopy, *J. Phys. Chem. Lett.*, 2011, *2*, 3118–3123.

[30] Brown, LV; Zhao, K; King, N; Sobhani, H; Nordlander, P; Halas, NJ. Surface-Enhanced Infrared Absorption Using Individual Cross Antennas Tailored to Chemical Moieties, *J. Am. Chem. Soc.*, 2013, 135, 3688– 3695.

[31] Lim, DK; Jeon, KS; Hwang, JH; Kim, H; Kwon, S; Suh, YD; Nam, JM. Highly Uniform and Reproducible Surface-Enhanced Raman Scattering from DNA-Tailorable Nanoparticles with 1-nm Interior Gap *Nat. Nanotechnol.*, 2011, 6, 452– 460.

[32] Ji, W; Spegazzini, N; Kitahama, Y; Chen, YJ; Zhao, B; Ozaki, Y. pH-Response Mechanism of p-Aminobenzenethiol on Ag Nanoparticles Revealed By Two-Dimensional Correlation Surface-Enhanced Raman Scattering Spectroscopy *J. Phys. Chem. Lett.*, 2012, 3, 3204– 3209.

[33] Joseph, V; Engelbrekt, C; Zhang, JD; Gernert, U; Ulstrup, J; Kneipp, J. Characterizing the Kinetics of Nanoparticle-Catalyzed Reactions by Surface-Enhanced Raman Scattering *Angew. Chem., Int. Ed*, 2012, 51, 7592– 7596.

[34] Dijk, T; Sivapalan, ST; DeVetter, BM; Yang, TK; Schulmerich, MV; Murphy, CJ; Bhargava, R; Carney PS. Competition Between Extinction and Enhancement in Surface-Enhanced Raman Spectroscopy, *J. Phys. Chem. Lett.*, 2013, 4,1193–1196.

[35] Sivapalan, ST; DeVetter, BM; Yang, TK; van Dijk, T; Schulmerich, MVCarney, PS; Bhargava, R; Murphy, CJ. Off-Resonance Surface-Enhanced Raman Spectroscopy from Gold Nanorod Suspensions as a Function of Aspect Ratio: Not What We Thought, *ACS Nano*, 2013, 7, 2099– 210.

[36] Shamual, D; Yu, H; Ray, PC. Gold Nanoparticle Based Label-Free SERS Probe for Ultrasensitive and Selective Detection of Trinitrotoluene *J. Am. Chem. Soc.*, 2009, 131, 13806– 13812.

[37] Lu, W; Singh, AK; Khan, SA; Senapati, D; Yu, H; Ray, PC. Gold Nano-Popcorn-Based Targeted Diagnosis, Nanotherapy Treatment, and *In Situ* Monitoring of Photothermal Destruction Response of Prostate Cancer Cells Using Surface-Enhanced Raman Spectroscopy *J. Am. Chem. Soc.*, 2010, 132, 18103– 18114.

[38] Singh, AK; Khan, SA; Fan, Z; Demeritte, T; Senapati, D; Kanchanapally, R; Ray, PC. Development of a Long-Range Surface-Enhanced Raman Spectroscopy Ruler, *J. Am. Chem. Soc.*, 2012, 134, 8662– 8669.

[39] Le Ru, EC; Etchegoin, PG. Single-Molecule Surface-Enhanced Raman Spectroscopy *Annu. Rev. Phys. Chem.*, 2012, 63, 65– 87.

[40] Haran, G. Single-Molecule Raman Spectroscopy: A Probe of Surface Dynamics and Plasmonic Fields *Acc. Chem. Res.*, 2010, 43, 1135– 1143.

[41] Willets, KA; Stranahan, SM; Weber, ML. Shedding Light on Surface-Enhanced Raman Scattering Hot Spots through Single-Molecule Super-Resolution Imaging *J. Phys. Chem. Lett.*, 2012, 3, 1286– 1294.

[42] Panikkanvalappil, SR; Mackey, MA; El-Sayed, MA. Probing the Unique Dehydration-Induced Structural Modifications in Cancer Cell DNA using Surface Enhanced Raman Spectroscopy *J. Am. Chem. Soc.*, 2013, 135, 4815– 4821.

[43] Sean Murphy, Libai Huang, Prashant V. Kamat, Reduced Graphene Oxide–Silver Nanoparticle Composite as an Active SERS Material, *J. Phys. Chem. C*, 2013, 117, 4740–4747.

[44] Ling, X; Xie, LM; Fang, Y; Xu, H; Zhang, HL; Kong, J; Dresselhaus, MS; Zhang, J; Liu, ZF. Can Graphene Be Used As a Substrate for Raman Enhancement? *Nano Lett.*, 2010,10, 553– 561.

[45] Sun, YH; Liu, K; Miao, J; Wang, ZY; Tian, BZ; Zhang, L; Li, QQ; Fan, SS; Jiang, KL. Highly Sensitive Surface-Enhanced Raman Scattering Substrate Made from Superaligned Carbon Nanotubes, *Nano Lett.*, 2010, 10, 1747– 1753.

[46] Thrall, ES; Crowther, AC; Yu, Z; Brus, LE. R6G on Graphene: High Raman Detection Sensitivity, Yet Decreased Raman Cross-Section. *Nano Lett.*, 2012, 12, 1571– 1577

[47] Ren, W; Fang, Y; Wang, EA. Binary Functional Substrate for Enrichment and Ultrasensitive SERS Spectroscopic Detection of Folic Acid Using Graphene Oxide/Ag Nanoparticle Hybrids *ACS Nano*, 2011, 5, 6425– 6433.

[48] , SK; Chu, Y; Rappoport, D; Crozier, KB; Aspuru-Guzik, A. Separation of Electromagnetic and Chemical Contributions to Surface-Enhanced Raman Spectra on Nanoengineered Plasmonic Substrates, *J. Phys. Chem. Lett.*, 2010, 1, 2740– 2746.

[49] Yu, X; Cai, H; Zhang, W; Li, X; Pan, N; Luo, Y; Wang, X; Hou, JG. Tuning Chemical Enhancement of SERS by Controlling the Chemical Reduction of Graphene Oxide Nanosheets, *ACS Nano*, 2011, 5, 952– 958.

[50] Angulo, AM; Noguez, C; Schatz, GC. Electromagnetic Field Enhancement for Wedge-Shaped Metal Nanostructures, *J. Phys. Chem. Lett.*, 2011, 2, 1978– 1983.

[51] Ai, KL; Liu, YL; Lu, LH. Hydrogen-Bonding Recognition-Induced Color Change of Gold Nanoparticles for Visual Detection of Melamine in Raw Milk and Infant Formula, *J. Am. Chem. Soc.*, 2009, 131, 9496– 9497.

[52] http://en.wikipedia.org/wiki/2008_Chinese_milk_scandal.

[53] http://en.wikipedia.org/wiki/2011_Taiwan_food_scandal.

[54] http://www.bbc.co.uk/news/world-europe-12120321.

[55] Li, XM; Luo, P; Tang, S; Beier, RC; Wu, X; Yang, L; Li, Y; Xiao, X. Development of an Immunochromatographic Strip Test for Rapid Detection of Melamine in Raw Milk, Milk Products and Animal Feed, *J. Agric. Foo Chem.*, 2011, 59, 6064– 6070.

[56] Kim, A; Barcelo, SJ; Williams, RS; Li, ZY. Melamine Sensing in Milk Products by Using Surface Enhanced Raman Scattering, *Anal. Chem.*, 2012, 84, 9303– 9309.

[57] Chen, LM; Liu, YN. Surface-Enhanced Raman Detection of Melamine on Silver-Nanoparticle-Decorated Silver/Carbon Nanospheres: Effect of Metal Ions, *ACS Appl. Mater. Interfaces*, 2011, *3*, 3091–3096.

In: Food Poisoning
Editor: Paresh C. Ray
ISBN: 978-1-63463-166-2

Chapter 10

NAPHTHALENE MOTHBALLS: A SILENT KILLER

Louis Z. G. Touyz
Periodontics; Faculty of Dentistry, McGill University,
Montreal QC, Canada

ABSTRACT

Mothballs are used globally to stop moth-larvae from damaging stored clothing and valuable furs.. Mothballs can be made of different insecticides, but the main one used is naphthalene. Naphthalene is a bicyclic aromatic compound used ubiquitously in industry agriculture and commerce. It is used for making other chemicals and exploited as an insecticide, soil fumigant or deodorant. Exposure occurs through chronic inhalation, skin contact or consumption in the food chain. The lungs and eyes are susceptible to toxic effects as are the kidney, brain and liver. Lens opacification and pulmonary histological changes are noted with poisoning. Naphthalene depletes glutathione, inhibits lipid peroxidation, increases DNA fragmentation and produces oxidative stress through production of superoxide anion and hydroxyl radicals. The ability to protect against toxic effects of naphthalene by using various anti-oxidants and free radical scavengers is known. Many households commonly use insecticides and pesticides domestically to control unwanted household infestations. Weather extremes demand that seasonal clothing be stored through changing cycles, to allow more than one seasons use. Naphthalene is a volatile substance which at room temperature releases a characteristic odoriferous gas which is toxic to moths. Unfortunately naphthalene vapours are also toxic to human cells and tissues. Various signs and symptoms described below derive from acute or chronic naphthalene poisoning. Frequently among the symptoms are haemolytic anaemia, ocular changes and pulmonary fibrosis. Methods of avoidance and palliative care of poisoning are discussed, and preventive and sociological strategies suggested for people to minimize risks from mothball poisoning.

BACKGROUND AND INTRODUCTION

Naphtha is a collective term for volatile liquid hydrocarbon mixtures that are inflammable. About 1820 coal-tar naphtha was distilled, (boiled with emanating vapours

cooled and collected) and the resultant substance formed was called naphthalene. Its pungent odour encouraged people to use it for many purposes including medicinal and biological applications. Since then many synonyms for naphthalene evolved into common use: Tar Camphor; White Tar; Moth Flakes; Albocarbon; Dezorator; Moth Balls; Mighty 150; Mighty RD1; Naphthene and Naphthalene under a variety of different phonetic spellings area used. For safety, health, disaster (fire and temperature changes) and economic purposes, it is important to know the chemistry and properties of naphthalene from the effects of handling, use, storage and transport.

Chemistry Formula, Structure and Properties

Chemically, naphthalene is classified as a polycyclic aromatic hydrocarbon (PAH) with a di-benzenoid structure. The positions on the molecule 1,4,5 and 8 are termed *alpha* positions, and 2,3,6 and 7 are termed *beta* positions. The electro-dynamic charges between the numbered atoms are in constant flux, and the carbon-carbon bonds in naphthalene are not of the same length. Accordingly, like benzene, naphthalene can undergo electrophilic aromatic substitution, which allows naphthalene to have more vigorous chemical reactions than benzene. Naphthalene can bond to other chemicals without accelerating catalysts to form new compounds. For example naphthalene binds to chlorine to form 1-chloronaphthalene without a catalyst. The *alpha sites* react more easily than the *beta sites*, and various combinations of add-on chemical produce isomer compounds with unique properties for each. Hydrogenation at raised temperatures yields other substance like *tetralin* and *decalin*, while oxidation with catalysts yields phthalic acid.

Properties: Molar mass=128.17052g/mol; Naphthalene is a white solid crystalline flake, easily compressed into a solid. Its density is 1.14g/cm^3, will melt 80.26^{o}C, boils at 218^{o}C and 30mg will dissolve in water at 25^{o}C. Its flash point is 79-87^{o}C and auto-ignition temperature is 525^{o}C. These properties relate to temperature at 25^{o}C and atmospheric pressure of 100kPa. [1, 2]

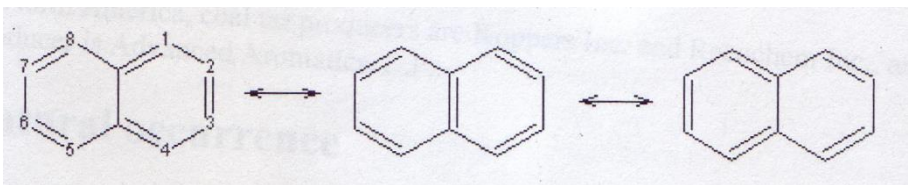

Figure 1. Chemical Structure. Naphthalene is composed of 2 joined benzene-like rings, fused together by sharing common central atoms. The molecular formula is $C_{10}H_8$.

Aim

This article appraises naphthalene properties, critiques its patho-biological effects deriving from accidental/abusive ingestion/incorporation into the human body, and suggests behavioural modification to minimize hazardous reactions, maximize benefits of use with

correct handling, and suggests possible mechanisms to optimise therapy from naphthalene intoxication. Focus is targeted to human reactions from chronic naphthalene poisoning.

Naphthalene in Biology, Nature and the Universe

Universally naphthalene is acknowledged as having strong reactive biological properties. It occurs naturally in small amounts in magnolias and in specific types of deer. Some wood termites (like those found in Formosa) produce it and some claim naphthalene acts against other ants, invading fungi and nematode worms. Not only do plants and arthropods produce naphthalene, but also varieties of fungi *like Muscodor albus*, and *Muscodor vitigenus.* Naphthalene exists in outer space between Cernis 52 and the constellation Perseus, and traces of it have been extracted from interstellar meteorites landing on earth. [1, 2]

Common Uses of Naphthalene

1,4dichlorobenzene is universally used in homes and storages as an insecticide. When enclosed the solid vaporizes rapidly to toxic lethal levels for adult moths and their larvae after hatching from eggs. It is not uncommon for people to *store clothes* in enclosing linen bags which allows diffusion of the naphthalene. Often it's placed as mothballs into closed domestic spaces like cupboards and chests and drawers, but it also escapes and pollutes household atmospheres.

Naphthalene is used in agriculture as a *fumigant pesticide*, and in/for other storage spaces like attics, storage depositories, costume wardrobes, museum cupboards and box-shelves to protect their specimen contents from attack by undesirable insect infestations. It has been used to *kill nematodes* (parasitic worms) in livestock. Naphthalene burns with thick black smoke and this is used in *pyrotechnical (fireworks) displays* and when making movies... It also *slows rust formation; consequently* bags of it are often kept in toolboxes. Also its *strong odour* is used in urinals toilets to mask ammoniacal smells. [1, 2]

Other Uses

Because it is solid at low industrial temperatures, it is used to create porosity in *grinding wheels* which are fired way above its melting, flash, and ignition point.

Naphthalene is also used in the chemical engineering field as a tool on the way to producing a variety of *insecticides and synthetic dyes*. Alkyl naphthalene sulfonates are used to disperse colloidal systems in aqueous media to make granular *agricultural formulations*, and processing textiles in *fabric* industries. It is used widely in processes for bleaching and dyeing *cloth*, making *pigments, pesticides, rubber* processing, and miscellaneous *chemicals and pharmaceuticals.* It is used as a plasticiser (dispersant) to make concrete and plaster board (wallboard and drywall); for *synthetic rubbers, tanning agents, and in making lead-acid battery plates.* [1, 2]

MEDICAL PROBLEMS AND CHALLENGES

Naphthalene is easily absorbed into the body. Rare cases have been reported through oral ingestion of the solid. More frequently poisoning occurs from vapours being absorbed through inhalation, [3, and 4] or dermal through skin by prolonged contact from handling. [4, 5, 6, 7]

Ocular contact with naphthalene will cause eye problems, [4] and exposed pregnant women put their foetuses at risk as naphthalene will cross the placental barrier. [8] Naphthalene affects pulmonary cells and induces chronic inflammation that results in pulmonary fibrosis. [9]

Red blood cells are particularly susceptible to naphthalene poisoning and anaemia results, with increased fragility of erythrocytes. [10] Haemoglobin is released in the serum after release from the imploding erythrocytes. Kidney, [11, 12] liver, [13] heart [14] and brain tissues react to naphthalene poisoning. Exposure has been associated with laryngeal and intestinal carcinoma. [15, 16].

It has a characteristic camphor-like smell of tar derived from coals. It is a volatile flammable solid that vaporizes at room temperature, and is detectable by the human nose (organoleptically, that is subjectively) at concentrations of 0.08ppm. [17] Workplace standards of air pollution with naphthalene have been put at a threshold time weighted value10ppm. [18]

Mechanisms and Pathophysiology

Understanding and controlling the molecule is essential to sustain health. *Naphthalene poisoning promotes oxidative stress in all tissues*. [19] It totally inactivates enzymes like glucose-6 dehydrogenase (G6PDH), and those with inherited deficiency of G6PDH are particularly susceptible to naphthalene poisoning and develop haemolytic anaemia. Glutathione is a strong anti-oxidant, and because of hereditary erythrocyte instability of glutathione, naphthalene poisoning with glutathione forms an epoxide metabolite (alpha naphthol) that mediates erythrocyte haemolysis. [9, 10, 20] Oxidative stress and lipid peroxidation with sulfur-groups in proteins leads to hepatic necrosis and ocular toxicity. [12] New borns are susceptible because they cannot conjugate both naphthalene and bilirubin, leading to neo-natal kernicterus (jaundice). The lens develops cataracts (precipitated protein). Depletion of glutathione also causes dose-dependant bronchiolar epithelial necrosis, inflammation and subsequent pulmonary fibrosis with breathing problems. [9]

Clinical Features

Toxic effects vary widely among patients [4, 21] Naphthalene is not a mammalian molecule and is incompatible with health.

Ingestion: When introduced into the body it acts as a disruptive poison. 2 grams ingestion over 2 days will be lethal to a 6 year old child. [3, 22, 23] The lethal dose for adults is between 5 and 15 grams depending on the weight of the subject [4].

Signs and Symptoms

Presentation: Unexplained headache, abdominal pain, nausea, vomiting, diarrhoea, fever, and profuse sweating are early features of naphthalene poisoning. Patients may develop optic neuritis, haemolytic anaemia, jaundice, pallor and hepatic necrosis.

Those with inherited G6DPD deficiency or sickle cell trait are more susceptible to haemolysis and methmaemoglobinaemia. [22]

Inhalation: Toxicity may be noted and is often encountered after a prolonged period of exposure. A wide variety of signs and/or symptoms may manifest from chronic exposure to naphthalene vapours, such as, headaches, bouts of mental confusion, and visual disturbances [22] chronic inhalation may produce varying degrees of nausea, loss of appetite, vomiting or disorientation. Delayed intra-vascular haemolysis may occur [4], and respiratory failure, pulmonary oedema, bouts of pneumonia and dyspnoea, respiratory distress and respiratory failure may present as a result. [13]

Local Effects

Eye, Ear, Nose and Throat : Corneal ulceration and cataracts may develop after exposure to naphthalene vapour or dust. Nasal and pharyngeal irritation with catarrh developing is noted with chronic exposure. Allergies to naphthalene are also reported but are rare. [4, 25]

Skin exposure: Continuous handling of naphthalene may produce a dermatitis characterised by itching, redness, scaling, weeping and crusting of the skin. [22]

Systemic Effects

Heart: The cardiac effects may show tachycardia and arrhythmias with hyperkalaemia and possible circulatory failure. [13, 24].

Blood analysis often includes a rapid fall of the RBC's count, the haemoglobin, and haematocrit, and a temporary increase in reticulocytes and normoblasts in the peripheral blood. Erythrocytes may contain Heinz bodies and show anisocytosis (variation in size) and poikilocytosis (irregular shapes). Deficiency of G6PDH can be demonstrated with a specific test (25).

Serum bilirubin is elevated. Consequently urine may vary in colour from reddish brown to dark brown bark black, and the metabolite alpha naphthol will be found in it. [11].

Pregnancy: a peculiarity of 'pica' (eating unusual abnormal substances as food) may occur during pregnancy. Pica-sucking of naphthalene in the third trimester has been reported with toxic haemolytic effects of the mother and baby. Withdrawal allowed for full recovery of mother and child. [8, 4]

Brain: Many types of insecticides interfere with neuro-transmission and ion channels. Naphthalene affects the brain and cognitive, pyramidal and extra-pyramidal, cerebellar functions may be compromised. Mild CNS effects are reversible. [26] Accommodation to the naphthalene fragrance also happens and consequent inhalation of vapors is unwittingly sustained. This may lead to any of the pathological reaction described.

Therapy and Treatment Strategies

Lens opacification and/or pulmonary histological changes are noted with poisoning, and naphthalene also depletes glutathione, inhibits lipid peroxidation, and increases DNA fragmentation. Naphthalene toxicity produces cellular oxidative stress through production of

superoxide anion and hydroxyl radicals. The ability to protect against toxic effects of naphthalene by using various anti-oxidants and free radical scavengers has been shown. [19]. Vit E, VitE-succinate, melatonin, curcumin, various L-cysteine pro-drugs, some aldose reductase inhibitors and spin-trapping agents, will counter to some extent the toxic effects. [19]

Resveretrol is an anti-oxidant found in red wines, grapes and many vegetables. Resveretrol treatment reverses most biochemical aberrations and histological damages induced by naphthalene toxicity. Resveretrol inhibits neutrophil infiltration, balance oxidant-antioxidant status, regulates generation of inflammatory mediators, and ameliorates oxidative organ injury due to naphthalene toxicity. [27]

Skin and eye exposure: Flush the affected area with lukewarm running water for at least 20 minutes. When handling the material, wearing impervious gloves is essential. [4]

Inhalation: Remove source and separate victim from the source. A thorough assessment of the respiratory airways, breathing and circulation is demanded. Administer oxygen if cyanosed and support ventilation. Cardio-pulmonary resuscitation may be indicated. With chronic poisoning frequent assessments of cardiopulmonary health is demanded with appropriate support to stabilize breathing and cardiac function. [11] A course of cortisone helps relieve symptoms. [25]

Ingestion: If more than 2 hours has passed gastric lavage is not effective [12]. Activated charcoal in slurry of water at 1 gram/kg up to 50 grams could prove useful. Fatty foods and dairy products should be avoided as they promote absorption [4, 12].

Prevention and Removal

The source of the vapours must be removed including all clothes or foodstuff that may have been exposed to the vapours. Relocating the victim and aerating their dwelling until no trace of the naphthalene is detected by smell; this is indicated to ensure cessatio of the offensive fumes.

Severe anaemia, kernicterus, convulsions, and renal dysfunction demand professional medical handling, and hospitalization with intense observation and symptomatic treatments are indicated.

DISCUSSION

All substances may be poison; it all depends on the dosage, frequency of exposure and quanta received.

The weight of victims, the form in which poisons are administered, and the time over which a poison is exposed, all impact on the body effects.

SOCIOLOGY AND IMPLICATIONS

From the wide range of industrial uses outlined above, it is easily possible for many people to be exposed to naphthalene and its deleterious effects. Children may play with it, and the ignorant may actually eat it. But by far the most prevalent domestic use is for protecting

clothes, woolen haberdashery (like blankets) and preserving other garments or furs against household moths. Naphthalene is manufactured into spheres (mainly) or other shapes of various sizes, and freely marketed to the public for household use. In spite of warnings on the packets, most people liberally use the products without appreciation for its potential harmful effects. For mothballs as naphthalene to be an effective fumigant, clothes should be enclosed in air-tight plastic bags. This ensures the vapours reach lethal levels for the moths and their larvae. Once removed, treated garments should be removed from their bags and aired out in fresh breeze until no camphorous odour can be detected.

People spending prolonged times in confined spaces with high concentrations of naphthalene vapours are prone to become mysteriously ill. *This frequently affects seniors who hibernate in winter in small apartments, and have laced their accumulated expensive garments with naphthalene*. Often the garment retainers are not air-tight and after a short period, the human nose accommodates to the naphthalene smell, and is tolerated or ignored.

Consequently complex symptoms arise and a medical diagnosis is obfuscated by many confounding variables and many a physician is flummoxed at the complexity of clinical findings. [11] Often the diagnosis of chronic naphthalene poisoning is arrived at too late to be able to implement effective curative therapy, and palliative therapy is all that is available. This is a challenge for both patient and treating physician.

Chronic naphthalene poisoning through inhalation may produce a sequence of minor but persistent signs and symptoms. Late onset anaemia, mild jaundice, urinary color changes, loss of mental acuity and heart problems may all manifest in mild or severe forms. Chronic poisoning may produce mild signs and symptoms, until threshold levels are reached, and positive therapeutic interference is indicated. This may demand cardiac, haematological or ocular therapies depending on which organ is in crisis.

Often the clues from toxicity are vague and obfuscated, but may be picked up in the presenting anamnesis (Medical History). A patient may report feeling much better after taking a boat cruise or other outdoor holidays. Others may claim they cannot stand the winters any more. Some say they breathe more comfortably outdoors but are limited because of the cold exposure. Friends may note the smell of naphthalene on victims' clothes, to which the victim may be oblivious. Affected foodstuffs may taste of naphthalene. If naphthalene poisoning is suspected a urinary test may vary in colour, and finding the metabolite alpha naphthol in it confirms toxic exposure. [11].

Courtesy, respect, possible ignorance of the deleterious effect and political correctness prevent friends from reporting or complaining about the offensive odour. Full medical workups may not be diagnostic or conclusive, and chronic naphthalene poisoning as a diagnosis may not initially be realized. Patients may develop a cardiac arrhythmia, anaemia and/or chronic pulmonary fibrosis as a result, and the best chances for preventive therapy may be missed. Only after symptomatic therapy and relocation to new lodgings will improvement be noted and a cohesive explanation for the symptoms realized.

CONCLUSION

People, especially seniors, who have used naphthalene, should be more aware of the possible dangers deriving from its toxic fumes. Everyone should be made aware of the

naphthalene dangers staying in an enclosed space without proper ventilation. Proper use and washout aeration of clothes moth protected by naphthalene are indicated. Mothballs are not so innocent; they may be a serious danger and a silent killer.

Declaration: The author has no conflict of interest to declare.

Dedication: This review is dedicated to the memory of *Edward Cohen Esq*. (1929-2010), a health care worker in psychiatry at the Douglas Hospital, Montreal PQ Canada. A true philanthropist whose early demise was too soon.

REFERENCES

[1] Naphthalene: http://en. Wikipedia.org/wiki/naphthalene. Accessed 04/01/2009

[2] Fernando R & Nissanaka S. Naphthalene. IPCS: INCHEM. INTOX 12 Meeting, Erfurt Germany. Sep 2000. MO Rambourg, Schepens. PIM 363. Wikipedia accessed 04/01/2009

[3] Santucci K and Shah B. Association of naphthalene with acute hemolytic anemia. *Acad. Emer. Med*. 2000. 7:42-47.

[4] Clinical Toxicology of Commercial Products. Gosselin, RE Smith, Hodge HC. Eds. II-153, III-307-310. Williams and Wilkins, Baltimore.

[5] Schafer WB. Acute hemolytic anemia related to naphthalene. Report of a case in a new-born infant. Pediatrics 1951. 7:172-174.

[6] Valaes T, Doxiades SA, Fessas P.Acute hemolysis due to naphthalene inhalation. *Jnl. of Pediatrics* 1963. 63:904-915.

[7] Fanbergh SJ. Exfoliative dermatitis due to Naphthalene. *Arch. Derm. Syph.* 1940. 43:53-56.

[8] Anziulewicz, Herman JD, Chiarulli EE. Trans-placental naphthalene poisoning. *Am. Jnl. Obstetrics and Gynecology* 1959. 78:519-521.

[9] Richieri PR, Buckpitt AR, Glutathione depletion by naphthalene in isolated hepatocytes and naphthalene oxide *in vivo*. *Biochem, Pharmacol.* 1988. 37: 2473-2478.

[10] Mackell JV, Rieders R, Brieger H & Bauer EL. Acute hemolytic anemia due to ingestion of naphthalene mothballs. *Pediatrics* 1951. 7:722-728.

[11] Weintraub E, Gandhi D, Robinson C. Medical complications due to mothball abuse. *South Med. Jnl.*93; 427-429.

[12] Choudri AN, Pasha MJ, Ali B. Acute renal failure following naphthalene poisoning. *J. Pak. Med. Assoc.* 1995; 45, 332-332.

[13] Siegel and Wason. Mothball Toxicity. Paediatric Clinics of North America. *Eds Blumer JL & Reed MD*. 1986, 33:369-374.

[14] Kouri N, Valti H, Papazoglou E et al. Severe hemolysis with severe metabolic disturbance after naphthalene Poisoning. EAPCCT Animal Scientific Meeting, Birmingham UK. May 1993. (Abstract)

[15] Wolf O. Naphthalene toxicity and Neoplastic Changes. *Deutsche Gesundheitswesen*, 1976. 31:996-7.

[16] IARC Monographs on Evaluation of Carcinogenic Risks in Humans. Some Traditional Herbal Medicines, some Mycotoxins, *Naphthalene and Styrene*. 2002. 82:367-8.

[17] Amoore JE, Hautala E. Odor as an aid to chemical safety: Odor thresholds compared with threshold limit values and volatiles for 214 industrial chemicals in air and water dilution. *Jnl. Applied Toxicol.* 1983, 3, 272-290.

[18] ACGIH- American Conference of Governmental Industrial Hygienists Inc. Documentation of the Threshold Limit Values and Biological Exposure Indices. 1986. 420-1. Cincinnati, Ohio, USA.

[19] Stohs SJ, Ohia S, Bagchi D. Naphthalene Toxicity and Antioxidant Nutrients. *Toxicology* 2002. 180 (1) 97-105.

[20] Haddad LM Shannon, Winchester JF. Clinical Management of Poisoning and Drug Overdose. Naphthalene Poisoning. 3rd Edition. 1998. WB Saunders Co.

[21] Dreisbach RH. In: Handbook of Poisoning. 6th edition. Hydrocarbons. Naphthalene. 1969, 152-3. Lang Medical Publications. Los Alto, California, USA.

[22] Dreisbach RH and Robertson WO. In: Handbook of Poisoning. Prevention diagnosis and treatment. 1987.,194-195. Appleton and Lange Los Altos Calif.

[23] Chun T, Perrone J, Osterhoudt K, Ugur S, Henretig F. Mothball blues; confusion in naphthalene toxicities and treatment. *Clin. Toxicol*. 1998.36:465 (abstract).

[24] Kurz JM. Napthalene poisoning. Critical care nursing techniques. *Dimensions Crit. Car. Nurs.* 1987.6:264-270.

[25] Hayes WJ. In: Pesticide studies in Man. 1982. 136-137. Williams and Wilkins. Baltimore. Md USA.

[26] Cheong R, Wilson RK, Cortese IC, Newman-Toker DE. Mothball withdrawal encephalopathy: case report and review of para dichlorobenzene neurotoxicity. *Subst. Abus.* 2006. 27, 63-7.

[27] Sehirli O, Tozan A, Omurtag GZ, Cetinel S, Contuk G, Gedik N, Sener G. Protective effect of Resveretrol against naphthalene induced oxidative stress in mice. *Ecotoxicol. Environ. Saf.* 2008. 71, 301-308.

INDEX

B

C

D

E

F

G

H

I

J

K

L

M

N

O

P

Q

R

S

T

U

V

W

Y

Z